S

Self-Assembled Monolayer

Kazue Kurihara
WPI-AIMR (Advanced Institute for Materials Research) and Institute of Multidisciplinary Research for Advanced Materials (IMRAM), Tohoku University, Sendai, Japan

Synonyms

SAM

Definition

Monolayer immobilized on a solid surface by chemical adsorption and/or chemical reaction.

Why SAM? From LB Films to SAM

Amphiphilic molecules, which bear a hydrophilic and a hydrophobic group such as a long hydrocarbon chain, form monolayers orienting their hydrophilic groups to water and the hydrophobic part to air at the air–water interface when they are spread from their solutions [1]. These monolayers can be transferred on the solid substrates at desired thickness by repeated transfer cycles. These transferred mono- and multilayers are called Langmuir–Blodgett (LB) films after the names of Irving Langmuir and Katherine Blodgett who developed the method in the 1930s. It was already demonstrated at the time of Langmuir and Blodgett that the LB film coating of silica glass reduces the reflection of the glass surface. The advantages of LB films for developing well-organized films in the molecular dimension attracted much attention in the 1970s and 1980s after Kuhn and Mobius demonstrated a sophisticated way of regulating the photoinduced energy transfer of cyanine dyes incorporated in LB films [2]. Such molecular organized systems have been active research targets for designing novel molecular devices. Although assembling molecules at the air–water interface and subsequently transferring them on solid surfaces are simple in principle, these processes require a relatively complicated instrument, an LB trough, experimental skills, and long labor.

Preparation and Applications

It was natural; therefore, preparation of similar organized structures by much simpler procedures was attempted and realized by J. Sagiv in 1979 [3]. The physical and chemical adsorption of amphiphiles was a tool for preparing monolayers at the solid–fluid interface. The earliest and popular way for immobilizing monolayers is the silane coupling reaction as shown in Fig. 1. A trichlorosilane-based "head group," for example, in an OTS (octadecyltrichlorosilane, R = octadecyl) molecule, reacts with a hydroxyl
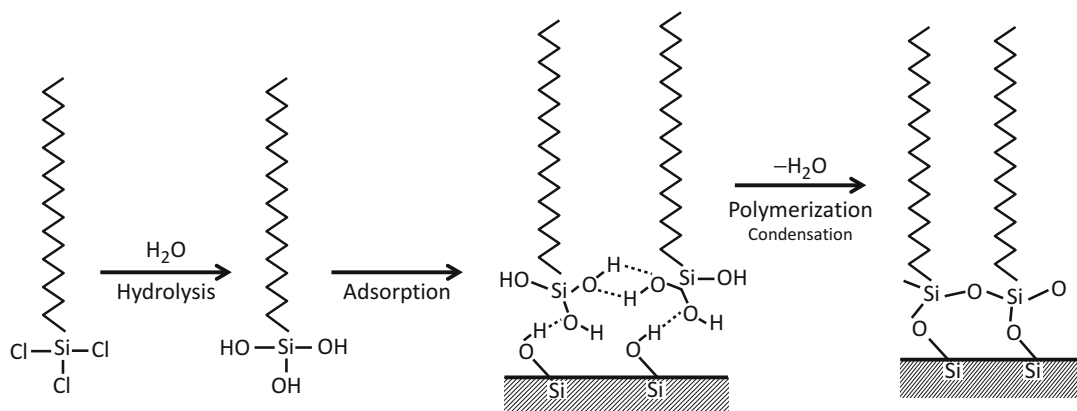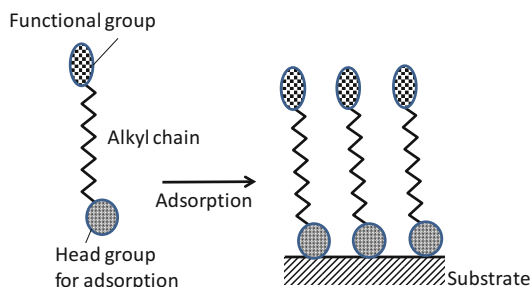
Self-Assembled Monolayer, Fig. 1 Chemisorption of *n*-octadecyltrichlorosilane (OTS) on glass [3]

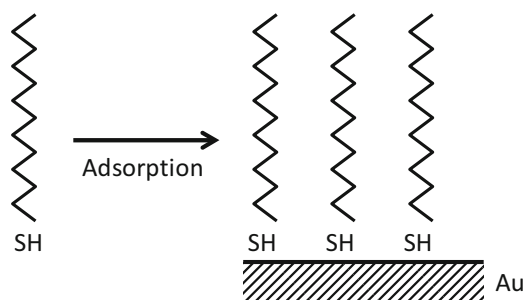**Self-Assembled Monolayer, Fig. 2** Formation of a self-assembled multilayer
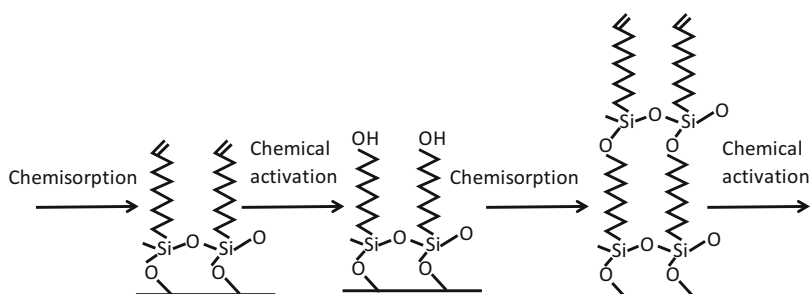
group on a substrate and forms a very stable covalent bond [R–Si–*O*-substrate]. The monolayers thus formed exhibit a high degree of perfection in terms of molecular density, packing and orientation, and homogeneity even when it contains dyes and another active component, which is similar to the LB films [3]. It is possible to recognize hydrocarbons of optimized length when defects are created in SAM [4]. Multilayer formation is possible to prepare interlayer polymerization as shown in Fig. 2 [5]. Subsequently, various variants of adsorbed groups are developed to form such monolayers, and monolayers prepared are called self-assembled monolayers (SAM) (see Fig. 3). Selecting the type of head group depends on the application of the SAM, mostly on substrates. Typically, head groups (i.e., –OH, −NH2, −COOH, or –SH groups) are connected to a molecular chain. Substrates can be planar surfaces, such as silicon

Self-Assembled Monolayer, Fig. 3 A typical example of a self-assembled monolayer

and metals, or curved surfaces, such as nanoparticles. Perhaps the most popular SAM is systems utilizing the SH groups as head groups for adsorption to gold and silver substrates as shown in Fig. 4 [6]. Thiol–metal bonds are fairly stable in a variety of temperature, solvents, and potentials. SAMs are widely used for introducing functional groups and changing the surface

Self-Assembled Monolayer, Fig. 4 Formation of a thiol self-assembled monolayer on gold

characteristics such as wettability and contact angles. Macro-imprinting method using PDMS (poly(dimethylsiloxane)) as a stamp and a SAM-forming solution as an ink is often used for preparing patterned surfaces such as hydrophobic and hydrophilic patterns [7]. Self-assembled monolayers are considered as essential elements for constructing nano- and micro-devices.

Related Entries

► Langmuir-Blodgett (LB) Film

References

1. Michael PC (1996) Langmuir-Blodgett films: an introduction. Cambridge University Press, Cambridge
2. Kuhn H, Möbius D (1971) Systems of Monomolecular Layers–Assembling and Physico-Chemical Behavior. Angew Chem Int Ed Engl 10:620
3. Sagiv J (1980) Organized monolayers by adsorption. 1. Formation and structure of oleophobic mixed monolayers on solid surfaces. J Am Chem Soc 102:92
4. Tabushi I, Kurihara K, Naka K, Yamamura K, Hatakeyama H (1987) Supramolecular Sensor Based on SnO_2 Electrode Modified with Octadecylsilyl Monolayer Having Molecular Binding Sites. Tetrahedron Lett 28:4299
5. Netzer L, Iscovici R, Sagiv J (1983) Adsorbed monolayers versus Langmuir-Blodgett monolayers-Why and how? I: From monolayer to multilayer, by adsorption. Thin Solid Films 99:235
6. Nuzzo RG, Allara DL (1983) Adsorption of bifunctional organic disulfides on gold surfaces. J Am Chem Soc 105:4481
7. Xia YN, Whitesides GM (1998) Soft Lithography. Angew Chem Int Ed 37:551

Self-Assembly of Hyperbranched Polymers

Yongfeng Zhou and Deyue Yan
School of Chemistry and Chemical Engineering, State Key Laboratory of Metal Matrix Composites, Shanghai Jiao Tong University, Shanghai, P. R. China

Synonyms

Block copolymers; Dendritic polymers; Supramolecular chemistry

Definition

Self-assembly of hyperbranched polymers is a process in which amphiphilic hyperbranched polymers spontaneously form ordered aggregates at all scales and dimensions by intermolecular noncovalent interactions including van der Waals interaction, Coulomb interaction, hydrophobic interaction, π–π stacking, and so on.

Introduction

Dendritic polymers, including dendrimers and hyperbranched polymers (HBPs), are the new emerging polymer architectures following the linear, branched, and cross-linking polymers. HBPs, consisting of dendritic units, linear units, and terminal units, are highly branched macromolecules with a three-dimensional dendritic architecture [1–4]. In fact, the hyperbranched structure also widely exists in nature, such as in the lightings, rivers, mountains, trees, corals, glycogens, neurons, and blood vessels. The reason for nature to select hyperbranched structure is certainly related with the unique property advantages originating from such a highly branched structure. As a matter of fact, HBPs have the properties of non/low-entanglement, low viscosity, good solubility, compact structure, and

S
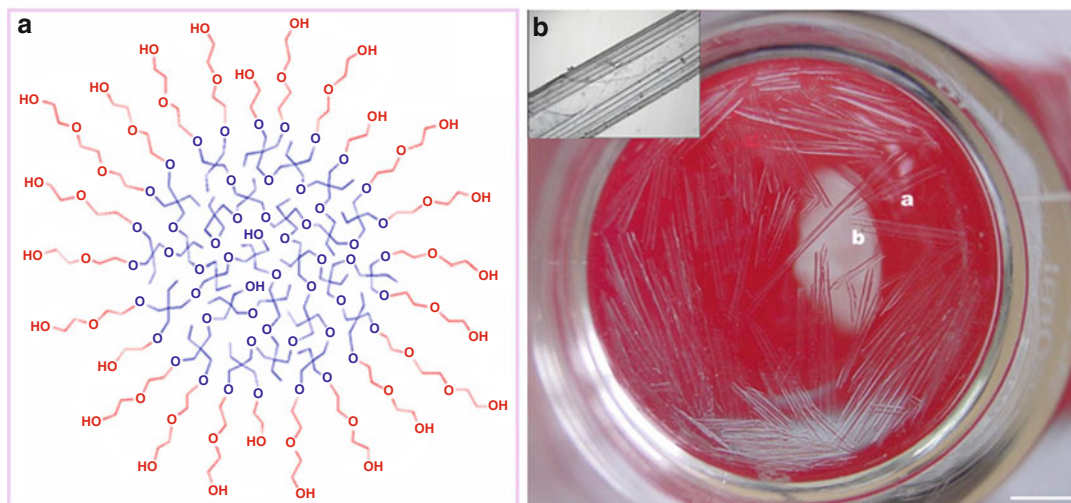
Self-Assembly of Hyperbranched Polymers, Fig. 1 (**a**) Schematic structure of the hyperbranched multiarm copolymer of HBPO-star-PEO. The HBPO core is in *blue* and the PEO arms are in *red*. (**b**) The digital photograph of the self-assembled macroscopic multiwalled tubes in acetone. The scale bar represents 1 cm. The *inset* shows the optical micrograph of the tubes (Reproduced with permission of the American Association for the Advancement of Science from Ref. [8])

a large number of terminal functional groups. Thus, HBPs can act as processing additives for linear polymers, for improving rheology and flow and for surface modification, which is very useful for processing polymers such as PVC with small temperature windows. In addition, due to the large number of functional groups, HBPs can act as highly efficient cross-linkers or as reactive components in coating and resin formulations. Moreover, HBPs can act as molecular templates to direct the self-assembly and growth of inorganic molecules to produce nanomaterials.

Molecular self-assembly is a hot research area in recent year. Generally, the reported precursor molecules used in self-assembly often possess well-defined molecular structures, such as small amphiphiles, dendrimers, and linear block copolymers. Through the self-assembly of these precursors, many elaborate microscopic or mesoscopic supramolecular objects have been observed over the last two decades, including nano- or microscale micelles, vesicles, ribbons, films, fibers, tubules, and so on [5–7]. Compared with these well-defined polymer precursors, HBPs have a rather irregular structure, and thus their self-assembly behaviors have been neglected for a long time. In year 2004, Yan and Zhou have found that an amphiphilic hyperbranched multiarm copolymer of HBPO-star-PEO with a hydrophobic hyperbranched poly(3-ethyl-3-oxetanemethanol) (HBPO) core and many hydrophilic poly(ethylene oxide) (PEO) arms can self-assemble into macroscopic tubes in a selective solvent of acetone (Fig. 1), which paves a new way in the self-assembly for HBPs [8]. Subsequently, many delicate supramolecular structures at all scales and dimensions have been reported by direct solution self-assembly, interfacial self-assembly, and hybrid self-assembly of amphiphilic HBPs.

## Multidimensional and Multi-scale Self-Assembly of HBPs

HBPs should have an amphiphilic character in order to realize the self-assembly. Up to now, both the covalent or noncovalent methods have been used to synthesize amphiphilic HBPs. For a covalent method, the hyperbranched multiarm

copolymer consisting of a hyperbranched core and many polymeric arms or functional groups has been synthesized, and the synthesis is performed by grafting polymerization of monomers initiated by the terminal groups of the hyperbranched core (so-called graft from method) or coupling the small molecules or oligomers to the terminal groups (so-called graft to method). Up to now, the hyperbranched cores are generally based on the hydrophobic HBPO, hydrophilic hyperbranched polyglycerol (HPG), hyperbranched polyesters such as the hydrophilic hyperbranched polyphosphate and commercially available hydrophobic Boltorn Hx (x = 20, 30, 40), and hydrophilic hyperbranched polyethylenimine (HPEI). The linear arms grated to these hyperbranched cores include PEO, poly (N-isopropylacrylamide) (PNIPAM), poly (acrylic acid) (PAA), poly(γ-benzyl-L-glutamate) (PBLG), poly[2-(dimethylamino)ethyl methacrylate] (PDMAEMA), poly(propylene oxide) (PPO), long alkyl chains, polystyrene (PS), and so on [9–12]. For the noncovalent method, the hyperbranched core and linear arms are connected together to form the amphiphilic HBP through the noncovalent bondings, such as the host–guest interaction, Coulomb interaction, and hydrogen bonding. For example, Zhou and coworkers have synthesized a linear-hyperbranched supramolecular polymer through the noncovalent coupling of adamantane (AD)-functionalized long alkyl chain and HPG grafted from β-cyclodextrin (CD-g-HPG) by the specific AD/CD host − guest interactions (Fig. 2a) [13]. Very recently, they also prepared supramolecular Janus hyperbranched polymer by the noncovalent coupling between the hydrophobic HBPO with an apex of an azobenzene (AZO) group and hydrophilic CD-g-HPG with a CD apex through the specific AZO/CD host − guest interactions (Fig. 2b) [14].

The synthesized amphiphilic HBPs can be used as the polymeric precursors in self-assembly. Although many kind of delicate supramolecular structures have been reported through the self-assembly of small amphiphiles and linear block copolymers, the size of these self-assemblies is generally limited to microscopic or mesoscopic scale. In other words, most of the works are based on microscopic or mesoscopic molecular self-assembly, and the macroscopic molecular self-assembly phenomenon has seldom been reported. In year 2004, Zhou and Yan reported macroscopic multiwalled tubes of millimeters in diameter and centimeters in length through the self-assembly of amphiphilic HBPO-star-PEO in acetone (Fig. 1b). For the self-assembly mechanism, the polymers spontaneously aggregated into macroscopic membranes with a lamellar structure consisting of an alternate packing of a hydrophobic HBPO core layer and hydrophilic PEO arm layer induced by phase separation, which further folded into macroscopic multiwall tubes [8]. In addition, the tubes could be cross-linked by epichlorohydrin to form super-macromolecules with unusually large molecular weight. This work not only realized the self-assembly of HBPs but also make the molecular self-assembly advance into the macroscopic scale. Ever since this groundbreaking work, there has been an explosive growth of interest in supramolecular self-assembly of HBPs. Many impressive molecular aggregates at all scales and dimensions, such as physical gels, micro- or nanovesicles, fibers, spherical micelles, honeycomb-patterned films, and large compound vesicles, have been reported by direct solution self-assembly, interfacial self-assembly, and hybrid self-assembly of HBPs (Fig. 3) [9–12].

Besides the covalently synthesized amphiphilic HPBs, very recently, supramolecular HBPs have also been found to demonstrate interesting self-assembly behaviors. For example, Zhou and coworkers had found the synthesized linear-hyperbranched supramolecular polymers (Fig. 2a) could self-assemble into unilamellar vesicles in water [13]. The vesicles showed a great ductility with a deformation of more than 300 % under external force and would disassemble readily under a competitive host of β-CD. Besides, Zhou and coworkers also found the supramolecular Janus hyperbranched polymers (Fig. 2b) could self-assemble into bilayer vesicles with narrow size distribution [14].
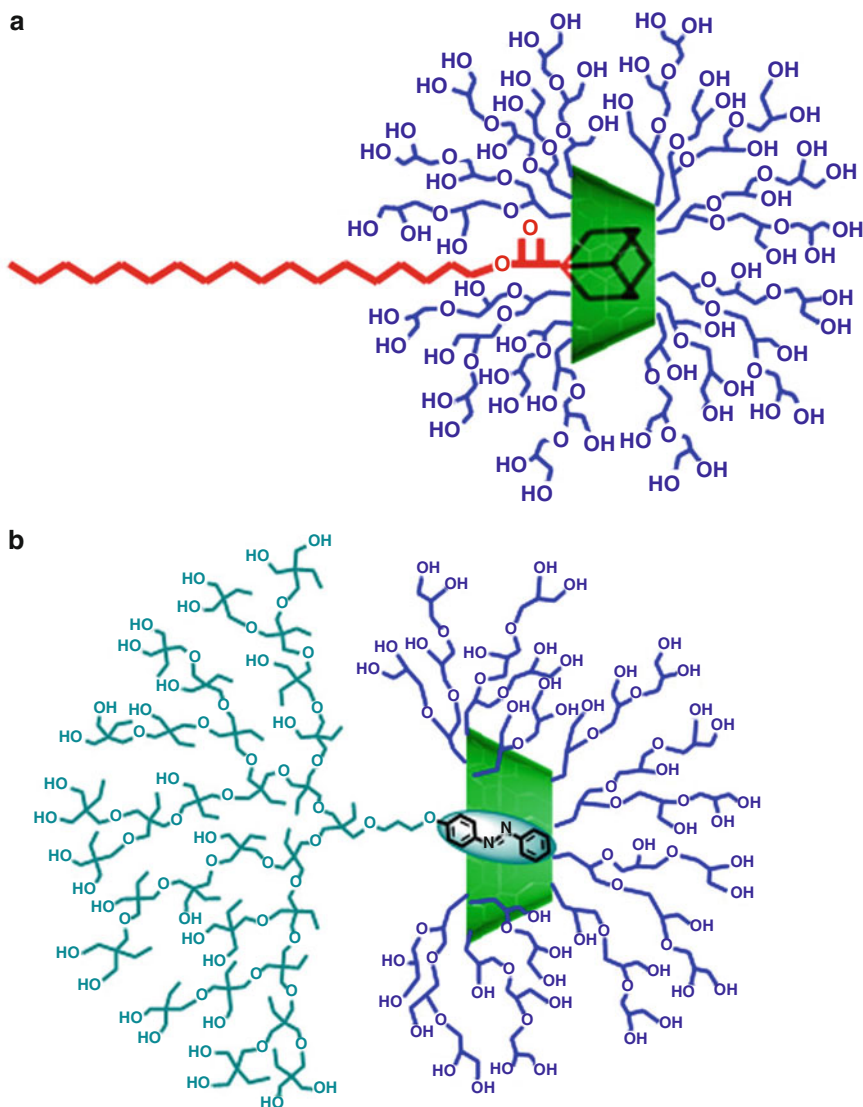
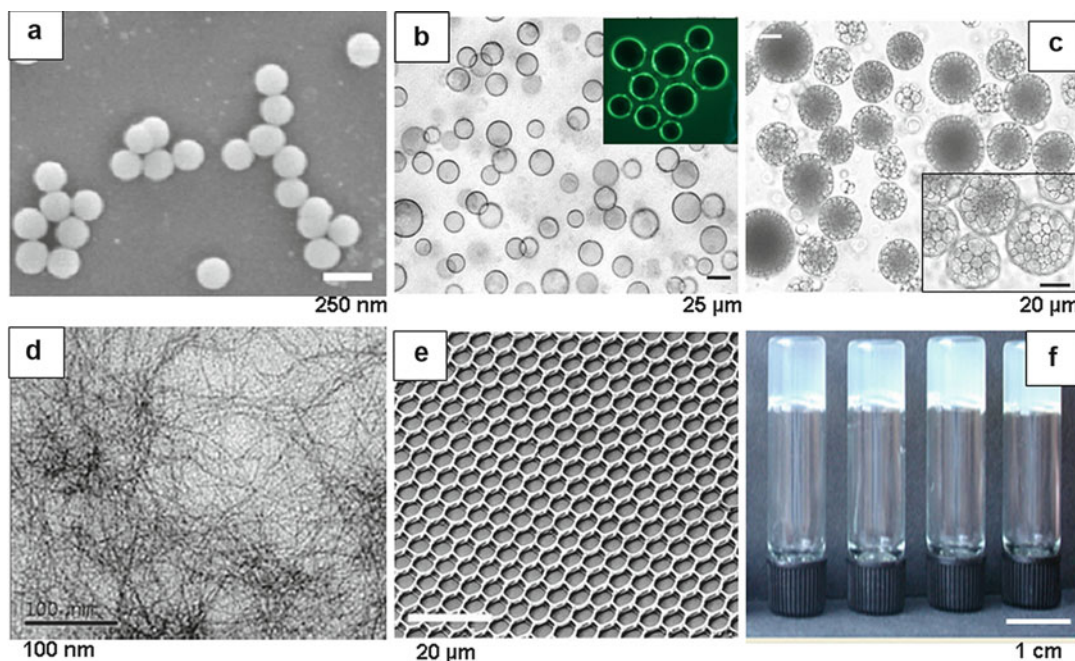**Self-Assembly of Hyperbranched Polymers, Fig. 2** Hyperbranched-based supramolecular polymers with a linear-hyperbranched structure (**a**) and a Janus hyperbranched structure (**b**) (Reproduced with permission of the American Chemical Society from Refs. [13] and [14])

The obtained vesicles could further aggregate into colloidal crystal-like close-packed arrays under freeze-drying conditions due to the almost monodisperse size and would disassemble reversibly under the irradiation of UV light due to the *trans-to-cis* isomerization of the AZO groups. The vesicles with a very good ductility or with a narrow size distribution are difficult to be achieved through the self-assembly of covalently synthesized HBPs. Such the special advantages can be attributed to the dynamic character of the supramolecular polymers.

Specialties in the Self-Assembly of HBPs

Compared with the linear block copolymers, HBPs have demonstrated several advantages or specialties in self-assembly behaviors, including abundant self-assembly morphologies or

Self-Assembly of Hyperbranched Polymers, Fig. 3 Some selected supramolecular structures obtained through the self-assembly of hyperbranched polymers. (**a**) Spherical micelles; (**b**) vesicles; (**c**) large compound vesicles; (**d**) fibers; (**e**) honeycomb-patterned film; (**f**) physical gel (Reproduced with permission of the American Chemical Society from (Ref. [18]; Langmuir 2007, 23, 5127) Wiley (Angew Chem Int Ed 2004, 43, 4896; Small 2007, 3, 1170; Angew Chem Int Ed 2007, 46, 4128) and Royal Society of Chemistry (Chem Commun 2007, 2587))

structures, special properties, and characteristic self-assembly mechanism [10].

Structure or Morphology Diversity

HBPs can self-assemble into various supramolecular objects owing to the special topological structure of the polymers. HBP has a three-dimensional globular structure. A small change in the molecule architecture of HBPs will give rise to a big change in topology due to an enlarged effect of the highly branched structure, which leads to a variable of designable self-assembly morphologies and structures. In addition, HBPs are more flexible than the linear analogs and can adopt any kind of chain conformation in response to the environmental stimuli during the microphase separation process, which is also favorable to the abundant self-assembly behaviors. Such a unique characteristic has been denoted as "topological amplification effects" [12]. It is much easier to understand such an effect if we take the tree as an example. The tree has a typical hyperbranched structure. There are uncountable trees on the earth, however, almost each tree has its one shape and it is difficult to find two trees with the same structure and morphology. In other words, like the trees, numerous hyperbranched polymers with different structures can be obtained, which will certainly lead to the diversity in the self-assembly morphologies. Typically, for HBPs, degree of branching (DB) is one of the most important intrinsic parameters to describe the branching topological structure, which not only greatly influences the physical and chemical properties of the polymers but also has a pronounced effect on the self-assembled behaviors. For example, in the self-assembly of HBPO-star-PEO, with the increase of the DB in HBPO cores, the polymers changed from the linear polymer brushes to spherical hyperbranched star copolymers, while the self-assembly structures
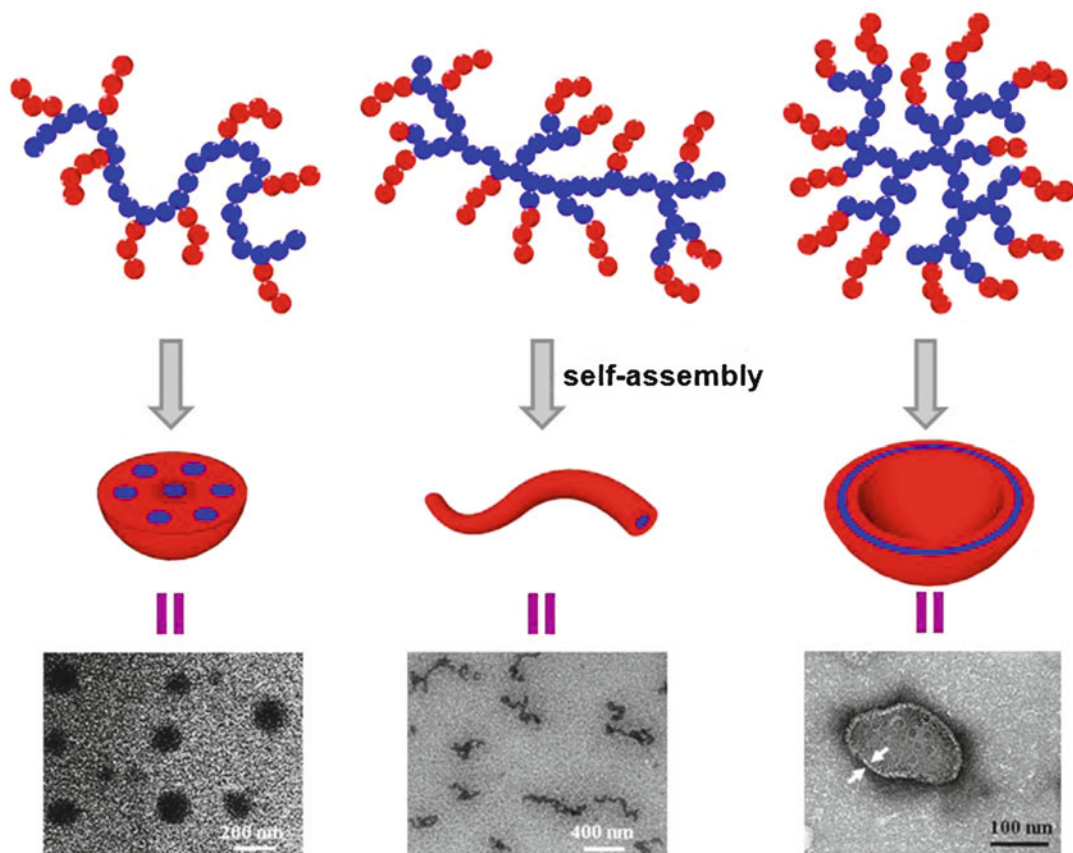
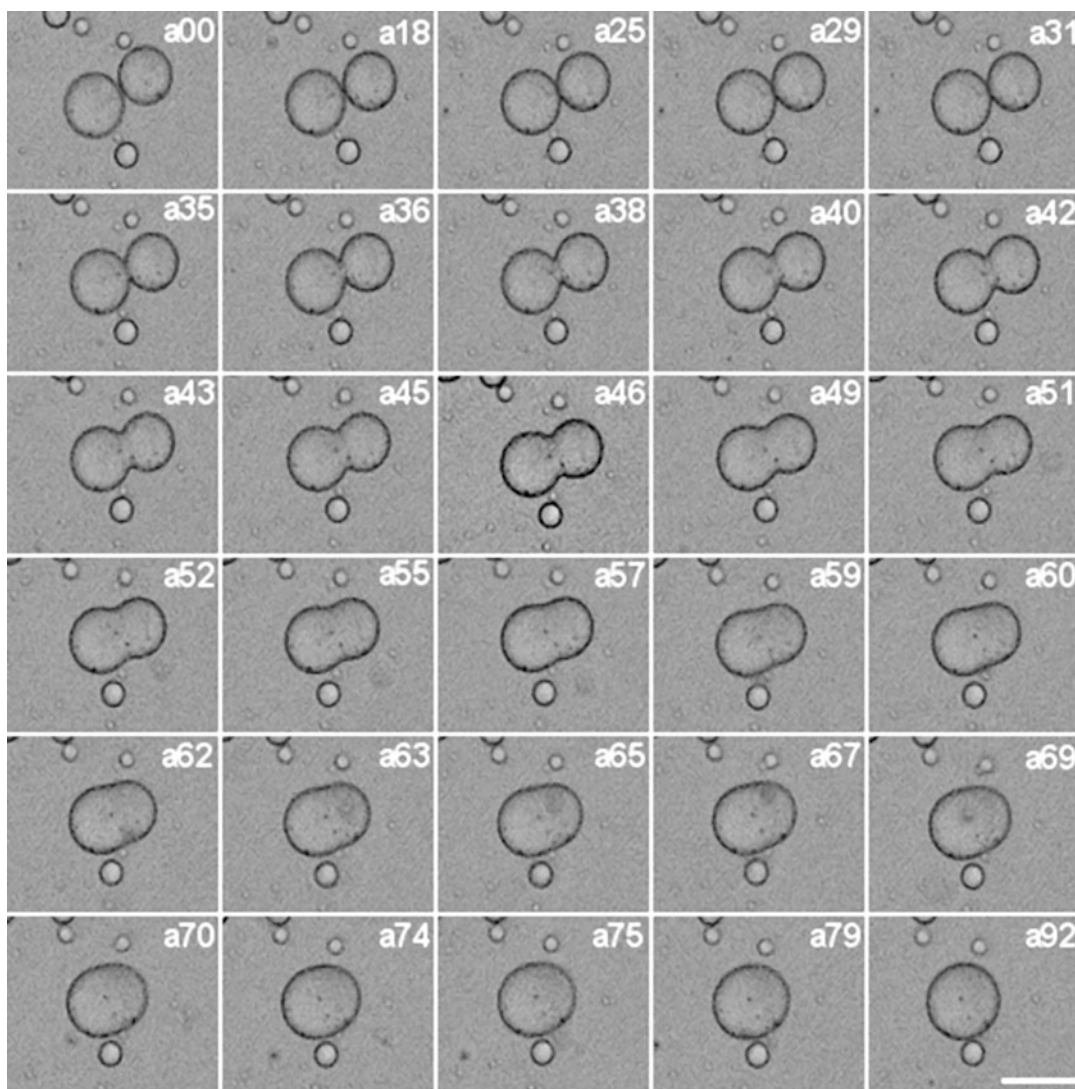**Self-Assembly of Hyperbranched Polymers, Fig. 4** Morphology transformations in the self-assembly of HBPO-star-PEOs with variable DBs in HBPO cores (Reproduced with permission of the Royal Society of Chemistry from Ref. [12])

changed from spherical micelles to rods to vesicles (Fig. 4) [15]. Such an example can illustrate the "topological amplification effects" of HBPs in the self-assembly process.

Special Properties of the Self-Assemblies

Beside the morphology diversity, the properties of the obtained self-assemblies from HBPs are also special. As mentioned above, HBPs themselves have some special properties when compared with the linear analogous. For the self-assembly studies, the most important property characters of HBPs are the very good flexibility and many functional groups. The good chain flexibility is useful for the HBPs to form various self-assemblies and endow them with very good flexibility. For example, it has been found that the polymer vesicles self-assembled from HBPs have very good stability, flexibility, and fluidity and can be used as the excellent model systems to mimic biomembranes, such as membrane fusion (Fig. 5), fission, aggregation, budding, and breathing [10–12]. In addition, since there are many functional groups, HBPs and their self-assemblies have demonstrated very good sensitivity in response to environmental stimuli. As a typical example, Zhou and Yan found HBPO-star-PEO could self-assemble into thermosensitive polymer vesicles, and these polymer vesicles showed sharp phase transitions at the lower critical solution temperature (LCST) [16]. Although, the molecular weight difference is only about 36,300 between the smallest and largest polymers, the LCST span is

Self-Assembly of Hyperbranched Polymers, Fig. 5 Real-time vesicles fusion process. The number in the symbol labeled on each image denotes the elapsed time (in seconds), and the time of first image is set as zero. The scale bar represents 50 μm (Reproduced with permission of the American Chemical Society from (J Am Chem Soc 2005, 127, 10468))

over 70 °C from 8 °C to 81 °C. Such a broad LCST dependence on the molecular weight is unusual and has not been found for the linear thermosensitive polymers, which is highly related with the hyperbranched topology and many functional groups. In fact, besides temperature, HBPs have also shown better sensitivity toward the solution pH, magnetic field, and photo than the linear counterparts. Furthermore, the large number of functional groups also makes

the HBP assemblies easy to be functionalized, which highly broaden their properties as well as the application areas.

These property advantages make HBPs very potential to be used as the smart drug carriers and chemical sensors. For example, PDMAEMA is a well-known cationic polymer candidate for nonviral gene vectors. However, the high cytotoxicity is still the major drawback to restrain their applications into clinical evaluation.

Very recently, hyperbranched structures have been introduced to modify PDMAEMA. A series of hyperbranched multiarm copolymers of HBPO-*g*-PDMAEMAs with the hydrophobic DB-variable HBPO cores and length-variable PDMAEMA arms were synthesized [17]. The obtained copolymers showed excellent gene transfection efficiency higher than that of branched polyethylenimine (PEI) and PDMAEMA homopolymers. In addition, the structure–property relationship inside it was also disclosed by studying the effects of DBs of the PEHO cores and PDMAEMA arm lengths on the gene transfection behavior, including the buffering ability, DNA compaction, self-assembly, cytotoxicity, and gene transfection efficiency. The detailed description on the biomedical application of HBPs and their self-assemblies can also be found in a recent review article [12]. In short, HBPs and their self-assemblies have shown unique properties, which make them very useful in polymer industry and biomedical areas such as drug delivery, protein purification/detection/delivery, gene transfection, antibacterial/antifouling materials, and bioimaging.

Special Self-Assembly Mechanism

Apart from the structure and property, the self-assembly mechanism of HBPs is also special. Up to now, many delicate supramolecular structures, such as spherical micelles, vesicles, tubes, fibers, films, and sheets, have been prepared through the self-assembly of HBPs. However, it is not special, and the same supramolecular structures have already been made through the self-assembly of linear block copolymers. The speciality lies in the self-assembly mechanism. Almost all self-assemblies from HBPs have the different forming mechanism when compared with those of the linear block copolymers owing to the special topological structure of HBPs. The most typical example is the self-assembly of spherical micelles. The linear block polymers can self-assemble into normal micelles consisting of the cores from the hydrophobic blocks and shells from the hydrophilic blocks. Such a micelle is about two-molecule lengths in diameter and often smaller than 50 nm. Besides, the linear block polymers can also form large multimolecular micelles around 100 nm aggregated from the small reverse micelles or normal micelles, and the typical self-assembly mechanisms are summarized as the large compound micelle (LCM) mechanism and multicompartment micelle mechanism. However, HBPs generally form unimolecular micelles in solution, and sometimes they will form the large multimolecular micelles around or above 100 nm. In 2005, Zhou and Yan suggested that these large multimolecular micelles from HBPs might be a kind of multimicelle aggregates (MMAs), in which HBPs first self-assembled into small micelles and then the small micelles further aggregated into large ones [18]. Subsequently, the experimental evidence has proved the MMA mechanism is right, and the building blocks for the large MMA can either be unimolecular micelles below 10 nm or small micelles around 20 nm. Very recently, such a MMA mechanism has also been proved in a theoretical level by dissipative particle dynamics simulations [19]. In this simulation work, the MMA mechanism is divided into two parts. One is called the unimolecular micelle aggregate (UMA) mechanism, which describes the formation of large multimolecular micelles from direct aggregation of unimolecular micelles (Fig. 6a); the other is called the small micelle aggregate (SMA) mechanism, which shows that the dendritic multiarm copolymers first self-assemble into small micelles and then the small micelles further aggregate into large multimolecular micelles (Fig. 6b). For the UMA mechanism, the key character is that there is no microphase separation during the self-assembly process, and such a self-assembly mechanism is unique for dendritic polymers. For the SMA mechanism, the dendritic multiarm copolymers first undergo a spherical-to-cone microphase separation during the formation of the small micelles before the secondary aggregation. So the SMA mechanism is something like the multicompartment micelle mechanism.

The MMA structure also has some special application. For example, it is textbook knowledge that chromophore aggregation generally quenches light emission, which is called as the

Self-Assembly of Hyperbranched Polymers, Fig. 6 The mechanism for the self-assembly of large multimolecular micelles from dendritic polymers. (**a**) Unimolecular micelle aggregate (*UMA*) mechanism. (**b**) Small micelle aggregate (*SMA*) mechanism (Reproduced with permission of the Royal Society of Chemistry from Ref. [19])
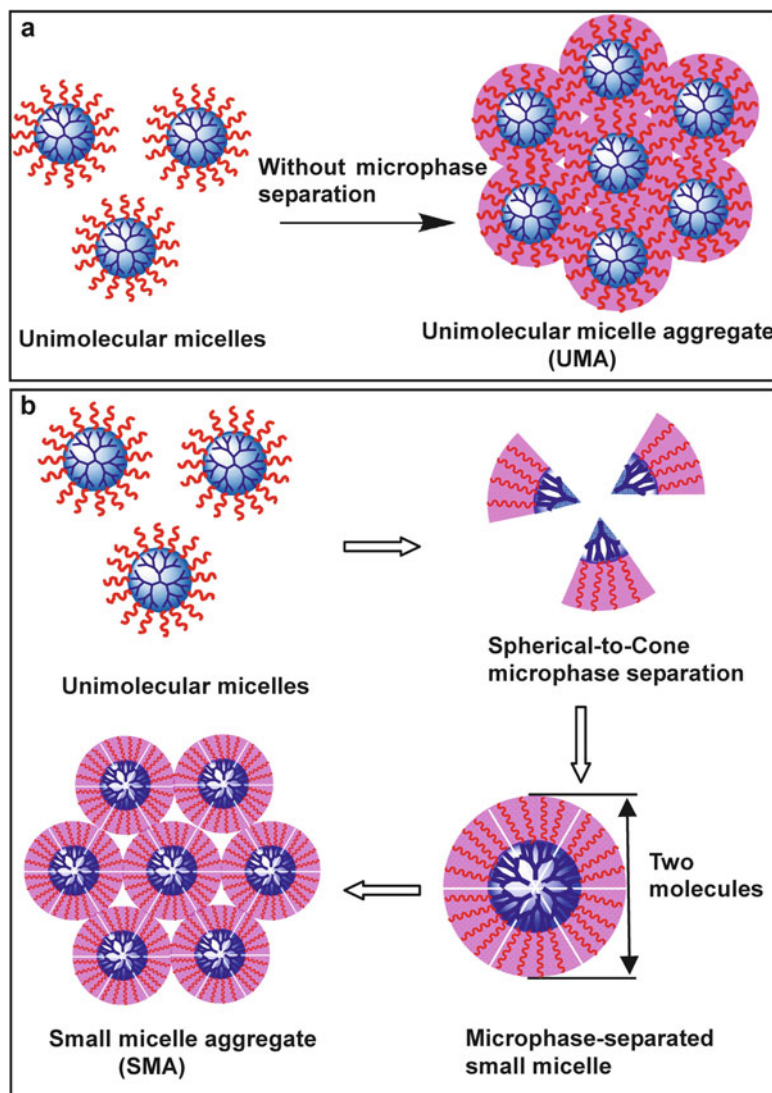
aggregation-caused quenching (ACQ) phenomenon. The reason for ACQ is due to the strong π–π stacking interactions between the chromophores. So, the ACQ molecules are generally used in a diluted state in order to get strong fluorescence. However, if the ACQ molecules can form the UMA structures, each molecule is isolated from one another in a molecular level, which can greatly inhibit the π–π stacking in spite that these molecules are aggregated into large micelles. In other words, the fluorescence emission will be great enhanced in such a UMA system. As proof-of-principle experiments, Zhu

and coworkers constructed the UMAs from the self-assembly of a hyperbranched multiarm copolymer with a hyperbranched conjugated polymer (HCP) core and many linear PEO arms. They found the UMAs displayed an emission enhancement phenomenon in spite that the polymers are one of the typical ACQ molecules [20].

Outlook on the Self-Assembly of HBPs

Although still being at an early stage, hyperbranched polymers have demonstrated

great potential to be excellent precursors in supramolecular self-assembly, and many kinds of delicate supramolecular at all dimensions and scales have been prepared through the solution, interfacial, and hybrid self-assembly process. The self-assembly behavior of hyperbranched polymers also displays some specialities or unique advantages when compared with that of linear block copolymers, including the morphology diversity, special property, and special self-assembly mechanism. In addition, both the hyperbranched polymers and their self-assemblies have shown very promising applications in the biomedical areas. All these aspects have made hyperbranched polymers become a very important interdisciplinary branch among the supramolecular science, polymer science, and material science and have attracted more and more attention from the scientific and engineering points of view in recent year. Nevertheless, there are still many problems that should be solved in the near future, for example, the theoretical studies on the self-assembly of hyperbranched polymer have been greatly lagging behind; the structure and property relationship has not been fully disclosed; and the application is still at the very beginning stage. So, an enduring attention should be paid for the further development of such a very young research area.

Related Entries

▶ Cyclodextrins-Based Supramolecular Polymers
▶ Dendrimers and Hyperbranched Polymers in Medicine
▶ Micelles and Vesicles
▶ Molecular Self-Organization
▶ Synthesis of Hyperbranched Polymers

References

1. Gao C, Yan DY (2004) Hyperbranched polymers: from synthesis to applications. Prog Polym Sci 29:183–275. doi:10.1016/j.progpolymsci.2003.12.002
2. Carlmark A, Hawker C, Hult A, Malkoch M (2009) New methodologies in the construction of dendritic materials. Chem Soc Rev 38:352–362. doi:10.1039/b711745k
3. Voit BI, Lederer A (2009) Hyperbranched and highly branched polymer architecture – synthetic strategies and major characterization aspects. Chem Rev 109:5924–5973. doi:10.1021/cr900068q
4. Yan DY, Gao C, Frey H (2011) Hyperbranched polymers. Wiley, Hoboken
5. Riess G (2003) Micellization of block copolymers. Prog Polym Sci 28:1107–1170. doi:10.1016/S0079-6700(03)00015-7
6. Rodríguez-Hernández J, Chécot F, Gnanou Y, Lecommandoux S (2005) Toward 'smart' nano-objects by self-assembly of block copolymers in solution. Prog Polym Sci 30:691–724. doi:10.1016/j.progpolymsci.2005.04.002
7. Mai YY, Eisenberg A (2012) Self-assembly of block copolymers. Chem Soc Rev 41:5969–5985. doi:10.1039/c2cs35115c
8. Yan DY, Zhou YF, Hou J (2004) Supramolecular self-assembly of macroscopic tubes. Science 303:65–67. doi:10.1126/science.1090763
9. Peleshanko S, Tsukruk VV (2008) The architectures and surface behavior of highly branched molecules. Prog Polym Sci 33:523–580. doi:10.1016/j.progpolymsci.2008.01.003
10. Zhou YF, Yan DY (2009) Supramolecular self-assembly of amphiphilic hyperbranched polymers at all scales and dimensions: progress, characteristics and perspectives. Chem Commun 10:1172–1188. doi:10.1039/b814560c
11. Zhou YF, Huang W, Liu JY, Zhu XY, Yan DY (2010) Self-assembly of hyperbranched polymers and its biomedical applications. Adv Mater 22:4567–4590. doi:10.1002/adma.201000369
12. Jin HB, Huang W, Zhu XY, Zhou YF, Yan DY (2012) Biocompatible or biodegradable hyperbranched polymers: from self-assembly to cytomimetic applications. Chem Soc Rev 41:5986–5997. doi:10.1039/c2cs35130g
13. Tao W, Liu Y, Jiang BB, Yu SR, Huang W, Zhou YF, Yan DY (2012) A linear-hyperbranched supramolecular amphiphile and its self-assembly into vesicles with great ductility. J Am Chem Soc 134:762–764. doi:10.1021/ja207924w
14. Liu Y, Yu CY, Jin HB, Jiang BB, Zhu XY, Zhou YF, Lu ZY, Yan DY (2013) A supramolecular Janus hyperbranched polymer and its photoresponsive self-assembly of vesicles with narrow size distribution. J Am Chem Soc 135:4765–4770. doi:10.1021/ja3122608
15. Cheng HX, Yuan XJ, Sun XY, Li KP, Zhou YF, Yan DY (2010) Effect of degree of branching on the self-assembly of amphiphilic hyperbranched multiarm copolymers. Macromolecules 43:1143–1147. doi:10.1021/ma902452p
16. Zhou YF, Yan DY, Dong WY, Tian Y (2007) Temperature-responsive phase transition of polymer vesicles: real-time morphology observation and molecular mechanism. J Phys Chem B 111:1262–1270. doi:10.1021/jp0673563

17. Wang YL, Li B, Zhou YF, Lu ZY, Yan DY (2013) Dissipative particle dynamics simulation study on the mechanisms of self-assembly of large multimolecular micelles from amphiphilic dendritic multiarm copolymers. Soft Matter 9:3293–3304. doi:10.1039/c3sm27396b

18. Mai YY, Zhou YF, Yan DY (2005) Synthesis and size-controllable self-assembly of a novel amphiphilic hyperbranched multi-arm copolyether. Macromolecules 38:8679–8686. doi:10.1021/ma051377y

19. Yu SR, Chen JX, Dong RJ, Su Y, Ji B, Zhou YF, Zhu XY, Yan DY (2012) Enhanced gene transfection efficiency of PDMAEMA by incorporating hydrophobic hyperbranched polymer cores: effect of degree of branching. Polym Chem 3:3324–3329. doi:10.1039/c2py20487h

20. Qiu F, Tu CL, Wang RB, Zhu LJ, Chen Y, Tong GS, Zhu BS, He L, Yan DY, Zhu XY (2011) Emission enhancement of conjugated polymers through self-assembly of unimolecular micelles to multi-micelle aggregates. Chem Commun 47:9678–9680. doi:10.1039/c1cc13587b

Self-Consistent Field Theory

An-Chang Shi
Department of Physics and Astronomy,
McMaster University, Hamilton, ON, Canada

Synonyms

Mean-field theory; SCFT; Self-consistent mean-field theory

Definition

Self-consistent field theory is a theoretical framework for the study of many-body systems. The self-consistent field theory of polymers describes the thermodynamic properties of inhomogeneous polymeric systems such as polymer blends and block copolymers.

Introduction

The essence of self-consistent field theory (SCFT) is to transform the problem of a complex interacting many-body system into a one-body problem in a conjugate field, whereas the conjugate field is in turn determined self-consistently from the solution of the one-body problem. In its most general form, the SCFT is a flexible theoretical framework applicable to any particle-based statistical and quantum mechanical systems. One of the most successful applications of SCFT is the study of the behavior of inhomogeneous polymeric systems including polymer blends, polymer solutions, and block copolymers.

The self-consistent field theory of polymers originated from the work of Edwards in the 1960s [1]. The most successful application of SCFT is the study of block copolymers, which form complex ordered nanodomains or microphases. This theoretical framework was explicitly adapted to treat block copolymers by Helfand in 1975 [2]. Because of the complexity of the theory, numerical techniques are in general required to obtain exact solution of the SCFT equations. The earliest attempts to obtain numerical solutions were made by Helfand and coworkers [3]. The first exact three-dimensional solutions of the SCFT equations were obtained by Matsen and Schick in 1994 [4]. Since then various numerical techniques to solve the SCFT equations in real space [5] and reciprocal space [4, 6] have been developed. With these developments the self-consistent field theory has become a powerful platform for the study of the phase behavior of inhomogeneous polymeric systems.

Formulation of Self-Consistent Field Theory

Details of the SCFT depend on specific microscopic models being investigated [7]. In what follows the SCFT of diblock copolymers is used to illustrate the theory. Extension to other polymer models as well as block copolymer blends and solutions is straightforward. For diblock copolymers, theoretical studies of their phase behavior are mostly based on the so-called standard model, in which the polymer chains are modeled as flexible Gaussian chains, and the interactions between the different monomers are

S

modeled by short-range contact potentials [8]. Furthermore, the hard-core repulsive interactions are approximated by the incompressibility condition.

The system consists of n_c diblock copolymer chains in a volume V, where each copolymer chain is composed of N monomers of species $\alpha = A, B$. The compositions of the blocks are $N_\alpha = f_\alpha N$ with $f_A + f_B = 1$. The block is further characterized by a Kuhn length $b_\alpha = \sigma_\alpha b$, where

b is a reference Kuhn length, and a monomer density, ρ_0. We will use the convention that all lengths are scaled by the radius of gyration of the copolymer chain, $R_g = \sqrt{N/6}b$. The chain arc length is scaled by the chain degree of polymerization N. Within the SCFT framework, the partition function of the system can be expressed as a functional integral over the monomer density $\phi_\alpha\left(\vec{r}\right)$ and their auxiliary field $\omega_\alpha\left(\vec{r}\right)$ [7, 8],

$$\mathcal{Z} = \int \prod_\alpha [\mathcal{D}\{\phi_\alpha\}\mathcal{D}\{\omega_\alpha\}] \prod_{\vec{r}} \delta\left(\phi_A\left(\vec{r}\right) + \phi_B\left(\vec{r}\right) - 1\right) e^{-F(\{\phi\},\{\omega\})},$$

where $F(\{\phi\}, \{\omega\})$ is the free energy functional, or, more precisely, the "Hamiltonian," of the system. Specifically $F(\{\phi\}, \{\omega\})$ is the energy

cost of a particular set of $\phi_\alpha\left(\vec{r}\right)$ and $\omega_\alpha\left(\vec{r}\right)$. For a diblock copolymer melt, this free energy has the form

$$F(\{\phi\},\{\omega\}) = \frac{\rho_0 R_g^3}{N}\left\{\int d\vec{r}\left[\chi N\phi_A\left(\vec{r}\right)\phi_B\left(\vec{r}\right) - \sum_\alpha \phi_\alpha\left(\vec{r}\right)\omega_\alpha\left(\vec{r}\right)\right] - V\ln Q_c(\{\omega\})\right\},$$

where χ is the Flory-Huggins parameter quantifying the effective interaction between A and B segments. The quantity $Q_c(\{\omega\})$ in the above expression is the single-chain partition function in the external field $\omega_\alpha\left(\vec{r}\right)$, which is a functional of the field $\omega_\alpha\left(\vec{r}\right)$. The single-chain partition function can be expressed in terms of the chain propagators $Q_\alpha\left(\vec{r}, s|\vec{r}'\right)$, which represents the conditional probability distribution of monomer s at $\vec{r}$, given that monomer 0 at $\vec{r}'$, in the presence of an external field $\omega_\alpha\left(\vec{r}\right)$. For Gaussian chains, the propagators can be obtained from the following modified diffusion equations:

$$\frac{\partial}{\partial s}Q_\alpha\left(\vec{r}, s|\vec{r}'\right) = \sigma_\alpha^2 \nabla^2 Q_\alpha\left(\vec{r}, s|\vec{r}'\right)$$
$$- \omega_\alpha\left(\vec{r}\right)Q_\alpha\left(\vec{r}, s|\vec{r}'\right),$$

with the initial conditions, $Q_\alpha\left(\vec{r}, 0|\vec{r}'\right) = \delta\left(\vec{r} - \vec{r}'\right)$. In many applications of the theory, it is convenient to introduce two end-integrated propagators, $q_\alpha\left(\vec{r}, s\right)$ and $q_\alpha^+\left(\vec{r}, s\right)$, defined by

$$q_\alpha\left(\vec{r}, s\right) = \int d\vec{r}' Q_\alpha\left(\vec{r}, s|\vec{r}'\right),$$

$$q_\alpha^+\left(\vec{r}, s|\vec{r}''\right) = \int d\vec{r}' d\vec{r}'' Q_\alpha\left(\vec{r}, s|\vec{r}'\right) Q_\beta\left(\vec{r}', f_\beta|\vec{r}''\right),$$

where $\beta = B$ if $\alpha = A$ and vice versa. These end-integrated propagators satisfy the same differential equation as $Q_\alpha\left(\vec{r}, s|\vec{r}'\right)$, with different initial conditions, $q_\alpha\left(\vec{r}, 0\right) = 1$ and $q_\alpha^+\left(\vec{r}, 0\right) = q_\beta\left(\vec{r}, f_\beta\right)$, where $\beta = B$ if $\alpha = A$ and vice versa. In terms of the end-integrated

propagators, the single-chain partition function $Q_c(\{\omega\})$ is given by

$$Q_c = \frac{1}{V}\int d\vec{r}\; q_\alpha^+\left(\vec{r},f_\alpha\right).$$

The free energy functional obtained above is exact, and it forms the basis for further development. What makes the SCFT tractable is that the effect of the many-body interactions between the different chains is reduced to the problem of the partition function, $Q_c(\{\omega\})$, of one chain in external fields $\omega_\alpha\left(\vec{r}\right)$.

Because exact evaluation of the partition function is in general not possible, a variety of approximate methods have been developed [7, 8]. The most fruitful approximate method is the mean-field theory, which amounts to evaluating the functional integral using a saddle-point technique. Technically, the mean-field equations or the SCFT equations are obtained by minimizing the free energy functional of the system with respect to the density distributions $\phi_\alpha\left(\vec{r}\right)$ and their conjugate fields $\omega_\alpha\left(\vec{r}\right)$. This procedure leads to a set of coupled equations determining the mean concentration density $\phi_\alpha\left(\vec{r}\right)$ and their conjugate fields $\omega_\alpha\left(\vec{r}\right)$:

$$\phi_\alpha\left(\vec{r}\right) = \frac{1}{Q_c}\int_0^{f_\alpha} ds\, q_\alpha\left(\vec{r},s\right)q_\alpha^+\left(\vec{r},f_\alpha - s\right)$$

$$\omega_\alpha\left(\vec{r}\right) = \chi N\left[\phi_\beta\left(\vec{r}\right) - f_\beta\right] + \eta\left(\vec{r}\right),$$

where $\beta = B$ if $\alpha = A$ and vice versa and $\eta\left(\vec{r}\right)$ is a Lagrangian multiplier which is introduced to ensure the incompressibility condition, $\phi_A\left(\vec{r}\right) + \phi_B\left(\vec{r}\right) = 1$. The single-chain partition function is given by

$$Q_c = \frac{1}{V}\int d\vec{r}\, q_A^+\left(\vec{r},f_A\right) = \frac{1}{V}\int d\vec{r}\, q_B^+\left(\vec{r},f_B\right).$$

The end-integrated propagators, $q_\alpha\left(\vec{r},s\right)$ and $q_\alpha^+\left(\vec{r},s\right)$, are solutions of the modified diffusion equations in the mean fields $\omega_\alpha\left(\vec{r}\right)$:

$$\frac{\partial}{\partial s}q_\alpha\left(\vec{r},s\right) = \sigma_\alpha^2\nabla^2 q_\alpha\left(\vec{r},s\right) - \omega_\alpha\left(\vec{r}\right)q_\alpha\left(\vec{r},s\right),$$

with the initial conditions, $q_\alpha\left(\vec{r},0\right) = 1$ and $q_\alpha^+\left(\vec{r},0\right) = q_\beta\left(\vec{r},f_\beta\right)$, where $\beta = B$ if $\alpha = A$ and vice versa. Because both $\phi_\alpha\left(\vec{r}\right)$ and $\omega_\alpha\left(\vec{r}\right)$ are determined self-consistently from the above self-consistent equations, the mean-field approximation is often referred as the self-consistent mean-field theory. In the literature, the self-consistent mean-field theory is often referred simply as the self-consistent field theory (SCFT). It should be pointed out that within the mean-field approximation, fluctuations in the monomer compositions or the conjugate fields are ignored. However, fluctuation of the polymer trajectories subjected to the mean fields is fully accounted for via the solution of the modified diffusion equations.

Within the mean-field approximation, the free energy per chain of the system is obtained by inserting the mean-field solution into the free energy expression

$$f = \frac{N}{\rho_0 R_g^3 V}F(\{\phi\},\{\omega\})$$
$$= \frac{1}{V}\int d\vec{r}\left[\chi N\phi_A\left(\vec{r}\right)\phi_B\left(\vec{r}\right) - \sum_\alpha \phi_\alpha\left(\vec{r}\right)\omega_\alpha\left(\vec{r}\right)\right]$$
$$- \ln Q_c(\{\omega\}).$$

The parameters entering the theory are the combination χN, the block volume fraction $f_A = 1 - f_B$, and the effective Kuhn lengths σ_α. The thermodynamic properties of a diblock copolymer melt are completely specified by the set of parameters $\{\chi N, f_A, \sigma_A, \sigma_B\}$ within the self-consistent mean-field theory.

Methods of Solution

Because of the complexity of the theory, analytic solutions of the SCFT equations can only be

obtained within the numerical accuracy under special conditions. The simplest solution of the mean-field equations is obtained for a homogeneous phase, in which the polymer concentrations and the mean-field potentials are constants, $\phi_\alpha\left(\vec{r}\right) = f_\alpha, \omega_\alpha\left(\vec{r}\right) = 0$, leading to the trivial solution, $q_\alpha\left(\vec{r}, s\right) = q_\alpha^+\left(\vec{r}, s\right) = 1$. The free energy per chain of a homogeneous phase is therefore given by $f_H = \chi N f_A(1 - f_A)$.

The most fruitful approach to SCFT has been numerical methods, which gives exact solutions within the numerical accuracy. With the availability of increasing computing power and new numerical techniques, computational methods of SCFT have been developed to the level that they can be used to explore the possible phases for a given block copolymer architecture [7]. The method to solve the SCFT equations numerically is conceptually straightforward. The first step is to make an initial guess of the mean fields $\omega_\alpha\left(\vec{r}\right)$, which may bear the symmetry of the ordered phase under investigation or be generated randomly. The modified diffusion equations with appropriate initial and boundary conditions are then solved to obtain the propagators, $q_\alpha\left(\vec{r}, s\right)$ and $q_\alpha^+\left(\vec{r}, s\right)$. These propagators can then be used to compute the mean-field concentrations, $\phi_\alpha\left(\vec{r}\right)$. The next step is to adjust the mean fields $\omega_\alpha\left(\vec{r}\right)$ according to an iterative procedure so as to satisfy the self-consistent equations and the incompressibility condition. For a given set of controlling parameters such as $\{\chi N, f_A, \sigma_A, \sigma_B\}$ for a diblock copolymer melt, there are many solutions to the SCFT equations, corresponding to different morphologies. The phase diagram is constructed by finding the structures with the lowest free energy density.

Numerical methods of SCFT can be loosely classified into two categories based on whether the theory is casted in real space or reciprocal space. In the reciprocal space or spectral method, the spatially varying functions are expanded in terms of a set of basis functions [4, 6].

For ordered phases with known symmetries, the basis functions can be constructed from the known symmetry [4], leading to accurate and efficient numerical methods. On the other hand, the basis functions can be taken as a generalized Fourier series [6], leading to a generic method for the study of inhomogeneous polymeric systems. Parallel to the development of the reciprocal-space methods, numerical techniques of SCFT in real space have been proposed. Numerous implementations of real-space SCFT have been developed by solving the SCFT equations in a large box or in an arbitrary unit cell [5–7]. Both the real-space and reciprocal-space methods are capable of describing and predicting ordered phases of block copolymers [9].

The self-consistent field theory has been applied to various inhomogeneous polymeric systems including polymer adsorption, polymer interfaces, and polymer brushes. The most successful application of SCFT to polymeric system is the study of nanodomain formation from block copolymers, leading to a large body of literatures on the study of equilibrium phase behavior of block copolymers [7, 8, 10, 11]. These studies have established a quantitative relation between molecular architecture, composition, and equilibrium phase behavior. A good understanding of the block copolymer phase behaviors has emerged from these studies. The understanding gained from the SCFT studies has been very successful in helping to explain the complex ordered phases experimentally observed in block copolymer systems.

Summary

The self-consistent field theory is a flexible and versatile theoretical framework for the study of many-body systems. A diblock copolymer melt is used as a model system to illustrate the theory. The theoretical methods and numerical techniques can be extended to more complex block copolymers. The formulation allows a systematic analysis of the thermodynamic properties of block copolymer systems. The equilibrium

phases and phase diagrams can be obtained by solving the SCFT equations, while the stability of the ordered phases can be analyzed within the SCFT framework. The SCFT can be taken as a numerical platform that is capable of predicting the phases and phase diagrams for complex polymeric systems.

Related Entries

References

1. Edwards S (1965) The statistical mechanics of polymers with excluded volume. Proc Phys Soc 85:613
2. Helfand E (1975) Theory of inhomogeneous polymers: Fundamentals of the Gaussian randomwalk model. J Chem Phys 62:999; (1975) Block copolymer theory. III. Statistical mechanics of the microdomain structure. Macromolecules 8:552
3. Helfand E, Wasserman ZR (1976) Block copolymer theory. **4**. Narrow interphase approximation. Macromolecules 9:879
4. Matsen MW, Schick M (1994) Stable and unstable phases of a diblock copolymer melt. Phys Rev Lett 72:2041
5. Drolet F, Fredrickson GH (1999) Combinatorial screening of complex block copolymer assembly with self-consistent field theory. Phys Rev Lett 83:4317; Bohbot-Raviv Y, Wang ZG (2000) Discovering new ordered phases of block copolymers. Phys Rev Lett 85:3428; Tzeremes G, Rasmussen KO, Lookman T, Saxena A (2002) Efficient computation of the structural phase behavior of block copolymers. Phys Rev E 65:041806
6. Guo Z, Zhang G, Qiu F, Zhang H, Yang Y, Shi A-C (2008) Discovering ordered phases of block copolymers: New results from a generic Fourier-space approach. Phys Rev Lett 101:028301
7. Fredrickson GH (2006) The equilibrium theory of inhomogeneous polymers. Oxford University Press, New York
8. Matsen MW (2002) The standard Gaussian model for block copolymer melts. J Phys Condens Matter 14:R21
9. Xu W, Jiang K, Zhang P, Shi A-C (2013) A strategy to explore stable and metastable ordered phases of block copolymers. J Phys Chem B 117:5296
10. Schmid F (1998) Self-consistent-field theories for complex fluids. J Phys Condens Matter 10:8105
11. Shi A-C (2004) Self-consistent field theory of block copolymers. In: Hamley IW (ed) Developments in block copolymer science and technology. Wiley, Chichester

Self-Decomposing Dendrimers

Liat Frid and Roey J. Amir
School of Chemistry, Tel Aviv University,
Tel Aviv, Israel

Synonyms

Domino dendrimers; Self-immolative dendrimers

Definition

Self-decomposing dendrimers are degradable dendrimers that are based on an active dendritic framework and are designed to disassemble spontaneously upon a single triggering event. The trigger group, which is used to initiate the spontaneous breakdown of the dendrimer, can be located at either the periphery or the focal point of the dendrimer. Activation of the trigger reveals an active functional group that starts a cascade of spontaneous reactions, which lead eventually to the complete disassembly of the dendritic structure into its monomers or larger dendritic fragments. Self-decomposing dendrimers are distinctive from other types of degradable dendrimers that require multiple independent degradation reactions to achieve complete decomposition.

Introduction

Dendrimers are very unique macromolecules due to their highly branched and precise modular structure, high number of functional end groups, overall globular shape, and monodispersity [1].

S

These distinctive features have made dendrimers extremely attractive platforms for delivery applications, which rely mostly on their utilization as a passive scaffold that can be loaded with active drugs or probe-molecules [2]. The loading of active molecular cargo can be achieved either by its encapsulation within the internal cavities of the dendrimer or by covalent binding to the periphery end groups of the dendrimer. These applications rely mostly on the multivalency, spherical shape and porosity of the dendritic architecture, which serves as a passive macromolecular framework [3]. In contrast, when looking at dendritic structures or architectures in nature, such as trees, one cannot ignore the active role of the dendritic structure in the overall functionality of the tree, as the branches are used not only to hold the leaves but also to serve as a network that allows the transformation of water and nutrients between the roots and the leaves. Inspired by the active role of natural dendritic structures, self-decomposing dendrimers are based on an active dendritic framework that allows a decomposition cascade to propagate along the dendritic structure, leading eventually to its decomposition [4]. Such dendrimers can have a great potential in biomedical applications as their highly controlled degradation is of great importance for the release of active cargo molecules, the degradation and

clearance of the dendritic carrier after its delivery task was accomplished [5].

Fundamental Decomposition Pathways

The first examples of self-decomposing dendrimers were published almost simultaneously in 2003 by the three independent groups of Shabat [6], de Groot et al. [7], and McGrath [8]. In principle, the self-decomposition of such dendrimers can be divided into two major types: convergent and divergent pathways. In the convergent disassembly, the decomposition cascade propagates from a trigger group, which is located on the periphery of the dendrimer, towards the core of the dendrimer (Fig. 1). This type of decomposition does not propagate in a dendritic manner as the decomposition cascade occurs along a linear vector that connects the trigger to the core of the dendrimer and therefore may result in relatively larger dendritic fragments [9].

In the second type of self-decomposing dendrimers, the cleavage cascade is initiated at a trigger group that is located at the core of the dendrimer. The decomposition cascade then propagates divergently towards the peripheral end groups, leading to the complete disassembly


Self-Decomposing Dendrimers, Fig. 1 Convergently self-decomposing dendrimer. Upon trigger activation, the degradation cascade propagates along a linear vector that connects the trigger and the core of the dendrimer. The overall decomposition results in the fragmentation of the dendrimer and release of an active molecule from its core.
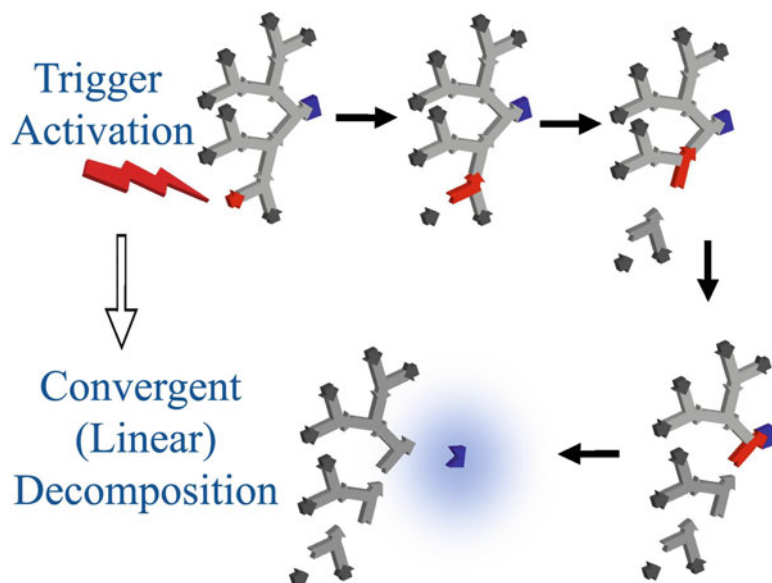
Self-Decomposing Dendrimers, Fig. 2 Divergently self-decomposing dendrimer. Upon trigger activation, the degradation cascade is amplified as it propagates along the dendritic framework, leading to the full decomposition of the dendrimer and release of all the active end groups.
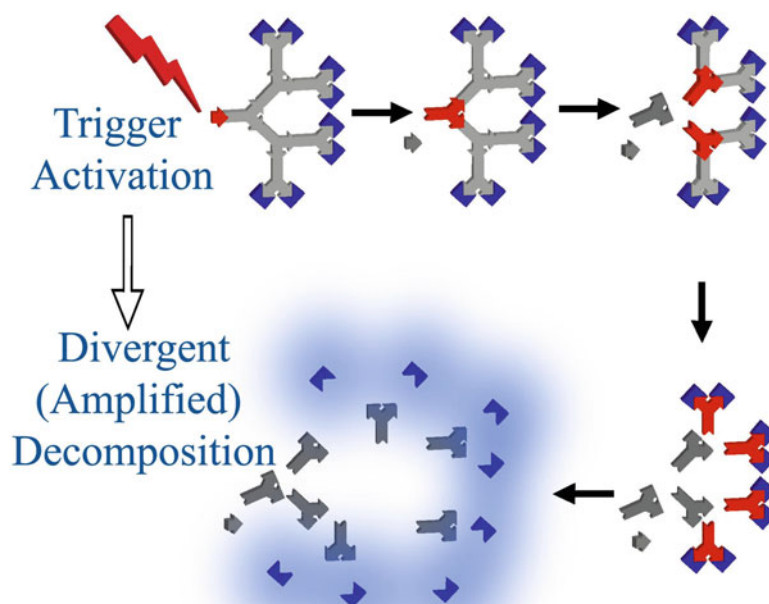
of the dendrimer to its monomeric building blocks and release of all its end groups (Fig. 2). This type of decomposition takes full advantage of the inherent structural amplification of dendrimers that rises from the exponential increase in the number of branching units and peripheral end groups [10].

Self-Decomposing Mechanisms

The active framework of the self-decomposing dendrimers is based on branched self-immolative linkers [11] that are designed to transduce a cleavage signal from the head of the monomer (input) to its tail (output). In the case of convergent decomposition, the monomer unit is required to have at least one input and one output functionalities (Fig. 3) that are fundamental to its capability to transduce a cleavage signal along a linear vector, which starts at the trigger group and ends at the core of the dendrimer [9].

In the case of the divergent disassembly, a monomer unit is required to have at least one input and two output functionalities (Fig. 4) in

order to achieve the dendritic amplification of the cleavage signal [4].

In order to study the dendrimers' decomposition, reporter groups were attached either to the core in the case of convergent decomposition or to the peripheral end groups in the case of divergent disassembly. Activation of the trigger leads to disassembly of the dendrimers and release of active reporter groups, which can be easily monitored (Figs. 1 and 2). While various self-decomposing monomers (Figs. 3 and 4) and dendrimers were published [10], there is great similarity in their release or decomposition mechanisms. In all these reports, the monomers' activity is based on quinone methide (QM) or aza-QM rearrangements. For example, in the case of a first-generation Shabat-type dendrimer (Fig. 5), cleavage of the trigger leads to the exposure of a phenol derivative that spontaneously undergoes a QM rearrangement (1,4 elimination) to release the first reporter group. The electrophilic QM is then attacked by a nucleophile (water molecule) to regenerate a phenol, which undergoes a second QM rearrangement (1,4 elimination) to release the second reporter group [6].
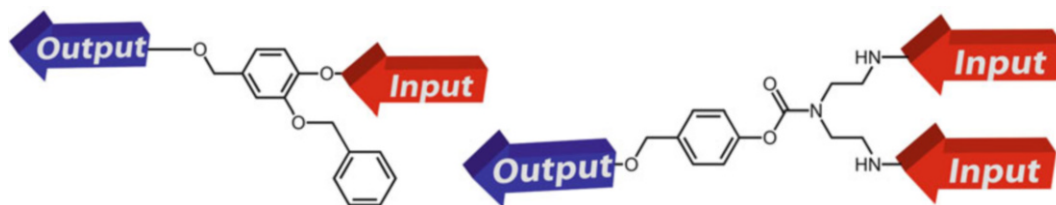
Self-Decomposing Dendrimers, Fig. 3 Convergent self-decomposing monomeric building blocks: An ABC-type branching unit (*left*) with one input functionality, one nonfunctional end group, and one output functionality and an AB$_2$-type monomer (*right*) with two inputs and one output functionalities.
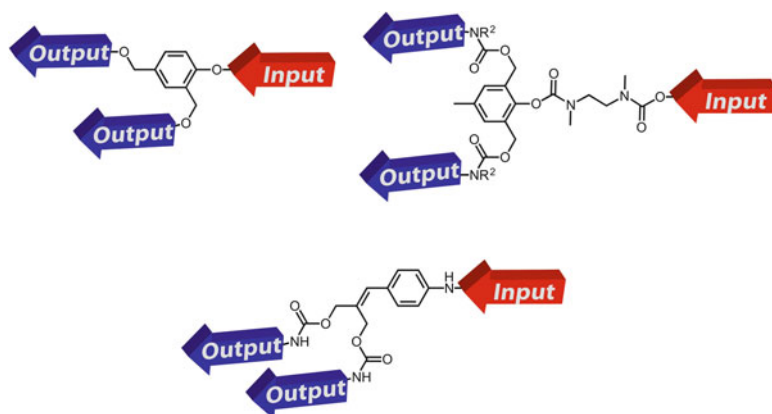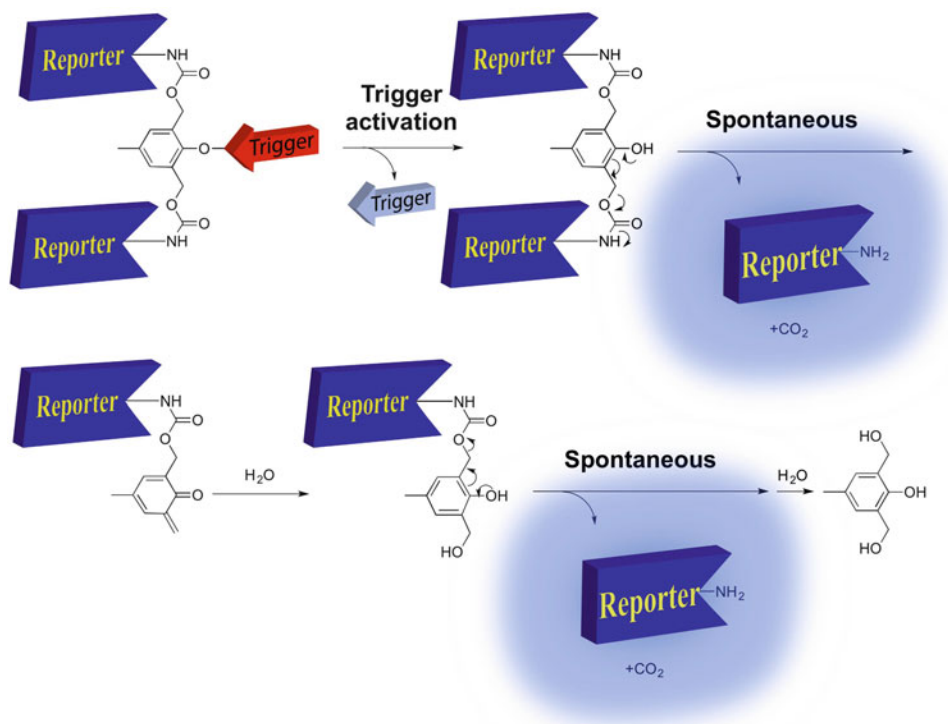

Self-Decomposing Dendrimers, Fig. 4 Divergent AB$_2$-type self-decomposing building blocks with one input and two outputs that enable the dendritic amplification.

In higher generation dendrimers, the output ports (tails) of the first branching monomer are attached to the input ports (heads) of the next layer of branching monomers. An example of a second-generation dendrimer that is composed from both convergently and divergently self-decomposing dendrons and its disassembly mechanism are presented in Fig. 6. Activation of one of the triggers initiates a series of cyclizations and QM rearrangements (1,6- and double 1,4 eliminations) that lead to the release of first-generation dendrons, which, upon exposure of their head group, go through additional QM rearrangement (double 1,4 elimination) to release their reporter groups [10].

Examples for Applications of Self-Decomposing Dendrimers

The triggered degradation of self-decomposing dendrimers should facilitate their clearance from the body after delivering their molecular cargo. This controlled decomposition makes them very attractive platforms for various biomedical applications such as drug delivery [12]. Shabat and coworkers achieved major advantages over other types of degradable dendrimers by attaching multiple drug molecules to the peripheral end groups of divergently decomposing dendrimers with an enzymatically cleavable trigger [13]. One advantage is the ability to release multiple drug molecules from the periphery of the dendrimer upon a single triggering event at its core. This is a highly important feature for drug delivery, as in many cases, the enzymes that are needed to activate or release the drug molecules from drug delivery systems are present in low concentrations, which limit the amounts and release rates of the carried drugs. By utilizing a divergently self-decomposing dendrimer as a delivery platform, the enzymatic activation can be amplified as the degradation cascade propagates through the dendritic structure. This dendritic amplification was shown to result in a significant increase in the amount and

Self-Decomposing Dendrimers, Fig. 5 A double 1,4 elimination as a quinone methide-based amplification mechanism of a single activation event (Shabat-type dendrimer). Cleavage of the trigger at the head of a first-generation dendrimer exposes a phenol that undergoes two subsequent QM rearrangements to release two reporter units.

release rate of drug molecules that were attached to the end group of a self-decomposing dendrimer. Another example for a dendritic delivery system based on a double 1,8 eliminations (Fig. 4) that could degrade to release four paclitaxel molecules upon trigger activation was published by de Groot and coworkers [7]. Self-decomposing dendrimers can be further utilized as a delivery platform that can simultaneously release a combination of different drugs. This was demonstrated by Shabat and coworkers, which reported the synthesis of a dendrimer loaded with three different anticancer drugs. This dendritic tri-prodrug showed enhanced activity compared to the mixture of the three individual prodrugs [10].

Amir and Shabat utilized convergent self-decomposing dendrimers as molecular logic gates. Multi-triggered dendrimer (Fig. 3) with two different enzymatic triggers was shown to serve as an OR logic gate, enabling the release of doxorubicin by two different enzymes [14]. This concept may be particularly important in the field of prodrug therapy in circumstances that require the activation of prodrugs by more than one tumor-associated enzyme.

Summary

"If a good idea for scientific innovation emerges, you can be sure that several teams of researchers will be quickly on the case." was the first sentence of a highlight in "Nature" [15] that emphasized the almost simultaneous publication of the first papers on self-decomposing dendrimers by the
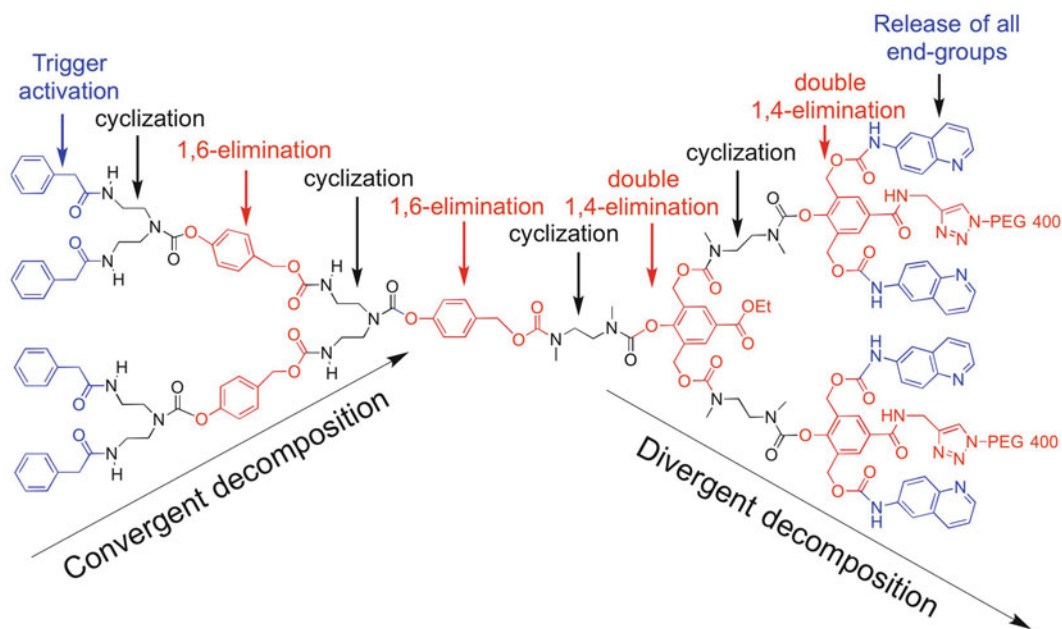
Self-Decomposing Dendrimers, Fig. 6 A second-generation dendrimer, composed from both convergently and divergently decomposing dendrons. Activation of any one of the triggers initiates a cascade of cyclizations and QM rearrangements that propagates convergently towards the core of the dendrimer. The disassembly cascade is then amplified by divergent decomposition that eventually leads to the full degradation of the dendrimer and release of its four end groups.

independent groups of Shabat, de Groot, and McGrath. Since these first publications, various self-decomposing dendrimers with different release mechanisms, triggers, and cargo molecules were synthesized and studied. Their controlled degradation and more importantly the dendritic amplification made them especially attractive as drug delivery platforms and as diagnostic probes. Moreover, the monomers that enable the self-decomposition were further applied in other polymeric systems to induce improved decomposition capabilities [16].

Related Entries

▶ Dendrimers and Hyperbranched Polymers in Medicine
▶ Drug and Gene Delivery Using Hyperbranched Polymers
▶ Stimuli-Responsive Polymers

References

1. Caminade AM, Turrin CO, Laurent R, Ouali A, Delavaux-Nicot B (eds) (2011) Dendrimers: towards catalytic, material and biomedical uses. Wiley, Chichester. doi:10.1002/9781119976530.
2. Soliman GM, Sharma A, Maysinger D, Kakkar A (2011) Dendrimers and miktoarm polymers based multivalent nanocarriers for efficient and targeted drug delivery. Chem Commun 47:9572–9587. doi:10.1039/C1CC11981H.
3. Calderón M, Quadir MA, Strumia M, Haag R (2010) Functional dendritic polymer architectures as stimuli-responsive nanocarriers. Biochimie 92:1242–1251. doi:10.1016/j.biochi.2010.02.017.
4. Amir RJ, Shabat D (2006) Domino dendrimers. In: Satchi-Fainaro R, Duncan R (eds) Polymer therapeutics I. ADV Polym Sci, vol 192. Springer, Berlin/Heidelberg, pp 59–94. doi:10.1007/11547761.
5. Wong AD, DeWit MA, Gillies ER (2012) Amplified release through the stimulus triggered degradation of self-immolative oligomers, dendrimers, and linear polymers. Adv Drug Deliv Rev 64:1031–1045. doi:10.1016/j.addr.2011.09.012.
6. Amir RJ, Pessah N, Shamis M, Shabat D (2003) Self-immolative dendrimers. Angew Chem Int Ed 42:4494–4499. doi:10.1002/anie.200351962.

7. de Groot FMH, Albrecht C, Koekkoek R, Beusker PH, Scheeren HW (2003) Angew Chem Int Ed 42:4490–4494. doi:10.1002/anie.200351942.

8. Szalai ML, Kevwitch RM, McGrath DV (2003) Geometric disassembly of dendrimers: dendritic amplification. J Am Chem Soc 125:15688–15689. doi:10.1021/ja0386694.

9. McGrath DV (2005) Dendrimer disassembly as a new paradigm for the application of dendritic structures. Mol Pharm 2:253–263. doi:10.1021/mp050047x.

10. Avital-Shmilovici M, Shabat D (2010) Self-immolative dendrimers: a distinctive approach to molecular amplification. Soft Matter 6:1073–1080. doi:10.1039/B922341J.

11. Blencowe CA, Russell AT, Greco F, Hayes W, Thornthwaite DW (2011) Self-immolative linkers in polymeric delivery systems. Polym Chem 2:773–790. doi10.1039/C0PY00324G.

12. Timko BP, Dvir T, Kohane D (2010) Remotely triggerable drug delivery systems. Adv Mater 22:4925–4943. doi:10.1002/adma.201002072.

13. Wang RE, Costanza F, Niu Y, Wu H, Hu Y, Hang W, Sun Y, Cai J (2012) Development of self-immolative dendrimers for drug delivery and sensing. J Control Release 159:154–163. doi:10.1016/j.jconrel.2011.11.032.

14. Amir RJ, Popkov M, Lerner RA, Barbas CF III, Shabat D (2005) Prodrug activation gated by a molecular "OR" logic trigger. Angew Chem Int Ed 44:4378-4381. doi:10.1002/ange.200500842.

15. Meijer EW, van Genderen MHP (2003) Chemistry: dendrimers set to self-destruct. Nature 426:128–129. doi:10.1038/426128a.

16. Peterson GI, Larsen MB, Boydston AJ (2012) Controlled depolymerization: stimuli-responsive self-immolative polymers. Macromolecules 45:7317–7328. doi:10.1021/ma300817v.

Self-Healing Polymers

Yoshinori Takashima and Akira Harada
Department of Macromolecular Science,
Graduate School of Science, Osaka University,
Machikaneyama, Toyonaka, Osaka, Japan

Synonyms

Remendable polymers; Reversible bond formation; Self-repairing; Self-restoring

Definition

Self-healing polymers have the ability to transform physical energy into a chemical and/or physical response to heal the damage. Self-healing polymers response to external stimulus to recover the initial material properties.

Introduction

The living organism has an excellent self-defense system, which are autoimmunity mechanism to protect themselves from bacteria, and virus etc., and a self-repair mechanism to prevent degradations and damages of themselves. If industrial materials have a self-healing property like the living organism, safety, efficacy, and reliability for materials significantly are improved and human societies will prevent tragic incidents, such as airplane and nuclear reactor disasters, in daily life. Recently, renewable materials have attracted much attention from the viewpoints of environmental protection and efficient utilization of natural resources. To realize the dream, self-healing materials have been investigated to create from many approaches (self-healing composites, concrete, ceramics, and fabrics) [1–4]. Self-healing polymeric materials have recently enjoyed increasing attention. Studies on self-healing polymeric materials have been increased over the last decade [5–8]. This may be because expanding the useful lifespan of materials is becoming highly desirable due to modern environmental and energy concerns. Thus, self-healing and self-repairing materials should become valuable commodities. On the other hand, polymeric materials, which mainly are used as reinforcement materials (but it used to say that polymeric materials is stronger than steel), developed "disposable materials" with little regard for unexpected degradations and damages of themselves. It is because polymeric materials constructed by covalent bonds hardly recover to an initial form and material strength when damaging. Conventional polymers have difficulty in self-healing because they do not

S

reform covalent bonds, and their cut surfaces do not readhere unless specific groups are introduced into the polymeric materials.

To create self-healing materials, there are three approaches: the storage of healing agents, reversible covalent bond formation with external stimuli, and healing material constructed by non-covalent bonds (Fig. 1). Healing agent storage methods effectively produce self-healing materials by using microcapsules. Although the healing agent storage methods fill gaps and cracks, disconnected functional groups on the cut surfaces do not reform the initial covalent bonds.

The focus of the current review is to discuss the important aspects of and trends in the relatively new field of self-healing materials using non-covalent interaction. The later review will focus on supramolecular polymeric materials consisting of cyclic host and guest complexes.

Thermoresponsive Self-Healing Materials

The Diels–Alder (DA) cycloaddition reaction is one of the most important reactions in a thermoresponsive self-healing method [9–14] (Fig. 2). The DA reaction is a cycloaddition reaction between a conjugated diene and a substituted alkene. One of the most relevant aspects of the Diels–Alder (DA) reaction is its thermal reversibility, known as the retro-Diels–Alder (rDA) reaction. There are two approaches to create remendable polymeric materials: (i) polymers cross-linked with the pendant groups through DA reactions and (ii) polymers prepared by DA reactions involving multifunctional complementary monomers. These polymeric materials prepared by DA reactions have healed crack damage relying on external stimuli (heat, light, pressure, etc.).

A material from tetra-linker furan (diene)- and a tri-linker maleimide (dienophile)-based monomers
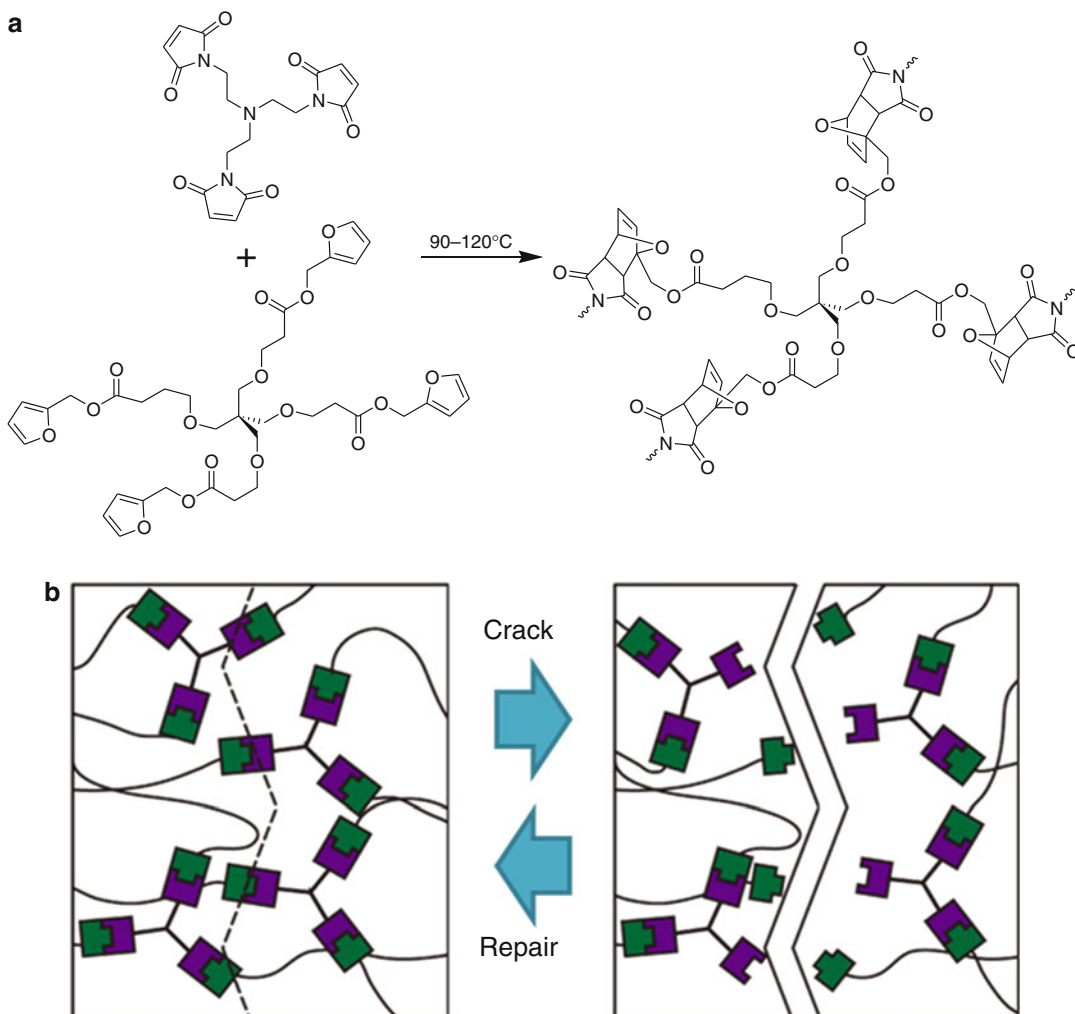
Self-Healing Polymers, Fig. 3 Preparation of furan–maleimide-based self-healing polymer network

gave cross-linked a polymeric network material (Fig. 3) [9]. The polymeric materials showed thermally remendable polymers through the DA/rDA strategy [9, 10]. When cracking, the polymeric network material healed above 120 °C. The polymeric network material was stressed to complete failure and subsequently healed by heating to ca. 90–120 °C, followed by cooling to room temperature. The healed polymer recovered to ca. 57 % of the initial material strength. Subsequently, the next generation of highly cross-linked remendable polymers consisting of 1,8-bis(maleimido)-1-ethylpropane and a tetrafuran monomer exhibited crack healing with as much as 83 % recovery of the initial material strength [10].

The DA/rDA reactions provide a simple and efficient way to prepare remendable polymers, which can go through repeated cycles of cracking and remending at the same site. On the other hand, the working temperature of the materials (85–150 °C) limits in the DA/rDA reactions.

Self-/Re-healing Materials Through Non-covalent Bonds

One of the most efficient ways to produce autonomously self-healing materials is non-covalent bond system where the polymerization and/or the cross-linking occurs by intermolecular interactions of the

a Fatty acids

b Urea derivatives

Amidoethylimidazolidone

Di(amidoethyl)urea

Diamidotetraethyltriurea

c
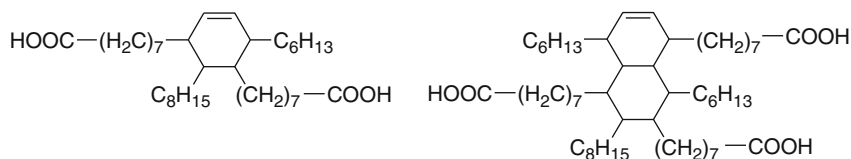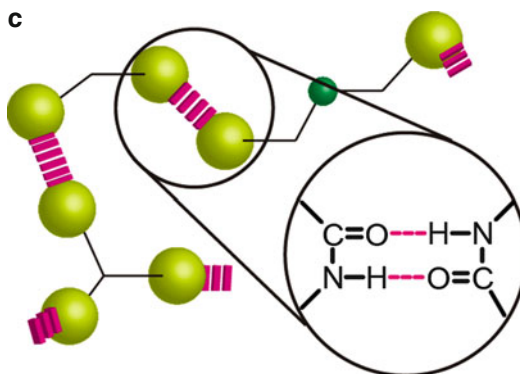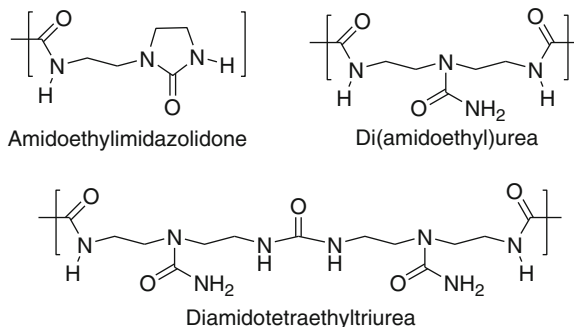
Self-Healing Polymers, Fig. 4 Fatty acids condensed with diethylene triamine and subsequently with a urea derivative to give a self-healing supramolecular network via hydrogen bonding

monomer units and/or the side chains by using hydrogen bonds [15], π-π stacking interactions, certain metal–ligand coordination bonds [16], or ion interactions [17]. The reversibility of non-covalent bonds allows repair to take place at the molecular level to fully restore the original material properties. Moreover, the crack and adhesions can be carried out repeatedly.

Polymeric materials based on rubber-like supramolecular network composed of low-molecular-weight hydrogen-bonding molecules, which are functionalized fatty di- and triacids, showed effective self-healing properties (Fig. 4). Fatty dimer acids were condensed with diethylene triamine and then reacted with urea. Hydrogen-bonding

motifs (amidoethyl imidazolidone, di(amido ethyl)urea and diamido tetraethyl triurea) formed the self-healable elastomers. When a rod-shaped rubber was cut in half using a razor, the cut rubber immediately mends after being broken; the gel can be lifted against its own weight. The repaired rubber adheres strongly to each other without a crack by extension and shrinkage [15].

Self-Healing Materials Through Host–Guest Interactions

Supramolecular materials consisting of host and guest polymers have unique features due
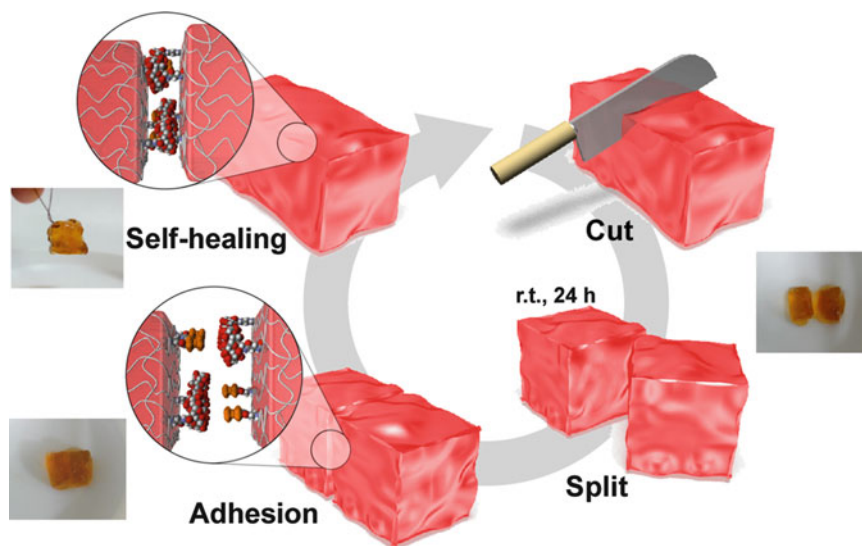
Self-Healing Polymers, Fig. 5 Schematic illustration of self-healing behavior of supramolecular materials through host–guest interactions

to selective complementary interactions. Host–guest interactions are versatile and can be used to prepare supramolecular materials, which have easily tuned switching efficiencies and functions. Self-healing and self-repairing properties are achieved using supramolecular materials that consist of host and guest polymers. The duality of supramolecular materials, which possess both switching and self-healing properties, has attracted both supramolecular chemists and materials scientists.

Poly(acrylic acid) modified with cyclodextrins (CD) as a host polymer and pAA with ferrocene as a guest polymer formed supramolecular materials by host–guest interactions. Supramolecular materials, which consist of host and guest polymers cross-linked by host–guest interactions, exhibit self-healing properties, which reach 84 % of the initial gel's strength on the cut gel surfaces. Redox stimuli can control self-healing properties such as readhesion between cut surfaces (Fig. 5) [18]. Polymerization of inclusion complexes of CD host and aliphatic guest monomers in aqueous solutions forms non-covalent cross-links between polymer chains to yield supramolecular hydrogels. When the gels are cut, cooperative host–guest complexation on the cut surfaces should quantitatively recover the

material strength [19]. When freshly cut surfaces are brought into contact, the free CD host and aliphatic guest units on the cut surface find the partner to form complementary complexes. This process is important to recover the material's original mechanical properties. Furthermore, a freshly cut surface does not adhere to the uncut surfaces at room temperature, indicating the need for non-associated units at the surface in the healing process.

Related Entries

▶ Molecular Self-Organization
▶ Supramolecular Hydrogels
▶ Supramolecular Polymers (Host-guest Interactions)

References

1. Dry CM (1992) Smart building materials which prevent damage and repair themselves. In: Smart materials fabrication and materials for micro-electro-mechanical systems, San Francisco, symposium held 28–30 Apr 1992. In series Materials Research Society proceedings, vol 276. MRS, Philadelphia, p 331

2. Wool RP (2008) Self-healing materials: a review. Soft Matter 4:400–418. doi:10.1039/B711716G
3. Bergman SD, Wudl F (2008) J Mater Chem 18:41
4. Marek WU (ed) (2011) Handbook of stimuli-responsive materials. Wiley-VCH Verlag GmbH, Weinheim
5. Caruso MM, Davis DA, Shen Q, Odom SA, Sottos NR, White SR, Moore JS (2009) Mechanically-induced chemical changes in polymeric materials. Chem Rev 109:5755
6. Yan X, Wang F, Zheng B, Huang F (2012) Stimuli-responsive supramolecular polymeric materials. Chem Soc Rev 41:6042
7. Schmidt FG, Barner-Kowollik C (2012) Current trends in the field of self-healing materials. Macromol Chem Phys 213:131
8. Herbst F, Döhler D, Michael P, Binder WH (2013) Self-healing polymers via supramolecular forces. Macromol Rapid Commun 34:203
9. Chen X, Dam MA, Ono K, Mal A, Shen H, Nutt SR, Sheran K, Wudl F (2002) Science 295:1698
10. Chen X, Wudl F, Mal AK, Shen H, Nutt SR (2003) Macromolecules 36:1802
11. Liu YL, Hsieh CY (2006) J Polym Sci Polym Chem 44:905
12. Watanabe M, Yoshie N (2006) Polymer 47:4946
13. Liu YL, Chen YW (2007) Macromol Chem Phys 208:224
14. Plaisted TA, Nemat-Nasser S (2007) Acta Mater 55:5684
15. Cordier P, Tournilhac F, Soulié-Ziakovic C, Leibler L (2008) Nature 451:977
16. Burnworth M, Tang L, Kumpfer JR, Duncan AJ, Beyer FL, Fiore GL, Rowan SJ, Weder C (2011) Nature 472:334
17. Wang Q, Mynar JL, Yoshida M, Lee EJ, Lee MS, Okuro K, Kinbar K, Aida T (2010) Nature 463:339
18. Nakahata M, Takashima Y, Yamaguchi H, Harada A (2011) Nat Commun 2:511
19. Kakuta T, Takashima Y, Nakahata M, Otsubo M, Yamaguchi H, Harada A (2013) Adv Mater 25:2849

Silica

Hiromitsu Kozuka
Faculty of Chemistry, Materials and Bioengineering, Kansai University, Suita, Osaka, Japan

Synonyms

Silicon dioxide; Silicon oxide; SiO_2

Definition

Silica is a material represented by a chemical formula, SiO_2, and is in solid state at the ambient temperature and pressure. Even when not represented exactly by the formula SiO_2, some materials are conventionally called silica as in the case of silica gels and colloidal silica, which contain at least hydrogen atoms and in some cases carbon atoms.

Introduction

Silica is a material represented by a chemical formula, SiO_2, and is in solid state at the ambient temperature and pressure. It is a colorless and transparent material but is colored when it contains impurity atoms or ions, and looks white and opaque when it scatters light, for instance, in the form of powders.

Silica exists either in crystalline or in amorphous (noncrystalline) form. Crystalline silica is thermodynamically stable and has an ordered and periodic atomic arrangement, while amorphous silica is metastable and has a disordered atomic arrangement. Although destined to transform into crystalline silica, amorphous silica practically remains as it is in the ambient atmosphere because such transformation requires atomic rearrangement, which can only be activated by thermal energy. This is why we can utilize amorphous silica as applied materials in the ambient atmosphere.

Crystalline silica has a number of polymorphs, that is, the crystals with the same chemical formula with different atomic arrangements, depending on temperature and pressure. α-Quartz is the thermodynamically stable polymorph at the ambient temperature and pressure, and utilized, for example, as an oscillator in watches. Silica glass, on the other hand, is typical amorphous silica, and the optical fibers in optical communication are the example of its use.

In this entry, first the structure, stability, and formation of crystalline silica and silica glass are illustrated. Second, the properties and applications of α-quartz and silica glass are described.

Finally, the brief introduction is given for the formation and properties of colloidal silica, silica gel, and mesoporous silica, which are other types of amorphous silica.

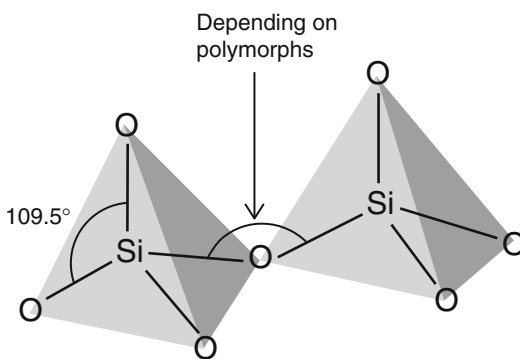## Crystalline Silica: Structure and Thermodynamic Stability

Crystalline silica has a number of polymorphs, i.e., the crystals with the same chemical formula, SiO_2, with different atomic arrangements. Most of them comprise SiO_4 tetrahedra that are linked to each other by sharing corners (O atoms) as shown in Fig. 1. Silicon atoms form sp^3 hybrid orbitals, leading to the formation of SiO_4 tetrahedra, and the O–Si–O bond angle is fixed at 109.5°, irrespective of polymorphs. On the other hand, the Si–O bond is rotatable, and the Si–O–Si bond angle is flexible, ranging from 140° to 180°, depending on the crystal structure.

β-Cristobalite (or high cristobalite), which belongs to the cubic crystal system, is one of the high-temperature polymorphs of silica, the structure of which is the most easy to be presented as shown in Fig. 2. As seen in Fig. 2, each SiO_4 tetrahedron is linked to each other by sharing O atoms, where the Si–O–Si bond angle is fixed at 151°. The crystalline silica that is thermodynamically stable at the ambient temperature and pressure is α-quartz (or low quartz), which belongs to the rhombohedral crystal system, and has the Si–O–Si bond angle of 144° (Fig. 3). Although "quartz" is a term for a crystalline
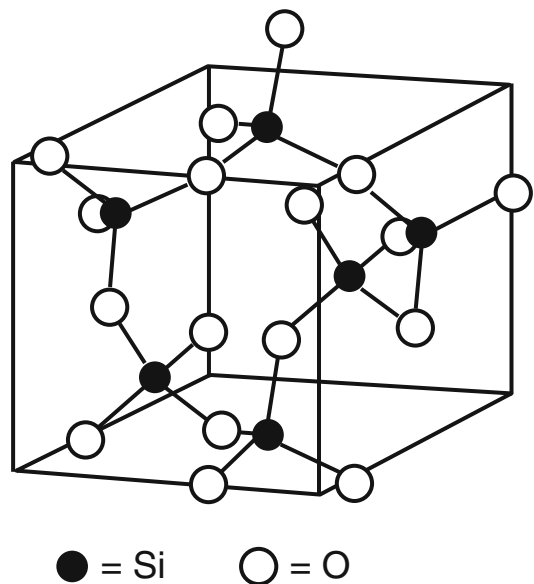
material, silica glass, an amorphous material, is often called "quartz glass" or just "quartz" especially in laboratories. "Quartz" to represent silica glass is a wrong terminology because silica glass is not crystalline. "Quartz glass" sounds scientifically strange but may be acceptable because the term "glass" represents the amorphous state. However, you should be careful when you see
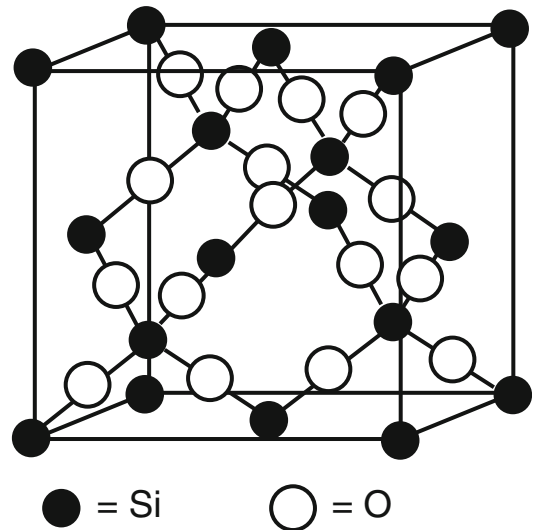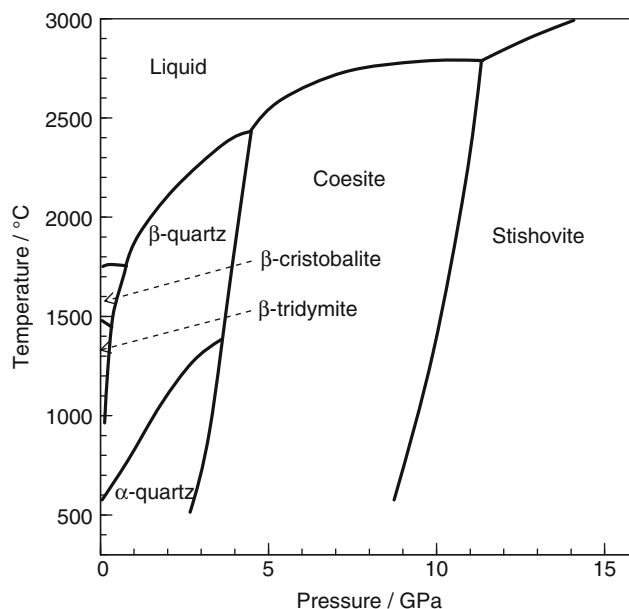

Silica, Fig. 2 Crystal structure of β-cristobalite

Silica, Fig. 3 Crystal structure of α-quartz

Silica, Fig. 1 SiO_4 tetrahedra sharing their corners

Silica, Fig. 4 Phase diagram of silica after Ref. [1]

Silica, Table 1 Crystal system, Si–O–Si bond angle, and density of silica polymorphs. The bond angle and density are shown also for silica glass

Silica	Crystal system	Si–O–Si bond angle/°	Density/g cm^{-3}
α-Quartz	Rhombohedral	144	2.65
β-Quartz	Hexagonal	153	2.53
β-Tridymite	Hexagonal	180	2.18
β-Cristobalite	Cubic	151	2.21
Coesite	Monoclinic	137, 143, 144, 150, 180	2.92
Stishovite	Tetragonal	131 (SiO_6 octahedra)	4.29
Silica glass	(Amorphous)	130–160	2.20

or hear the term "quartz" in laboratories or even in academic papers and should examine whether the term represents crystalline silica or not.

β-Quartz, α-cristobalite, α- and β-tridymite, coesite, and stishovite are the other examples of polymorphs of crystalline silica. Figure 4 shows the phase diagram of silica [1]. Amorphous silica is not seen in the diagram, of course, because it is not a thermodynamically stable phase. As seen in the diagram, α-quartz transforms into β-quartz, β-tridymite, and then β-cristobalite as temperature increases under the ambient pressure. The Si–O–Si bond angles and density of these polymorphs are summarized in Table 1. As seen in Table 1, the higher-temperature silica phases tend to have lower densities, i.e., more open structures. The melting point of silica is 1,713 °C, and β-cristobalite transforms into silica liquid at this temperature (Fig. 4). On the other hand, silica glass, an amorphous silica, has no melting point but glass transition temperature as illustrated later.

Coesite and stishovite are polymorphs that are thermodynamically stable under high pressures. Coesite is also composed of SiO_4 tetrahedra while stishovite exceptionally consists of SiO_6 octahedra as shown in Fig. 5, i.e., the coordination number of silicon is six, and its crystal structure is identical to rutile (TiO_2 and SnO_2). Coesite and stishovite are high-pressure phases, which results in their higher densities: 2.92 (coesite) and 4.29 (stishovite) g cm^{-3}.
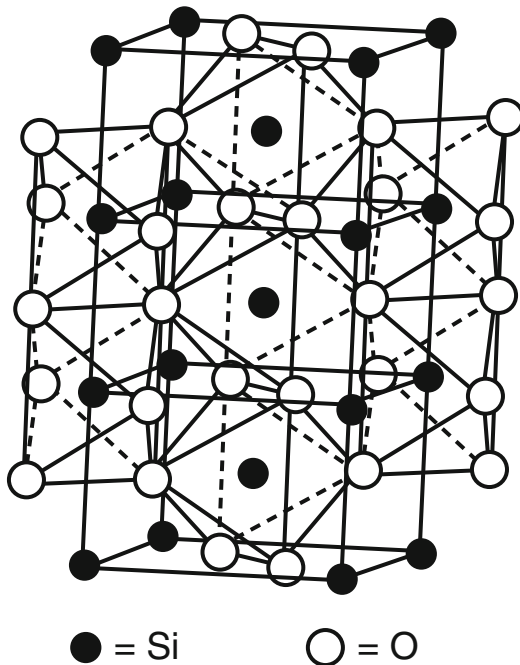
Silica, Fig. 5 Crystal structure of stishovite

● = Si   ○ = O

Silica Glass: Structure and Formation

Figure 6 shows the volume–temperature relationship for general materials. Starting from the liquid state, the volume decreases with decreasing temperature. When the temperature reaches the melting point, T_m, the liquid is "solidified," i.e., transforms into crystals; the thermodynamically stable solid is crystals and not amorphous. At this stage, the volume decreases abruptly. (Water is an exceptional material and increases in volume on solidification.) The volume of the crystals further decreases with decreasing temperature.

The atomic arrangement in a liquid is disordered and not static with time while that in a crystal is ordered and static. (The atoms are vibrating in crystals, but the time-averaged locations of atoms are unchanged with time). Therefore, the liquid-to-solid transformation (liquid-to-crystal transformation) is a drastic change from the viewpoint of atomic arrangement. Such a liquid-to-crystal transformation does not occur simultaneously throughout the bulk but via "nucleation" and "crystal growth."
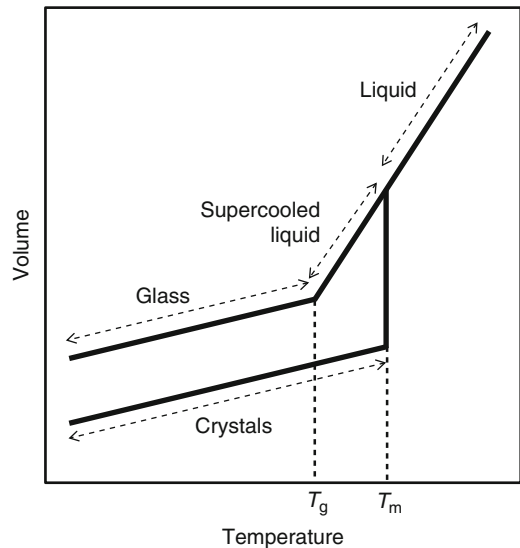

Silica, Fig. 6 Volume–temperature relationship for materials in general

A "crystal nucleus" is a small region where the atomic arrangement is ordered, and such a region increases in volume with time, which is called "crystal growth."

When the liquid is cooled slowly, "nucleation" and "crystal growth" occur, leading to crystallization, i.e., transformation into crystals. When the liquid is cooled at high rates, insufficient time is given for "nucleation" and "crystal growth" to occur, and as a result, the liquid is cooled down below T_m without being crystallized, becoming what is called "supercooled liquid." The supercooled liquid retains fluidity and disorder in atomic arrangement, and when it is further cooled down, the volume–temperature relation exhibits deflection at a certain temperature (Fig. 6). This temperature is called "glass transition temperature, T_g," where the supercooled liquid loses the fluidity and the change in atomic location with time. The solid material thus formed is called "glass."

Liquids are solidified into either crystals or glass on cooling, depending on cooling rates, as illustrated above. However, the tendency for glass formation also depends on materials. The cooling rate that is needed for glass formation is defined as critical cooling rate for glass formation, and silica is known to have a very low

Silica, Fig. 7 Schematic illustration of the atomic arrangement (**a**) in α-quartz and (**b**) in silica glass after Ref. [3] (With permission from John Wiley & Sons)
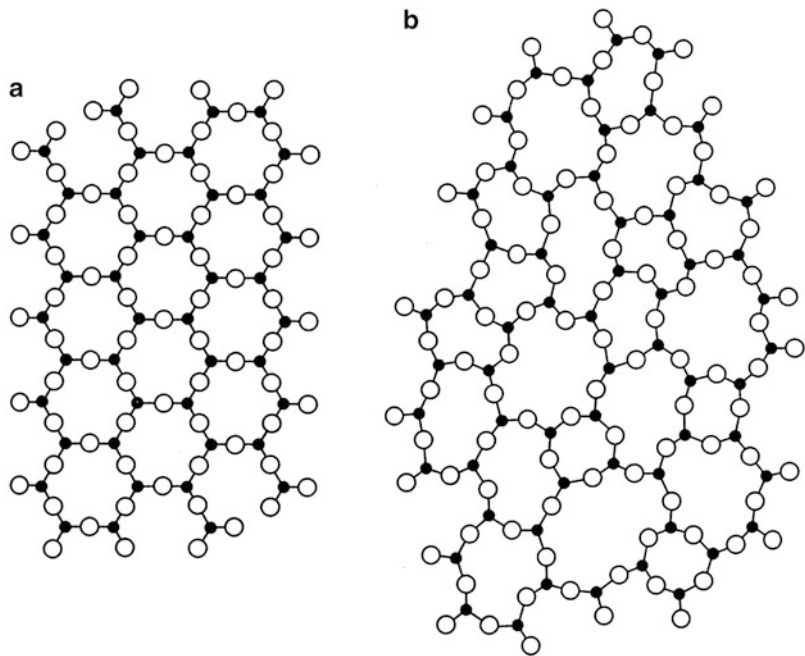
critical cooling rate around 10^{-4}–10^{-3} K/s. This indicates that silica has very high tendency for glass formation. Boron trioxide (B_2O_3), germania (GeO_2), and phosphorus pentoxide (P_2O_5) also have very low critical cooling rates and are called "glass formers" as well as silica.

Although the atomic arrangement is disordered in glass, there is what is called a short-range order. Silica glass is built up with SiO_4 tetrahedra with an O–Si–O bond angle of $109.5°$ as in the case of α-quartz, a crystal (Fig. 1). The Si–O bond distance of 0.16 nm and the O–O distance of 0.26 nm are also comparable to those of α-quartz. Then silica glass can be said to have short-range order in atomic arrangement. The only difference in atomic arrangement is the Si–O–Si bond angle. The Si–O–Si bond angle has distribution and ranges from $130°$ to $160°$ in silica glass [2] while α-quartz has a fixed bond angle of $144°$ (Table 1). The average Si–O–Si bond angle in silica glass, however, lies around $144°$, which is equal to the angle fixed in α-quartz. This results in the distribution of the Si–Si distance in silica glass, while α-quartz has a specific distance. This is why silica glass is said to have short-range order without long-range order in atomic arrangement.

Such a contrast in atomic arrangement is schematically represented in Fig. 7, which is given by W. H. Zachariasen and is very familiar in glass science [3]. Since each silicon atom is coordinated not by four but by three oxygen atoms in Fig. 7, the illustration is not an exact one. However, the illustration well describes the existence of the SiO_4 tetrahedra and the identical O–Si–O bond angle both in α-quartz and in silica glass. The illustration also well represents the fixed Si–O–Si bond angle in α-quartz and its distribution in silica glass.

Silica glass has a density of 2.20 g/cm^3, a smaller value than that of α-quartz, 2.65 g/cm^3, indicating that silica glass has more open structure than α-quartz (Table 1). A term "n-membered ring" is often used to describe the structure of silica, representing a ring structure that is composed of n SiO_4 tetrahedra that is linked to each other by sharing corners. α-Quartz is composed of 6-membered rings. In the case of silica glass, on the other hand, the majority is 6-membered rings, but n has distribution. Three- and 4-membered rings are sometimes called "defects" in silica glass structure, which is a terminology different from that in crystallography.

Silica glass is thermodynamically metastable and hence tends to transform into crystalline silica. However, such transformation does not occur at the ambient temperature because the transformation needs the rearrangement of atoms and the diffusion coefficient of atoms is too small at such low temperatures. When silica glass is heated, on the other hand, the diffusion coefficient increases, and silica glass is crystallized near at the glass transition temperature. This is an irreversible change, and in order to recover the glass state, the crystallized silica should be melted by heating over its melting point.

As described above, silica glass is formed by cooling silica liquid. However, silica glass can also be prepared without the melting process. It can be prepared even from solutions and gaseous species as illustrated in section "Production of α-Quartz and Silica Glass," where the processing temperatures are lower than the melting point of silica.

Properties of α-Quartz and Silica Glass

As illustrated in the above sections, both α-quartz and silica glass have the same chemical formula, SiO_2, and are composed of SiO_4 tetrahedra linked to each other by sharing oxygen atoms. The only difference is whether or not they have the long-range order in atomic arrangement and distribution in Si–O–Si bond angles, which provides similar properties to α-quartz and silica glass. As shown in Table 2, α-quartz and silica glass have similar optical absorption edge wavelength around 150 nm, thermal conductivity around 2–3 Wm^{-1} K^{-1}, and Young's modulus around 70 GPa, and both are electrical insulators.

On the other hand, because of the more open structure, which is revealed in lower density, silica glass has a lower refractive index (1.46) than α-quartz (1.55) as seen in Table 2. Difference is also seen in thermal expansion coefficient. Silica glass has much lower thermal expansion coefficient $(0.5 \times 10^{-6}$ $K^{-1})$ than α-quartz $(12 \times 10^{-6}$ $K^{-1})$, which is also due to its more open structure. The Si–O bond length increases with increasing temperature but is compensated by the change in Si–O–Si bond angle, resulting in low thermal expansion coefficient of silica glass.

As far as the chemical properties are concerned, both α-quartz and silica glass have high durability in organic solvents, water, and acids except for hydrofluoric acid. Silica is attacked by hydrofluoric acid (HF) to produce hexafluorosilicic acid (H_2SiF_6):

$$SiO_2 + 6HF \rightarrow 2H^+ + SiF_6{}^{2-} + 2H_2O$$

In contrast, both α-quartz and silica glass have low durability in basic solutions. Dissolution occurs by nucleophilic attack on silicon atoms by hydroxide ions (OH^-).

Applications of α-Quartz and Silica Glass

Silica glass has high thermal shock resistance due to its low thermal expansion coefficient. Therefore, silica glass or glasses with high silica contents can be used as applied materials that experience rapid and large changes in temperature. The tubes for tube furnaces and the crucibles for melting materials are examples, often used in laboratories. Due to the large bandgap energy and high transparency at ultraviolet (UV) wavelengths, silica glass is used as window materials and optics components in

Silica, Table 2 Properties of α-quartz and silica glass

| Silica	Density/ g cm^{-3}	Refractive index	Bandgap energy/eV	Optical absorption edge/nm	Thermal expansion coefficient/ 10^{-6} K^{-1}	Thermal conductivity/ Wm^{-1} K^{-1}	Young's modulus/GPa	Resistivity/ Ωm
α-Quartz	2.65	1.55	8.4	148	0.4	2.7	70	10^{12}–10^{18}
Silica glass	2.20	1.46	7.8	159	12.3	2.2	73	$>10^{18}$

various fields that require high UV transmittance. Silica glass has high transparency at infrared (IR) wavelengths particularly around 1.5 μm as well, which benefits their use as optical fibers in optical communications. Practically, the core and cladding, which have higher and lower refractive indices, respectively, should be made in optical fibers to allow the light transmission; dopants like germania (GeO_2), alumina (Al_2O_3), boron oxide (B_2O_3), and fluorine (F) are introduced in silica glass.

An applied mechanical stress generates a voltage in α-quartz, and an applied voltage changes its dimension. In other words, α-quartz has piezoelectric property (piezoelectricity). Silica glass exhibits no piezoelectricity, and this is a unique property of α-quartz. Due to this unique property, α-quartz is used in devices that generate sound, high voltages, and electronic frequency. α-Quartz as an oscillator in electric circuits in watches and computers is used in our daily life.

Production of α-Quartz and Silica Glass

α-Quartz occurs in nature via crystallization of molten magma. However, natural α-quartz that is pure enough for use in industry is quite rare and hence expensive. Therefore, highly pure α-quartz is synthesized by hydrothermal process for industrial use. The solubility of silica in water is known to be maximized at 340 °C. Utilizing this temperature dependence of solubility, natural quartz is dissolved in hot water in an autoclave (pressure vessel) with α-quartz seeds, and single-crystal α-quartz is grown by controlling the temperature.

Silica glass produced in industries is classified into "fused silica glass" and "synthetic silica glass." Fused silica glass is produced by purifying natural quartz (silica stone or silica sand) with reagents or halide gas and then melting it at temperatures over 2,000 °C. Synthetic silica glass, on the other hand, is produced by chemical vapor deposition (CVD) where vaporized silicon tetrachloride ($SiCl_4$) is hydrolyzed in oxyhydrogen flame:

$$SiCl_4 + 2H_2 + O_2 \rightarrow SiO_2 + 2HCl$$
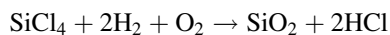
Fine silica particles thus obtained are called "fumed silica," which are deposited on a material in the CVD process. Then the deposited fumed silica is heated in a controlled atmosphere to remove the voids between particles, leading to synthetic silica glass products. Synthetic silica glass has higher purity than fused silica glass due to the high purity of the starting material, and the residual OH groups can be lowered by controlling the atmosphere in the heating process. Due to the higher purity, silica glass fibers for optical communication are produced from synthetic silica glass.

Silica gels can also be converted into silica glass by heating them at temperatures as high as 1,000 °C as will be illustrated in section "Silica Gel."

Colloidal Silica

Colloidal silica is amorphous silica particles of 1–100 nm in size that are suspended in liquids typically in aqueous solutions [4]. Such suspensions are called "silica sols." Colloidal silica particles are covered with a number of silanol groups (Si–OH groups). Therefore, the chemical formula of colloidal silica is not SiO_2 but $SiO_{2-x}(OH)_{2x}$ although it is called silica. When the surface of colloidal silica is modified by organic species, the chemical formula turns different further from $SiO_{2-x}(OH)_{2x}$.

Colloidal silica is produced in industries by neutralizing aqueous sodium silicate, which is called water glass:

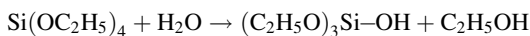$$Na_2SiO_3 + 2H^+ \rightarrow SiO_2 + 2Na^+ + H_2O$$
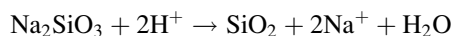
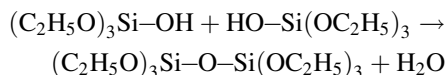Protonated ion exchange resins are used for the neutralization.

Colloidal silica can also be prepared by hydrolyzing silicon alkoxides [5]. Silicon alkoxides like tetraethoxysilane also called tetraethylorthosilicate and silicon tetraethoxide are hydrolyzed, and the hydrolyzed species undergo condensation

reaction to form siloxane bonds (Si–O–Si bonds) in alcoholic media:

<Hydrolysis>

$$Si(OC_2H_5)_4 + H_2O \rightarrow (C_2H_5O)_3Si–OH + C_2H_5OH$$

<Condensation>

$$(C_2H_5O)_3Si–OH + HO–Si(OC_2H_5)_3 \rightarrow$$
$$(C_2H_5O)_3Si–O–Si(OC_2H_5)_3 + H_2O$$

These reactions repeatedly proceed, and colloidal silica particles are formed in solutions. Instead of colloidal silica, polymer-like silica (polymeric silica) is also formed by controlling the pH and amount of water for the hydrolysis reaction. There is no clear boundary between colloidal and polymeric silica, and the siloxane species thus formed are characterized by fractal dimension; colloidal silica has fractal dimensions near 3 and polymeric silica around 1 and 2. Such reactions to form siloxane polymers or colloids utilizing alkoxides are often called "sol–gel reaction."

Colloidal silica has a number of industrial applications including the polishing slurries for silicon wafer polish, the binders for catalysts, the binders of molds for investment casting, the fillers for polymeric resins, and so on.

Silica Gel

Suspensions of colloidal silica (silica sols) have fluidity. When colloidal silica particles come to touch each other, which can be achieved by changing the pH or by removing the solvent, the suspension loses fluidity. Such materials that have lost fluidity are called silica gels. In other words, silica gels are materials that are composed of colloidal silica particles and behave like a solid. Because silica gels are composed of colloidal silica particles, their chemical formula is not SiO_2 but $SiO_{2-x}(OH)_{2x}$ again. Silica gels can also be obtained from alkoxide solutions, where colloidal silica or siloxane polymers grow by the progress of sol–gel reaction. Such alkoxide-derived silica gels usually contain alkoxy groups remaining unreacted. In such a case, the chemical formula is different even from $SiO_{2-x}(OH)_{2x}$.

Silica gels are transformed to silica glass when heated up to temperatures as high as 1,000 °C. During heating, the solvent evaporates, the silanol groups on the particle surface are further condensed to form siloxane bonds, and the pores shrink and collapse.

Silica gels have high specific surface area over hundred m²/g because they are built up with tiny colloidal silica particles. The surface of the colloidal silica particles also recognized as the pore walls is covered with silanol groups. Since water molecules and silanol groups form hydrogen bonds, and due to the high specific surface area, silica gels absorb water vapor in the atmosphere. This is why silica gels are used as desiccants.

Utilizing the porous nature, silica gels are also used as the stationary phase in column chromatography. Silica gels are safe materials and are used widely in the food industry as anticaking agents, defoaming agents, stabilizers, adsorbents, carriers, conditioning agents, chillproofing agents, filter aids, emulsifying agents, viscosity control agents, and anti-settling agents.

Mesoporous Silica

Pores in materials are classified by their diameters. Pores with diameters less than 2 nm, of 2–50 nm, and over 50 nm are called micropores, mesopores, and macropores, respectively. Mesoporous silica that is attracting much attention in materials science is amorphous silica with periodic mesopores that are homogeneous in diameter (Fig. 8) [6]. Prof. Kuroda's group at Waseda University first synthesized the mesoporous silica. Mobil Corporation later prepared mesoporous silica using surfactants as templates. When a surfactant is dissolved in aqueous solution at a certain concentration, micelles are formed, followed by the formation of their closely packed aggregation. When silicon alkoxides are added with catalysts, sol–gel reaction takes place at the periodic voids between the

S
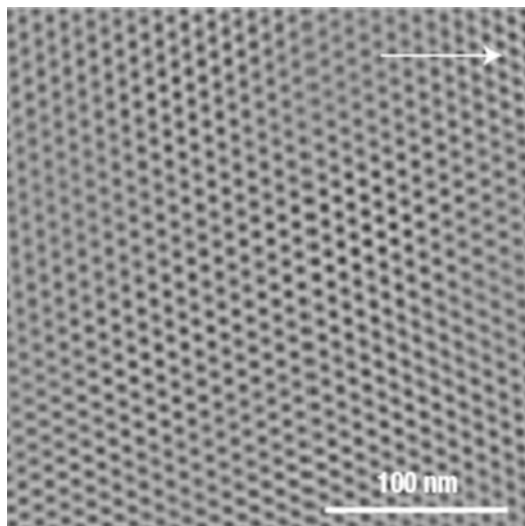
Silica, Fig. 8 Transmission electron microscopic image of mesoporous silica after Ref. [6] (With permission from Nature Publishing Group)

aggregates, leading to the formation of mesoporous silica.

Since mesoporous silica is a new type of material with well-controlled and periodic pores of nanometer in size, it attracts much attention as catalysts, adsorbents, optical devices, and gas sensors.

Related Entries

▶ Inorganic Nano-Fillers for Polymers
▶ Inorganic Polymers: Overview
▶ Layered Silicate-Based Rubber Nanocomposites
▶ Organic-Inorganic Hybrid Materials: Sol-Gel Reactions
▶ Polyhedral Oligomeric Silsesquioxanes (POSS)
▶ Polysiloxanes
▶ Silica Reinforcement

References

1. Swamy V, Saxena SK, Sundman B, Zhang J (1994) A thermodynamic assessment of silica phase diagram. J Geophys Res 99:11787–11794. doi:10.1029/93JB02968
2. Allen SM, Thomas EL (1999) The structure of materials. Wiley, New York
3. Kingery WD, Bowen HK, Uhlmann DR (1976) Introduction to ceramics. Wiley, New York
4. Iler RK (1979) The chemistry of silica: solubility, polymerization, colloid and surface properties and biochemistry of silica. Wiley, New York
5. Brinker CJ, Scherer GW (1990) Sol–gel science: the physics and chemistry of sol–gel processing. Academic, Boston
6. Miyata H, Suzuki T, Fukuoka A, Sawada T, Watanabe M, Noma T, Takada K, Mukaide T, Kuroda K (2004) Silica films with a single-crystalline mesoporous structure. Nat Mater 3:651–656. doi:10.1038/nmat1184

Silica Reinforcement

Wilma K. Dierkes[1] and Anke Blume[1,2]
[1]Department of Elastomer Technology and Engineering, Faculty of Engineering Technology, University of Twente, Enschede, The Netherlands
[2]Applied Technology Rubber and Tire, Evonik Industries AG, Wesseling, Germany

Synonyms

Dynamic-mechanical properties; Natural rubber; Reinforcement; Silane; Silica; Styrene-butadiene rubber; Tires

Definition

Silica reinforcement is the strengthening of elastomers by the addition of a filler system based on silica and a coupling agent. By the addition of reinforcing fillers, the physical as well as the dynamic-mechanical properties change: the material gets stronger and elasticity is reduced. Different types and amounts of fillers allow tailoring the properties of rubber.

History

Silica as a reinforcing filler in rubber is widely used in tires; more than 80 % of the original

equipment tires in Europe contain this particular filler [1]. The first tire producer who introduced silica was Michelin in their "Green Tires" in the early 1990s, containing a silica-coupling agent combination instead of carbon black. The reason for the replacement of the traditionally used carbon black by silica was the improvement in rolling resistance and wet grip. Earlier, silica had only marginal importance; it was, and still is, used in non-tire applications such as shoe soles, belts, hoses, or cable jackets. Shoe soles were the main application in the past, as silica makes rubber a nonstaining material with high abrasion, tear, and flex resistance [1].

Properties of Silica-Reinforced Material

Compared to carbon black, silica as such is characterized by weaker filler-polymer interactions and stronger filler-filler interactions with, as a consequence, higher compound viscosity, higher modulus at low strain amplitudes, lower modulus at high strain amplitudes, and lower bound rubber content [2]. The combination of silica with a coupling agent results in a higher reinforcing effect and different dynamic-mechanical and physical properties compared to carbon black. The main influence on physical properties is found for resilience, heat buildup,

wear, heat resistance, tear strength, flex stability, hardness, stiffness, modulus, and tack. The changes in tire-related properties when successively replacing carbon black by a silica-silane filler system are given in Figs. 1 and 2. The measurements to predict wet grip were performed on a Laboratory Abrasion Tester, LAT100, in which a small rubber wheel is tested on a turning disk representing the road surface. Rolling resistance is commonly predicted by measurement of the tan δ values at 60 °C and 10 Hz. In this study, the highly reinforcing carbon black type N234 is successively replaced by a highly dispersible silica and a disulfide silane (bis(triethoxysilylpropyl) disulfide) filler system, in a polymer matrix of solution-SBR with 25 % styrene and 50 % vinyl content. This leads to significant improvements in wet grip (Fig. 1) and tan δ as an indication of rolling resistance (Fig. 2) with increasing concentration of silica. Besides, it shows the improvement in heat buildup. The results of wear measurements done on the LAT100 as shown in Fig. 1 are rather indifferent and demonstrate the difficulty to get reliable data for wear prediction.

The strong reinforcing effect of silica compared to carbon black allows the reduction of the filler content without any negative influence on the property profile, but with an additional positive effect on elasticity due to the higher
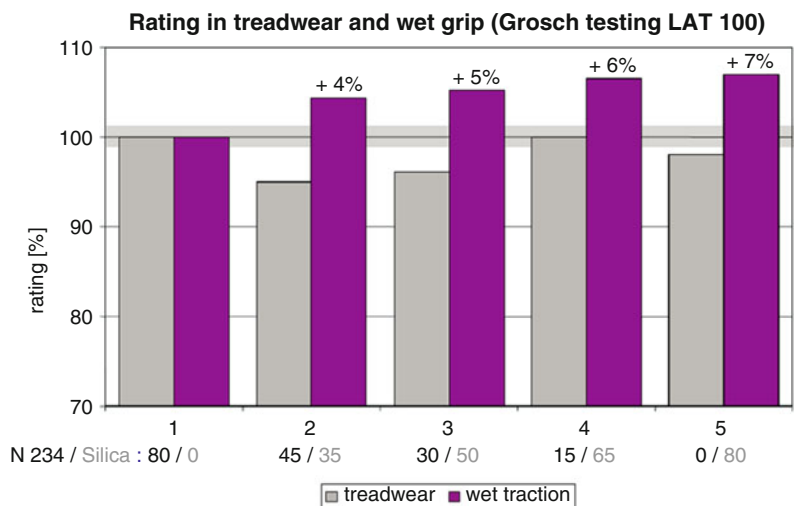
Silica Reinforcement, Fig. 1 Influence of carbon black/silica ratio on wet grip and treadwear

Silica Reinforcement, Fig. 3 Commonly used silane for
tire tread applications (x = 3.7)
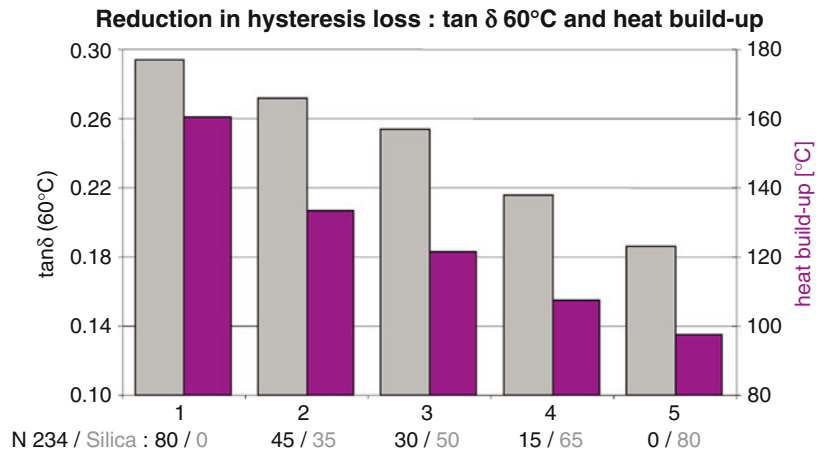
ratio of elastic component to damping filler. This results in an additional reduction of the rolling resistance.

The stability of the covalent silica-polymer network causes a lower rate of breaking and reformation of the silica-polymer bonds compared to the carbon black-polymer network during a deformation cycle, resulting in a decrease of the loss modulus. A low value of the loss modulus together with a high value of the storage modulus results in a low value of the phase angle. As both loss and storage modulus depend on deformation, the phase angle is also influenced by the applied strain: it increases with increasing deformation [3].

## Silica Types, Coupling Agents, and Polymers

Silica types used for rubber reinforcement are characterized by their surface area accessible for large molecules such as polymers (CTAB surface) and the total surface area (BET surface), which both vary between 50 and 250 m^2/g, and the primary particle size, which is in a range between 5 and 50 nm [4]. In a rubber matrix, silica particles form grapelike aggregates or clusters of 30–150 nm in size. Often, a correlation between the diameter of the primary particles and the mean diameter of aggregates is found; however, new types of silica combine very small particle sizes (high surface area) with extraordinarily large aggregate dimensions [5]. They are

reported to result in improved rolling resistance performance, longer tread life, higher dispersibility, and better handling [6]. Studies have shown that wet skid resistance is expected to improve with smaller aggregate size, while the loss angle (tan δ) at 60 °C as an indication for rolling resistance is reduced with increasing silica aggregates, thus reducing rolling losses [7]. Another key property is the structure of the silica, the extent to which it aggregates in a grapelike structure: the stronger the reinforcing effect, the higher the structure. Besides, the structure influences the dynamic properties: the higher the structure of the silica, the higher the amount of the complex modulus.

In most of the cases, silica is used together with a coupling agent. Coupling agents are bifunctional silanes. They contain a chemical group which can couple to the filler, as well as a moiety reacting with the polymer. The most commonly used silane is bis(triethoxysilylpropyl) tetrasulfide (Fig. 3). This silane has a high sulfur content which poses the risk of vulcanization during processing (scorch). An alternative with a reduced scorch risk is the

OR
|
RO — Si —(CH₂)₃— SH
|
OR
with R = C₂H₅ or Alkylpolyether
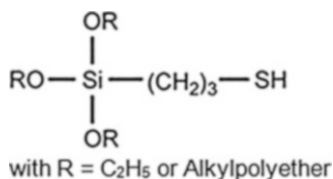
Silica Reinforcement, Fig. 4 Newly developed silane for tire tread applications

corresponding disulfide. These silanes form a covalent bond between the filler and the polymer during the vulcanization step, resulting in interpenetrating networks of polymer-polymer and polymer-filler bonds [8]. The particular network structure gives the material its unique property profile with improved dynamic properties and, as a consequence, better performance when used in a tire. However, there is a limit to the bond density for optimal properties: rubber with a high density of weak physical bonds with occasional strong chemical bonds performs best [9]. The chemical bonds are crucial for the properties: only physical interaction as achieved with silica grafted with alkyl chains shows a lower reinforcing effect [10].

Recent developments in coupling agents focus on improved properties of the elastomeric material in tire applications, especially wet grip and rolling resistance, and one of the latest silanes contains a free mercaptogroup shielded by bulky side groups as given in Fig. 4.

The main application for silica is rubber for treads of passenger car tires, and therefore it is mostly used together with styrene-butadiene rubber (SBR) and butadiene rubber (BR). Recently, modified SBR types were introduced with a better compatibility and interaction with silica and, as a consequence, improved tire properties. Examples of these modifications are dithiol- or carboxyl-backbone modification [11].

The silica-silane filler system has a low compatibility with natural rubber (NR); therefore its use in truck tire treads is so far rather limited. The nonrubber constituents in NR, mainly proteins in a concentration of app. 6 %, are interfering with the silica-silane reaction. They are adsorbed on the silica surface and thus improve the dispersion of the silica, but they do not couple to the polymer. As a consequence, the physical and dynamic properties of a NR-silica-silane composite material are rather poor [12]. Epoxidized NR was used in order to enable a direct chemical reaction between the polymer and the filler. The epoxidation influences processing and properties of the rubber, as it reduces the filler-filler interaction. However, an extra addition of silane to the compound is still necessary [13].

For most applications, silica is used in polymer blends. In tires, blends of SBR with BR and NR are often used. In such a blend, the silica distribution within the different polymers is unbalanced and determined by the surface energy and wetting behavior of the polymer towards the silica: the final concentration of silica after the mixing process will be higher in SBR compared to NR [14]. Flocculation, a phenomenon observed in silica compounds upon heating, and reformation of a filler-filler network is also determined by the surface energetic properties [15].

Processing

Mixing of silica compounds is rather time-consuming, and the most critical aspects are the generation of ethanol, the low dispersibility of the filler, and the risk of scorch.

During mixing of silica-silane reinforced compounds, a chemical reaction between the filler and the silane has to take place, as shown in Fig. 5. Ethanol is generated during this reaction, which hampers the further silanization reaction and complicates the mixing process. Lower concentrations of ethanol in the compound make the silanization reaction more efficient, and one measure to achieve this is fast removal of ethanol out of the mixer [16]. Another possibility for reducing the ethanol generation and enhancing the hydrophobation reaction is the use of silanes with a lower number of ethoxy groups, e.g., with one instead of three ethoxy groups. This silane leads to changes of dynamic properties, especially of the indicators for rolling resistance and wet grip, which both are expected to improve. A low concentration of ethanol in the compound

S

Silica Reinforcement, Fig. 5 The chemical reaction between the first ethoxy group of the silane with silanol groups of the silica (primary reaction, *left*) and the reaction with the remaining ethoxy groups (secondary reaction, *right*) [17]

also reduces the risk of porosity during further processing of the material.

The trend of using silica types with very small primary particle sizes leads to more difficulties in dispersion of the filler, but specially developed silica types with small particles, but large aggregate sizes reverse this trend and show easy dispersibility [5].

Another critical point of mixing of silica compounds is the scorch risk due to the presence of sulfur in the coupling agents. This can significantly be reduced by the addition of zinc oxide, an activator for the vulcanization, at a later mixing stage instead of the normally applied addition in the first mixing step [18].

Outlook

Tire technology is the leading area for the R&D efforts on elastomers, and the main topics in this field currently are sustainability, durability, and safety. For passenger car tires, significant improvements are achieved in the past 30 years by replacing carbon black by a silica-silane filler system. The development work is still going on, with nowadays focus on modified elastomers and special silica and silane types for tailored filler-polymer interaction. An important field in this area is natural rubber: truck tire treads mainly contain NR as polymer, and improving the compatibility with the silica-silane system would enable the truck tire manufacturers to produce tires with lower rolling resistance and better wet traction while maintaining good abrasion resistance. However, the polar nonrubber constituents interfere with the equally polar filler, and this influence makes the combination of natural rubber with silica and silane a great challenge.

Related Entries

▶ Controlling Performance of Filled Rubbers
▶ Dynamic Mechanical Properties
▶ Elastomer Blends: The Role of Nanoparticles on Properties
▶ Filler Dispersion and Filler Networks

▶ Inorganic Nano-Fillers for Polymers
▶ Mechanical Behavior of Filled Rubbers
▶ Natural Rubber
▶ Rubber Nanocomposites
▶ Synthetic Rubbers
▶ Vulcanization

References

1. Blume A, Luginsland H-D, Meon W, Uhrlandt S (2004) Rubber compounding, Chapter 7, CRC Press, Boca Raton
2. Wolff S, Wang M-J, Tan E-H (1994) Surface energy of fillers and its effect on rubber reinforcement. Part 2. Kautsch Gummi Kunstst 47(2):873–884
3. Wolff S, Görl U, Wang M-J, Wolff M (1994) Silica-based tread compounds. Eur Rubber J 16:16–19
4. Röthemeyer F, Sommer F (2013) Kautschuk Technologie. Hanser, München
5. Guy L, Cochet P, Bomal Y (2009) New insights in the dynamic properties of precipitated silica filled rubber using a new high surface silica. Kautsch Gummi Kunstst 62(7–8):383–391
6. http://www.rhodia.com/en/binaries/rhodia_tire_solutions_leaflets_en.pdf. Accessed 8 Jan 2014
7. Cichomski E, Tolpekina T, Schultz S, Dierkes W, Noordermeer J (2013) Influence of the silica surface area and structure on rolling and wet skid resistance of a passenger car tire tread. Lecture at the Eurofillers Conference, Bratislava, Slovakia
8. Leblanc JL (2010) Filled polymers. CRC Press, Boca Raton
9. Hamed GR (2000) Reinforcement of rubber. Rubber Chem Technol 73:526–533
10. Donnet JB (1998) Black and white fillers and tire compound. Rubber Chem Technol 71:323–341
11. Hogan TE, Randall A, Hergenrother WL, Lin CJ (2010) The role of functional polymers in improving tire performance. Rubber World 242(6):38–44
12. Sarkawi SS (2013) Nano-reinforcement of tire rubbers: silica technology for natural rubber. Wöhrmann Print Service, Zutphen
13. Kwaesakul W (2013) Silica-reinforced natural rubber for low rolling resistance, energy-saving tyres. Wöhrmann Print Service, Zutphen
14. Le HH, Kleer M, Hristov M, Ilisch S, Xuan TH, Do QK, Pham T, Stöckelhuber K-W, Heinrich G, Radusch H-J (2013) Selective wetting and localization of silica in binary and ternary blends based on styrene butadiene n rubber, butadiene rubber, and natural rubber. Macromol Mater Eng 298:1085–1099
15. Stöckelhuber KW, Svistikov AS, Pelevin AG, Heinrich G (2011) Impact of filler surface modification on large scale mechanics of styrene butadiene/silica rubber composites. Macromolecules 44:4366–4381
16. Dierkes W (2005) Economic mixing of silica-rubber compounds. Print Partners Ipskamp, Enschede

S

17. Hunsche A, Görl U, Mueller A, Knaack M, Goebel T (1997) Investigation concerning the reaction silica-organosilane and organosilane/polymer. Kautsch Gummi Kunstst 50:881–889
18. Reuvekamp LAEM (2003) Reactive mixing of silica and rubber for tyres and engine mounts. Twente University Press, Enschede

Silk Fibroin

Tetsuo Asakura[1] and Yu Suzuki[2]
[1]Department of Biotechnology, Tokyo University of Agriculture and Technology, Koganei-shi, Tokyo, Japan
[2]Tenure-Track Program for Innovative Research, University of Fukui, Fukui-shi, Fukui, Japan

Synonyms

Cocoon; Silkworm silk

Definition

Silk fibroin is a major component protein of the silkworm silk and its conformation dramatically changes between before and after spinning of silkworm.

Background

The silk of domestic silkworm, *Bombyx mori (B. mori)*, is composed of two proteins: fibroin and sericin. Silk fibroin is encased in silk sericin coat, a family of glue-like protein that holds two silk fibroin fibers together to form the composite fibers of the cocoon. Silk fibroin is secreted into the posterior silk gland as an aqueous solution. Then the silk fibroin stored in the middle silk gland, called "liquid silk," is spun out through the anterior silk gland and converted into silk fiber.

Mechanical Character

The stiffness, strength, and strain values at break of *B. mori* silk fibroin fiber along with values for

Silk Fibroin, Table 1 Comparison of mechanical properties of *B. mori* silk fibroin fiber and of spider silk to several types of biomaterial fibers and man-made fibers [1, 2]

| Material	Strength (Mpa)	Stiffness (Gpa)	% Strain at break
B. mori silk fibroin	610–690	15–17	4–16
N. clavipes spider silk	875–972	11–13	17–18
Wool	200	0.5	50
Collagen	0.9–7.4	0.0018–0.046	24–68
Tendon collagen	150	1.5	12
Bone	160	20	3
PLA	28–50	1.2–3.0	2–6
Nylon fiber	950	5	18
Carbon fiber	4,000	300	1.3

other biomaterials and selected man-made materials are summarized in Table 1. A comparison of the mechanical properties suggests that *B. mori* silk fibroin fibers provide an excellent combination of the strength and toughness. The features of the spider silks are the high strength in combination with elasticity in comparison with other biomaterials [1, 2].

Primary Structure

Silk fibroin molecule consists of a heavy (H) chain of 390 kDa and a light (L) chain of 26 kDa connected by a disulfide bond. The amino acid composition of the H chain showed the predominance of four amino acids: Gly (42.9 %), Ala (30.0 %), Ser (12.2 %), and Tyr (4.8 %). Detailed primary structure is unusually repeated sequence in the H chain of *B. mori* silk fibroin as shown in Fig. 1 [3]. An analysis of the primary structure of H chain indicated that the sequence may be roughly divided into four modular motifs: i.e., module (i) contains a highly repetitive GAGAGS (single letter code of amino acid is used) sequence and comprises the crystalline regions; module (ii) contains relatively less repetitive sequences with hydrophobic and/or aromatic residues – GAGAGY, GAGAGV, and GAGAGVGY – and make up the semicrystalline

Silk Fibroin,
Fig. 1 Schematic representation of the organization of the 12 repetitive domains and 11 amorphous repeated motifs in the primary structure of *B. mori* silk fibroin H chain. The repetitive domains are composed of 1–8 repeats of repetitive unit R, which consists of three repeated elements of the sequence motifs
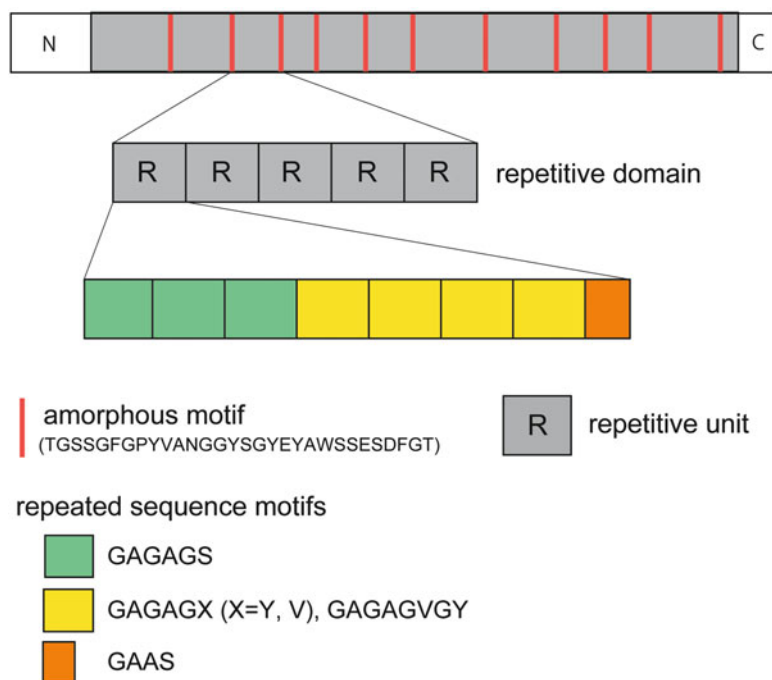
regions; module (iii) is very similar to module (i) except for the presence of an AAS motif; and module (iv) constitutes the amorphous regions containing negatively charged, polar, bulky hydrophobic, and/or aromatic residues, e.g., TGSSGFGPYVANGGYSGYEYAWSSES-DFGT.

Higher-Order Structure

Structure of *B. mori* Silk Fibroin After Spinning (Silk II)

In the solid state, two kinds of the crystalline modifications, Silk I and Silk II, have been reported [4]. The Silk II structure formed after silk spinning was proposed as a regular array of antiparallel β-sheet firstly, based on X-ray fiber diffraction study of native *B. mori* silk fibroin fiber [5]. Later, some intrinsic structural disorder in the Silk II structure was pointed out by several researchers [6–8] although the general features of this antiparallel β-sheet model were supported essentially. Atomic-level conformational analysis of Silk II was performed for $(AG)_{15}$ which is the model peptide for crystalline region of

B. mori silk fibroin. A lamellar structure has been proposed, based on changes in the intensities of asymmetric $Ala^{13}C\beta$ peaks in the ^{13}C CP/MAS NMR spectra coupled with selective ^{13}C labeling of different Ala methyl carbons [9]. The relative intensities of the peaks at 16.7 ppm which were assigned to the distorted β-turn structure change largely depending on the labeled position of the Ala residue. When the relative intensity was plotted against the residue number of the labeled $[3\text{-}^{13}C]Ala$, the plot indicates two maxima at the positions 9 and 19 of $(AG)_{15}$. This implies the appearance of the folded lamellar structure with a β-turn at these positions as shown in Fig. 2. X-ray diffraction data also propose such a lamellar structure and eight amino acid residues contribute to the β-sheet structure for $(AG)_n$ [10]. This is in agreement with the NMR result.

Structure of Silk Fibroin Before Spinning (Silk I)

Silk I is the structure of *B. mori* silk fibroin in the solid state obtained from the middle silk gland after drying. The backbone structure of the Silk I conformation for $(AG)_n$ was determined to be a

S

Silk Fibroin, Fig. 2 The
lowest energetic model of
$(AG)_{15}$ with lamellar
structure obtained from
combination of solid-state
NMR measurements and
statistical mechanical
calculations
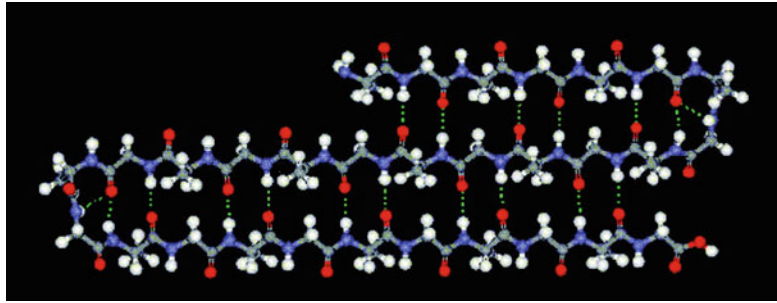
repeated type II β-turn structure by combining several solid-state NMR techniques, and the torsion angles were determined to be ($\phi = -62°$ $\varphi = 125°$) for the Ala residue and ($\phi = 77°$ $\varphi = 10°$) for the Gly residue [11] (Fig. 3). The solution structure of native liquid silk was determined with solution NMR, for tandem repeated sequences with $(GAGXGA)_n$ (X = S, Y, V) and GAASGA motifs in *B. mori* silk fibroin. A type II β-turn structure for liquid silk which is close to the structure determined from solid-state NMR for the motif $(GAGXGA)_n$ was determined, while the motif GAASGA is disordered in its conformation and most probably forms a flexible segment [12].

Structure of N-Terminal Domain of Silk Fibroin

B. mori fibroin includes a non-repetitive 151 residue header sequence and a 58 residue C-terminal sequence. The header sequence is homologous to the N-terminal sequence of other fibroins with a difference crystalline region. A crystal structure of the N-terminal domain of *B. mori* silk fibroin was determined an entangled β-sheet dimer. It is shown that N-terminal domain undergoes a pH-responsive conformational transition from random coil to β-sheets at around pH 6.0. This implies that N-terminal domain functions as a pH-responsive self-assembly module that could prevent premature β-sheet formation at neutral pH yet could initiate fibroin assembly as pH decreases along the lumen of the posterior silk gland to the anterior silk gland [13].

Silk Fibroin as Biomedical Materials

Silk has been used in biomedical applications for centuries, primarily for suturing. Silk is susceptible to proteolytic degradation in vivo and is absorbed slowly. Fibroin provides an antithrombotic surface and serves as a scaffold for various cell types in tissue engineering [14]. The regenerated silk solutions have been used to form a variety of biomaterials, such as gels, sponges, and films, for medical applications. Silks can be chemically modified through amino acid side chains to alter surface properties or to immobilize cellular growth factors. Molecular engineering of silk sequences has been used to modify silks with specific features, such as cell recognition or mineralization [15].

As the application for biomedical materials, the efficiency of silk fibroin as a material for small-diameter vascular grafts was evaluated [14]. When it was implanted in rat abdominal aorta, the patency of the silk fibroin grafts at 1 year after implantation was significantly higher than that of PTFE grafts (85.1 % vs. 48 %, $P < 0.01$) (Fig. 4a). Endothelial cells and smooth muscle cells migrated into the fibroin graft early after implantation and became organized into endothelial and medial layers. The content of collagen significantly increased at 1 year after implantation, with a decrease in fibroin content (Fig. 4b). These results indicate fibroin would be a promising material to engineer vascular prostheses for small arteries.
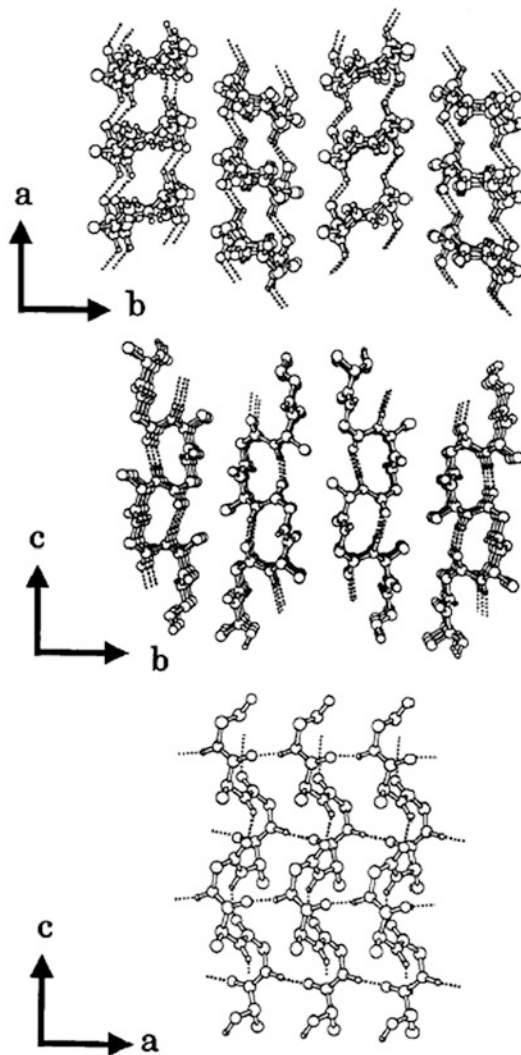
Silk Fibroin, Fig. 3 The molecular arrangement of the Silk I structure determined by several solid-state NMR and X-ray diffraction measurements

Other Silks

Spider Silks

Spider silk is one of the toughest biopolymers. Spider silk from *N. clavipes* has been studied extensively and is characterized by its remarkable mechanical strength and thermal stability in fiber form. The different types of silks formed by spiders serve various functions. The mechanical

properties of the different silks are due to structural differences derived from different amino acid compositions and sequences. Dragline silk for safety and web construction is one of the strongest natural materials and is composed of two proteins: major ampullate spidroins protein 1 and 2 (MaSp1 and MaSp2) [15].

The amino acid composition of dragline silk, MaSp1 from *N. clavipes*, consists mainly of Gly and Ala, like *B. mori* silk, while Glu, Pro, and Arg are also significant in content. This silk consists of repetitive blocks of peptides which give rise to the unique structural properties. The crystalline domains, which contribute to the tensile strength, contain repeats of Ala or Ala-Gly in MaSp1 and MaSp2. Another motif consisting of GPGXX (where X is most likely Gln) found only in MaSp2 is responsible for β-turn spiral and results in the elasticity of silk. Flagelliform silk from *N. clavipes* is rich in this motif and is highly elastic to serve its function in prey capture. Another motif, GGX, a glycine helix found in MaSp1, is responsible for the less crystalline regions of the silk structure. These domains also give rise to elasticity of dragline silk. At the N- and C-termini of the protein, non-repetitive sequences are found which have been proposed to have a role in assembly of the protein [16, 17].

Wild Silkworm Silks

While the vast majority of studies of silk has been done on silkworm and spider silks, silk is a natural protein fiber that is produced by numerous insects and arthropods. Wild silkworm silks are also interesting. The amino acid composition of silk fibroin from a wild silkworm, *S. c. ricini* or *A. pernyi*, is considerably different from that of *B. mori* silk fibroin. The proportion of Gly residues is greater in *B. mori* silk fibroin, while the content of Ala residues is greater in *S. c. ricini* silk fibroin. The solution structure of *S. c. ricini* silk fibroin has been studied with solution NMR [18]. The fast exchange in the NMR timescale between helix and coil forms of the poly-Ala region has been observed during the helix-to-coil transition with changing
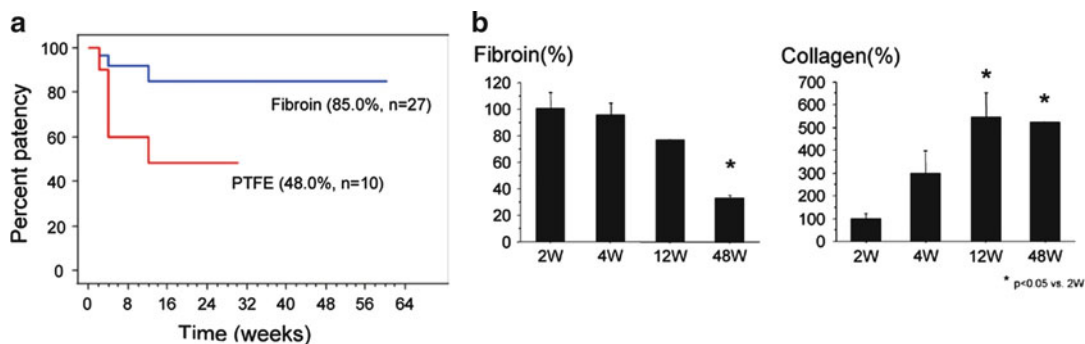
Silk Fibroin, Fig. 4 (**a**) Patency for 27 fibroin and 10 PTFE grafts implanted into rat aortas at 2–60 weeks. (**b**) The content of fibroin gradually decreased while collagen content increased after implantation

temperature. Moreover, solid-state NMR analysis of model peptides leads to the precise silk structure before spinning, where the poly-Ala sequence takes a typical α-helix pattern with a tightly wound helical structure at both terminal regions of the poly-Ala sequence [19]. Wild silkworm silks are also studied for application of biomedical materials. Silk fibroin of *A. pernyi*, *A. yamamai*, and *A. mylitta* contain Arg-Gly-Asp sequence in the primary structure. Integrin, the cell surface molecule, binds the RGD sequence. It was shown that the RGD sequence elevated cell adhesion and proliferation activity in vitro study [20]. Therefore, wild silkworm silk might be promising materials for biomedical application as well as *B. mori* silk fibroin.

Summary

B. mori silk fibroin fiber is prepared from an aqueous silk fibroin solution by spinning. The structure of fibroin before spinning (Silk I) and after spinning (Silk II) revealed that the recombination of hydrogen bond from intramolecular to intermolecular leads the dynamic conformational transition at fiber formation. Recent advances in the role of N- and C-terminal domain facilitate revealing the profound fiber formation mechanism. Also, many researchers are applying fibroin for biomedical devices such as artificial vascular grafts, drag delivery materials, and scaffold for bone and teeth regeneration. Certainly,

a better understanding of fiber formation mechanism has broad impact on application of fibroin-based biomedical devices as well as fiber processing technology.

Related Entries

▶ Biodegradable Materials

References

1. Altman GH, Diaz F, Jakuba C, Calabro T, Horan RL, Chen J, Lu H, Richmond J, Kaplan DL (2003) Silk-based biomaterials. Biomaterials 24:401–416
2. Gosline JM, Guerette PA, Ortlepp CS, Savage KN (1999) The mechanical design of spider silks: from fibroin sequence to mechanical function. J Exp Biol 202:3295–3303
3. Zhou CZ, Confalonieri F, Jacquet M, Perasso R, Li ZG, Janin J (2001) Silk fibroin: structural implications of a remarkable amino acid sequence. Proteins Struct Funct Genet 44:119–122
4. Asakura T, Kaplan D (1994) Silk production and processing. In: Charles Arntzen (ed) Encyclopedia of agricultural science, 4th edn. Academic Press, pp 1–11
5. Marsh RE, Corey RB, Pauling L (1955) An investigation of the structure of silk fibroin. Biochim Biophys Acta 16:1–34
6. Fraser RD, MacRae TP, Stewart FH (1966) Poly-l-alanylglycyl-l-alanylglycyl-l-serylglycine: a model for the crystalline regions of silk fibroin. J Mol Biol 19:580–582
7. Lotz B, Cesari FC (1979) Chemical-structure and the crystalline-structures of *Bombyx-mori* silk fibroin. Biochimie 61:205–214

8. Takahashi Y, Gehoh M, Yuzuriha K (1999) Structure refinement and diffuse streak scattering of silk (*Bombyx mori*). Int J Biol Macromol 24:127–138

9. Asakura T, Sato H, Moro F, Nakazawa Y, Aoki A (2007) Lamellar structure in Poly(Ala-Gly) determined by solid-state NMR and statistical mechanical calculations. J Am Chem Soc 129:5703–5709

10. Panitch A, Matsuki K, Cantor EJ, Cooper SJ, Atkins EDT, Fournier MJ, Mason TL, Tirrell DA (1997) Poly(*L*-alanylglycine): multigram-scale biosynthesis, crystallization, and structural analysis of chain-folded lamellae. Macromolecules 30:42–49

11. Asakura T, Ohgo K, Komatsu K, Kanenari M, Okuyama K (2005) Refinement of repeated β-turn structure for silk I conformation of *Bombyx mori* silk fibroin using ^{13}C solid-state NMR and X-ray diffraction methods. Macromolecules 38:7397–7403

12. Suzuki Y, Yamazaki T, Aoki A, Shindo H, Asakura T (2013) NMR study of the structures of repeated sequences, GAGXGA (X = S, Y, V), in *Bombyx mori* liquid silk. Biomacromolecules 15:104–112

13. He YX, Zhang NN, Li WF, Jia N, Chen BY, Zhou K, Zhang JH, Chen YX, Zhou CZ (2012) N-terminal domain of *Bombyx mori* fibroin mediates the assembly of silk in response to pH decrease. J Mol Biol 418:197–207

14. Enomoto S, Sumi M, Kajimoto K, Nakazawa Y, Takahashi R, Takabayashi C, Asakura T, Sata M (2010) Long-term patency of small-diameter vascular graft made from fibroin, a silk-based biodegradable material. J Vasc Surg 51:155–164

15. Vepari C, Kaplan DL (2007) Silk as a biomaterial. Prog Polym Sci 32:991–1007

16. Askarieh G, Hedhammar M, Nordling K, Saenz A, Casals C, Rising A, Johansson J, Knight SD (2010) Self-assembly of spider silk proteins is controlled by a pH-sensitive relay. Nature 465:236–238

17. Hagn F, Eisoldt L, Hardy JG, Vendrely C, Coles M, Scheibel T, Kessler H (2010) A conserved spider silk domain acts as a molecular switch that controls fibre assembly. Nature 465:239–242

18. Asakura T, Kashiba H, Yoshimizu H (1988) Nmr of silk fibroin. 8. C-13 Nmr analysis of the conformation and the conformational transition of Philosamia-cynthia-ricini silk fibroin protein on the basis of Bixon-Scheraga-Lifson theory. Macromolecules 21:644–648

19. Nakazawa Y, Asakura T (2003) Structure determination of a peptide model of the repeated helical domain in *Samia cynthia ricini* silk fibroin before spinning by a combination of advanced solid-state NMR methods. J Am Chem Soc 125:7230–7237

20. Kundu SC, Kundu B, Talukdar S, Bano S, Nayak S, Kundu J, Mandal BB, Bhardwaj N, Botlagunta M, Dash BC, Acharya C, Ghosh AK (2012) Invited review nonmulberry silk biopolymers. Biopolymers 97:455–467

Smart Materials

Takao Aoyagi
International Center for Materials Nanoarchitectonics, National Institute for Materials Science, Tsukuba, Ibaraki, Japan

Synonyms

Intelligent materials; Stimuli-responsive materials

Definition

Smart materials are one of the functional materials that respond to against the environmentally internal or external stimuli, such as application of electric/magnetic field, changing in temperature and pH, or light irradiation. Stimuli-responsive materials or intelligent materials have almost same sense.

Introduction

So much attention has been paid to the smart polymeric materials, because these materials can show sensitive response against many kinds of stimuli such as application of electric/magnetic field, changing in temperature and pH or light irradiation, and so on. Among them, the most famous smart polymeric materials are poly(*N*-isopropylacrylamide) (abbreviated as PNIPAAm) and its PNIPAAm-based materials including some other materials modified with PIPAAm. Until now, there are many researches that have been done that include physicochemical analyses of the response mechanism and diverse applications. Its lower critical solution temperature (abbreviated as LCST) is 32 °C [1], and the LCST of PNIPAAm-based materials can be easily and precisely controlled to near body temperature by copolymerization or functionalization. Owing to the LCST near body temperature,

applications of PNIPAAm have been extensively focused on biotechnology, diagnosis, biomaterial, medicine, or tissue engineering [2, 3]. Moreover, recent precise-polymerization methods, such as atom transfer polymerization (abbreviated as ATRP) or reversible addition-fragmentation chain transfer (abbreviated as RAFT) polymerization, surely have contributed to develop well-designed and well-characterized smart materials [4, 5]. Cooperative dehydration and hydration of polymer chains with uniform chain length contribute sensitive response against the kinds of stimuli that exemplified above.

PNIPAAm-Based Smart Materials

Recent progresses of nanotechnologies also relate to the new smart materials studies. Macro-sized PNIPAAm hydrogel has a relatively slow response to temperature change. So, to get quickness, nanostructures have attracted great attention because of their fast rate of response to temperature change due to nano-sized structure [6]. Nanoparticle, nanofiber, ultrathin layer, bioconjugate, and so on are exemplified [7–9]. Among many types of them, recently, smart nanofiber is focused for biomedical application, because of its biomimetic structure, high specific surface area, high molecular alignment, and high porosity compared to conventional films or hydrogels. As the most widely employed method for preparation of nanofibers, electrospinning is an adaptable method of generating them by optimizing an electrical charged voltage to polymer solution [10]. The diameter can be controlled by electrospinning parameters such as concentration of polymer solution, distance between tip to collector, voltage, and feeding speed [11]. It is easily understood that nanofibers comprised of PNIPAAm and is completely soluble in aqueous solution below the LCST. To design the reversible transition against the repeating temperature change, the materials should not be soluble even below LCST. To solve the problem, PNIPAAm-based smart polymers cross-linkable by photo irradiation or thermal treatment were studied [12]. To achieve this purpose, newly designed photoreactive copolymer NIPAAm-2-carboxyisopropylacrylamide (abbreviated as NIPAAm-co-CIPAAm) was prepared by free radical polymerization followed by introduction of 4-aminobenzophenone (BP) into copolymer as a chemical cross-linker [8]. Figure 1 shows the synthetic scheme of the photoreactive polymer. After the UV light irradiation, such smart materials showed perfectly reversible size and tensile strength change against the repeating temperature changing.

To obtain the thermal cross-linking type of PIPAAm-based smart materials, simple
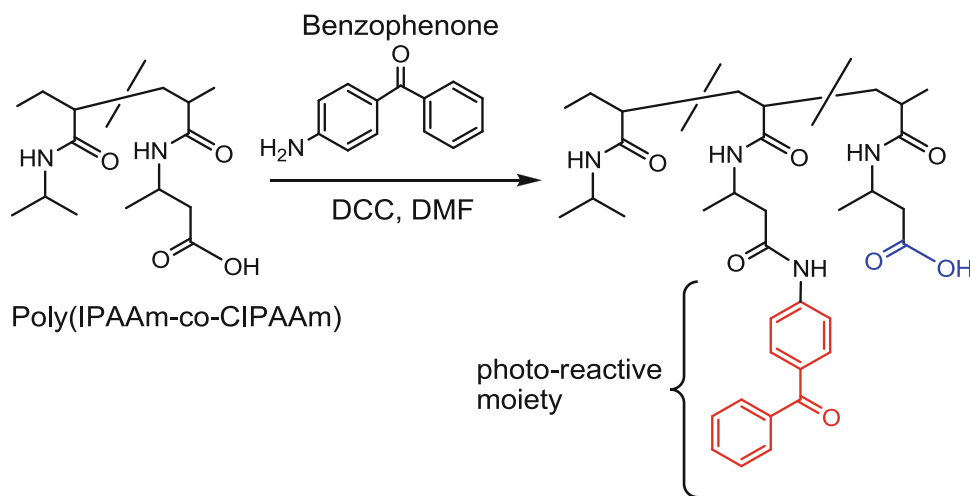
Smart Materials, Fig. 1 Synthetic scheme of PIPAAm-based photoreactive polymer for smart nanofiber

copolymer poly(NIPAAm-co-N-hydroxymethy-lacrylamide) (abbreviated as poly(NIPAAm-co-HMAAm)) was synthesized by free radical polymerization [13]. HMAAm was chosen for post thermal cross-linking, because its hydroxymethyl group can be chemically cross-linked by self-condensation of intra- or intermolecular chains with only heating [14, 15]. By thermal curing, the methylol groups in HMAAm transformed to bis(methylene ether) and methylene bridges. The unreacted remaining hydroxymethyl group plays a role of modulating LCST. The chemical cross-linking of the nanofiber was carried out by thermal curing of the OH groups of HMAAm.

Two types of nanofibers described above were supplied to biomedical application such as cell capture [12] and release aiming at cell container and cancer therapy [12]. About the use for anti-cancer, self-heating and temperature-responsive nanofiber incorporated magnetic nanoparticles (MNPs) were developed because of their self-heating property by applying alternative magnetic field (AMF). In Fig. 2, synthetic scheme is shown. Specifically, polymer composite nanofiber composed of poly(NIPAAm-co-HMAAm), MNPs, and anticancer drug, doxorubicin (abbreviated as DOX), were prepared by electrospinning followed by the cross-linking reaction. To test both thermotherapy and chemotherapy effects of the composite nanofiber in vitro, the cytotoxicity to human melanoma cell line COLO 679 cells were evaluated by MTT assay. Eventually, in case of the DOX/MNP nanofiber, cell viability decreased to 70 % by AMF application. Although the thermotherapy effect itself showed a minor anticancer effect for a short duration AMF application, cooperative DOX released from the nanofibers induced the damages of cancer cells due to a synergistic effect in combination with thermotherapy.

Surface Shape Memory Materials by Smart Polymers

There are many researches on shape memory materials [16]. In general, transition between
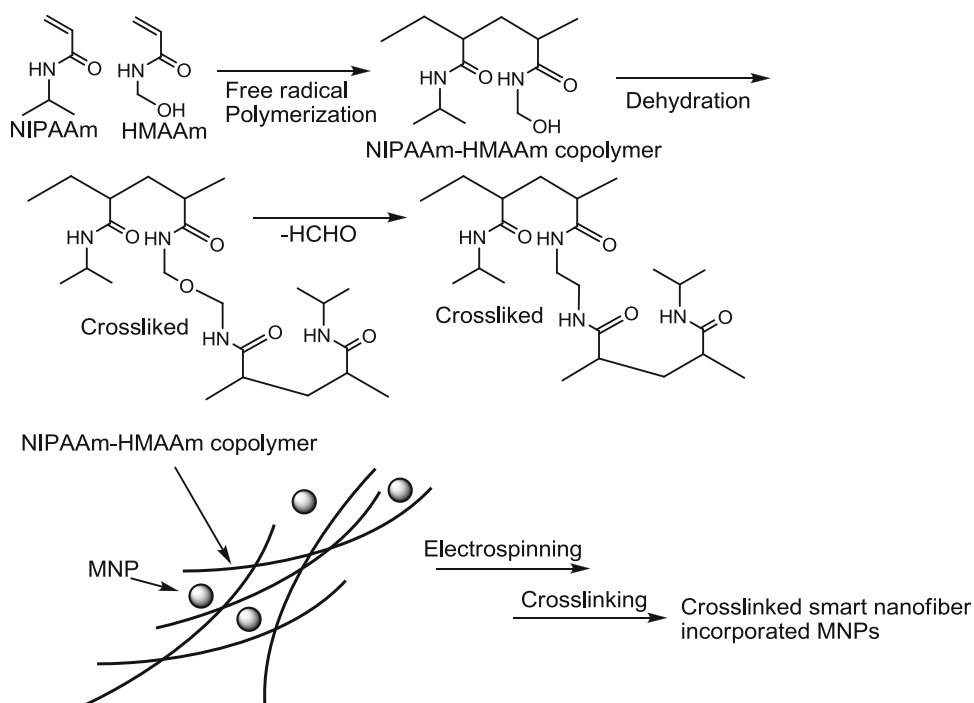
Smart Materials, Fig. 2 Preparative scheme of smart nanofiber incorporated magnetite nanoparticle
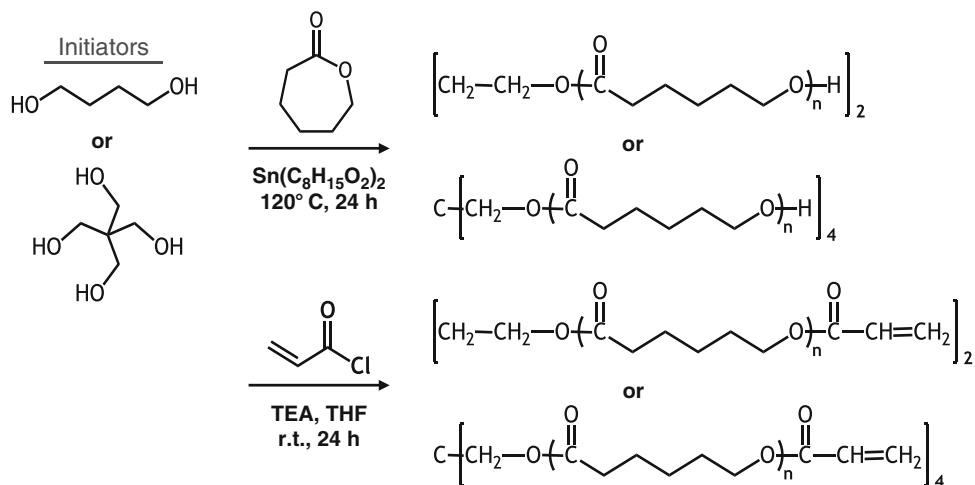
Smart Materials, Fig. 3 Macromonomer syntheses of linear and branched PCL

crystallization and melting of polymer crystalline is used for holding temporary shape and recovery to permanent one. Recently, mechanobiology attracts much attention [17], and developments of surface shape memory materials would contribute to study them. Actually, the use of such material is essential to study dynamic surface topography on cell function control, because external stimulus, for example, just heating, can erase the surface pattern or alter the pattern geometry [18]. Moreover, the effect of materials elasticity on cell attachment, proliferation, and differentiation also has been investigated using such materials. Our group investigated cross-linked PCL whose softening points are near body temperature [19]. Preparative scheme is shown in Fig. 3. It is well known that PCL is a semicrystalline polymer and its melting point is around 60 °C. To adjust the softening point near body temperature, crystallinity control is surely critical. Precise molecular design, for example, control of ratio in mixing of linear and branched PCL macromonomers or molecular weights, succeeded to modulate the temperatures of cured materials around 20–40 °C [19].

To prepare shape memory surfaces with permanent surface patterns, a PCL macromonomer solution with adequate mixing of the linear and branched ones was injected between a glass master and a flat slide glass with Teflon spacer and cured by heating. The curing was done by reaction of each acryl groups at the chain ends. To program temporary surface patterns, the cross-linked film-type materials were compressed in a thermo chamber followed by cooling. The permanent grooved topography quickly appeared after heating. It was also succeeded that shape memory transition from a grooved pattern to another one. Thus, temporary surface patterns can be easily programmed into the films, and the recovery to the permanent surface patterns is rapid and complete, irrespective of the temporary or permanent pattern.

To investigate the role of dynamic and reversible surface patterns on cell proliferation, specifically cell alignment on the PCL films before and after a topographic change, NIH 3 T3 fibroblasts were seeded on fibronectin-coated PCL films with a temporary grooved topography and cultured. Cells migrated and grew horizontally to the surface grooves with cultivation time. Upon changing from the grooved topography to a flat surface by heating over transition temperature, cell alignment was lost and random cell migration and growth ensued [18]. These results suggested such surface shape memory materials could contribute to mechanobiology. The cross-linked PCL smart materials are also very useful to investigate the relation of materials elasticity and cell functions [20].

References

1. Schild HG (1992) Poly (*N*-isopropylacrylamide) – experiment, theory and application. Prog Polym Sci 17:163–249
2. Miyata T, Asami N, Uragami T (1999) A reversibly antigen-responsive hydrogel. Nature 399:766–769
3. Ebara M, Hoffman JM, Hoffman AS, Stayton PS (2006) Switchable surface traps for injectable bead-based chromatography in PDMS microfluidic channels. Lab Chip 6:843–848
4. Nagase K, Watanabe M, Kikuchi A, Yamato M, Okano T (2011) Thermo-responsive polymer brushes as intelligent biointerfaces: preparation via ATRP and characterization. Macromol Biosci 11:400–409
5. Kotsuchibashi Y, Ebara M, Idota N, Narain R, Aoyagi T (2012) A 'smart' approach towards the formation of multifunctional nano-assemblies by simple mixing of block copolymers having a common temperature sensitive segment. Polym Chem 3:1150–1157
6. Kabra Bg, Gehrke Sh (1991) Synthesis of fast response, temperature-sensitive poly(*N*-isopropylacrylamide) gel. Polym Commun 32:322–323
7. Maya S, Sarmento B, Nair A , Rejinold NS, Nair, SV and Jayakumar R (2013) Smart stimuli sensitive nanogels in cancer drug delivery and imaging: a review. Current Pharm Des 19: 7203-7218
8. Matsukuma D, Yamamoto K, Aoyagi T (2006) Stimuli-responsive properties of *N*-isopropylacrylamide-based ultrathin hydrogel films prepared by photo-cross-linking. Langmuir 22:5911–5915
9. Li M, De P, Gondi SR, Sumerlin BS (2008) Responsive polymer-protein bioconjugates prepared by RAFT polymerization and copper-catalyzed azide-alkyne click chemistry. Macromol Rapid Commun 29:1172–1176
10. Ramakrishna S, Fujihara K, Teo W-E, Yong T, Ma Z, Ramaseshan R (2006) Electrospun nanofibers: solving global issues. Mater Today 9:40–50
11. Yarin AL, Kataphinan W, Reneker DH (2005) Branching in electrospinning of nanofibers. J Appl Phys 98:064501
12. Kim YJ, Ebara M, Aoyagi T (2012) A smart nanofiber web that captures and releases cells. Angew Chem Intern Ed 51:10537–10541
13. Kim YJ, Ebara M, Aoyagi T (2012) Temperature-responsive electrospun nanofibers for 'on-off' switchable release of dextran. Sci Technol Adv Mater 13:064203
14. Yocum RH, Nyquist EB(eds) (1973) Functional monomers. Marcel Dekker, New York
15. Krishnan S, Klein A, El-Aasser MS, Sudol ED (2003) Influence of chain transfer agent on the cross-linking of poly(*n*-butyl methaerylate-*co*-N-methylol acrylamide) latex particles and films. Macromolecules 36:3511–3518
16. Sun L, Huang WM, Ding Z, Zhao Y, Wang CC, Purnawali H, Tang C (2012) Stimulus-responsive shape memory materials: a review. Mater Design 33:577–640
17. Tatsumi R (2010) Mechano-biology of skeletal muscle hypertrophy and regeneration: possible mechanism of stretch-induced activation of resident myogenic stem cells. Animal Sci J 81:11–20
18. Ebara M, Uto K, Idota N, Hoffman JM, Aoyagi T (2012) Shape-memory surface with dynamically tunable nano-geometry activated by body heat. Adv Mater 24:273–278
19. Uto K, Yamamoto K, Hirase S, Aoyagi T (2006) Temperature-responsive cross-linked poly(epsilon-caprolactone) membrane that functions near body temperature. J Contr Rel 110:408–413
20. Tam KV, Uto K, Ebara M, Pagliari S, Forte G, Aoyagi T (2012) Mesenchymal stem cell adhesion but not plasticity is affected by high substrate stiffness. Sci Technol Adv Mater 13:064205

Star Polymers as Biofunctional Coatings

Jürgen Groll[1] and Martin Möller[2]
[1]Department for Functional Materials in Medicine and Dentistry, University of Würzburg, Würzburg, Germany
[2]DWI – Leibniz Institute for Interactive Materials and Institute for Technical and Macromolecular Chemistry, RWTH Aachen University, Aachen, Germany

Synonyms

PEG, poly(ethylene glycol); PEO, poly(ethylene oxide)

Definition

Star polymer = polymer with at least three polymer chains originating from a central core.

Introduction

Materials that are intended for interaction with biological systems, either in vitro or in vivo, are usually endowed with bioactive molecules in order to stimulate specific interactions between material and biology. For sensors, a selective

S

interaction with the analyte is desired, while in the case of biomaterials, a preferred adhesion and growth of the target tissue cells or respective influence on the adhesion and differentiation of stem cells is intended. However, despite the functionalization with bioactive molecules, when artificial materials get in contact with complex biological fluids, they are usually rapidly decorated with adsorbing biomolecules, predominantly proteins. These proteins can denature especially on hydrophobic surfaces, which is the initial and decisive step that leads to loss of control on the material-biosystem interface. For sensors this means bad signal-to-noise ratios, poor sensitivity, or even false-positive signals, while for biomaterials this may trigger the immune system and influence wound healing.

Biofunctional coatings are thus of major importance for the performance of biosensors, biomedical devices, cell culture scaffolds, and biomaterials. Especially the combination of overcoming nonspecific protein adsorption while at the same time generating specific biointeraction sites is a key factor and a major challenge for biointerface design. The general strategy to achieve this aim is to introduce a coating layer that prevents protein adsorption either thermodynamically, so that attractive surface interactions are overcompensated by repulsive interactions with the layer, or at least kinetically by creating a free energy barrier of sufficient height that cannot be overcome on relevant time scales [1]. This chapter focuses on general strategies for the covalent grafting of polymer chains to surfaces with a special focus on the effect of macromolecular architecture, especially linear versus star-shaped molecules, on the resulting films. The well-established NCO-sP(EO-stat-PO) system will be taken as example for a star polymer-based coating system to demonstrate advantages and possible strategies for biofunctionalization.

alternatives such as polyoxazolines, polyglycidols, or polybetainic structures have recently shown promising results, the most established and most extensively used polymer as basis for biofunctional coatings is poly(ethylene oxide) (PEO). PEO is hydrophilic and uncharged and has been recognized as particularly efficient for achieving protein-resistant surfaces; moreover, it is approved by the United States Food and Drug Administration (FDA) for application in humans [2]. It is worthwhile mentioning that the mechanism of how PEO acts and why it exhibits extraordinary low protein interaction on surfaces is still not clearly understood. For thicker layers, the entropic penalty for a protein penetrating a hydrated hydrophilic polymer layer which results in the release of numerous water molecules is often taken as simplistic explanation. However, the special conformation of PEO chains in water with the multiple possibilities of hydrogen bridge formation is known to be important, and the fact that self-assembled alkylthiol monolayers with only three ethylene oxide units per alkyl chain at the water interface are sufficient to minimize the interaction with proteins demonstrates that the overall mechanism is complex. Yet, from experimental studies it is clear that the key demand for minimization of unspecific protein adsorption is the generation of a high polymer segment density on the surface [3]. Grafting density and chain length are thus the two essential experimental control parameters by which the degree of protein resistance is governed [4]. It has recently been shown that for molecular weights between 600 and 2,000 g/mol, a grafting density of 0.5 linear OH-terminal PEO chains/nm^2 is the threshold for minimal protein adsorption [5]. As this chapter rather concerns effects of macromolecular architecture than evaluation of different polymer backbones, the following sections will focus on PEO-based polymers.
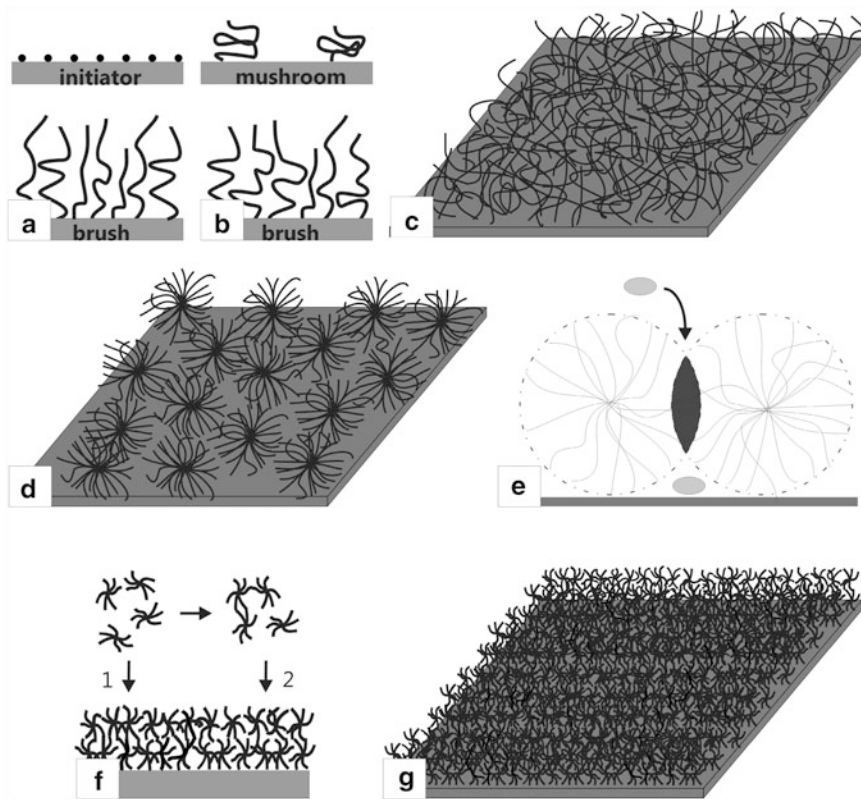
PEO as Basis for Minimal Interaction

A number of different types of (bio-)polymers have been used to render surfaces non-adsorptive for proteins. Although

Strategies for Surface Grafting of Polymers

Different strategies may be pursued to covalently cover a substrate by a layer of polymer

Star Polymers as Biofunctional Coatings, Fig. 1 *Strategies for surface grafting of polymers.* (**a**) "Grafting from" techniques take advantage of the dense grafting that can be achieved by the surface immobilization of low-molecular-weight initiators, followed by polymerization of polymer chains from the surface. (**b**) "Grafting to" techniques with linear chains rely on the grafting of ready polymer chains via one reactive end to a surface. While the variation of molecular weight is bigger, it is harder to achieve a high grafting density that results in a polymer brush. (**c**) The resulting surface coatings are limited to monomolecular layers but may be generated with high polymer segment density. (**d**) Branched structures such as star polymers possess the advantage of a high number of functional groups per molecule. However, a monolayer of high-molecular-weight multi-arm stars results in a dense sphere-like structure with defects and an overall polymer segment density lower than that for linear grafted chains (**e**). (**f**) In contrast, the use of low-molecular-weight star molecules with fewer arms and reactive end groups that allow interpolymeric cross-linking results in a dense polymer network. Cross-linking between the polymers can be performed after coating on the substrate (**f1**) or already be initiated in solution so that oligomers and activated prepolymers are immobilized on the substrate during the coating procedure (**f2**). (**g**) Due to the high number of functional groups and the cross-linking reaction, these films are not limited in thickness to monomolecular layers and possess a high polymer segment density. Moreover, functional groups that cannot take part in network formation due to steric constraints remain in the film and may be used for functionalization

chains (Fig. 1). Immobilization of low-molecular-weight initiators followed by polymerization of polymer chains from the surface ("grafting from") is an elegant way to achieve such films. As the packing density that can be achieved with the initiators is high, the resulting grafting density of the polymer chains is equally high. This method has extensively been used using radical polymerization techniques for PEO-modified (meth-)acrylate monomers [6] but is not directly applicable to PEO. Layer thickness of such coatings is limited due to increasingly hindered monomer diffusion during polymerization in the densely grafted film but can be achieved high enough to obtain coatings with minimal unspecific protein adsorption.

Following an alternative strategy, protein-repellant PEO coatings are frequently prepared by covalently grafting long, randomly coiling, ready linear chains via their terminus to the surface. While this method has the advantage of using ready polymer chains, it is much harder to achieve high grafting densities. Each polymer chain that is anchored on the substrate acts as steric hindrance for subsequent grafting of other chains. As PEO is hydrophilic and highly swollen under normal conditions in water, the steric restriction is significant and results in a surface decoration with PEO chains that are separated from each other and do not fully cover the substrate. The so-called mushroom regime of grafting density is not efficient for reducing the ability of proteins to adsorb. As mentioned above, a high polymer segment density is the key criterion. To achieve this, the grafting density of the polymer chains has to be high, so that the polymer chains cannot fill a maximum volume around the grafting point at the surface but are forced to stretch out perpendicularly to the surface in order to avoid unfavorable monomer-monomer interactions and maintaining optimal salvation. Only in this so-called brush regime the grafted chains provide adequate coverage and thickness to form a very effective steric barrier against protein adsorption. Such layers may be achieved by grafting the POE chains at critical solubility with minimal hydrodynamic radius per chain, for example, by changing the temperature and adding salt [7]. The steric restriction during grafting is minimized under such conditions, and switching back to standard conditions after grafting results in a polymer brush.

Star-Shaped Molecules

Star-shaped PEO molecules (star PEO) have a central core region from which the PEO arms extend. Due to this constraint, their density is higher than that of a linear chain, offering the opportunity to produce PEO surfaces with higher grafting density. Moreover, the ends of the arms are preferentially located near the periphery due

to the steric constraints in the interior of the star. Therefore, the probability is increased for end-functionalized groups to bind to the surface. However, the overall molecular weight of the star molecules, the number of arms, and the chemical reactivity are crucial parameters that determine the effectiveness of resulting coatings to resist the adsorption of proteins. There are studies of star PEO molecules with a rigid poly-divinylbenzene core bearing at least 24 arms and overall molecular weight of at least 230 kDa that have been used for grafting to substrates by covalently attaching the star PEO molecules to the surface without intermolecular cross-linking [8, 9]. These molecules pack closely on the surface and strongly reduce protein adsorption for larger proteins, but the efficiency is lower for small proteins such as cytochrome c. This is explained by the spherical shape of the high-molecular-weight PEO stars with their rigid core that form a packing of spheres on the surface so that gaps remain between the molecules. These areas of little or no polymer coverage appear sufficiently large for small proteins to reach the surface and adsorb to it.

Based on these findings, protein-resistant properties of star PEO coatings may be improved by using smaller molecules with a lower amount of arms and a more flexible core. In addition, functionalization of the star molecules with reactive groups at the distal ends of the arms that enable intermolecular cross-linking will result in a more homogeneous lateral PEO density profile and higher surface coverage. This will also be of advantage for functionalization with molecules that may be introduced through reaction with the end groups. Finally, this approach will not be restricted to monomolecular thin coatings as it will allow a three-dimensional chemical cross-linking of thicker layers.

An Example for Biofunctional Coatings Based on Star-Shaped Molecules

One example that meets these criteria is the NCO-sP(EO-*stat*-PO) coating system that is based on six-arm, star-shaped molecules with

a sorbitol core, a backbone of statistically copolymerized ethylene oxide and propylene oxide in a ratio of 4:1, a molecular mass of 2,000 g/mol per arm and reactive isocyanate end groups [10, 11]. The NCO-sP(EO-*stat*-PO) molecules can be dissolved in water, and coatings can be applied from aqueous solutions. When the NCO-sP(EO-*stat*-PO) material is dissolved in water, hydrolysis of the isocyanate groups at neutral pH leads to formation of amine groups that directly react with unreacted isocyanate groups to form urea bridges between the NCO-sP (EO-*stat*-PO) molecules. Since the kinetics of amine addition to isocyanate is much faster than hydrolysis, urea bridge formation occurs preferentially until steric restrictions significantly lower the reaction probability. The aqueous NCO-sP(EO-*stat*-PO) solution can be used for coating surfaces by either simple dip, spin, or spray coating. After coating, the system requires at least 12 h for completion of the cross-linking reaction within the layer. During this time, all isocyanate groups hydrolyze and then either react with other isocyanate groups to form urea bridges or remain as free amino groups. These layers have proven extremely efficient in minimizing protein adsorption even under single-molecule fluorescence conditions [10]. For reducing cell adhesion under standard cell culture conditions, it has been shown that the possibility to increase layer thickness through adjusted coating conditions and subsequent three-dimensional cross-linking of the layer is important. Only for layers thicker than 10 nm, adhesion of cell lines or primary dermal fibroblasts and mesenchymal stem cells is fully prevented in standard cell culture conditions [11]. Another advantage of the intermolecular cross-linking is the reduced demand on the substrate to achieve homogeneous coatings. While many high-performance surface modifications are limited to ultraflat model surfaces (e.g., self-assembled monolayers), the NCO-sP(EO-stat-PO) system can be applied to large-sized objects and complicated 3D structures. Moreover, a rather low density of functional groups on the substrate for chemical attachment of the layer is needed for good overall film adhesion.

For the preparation of biofunctional coatings, one particular advantage of the NCO-sP (EO-*stat*-PO) system is the change in reactivity from isocyanate groups, which are reactive towards nucleophilic groups such as alcohols, amines, and thiols, to amine groups during the layer preparation and curing of the coating. This enables to use the reactive isocyanate groups for functionalization at two different timepoints, in solution and in freshly prepared coatings. Addition of water-soluble compounds that bear nucleophilic groups to the aqueous NCO-sP (EO-*stat*-PO) solution before coating results in covalent attachment of these molecules to the reactive prepolymers and to covalent embedding of these compounds in the resulting polymer layer (Fig. 2). After complete hydrolysis of the isocyanate groups, these compounds are isotropically distributed in a coating that inhibits nonspecific interactions with proteins and cells, so that the immobilized molecules can interact specifically with their interaction partners, for example, carbohydrates, proteins, or cells. This feature is achieved in a one-step layer preparation without the use of further chemical blocking agents. As one example, when biocytin is introduced into the coatings in this way, surfaces can be produced where biotinylated proteins may be specifically immobilized via streptavidin. Due to the minimal interaction between non-bound proteins and the polymer-covered surface, such coatings may then be used for protein folding and interaction studies down to single-molecule level [12, 13].

NCO-sP(EO-stat-PO) coatings can also be functionalized with lateral control over distribution of the bioactive compounds. This can be achieved by standard patterning methods such as soft lithography (microcontact printing) or automated deposition of small droplets of a solution containing the compound to be immobilized onto freshly prepared coatings that still contain reactive NCO groups. After completed reaction of the NCO groups, the resulting coatings exhibit the same kind of specific interaction between the immobilized compounds as described above, however, with the difference that the bioactive molecules are now anisotropically distributed over the surface according to the
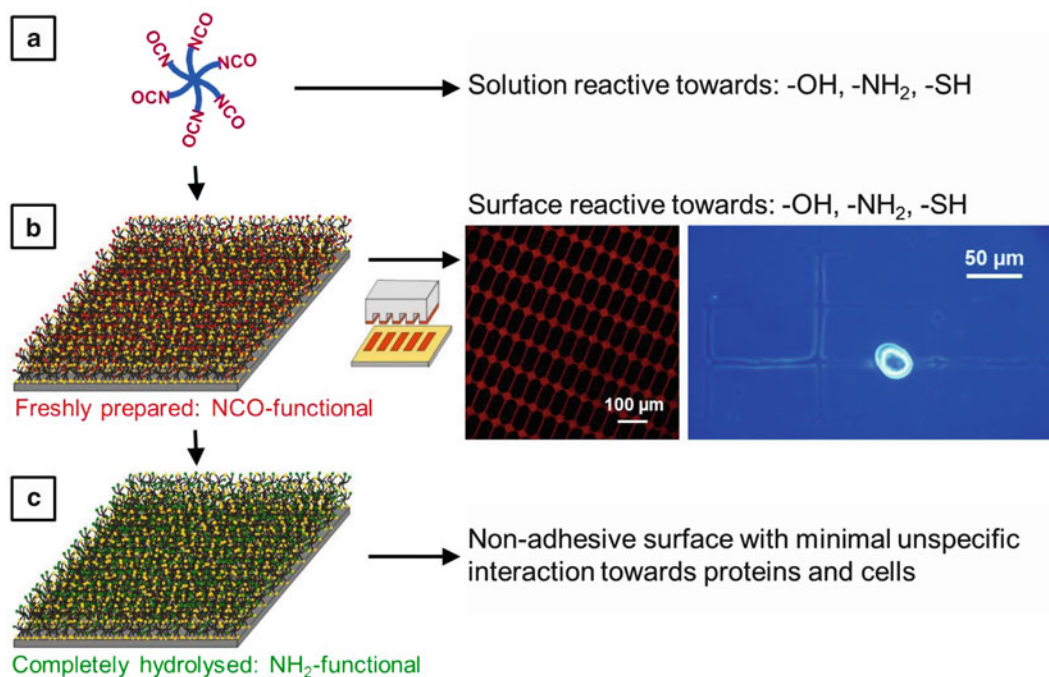
Star Polymers as Biofunctional Coatings, Fig. 2 *NCO-sP(EO-stat-PO) coating and bioactivation possibilities*. (**a**) Molecules to be immobilized in the coating can be added to the NCO-sP(EO-*stat*-PO) solution prior to casting. The NCO groups (*red*) are reactive towards nucleophilic functional groups such as thiols (most rapid reaction), amines (rapid), and also alcohols (moderate reaction kinetics). This one-step strategy towards biofunctional coating results in a random distribution of the molecules in the resulting layer. (**b**) Freshly prepared NCO-sP(EO-stat-PO) coatings retain their reactivity towards nucleophilic groups for several hours, so that patterning strategies like microcontact printing or spotting can be used for bioactivation with control over lateral distribution of the bioactive ligands. The fluorescence microscopy image shows microcontact printed red fluorescence labeled Concanavalin A that was patterned by microcontact printing, and the digital image on the right shows selective adhesion and growth of an insect neuron cell on this patterned surface. This also demonstrates the nonadhesiveness of the unfunctionalized polymer coating in between the Concanavalin A pattern. (**c**) After approximately 8 h, the NCO groups are reacted (through either hydrolysis to amine groups or aminolysis to result in a urea linkage between two star molecules), and a passive and nonadhesive dense polymer layer results that bears free amino groups (*green*) and urea bridges between the stars (*yellow*), respectively

desired pattern. Using microcontact printing, this approach has been used to bind proteins such as fibronectin or also the lectin Concanavalin A, which are specifically recognized by cells on the surface. In the case of Concanavalin A, insect neurons selectively grow along the micropatterns of immobilized proteins, which could be used to generate patterns of functional insect neuronal networks on the surfaces. In the case of fibronectin, different cell types have been used to demonstrate specific recognition of the patterns and geometric control of cell adhesion and migration. Also soft and deformable substrates such as PDMS have been surface modified this way, and myoblast cells were seeded and grown on the substrates. Mechanical stimulation of the substrates could show a dependency on the effect of cellular behavior and differentiation on the orientation of linear deformation towards the line pattern [14]. Automated spotting has been used to

immobilize an array of probe-target pairs of oligonucleotides on the coatings. Due to the minimal interaction with proteins, and since the immobilized oligonucleotides were automatically separated from the surface by a 2 kDa spacer which reduced steric hindrance, taq DNA polymerase could be used for on-chip single-base extension of the surface-bound oligonucleotides. This way, a complete biochip could be developed that enabled the unambiguous identification of single-nucleotide polymorphisms [15].

Conclusions

The discussed model system and the presented application examples demonstrate the advantage of low-molecular-weight, flexible, and multifunctional star-shaped molecules as basis for the generation of biofunctional coatings. Star molecules which are endowed with reactive chemical groups at the distal ends combine high polymer segment density with high chemical functionality, and intermolecular cross-linking has been identified as important advantage over traditional grafting methods regarding versatility of the system and application to a broad range of materials and geometries.

Related Entries

► Dendrimers and Hyperbranched Polymers in Medicine
► Polymer Brushes
► Self-Assembled Monolayer
► Self-Assembly of Hyperbranched Polymers
► Synthesis of Star Polymers

References

1. Halperin A (1999) Polymer brushes that resist adsorption of model proteins: design parameters. Langmuir 15:2525–2533
2. Harris JM, Zalipsky S (eds) (1997) Poly(ethylene glycol): chemistry and biological applications. American Chemical Society, Washington, DC
3. Szleifer I, Carignano MA (2000) Tethered polymer layers: phase transitions and reduction of protein adsorption. Macromol Rapid Commun 21:423–448
4. Malmsten M, Emoto K, Alstine JMV (1998) Effect of chain density on inhibition of protein adsorption by poly(ethylene glycol) based coatings. J Colloid Interface Sci 202:507–517
5. Unsworth LD, Sheardown H, Brash JL (2008) Protein-resistant poly(ethylene oxide)-grafted surfaces: chain density-dependent multiple mechanisms of action. Langmuir 24:1924–1929
6. Barbey R, Lavanant L, Paripovic D, Schüwer N, Sugnaux C, Tugulu S, Klok H-A (2009) Polymer brushes via surface-initiated controlled radical polymerization: synthesis, characterization, properties, and applications. Chem Rev 109(11):5437–5527
7. Kingshott P, Thissen H, Griesser H (2002) Effects of cloud-point grafting, chain length, and density of PEG layers on competitive adsorption of ocular proteins. Biomaterials 23:2043–2056
8. Sofia SJ, Premnath V, Merrill EW (1998) Poly(ethylene oxide) grafted to silicon surfaces: grafting density and protein adsorption. Macromolecules 31:5059–5070
9. Irvine DJ, Mayes AM, Satija KS, Barker GJ, Sofia-Allgor SJ, Griffith LG (1998) Comparison of tethered star and linear poly(ethylene oxide) for control of biomaterials surface properties. Biomed Mater Res 40:498–509
10. Heyes CD, Groll J, Moeller M, Nienhaus GU (2007) Synthesis, patterning and applications of star-shaped poly(ethylene glycol) biofunctionalized surfaces. Mol Biosys 3:419–430
11. Gasteier P, Reska A, Schulte P, Salber J, Offenhaeusser A, Moeller M, Groll J (2007) Surface grafting of PEO-based star-shaped molecules for bioanalytical and biomedical applications. Macromol Biosci 7:1010–1023
12. Groll J, Moeller M (2010) Star polymer surface passivation for single molecule detection. Methods Enzymol 472:1–18
13. Groll J, Moeller M (2013) Surface passivation for single molecule detection. In: Roberts GCK (ed) Encyclopedia of biophysics. Springer, New York, p 2536
14. Ahmed W, Wolfram T, Goldyn A, Bruellhoff K, Rioja BA, Möller M, Spatz JP, Saifa TA, Groll J, Kemkemer R (2010) Myoblast morphology and organization on biochemically micropatterned hydrogel coatings under cyclic mechanical strain. Biomaterials 31(2):250–258
15. Geistlinger J, Du W, Groll J, Liu F, Hoegel J, Foehrl KJ, Pasquarelli A, Schneider M (2012) P2RX7 genotype association in severe sepsis identified by a novel multi-array for rapid screening and replication of risk SNPs. Clin Chim Acta 413(1–2):39–47

S

Star Polymers as Unimolecular Containers

Chuan Wei and Haifeng Gao
Department of Chemistry and Biochemistry,
University of Notre Dame, Notre Dame, IN, USA

Synonyms

Core-shell; Star polymer; Unimolecular container

Definition

Star polymers composed of multiple radiating arms and one central core represent a simple arrangement of linear chains to form polymers with branched architectures. Based on the chemical composition of the arms, star polymers include homoarm star polymers and miktoarm star polymers [1]. The homoarm stars (normal stars, Fig. 1a) have arms with the identical chemical composition and similar molecular weights, while the miktoarm stars (or heteroarm stars, Fig. 1b) contain several arm species with different chemical compositions and/or molecular weights in one star molecule. The number of arms in one star molecule could be controlled during the synthesis and varies from a few to several hundred when small molecules, oligomers, or hyperbranched polymers are used to form the star core.

The core-shell structure and globular shape (Fig. 1c) of star polymers provide a promising nanostructured platform when polymer carriers are required for functions of encapsulation, protection, and controlled release. Since all linear chains and central branched core are covalently connected, instead of physically assembled, star polymers are a type of unimolecular containers that benefit high stability under harsh and dilution conditions. Furthermore, the hierarchical structure of star polymers allows selective functionalization of different segments, e.g., core, shell, and arm-end periphery, in the star molecules,
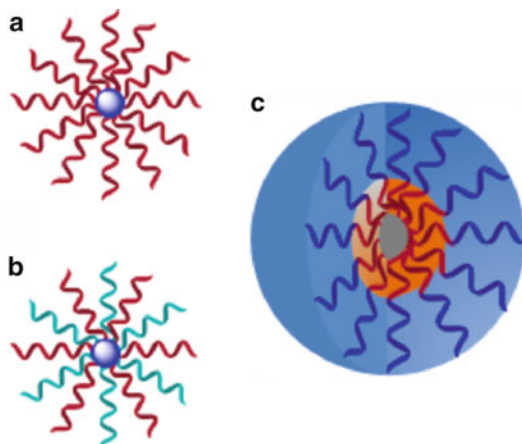
Star Polymers as Unimolecular Containers, Fig. 1 Illustration of (**a**) homoarm star polymer, (**b**) miktoarm star polymer, and (**c**) the feature of core-shell structure in a star molecule for potential applications

which is important for potential applications in catalysis, diagnostic, and therapeutic delivery.

Synthesis

Star polymers are commonly synthesized using living/controlled polymerization techniques, such as anionic, cationic, and radical polymerizations [2]. The success of star polymer synthesis, characterized by the star yield and star uniformity (molecular weight distribution), is significantly determined by the degree of the preserved chain-end functionality in the linear arm precursors. So far, living anionic polymerizations, living cationic polymerizations, and controlled radical polymerizations, further including atom transfer radical polymerization (ATRP), nitroxide-mediated polymerization (NMP), and reversible addition fragmentation chain transfer (RAFT) polymerization, are among the most popular techniques for synthesis of various types of arm precursors and star polymers. All these techniques have the features of fast initiation and limited chain breaking reactions (e.g., chain transfer and termination reactions), which produce linear chains with the best preservation of chain-end groups and star polymers with well-controlled molecular structure.

Star Polymers as Unimolecular Containers, Fig. 2 Three routes for synthesis of star polymers: (**a**) "core-first," (**b**) "coupling-onto," and (**c**) "arm-first" methods
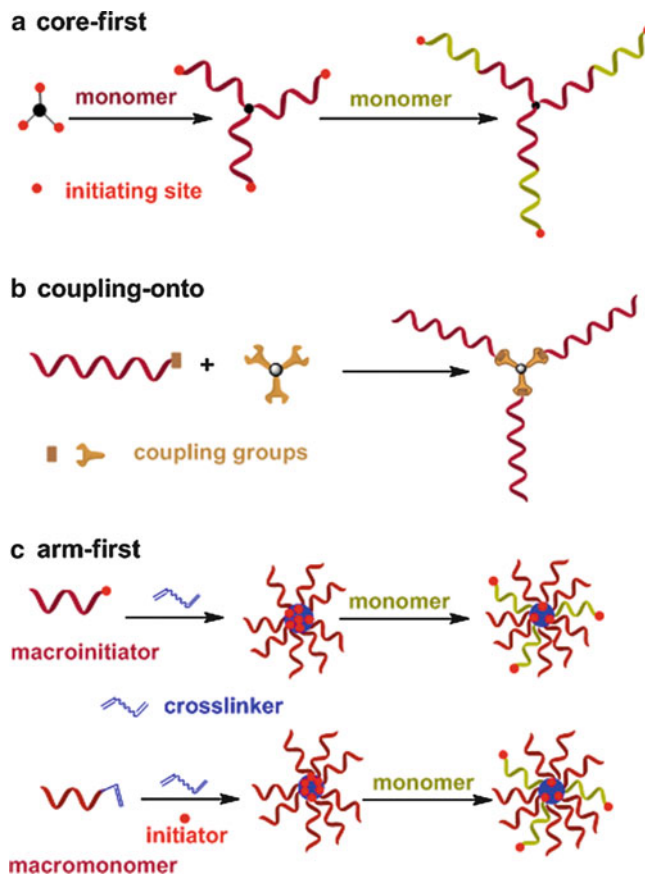
Depending on the formation sequence of arms and cores, star polymers can be synthesized using one of three strategies: "core-first," "coupling-onto," and "arm-first" (Fig. 2). The "core-first" method involves the use of a multifunctional initiator (core) that can be small molecule, oligomer, and hyperbranched polymer (Fig. 2a). The polymerization of monomer from the initiating sites on the core generates a star molecule with preserved initiating site at the chain end of each arm, which can be further used for chain extension when polymerizing a second monomer to form star block copolymer. Due to the use of multifunctional initiators, a potential concern in the "core-first" method is the chain-end termination reactions which become particularly significant in radical-based polymerizations. The undesired radical-radical coupling reactions between two star molecules could produce

coupled product and broaden the molecular weight distribution of the final product.

In the "coupling-onto" method (Fig. 2b), a star polymer is synthesized by coupling linear polymeric chains (arms) containing a reactive chain-end group with a multifunctional agent (core). Due to the slow reaction between the polymer chain ends and the multifunctional core, an organic reaction with high coupling efficiency and benign experimental condition is highly recommended. For example, several types of highly efficient "click reactions" [3] are recently developed for synthesis of various kinds of star and miktoarm star polymers with predetermined structure and high star yield.

In the "arm-first" method (Fig. 2c), the linear arms of the star polymers are synthesized first, followed by binding of the arms to form the core, usually using a divinyl cross-linker. The resulting

star polymers have a statistical distribution of the number of arms and a highly cross-linked core. The preformed arms can be either linear macroinitiator or macromonomer, and the star formation can occur either in a homogeneous solution or in a heterogeneous micelle system. The preserved initiating sites in the star cores can be further employed to initiate the polymerization of another monomer and form miktoarm star copolymers. The versatile feature of the "arm-first" method allows the cross-linking reaction of a mixture of different macroinitiators and macromonomers as arm precursors, thus producing miktoarm star polymers in one pot.

Application of Star Polymers as Unimolecular Containers

Star polymers with three-dimensional shape and core-shell structure represent a promising nanoobject that can be used as discrete carriers for cargo molecules or as template reactors for synthesis of hybrid materials [4]. The core domain surrounded by the dangling arms can have tunable size and chemical compositions, which create potentials to apply star polymers in drug delivery, [5] catalysis, [6] and templates for inorganic nanoparticles.

Star Polymer as Catalyst Carrier

Star polymer catalysts in well-defined nanostructures could solve the intrinsic problems in the traditional homogeneous and heterogeneous catalysts. The macromolecular nature of the star polymer allows efficient separation and recovery of catalyst from small molecular substrates and products. At the same time, the nanoscaled dimension of a star molecule has specific surface area (m^2/g) thousands of times larger than that of a micrometer-sized polymer bead, which minimizes the diffusion barrier of small molecules in and out of the star polymer support. Compared to linear polymers, star-shaped polymers benefit from their core-shell structure and multiple chain-end groups. These features not
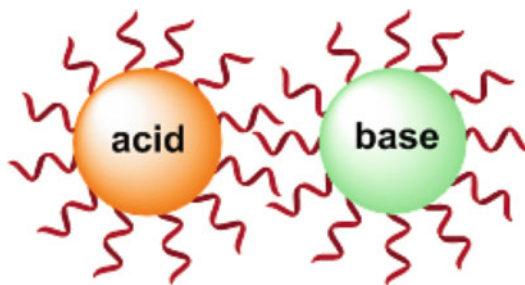
Star Polymers as Unimolecular Containers, Fig. 3 Cascade reaction by star polymer catalyst

only provide the possibility to increase catalyst loading but also create a different microenvironment in the core from the dispersing medium.

Sawamoto et al. reported direct encapsulation of ruthenium (Ru) catalysts into star polymers in the "arm-first" star synthesis. The catalysts that were functioning for polymerization could be encapsulated into the star core when ligand-functionalized monomers were used during the core formation step [7]. Star polymers with encapsulated Ru catalysts showed comparable catalysis efficiency as small molecule catalyst in oxidation of alcohol to ketone. The inner metal catalyst can also be exchanged to other metals via a replacement reaction [8]. Fréchet group applied the feature of site isolation of star polymers to demonstrate the coexistence of incompatible catalysts in one reactor by finishing a cascade reaction. The core-shell structure of star polymers served as a scaffold that can effectively isolate functional catalysts in the core domain. For instance, acid and base catalysts covalently grafted into the core domains of different star polymers could coexist in the medium due to the steric shielding from the surrounding arms (Fig. 3) [9].

Star Polymer for Drug Delivery

Since the concept of using functional polymers for drug delivery was reported in the 1980s, [10] a variety of synthetic polymers have been explored for controlled delivery of therapeutic and diagnostic drug molecules. Compared to the widely explored micelle systems, amphiphilic

PEG arms

Tumor targeting ligands

Conjugated drug
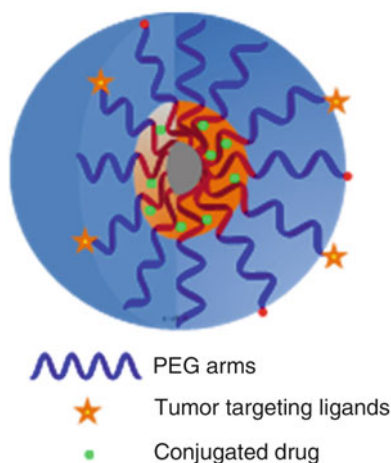
Star Polymers as Unimolecular Containers, Fig. 4 Functional star polymers as drug carriers

star polymers with hydrophilic arms and hydrophobic core enjoy higher stability under dilution and shearing conditions due to the covalent structure (Fig. 4). The outer shell arms could be neutral polymers or polyelectrolytes. So far, polyethylene glycol (PEG) and derivatives are extensively used as the hydrophilic arms because PEG is FDA approved and satisfies the basic requirements of biocompatibility and low toxicity for synthetic biomaterials. Additional advantages of PEG polymers include its capability to interfere with opsonin proteins in bloodstream, which slows the recognition of polymer conjugates by the macrophages of the mononuclear phagocyte system [11]. Model drugs, such as the toxic hydrophobic cancer drugs, can be encapsulated in the highly branched cores by either physical or chemical bonds.

Star polymers, usually having higher molecular weight than the linear polymers, can circulate in the bloodstream longer and be selectively captured into tumor tissues due to the enhanced permeation and retention (EPR) effect [12]. On the other hand, degradability of the polymer carriers in physiological conditions should also be considered to avoid the permanent accumulation of polymers in the body. For this purpose, functional groups, e.g., disulfide, acetal, and ketal groups, are often used during the core construction to introduce the feature of

degradability into the polymer carriers [13]. The degradation of star polymers produces low molecular weight oligomers and small molecules, which can be easily removed from the body through kidney and urines. For example, Boyer and coworkers reported uniform star polymers with functional PEG as shell using arm-first method [14]. The presence of functional aldehyde groups in the core was designed as acid labile linkers for anticancer drug conjugation. In vivo release experiment showed clearly pH responsive behavior without burst release.

Star Polymer as Nanoparticle Template

Metal nanoparticles, such as Au, Ag, and Pt, represent important inorganic nanomaterials due to their intriguing optical, electronic, and catalytic properties. Many physical and chemical methods have been developed for the preparation of various metal nanoparticles with different sizes, shapes, and morphologies [15]. Among these methods, template-directed synthesis received broad attention, which refers to the use of a prefabricated nanostructured object to influence the placement of building blocks (e.g., atomic or molecular species) during the growth of inorganic materials. To use the core-shell-structured star polymers as templates, a designing principle is that the metal ion precursors should only complex with the inner blocks of the star copolymers, which confine the formation of nanoparticles within the star interior when reducing agents are added (Fig. 5). Due to the hydrophilic nature of the metal precursor ions, all of the star block copolymers have a hydrophilic inner domain and hydrophobic outer block. Thus, the star copolymers are dissolved in nonpolar solvent mimic inverse micelles [16–18]. The inner block polymer could contain pyridine groups and ethylene oxide groups, which interact with anionic precursors, such as $AuCl_4^-$. Alternatively, it could also be carboxylic acid groups and ethylene oxide groups, which are able to complex with cationic precursors, such as Ag^+, Pd^{2+}, and Pt^{4+}. After

S
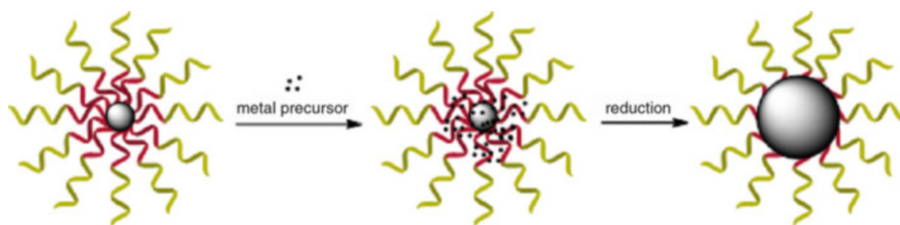
Star Polymers as Unimolecular Containers, Fig. 5 Star polymers as nanoparticle template

reduction, the stability of formed inorganic nanoparticles is expected to be dependent on the length of outer shell blocks.

Summary

Star polymers containing a central core and multiple radiating arms represent an intriguing unimolecular platform as nanocontainers in applications of drug delivery, catalysis, and templates for hybrid nanomaterials. In the synthesis of star polymers, it is a key step to accurately control the size and composition distribution in each segment, which is becoming a rapidly growing research area, encompassing knowledge from the disciplines of polymer chemistry, physical chemistry, and materials science. Future development of star polymers needs new synthetic methodologies that can accurately incorporate multiple functional groups into different domains of a star molecule without losing the feature of facile synthesis. It is believed that the development in synthetic technology, as well as the advancing knowledge on the controlled polymerization techniques, is going to lay the foundation for building star polymers with more sophisticated structures and broader applications.

Related Entries

▶ Dendrimer-Like Star Branched Polymers
▶ Dendrimers and Hyperbranched Polymers in Medicine
▶ Drug and Gene Delivery using Hyperbranched Polymers
▶ Synthesis of Hyperbranched Polymers
▶ Synthesis of Star Polymers

References

1. Hadjichristidis N, Pitsikalis M, Pispas S, Iatrou H (2001) Polymers with complex architecture by living anionic polymerization. Chem Rev 101:3747–3792
2. Gao H, Matyjaszewski K (2009) Synthesis of functional polymers with controlled architecture by CRP of monomers in the presence of cross-linkers: from stars to gels. Prog Polym Sci 34:317–350
3. Binder WH, Sachsenhofer R (2007) "Click" chemistry in polymer and materials science. Macromol Rapid Commun 28:15–54
4. Gao H (2012) Development of star polymers as unimolecular containers for nanomaterials. Macromol Rapid Commun 33:722–734
5. Kreutzer G, Ternat C, Nguyen TQ, Plummer CJG, Mnson J-AE, Castelletto V, Hamley IW, Sun F, Sheiko SS, Herrmann A, Ouali L, Sommer H, Fieber W, Velazco MI, Klok H-A (2006) Water-soluble, unimolecular containers based on amphiphilic multiarm star block copolymers. Macromolecules 39:4507–4516
6. Ouchi M, Terashima T, Sawamoto M (2008) Precision control of radical polymerization via transition metal catalysis: from dormant species to designed catalysts for precision functional polymers. Acc Chem Res 41:1120–1132
7. Terashima T, Kamigaito M, Baek K-Y, Ando T, Sawamoto M (2003) Polymer catalysts from polymerization catalysts: direct encapsulation of metal catalyst into star polymer core during metal-catalyzed living radical polymerization. J Am Chem Soc 125:5288–5289
8. Terashima T, Nomura A, Ito M, Ouchi M, Sawamoto M (2011) Star-polymer-catalyzed living radical polymerization: microgel-core reaction vessel by tandem catalyst interchange. Angew Chem Int Ed 50:7892
9. Helms B, Guillaudeu SJ, Xie Y, McMurdo M, Hawker CJ, Fréchet JMJ (2005) One-pot reaction cascades using star polymers with core-confined catalysts. Angew Chem Int Ed 44:6384–6387
10. Duncan R, Kopecek J (1984) Soluble synthetic polymers as potential drug carriers. Adv Polym Sci 57:51–101

11. Moghimi SM, Hunter AC, Murray JC (2001) Long-circulating and target-specific nanoparticles: theory to practice. Pharmacol Rev 53:283–318

12. Fox ME, Szoka FC, Fréchet JMJ (2009) Soluble polymer carriers for the treatment of cancer: the importance of molecular architecture. Acc Chem Res 42:1141–1151

13. Syrett JA, Haddleton DM, Whittaker MR, Davis TP, Boyer C (2011) Functional, star polymeric molecular carriers, built from biodegradable microgel/nanogel cores. Chem Commun 47:1449–1451

14. Liu J, Duong H, Whittaker MR, Davis TP, Boyer C (2012) Synthesis of functional core, star polymers via raft polymerization for drug delivery applications. Macromol Rapid Commun 33:760–766

15. Rozenberg BA, Tenne R (2008) Polymer-assisted fabrication of nanoparticles and nanocomposites. Prog Polym Sci 33:40–112

16. Youk JH, Park M-K, Locklin J, Advincula R, Yang J, Mays J (2002) Preparation of aggregation stable gold nanoparticles using star-block copolymers. Langmuir 18:2455–2458

17. Filali M, Meier MAR, Schubert US, Gohy J-F (2005) Star-block copolymers as templates for the preparation of stable gold nanoparticles. Langmuir 21:7995–8000

18. Xu H, Xu J, Zhu Z, Liu H, Liu S (2006) In-situ formation of silver nanoparticles with tunable spatial distribution at the poly(N-isopropylacrylamide) corona of unimolecular micelles. Macromolecules 39:8451–8455

Starch and Dextran

Shinichi Kitamura and Shiho Suzuki
Graduate School of Life and Environmental
Sciences, Osaka Prefecture University, Sakai,
Osaka, Japan

Synonyms

(1 → 4)-α-D-glucan; α-(1 → 6)-branched (1 → 4)-α-D-glucan; Amylopectin; Amylose; Branched (1 → 6)-α-D-glucan

Definition

Starch is made up of granules consisting of two carbohydrate polymers, amylose and amylopectin, which are synthesized in plants. Dextran is branched (1 → 6)-α-D-glucan produced by bacteria. We focus on these two polysaccharides and especially how we can use them as nanomaterials by reviewing recent related papers.
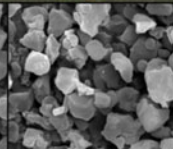
Starch
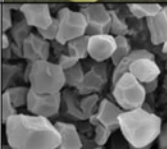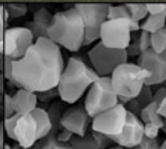
Starch, one of the most abundant bio-polymeric materials, occurs in the form of water-insoluble particles (starch granules) in the seeds, tubers, and other parts of plants. It consists mainly of two chemically distinguishable polysaccharides: amylose, an essentially linear (1 → 4)-α-D-glucan, and amylopectin, a branched glucan that contains largely α-(1 → 4) linkages but with branched glucans attached by α-(1 → 6) linkages. However, starches from waxy varieties of maize, potato, and rice contain virtually no amylose. In contrast, certain varieties of hybrid corn, such as amylomaize, have starch with more than 75 % amylose. Over the past two decades, attempts have been made to alter the ratio of amylose and amylopectin in starch by genetic modification [1]. For example, Schwall reported that the simultaneous inhibition of two isoforms of starch branching enzyme results in very high amylose potato starch containing insignificant levels of highly branched amylopectin [2].
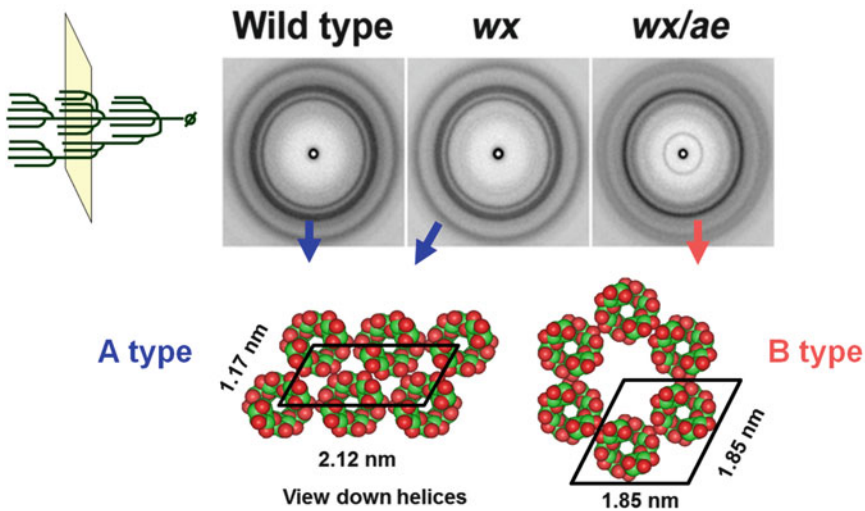
The ratio of amylose to amylopectin and the unit chain length of amylopectin have a great influence on the physical properties of starch and its film, gels, and solutions. Kubo et al. showed that the starch from double mutant rice contains only amylopectin with relatively longer unit chains, resulting in large changes in its physicochemical properties [3]. Figure 1 shows physical properties and digestibility of starch granules isolated from wild-type, *wx*, and *wx*/*ae* rice. X-ray diffraction and molecular models for each starch are shown in Fig. 2.

It is sometime advantageous to use "designed starch" polysaccharides that can be synthesized using enzyme reactions. Studies of such polysaccharides, especially synthetic amylose, will also be covered in this article [4].

Starch has wide application, including uses in food, paper, packaging, textile chemicals, and the

S

Starch and Dextran, Fig. 1 Physical properties and digestibility of starch granules isolated from wild-type (WT), *wx*, and *wx*/*ae* rice

	WT	wx	wx/ae
Rice grain			
Starch granule morphology (SEM image)			
Grain size	5.37 mm	4.68 mm	3.96 mm
Starch granule size	5 µm (3-7 µm)	5 µm (3-7 µm)	4 µm (1-7 µm)
Crystal structure	A type	A type	B type
Gelatinization temperature	65.8°C	68.0°C	82.9°C
Digestibility	High	High	Low (40%)

Starch and Dextran, Fig. 2 X-ray diffraction and molecular models for each starch isolated from wild-type, *wx*, and *wx*/*ae* rice. Amylopectin double-helical chains can either form the denser *A-type* crystallites, with staggered monoclinic packing, or the more open hydrated *B-type* hexagonal crystallites, dependent on the plant source of the granules. The water molecules are not shown in the molecular models

pharmaceutical industries. New industrial uses of starch, particularly in relation to nanotechnology, make it a renewable source of increasing significance [5].

Crystalline Particle Formation from Solution

Low-molecular weight amylose can be recrystallized into A and B crystalline particles in aqueous solution. Long chains and low recrystallization temperatures induce B-type crystalline form, while high concentrations, high temperatures, and short chains induce A-type crystallization. Most recently, Montesanti successfully prepared A-type amylose single crystals using enzymatically synthesized amylose with DP from 17 to 20 [6]. The retrograded higher DP amyloses consist of particles with a surprising uniformity in size, with the volume of each
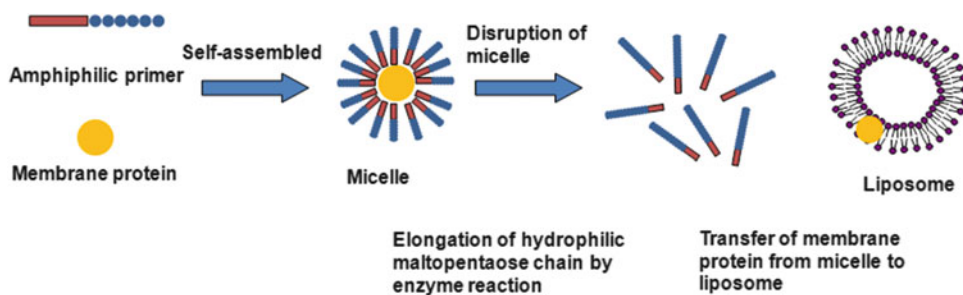
Starch and Dextran, Fig. 3 Schematic presentation of the transfer of membrane protein from micelle to liposome

particle increasing proportionally with the degree of retrogradation, because the formation of amylose particles proceeds via a nucleation process which is complete within a short time after the onset of retrogradation. X-ray diffraction patterns of these amylose particles show only an amorphous halo with weak B crystalline peaks [4].

Gel Formation

Amylose gels are three-dimensional hydrophilic networks formed either by a junction zone of double helices (physical gel) or by covalent bond cross-links (chemical gel) where water molecules are trapped and immobilized. When an aqueous suspension of starch granules is heated above a certain temperature, the granules irreversibly swell and the amylose fraction leaches out to some extent. Upon cooling, the amylose in solution undergoes a process called retrogradation. If the concentration is high enough, this process results in the formation of a network which renders the solution into a gel. Starch gel conforms to the filler-in-matrix model, where the filler is swelled starch granules and the matrix is the leached starch component from starch granules [7]. The matrix is predominantly composed of amylose.

The properties of starch gel are mainly determined by plant sources, but they can be changed to a significant extent by small modifications of the starch. Limited hydrolysis of insoluble cassava starch granules results in enhanced gelling properties. These enhanced gelling properties are due to altered composition of the leached material (matrix) from swelled starch granules (filler). In other words, nanoscale junction structure

appears faster in treated-starch gel than in native starch gel, as revealed by SAXS [8].

While physical starch gels change their physical properties with age, chemically linked starch gels are stable and thus have more potential for biomedical applications, especially drug delivery systems (DDS). pH-sensitive hydrogels and aerogels made from cross-linked starches have already been proposed for use in DDS [9, 10].

Akiyoshi et al. developed an amylose based nano-gel. The self-assembly of amphiphilic methoxy poly(ethylene oxide)-block-amylose forms a complex with both iodine in water and methyl orange in chloroform [11]. An enzyme-responsive molecular assembly system with amylose-primer surfactants has been developed [12]. The association of amylose-primer surfactants is controlled by changing the amphiphilicity with a chain-elongation reaction triggered by the addition of phosphorylase. Figure 3 shows a schematic presentation of the transfer of membrane protein from micelle to liposome.

Phenylcarbamate derivatives of amylose immobilized onto silica gel are used as chiral stationary phases for high-performance liquid chromatography. Most recently, Arakawa et al. [13] showed that both dimensions and intrinsic viscosities of amylose tris(n-butyl carbamate) in D-ethyl lactate are appreciably larger than in L-ethyl lactate. The content of intramolecular hydrogen bonding C=O groups in D-ethyl lactate is about 15 % more than that in L-ethyl lactate, as estimated by isothermal titration calorimetry. This shows how amylose derivatives can interact with chiral compounds at the molecular level.

Starch and Dextran,
Fig. 4 Molecular model of
the complex of iodine with
amylose
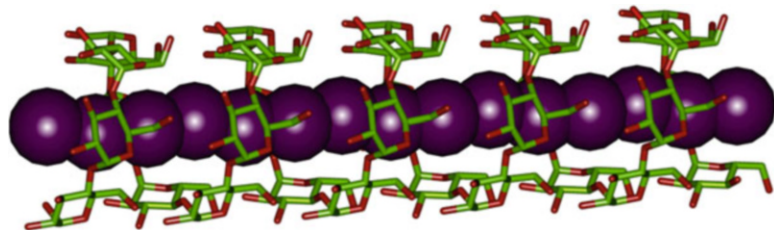
Functional Films

The mechanical properties of film made from
amylose are much better than those of film
made from amylopectin. Adding small amounts
of chitin (less than 10 %) to synthetic amylose
film increases the permeability of gases and
improves its mechanical properties. In addition,
this blended amylose film shows strong
antibacterial action, suggesting a morphological
change in the chitin molecules on the film
surface [14]. It is well known that amylose
forms complexes with iodine, butanol, and other
organic reagents. Figure 4 shows a molecular
model of the complex of iodine with amylose.
Molecular hyperpolarizability is enhanced by
forming a supramolecular amylose–dye inclusion
complex. Polarized amylose film can be made by
extending transparent synthetic amylose film that
has been doped with iodine vapor molecules.

Starch-Based Nanocomposites

Nanocomposites can be classified into two types
according to filler material shape: elongated
particles and layered materials. Good examples
of elongated particles are cellulose nanofibrils
and carbon nanotubes. Layered polymer
nanocomposites are classified into three types:
intercalated, exfoliated, and phase-separated.
These three types of nanocomposites are
constructed from starch polymers and clays
[4, 15, 16].

Dextrans

Dextran is an extracellular bacterial polysaccha-
ride composed of glucose residues mainly linked
by α-(1 → 6)-linkages, with 5–35 % of the glu-
cose units in the polymer branched at the O-3,

O-2 and/or O-4 atoms of the backbone depending
on the bacterial strain. The most well-known
dextran is produced by *Leuconostoc
mesenteroides* NRRL B-512 and has 5 % of its
branch linkages at O-3. Its molecular chain has a
few very long branches, distributed randomly in
the molecule. This branching structure is of great
importance in determining its solution properties.
Kuge et al. has shown that the long branch con-
tent increases with increasing molecular
weight [17].

Most recently, Suzuki et al. showed that the
Mark-Houwink-Sukurada equation for linear
dextran, $[\eta] = 1.39 \times 10^{-2} M^{0.78}$, holds, where
$[\eta]$ is the intrinsic viscosity and M is the molec-
ular weight. The exponent of M, 0.78, suggests
that the chain behaves like a random coil in rich
solvent with large conformational freedom.
The flexibility of dextran is due mainly to its
α-(1 → 6) glycosidic linkages which contain
three bonds (C-5′, C-6′, O, C-1) between each
pair of glucose residues (see Fig. 5). Dextrans
have high water solubility and the solutions
behave as Newtonian fluids [18].

Clinical grades of dextrans with a molecular
weight range of $75–100 \times 10^3$ have been used as
plasma volume expanders. They work by restor-
ing blood plasma lost through severe bleeding.
Aqueous two-phase systems of dextran and poly-
ethylene glycol have been used for the separation
of cell components. Fluorescein conjugates of
dextran are used as a fluorescent probe to study
cell processes such as cell permeability, phago-
cytosis, and endocytosis. Chemically cross-
linked dextran beads are widely used for gel
chromatography in biochemical research and
industry.

More recently, dextran derivatives have been
synthesized for nanotechnology and medical

Starch and Dextran,
Fig. 5 Disaccharide unit
for dextran main chain
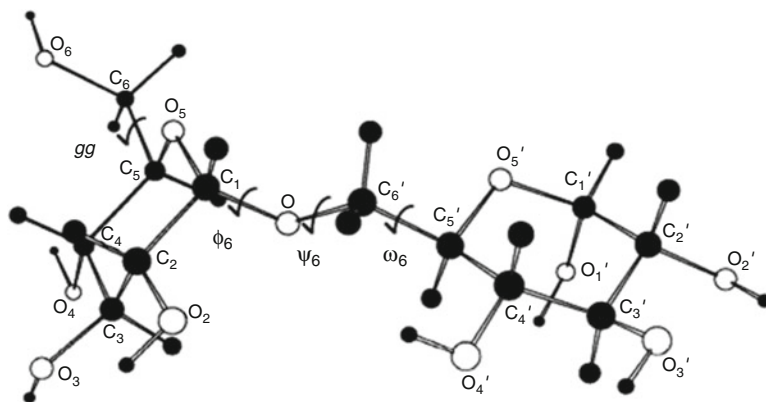
applications. For example, two oppositely charged dextran derivatives incorporating 2-bromoethylamine and chloroacetic acid self-assemble into microsize tubes. These tubular self-assemblies are sensitive to both pH and salt concentrations [19]. Microscopic observations confirm that the tubes have hollow structures up 100 μm long with a diameter between 600 nm and 2 μm. Dextran hydrogels are soft and pliable, offering opportunities for medical applications. Sun et al. [20] showed that dextran hydrogel scaffolds enhance angiogenic response and promote complete skin regeneration during burn wound healing. This line of work is promising for medical applications of dextran.

In conclusion, we emphasize that starch and dextran are composed of the same monomer unit, glucose, but have different glycosidic bonds. This difference leads to different physical and functional properties and key functions, notably their ability to increase viscosity and form gels and films. Their versatile derivatization can be performed though OH groups in the glucose unit. These physical and chemical properties can be readily exploited in a broad range of industrial applications. With increasing knowledge of enzymes and genetic engineering, new related materials are emerging and will be used for tailor-made "polymeric nanomaterials." Among them, cyclic amylose and dextran synthesized by enzymatic reactions are of interest, although we do not touch upon that in this article.

Related Entries

▶ Biodegradable Materials
▶ Cellulose
▶ Chitin and Chitosan
▶ Pullulan

References

1. Keeling PL (1997) Plant biotechnology: technical barriers to starch improvement. In: Frazier PJ, Donald AM, Richmond P (eds) Starch. Structure and functionality. The Royal Society of Chemistry, Cambridge
2. Schwall GP, Safford R, Westcott RJ, Jeffcoat R, Tayal A, Shi YC, Gidley MJ, Jobling SA (2000) Production of very-high-amylose potato starch by inhibition of SBE A and B. Nat Biotechnol 18:551–554
3. Kubo A, Akdogan G, Nakaya M, Shojo A, Suzuki S, Satoh H, Kitamura S (2010) Structure, physical, and digestive properties of starch from *wx ae* double-mutant rice. J Agric Food Chem 58:4463–4469. doi:10.1021/Jf904074k
4. Kitamura S (1996) Starch polymers, natural and synthetic. In: Salamone JC (ed) Polymeric materials encyclopedia. CRC Press, Boca Raton
5. Medeiros ES, Dufresne A, Orts WJ (2010) Starch-based nanocomposites. In: Bertolini AC (ed) Starches. Characterization, properties, and applications. CRC press, Boca Raton
6. Montesanti N, Veronese G, Buleon A, Escalier PC, Kitamura S, Putaux JL (2010) A-Type crystals from dilute solutions of short amylose chains. Biomacromolecules 11:3049–3058. doi:10.1021/Bm1008712
7. Goesaert H, Brijs K, Veraverbeke WS, Courtin CM, Gebruers K, Delcour JA (2005) Wheat flour constituents: how they impact bread quality, and how to impact their functionality. Trends Food Sci Technol 16:12–30. doi:10.1016/j.tifs.2004.02.011

S

8. Ichihara T, Fukuda J, Takaha T, Yuguchi Y, Kitamura S (2014) Limited hydrolysis of insoluble cassava starch granules results in enhanced gelling properties. J Appl Glycosci 61:15–20

9. Kennedy JF, Knill CJ, Liu L, Panesar PS (2011) Starch and its derived products: biotechnological and bio-medical applications. In: Williams PA (ed) Renewable resources for functional polymers and biomaterials. RSC Publishing, Cambridge

10. Mehling T, Smirnova I, Guenther U, Neubert RHH (2009) Polysaccharide-based aerogels as drug carriers. J Non-Cryst Solids 355:2472–2479. doi:10.1016/j.jnoncrysol.2009.08.038

11. Akiyoshi K, Kohara M, Ito K, Kitamura S, Sunamoto J (1999) Enzymatic synthesis and characterization of amphiphilic block copolymers of poly(ethylene oxide) and amylose. Macromol Rapid Commun 20:112–115. doi:10.1002/(Sici)1521-3927(19990301)20:3<112::Aid-Marc112>3.0.Co;2-Q

12. Morimoto N, Ogino N, Narita T, Kitamura S, Akiyoshi K (2007) Enzyme-responsive molecular assembly system with amylose-primer surfactants. J Am Chem Soc 129:458–459. doi:10.1021/ja065966a

13. Arakawa S, Terao K, Kitamura S, Sato T (2012) Conformational change of an amylose derivative in chiral solvents: amylose tris(n-butylcarbamate) in ethyl lactates. Polym Chem 3:472–478

14. Suzuki S, Shimahashi K, Takahara J, Sunako M, Takaha T, Ogawa K, Kitamura S (2005) Effect of addition of water-soluble chitin on amylose film. Biomacromolecules 6:3238–3242. doi:10.1021/Bm050486h

15. Kvien I, Sugiyama J, Votrubec M, Oksman K (2007) Characterization of starch based nanocomposites. J Mater Sci 42:8163–8171. doi:10.1007/s10853-007-1699-2

16. McGlashan SA, Halley PJ (2003) Preparation and characterisation of biodegradable starch-based nanocomposite materials. Polym Int 52:1767–1773. doi:10.1002/Pi.1287

17. Kuge T, Kobayashi K, Kitamura S, Tanahashi H (1987) Gpc analyses of polysaccharides 2. Degrees of long-chain branching in dextrans. Carbohydr Res 160:205–214. doi:10.1016/0008-6215(87)80312-9

18. Suzuki S, Yukiyama T, Ishikawa A, Yuguchi Y, Funane K, Kitamura S (2014) Conformation and physical properties of cycloisomaltooligosaccharides in aqueous solution. Carbohydr Polym 99:432–437. doi:10.1016/j.carbpol.2013.07.089

19. Sun GM, Chu CC (2009) Self-Assembly of chemically engineered hydrophilic dextran into microscopic tubules. ACS Nano 3:1176–1182

20. Sun GM, Zhang XJ, Shen YI, Sebastian R, Dickinson LE, Fox-Talbot K, Reinblatt M, Steenbergen C et al (2011) Dextran hydrogel scaffolds enhance angiogenic responses and promote complete skin regeneration during burn wound healing. Proc Natl Acad Sci U S A 108:20976–20981. doi:10.1073/pnas.1115973108

Statistical Thermodynamics of Polymeric Networks

V. G. Rostiashvili and T. A. Vilgis
Polymer Theory Group, Max Planck Institute for Polymer Research, Mainz, Germany

Synonyms

Chemical and physical gels; Entanglements; Material failure; Nano-self-assembly; Supramolecular networks

Definition

The statistical thermodynamics of polymer networks with permanent cross-links (chemical gels) as well as with links that have a finite lifetime (physical gels) is briefly outlined. The theory of chemical gels is usually based on the so-called replica trick which enables to average the free energy functional over the frozen cross-link distribution. The physical gel paradigm goes actually beyond the polymeric networks and embraces the patchy colloids and nano-self-assembly. We discuss the phase diagram of such systems as well as the dynamical scattering function which shows a generic two-step decay behavior. Finally, we address shortly the deformation and failure of physical gels.

Introduction

The statistical thermodynamics of heterogeneous networks is a long-standing problem in the context of polymer chemical physics. Considerations were based typically on the calculation of the appropriate partition function (as is customary in statistical mechanics!) with permanent, randomly distributed cross-links which give rise to the inherent inhomogeneity in the network. To treat such permanent (or "frozen") disorder in the system, one needs a special technique which is
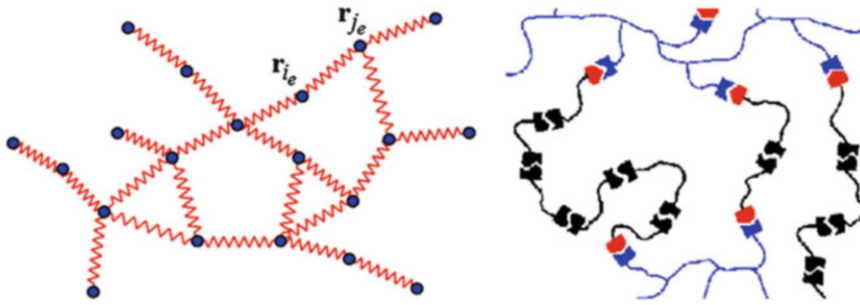
Statistical Thermodynamics of Polymeric Networks, Fig. 1 Schematic representation of a chemical gel with permanent bonds between monomers (*left panel*) and a physical gel where bonds are characterized by a finite lifetime so that cluster motion is accompanied by polymer rearrangements (*right panel*)

Chemical Gels

The Standard Edwards Formulation: Non-Gibbsian Statistical Physics

The standard rubber model was introduced by Edwards in the context of quenched disorder [1, 16] formed by the fixed cross-links, which introduce a non-Gibbsian statistical physics. The partition function of a given (quenched) cross-link configuration of the chain is given by

$$Z(\mathbf{C}) = \int_V D\mathbf{R}\, e^{-\beta(H_W + H_I)} \prod_{e=1}^{M} \delta\big(\mathbf{R}_{i_e} - \mathbf{R}_{j_e}\big), \quad (1)$$

where the monomer positions are given by a set of vectors $\mathbf{R}_i$ and the index i runs over all monomers along the contour, i.e., $i = 0, \ldots, N$. There are M cross-links which join monomers i_e and j_e ($e = 1, 2, \ldots M$), so that $\mathbf{R}_{ie} = \mathbf{R}_{je}$. The network partition function now depends on the cross-link distribution $\{i_e, j_e\}$. The Edwards Hamiltonian contains two important contributions. The first defines the connectivity of the chain and is expressed by a discrete Wiener measure:

$$\beta H_W = \frac{d}{2a^2} \sum_{i=1}^{N} (\mathbf{R}_i - \mathbf{R}_{i-1})^2. \quad (2)$$

The second contribution is defined by the excluded volume of the different monomers, i.e.,

$$\beta H_I = \upsilon \sum_{0 \leq i < j}^{N} \delta\big(\mathbf{R}_i - \mathbf{R}_j\big). \quad (3)$$

called "replica trick" that has been suggested in the Deam and Edwards seminal paper [1]. This approach has been developed further within a much more comprehensive statistical physics context of permanent or chemical gels [2, 3] (see Fig. 1, left panel).

In the course of further investigations, a broad spectrum of polymer network behaviors has been discussed: stress relaxation close to the sol–gel phase transition [4, 5], structural arrest and glass transition [6–8], viscoelastic properties [9–11], etc. Finally, the elastic properties of cross-linked directed polymers [12], nematic elastomers, and networks build up of semiflexible polymers [13] as well as nematic elastomers [14] have been investigated within the "replicated" statistical mechanics. An overview of polymer network dynamics (in both Rouse and Zimm cases) can be found in a recent review paper [15].

The aforementioned polymer networks with permanent bonds (or cross-links) are referred to sometimes as **chemical gels**. In contrast, the **physical gels** are typically made of molecules forming a stress-sustaining network but with bonds that have a finite lifetime (see Fig. 1, right panel). Below in sect. "Chemical Gels," we will discuss first the statistical thermodynamics of frozen polymer networks (chemical gels), and then in sect. "Physical Gels and Nano-Self-Assembly," we address the dynamic behavior of physical gels and nano-self-assembly. Finally, in sect. "Deformation and Failure of Polymer Networks," the mechanical response and material failure will be discussed in terms of strain-induced nucleation, followed by the accumulation and growth of microcracks.

S

The main issue of the problem is the handling of the cross-link constraints which are expressed in the multiple delta function in Eq. 1. This hard constraint represents the quenched disorder, which imposes that monomer at the position vector $\mathbf{R}_{ie}$ is always linked to monomer at $\mathbf{R}_{je}$. Thus, the free energy of the network depends on the actual cross-link configuration, $C: \{i_e, j_e\}$, i.e., $F(C) = -k_B T \ln Z(C)$, and must then be averaged over its distribution, i.e.,

$$F = \langle F(C) \rangle_C = -k_B T \langle \ln Z(C) \rangle_C. \qquad (4)$$

The usual way to treat the cross-link term is to employ the so-called replica trick, which allows

to average the quenched system (i.e., the system with a frozen disorder). Using the formal mathematical identity in $\ln\ Z = \lim_{n \to 0} \frac{1}{n}(Z^n - 1)$ allows to average a power of the partition function, and the evaluation of the generalized partition function reads

$$\begin{aligned} \exp(\beta F(n)) &= \langle Z^n(C) \rangle_C \\ &= \int\limits_V \prod_{\alpha=1}^{n} D\mathbf{R}^\alpha \frac{1}{2\pi i} \oint \frac{d\mu M!}{\mu^{M+1}} \exp^{-\beta H_{\text{eff}}(n,\,\mu)} \end{aligned}$$

$$(5)$$

where the effective Hamiltonian is given by

$$H_{\text{eff}} = \sum_{\alpha=1}^{n} \left(\frac{d}{2a^2} \sum_{i=1}^{N} \left(\mathbf{R}_i^\alpha - \mathbf{R}_{i-1}^\alpha \right)^2 + \upsilon \sum_{0 \le i < j}^{N} \delta\left(\mathbf{R}_i^\alpha - \mathbf{R}_j^\alpha \right) \right) + \mu \sum_{0 \le i < j}^{N} \prod_{\alpha=1}^{n} \delta\left(\mathbf{R}_i^\alpha - \mathbf{R}_j^\alpha \right). \qquad (6)$$

In Eq. 5, the grand canonical representation for the cross-link constraints has been used, i.e., $(A)^M = (M!/2\pi i) \oint d\mu \exp (\mu A)/\mu^{M+1}$, where $A = \sum_{0 \le i \le j}^{N} \delta(\mathbf{R}_i^\alpha - \mathbf{R}_j^\alpha)$ and μ stands for the chemical potential. In order to calculate the free energy in Eq. 5, one has to evaluate the functional integral over configurations $\{\mathbf{R}_i^\alpha\}$. This is a formidable task, and therefore, one should transform the problem into a more tractable one by going to a field theoretical representation followed by a mean field treatment. In this term, one could discuss the amorphous solid-state formation [2], the density correlation functions in heterogeneous structures of networks upon stretching, and some other interesting questions [3].

Gaussian Network

Historically, the classical theory of high elasticity of rubbers was developed in 40 years of the last century [17]. The theory is based on some basic assumptions:

- Each subchain which forms the network is "phantom"; i.e., all surrounding polymers do not restrict conformations which are compatible with the end-to-end distance of our subchain.

- The statistics of all subchains is Gaussian. This assumption can be justified by the fact that networks are usually rather concentrated systems, where (as, e.g., in a concentrated solution) chains are governed by Gaussian statistics [18].
- The deformations on nanoscopic scales are the same as on macroscopic scales. This property is usually referred as the affine deformation of rubber network.
- The density of the network is well behaved.

The realistic cross-linked polymer melt can be made solid by adding a reagent which joins each chain to neighbors. Upon the network formation, however, many structural elements, such as entanglements, loops, and dangling ends (i.e., subchains which are cross-linked only once), become frozen as it is shown in Fig. 2.

As a result, in the Gaussian network theory, the high elasticity is defined by entropic contribution of subchains (i.e., chain fragments between two cross-links). The entropy of a subchain with an end-to-end vector $\mathbf{R}$ reads

$$S(\mathbf{R}) = k_B \ln P_N(\mathbf{R}) \qquad (7)$$
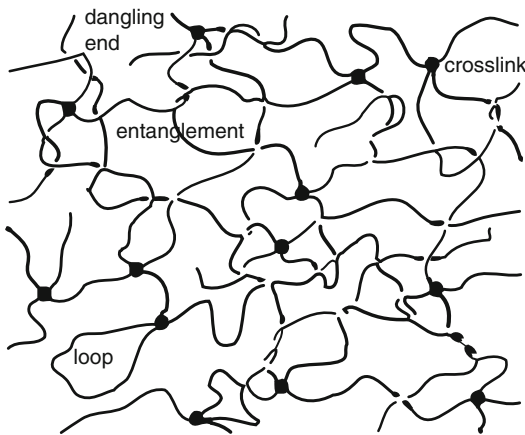
Statistical Thermodynamics of Polymeric Networks, Fig. 2 Structural elements in a network

where $P_N(\mathbf{R})$ is the end-to-end vector distribution function for a Gaussian chain with a chain length N [18]. Note that because the internal energy U could be neglected, the total free energy $F(\mathbf{R}) = -TS(\mathbf{R})$ and we have

$$F(\mathbf{R}) = k_B T \frac{3R^2}{2b^2N} - \frac{3}{2} k_B T \ln\left(\frac{3}{2\pi b^2 N}\right). \quad (8)$$

The corresponding deformation force is then given by

$$f = \frac{\partial F}{\partial \mathbf{R}} = k_B T \frac{3}{b^2 N} \mathbf{R}. \quad (9)$$

Although this is a very simple formula, it has some interesting features. Firstly, it resembles a Hooke's law, where the force is proportional to the extension. Secondly, the force increases with increasing temperature. This is different than in ordinary elasticity (e.g., in metals) where the force decreases with temperatures. The physical reason for this is an entropic nature of elastic effects, so that that for higher temperatures normally, more conformations are accessible. Moreover, Eq. 9 shows that the elasticity modulus goes as $\sim 1/N$, i.e., is very small.

In the same way as for chain extension, the chain compression costs entropy. Confining a chain of

a natural size $R \simeq bN^{1/2}$ to any other (smaller) size R can be estimated by the entropy penalty [18]:

$$F_{\text{conf}} = k_B T \frac{b^2 N}{R^2}. \quad (10)$$

The combination of this equation with Eq. 8 leads to the total free energy:

$$F(R) = k_B T \left(\frac{R^2}{b^2 N} + \frac{b^2 N}{R^2}\right). \quad (11)$$

The minimum of this free energy comes of course at the well-known size $R \simeq bN^{1/2}$.

This simple preliminary consideration based on a single-chain deformation behavior enables to construct the theory of Gaussian networks. To this end, let us introduce a diagonal deformation matrix

$$\boldsymbol{\lambda} = \begin{bmatrix} \lambda_x & 0 & 0 \\ 0 & \lambda_y & 0 \\ 0 & 0 & \lambda_z \end{bmatrix} \quad (12)$$

where the deformations $\boldsymbol{\lambda}_{x,y,z}$ correspond to the three principal axes. Each of these parameters describes the ratio of final and initial length of the rubber as well as the individual deformation of chains on the nanoscopic length scale, i.e.,

$$\mathbf{R}(\boldsymbol{\lambda})_i = \boldsymbol{\lambda} \cdot \mathbf{R}_i \quad (13)$$

where $\mathbf{R}_i$ is the undeformed end-to-end distance of the i-th chain in the network. Then the free energy of a deformed rubber which consists of n_c cross-linked chains can be described as

$$F(\{\boldsymbol{\lambda} \cdot \mathbf{R}_i\}) = k_B T \frac{3}{2b^2 N} \sum_{i=1}^{n_c} (\boldsymbol{\lambda} \cdot \mathbf{R}_i)^2. \quad (14)$$

Note that the free energy as it stands in Eq. 14 still contains "microscopic" variables, i.e., the individual chain end-to-end distances $\mathbf{R}i$. In order to obtain the free energy of the total network, one should average the free energy over all subchains (this actually corresponds to the non-Gibbsian statistical mechanics which was discussed in sect. "The Standard Edwards

Formulation: Non-Gibbsian Statistical Physics"). Taking into account that $\langle \mathbf{R}_i^2 \rangle = b^2 N/3$, we arrive at

$$F(\boldsymbol{\lambda}) = \frac{1}{2} k_B T n_c \boldsymbol{\lambda} \cdot \boldsymbol{\lambda}^T. \qquad (15)$$

As a simple diagonal form of the deformation matrix has been chosen, the last equation can be written in a standard form

$$F(\boldsymbol{\lambda}) = \frac{1}{2} k_B T n_c \left(\boldsymbol{\lambda}_x^2 + \boldsymbol{\lambda}_y^2 + \boldsymbol{\lambda}_z^2 \right). \qquad (16)$$

This free energy enables us to calculate a simple equation of state which is here a force–extension relationship. For this end, we remark that the cross-linked polymer materials are (in the absence of any solvent) incompressible. Therefore, for a uniaxial deformation experiment, we can use the following relation:

$$\begin{aligned} \boldsymbol{\lambda}_z &= \boldsymbol{\lambda} \\ \boldsymbol{\lambda}_x &= \lambda_y = \lambda^{-1/2} \end{aligned} \qquad (17)$$

which yields immediately the force–extension relation

$$f = n_c k_B T \left(\lambda - \frac{1}{\lambda^2} \right). \qquad (18)$$

Equation 18 is one of the main results of the classical rubber elasticity theory [17]. It is interesting that this formula predicts not only the linear deformation regime (for $\boldsymbol{\lambda} - 1 << 1$) but also some nonlinear properties. In a more general case, one could also take into account the compression terms which make the free energy function more

complicate. Here we only mention that in this case, the additional terms $1/\lambda_x^2 + 1/\lambda_y^2 + 1/\lambda_z^2$ and $\lambda_x^2/\lambda_y^2\lambda_z^2 +$ perm (x, y, z) will appear. In the more general mathematical theory, it is postulated that the deformation free energy depends only on the three tensor deformation invariants $I_1 = \lambda_x^2 + \lambda_y^2 + \lambda_z^2, 1/\lambda_x^2 + 1/\lambda_y^2 + 1/\lambda_z^2$ and $I_3 = \lambda_x \lambda_y \lambda_z$.

The free energy function discussed above ignores all sorts of defects shown in Fig. 2. For example, the phantom chain model does not take into account the topological constraints or chain entanglements. Moreover, the chain has a maximum extension $\lambda_{\max} = \sqrt{N}$, which appears often far too large as measured in reality. As soon as the deformation $\lambda \to \lambda_{\max}$, the force becomes very large, the fact which was ignored in the Gaussian theory.

Entanglements and a Simple Tube Model: A Material Law

The tube model goes back to de Gennes, and Edwards is a relatively simple representation of topological restrictions in a cross-linked melt [18, 19]. Tube model introduces a new length scale, tube diameter, or the mean distance between entanglements, which governs physical behavior (cf. Fig. 3) On the other hand, the entanglement can be seen as a local topological constraint as it is pictured in Fig. 4. Two conformations, shown in Fig. 4, are not equivalent since they cannot be transformed to each other. This is due to excluded volume which makes chain of a finite thickness. This must have strong influences on the mechanical behavior. One could expect that these topological constraints act at two different regimes. First, at
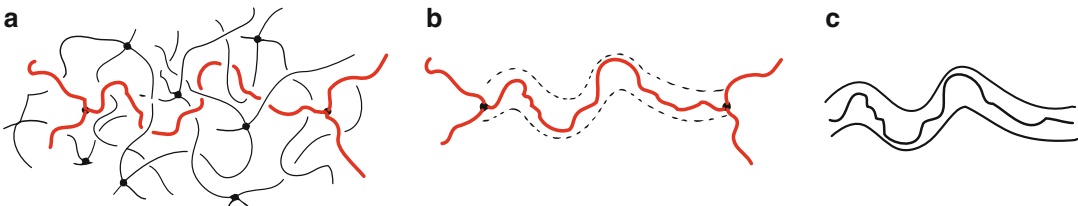
Statistical Thermodynamics of Polymeric Networks, Fig. 3 Chains trapped in tubes as simple mean field model for entangled states in networks. Figures (**a**), (**b**), and (**c**) show successively how the notion of a tube can be inferred
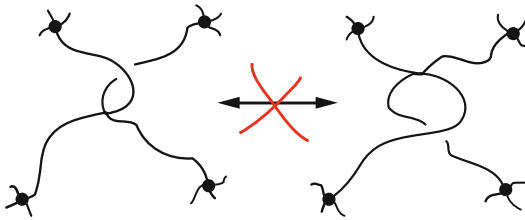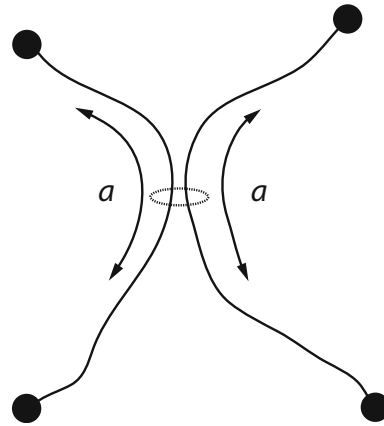
Statistical Thermodynamics of Polymeric Networks, Fig. 4 Locally constrained chains. There is now way to transform the two chain conformations to each other

Statistical Thermodynamics of Polymeric Networks, Fig. 5 Locally constrained chains. The chains are trapped and the conformation cannot be resolved

small deformations, the sliding of entanglements is relevant, whereas at larger deformation, the tube geometry governs the mechanical behavior. These two points are the subject of the rest of this section where we mainly follow Refs. [20, 21].

The effects of the entanglements at low deformation can be mainly described by the entanglement sliding. As mentioned before, we have already intuitively see that the entanglement can be seen as a kind of "soft cross-link." Schematically, this can be drawn as Fig. 5. Here the cross-links at the end of subchains act as full constraint, whereas the entanglement has been replaced by a ring, which can slide along the chains at certain distance a. This distance a is of the order of the mean distance between entanglements. Of course, such kind of sliding might happen anywhere in the network, and for a moment, we assume that there are N_s such slip-links in the rubber. The number N_s of slip-links and the number of cross-links N_c are assumed to be given, so that we are dealing with a two-parameter theory. Recently, the new powerful numerical development using a detailed primitive path analysis (which also enables to calculate N_c) has been developed by Everaers and Kremer [22].

The mathematical description of the statistical mechanics of this model is rather complicated, and we are not going to report this here. Instead, we provide a more simplified version, along the line given above in the theory of Gaussian single-chain elasticity. We present a much simpler but nevertheless adequate derivation, following Ref. [23]. It will turn out that this kind of approach is easier to generalize when one needs also to discuss the finite extensibility of chains.

We assume that the chain is Gaussian, with an end-to-end separation probability written in the form

$$P(\mathbf{R},N) = \prod_{i=x,y,z} \int d\tau \chi(\tau) \left(\frac{3}{2\pi b^2(N+\tau)} \right)^{3/2}$$
$$\times \exp\left(-\frac{3R_i^2}{2b^2(N+\tau)} \right). \tag{19}$$

The variable τ describes the number of segments which are gained or lost as a result of the slippage. The distribution $\chi(\tau)$ describes the probability of the slippage, which for simplicity can be taken as a rectangular function, i.e.,

$$\chi(\tau) = 1 \quad \text{for} \quad -a < \tau \quad < a. \tag{20}$$

Then we may write

$$P(\mathbf{R},N) = \prod_{i=x,y,z} \int_{-a}^{+a} d\tau \chi(\tau) \left(\frac{3}{2\pi b^2(N+\tau)} \right)^{3/2}$$
$$\times \exp\left(\frac{3R_i^2}{2b^2(N+\tau)} \right). \tag{21}$$

Following the recipe to calculate the free energy, we have

$$F = -k_B T \int d^3 R\, P(\mathbf{R}, N) \ln P(\boldsymbol{\lambda} \cdot \mathbf{R}) \qquad (22)$$

which after some calculation gives

$$
\frac{F}{k_B T} = \frac{1}{2} N_c \sum_{i=x,y,z} \lambda_i^2
$$
$$
+ \frac{1}{2} N_s \sum_{i=x,y,z} \left\{ \frac{(1+\eta)\lambda_i^2}{(1+\eta)\lambda_i} + \log\left(1 + \eta \lambda_i^2\right) \right\}.
$$
$$(23)$$

In Eq. 23, we have added the cross-link and the slip-link contributions. The parameter η is proportional to a. This result is consistent with the more complicated theory based on non-Gibbsian statistical physics by Ball et al. [24].

The free energy (Eq. 23) is quite a simple result. The main effect is a reduced macroscopic slip variable η, which is proportional to the mesoscopic variable a. Assuming the slip takes place between two neighboring cross-links, an estimation η suggests values between zero and one. Two limiting cases should be discussed. Firstly, if the slippage becomes zero ($\eta = 0$), the slip-link turns into a cross-link and fully contributes to the modulus. The free energy is then

$$\frac{F}{k_B T} = \frac{1}{2} \ (N_c + N_s) \sum_{i=x,y,z} \lambda_i^2. \qquad (24)$$

The other significant limit is given by infinite slippage, $\eta \rightarrow \infty$. For large values of η, the constraints act less severe. Such cases can be addressed to swollen networks, when the chain segments are pushed away from each other as far as possible. Then the free energy reads as

$$\frac{F}{k_B T} = \frac{1}{2} \ N_c \sum_{i=x,y,z} \lambda_i^2 + \frac{1}{2} \ N_s \ln \prod_{i=x,y,z} \lambda_i, \qquad (25)$$

and the modulus depends mainly on the number of cross-links.

Discussion of the physical behavior should now clarify major counterintuitive points. The intuitive picture of the behavior of a slip-link

under stress is that it will respond by moving until it locks to another entanglement or cross-link and behaves as a cross-link perhaps of higher functionality. This means that a slip-link hardens, but a finite value of η in Eq. 23 suggests softening. This result is reasonable if one accounts for the increase of phase space during deformation for the slippage a. As the slipping distance increases, the more conformations will be accessible, so that the link weakens. This can only be true of course if the deformation is not too large, i.e., long before the polymers are drawn taut.

Physical Gels and Nano-Self-Assembly

Molecular or nano-self-assembly of the constituents could form a reversible gel upon heating or cooling [25]. This versatile state of matter, which exhibits viscoelasticity as well as glassy behavior, is ubiquitous in nature, ranging from colloids, emulsions, and food technology products [26] up to spectrin (the cytoskeleton of living organisms) [27–29]. Recently, thermoreversible rubber has been obtained by supramolecular assembly of two and three functional molecular groups via hydrogen bonding [30]. In contrast to conventional cross-linked or thermoreversible rubbers, this system can be simply repaired when broken or cut by bringing together fractured surfaces by means of self-healed at room temperature.

Another interesting system which exhibits the properties of thermoreversible gels is oil-in-water microemulsions, modified with bridging telechelic polymers [31–33]. The authors coarse-grained the telechelic polymer molecules (with hydrophobic heads), retaining only their ability as linkers, and allowed for the effective interactions between interconnected droplets, as is shown in Fig. 6. Despite the particular oil-in-water microemulsion context, this model helps to elucidate connections between related generic phenomena: geometric percolation, glass transition, and phase separation. The corresponding model is built up from soft spherical droplets (with a direct interaction potential $V_1(r_{ij}) = \in_1 (\sigma/r_{ij})^{14}$) subjected to bonding
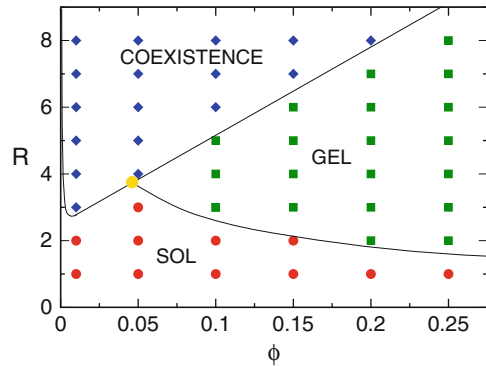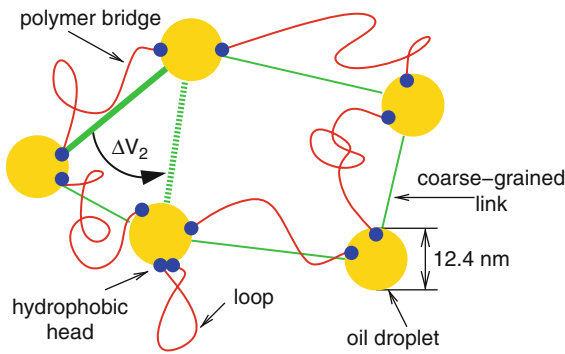
Statistical Thermodynamics of Polymeric Networks, Fig. 6 *Left panel*: Sketch of an oil-in-water microemulsion. The bridging telechelic polymers are replaced by coarse-grained effective links (*green*). The thicker and dashed links represent a Monte Carlo move (with potential energy change ΔV_2) for the connectivity matrix. *Right panel*: The corresponding phase diagram (Reprinted with permission from Ref. [32])

interaction (with a FENE-like potential $V_2(r_{ij}) = -\epsilon_2 \ln(1 - (r_{ij} - \sigma)^2/l^2)$ where $r_{ij} < l$). The bonding configuration is described by a $N \times N$ matrix, $\{C_{ij}\}$, where C_{ij} is the number of bonds between droplets i and j. The resulting Hamiltonian reads

$$H = \sum_{i=1}^{N} \left(\frac{m v_i^2}{2} + C_{ii}\,\epsilon_0 + \sum_{j>i} \left[V_1(r_{ij}) + C_{ij} V_2(r_{ij}) \right] \right)$$

(26)

where ϵ_0 represents the energy cost of loops. The studies were performed by molecular dynamics (MD) simulation, whereas a Monte Carlo (MC) simulation has been used to evolve the connectivity matrix C_{ij}: each particular random move of a bond is accepted with rate $\tau_{\text{link}}^{-1}\min[1, \exp(-\Delta V_2)]$ (see the left panel in Fig. 6). The resulting phase diagram is shown in Fig. 6, right panel, in terms of the control parameters: number of telechelic heads per droplets, $R = 2N_p/N$, and the droplet volume fraction ϕ. The "sol" region marks a dilute assembly of relatively small clusters. As the parameter R grows, the effective attraction increases and phase separation comes about ("coexistence"). For $\phi > 0.05$, a broad gel region exists between the sol phase and phase separation. In the gel phase, a system-spanning cluster of telechelically connected droplets emerges, which endows the fluid with viscoelastic properties. To show that

the gel phase indeed behaves dynamically as a soft viscoelastic fluid, the authors have measured the self-intermediate scattering functional [33]:

$$F_s(q,t) = \frac{1}{N} \sum_{j=1}^{N} \left\langle \exp\left[i\mathbf{q}\left(\mathbf{r}_j(t) - \mathbf{r}_j(0)\right) \right] \right\rangle.$$

(27)

Figure 7 shows the results of these measurements for different parameters R (i.e., effective attraction) and ϕ (which is responsible for the effective repulsion). At $\phi = 0.5$ and growing R, one could observe a generic two-step decay with a plateau height controlled by R and a final slow decay, depending on characteristic time τ_{link}. This behavior reflects the vibration of the increasingly stiffer network of connected particles, followed by a slow reorganization of the transient network. It is interesting that in this "bonded glass" even for very large $R = 50$, the behavior is ergodic albeit the relaxation time increases smoothly with R. Thus, there is no evidence of an "ideal" gel (or "bonded" glass) as predicted theoretically (on the basis of the mode coupling theory (MCT)) for colloidal suspensions with attractive interactions [34, 35].

In the opposite limit where $R = 0$ and the volume fraction becomes large, the microemulsion or colloidal system turns into a standard dense glass (see Fig. 7b). Here the plateau appearance
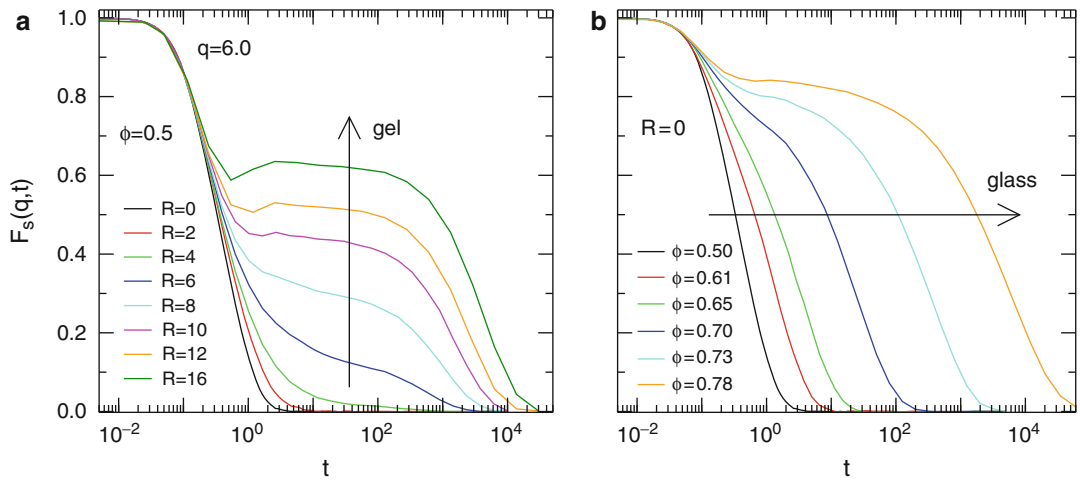
Statistical Thermodynamics of Polymeric Networks, Fig. 7 Time dependence of $F_s(q, t)$ for $q = 6.0$ (**a**) Gelation at $\phi = 0.5$, $\tau_{\text{link}} = 10^2$, and increasing parameter *R*. (**b**) Glass transition at $R = 0$ and increasing ϕ (Reprinted with permission from Ref. [33])

Statistical Thermodynamics of Polymeric Networks, Fig. 8 Examples of patchy particles with located sticky spots used in the MD simulation (Reprinted with permission from Ref. [37])
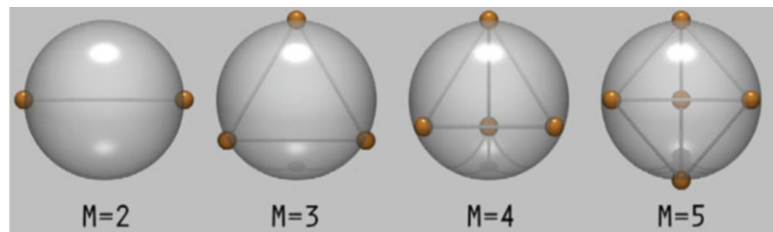
and the two-step decay stem from the transient cage, formed by the neighbors, followed by a slow structural relaxation. As usual for such "repulsive glass," the relaxation time increases dramatically with ϕ, while the plateau height remains constant [36].

Patchy Colloids

Besides the colloidal suspensions with attractive interactions [34, 35], the colloids with limited valence, or patchy colloids, recently attracted interest as a new class of material to build, among various issues, ideal colloidal gels. An example of experimental patchy colloid, which was used in a theoretical study [37], is shown in Fig. 8. An interesting review devoted to colloidal gels, including the patchy colloids, can be found in Ref. [38]

In these models, particles interact via a simple square well (SW) potential but only with a predefined maximum number of attractive neighbors, N_{max}, while hard-core interactions have no such limitations. The limited-valence condition is imposed by adding a *bonding constraint*. For two particles to be bonded, two conditions should be obeyed: (i) particles' centers must be within the attraction interval $\sigma < r < \sigma + \Delta$, and (ii) each of the particles should have less than N_{max} bonds. The resulting Hamiltonian of the system has many-body terms containing information on the existing bonds. As a result, at any step of the simulation, not only coordinates and velocities should be saved but also the *bond list*. The phase diagram substantially depends on the N_{max} value. Namely, small values of N_{max} reduce the tendency of the system to phase separate (see Fig. 9).

To elucidate how the structural arrest transition manifests itself on different length scales (or different wave vectors **q**), the authors of

Ref. [39] studied the density autocorrelation function $F_q(t) = \rho_q(t)\rho_{-q}(0)$. Recall that large q indicates typically nearest-neighbor distances which are relevant for the bond breaking–healing processes in case of transient networks as well as of the cage reorganization ("hopping process" in terms of W. Götze). In contrast, the low-q area is responsible for the ergodic–nonergodic (NEN) transition which is predicted by MCT [36]. Indeed, looking at the full decay of density auto-correlation function $F_q(t)$, one observes that in
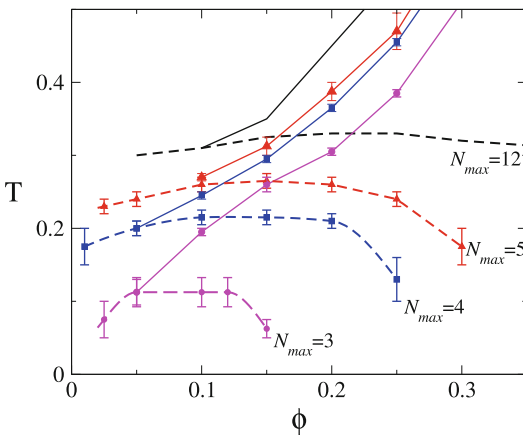
Statistical Thermodynamics of Polymeric Networks, Fig. 9 Phase diagram variation: with decreasing N_{max}, the phase separation is shifted to lower temperatures and lower densities. Percolation and spinodal are marked by *solid and dashed lines*, respectively (Reprinte7d with permission from Ref. [39])

the gel phase, for $q\sigma \approx 7$, no slowing down is detected at all, while a clear plateau is observed (upon cooling) for smaller q, as can be seen in Fig. 10 (left panel). Therefore, with respect to glasses, experimental studies have to focus strictly in the low-q area.

The nonergodic behavior is characterized by the *nonergodic parameter f_q*, the amplitude in the stretched exponential fitting $F_q(t) = f_q \exp [-(t/\tau_q)^{\beta q}]$ of the long-time decay. Figure 10 (right panel) shows f_q at different packing fractions ϕ. At low ϕ, the nonergodic parameter f_q is largest at $q \to 0$ and goes to zero within the interval $0 < q\sigma < 5$. With increasing ϕ, a small peak starts to form at larger q which is still of the order of few $q\sigma$. This behavior roughly follows that of the static structure factor $S(q) = \langle|\rho_q(0)|^2\rangle$. At large ϕ, the shape of f_q closely resembles $S(q)$ of a hard sphere system with a first peak around $q\sigma \approx 2\pi$, i.e., the nearest-neighbor length scale.

Figure 10 (right panel) shows that within $0.45 < \phi < 0.55$, there occurs a *gel-to-glass* transition which becomes evident from the behavior of the nonergodicity parameter f_q. It is also instructive to discuss the static structure fac-tor $S(q)$ behavior at different temperatures T, shown in Fig. 11. First of all, the function $S(q)$ displays progressively pronounced peaks at $q \sim 2\pi/\sigma$ and some other $q\sigma$ values as T decreases. Most importantly, an increase of $S(q)$ in the low-q area is observed which saturates
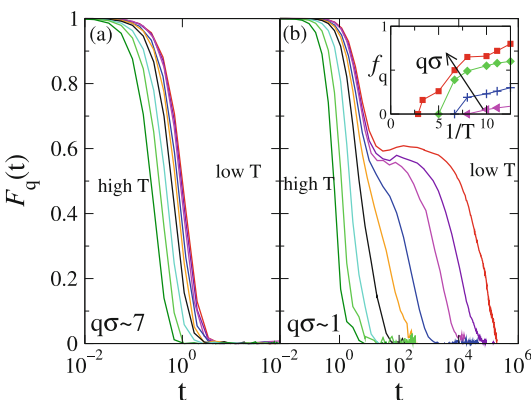

Statistical Thermodynamics of Polymeric Networks, Fig. 10 *Left panel*: $F_q(t)$ behavior with T at $\phi = 0.2$ and $N_{\max} = 3$. *Right panel*: Nonergodicity parameter f_q for
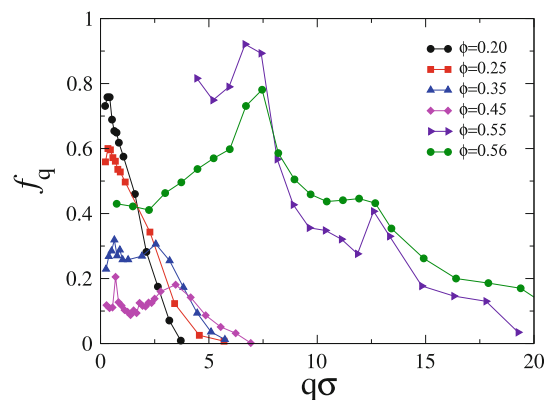
different packing fractions ϕ (Reprinted with permission from Ref. [38])

Statistical Thermodynamics of Polymeric Networks, Fig. 11 Structural factor $S(q)$. Below $T \leq 0.1$, the system displays an equilibrium gel transition (see behavior at $q \to 0$) (Reprinted with permission from Ref. [38])
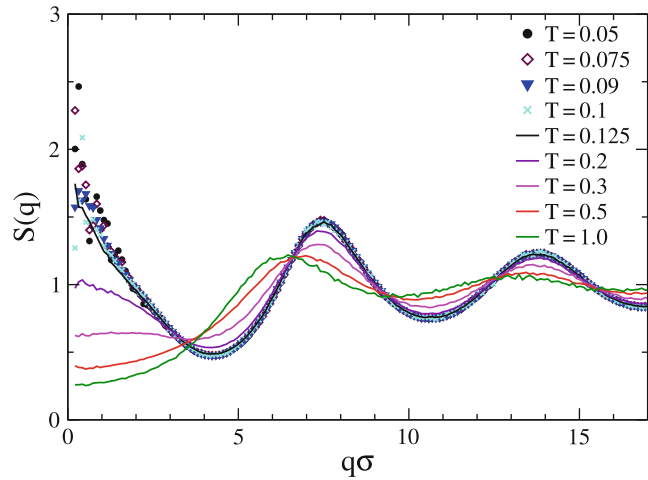
at $T \leq 0.1$. This increase reflects the phase separation at $T \approx 0$ J and indicates that the system is highly compressible and inhomogeneous. As a result, one may specify the following physical gel features with respect to standard glasses:

1. The structural arrest in physical gels occurs at much smaller packing fraction than in standard glasses (see Fig. 9).
2. Localization length in physical gels is much larger (see Fig. 10 right panel).
3. Nonergodicity properties strongly depend on the length-scale observation (see Fig. 10 left panel). The function $F_q(t)$ displays nonergodic features (i.e., the emergence of a clear plateau) first at very small q and then upon decreasing T, for larger and larger q. Thus, the gel transition temperature strongly depends on the wavelength of observation, in contrast to what is typical in standard glasses, where all length scales become nonergodic at a single transition temperature T_c.
4. The static structural factor shows growth at small wave vectors q (see Fig. 11).

Supramolecular Polymer Networks

Recently, a new class of polymeric materials was developed, supramolecular polymer networks, which are formed by highly directed supramolecular bonds such as hydrogen bonds, π–π interactions, or metal complexes. These bonds either form a network from non-covalently associating

monomers or associate together (acting as non-covalent side groups) precursor polymer chains [40]. In the last case, the dynamic behavior could be treated within the "sticky" reptation model [41]. The presence of stickers significantly modifies the self-diffusion coefficient and the stress relaxation. For example, when the chain is strongly stuck, the chain self-diffusion coefficient $D_{\text{self}} \propto a^2/\tau_s S^2$, where S is the number of stickers per chain and τ_s is the sticker lifetime. As one could see in this case, D_{self} is chain length independent. Moreover, the presence of the sticker lifetime τ_s (besides the Rouse time $\tau_R \propto N^2$ and the terminal time $\tau* \propto N^3$, where N is the chin length) brings into existence two plateaus in the dynamic modulus $G(t)$. One plateau is related with the classical reptation, whereas the second one is due to the additional reversible chain association.

Deformation and Failure of Polymer Networks

Deformation and failure of polymer networks are two related problems of great practical and fundamental importance. The models of physical gels (or transient networks), which we discussed in the previous section, can be also used for investigation of material failure. Despite the large amount of experimental data and the considerable efforts based mainly on computer
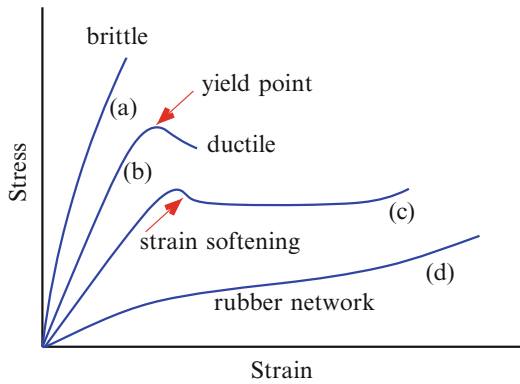
Statistical Thermodynamics of Polymeric Networks, Fig. 12 Typical stress–strain curves of polymers tested at different temperatures: curves (**a**)–(**c**) represent glassy polymers (i.e., temperature interval $T < T_g$) with increasing temperature from (**a**) to (**c**). The curve (**d**) corresponds to the rubber state, i.e., to $T > T_g$. Ends of the curves indicate the points of material failure: (**a**) brittle and (**b**)–(**d**) ductile

simulations, many questions concerning a physical picture of material failure have not yet been answered Before we proceed with the model consideration, let us recall some basic notions related to polymer fracture phenomenology [42].

When temperature T is sufficiently low, the system behaves as elastic one until breaking and fracture is observed *brittle* (see Fig. 12a). Usually, the tensile strain at the "brittle" breaking point is about $1 \div 5$ %. At higher temperatures, materials go through a *yield point* which defines the onset of irreversible plastic deformation and results in ductile fracture (see Fig. 12b). In curve (*c*), the yield point is followed by the occurrence of necking which propagates along the sample at almost constant stress. In this case, the polymer material develops inhomogeneous deformations, necks, or shear bands, which also depend on the sample geometry. Finally, at even higher temperatures, $T > T_g$, the polymer undergoes a transition from glassy- to rubberlike state (see Fig. 12d). Here rupture can be understood by visualization of rubber as a network (or a cross-linked polymer) degradation. Small cracks nucleate at the weakest bonds until one dominating crack (or the main cluster of broken bonds) tears the material apart. In the next subsection on the basis

of a simple transient network model with driven external force, we discuss the generic features of this last scenario.

Fracture in Two-Dimensional Network Model

The fracture behavior of materials has been a focus of large amount of research. MD simulation has become an important tool for these investigations. However, simulations face a problem: the fracture process involves long time and spatial scales of atomic deformation, which are difficult to simulate. Most simulations overcome this problem by studying fracture with a *preexisting crack*. Only few simulations have been used to study the formation of cracks at nonzero temperature without preexisting crack. For example, void formation has been observed in a $3D$ system of driven binary Lennard–Jones system [43]. Some simulations of rate crack nucleation have been performed in a $2D$ spring network [44].

Fracture in network models, being seen as a kind of dynamic phase transition, represents a challenge to nonequilibrium statistical mechanics. In this sense, one could expect an interplay over many length scales (in our case the interplay of small clusters of broken bonds with a main cluster).

Systematic study of these problems is still lacking. One of the interesting MD simulations, based on a simple $2D$ model and intended to elucidate the analogy with a phase transition, was undertaken in Ref. [45, 46]. This model represents a triangular lattice, shown in Fig. 13; particles (nods) i and j interact with central force:

$$f_{ij} = F\big(|\mathbf{r}_i - \mathbf{r}_j|\big) \frac{\mathbf{r}_i - \mathbf{r}_j}{|\mathbf{r}_i - \mathbf{r}_j|} \qquad (28)$$
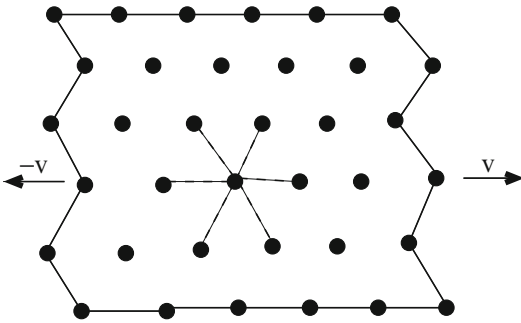
Both linear (harmonic potential)

$$F(r) = -\alpha(r - a) \qquad (29)$$

and Lennard–Jones (LJ) type of force have been considered:

$$F(r) = \frac{\alpha a}{6} \left[\left(\frac{a}{r}\right)^{13} - \left(\frac{a}{r}\right)^7 \right] \qquad (30)$$

The bond is considered broken as soon as the mutual distance becomes larger than a reasonable

Statistical Thermodynamics of Polymeric Networks,
Fig. 13 Sketch of the molecular dynamics experiment.
The *dashed lines* refer to the interactions involving a given
site with its nearest neighbors. The *left* and *right* bound-
aries are pulled apart with velocity v. Free boundary con-
ditions are assumed along the upper and lower borders
(Reprinted with permission from Ref. [45])

threshold a^*. In terms of parameter a, the thresh-
old a^* was taken between 1.1 and 1.8. The exter-
nal stretching is implemented by pulling the left
and right boundaries apart with velocity v (see
Fig. 13) so that the strain follows the law: $d = vt/L$
(L is size of the lattice). Free boundary conditions
were chosen for the upper and lower boundaries.
The model contains also an inherent disorder:
some fraction c of bonds has been cut in advance.
At $c = 0$, the model is a perfectly homogeneous
lattice.

The stress–strain curves of this model show a
well-pronounced peak at a characteristic strain d_c
which corresponds to the "yield point," marked in
Fig. 12. Above d_c, the onset of microcracks leads
to a rearrangement of the lattice in order to with-
stand the imposed strain which leads to
a decrease of the stress.

The number of broken bonds $N(d)$ as
a function of d has been studied. It is natural to
use the fraction

$$\langle n(d) \rangle = \left\langle \frac{N(d)}{N_b} \right\rangle \tag{31}$$

as a possible order parameter. Here N_b is the final
number of broken bonds in a given realization,
and $\langle \ldots \rangle$ is the average over different realizations
of disorder. Plotting of this order parameter $\langle n(d) \rangle$
versus the control parameter, $\Delta = (d - d_c)L$, is
reminiscent of the second-order phase transition.

Another interesting problem which was stud-
ied was the dependence of the total number of
broken bonds $N_b(L)$ on the system size L. The aim
was to characterize the possible fractal nature of
the process. This investigation revealed a clear
power-law dependence $N_b \propto L^{\beta}$, where $\beta = 1.35$
± 0.03.

The crack length cannot be shorter than
a straight line so that $1 < \beta < 2$. On the other
hand, it is necessary to understand whether the
value $\beta > 1$ is attributed to the structure of the
main crack, or to the distribution of microcracks.
For this purpose in Ref. [45], the number $N_b^{(i)}$ and
$N_b^{(o)}$ of broken bonds inside and outside the main
cluster (crack), respectively, was investigated
separately. The results show that $N_b^{(i)}$ scales
approximately in the same way as the total bro-
ken bond number N_b, namely, as $N_b^{(i)} \propto L^{1.31}$. The
scaling law for the number of bonds outside the
main cluster reads $N_b^{(o)} \propto L^{1.52}$, but on the other
hand, it was found that $N_b^{(i)} \gg N_b^{(o)}$. This leads to
the interesting conclusion that if the scaling
behavior remains unchanged in larger lattices,
the majority of broken bonds will be eventually
found outside of the main cluster.

Conclusion

Classical and fundamental theories of polymer
networks have been discussed to derive constitu-
tive relations for material science. We have
shown that the statistical physics gives a solid
evidence for such a derivation. Indeed, perma-
nently cross-linked networks were the first phys-
ical systems with quenched disorder which has
been treated by means of non-Gibbsian statistical
physics and the replica trick. Since that time,
many problems in the physics of network still
remain to be investigated. For example, the role
of entanglements and other topological con-
straints is not solved in all details. On the other
hand, the studies of physical networks in biolog-
ical systems and in self-assembly open new ave-
nues in living matter and material science.
Transient and self-healing networks need new
theoretical methods and approaches, especially
under the aspect of nonequilibrium processes.

Despite the long-standing investigations, the statistical physics of network remain an exciting field of the scientific activity.

Related Entries

▶ Material Laws of Rubbers
▶ Molecular Modeling of Elastomers
▶ Supramolecular Network Polymers

References

1. Deam RT, Edwards SF (1976) The theory of rubber elasticity. Phylos Trans R Soc London Ser A 280:317
2. Goldbart PM, Castillo HE, Zippelius A (1996) Randomly crosslinked macromolecular systems: vulcanization transition to and properties of the amorphous solid state. Adv Phys 45:393
3. Panyukov SV, Rabin Y (1996) Statistical physics of polymer gels. Phys Rep 269:1
4. Broderix K, Aspelmeier T, Hartmann K, Zippelius A (2001) Stress relaxation of near-critical gels. Phys Rev E 64:021404
5. Broderix K, Löwen H, Müller P, Zippelius A (2001) Anomalous stress relaxation in random macromolecular networks. Physica A 302:279
6. Wald C, Zippelius A, Goldbart PM (2005) Glassy states and microphase separation in cross-linked homopolymer blends. Europhys Lett 70:843
7. Ulrich S, Mao X, Goldbart PM, Zippelius A (2006) Elasticity of highly cross-linked random networks. Europhys Lett 76:677
8. Mao X, Goldbart PM, Xing X, Zippelius A (2007) Elastic heterogeneity of soft random solids. Europhys Lett 80:26004
9. Löwen H, Müller P, Zippelius A (2005) Rheology of gelling polymers in the Zimm model. J Chem Phys 122:014905
10. Küntzel M, Löwen H, Müller P, Zippelius A (2003) Diffusion of gelation clusters in the Zimm model. Eur Phys J E 12:325
11. Broderix K, Löwen H, Müller P, Zippelius A (1999) Shear viscosity of a crosslinked polymer melt. Europhys Lett 48:421
12. Ulrich S, Zippelius A, Benetatos P (2010) Random networks of cross-linked directed polymers. Phys Rev E 81:021802
13. Kiemes M, Benetatos P, Zippelius A (2011) Orientational order and glassy states in networks of semiflexible polymers. Phys Rev E 83:021905
14. Xing X, Pfahl S, Mukhopadhyay S, Goldbart PM, Zippelius A (2008) Nematic elastomers: From a microscopic model to macroscopic elasticity theory. Phys Rev E 77:051802
15. Löwen H, Müller P, Zippelius A (2005) Dynamics of gelling liquids: a short survey. J Phys Cond Mat 17:S1659
16. Edwards SF (1982) The theory of glass quenched from the melt. Ann NY Soc 371:210
17. Treloar LRG (1975) The physics of rubber elasticity. Clarendon, Oxford
18. de Gennes PG (1979) Scaling concepts in polymer physics. Cornell University Press, Ithaca
19. Doi M, Edwards SF (1986) The theory of polymer dynamics. Clarendon, Oxford
20. Edwards SF, Vilgis TA (1988) The tube model theory of rubber elasticity. Rep Prog Phys 51:243
21. Edwards SF, Vilgis TA (1986) The effect of entanglements in rubber elasticity. Polymer 27:483
22. Everaers R, Sukumaran SK, Grest GS, Svaneborg C, Sivasubramanian A, Kremer K (2004) Rheology and microscopic topology of entangled polymer liquids, Science 303:823.
23. Wall FT, Flory JP (1951) Statistical thermodynamics of rubber elasticity. J Chem Phys 19:1435
24. Ball RC, Doi M, Edwards SF, Warner M (1981) Elasticity of entangled networks. Polymer 22:1010
25. Tanaka F (2011) Polymer physics: application to molecular association and thermoreversible gelation. Cambridge University Press, Cambridge
26. Blanshard JMV, Lillford PI (1987) Food structure and behavior. Academic, New York
27. MacKintosh FC, Käs J, Jammey PA (1995) Elasticity of semiflexible biopolymer networks. Phys Rev Lett 75:4425
28. Hinner B, Tempel M, Sackmann E, Kroy K, Frey E (1998) Entanglement, elasticity, and viscous relaxation of actin solutions. Phys Rev Lett 81:2614
29. Lieleg O, Schmoller KM, Claessens MMAE, Bausch AR (2009) Cytoskeletal polymer networks: viscoelastic properties are determined by the microscopic interaction potential of cross-links. Biophys J 96:4725
30. Cordier P, Tournilhac F, Soulié-Ziakovic C, Leibler L (2008) Self-healing and thermoreversible rubber from supramolecular assembly. Nature 451:977
31. Hurtado PI, Berthier L, Kob W (2007) Heterogeneous diffusion in a reversible gel. Phys Rev Lett 98:135503
32. Hurtado PI, Berthier L, Kob W (2009) Static and dynamic properties of a reversible gel. AIP Conf Proc 1091:166
33. Chaudhuri P, Berthier L, Hurtado PI, Kob W (2010) When gel and glass meet: A mechanism for multistep relaxation. Phys Rev E 81:040502(R)
34. Bergenholz J, Fuchs M (1999) Nonergodicity transitions in colloidal suspensions with attractive interactions. Phys Rev E 59:5706
35. Dawson K, Foffi G, Fuchs M, Götze W, Sciortino F, Sperl M, Tartaglia P, Voigtmann T, Zaccarelli E (2000) Higher-order glass-transition singularities in colloidal systems with attractive interactions. Phys Rev E 63:011401
36. Binder K, Kob W (2005) Glassy materials and disordered solids. World Scientific, Singapore

S

37. Bianchi E, Largo J, Tartaglia P, Zaccarelli E, Sciortino F (2006) Phase diagram of patchy colloids: towards empty liquids. Phys Rev Lett 97:168301
38. Zaccarelli E (2007) Colloidal gels: equilibrium and non-equilibrium routes. J Phys Cond Mat 19:323101
39. Zaccarelli E, Boldyrev SV, La Nave E, Moreno AJ, Saika-Voivod I, Sciortino F, Tartaglia P (2005) Model for reversible colloidal gelation. Phys Rev Lett 94:218301
40. Seiffert S, Sprakel J (2012) Physical chemistry of supramolecular polymer networks. Chem Soc Rev 41:909
41. Leibler L, Rubinstein M, Colby RH (1991) Dynamics of reversible networks. Macromolecules 24:4701
42. Herrmann HJ, Roux S (eds) (1990) Statistical models for the fracture of disordered media. North-Holland, Amsterdam
43. Lorenz CD, Stevens MJ (2003) Fracture behavior of Lennard-Jones glasses. Phys Rev E 68:021802
44. Santucci S, Vanel L, Guarino A, Scorretti R, Ciliberto S (2003) Thermal activation of rupture and slow crack growth in a model of homogeneous brittle materials. Europhys Lett 62:320
45. Politi A, Zei M (2001) Fractures in heterogeneous two-dimensional systems. Phys Rev E 63:056107
46. Meacci G, Politi A, Zei M (2004) Fracture precursors in disordered systems. Europhys Lett 66:55

Step Polyaddition Polymerizations, an Overview

Brian R. Donovan and Derek L. Patton
School of Polymers and High Performance Materials, The University of Southern Mississippi, Hattiesburg, MS, USA

Synonyms

Step-addition polymerization; Step-growth addition polymerization; Step-growth polymerization

Definition

Step polyaddition polymerizations are stepwise reactions between bifunctional and polyfunctional monomers that yield macromolecules without the loss of a small-molecule byproduct.

Introduction

The terms "addition polymer" and "condensation polymer" were first defined by Wallace Carothers, respectively, as a macromolecule whose structural unit has the same molecular formula as its monomer, or as a macromolecule whose structural unit differs from the molecular formula of the monomer due to the loss of condensation byproducts [1]. Thus, the corresponding polymerization reactions used to produce the respective polymer types were coined as either *addition polymerizations* or *condensation polymerizations*. Considering the breadth of contemporary polymer chemistry, these terms are often ambiguous and fail to accurately capture and describe all polymerization mechanisms. Presently, polymerization processes are more accurately categorized according to the polymerization mechanism, i.e., *chain growth*, where polymer formation occurs as monomers successively add to an active center of a growing polymer chain with distinct initiation, propagation, and termination steps, or *step growth*, where polymer forms by a stepwise reaction of bifunctional (or polyfunctional) monomers to first form dimers, trimers, and longer oligomers, then high molecular weight polymers after many steps (i.e., high functional group conversion) [2]. Step-growth polymerizations, in general, may be broken down into two categories – (i) step polycondensation and (ii) step polyaddition. As the name implies, step polycondensation refers to the formation of polymers by stepwise condensation reaction of bifunctional or polyfunctional monomers with elimination of a small-molecule byproduct at each step. A detailed discussion of step polycondensation polymerization is the subject of another entry and will not be included in this overview. In contrast, the synthesis of macromolecules by step polyaddition polymerization proceeds through a series of stepwise addition reactions between bifunctional and polyfunctional monomers without the loss of a small-molecule byproduct. As a general step-growth process, high molecular weight polymer in step polyadditions may only be achieved at high monomer conversion and

under stoichiometric monomer conditions. As a consequence of the step-growth mechanism, each reaction product in the system, from oligomer to high polymer, retains the same functional and reactive end groups as the original monomer. In step polyaddition polymerizations, the addition reaction to link monomers usually involves either the migration of a hydrogen atom at each addition step – as in the addition of an amine to an isocyanate or a cycloaddition at each addition step – as in a Diels-Alder cycloaddition between a diene and a dienophile.

For a more involved discussion of step-growth polymerization kinetics, molecular weight control, and advanced topics, the reader is referred to other excellent resources on the subject [2, 3], as it is outside the scope of this entry to provide comprehensive details on general step-growth polymerizations. Instead, this entry aims to provide the reader with a basic understanding and overview of several types of step polyaddition polymerizations. First, the traditional step polyaddition reactions that yield polyurethanes and Diels-Alder polymers are discussed,

followed by a brief discussion of the more contemporary thiol-ene reaction that yields polythioethers. For brevity, additional examples of contemporary step polyaddition reactions – such as copper-catalyzed azide-alkyne Huisgen cycloadditions – as a route to polytriazoles are not discussed [4].

Polyurethanes

Polyurethanes (PUs) are a class of macromolecules in which the repeating motif in the polymer backbone is joined by urethane (or carbamate) linkages. PUs were first developed in the 1940s by Otto Bayer and presently find broad use as foams, fibers, thermoplastic elastomers, and coatings. Linear PUs are predominately synthesized by the step polyaddition reaction of difunctional isocyanates with difunctional alcohols (diols), as generically shown in Fig. 1a. Several of the most common and industrially important diisocyanate monomers are shown in Fig. 1b, including tolylene-2,4-diisocyanate (TDI), 4,4'methylenebis(phenyl
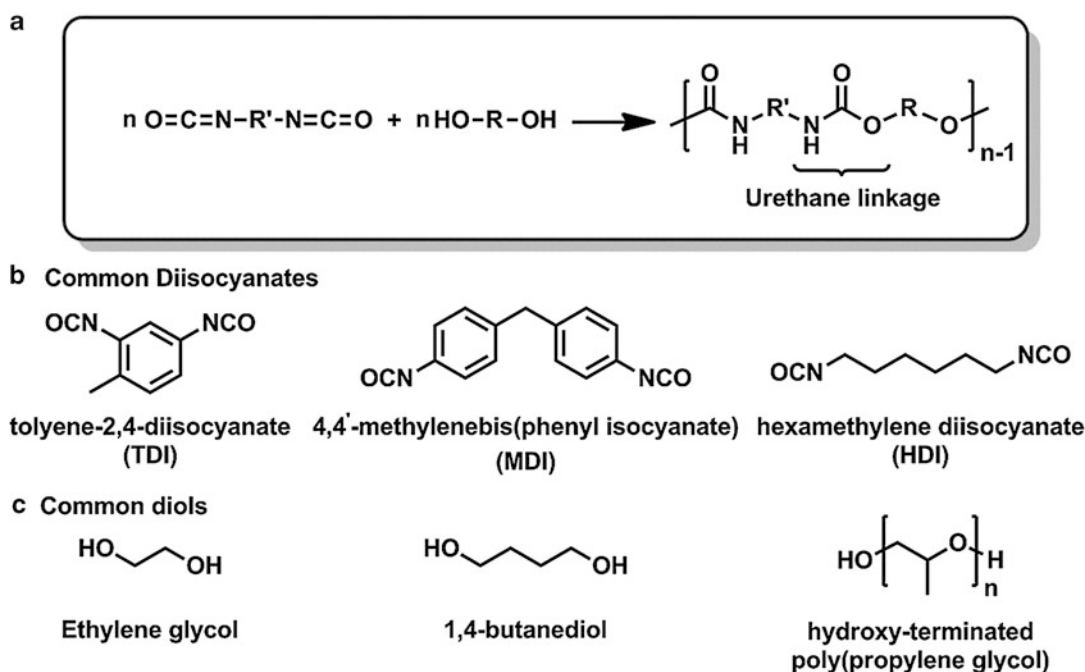
Step Polyaddition Polymerizations, an Overview, Fig. 1 (**a**) General reaction scheme for the synthesis of a polyurethane. (**b**) Common diisocyanate and (**c**) diol monomers used in the synthesis of polyurethanes

isocyanate) (MDI), and hexamethylene-1,6-diisocyanate (HDI). Likewise, common diol monomers, such as ethylene glycol, 1,4-butanediol, and dihydroxy-terminated poly(propylene glycol), are shown in Fig. 1c. The ability to control the chemical structure of the repeating motif via judicious choice of the organic constituents of the isocyanate (R') and alcohol (R) as well as the ability to fine-tune polymer chain flexibility and morphology facilitate the use of these step polyaddition polymers for a variety of applications [5].

Much of the commercial success of PUs can be attributed to the rich chemistry of the isocyanate. The electronegativity of the nitrogen and oxygen atoms serves to polarize the isocyanate functional group by pulling electron density away from the central carbon atom, leaving it susceptible to nucleophilic attack. In general, aromatic diisocyanates are typically more reactive than aliphatic diisocyanates. The isocyanate group is highly reactive toward nucleophiles, such as alcohols, amines, and thiols, and weaker nucleophiles such as water. Reaction between isocyanate and water yields an unstable carbamic acid linkage, which gives an amine upon loss of carbon dioxide. Amines then react with isocyanates to form urea linkages. The high reactivity of

isocyanates and the nucleophilicity of the reaction products, such as urethane and urea groups, make side reactions commonplace in polyurethane synthesis. The reaction of isocyanate with urea and urethane groups yields biuret and allophanate groups, respectively. In addition, isocyanates can undergo dimerization and trimerization to give uretidinedione and isocyanurate, respectively. In some cases, these side reactions are desirable to obtain different properties. For example, in the synthesis of rigid PU foams, a high concentration of isocyanurate resulting from isocyanate trimmers is needed to obtain higher cross-link densities. Step polyaddition polymerization of urethanes can be carried out in the bulk or in solution and is typically catalyzed by tertiary amines or organotin compounds.

Linear segmented polyurethanes are an incredibly versatile material. A typical two-step synthetic route to segmented PUs, as shown in Fig. 2, includes the polymerization of an oligomeric diol with a diisocyanate "capper," commonly referred to as the prepolymer method. The NCO-functionalized prepolymer is then reacted with a short-chain diol that acts as a chain extender. The result is a segmented block
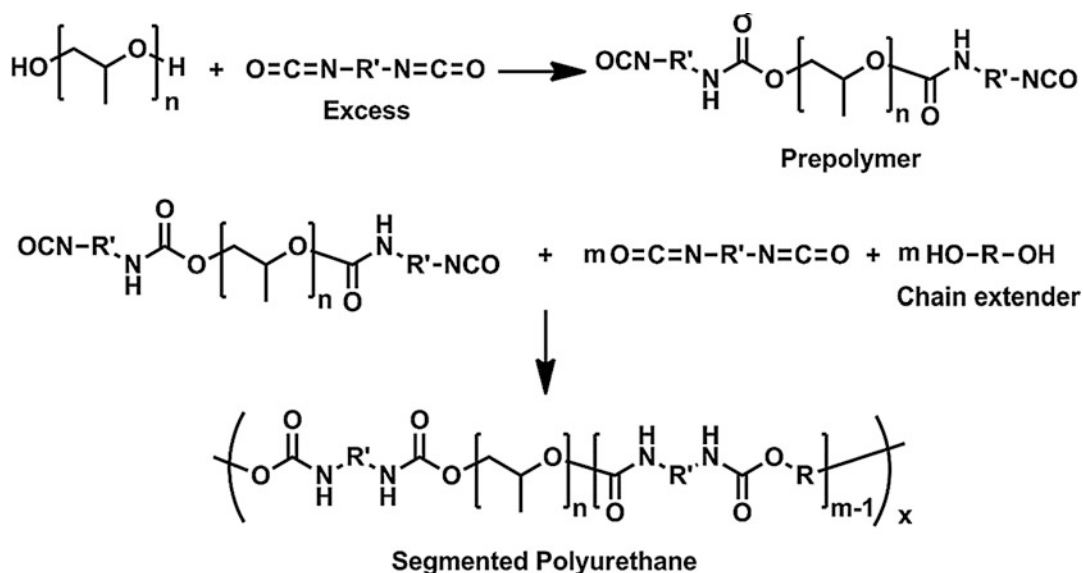
Step Polyaddition Polymerizations, an Overview, Fig. 2 General reaction scheme for the synthesis of segmented polyurethanes

copolymer usually consisting of a hard block (derived from the diisocyanate monomer) and a soft block (derived from the isocyanate capper diol prepolymer). The salient properties of segmented PUs can be attributed to the intermolecular hydrogen bonding between the urethane and urea groups, which also contributes to the crystallinity. The hydrogen-bonding interaction in urethane linkages is weaker than urea and amide groups; thus, PUs often have lower softening temperature than polyureas and polyamides. The prevalent hydrogen-bonding unit within the hard segment block gives rise to the high glass transition temperature (Tg) and the microphase separated morphology typically observed in segmented PUs. The extent of hydrogen bonding and morphology of the segmented PUs depend extensively on the choice of diol chain extender. Thermoplastic polyurethanes (TPUs) exploit strong hydrogen-bonding interactions to impart outstanding elastomeric properties.

Diels-Alder Cycloaddition

One of the most widely employed cycloaddition reactions in the context of step polyaddition polymerization is the Diels-Alder (DA) cycloaddition [6]. The DA reaction was first discovered in 1928 by Otto Diels and Kurt Alder. The DA reaction is a [4 + 2] cycloaddition reaction involving the reaction of a 4π electron 1,3-diene with a 2π electron dienophile to form a cyclohexene adduct. Dienes are typically activated by electron-donating groups (i.e., ether linkage in furan), while dienophiles are activated by electron-withdrawing groups (i.e., imide) [6].

Figure 3 shows an example of a highly utilized DA reaction involving a bisfuran (diene) and bismaleimide (dienophile) [7]. The step cycloaddition polymerization occurs at relatively low temperatures (~60 °C); however, molecular weight of the polymer can be limited by the retro-Diels-Alder reaction that takes place at higher temperatures (~100 °C) [7]. The temperature of the DA and retro-DA reaction and thus the stability of the polymer can be somewhat tuned by monomer substituents. The low retro-DA temperature makes the furan-maleimide DA reaction an ideal linkage in self-healing or recyclable polymers, where it has found much interest [7]. While DA cycloaddition polymerizations have not found much industrial utility, the polymeric products exhibit interesting structures, such as the fused-ring, ladder-type polymer resulting from DA polymerization of 2-vinyl-1,3-butadiene and quinone, as shown in Fig. 4. Ladder polymers are unique in that they tend to have high chemical, thermal, and mechanical stability making these structures attractive synthetic targets [8]. DA step cycloaddition polymerization enables a synthetically mild approach to generate near-perfect ladder structure polymers.

Thiol-Mediated Additions

Thiol-mediated reactions have generated great interest as a route for polymer synthesis, polymer network formation, and polymer modification [9–12]. Specifically, thiols readily react in an addition manner with electron-rich alkenes (radical-mediated), alkynes (radical-mediated), electron-poor alkenes (amine or phosphine-catalyzed), isocyanates (amine-catalyzed), and
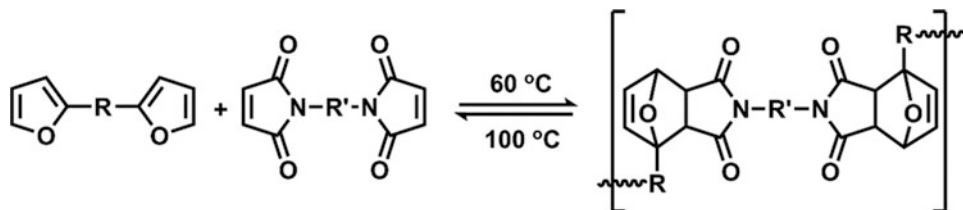
Step Polyaddition Polymerizations, an Overview, Fig. 3 Diels-Alder reaction of a diene, furan, with a dienophile, maleimide
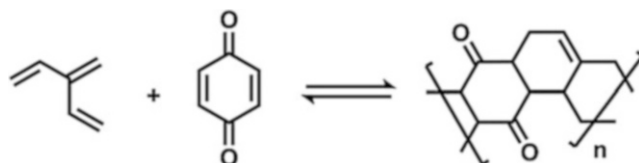
Step Polyaddition Polymerizations, an Overview, Fig. 4 Step-growth DA polymerization of 2-vinyl-1,3-butadiene and quinone to form a ladder polymer
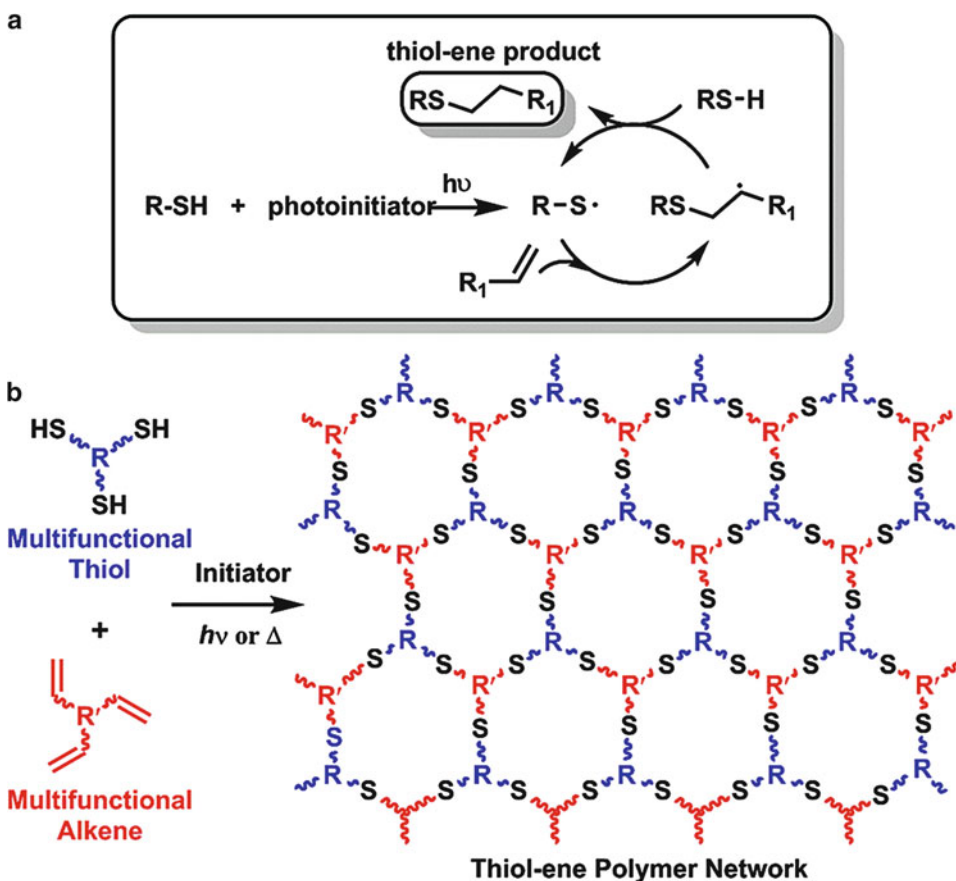
Step Polyaddition Polymerizations, an Overview, Fig. 5 Free-radical, step-growth thiol-ene polymerization mechanism and the resulting homogeneous network structure when polymerizing multifunctional thiol and alkene monomers

epoxies (amine-catalyzed S_N2 ring opening) resulting in a diverse set of reactions for polymer chemists. Thiol-mediated reactions are advantageous for polymer synthesis in that they proceed at room temperature with high efficiency and rapid kinetics, in the presence of oxygen/water, without expensive and potentially toxic catalysts, and are highly tolerant of a wide range of functional groups [10]. In the context of this overview, the discussion of thiol-ene will be limited to the radical-mediated hydrothiolation reaction for polymer and network synthesis. Radical-mediated hydrothiolation can be conducted under thermal initiation conditions; however, the reaction is most often induced using light. Under photochemical conditions, as shown in Fig. 5a,

the reaction proceeds via a radical step polyaddition mechanism – representing the only example when radical addition occurs in a step-growth manner. Overall, the process occurs with typical steps observed in chain processes with (i) initiation (homolytic cleavage of the thiol to generate a sulfur-centered radical), (ii) propagation (direct addition of the sulfur-centered radical across the alkene to give a carbon-centered radical followed by chain transfer to another thiol), and (iii) termination (radical-radical coupling). Consequently, molecular weight grows with typical step-growth kinetics, but with more rapid reaction rates [13].

While the thiol-ene reaction has been utilized for the synthesis of linear polythioethers, the reaction is more known for the synthesis of highly uniform polythioether networks using polyfunctional alkenes and thiols (Fig. 5b) [11]. The homogeneity of thiol-ene networks, in comparison to traditional polyacrylate networks, is a consequence of the step polyaddition process leading to delayed onset of gel formation. The homogenous network structure provides thermosets with very well-defined mechanical and thermomechanical properties that can be readily tuned by judicious choice of thiol and alkene monomers. Thiol-ene-based polymer networks have found use as optical adhesives, coatings, and as potential energy-dampening materials.

Summary

Step polyaddition polymerizations proceed via a series of stepwise addition reactions between bifunctional and polyfunctional monomers without the loss of a small-molecule byproduct, while following the general step-growth kinetic rate laws (i.e., molecular weight builds slowly with monomer conversion). Some of the most widely used polymer products of step polyaddition polymerizations include polyurethanes and Diels-Alder polymers. Contemporary step polyaddition reactions, such as the thiol-ene click reaction, are finding widespread use as synthetic routes to functional polymer materials. The library of step polyaddition polymerization continues to grow as these reactions continue to provide both unique and effective solutions to interdisciplinary materials problems.

Related Entries

▶ Chain-Growth Copolymerization (Overview)
▶ Polymer Synthesis via Click Reactions
▶ Polymerization Reactions (Overview)
▶ Polyurethane Synthesis

References

1. Carothers WH (1929) Studies on polymerization and ring formation I. An introduction to the general theory of condensation polymers. J Am Chem Soc 51(8):2548–2559
2. Odian G (2004) Principles of polymerization. Wiley, Hoboken
3. Braun D, Cherdron H, Ritter H (2001) Polymer synthesis: theory and practice, fundamentals, methods, experiments, 3rd edn. Springer, New York
4. Qin A, Lam JWY, Tang BZ (2010) Click polymerization. Chem Soc Rev 39(7):2522–2544. doi:10.1039/B909064A
5. Lyman DJ (1972) Polyurethanes – the chemistry of the diisocyanate-diol reaction. In: Solomon DH (ed) Step-growth polymerizations, vol 3. Marcel Dekker, New York, pp 95–156
6. Bailey WJ (1972) Diels-Alder polymerization. In: Solomon DH (ed) Step-growth polymerizations, vol 3. Marcel Dekker, New York, pp 279–332
7. Gandini A (2013) The furan/maleimide Diels–Alder reaction: a versatile click–unclick tool in macromolecular synthesis. Prog Polym Sci 38(1):1–29
8. Schlüter A-D (1991) Ladder polymers: the new generation. Adv Mater 3(6):282–291
9. Thiol-X Chemistries in Polymer and Materials Science (2013) Royal society of chemistry. Cambridge, Cambridge
10. Hoyle CE, Bowman CN (2010) Thiol-Ene click chemistry. Angew Chem Int Ed 49(9):1540–1573
11. Hoyle CE, Lee TY, Roper T (2004) Thiol-enes: chemistry of the past with promise for the future. J Polym Sci Part A-Polym Chem 42(21):5301–5338
12. Hoyle CE, Lowe AB, Bowman CN (2010) Thiol-click chemistry: a multifaceted toolbox for small molecule and polymer synthesis. Chem Soc Rev 39(4):1355–1387
13. Lowe AB (2010) Thiol-ene "click" reactions and recent applications in polymer and materials synthesis. Polym Chem 1(1):17–36

S

Stereocomplexed Polylactides

Marek Brzeziński and Tadeusz Biela
Department of Polymer Chemistry, Centre of
Molecular and Macromolecular Studies, Polish
Academy of Sciences, Lodz, Poland

Synonyms

PLA stereocomplex; Stereocomplex formation;
Stereocomplexation

Definition

Macromolecules of identical chemical composition but different configuration of repeating units are able to form an intermolecular complex called stereocomplex. Stereocomplex forms in the solid-state crystalline structure melting at higher temperature (T_m) than that of the homochiral components alone. Stereocomplexation or stereocomplex formation of polylactides (PLA) occurs due to non-covalent interactions of enantiomeric chains of poly(L-lactide) (PLLA) and poly(D-lactide) (PDLA).

Introduction

Macromolecules composed of repeating units with complementary attracting sites can form intermolecular complexes. Typical examples are provided by natural macromolecules such as polysaccharides, polypeptides, or nucleic acids. Taking a lesson from biology, synthetic polymer chemistry developed a variety of supramolecular systems in which complementary interactions lead to materials with enhanced physicochemical properties [1–3]. Macromolecules of identical chemical composition but different configuration of repeating units are also able to form intermolecular complexes called stereocomplexes [4]. Macromolecular stereocomplexes usually form crystalline structures melting at higher temperature (T_m) than

their homochiral components. Moreover, the PLLA/PDLA equimolar mixture is able to form stereocomplex, both from the melt and from the solution [5].

Microstructure of PLA Stereocomplex

PLAs have an asymmetric carbon atom in each lactate repeating unit, and depending on the monomer used in polymerization (L,L-lactide (L,L-LA), D,D-lactide (D,D-LA), racemic [1:1 (L,L)/(D,D)-lactide], or meso (L,D)-lactide (L,D-LA)), semicrystalline PLLA and PDLA or amorphous PDLLA polymers are obtained as it was shown in Fig. 1.

As it was discovered by Ikada and Tsuji in 1987, the intermolecular interactions of enantiomeric PLA chains of the opposite configuration PLLA and PDLA lead to the corresponding stereocomplex (sc-PLA) formation [5]. The minimum chain length for stereocomplex formation is seven lactyl units, whereas individual enantiomeric lactide oligomers crystallize at a degree of polymerization (DP) equal to 11. This difference is due to the different crystal structures of homopolymers and stereocomplexes. It has been reported that the crystals in the homopolymers of PLLA (or PDLA) have a 10_3 helix structure (called also α helix), whereas the stereocomplex forms a more compact 3_1 helix (called also β helix). Obviously, one of the lactyl end groups which is directly attached to initiator is not able to participate in the crystallite formation. As a result, 11 units (not 10) are required to form a 10_3 helix, and consequently, to form the 3_1 helix, seven lactyl residues are needed.

Initially, van der Waals interactions were suspected to be responsible for stereocomplex formation, but finally a weak hydrogen bonding: $-CH_3 \cdot \cdot \cdot \cdot \cdot O = C <$ and $\equiv CH \cdot \cdot \cdot \cdot \cdot O = C <$ between the PLLA/PDLA chains has been found to keep two PLA helical chains with the opposite configuration together (cf. Fig. 2). Assuming multicentric interactions (each $C = O$ is bonding to one $-CH_3$ and one $\equiv CH$ group), a tentative calculation results in a hydrogen-bonding enthalpy $\Delta H_f = 5.2$ kJ/mol

Stereocomplexed Polylactides, Fig. 1 Structures of stereoisomers of lactide and PLAs

L,L-LA → PLLA (isotatic)

D,D-LA → PDLA (isotatic)

meso-LA → PLDLA (syndiotatic)
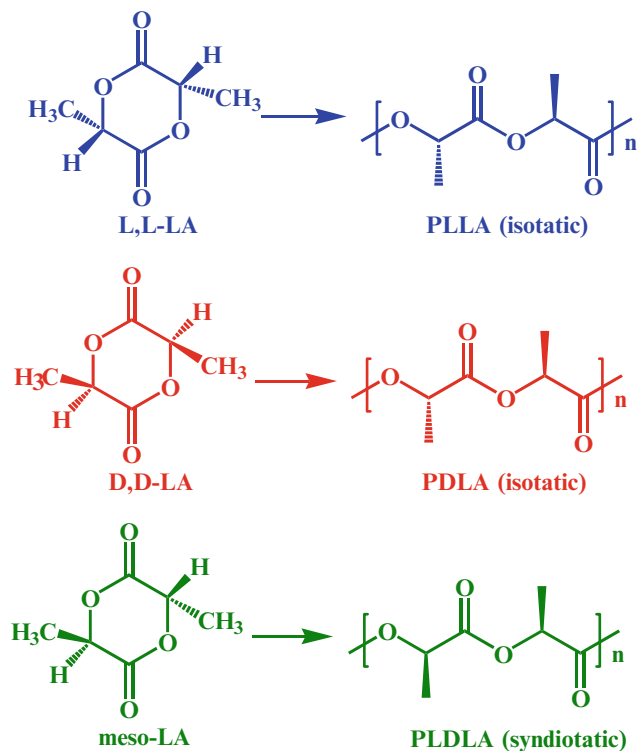
Stereocomplexed Polylactides, Fig. 2 PDLA (*top*) and PLLA (*bottom*) chains in parallel orientation, as located in the stereocomplex crystal. Hydrogen-bonding angles for the interactions suggested by FTIR are 120° and 150° for CR-H · · · O and CH$_3$ · · · O bonds, respectively, and hydrogen bond distance is about 2.9 Å (Reprinted with permission from Sarasua et al. [6]. Copyright (2005) American Chemical Society)
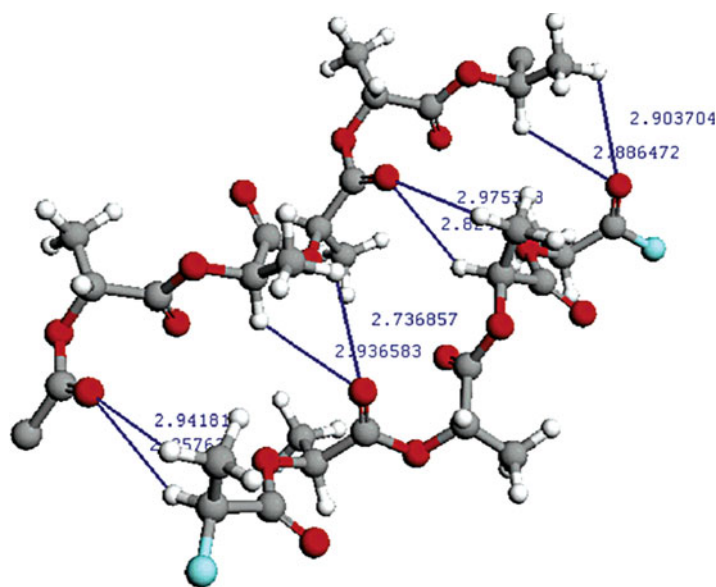
(1.2 kcal/mol). This value is also close to that obtained from ab initio calculations.

It should also be noted that two polylactide chains, because of its asymmetry, can interact in two manners: parallelly and antiparallelly. In the case of the linear sc-PLAs, both abovementioned types of geometry are possible, although according to Brizzolara et al.'s calculations [7],

interaction energy is higher for the parallelly oriented PLA helices.

Properties of PLA Stereocomplex

PLA, a biodegradable, biocompatible, nonvolatile, and odorless polymer, is classified as GRAS (generally recognized as safe) by the US Food and Drug Administration. However, in comparison with other commercial thermoplastics, it exhibits a low rate of crystallization and a relatively low melting temperature. Thus, the enhancement of the thermal stability of PLA is important to use this material in a various industrial applications [8]. Stereocomplexation seems to be one of the most important and relatively easy methods for improving the thermal properties of PLA.

Linear high molar mass ($M_n = 10^5$ g/mol) polylactide stereocomplexes are not able to survive melting to reform the stereocomplex crystallites, and after slow cooling from the melt, a mixture composed of homochiral crystallites and stereocomplex crystallites is formed. However, it has been shown that in the case of star-shaped high-molar-mass ($M_n \geq 10^5$) enantiomeric PLAs with more than six arms, the formation of the PLA stereocomplexes in the melt is complete and perfectly reversible, probably because of the "hardlock fruit"-type interactions (see Fig. 3).

The calculations giving the advantage of parallel interaction of PLLA and PDLA in the linear stereocomplexes, as mentioned above, may not apply to the star-shaped structures. In the star-shaped sc-PLA, chains may predominantly interact in the antiparallel geometry because of the better fitting of the complementary chains in this orientation [9]. The steric hindrance of the star cores crowded together rather excludes the parallel arm interactions as shown in Fig. 3.

However, the successful preparation of thermally stable stereocomplexes based on the linear high-molar-mass polylactides is still a strategic target. Recently, it has been found that covalently modified multi-walled carbon nanotubes (MWCNTs) can be used as initiators in the ring-opening polymerization of L- and D-lactides to
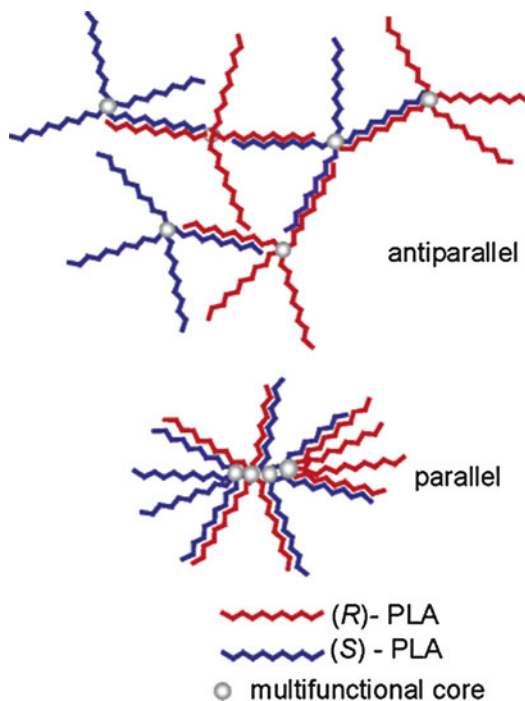
Stereocomplexed Polylactides, Fig. 3 Schematic structure of parallel and antiparallel PLA stereocomplexes of the star-shaped macromolecules ((R)-PLA corresponding to D-PLA and (S)-PLA to L-PLA) (Reprinted with permission from Biela [9]. Copyright (2006) American Chemical Society)

induce efficient dispersion of the MWCNTs in the PLA matrix. Moreover, the thermal properties of the prepared PLA/MWCNTs composites and the thermal stability of their stereocomplexes are highly enhanced. Furthermore, Purnama et al. proposed preparation of bio-stereocomplex nanocomposites with cellulose nanowhiskers (CNW). The sc-PLA-CNW materials exhibit excellent stereocomplex memory and are able to reform perfect sc-PLA crystallites after melting [10]. The ability to readily obtain the PLA stereocomplex with improved physicochemical properties such as thermal and mechanical properties is very important for their mass applications [11].

The combined effect of the influence of the nature of polylactide end groups and PLA architecture on the morphology and properties of stereocomplexes has also been extensively investigated. It has been shown that for
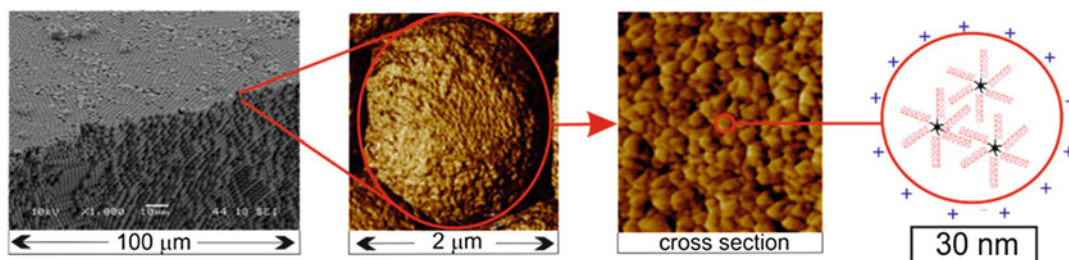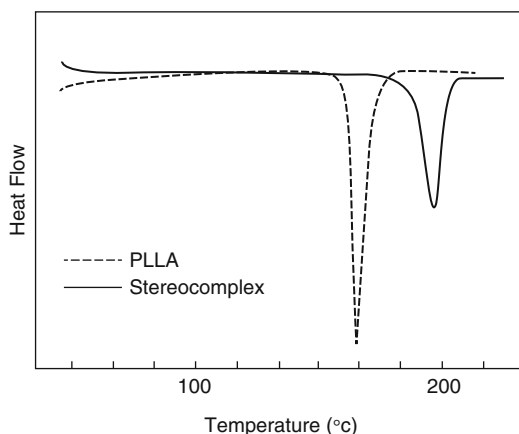
Stereocomplexed Polylactides, Fig. 4 Hierarchical structure of stereocomplex microspheres colloidal crystal (Reprinted with permission from Brzeziński et al. [12]. Copyright (2014) Wiley)

stereocomplexes of low-molecular-weight enantiomeric PLLA and PDLA, the nature of end groups can affect the morphology of stereocomplex particles precipitating from an organic solvent. Stereocomplex of PLLA/PDLA terminated with imidazolium ionic liquid derivative (PLA-IL) precipitated from 1,4-dioxane in the form of uniform microspheres. Stereocomplexation of star-shaped PLLA and linear PDLA functionalized with imidazolium ionic end groups in 1,4-dioxane leads to the formation of uniform microspheres which crystallize in the form of colloidal crystals. Analysis, using scanning electron microscopy (SEM) and atomic force microscopy (AFM), shows the interesting hierarchical structure of the system, starting from the nanometrical grains composed of few stereocomplex macromolecules that aggregate in uniform microspheres, ending with formation of colloidal crystals of microspheres as it is shown in Fig. 4.

Main Analytical Methods of sc-PLA Analysis

The formation of stereocomplex may be observed using different analytical methods, namely, differential scanning calorimetry (DSC), attenuated total reflectance Fourier transform infrared analysis (ATR FTIR), wide-angle X-ray scattering (WAXS), and cross-polarization/magic-angle spinning ^{13}C nuclear magnetic resonance (CP/MAS ^{13}CNMR).

The melting temperature of sc-PLA is higher than its enantiomeric components, and therefore,

Stereocomplexed Polylactides, Fig. 5 Typical DSC curves of PLLA (*dotted line*) and sc-PLA (*solid line*) (Reprinted with permission from Fukushima and Kimura [13]. Copyright (2014) Wiley)

DSC analysis can be used as a method to confirm stereocomplexation. DSC thermograms of the sc-PLA and one of its enantiomeric component are shown in Fig. 5. It should be mentioned that melting temperature of the enantiomeric components (PLLA or PDLA) is ~50 °C lower than that one of the stereocomplex. In the DSC thermogram of sc-PLA, one melting peak appeared at 223 °C. It means that the crystalline fraction of this material contains stereocomplex crystallites only.

A very useful and fast method to observe the stereocomplexation is also infrared analysis (ATR-FTIR). The significant changes in the conformation of PLA chains have been directly observed during this process. The α helix (wave number 921 cm^{-1}) which is characteristic for
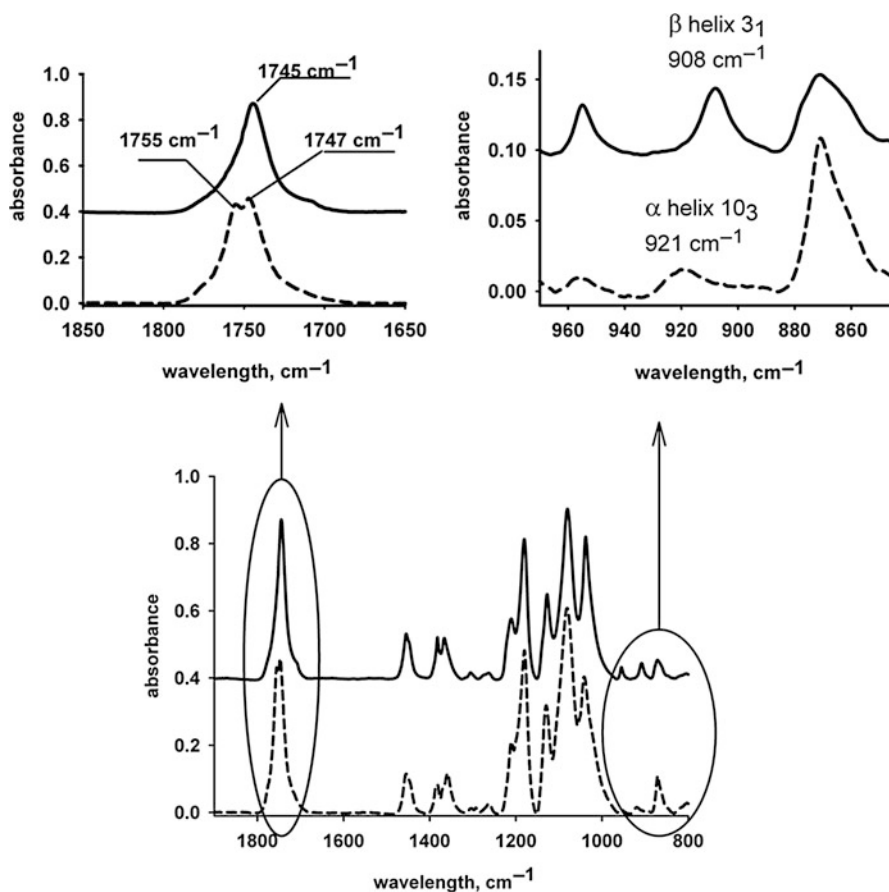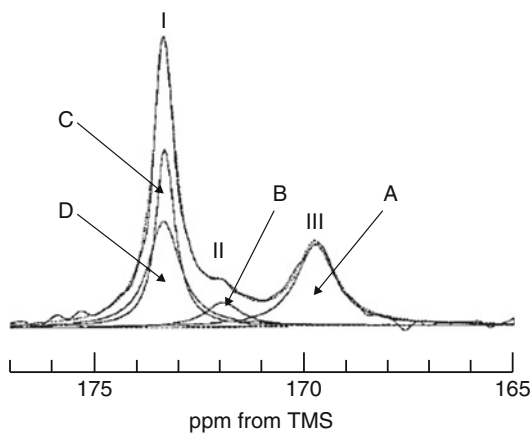
Stereocomplexed Polylactides, Fig. 6 The ATR-FTIR spectra of enantiomeric PLLA (*dashed line*) and stereocomplex sc-PLA (*solid line*) (Reprinted with permission from Brzeziński et al. [12]. Copyright (2014) Wiley)

both PLLA and PDLA enantiomers is transformed into the more compact β helix (wave number 908 cm^{-1}) of the stereocomplex, and a new band at 1,748 cm^{-1} also appears. In Fig. 6, the ATR-FTIR spectrum of the PLA stereocomplex compared with the spectrum of the PLLA enantiomer is shown. Regions of wavelength in which characteristic changes were observed at 1,700–1,800 cm^{-1} and at 970–850 cm^{-1} (stretching vibration of C = O group and skeletal stretching vibration of α and β helixes, respectively) are enlarged.

High-resolution solid-state CP/MAS ^{13}C NMR spectroscopy is also an effective method for tracing PLA stereocomplexation. The range of chemical shifts characteristic for the carbonyl

carbon atom (165–175 ppm δ) is particularly diagnostic. In ^{13}C NMR spectra (Fig. 7), the rigid stereocomplex crystalline component (C and D in line I) should give a signal at 173.3 ppm, because line I is not observed for the crystallized nonblended PDLA and PLLA precipitates. It can be assumed that the disordered stereocomplex crystalline component may also partly contribute to this peak. The amorphous component should give a peak at 169.7 ppm, whereas if the homocrystalline component B corresponds to line II (i.e., crystallites of individual enantiomeric macromolecules) is present, it should give a signal at 172 ppm because it has a very similar chemical shift to that one of precipitates of the nonblended PDLA or PLLA. In the

Stereocomplexed Polylactides, Fig. 7 Analysis of components *A–D* in resonance lines *I–III* for the total ^{13}C NMR spectrum of carbonyl carbon in the stereocomplex precipitate: *A* noncrystalline (amorphous) component (169.7 ppm); *B* homocrystalline component (172.0 ppm); *C* rigid stereocomplex crystalline component (173.3 ppm); *D* disordered stereocomplex crystalline component (173.3 ppm) (Reprinted with permission from Tsuji [5]. Copyright (2014) Wiley)

Stereocomplexed Polylactides, Fig. 8 WAXS profiles of equimolar blend of PLLA/PDLA and pure PLLA, respectively (Reprinted with permission from Fukushima and Kimura [13]. Copyright (2014) Wiley)

spectrum of PLA stereocomplex, the shoulder in the 169–172 ppm region (component A in line III) is clearly visible, indicating the contribution of the amorphous phase. Those results could be confirmed with the results from DSC analysis.

The supplementary examination confirming the formation of a stereocomplex is the WAXS analysis, which, like ATR-FTIR method, is clear and useful but time-consuming.

In the Fig. 8, the WAXS profiles of the PLA stereocomplex and one of its enantiomeric components are shown. The main peaks of PLLA and PDLA film that appear at 2θ values of 15, 17, and 19° are related to the α form of both enantiomeric PLAs, crystallized in a pseudo-orthorhombic unit cell of dimensions: a = 1.07 nm, b = 0.595 nm, and c = 2.78 nm, which contains two 10_3 helices. The most intense peaks of equimolar blend of PLLA/PDLA are observed at 2θ values of 12, 21, and 24°. These peaks are ascribed to the PLA stereocomplex crystallized in a triclinic unit cell of dimensions – a = 0.916 nm, b = 0.916 nm, and c = 0.870 nm – in which L-lactyl and D-lactyl unit sequences are packed

parallel taking 3_1 helical conformation (called also β helix). The lattice containing a PLLA or PDLA chain with a 3_1 helical conformation has the shape of an equilateral triangle, which is expected to form equilateral-triangle-shaped single crystals of the PLA stereocomplex.

Furthermore, Brizzolara et al. [7] compared the WAXS profiles from actual stereocomplexed specimens with a force-field simulated stereocomplex. They also proposed the growth mechanism of the stereocomplex equilateral-triangle-shaped single crystal.

Application of PLA Stereocomplex

PLA-based materials have been used mostly for short-time applications from drug carriers and implants to packaging and textiles [14]. However, poor mechanical and thermal properties of PLA exclude its use as an ordinary structural material. Stereocomplexation improves these properties and thus broaden the possible application of PLA-based materials.

S

The crucial issue for stereocomplex PLA-based materials is production costs of both L- and D-lactide acid, the main raw materials for the production of LA monomers. The L-lactide acid has been widely used as a food additive, and it is produced in the industrial scale. The discovery of sc-PLA caused the increase attention in the manufacturing technology of the D-lactide acid. Therefore, the reduction of D-lactide acid costs will solve, at least partially, the problem of producing sc-PLA materials on large scale and serve as an alternative for commercial polymeric materials.

Sc-PLA-based materials are already used in biomedicine as drug delivery systems (DDS) and hydrogels. Biodegradable stereocomplex-based microspheres and micelles are proposed for the transportation and delivery of biologically active agents. Stereocomplex self-assemblies exhibit strong thermodynamic and kinetic stability and slower drug release. Hydrogels are prepared from block and graft copolymers with hydrophilic segments and L- and D-lactide unit sequences.

Stereocomplex crystallites can act as nucleation agents for pure PLA crystallization. Moreover, narrowly dispersed stereocomplex nanocrystals are proposed for the all-poly(lactide acid) nanocomposites. Small size and high aspect ratio of nano-reinforcing agents will dramatically improve thermal and mechanical properties of PLA nanocomposite material. The same composition of the nanofiller and the matrix prevents from their incompatibility and increases their potential recyclability.

Sc-PLA could find higher applications in automotive, communication, and electronic industries. Sc-PLA is suitable for making fibers, films, rods, and other processed plastics [4]. Thermally stable sc-PLA fibers could be used for manufacturing woven and knitted products. On the other hand, sc-PLA films have found the application as optically transparent heat-resistant insulators. Moreover, PLA stereocomplex materials could have potential in single-use microwave applications. In the near future, sc-PLA will provide many applications as bio-based sustainable materials, for example, as "green" notebooks, cell phones, or panels for DVD drivers.

Nowadays, three companies produce bioplastics based on sc-PLA: Corbion Purac, Teijin, and Hycail. Teijin and Hyacil produce sc-PLA on the industrial scale and begin to apply sc-PLA for packaging, civil engineering and construction, and oil fields (the drilling phase in shale gas extraction, etc.). Corbion Purac prepares highly heat-resistant sc-PLA materials that can withstand temperatures up to 180 °C/ 356 °F. PURALACT® is ideal for bio-based beverage cups for hot drinks such as coffee, soup, hot chocolate, tea, etc.

Conclusions and Perspectives

Crystallization of the polylactide stereocomplex crystalline structure resulted in an increase of melting temperature of about 50 °C with respect to that obtained in homocrystalline samples as it was detected in DSC analysis. The WAXS profiles of stereocomplexed PLA revealed a more compact crystalline structure, and FTIR results provided new bands at 1,748 cm^{-1} (stretching vibration of C = O) and 908 cm^{-1} (skeletal stretching vibration), attributed to crystalline polylactide chains in the 3_1 helical conformation (called β helix). In addition, the spectral bands attributed to the interlamellar material indicate a truly amorphous phase, in contrast to the semi-ordered interphase found during crystallization of PLLA. Hence, crystallization mechanisms of PLLA and the stereocomplex revealed differences.

The thermal and mechanical properties of sc-PLA are similar to other bio-based polymers as it was shown in Table 1. The sc-PLA exhibits better thermal and mechanical properties even for not fully stereocomplexed materials (containing a certain amount of homocrystallites) formed using high-molecular-mass enantiomeric polymers. However, the usage of PLA nanocomposites paves the way for future stereocomplex products with excellent stereocomplex memory. Along with its heat resistance, sc-PLA has many other

Stereocomplexed Polylactides, Table 1 Mechanical and thermal properties of the representative bio-based polymers (Copyright (2010) Wiley)

	PLLA	sc-PLA	PGA	PHB
T_m (°C)	170–190	220–240	225–230	188–197
T_g (°C)	50–65	65–72	40	5
ΔH_m (J/g)	93–203	142–155	180–207	146
Density (g/cm^3)	1.25–1.30	1.21–1.342	1.50–1.69	1.18–1.26
Tensile strength (MPa)	120–2260	880	80–980	180–200
Young's modulus (GPa)	6.9–9.8	8.6	3.9–14	4.9–5.9
Elongation at break (%)	12–26	30	30–40	50–70

PGA poly(glycolic acid), *PHB* poly(3-hydroxybutyrate)

properties, including crystallinity, chemical resistance, transparency, and gas permeability, making it suitable for use as an engineering plastic material. The application of sc-PLA products has just started to replace conventional oil-based polymers and should have high potential as sustainable structural materials to make fibers, films, rods, and other processed plastics. Particularly, sc-PLA fibers show high thermal stability and can be subjected to dyeing and hot pressing by ordinary techniques. It has already been confirmed that a knit of sc-PLA withstands laundering above 180 °C. Because of its incombustible nature, sc-PLA could be potentially applied in housing of various electric appliances and automobile parts. Since both PLLA and PDLA are already commercially available and their market prices are gradually falling, stereocomplex manufacturing in the near future can be profitable. It is likely that soon, wide industrial applications of these materials will be possible.

References

1. Lehn J-M (1995) Supramolecular chemistry. VCH, Weinheim
2. Harada A (2012) Supramolecular polymer chemistry. Wiley, Weinheim
3. Ciferri A (2005) Supramolecular polymers. Taylor and Francis, New York/Basel
4 Hirata M, Kimura Y (2011) Structure and properties of stereocomplex-type poly(lactic acid). In: Auras RA, Lim L-T, Selke SEM, Tsuji H (eds) Poly(lactid) acid, vol 5. Wiley, Hoboken, p 528
5. Tsuji H (2005) Poly(lactide) stereocomplexes: formation, structure, properties, degradation, and applications. Macromol Biosci 5:560–597
6. Sarasua JR, Rodríguez NP, Arraiza LP, Meaurio E (2005) Stereoselective crystallization and specific interactions in polylactides. Macromolecules 38: 8362–8371
7. Brizzolara D, Cantow H-J, Diederichs K, Keller E, Domb AJ (1996) Mechanism of the stereocomplex formation between enantiomeric poly(lactide)s. Macromolecules 29:191–197
8. Tsuji H (2013) Poly(lactic acid). In: Kabasci S (ed) Bio-based plastics: materials and applications, vol 8. Wiley, Chichester, pp 171–240
9. Biela T, Duda A, Penczek S (2006) Enhanced melt stability of star-shaped stereocomplexes as compared with linear stereocomplexes. Macromolecules 39: 3710–3713
10. Purnama P, Kim SH (2014) Bio-based composite of stereocomplex polylactide and cellulose nanowhiskers. Polym Degrad Stab. doi:10.1016/j. polymdegradstab.2014.01.004
11. Brzeziński M, Biela T (2014) Polylactide nanocomposites with functionalized carbon nanotubes and their stereocomplexes: a focused review. Mater Lett 121:244–250
12. Brzeziński M, Biedroń T, Tracz A, Kubisa P, Biela T (2014) Spontaneous formation of colloidal crystals of PLA stereocomplex microspheres and their hierarchical structure. Macromol Chem Phys 215:27–31
13. Fukushima K, Kimura Y (2006) Stereocomplexed polylactides (Neo-PLA) as high-performance bio-based polymers: their formation, properties, and application. Polym Int 55:626–642
14. Raquez J-M, Mincheva R, Coulembier O, Dubois P (2012) Ring-opening polymerization of cyclic esters: industrial synthesis, properties, applications, and perspectives. In: Matyjaszewski K, Möller M (eds) Polymer science: a comprehensive reference, vol 4. Elsevier, Amsterdam/Oxford/Waltham, p 761

S

Stereospecific Polymerization

Tomohiro Hirano[1] and Takehiro Kitaura[2]
[1]Department of Chemical Science and
Technology, Institute of Technology and
Science, The University of Tokushima,
Tokushima, Japan
[2]Division of Chemistry, Graduate School of
Engineering Science, Osaka University,
Toyonaka, Osaka, Japan

Synonyms

Stereoselective polymerization

Definition

IUPAC recommendations have defined stereo-specific polymerization and related terms as follows [1–3]: "Stereospecific polymerization is polymerization in which a tactic polymer is formed. Tactic polymer is composed of tactic macromolecules. A tactic macromolecule is a regular macromolecule, in which essentially all the configurational repeating units are identical. A configurational repeating unit having defined configuration at all sites of stereoisomerism in the main chain is a stereorepeating unit. Stereoregular polymer is composed of stereoregular macromolecule that is a regular macromolecule essentially comprising only one species of stereorepeating unit. A stereoregular polymer is always a tactic polymer, but a tactic polymer is not always stereoregular because a tactic polymer need not have all sites of stereoisomerism defined." Consequently, stereospecific polymerization definitely includes polymerization in which a stereoregular polymer is formed.

Historical Background

With one preceding finding of stereoregular poly (vinyl ether) by Schildknecht in 1947, the field of stereospecific polymerization actually came into existence when Ziegler and Natta in the early 1950s developed new polymerization systems which exhibited unique stereoregulating powers in olefin polymerization [4, 5]. Tacticity determination of vinyl polymers by ^{1}H NMR was first achieved for poly(methyl methacrylate) (PMMA) by Bovey and Tiers, Nishioka et al., and Johnsen in the beginning of the 1960s, independently [6]. The NMR spectroscopic evidence is still the absolute measure of the stereochemical configuration of polymers. Thus, the field of stereospecific polymerization has been developing along with the progress of the NMR spectroscopy.

Vinyl Polymerization

α-Substituted and α, α-Disubstituted Vinyl Monomers

Definition of Tacticity
In polymers from α-substituted vinyl monomers $CH_2 = CH\text{-}X$ or α, α-disubstituted vinyl (vinylidene) monomers $CH_2 = CXY$, the main-chain carbons having substituent group(s) are termed "pseudo-asymmetric" since, if the chain ends are disregarded, such carbons do not have the four different substituents necessary to qualify for being truly asymmetric. Nevertheless, they have the possibility of relative handedness [4, 5, 7–10]. The simplest regular arrangements along a polymer chain are the isotactic (*it-*) stereostructure, in which all the substituents are located on the same side of the zigzag plane repeating the chain stretched out in an all-trans conformation. The structure is often represented by a "rotated Fischer projection" in which the main-chain skeleton is represented by a horizontal line (Fig. 1).

Another regular arrangement is the syndiotactic (*st-*) structure, in which the groups alternate from side to side and thus the configurations of the neighboring units are opposite (Fig. 1).

The smallest unit representing relative configuration of the consecutive monomeric units is termed a diad (or dyad in old literatures) (Fig. 2).

For a vinyl polymer, two types of diads should be considered, which are designated as meso (*m*)

Stereospecific
Polymerization,
Fig. 1 Zigzag chain
depiction and rotated
Fischer projection of
stereoregular vinyl
polymers

Isotactic polymer

(Rotated Fischer projection)

Syndiotactic polymer

(Rotated Fischer projection)

meso (m)
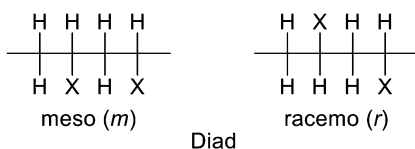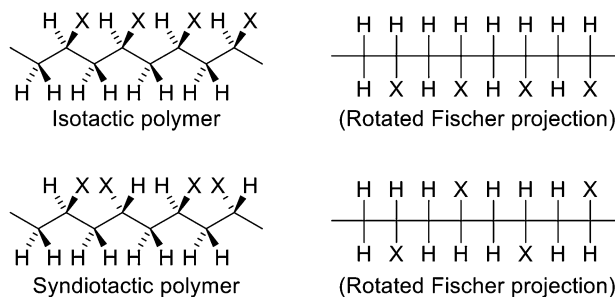
racemo (r)

Diad

Stereospecific Polymerization, Fig. 2 Diad stereoisomerism

and racemo (r). Using these notations, a sequence in an *it*-polymer can be represented as –*mmmmmm*– and that in an *st*-polymer as –*rrrrrr*–. In reality, however, purely isotactic or syndiotactic polymers are rarely obtainable, but the extent of regularity is always the question to be analyzed. "Tacticity" is the term used for defining such stereochemical features of polymers. The term "tacticity" is defined as "The orderliness of the succession of configurational repeating units in the main chain of a regular macromolecule, a regular oligomer molecule, a regular block or a regular chain."

By extending the notation of *m* and *r*, one can define relative configurations for the longer monomeric units along the polymer chain as triad, tetrad, and so on (*n*-ad in general). Figure 3 shows three possible triads, represented by *mm*, *rr*, and *mr* (*rm* triad is the same as *mr* triad in vinyl polymers and therefore not shown), which are also named isotactic, syndiotactic, and heterotactic triads, respectively. Similarly, for tetrad, the following six distinguishable sequences are possible: *mmm*, *mmr*, *rmr*, *rrr*, *rrm*, and *mrm*.

Isotactic Specific Polymerization
As described in the historical background, the field of stereospecific polymerization was actually opened by the findings of Ziegler-Natta

catalysis for *it*-specific olefin polymerization [4]. Although the industrial importance of the heterogeneous Ziegler-Natta catalysis has not been decreased to date, understandings of mechanistic aspects and thus rational catalyst design for stereostructure control have been developed drastically in the homogeneous system catalyzed by structurally defined, so-called single-site organometallic catalysts, such as metallocenes and related complexes.

In 1983, metallocenes such as **1** (Fig. 4) were reported as catalysts for rapid propylene polymerization, combined with methylaluminoxane (MAO). Stereoregularity of the obtained polymer was atactic. However, inspired by this discovery, polymers of a wide range of stereoregularities have been prepared with properly designed catalysts since then [9, 10].

One of the fundamental requirements for the stereospecific polymerization catalyst is recognition of monomer enantioface to control absolute configuration of emerging chiral carbons at growing chain ends. For instance, upon activation with MAO, two active sites of C_2 symmetric *ansa*-metallocenes (the term "*ansa*" is Greek for "handle," that is, "bridging" of two cyclopentadienyl groups in the complex) are both chiral and equivalent (homotopic) and enantioselective for the same monomer enantioface, leading to *it*-specific polymerization of propylene (Fig. 5).

Besides the C_2 *ansa*-metallocenes, C_1 symmetric one can also perform *it*-specific polymerization by the site-epimerization mechanism, which virtually prohibits availability of one of two sites (Fig. 6).

it-Polystyrenes are obtainable by heterogeneous Ziegler-Natta catalysis. Recent progress

S
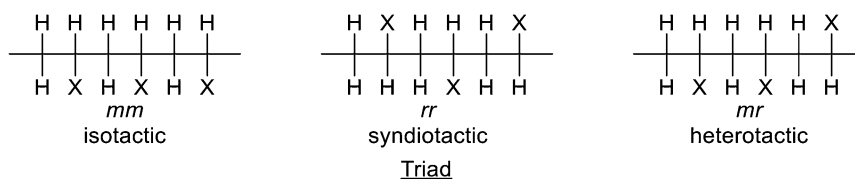
Stereospecific Polymerization, Fig. 3 Triad stereoisomerism

M = Zr, Hf, Ti etc.
X = alkyl, halogen etc.

1
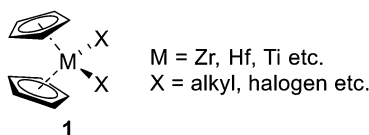
Stereospecific Polymerization, Fig. 4 Metallocenes

of homogeneous systems has enabled *it*-specific styrene polymerization catalyzed by the soluble complexes as shown in Fig. 7, as well as some C_2 *ansa*-zirconocenes.

Methacrylate is one of the most extensively studied classes of vinyl monomers, in regard to the stereoregularity of the obtained polymers. Methacrylates can be polymerized by the variety of polymerization systems including radical, anionic, and organometallic catalysis. The stereoregularity is a function of monomer structure, initiator, solvent, temperature, and so on.

Anionic polymerization of methacrylates with proper selection of the conditions allows preparation of a wide variety of stereoregular polymethacrylates [5]. Even at the beginning days of the stereospecific polymerization, the stereospecificity of the anionic polymerization of MMA was known to be strongly influenced by the solvent polarity; polar THF gave PMMA rich in syndiotactic, whereas nonpolar toluene produced isotactic-rich one. In the 1980s, highly *it*-specific anionic polymerization of MMA initiated with *t*-butylmagnesium bromide (t-C_4H_9MgBr/MgBr$_2$) was reported (Fig. 8). The polymerization proceeds in a living manner without side reactions and gives a highly isotactic polymer (*mm* > 95 %) with narrow molecular weight distribution (MWD).

Recently, a better control of tacticity has been realized by using combined anionic initiators comprised of a lithium ester enolate and a large

excess of lithium trimethylsilanolate (Me$_3$SiOLi) (Fig. 8). The system afforded highly isotactic PMMA, whose isotacticity reached *mm* of 98.9 %, at −95 °C.

The C_2 symmetric zirconocene-based complexes such as **2** (Fig. 9) combined with R$_2$Zn/Ph$_3$CB(C$_6$F$_5$)$_4$ also induced highly *it*-specific polymerization of MMA. Ester enolate type of zirconocene complex **3** (Fig. 9) formed *it*-PMMA (*mm* = 96.7 %) with fairly narrow MWD at ambient temperature.

Methacrylates with extremely bulky ester group such as triphenylmethyl methacrylate **4** (Fig. 10) give highly isotactic polymers with anionic polymerization and even radical one. The high stereospecificity was most probably derived from the sterically demanded "helical" conformations of the forming polymer chains by the bulky pendant groups (Fig. 11). The bulkiness-driven *it*-specificity was also observed in the radical polymerization of *N*-triphenylmethylmethacrylamide **5** (Fig. 10).

Stereoregulation in radical polymerization has been drastically developed in recent years [7]. For instance, addition of lanthanide Lewis acids such as Yb(OTf)$_3$, Lu(OTf)$_3$, and Sc(OTf)$_3$ induced *it*-specific radical polymerization of *N*-isopropylacrylamide (NIPAAm) (*m* = 92 %, with Yb(OTf)$_3$, in MeOH at −20 °C).

Vinyl ethers can be polymerized by cationic initiators; however, a limited number of reports on highly stereospecific cationic polymerization have been presented [8]. Cationic polymerization of *tert*-butyl vinyl ether with BF$_3$-based initiators in toluene gave *it*-polymer (*mm* = 79 %), which can readily be converted to *it*-poly(vinyl alcohol). *it*-Specific polymerization of less bulky isobutyl vinyl ether was reported by using a titanium complex [TiCl$_2$(OAr)$_2$, *m* = 90 %] or FeSO$_4$/*tert*-BuOH (*m* = 83 %).

P : Growing polymer chain end
□: Monomer coordination site
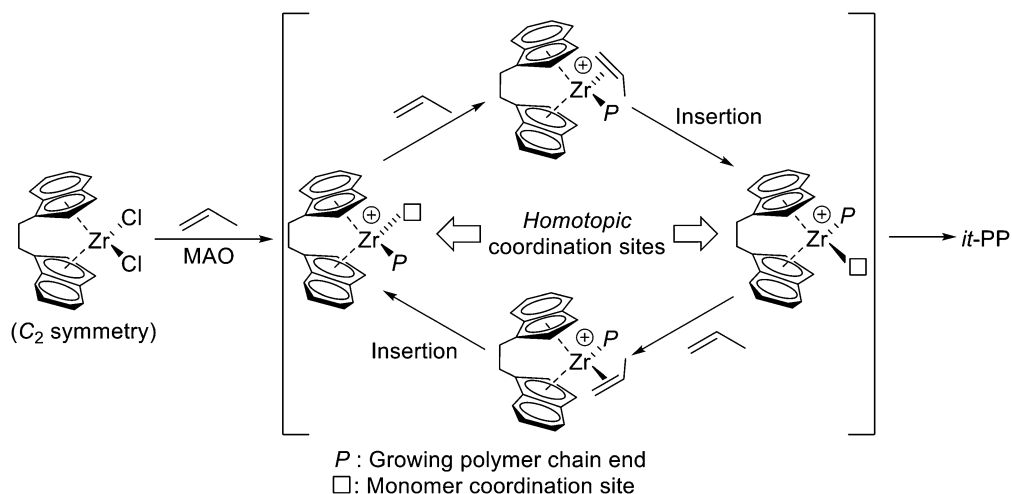
Stereospecific Polymerization, Fig. 5 *it*-Specific polymerization of propylene with C_2 symmetric *ansa*-zirconocene

Diastereotopic coordination sites
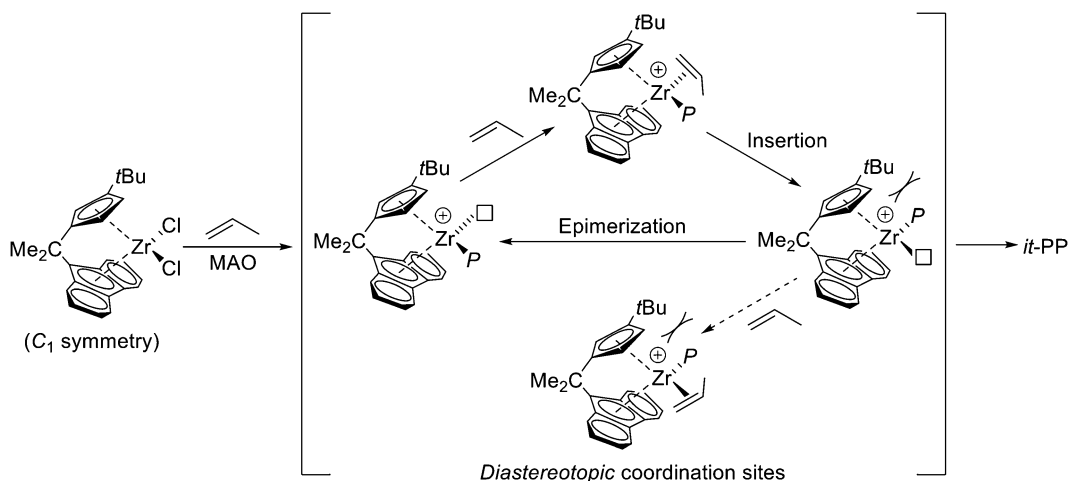
Stereospecific Polymerization, Fig. 6 *it*-Specific polymerization of propylene with C_1 symmetric *ansa*-zirconocene

S
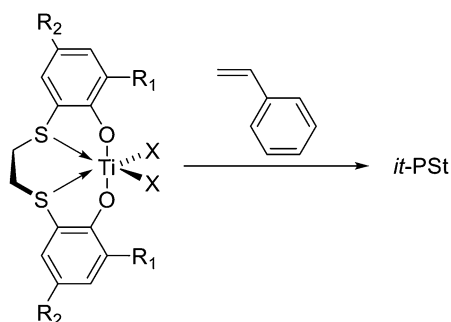
Stereospecific Polymerization, Fig. 7 *it*-Specific polymerization of styrene with a homogeneous catalyst

Syndiotactic-Specific Polymerization

In contrast to the *it*-specific propylene polymerization with C_2 *ansa*-metallocenes, *C*s symmetry of the catalyst can induce *st*-specificity, where two enantiotopic coordinating sites are alternately available during the polymerization process [9, 10]. Actually, *C*s symmetric zirconocenes performed high syndiotactic specificity in propylene polymerization (Fig. 12).

The *st*-specific polymerization of styrene was also realized by homogeneous catalysts, such as half-titanocene **6** (Fig. 13), combined with MAO.

Highly syndiotactic living anionic polymerization of MMA is realized by the use of combinations of t-C_4H_9Li and R_3Al in toluene at $-78\ °C$ [5]. The polymerization by t-C_4H_9Li alone gives an isotactic-rich polymer with broad MWD. When R_3Al such as $(n$-$C_4H_9)_3Al$ was added with the ratio of Al/Li $\geq$ 3, the syndiotacticities were around 90 % and the Mn values were close to those calculated from the amounts of t-C_4H_9Li. A bulky methacrylate, trimethylsilyl methacrylate (TMSMA) afforded highly syndiotactic polymers when polymerized with t-C_4H_9Li/bulky aluminum phenoxide **7** (Fig. 14) in toluene at low temperatures. The polymer obtained at $-95\ °C$ was 98 % syndiotactic in triad.

Organolanthanides such as **8** (Fig. 15) gave highly syndiotactic PMMA (rr = 95.3 %) with narrow MWD (M_w/M_n = 1.05). Eight-membered, MMA-dimerized species **9** (Fig. 15) was isolated, which was assumed to be a model of the active species.

Recently, some polar solvents have been recognized as good reaction media for effective stereoregulation in radical polymerization [7]. They can strongly interact with polar groups of monomers and propagating chain ends through hydrogen bonding. Fluorinated alcohol, which can act as a strong hydrogen donor, is one of the intensively studied categories of such solvents. Radical polymerization of vinyl acetate in **10** (Fig. 16) gave st-polymers [r = 73 % ($-78\ °C$), r = 62 % (20 °C)]. Syntheses of highly stereoregular PMMA in **11** (Fig. 16) (r = 88 %, 20 °C) and poly(N-methylmethacrylamide) in **12** (Fig. 16) (r = 98 %, $-78\ °C$) were reported. The stereospecificity was assumed to be derived from electrostatic repulsions between fluorinated alcohols hydrogen-bonding to polar groups (typically, carbonyl groups) at the propagating chain ends and the incoming monomers (Fig. 17).

Lewis basic solvents, or hydrogen acceptors, can also interact with monomers having hydrogen-donating groups to exert stereoregulation. Radical polymerization of 2-hydroxyethyl methacrylate in N,N-dimethylformamide gave st-polymers [r = 88 % (20 °C)], whereas st-polyNIPAAm was synthesized in hexamethylphosphoramide/toluene [r = 72 % ($-60\ °C$)].

Heterotactic-Specific Polymerization
The stereostructure of heterotactic (ht-) polymer is depicted as an ht-PMMA in Fig. 18.

ht-Specific polymerization requires higher-order stereoregulation than it- and st-specific ones, since m-addition and r-addition have to take place in an alternate manner. In fact, there have been a limited number of reports on the formation of highly ht-homopolymers by vinyl polymerization.
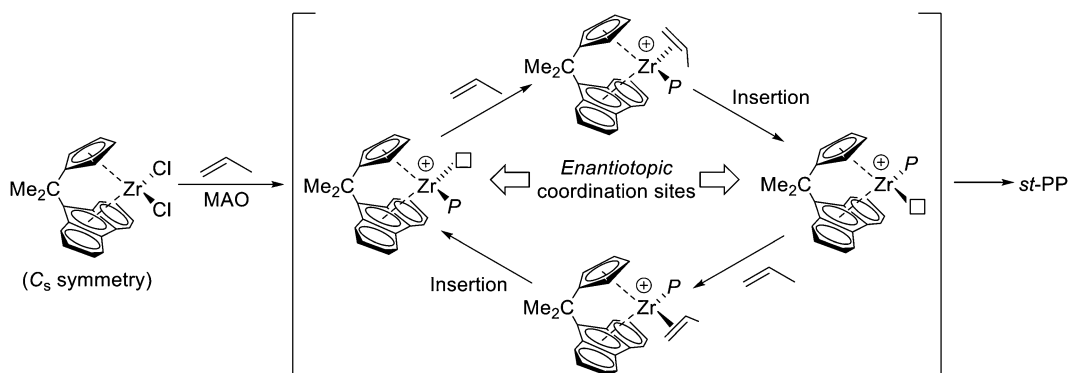

Stereospecific Polymerization, Fig. 9 it-Specific zirconocene-based polymerization catalysts

Stereospecific Polymerization, Fig. 8 it-Specific anionic polymerization of MMA
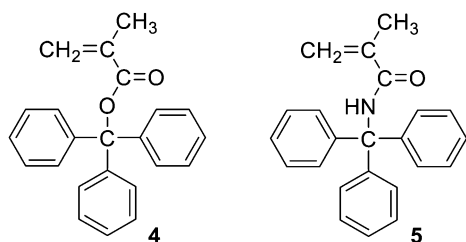
Stereospecific Polymerization, Fig. 10 Extremely bulky monomers for *it*-specific polymerizations

ht-Specific living anionic polymerization was reported on primary alkyl methacrylates with a combined system of *t*-C$_4$H$_9$Li and **7** in toluene at low temperatures. The *mr* triad content of the resulting polymer was up to 95 % under optimized conditions [5].

ht-Specific anionic polymerization of *N*, *N*-diethylacrylamide was also reported by using 1,1-bis(4′-trimethylsilylphenyl)-3,3-diphenylpropylpotassium/Et$_2$Zn at 18 °C in
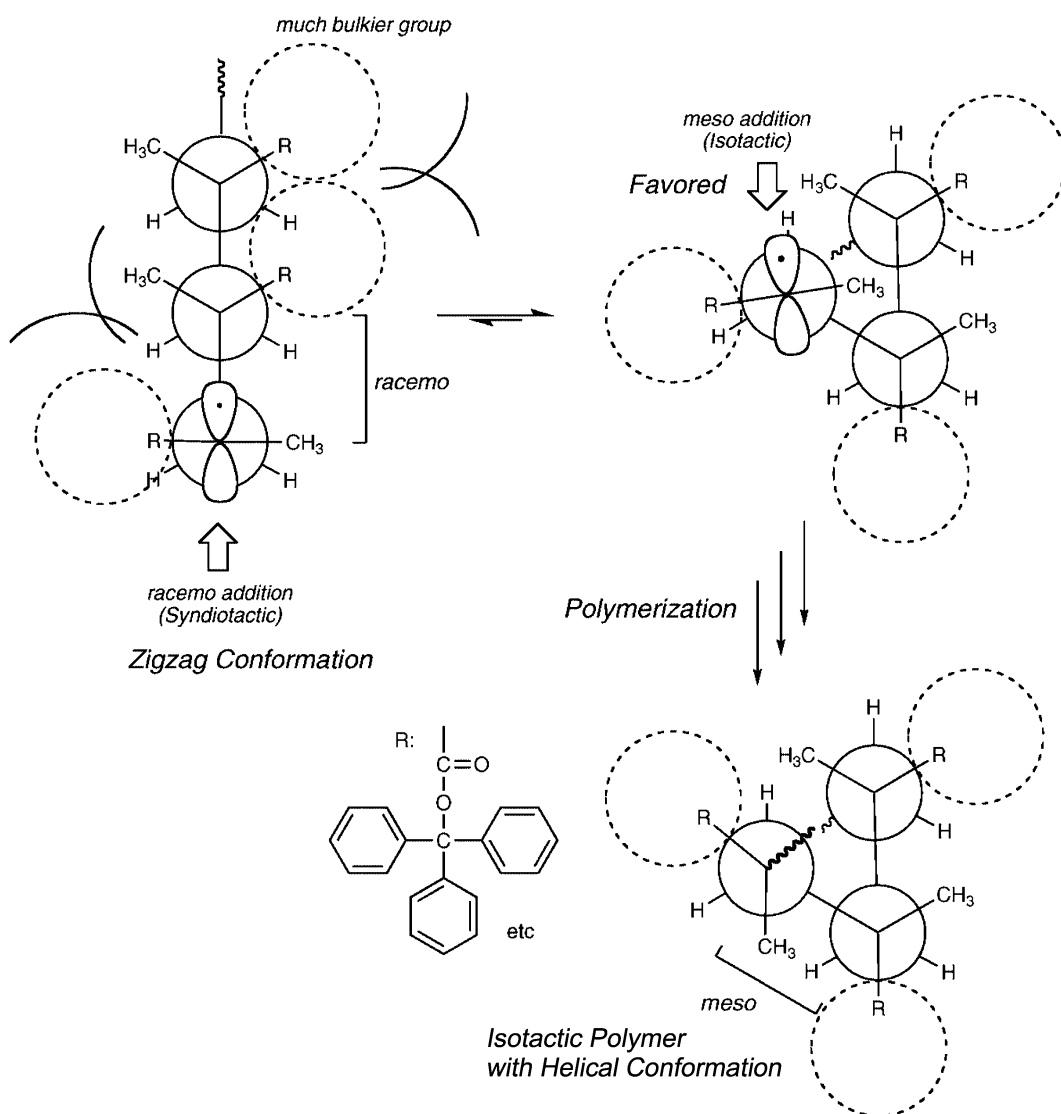
Stereospecific Polymerization, Fig. 11 Schematic model of *it*-specific propagation of bulky monomers (Reprinted with permission from Satoh and Kamigaito [7]. Copyright 2009 American Chemical Society)

Stereospecific Polymerization, Fig. 12 *st*-Specific polymerization of propylene with *C*s symmetric zirconocene

Stereospecific Polymerization, Fig. 13 Half-titanocene
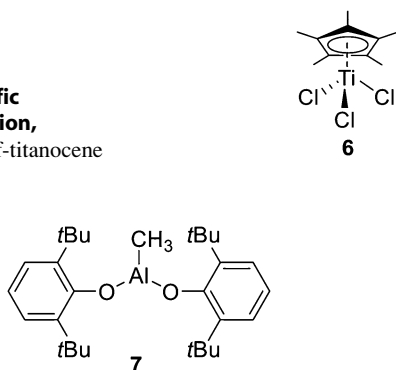
Stereospecific Polymerization, Fig. 14 Bulky aluminum phenoxide
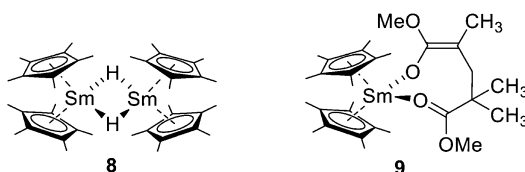
Stereospecific Polymerization, Fig. 15 Samarium-based complex for *st*-specific MMA polymerization and isolated MMA-dimerized species
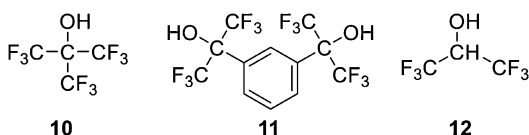
Stereospecific Polymerization, Fig. 16 Fluorinated alcohols employed for stereospecific radical polymerizations

THF. The addition of Et_3B instead of Et_2Zn was also effective in the *ht*-polymer formation.

In fluorinated alcohols as solvents, *ht*-specific radical polymerization was also reported [7]. Polymerization of vinyl pivalate with $(n\text{-}C_4H_9)_3B$ in the presence of a small amount of air in $(CF_3)_3COH$ at $-40\,^{\circ}C$ gave a *ht*-polymer with $mr = 61.0\,\%$. Polymerization of NIPAAm in toluene/fluorinated alcohol also gave *ht*-polymers at $-40\,^{\circ}C$ ($mr = 75\,\%$).

α,β-Disubstituted Vinyl Monomers

The α,β-disubstituted vinyl monomers (CHY = CHX) can give stereoregular polymers with "ditactic" stereosequences: *erythrodiisotactic*, *threodiisotactic*, *disyndiotactic*, and *diheterotactic* polymers (Fig. 19).

The examples of the ditacticity control of crotonates ($X = CO_2R$, $Y = CH_3$) are given [5]; triphenylmethyl crotonate afforded a threodiisotactic polymer with fluorenyllithium in toluene at $-78\,^{\circ}C$ in the presence of TMEDA (tetramethylethylenediamine). Group transfer polymerization of methyl crotonate gave a disyndiotactic polymer when 1-methoxy-1-(triethylsiloxy)-2-methyl-1-propene, HgI_2, and $(C_2H_5)_3SiI$ were used as an initiator, a catalyst, and a cocatalyst, respectively. *t*-Butyl crotonate gave an atactic polymer with $t\text{-}C_4H_9Li$ in THF at $-78\,^{\circ}C$ but a diheterotactic polymer with $(C_6H_5)_2Mg$ in toluene at $-78\,^{\circ}C$.

Stereospecific Polymerization, Fig. 17 Schematic model of solvent-mediated *st*-specific polymerization (Reprinted with permission from Chem. Rev. 2009;109(11):5120–5156. Copyright 2009 American Chemical Society)

Stereospecific Polymerization, Fig. 18 Stereostructure in *ht*-PMMA chains

Stereospecific Polymerization, Fig. 19 Rotated Fischer projections of ditactic polymers of α,β-disubstituted vinyl monomers

Dienes and Acetylenes

Butadiene, the simplest conjugated diene, can give polymers with 1,2- and 1,4-substructures. (in the case of asymmetric monomers (e.g., isoprene), 3,4-substructure is also possible) [11, 12]. Stereoregular polymers of butadiene are depicted

as follows: *cis*-1,4-, *trans*-1,4-, *it*-1,2-, and *st*-1,2-polymers (Fig. 20).

Ziegler-Natta catalysts such as TiX$_4$-R$_3$Al gave polymers with high *cis*-1,4 contents, whereas vanadium-based systems such as VX$_4$-R$_3$Al produced *trans*-1,4-polymers. Recently, complexes of lanthanides, Nd, Sm, Gd, etc., were reported as

Stereospecific Polymerization, Fig. 20 Stereoregular polybutadiene chains
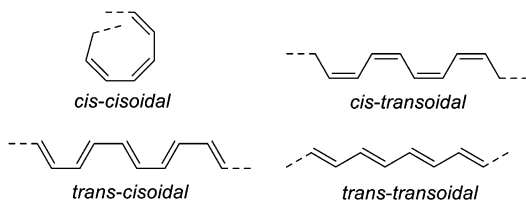
Stereospecific Polymerization, Fig. 21 Microstructures of polyacetylene
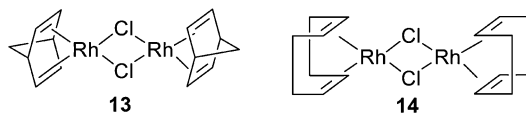
Stereospecific Polymerization, Fig. 22 Rhodium complexes for *cis*-specific polymerization of substituted acetylenes

catalysts for extremely high *cis*-1,4 selective polymerization (*cis*-1,4 > 99 %). Formation of *st*-1,2-polymers was also reported by using acetylacetonato complexes such as AlR$_3$–Co (acac)$_3$–CS$_2$ (*st*-1,2 > 99 %), whereas chromium-based systems such as AlR$_3$-Cr (C = NPh)$_6$ gave *it*-1,2-ones [11].

The microstructures of poly(acetylene) chains are normally depicted as shown in Fig. 21.

Acetylene can be polymerized with Ziegler-Natta catalyst [Ti(O^{n}Bu)$_4$-Et$_3$Al] to give *cis*-polymers at low temperatures (*cis* 98 % at −78 °C), whereas *trans*-polymers are obtained at high temperature (*trans* 100 % at 150 °C). Rhodium complexes such as **13** and **14** (Fig. 22) are effective for the polymerization of substituted
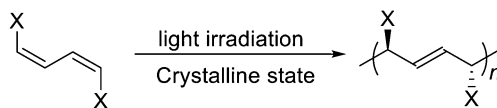
Stereospecific Polymerization, Fig. 23 Polymerization of muconic acid derivatives in crystalline state

acetylenes such as phenylacetylene to form *cis-transoidal* polymers [12].

Polymerization in Confined Media

Besides the solution polymerization, polymerization in confined media, where monomers are regularly aligned, is an attractive way to synthesize stereoregular polymers [13, 14]. Some kinds of muconic or sorbic acid derivatives can be polymerized by light irradiation in the crystalline state [13], giving "tritactic" stereoregular polymers (topochemical polymerization) (Fig. 23).

Inclusion polymerization is a solid process where monomer molecules are included as the guest in channel-like cavities of host clathrate crystals of urea, thiourea, etc. Under the irradiation of γ-ray, *st*-poly(vinyl chloride) and *it*-polyacrylonitrile were obtained.

Radical polymerization of MMA in a *st*-poly(-methacrylic acid) porous film gave *it*-PMMA [14]. The stereoregularity of PMMA prepared within the *st*-poly(methacrylic acid) "template" film was assumed to be due to stereocomplexation of these two polymers during the polymerization (Fig. 24).

Ring-Opening Polymerization (ROP)

Polymerization, in which stereoisomerism present in the monomer is merely retained in the polymer, is not regarded as stereospecific [3]. For example, the polymerization of a chiral monomer, e.g., (*R*)-propylene oxide [(*R*)-methyloxirane], with retention of configuration is not considered to be a stereospecific reaction. However, selective polymerization, with retention, of one enantiomer in a mixture of (*R*)- and (*S*)-propylene oxide is so classified.
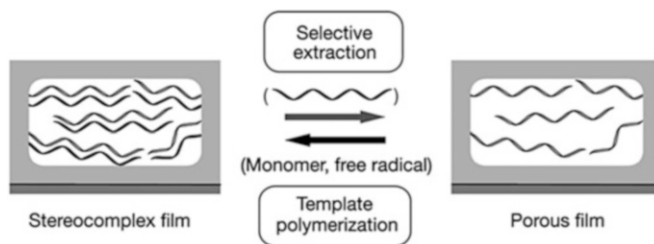
Stereospecific Polymerization, Fig. 24 Template polymerization of MMA within *st*-poly(methacrylic acid) porous films (Reprinted with permission from Macmillan Publishers Ltd: *Nature* 429(6987):52–55, Copyright (2004))
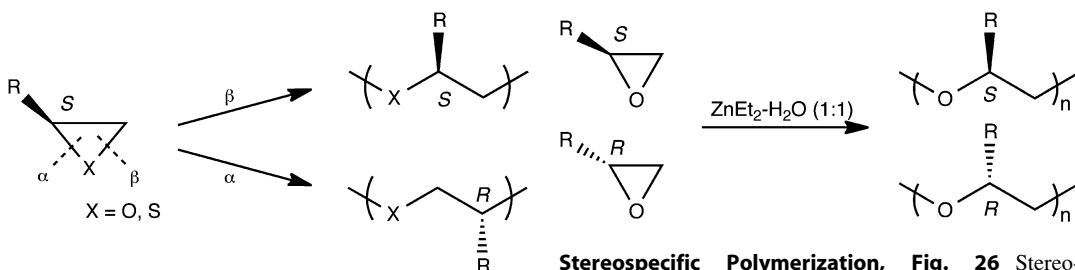
Stereospecific Polymerization, Fig. 25 Two kinds of ring-opening modes in the ROP of substituted oxiranes and thiiranes

Stereospecific Polymerization, Fig. 26 Stereoselective polymerization of substituted oxiranes with $ZnEt_2$-H_2O mixture (1:1)

Oxiranes and Thiiranes

The mechanism of ring opening of substituted oxiranes and thiiranes depends on the nature of an initiator used (Fig. 25) [15, 16].

When cationic-type initiators are used, the ring opening occurs to some extent at the α-position, leading not only to an inversion of configuration of the asymmetric carbon but also to the appearance of irregular linkages, e.g., head-to-head and tail-to-tail units.

Anionic initiators usually open the ring specifically at the β-position and produce polymers having more than 95 % head-to-tail linkages. If during the polymerization the ring is opened exclusively at the β-position, the configuration of the asymmetric atom remains unchanged and the polymer chain will be composed of repeating units of the *R* and *S* types, which are dependent on the absolute configuration of the chiral carbon atom in the monomer.

Systems obtained by partial hydrolysis or alcoholysis of organometallic compounds such as $MgEt_2$, $ZnEt_2$, $CdEt_2$, and $AlEt_3$ produce stereospecifically crystalline *it*-polymers through an "anionic-coordinated" mechanism. However, the stereospecificity of these initiators depends on the degree of hydrolysis or alcoholysis of the organometallic compounds. For instance, $ZnEt_2$-H_2O (1:1) is a more stereospecific system both for oxiranes and thiiranes (Fig. 26), than $ZnEt_2$-H_2O (1:0.5) which shows some cationic behavior. Cadmium tartrate shows very high stereospecificity in the case of thiiranes, in particular *tert*-butyl thiirane [15].

The first clear example of enantiomer-selective polymerization was demonstrated for propylene oxide (methyloxirane). Polymerization of racemic propylene oxide with a $ZnEt_2$/ (+)-borneol or $ZnEt_2$/(−)-menthol initiator system gave optically active polymers, and the unreacted monomer was rich in the (*S*)-isomer (Fig. 27) [16].

The enantiomer selectivity is generally higher in the polymerization of thiiranes than in that of oxiranes. For example, in the polymerizations with $ZnEt_2$/(*S*)-(−)-2,2′-binaphthol at room temperature, the consumption rate ratio of
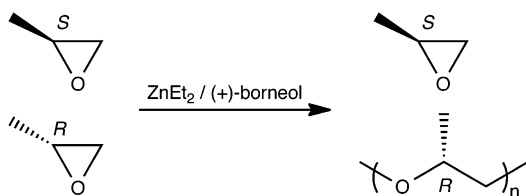
Stereospecific Polymerization, Fig. 27 Enantiomer-selective polymerization of propylene oxide with ZnEt$_2$/(+)-borneol initiator system
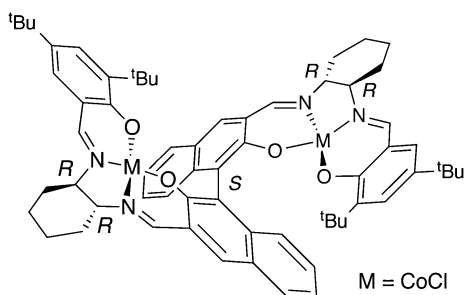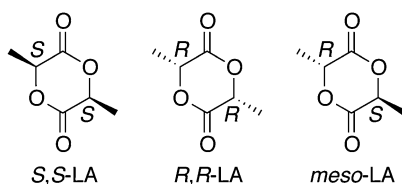

Stereospecific Polymerization, Fig. 28 Bimetallic complex for enantiomer-selective polymerization of oxiranes

Stereospecific Polymerization, Fig. 29 Lactide stereoisomers

(S)-propylene sulfide (methylthiirane) to (R)-one (k_S/k_R) was 20, whereas that of (S)-propylene oxide to (R)-one (k_S/k_R) was almost unity. However, it was recently found that bimetallic complex **15** (Fig. 28) exhibits high enantiomer selectivity for polymerizations of oxiranes, k_S/k_R up to 370 [16].

Lactide

Lactide is a cyclic dimer of lactic acid. Because there are two stereogenic centers in one lactide molecules, different stereoisomers of lactide are distinguished, (S,S)-LA, (R,R)-LA, and *meso*-LA (Fig. 29) [17, 18]. An equivalent mixture of (S,S)-LA and (R,R)-LA is referred to as *rac*-LA [17].

The ROP of lactide proceeds via different mechanisms, such as cationic, anionic, and coordination-insertion mechanisms, depending on the catalyst used. It is very difficult to obtain PLA with high molecular weights via a cationic mechanism. Anionic ROP of lactide has problems in controlling molecular structures of the PLA product, which is mainly caused by side reactions, such as epimerization, chain termination, and inter-/intramolecular transesterification reactions. Therefore, lactide polymerization via a coordination-insertion mechanism has become important from the viewpoint of controlling molecular structures.

Metal alkoxides are known to catalyze the ROP of lactide via a coordination-insertion mechanism, which involves four steps as depicted in Fig. 30: (i) coordination of the lactide monomer to the Lewis acid metal center, (ii) the lactide monomer inserts into the metal-alkoxide bond via nucleophilic addition, (iii) ring opening of the lactide monomer via acyl-oxygen cleavage, and (iv) continuous insertion of lactide monomers, followed by hydrolysis of the active propagating chain end.

Stereoregular PLA can be prepared from *rac*- or *meso*-LA via two different mechanisms. One is a chain-end-control mechanism. The configuration of the next inserted monomer in *rac*-LA polymerization or the cleavage site of the monomer in *meso*-LA polymerization is determined by the stereogenic center in the last repeating unit along the propagating chain. If the stereogenic center in the last unit favors a *meso*-enchainment, *it*-PLA is obtained from *rac*-LA (Fig. 31) and *ht*-PLA is obtained from *meso*-LA (Fig. 32).

If the stereogenic center in the last unit favors a *racemo*-enchainment, *ht*-PLA is obtained from *rac*-LA (Fig. 33) and *st*-PLA from *meso*-LA (Fig. 34).

The other is an enantiomorphic site-control mechanism. The configuration of the inserted monomer in *rac*-LA polymerization or the cleavage site of the monomer in *meso*-LA polymerization is determined by the configuration of the surrounding ligand, regardless of the stereogenic center in the last repeating unit along the

Stereospecific Polymerization, Fig. 30 Proposed mechanism of a coordination-insertion mechanism in the ROP of lactide
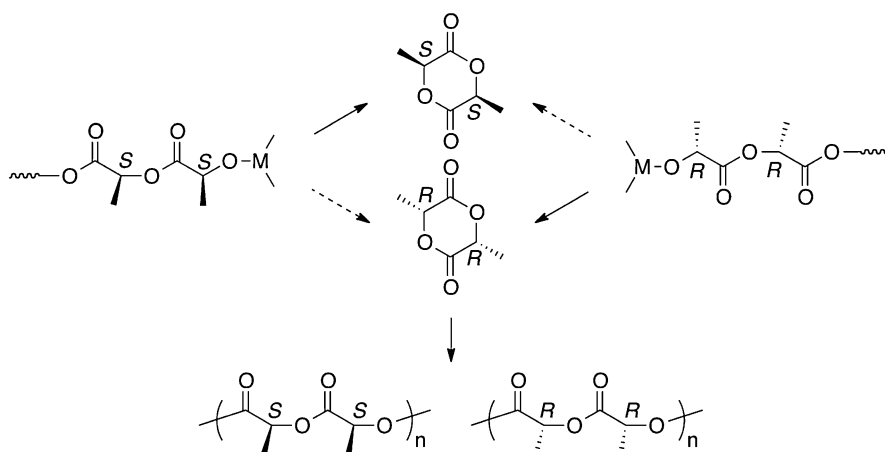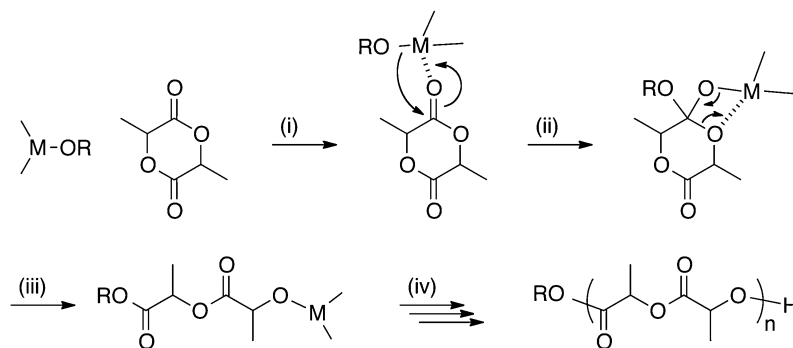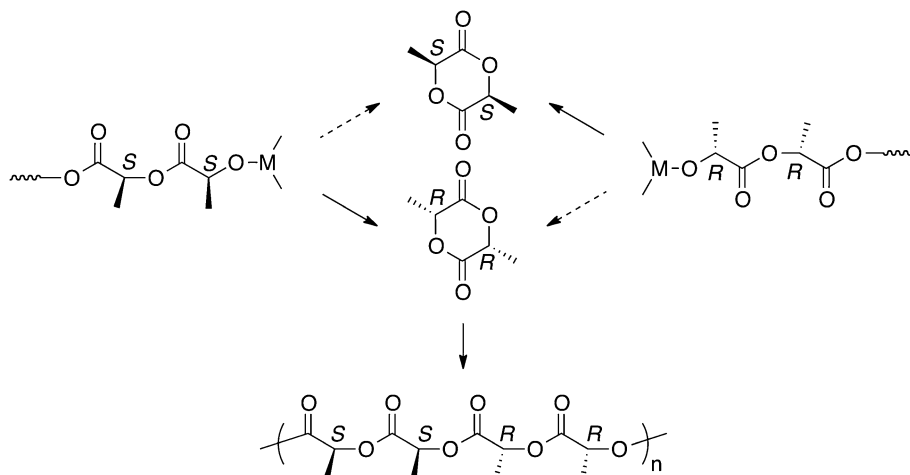

Stereospecific Polymerization, Fig. 31 Formation of *it*-PLA from *rac*-LA via a chain-end control mechanism
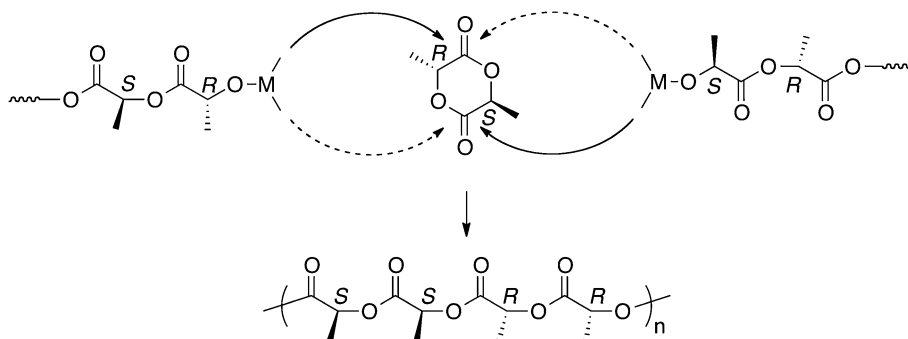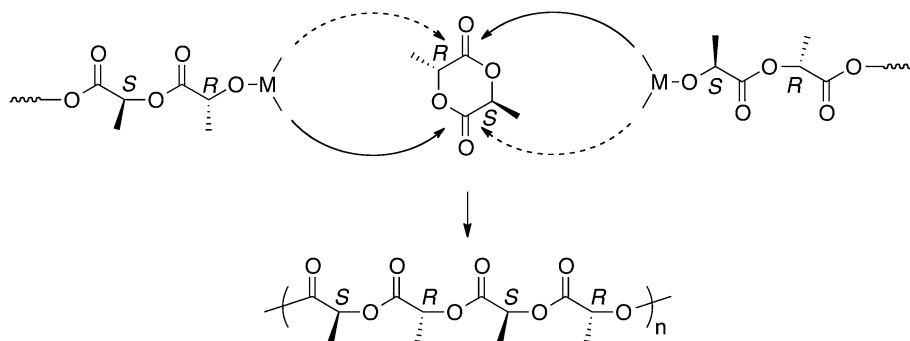

Stereospecific Polymerization, Fig. 32 Formation of *ht*-PLA from *meso*-LA via a chain-end control mechanism

propagating chain. In the lactide polymerization following an enantiomorphic site-control mechanism, *it*- and *st*-PLA can be solely obtained from *rac*- and *meso*-LA, respectively, unless the exchange reactions between the propagating polymer chains take place as mentioned below.

The ROP of *rac*-LA with an enantiomerically pure initiator, i.e., **16a** (Fig. 35), proceeds in an enantioselective manner. In this polymerization, at conversions less than 50 %, the polymer microstructure is predominantly isotactic, forming (*R*)-PLA. The reaction reached 100 % conversion
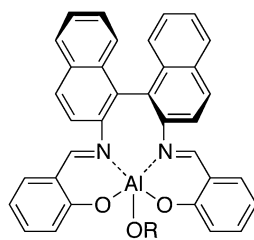
Stereospecific Polymerization, Fig. 33 Formation of *ht*-PLA from *rac*-LA via a chain-end control mechanism
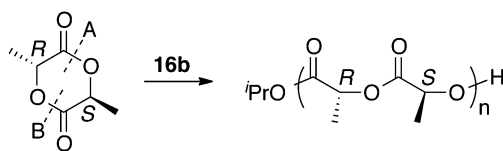

Stereospecific Polymerization, Fig. 34 Formation of *st*-PLA from *meso*-LA via a chain-end control mechanism

Stereospecific Polymerization, Fig. 35 Enantiomerically pure initiators for ROP of lactides

R = Me, **16a**; *i*Pr, **16b**

Stereospecific Polymerization, Fig. 36 Formation of *st*-PLA from *meso*-LA via an enantiomorphic site-control mechanism

very slowly due to the fact that the polymerization rate of (*S,S*)-LA is much lower than that of (*R,R*)-LA. The resulting PLA had a tapered stereoblock microstructure, in which the stereoblock distribution was changing from all (*R,R*)-units to all (*S,S*)-units over the polymer chain.

The presence of a bimetallic side product was discovered when preparing **16a**. In order to eliminate the formation of this bimetallic side product, **16b** (Fig. 35) was prepared [17]. The ROP of *meso*-LA with **16b** yielded *st*-PLA with syndiotacticity of 96 % by an enantiomorphic site-control mechanism (Fig. 36). The catalyst selected one of the two enantiotopic acyl-oxygen
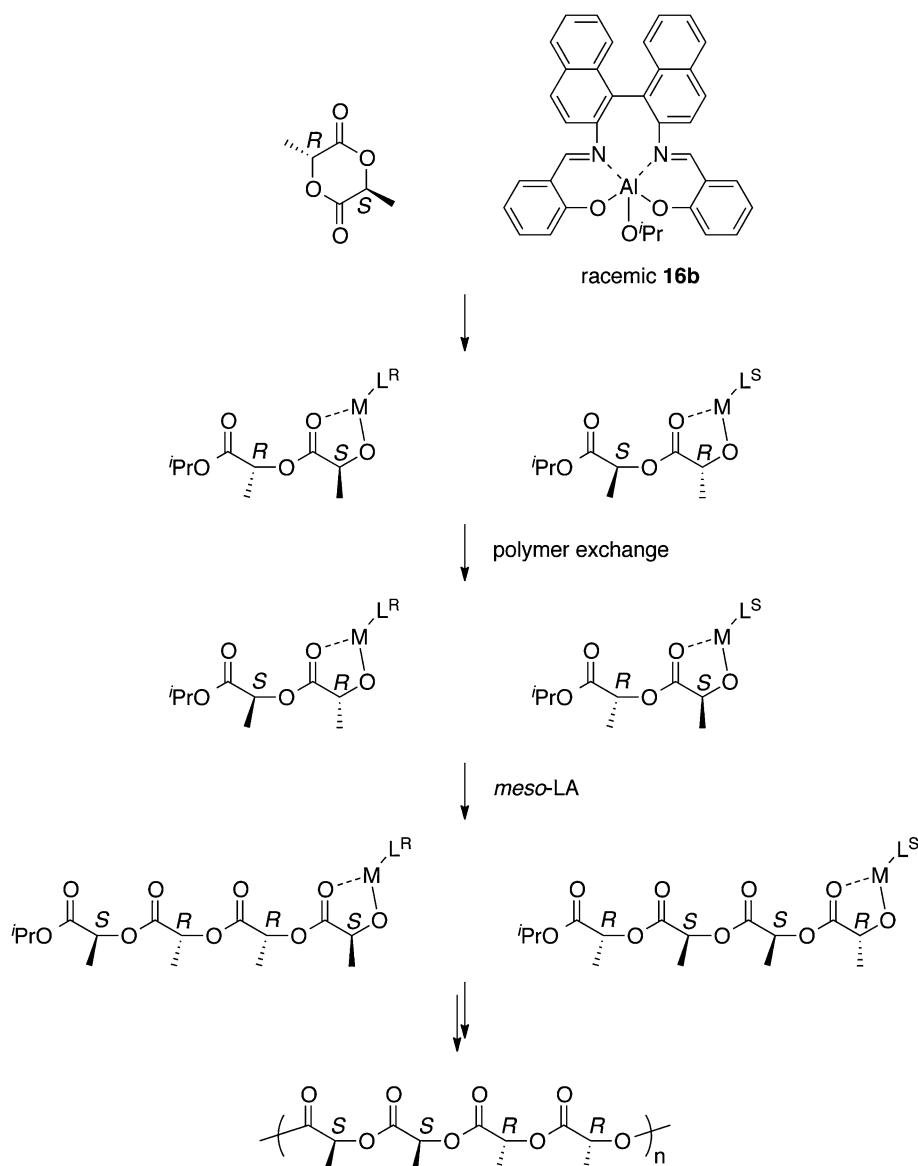
Stereospecific Polymerization, Fig. 37 Polymer exchange mechanism for the formation of *ht*-PLA from *meso*-LA

bonds at the initiation and the propagation. In fact, the stoichiometric reaction of **16b** with *meso*-LA underwent bond cleavage at site A with 97 % selectivity [18].

The ROP of *meso*-LA with racemic **16b** gave *ht*-polymer. To explain the novel formation of the *ht*-structure from *meso*-LA by using racemic **16b**, a polymer exchange mechanism was proposed, whereby each individual polymer chain

effectively switches between enantiomeric aluminum centers before the insertion of the next monomeric units (Fig. 37) [17].
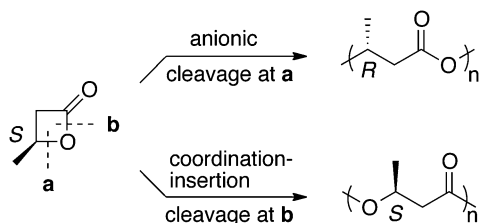
β-Lactones

Poly(3-hydroxybutyrate) (PHB) is a naturally occurring polyester produced by a wide variety of bacteria [18, 19]. Natural PHB consists of a repeating unit of *R* configuration at the

β-position of the ester carbon. PHBs can be prepared by the ROP of β-butyrolactone. It is well known that there are two mechanisms, i.e., anionic and coordination-insertion mechanisms, for the polymerization catalyzed by metal alkoxides. In the anionic mechanism, the alkyl-oxygen bond of β-butyrolactone (BL) gets detached, resulting in the inversion of the configuration at the β-carbon of the monomer (Fig. 38a). On the other hand, in the coordination-insertion mechanism, ring opening takes place via cleavage at the acyl-oxygen bond with retention of the asymmetric center configuration (Fig. 38b) [18].

The ROP of *rac*-BL via the coordination-insertion mechanism gives *it*- or *st*-polymers (Fig. 39). For example, achiral chromium(III) salophen complexes **17** (Fig. 40) and silica-supported Nd-bis(borohydride) species **18** (Fig. 40) produce the *it*-polymers. Alkyl tin compounds such as **19** (Fig. 41) and achiral Group 3 metal complexes such as **20–22** (Fig. 41) provide the *st*-polymers [19].

The ROP of *rac*-BL with a chiral initiator proceeds in an enantioselective manner. The first example is a combination of simple Group 12/13 alkylmetals, such as ZnEt₂ and AlEt₃, with (*R*)-3,3-dimethyl-1,2-butanediol. In this polymerization, the (*R*)-enantiomer of BL was preferentially incorporated in the polymer chain (Fig. 42) [19].

Ring-Opening Metathesis Polymerization (ROMP)

ROMP is a way of making polymers from a variety of cyclic olefins (Fig. 43) [20]. Strained monomers are best suited for ROMP, since secondary reactions of relatively unstrained C=C bonds in the resulting polymer can thereby be minimized. Norbornenes and 2,3-disubstituted norbornadienes have been popular, because they are relatively inexpensive and can be prepared in a large variety. The most basic features of the primary structure of all ROMP polymers are *cis* or *trans* C=C bonds between polymer repeating units. The relative stereochemistry between monomeric units (tacticity) is the next important structural component. Formation of a polymer with a single structure requires that the polymerization proceeds via a single propagation step that is a minimum of ~20 times faster than all other possible propagation steps.

### Norbornenes and Norbornadienes

Four regular structures of polynorbornene are possible as a consequence of a repeated single ROMP propagation step involving an achiral monomer (Fig. 44).

Well-defined olefin metathesis catalysts have been prepared: largely imido alkylidene catalysts based on Mo or W in the highest possible oxidation state or catalysts that contain Ru.
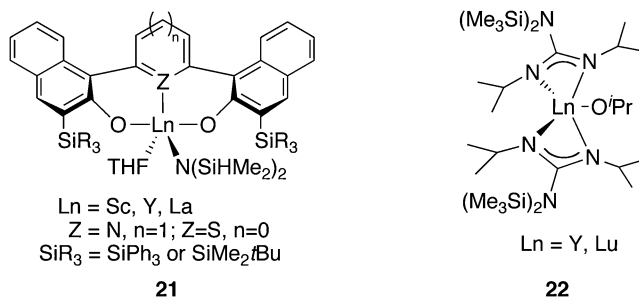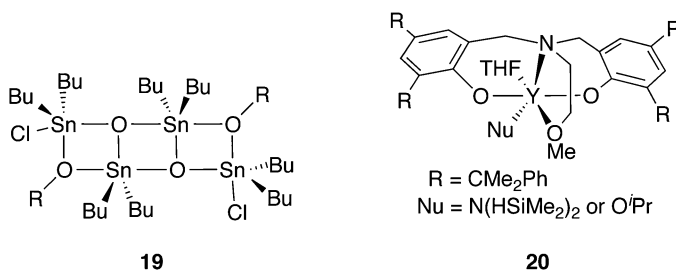

Stereospecific Polymerization, Fig. 38 Two kinds of ring-opening modes in ROP of β-BL

Stereospecific Polymerization, Fig. 39 Formation of *it*- or *st*-polymers from *rac*-BL
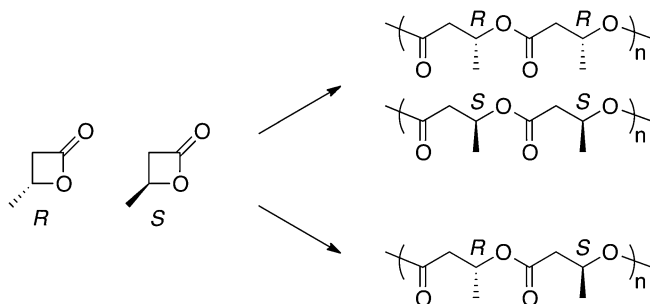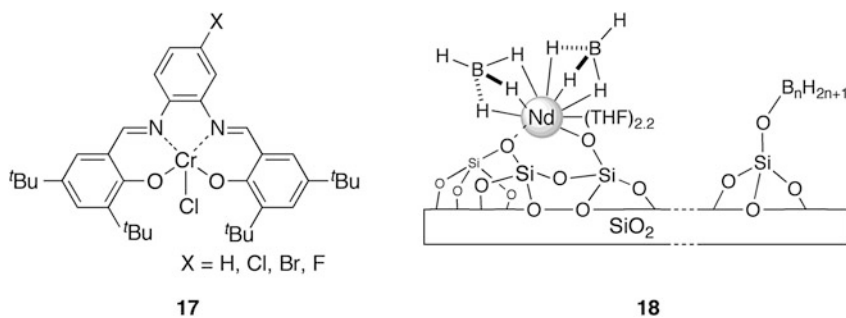
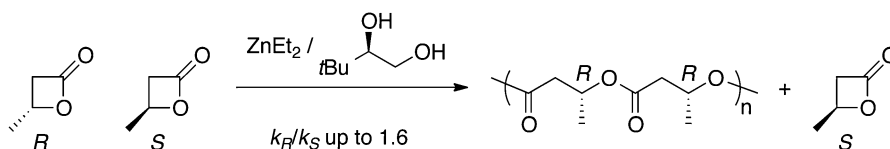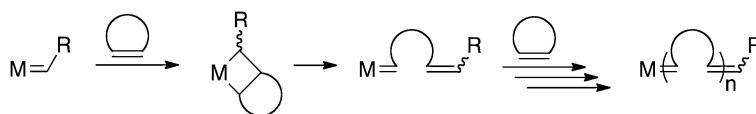**Stereospecific Polymerization, Fig. 40** *it*-Specific ROP catalysts for *rac*-BL
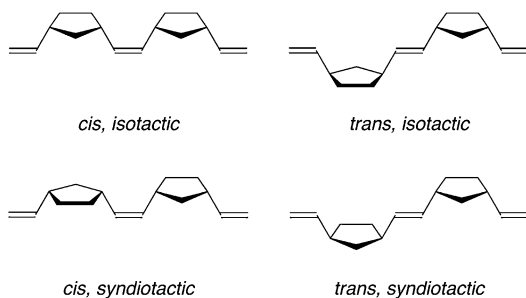

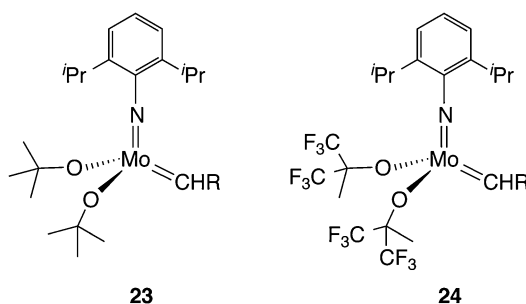**Stereospecific Polymerization, Fig. 41** Catalysts for *st*-specific ROP of *rac*-BL

Stereospecific Polymerization, Fig. 42 Enantiomer-selective polymerization of *rac*-BL with ZnEt$_2$/(*R*)-3,3-dimethyl-1,2-butanediol initiator system

Stereospecific Polymerization, Fig. 43 Proposed mechanism of the ROMP of a cyclic monomer

Stereospecific Polymerization, Fig. 44 The four regular structures of polynorbornene

Stereospecific Polymerization, Fig. 45 "First-generation" catalysts for ROMP

The *cis/trans* structures and tacticities of ROMP polymers have been mostly controlled by Mo and W catalysts.

Imido alkylidene catalysts for the type $M(NR)(CHR')(OR'')_2$ (M = Mo or W), such as **23** and **24** (Fig. 45), are called "first-generation" catalysts. "Second-generation" catalysts of the type $M(NR)(CHR')(diolate)$, where the diolate is a chiral and often enantiomerically pure biphenolate or binaphtholate such as **25** and **26** (Fig. 46), have been developed with a view toward enantioselective organic reactions. "Third-generation" catalysts of the type $M(NR)(CHR')(OR'')(Pyr)$ where Pyr is a pyrrolide or a substituted pyrrolide such as **27–29** (Fig. 47) are called MAP catalysts (for monoalkoxide pyrrolide or monoaryloxide pyrrolide) and are

the first examples that contain a stereogenic metal center.

Syn and *anti* alkylidene isomers are possible in all Mo and W imido alkylidene catalysts for a generic first-generation catalyst. When norbornene adds through its *exo* C=C face to the rear pseudotetrahedral face, which is formed by the alkylidene C_α, the imido N, and an alkoxide O atom at the corner (CNO) of the *syn* isomer catalyst, with its ring structure oriented toward the imido group ("ene$_{syn}$"), the metallacyclobutane intermediate is produced (Fig. 48a). The metallacycle should open to yield the *syn* + M_{cis} insertion product, if pseudorotation of the C—C(R') bond in the metallacycle is slower than the ring opening of the metallacycle (Fig. 48a). If the norbornene approaches in an ene$_{anti}$ fashion, the *anti* + M_{trans} insertion product should be formed (Fig. 48b). The two possible additions of norbornene to the *anti* isomer catalyst are also shown in Fig. 48c–d. Any addition of norbornene to the front CNO face would lead to the mirror image of one of the insertion products. Therefore, four energetically distinct pathways for the initiation are possible. A *trans* double bond is formed as a consequence of *syn*/ene$_{anti}$ or *anti*/ene$_{syn}$ steps, whereas a *cis* double bond is formed as a consequence of *syn*/ene$_{syn}$ or *anti*/ene$_{anti}$ steps. If the same CNO face is approached in each step in the polymerization process of *syn*/ene$_{syn}$ or *anti*/ene$_{anti}$, a *cis*, *it*-polymer is formed. If the alternating CNO faces are approached in each step, a *cis*, *st*-polymer is generated.

The *syn* and *anti* alkylidene isomers can interconvert at rates that vary by many orders of magnitude (Fig. 49). The *anti* isomers bind 2e donors such as THF more strongly and have been observed to be much reactive toward some ROMP monomers. The *syn* and *anti* isomers are key to controlling the manner in which a ROMP monomer is polymerized.

In a propagating process, the two M = C faces are different as a consequence of the chiral C_β in the alkylidene, so eight propagation pathways are possible. If any alkylidene rotates about the M=C

Stereospecific Polymerization, Fig. 46 "Second-generation" catalysts for ROMP

25

26

27

28

29
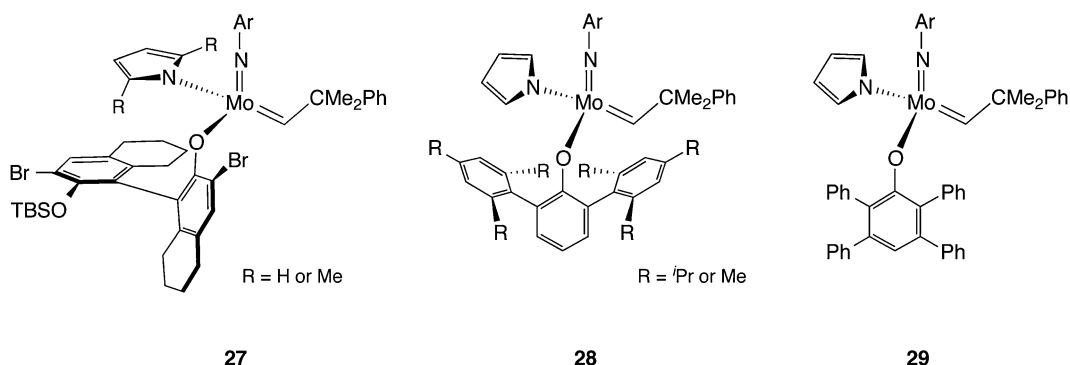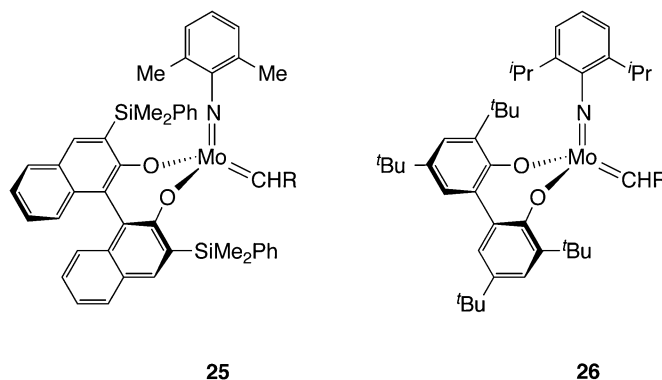
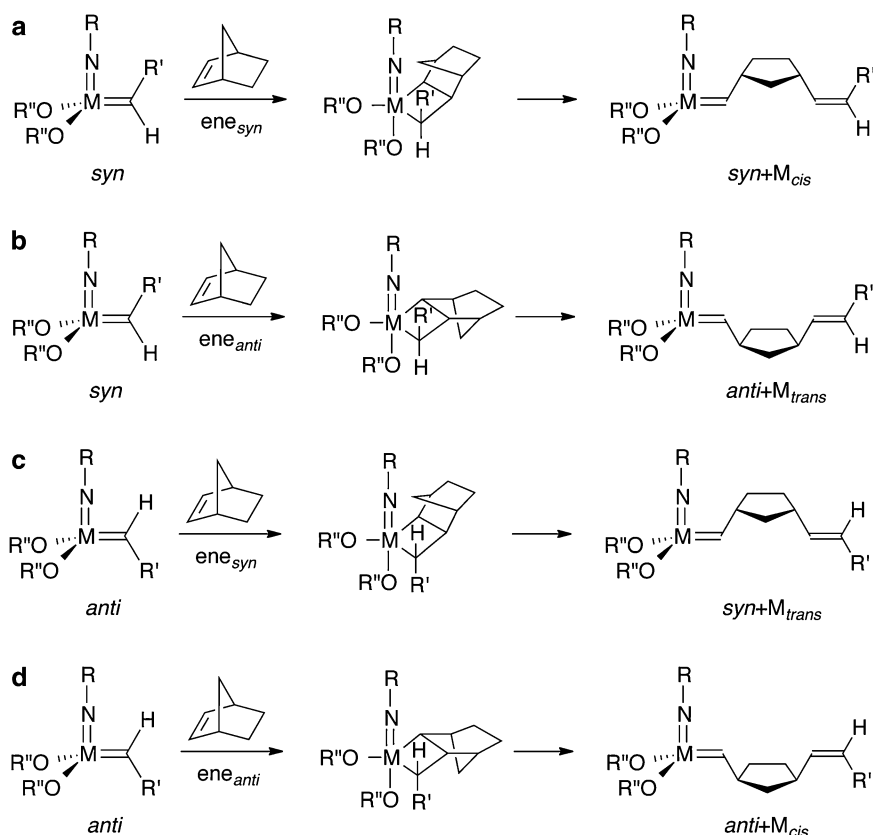**Stereospecific Polymerization, Fig. 47** "Third-generation" catalysts for ROMP

bond in the first insertion product (*anti → syn* or *syn → anti*), a mirror image of one of the remaining three insertion products is generated (Fig. 50); for example, if *anti* + M*trans* rotates 180° about the M=C bond, the mirror image of *syn* + M*trans* is generated. Therefore, one of the four regular structures could form in two ways. For example, *trans, st*-polynorbornene can form as shown in Fig. 50, if norbornene adds selectively to one M = C face in response to the chirality at the C$_\beta$ (chain-end control). The two mechanisms (*syn*/ene*anti* and *anti*/ene*syn*) are different, but each consists of a single type of the repeating monomeric unit. If other propagating processes are accessible, a polymer with a single structure would be less likely to be formed. In any

reaction between an achiral bisalkoxide and an achiral cyclic olefin, a single tacticity is a consequence of control via chirality at the C$_\beta$ in the alkylidene (chain-end control). It is not possible to form the *trans* C=C bond in a process that consists of one type of the propagation mechanism without converting one alkylidene isomer to the other before a subsequent addition of monomer.

Catalysts of the type M(NR)(CHR′)(diolate) were developed in order to provide a higher degree of tacticity control than that provided through chain-end control. The asymmetric nature of a chiral catalyst may control the stereochemistry of monomer addition more efficiently compared to the chiral C$_\beta$ in a chain end, and

S

Stereospecific Polymerization, Fig. 48 Four kinds of propagating steps in the ROMP of norbornene
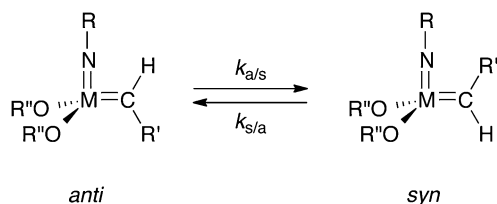
Stereospecific Polymerization, Fig. 49 Equilibrium between *syn* and *anti* alkylidene isomers

higher tacticity polymers would be expected. If a chiral metal complex forces the monomer to add to the same CNO face in each propagation step (enantiomorphic site control), an *it*-polymer will be formed.

An MAP catalyst has a stereogenic metal center. The configuration of the metal can invert via five-coordinate rearrangement processes. Thus, the stereochemistry at the metal inverts as

a consequence of each forward metathesis processes. A *cis*, *st*-polymer should be obtained, if the monomer approaches in an ene$_{syn}$ manner at the *trans* position to the pyrrolide and the chirality of the metal inverts with each step (Fig. 51). *cis*, *st*-Structures arise solely as a consequence of each monomer being forced to add in an ene$_{syn}$ manner to *syn* intermediates, i.e., to the alternating faces of the M=C bond.

The metal center is the only chiral element present in initiators. A stereogenic metal center was proposed to exert a powerful electronic control on a metal-based catalytic reaction. Thus, stereogenic metal control is electronic in origin and is distinct from enantiomorphic site control and chain-end control.

If the configuration at a stereogenic center of racemic monomer is the primary
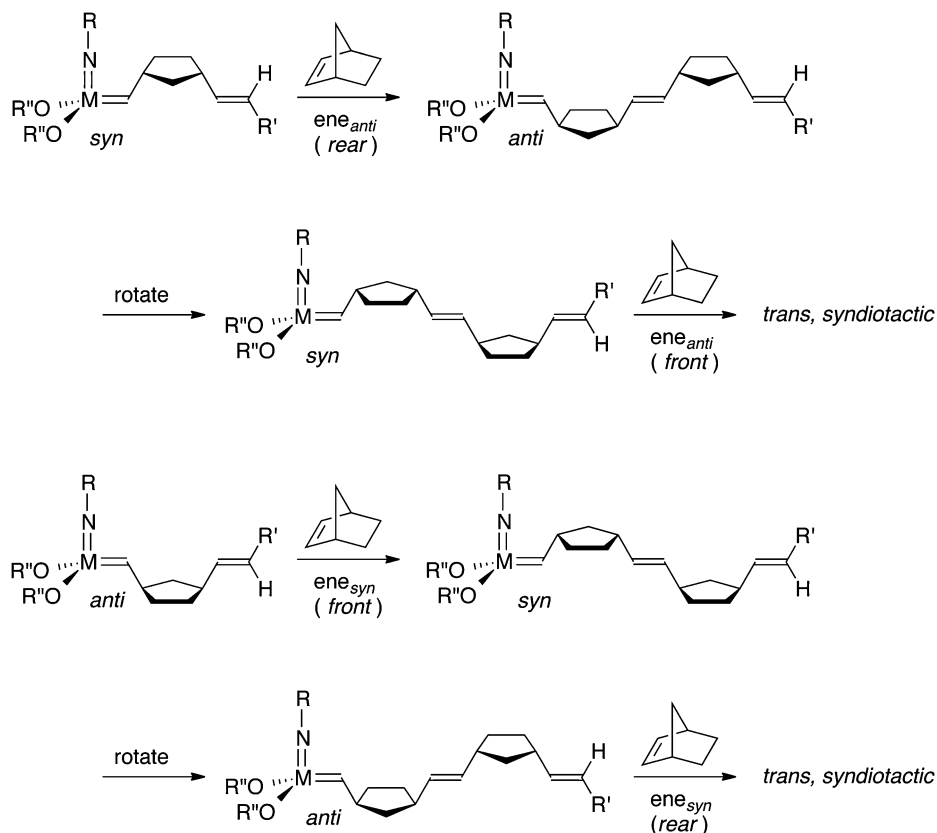
Stereospecific Polymerization, Fig. 50 Formation of *trans*, *st*-polynorbornene via a chain-end control mechanism
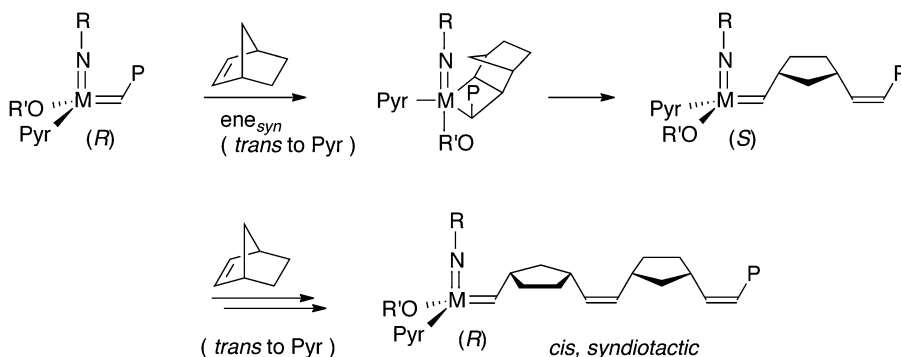
Stereospecific Polymerization, Fig. 51 Formation of *cis*, *st*-polynorbornene via a stereogenic-metal-control mechanism

determinant of which face of the M=C bond is attacked by a given ROMP monomer, a *cis*, *st*-polymer that contains alternating enantiomeric units in the chain will be formed (Fig. 52).

Cyclopropenes and Oxanorbornadienes

cis, *st*-Polymers could be obtained by ROMP of racemic derivatives of cyclopropenes or oxanorbornadienes with MAP catalysts via stereogenic metal control (Fig. 53).

Stereospecific Polymerization, Fig. 52 Formation of *cis*, *st*-polymers from racemic norbornene derivatives

Stereospecific Polymerization, Fig. 53 Formation of *cis*, *st*-polymers from racemic cyclopropene and oxanorbornadiene derivatives

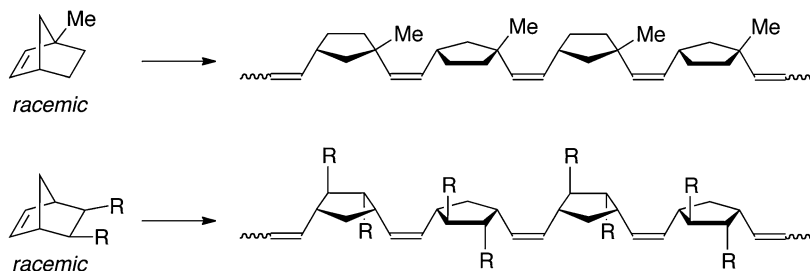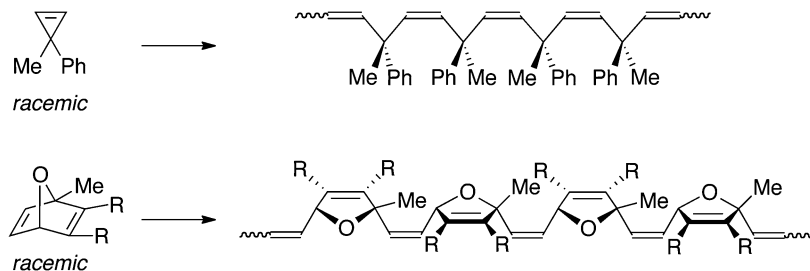## Related Entries

▶ Anionic Addition Polymerization (Fundamental)
▶ Anionic Ring-Opening Polymerization
▶ Asymmetric Polymerization
▶ Coordination Polymerization (Olefin and Diene)
▶ Coordination Polymerization (Styrene and Polar Vinyl Monomers)
▶ Free-Radical Addition Polymerization (Fundamental)
▶ Polymerization Reactions (Overview)
▶ Ring-Opening Metathesis Polymerization
▶ Ziegler-Natta Polymerization

References

1. IUPAC (1974) Basic definitions of terms relating to polymers 1974. Pure Appl Chem 40:477–492. doi:10.1351/pac197440030477
2. IUPAC (1981) Stereochemical definitions and notations relating to polymers (IUPAC recommendations 1980). Pure Appl Chem 53:733–752. doi:10.1351/pac198153030733
3. IUPAC (2008) Glossary of terms related to kinetics, thermodynamics, and mechanisms of polymerization (IUPAC recommendations 2008). Pure Appl Chem 80:2163–2193. doi:10.1351/pac200880102163
4. Mulhaupt R (2003) Catalytic polymerization and post polymerization catalysis fifty years after the discovery of Ziegler's catalysts. Macromol Chem Phys 204:289–327. doi:10.1002/macp.200290085
5. Kitayama T (2007) Tacticity. In: Matyjaszewski K, Gnanou Y, Leibler L (eds) Macromolecular engineering, vol 2. Wiley-VCH, Weinheim, pp 731–773
6. Hatada K, Kitayama T (2004) NMR spectroscopy of polymers. Springer, Berlin. doi:10.1007/978-3-662-08982-8
7. Satoh K, Kamigaito M (2009) Stereospecific living radical polymerization: dual control of chain length and tacticity for precision polymer synthesis. Chem Rev 109(11):5120–5156. doi:10.1021/cr900115u
8. Kanazawa A, Kanaoka S, Aoshima S (2010) A stepping stone to stereospecific living cationic polymerization: cationic polymerization of vinyl ethers using iron(II) sulfate. J Polym Sci Part A Polym Chem 48:3702–3708. doi:10.1002/pola.24144
9. Razavi A, Thewalt U (2006) Site selective ligand modification and tactic variation in polypropylene chains produced with metallocene catalysts. Coord Chem Rev 250:155–169. doi:10.1016/j.ccr.2005.07.006
10. Zohuri GH, Albahily K, Schwerdtfeger ED, Miller SA (2012) Metallocene alkene polymerization catalysts. In: Matyjaszewski K, Möller M (eds) Polymer science: a comprehensive reference, vol 3. Elsevier, Amsterdam, pp 673–697. doi:10.1016/B978-0-444-53349-4.00081-9
11. Ricci G, Sommazzi A, Masi F, Ricci M, Boglia A, Leone G (2010) Well-defined transition metal complexes with phosphorus and nitrogen ligands for 1,3-dienes polymerization. Coord Chem Rev 254:661–676. doi:10.1016/j.ccr.2009.09.023
12. Sanda F, Shiotsuki M, Masuda T (2012) Alkyne polymerization. In: Matyjaszewski K, Möller M (eds)

Polymer science: a comprehensive reference, vol 3. Elsevier, Amsterdam, pp 875–954. doi:10.1016/B978-0-444-53349-4.00088-1

13. Matsumoto A (2001) Stereospecific polymerization of 1,3-diene monomers in the crystalline state. Prog React Kinet Mech 26:59–109. doi:10.3184/007967401103165190

14. Serizawa T, Hamada K, Akashi M (2004) Polymerization within a molecular-scale stereoregular template. Nature 429(6987):52–55. doi:10.1038/nature02525

15. Spassky N, Dumas P, Sepulchre M, Sigwalt P (1975) Properties and methods of synthesis of several optically active polyoxiranes and polythiiranes. J Polym Sci: Polym Symp 52:327–349. doi:10.1002/polc.5070520127

16. Ito S, Nozaki K (2010) Asymmetric polymerization. In: Ojima I (ed) Catalytic asymmetric synthesis, 3rd edn. Wiley, Hoboken. doi:10.1002/9780470584248.ch13

17. Dijkstra PJ, Du H, Feijen J (2011) Single site catalysts for stereoselective ring-opening polymerization of lactides. Polym Chem 2:520–527. doi:10.1039/C0PY00204F

18. Nakano K, Kosaka N, Hiyama T, Nozaki K (2003) Metal-catalyzed synthesis of stereoregular polyketones, polyesters, and polycarbonates. Dalton Trans 4039–4050. http://www.rsc.org/Publishing/librarians/News/ChemCommDaltonTransactions.asp. doi:10.1039/B304690G

19. Carpentier J (2010) Discrete metal catalysts for stereoselective ring-opening polymerization of chiral racemic beta-lactones. Macromol Rapid Commun 31:1696–1705. doi:10.1002/marc.201000114

20. Schrock RR (2011) Synthesis of stereoregular ROMP polymers using molybdenum and tungsten imido alkylidene initiators. Dalton Trans 40:7484–7495. doi:10.1039/C1DT10215J

Stimuli-Responsive Bioconjugate

James J. Lai, Anthony J. Convertine and Patrick S. Stayton
Department of Bioengineering, University of Washington, Seattle, WA, USA

Abbreviations

ATRP	Atom transfer radical polymerization
BMA	Butyl methacrylate
CRP	Controlled radical polymerization
CTA	Chain transfer agent
DEAEMA	Diethylaminoethyl methacrylate
DMAEMA	Dimethylaminoethyl methacrylate
HPMA	N-(2-Hydroxypropyl) methacrylamide)
LCST	Lower critical solution temperature
LMWD	Low molecular weight drugs
NHSAc	N-Hydroxysuccinimide acrylate
PDS	Pyridyl disulfide
PEAA	Poly(ethylacrylic acid)
PEG	Polyethylene glycol
PEGMA	Polyethyleneglycol methacrylate
PGA	Poly(glutamic acid)
pNIPAM	Poly(N-isopropylacrylamide)
PPAA	Poly(propylacrylic acid)
RAFT	Reversible addition–fragmentation chain transfer polymerization
SA	Streptavidin

Synonyms

Smart conjugates; Stimuli-responsive nanoparticles; Stimuli-responsive polymer–protein conjugate

Definition

Stimuli-responsive bioconjugates are naturally produced biomolecules such as protein that are modified with stimuli-responsive polymers.

Introduction

Bioconjugates that utilize synthetic polymers to modify naturally produced macromolecules (e.g., protein, peptide, nucleic acid, etc.) have a relatively long history of being utilized for drug delivery, imaging, diagnostics, etc. For example, poly(ethylene glycol) (PEG) (or its biomolecules) exhibits nontoxic, nonimmunogenic, and biocompatible properties. Therefore, PEGylation that conjugates PEG to various biomolecules has been widely employed to tune the activity of the biomolecules or passively stabilizing the

S

biomolecules in vivo to allow increased blood circulation time or improved tumor targeting by the enhanced permeation and retention effect. Technologies, developed for PEGylation, have been adapted for other synthetic polymers, which may also enhance the stability and solubility of the biological component to which they are attached, while simultaneously providing responsive behavior and numerous sites for subsequent functionalization (e.g., to allow the attachment of cofactors, targeting ligands, imaging reagents, etc.).

Stimuli-responsive polymers sharply and reversibly respond to physical or chemical stimuli by changing their conformation and physical-chemical properties, i.e., changing from a hydrophilic state to a more hydrophobic state. Poly(N-isopropylacrylamide), pNIPAAm, the most extensively studied and utilized stimuli-responsive polymer, exhibits a lower critical solution temperature (LCST) behavior [1]. Below a defined temperature designated as the LCST, it is hydrophilic and highly solvated, while above the LCST, it is more hydrophobic and aggregated. This temperature transition is completely reversible and notably sharp around 32 °C. When the biomolecules such as proteins conjugated with the polymer, the stimuli-responsive transition properties are conferred to the biomolecules. The biggest impact of stimuli-responsive polymers has been in the biomedical field, where the versatility and usefulness of these polymers as molecular engineering tools have been demonstrated in the development of biological sensors, drug delivery vehicles, and tissue engineering. Here we present an overview of stimuli-responsive conjugates for therapeutic and in vitro diagnostic applications.
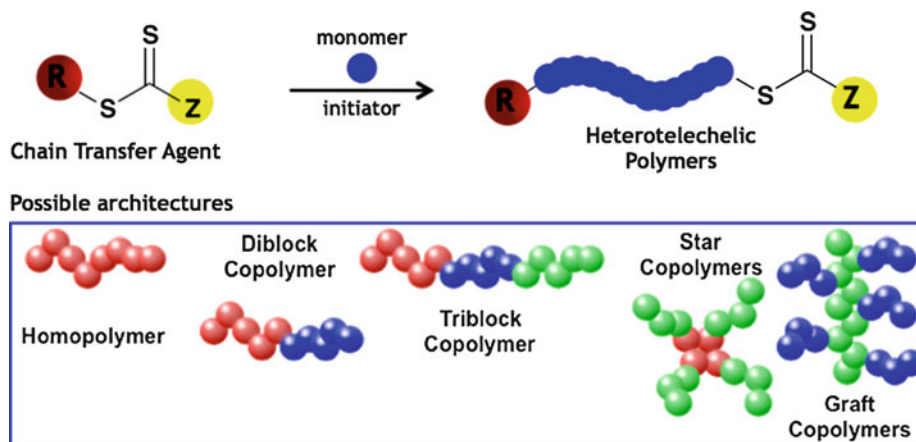
Stimuli-Responsive Bioconjugates for Therapeutic Applications

Currently, all proteins and peptide drugs target extracellular receptors because of the difficulty of intracellular delivery. The intracellular target universe is rich in disease application space, and many proteins/peptides are known to agonize or antagonize key intracellular targets connected with a corresponding wide variety of specific disease etiologies. The ability to deliver functional biologic drugs to intracellular space would also greatly enhance the capabilities of the molecular imaging field in both in vivo and in vitro applications. Viable therapeutic systems must integrate numerous modular components with different functional properties into a single well-defined nanoparticle format. These components include a pH-responsive segment that enhances membrane transport selectively in the low pH environment of the endosome, a targeting element that directs uptake into specific cells, and a versatile complexation element that allows for spontaneous association with the biologic drug or imaging agent. These individual functional requirements must remain active once integrated together into a total delivery system while maintaining good biocompatibility. Controlled radical polymerization (CRP) methodologies, including the versatile reversible addition–fragmentation chain transfer (RAFT) polymerization process, are rapidly moving to the forefront in construction of drug and gene delivery vehicles. RAFT polymerization in particular has allowed previously unattainable polymeric architectures to be prepared for pharmaceutically relevant conditions. This unprecedented synthetic latitude is for the first time allowing for the preparation of water-soluble or amphiphilic architectures with precise dimensions and appropriate functionality for attachment and targeted delivery of diagnostic and therapeutic agents.

Nanoparticle Synthesis

RAFT represents one of the most significant recent advances in synthetic chemistry and its application is revolutionizing a broad range of disciplines from traditional polymer science to biology. The versatility of RAFT lies in the elegant simplicity of the technique, broad chemical compatibility, and ease of use. RAFT employs a thiocarbonylthio compound as a degenerate chain transfer agent (CTA), which is most commonly a dithioester or trithiocarbonate. By simple manipulation of the initial monomer, CTA, and radical initiator stoichiometry, it is possible to prepare near-monodisperse materials

Stimuli-Responsive Bioconjugate, Fig. 1 Synthetic outline for the preparation of sophisticated polymeric architectures for drug delivery and diagnostic applications via RAFT polymerization

over a range of predefined molecular weights. These agents contain the general structure shown in Fig. 1, where R is a radical initiating group and Z stabilizes the thiocarbonyl towards radical addition. Through a series of chain transfer steps, polymerization proceeds in a controlled process with most polymer chains containing R and Z groups at their alpha and omega chain terminuses, respectively. Following polymerization of a given monomer or monomers, the resultant macroCTA can be isolated for use in subsequent block (co)polymerization steps.

Because this methodology does not require the use of any toxic metal catalysts, it is particularly well suited for use in biotechnology applications. Most commercially available RAFT CTAs, which contain carboxylic acid functionality, are modified using standard esterification/amidation reactions. Because the functional groups are introduced as part of the polymerization process, this strategy eliminates the need for costly and often ill-defined postpolymerization steps (simpler than modification reactions). One particularly exciting application of R-group functionalization involves coupling of an NHS-activated RAFT CTA onto resin bound oligopeptides [2]. Integrating this strategy into biologic drug delivery systems has tremendous potential because of the large number of potential therapeutic and cell-specific targeting peptides that can be generated via phage display.

Some examples of Z-functional RAFT CTAs have also been reported. However, the synthetic methodology needed to prepare these compounds is less facile than the simple R-group modification.

The distinction between R- and Z-group functionality can be an important criterion when designing a biologic drug delivery system where self-assembly of one of the polymeric segments can sequester the associated group from the aqueous phase. Localization of the desired functionality on the prescribed chain segment is not always possible through a simple reversal of the polymerization steps because many monomer families show a blocking order dependence. The thiocarbonylthio group that presents at the omega chain terminus is itself a versatile functional group, and numerous examples of its reduction to a biologically significant thiol group, either through hydrolysis or aminolyis (if primary amine is given as the reagent for aminolysis, then reagent for hydrolysis needs to be given), have been reported. The progress of these reactions can be conveniently monitored by following the disappearance of the thiocarbonylthio group absorbance at 310 nm. Recently, it has also been shown that a single discrete chemical functionality can be placed at the omega chain terminus through a chain extension approach. This strategy takes advantage of the inability of maleimides to homopolymerize under standard conditions and eliminates the need for thiocarbonylthio

cleavage, which can be important in biological applications where other potential degradable functionalities are present.

Drug Binding

The mechanism by which biologic drugs are tethered to the polymeric delivery system is dependent on the physiochemical nature of the biomacromolecule and the clinical application of the therapeutic construct. Nucleic acids such as siRNA and plasmid DNA have historically been tethered to polymer- and lipid-based synthetic vectors by means of strong ionic interactions between the negatively charged nucleic acid and positively charged polymeric polyamines. Polyplexes are particularly attractive as a means of drug binding because these are formed/obtained/prepared spontaneously simply by mixing the polymer and drug. This approach also eliminates the need for functionalized nucleic acids as well as complex conjugation reactions. In many cases, the synthetic polycations are formulated with excess positive charge relative to the nucleic acid in order to facilitate nonspecific uptake and endosomal escape via the so-called proton sponge effect. This approach however requires the polyplex, which formed spontaneously in aqueous solution, to dissociate upon entering the cytoplasmic compartment. Quaternary ammonium polymers containing associated ester functionality are employed to facilitate greater nucleic acid release. Upon entering the endosomal compartment, ester moieties are hydrolyzed causing a change in the polymeric repeat unit from cationic to zwitterionic. This change not only eliminates the strong charge–charge interaction between the polymer and the nucleic acid but also increases the biocompatibility of the polymer.

While a number of synthetic polycations, including poly(lysine), poly(ethyleneimine) (both linear and branchy), and acrylic amines, have been described, their clinical impact has thus far been limited because of significant in vivo toxicity. A number of elegant synthetic approaches have been proposed in order to enhance the biocompatibility of polycation-based delivery systems. These approaches include the incorporation of degradable linkages, such as disulfide and acetal, within the polymer backbone and the incorporation of neutral hydrophilic stabilizers such as polyethylene oxide. Despite these efforts, significant concerns regarding the ultimate in vivo fate of these agents remain. Polycation toxicity is mostly acute when drugs are administered via intravenous injection because of interaction with lung tissue. For these reasons, clinical impact of polycation-based vectors will likely be most significant in applications such as vaccines and cancer therapy where subcutaneous or intraperitoneal injections are possible.

Direct biologic drug conjugates have been proposed as an alternative mechanism for tethering the polymeric delivery system to the therapeutic agent. In these systems, a covalent bond is formed between the biologic drug and the polymeric scaffold. Ideally this bond is stable for some time in circulation, but upon entering the endosomal or cytoplasmic compartment, it is degraded via chemical or enzymatic intervention. Thiol-reactive pyridyl disulfide (PDS) groups have been combined with RAFT and "click" chemistry to prepare end-functionalized polymer-dendritic carbohydrate scaffolds [3]. This synthetic approach is amenable to a range of sugar functionalities and has been shown to efficiently bind siRNA. We have also employed pyridyl disulfide functional RAFT agents and monomers to prepare a variety of biologic conjugates including peptide, protein, and siRNA. For example, a pyridyl disulfide functional trithiocarbonate was employed to prepare a diblock copolymer containing a biocompatible HPMA segment for drug binding and an endosomal-releasing block. Conjugation and subsequent delivery of the Bak peptide resulted in pronounce increases in proapoptotic activity over controls. While degradation of the polymer-drug linkage is likely a required step for a number of therapeutic applications, it may not be necessary in all cases. Applications involving large therapeutic molecules such as antibodies and large peptides where the mechanism of action is far from the polymeric tether may function

effectively without cleavage from the delivery system. Other applications, such as protein vaccines, where peptide linkages within the biologic drug itself are degraded may provide an alternative means of drug release. Irreversible conjugates using model protein drugs have been prepared via a variety of chemistries including alkyne–azide click chemistry, NHS esters, and thioether.

Cytosolic Delivery

The major challenge associated with the use of biologic drugs is the need for these agents to be delivered "outside-in" to the cytoplasmic compartment of target cells. Traditional therapies based on low molecular weight drugs (LMWD) do not, in most cases, require the use of endosomal-releasing systems in order to reach the cytosol. These compounds are able to passively diffuse through biological membranes because of their hydrophobic nature and small size. In contrast to LMWDs, biologic drugs based on hydrophilic biomacromolecules are unable to penetrate cell membranes and therefore must contain some mechanisms of endosomal escape in order to reach the cytosol. Viruses and other pathogenic organisms such as Diphtheria have evolved highly effective delivery systems for getting nucleic acids and proteins to intracellular locations and targets. These vectors mediate endosomal escape by incorporating fusogenic proteins (e.g., hemagglutinin) on their viral coat that undergo a pH-induced conformational change from hydrophilic at physiological pH to hydrophobic in response to the acidic endosomal environment. At physiological pH (7.4), these proteins are in a "stealth-like" conformation, until they are brought into endosomes. As the pH of these compartments drops during endosomal trafficking to values of pH 5.5 or lower, a conformational change is triggered that exposes the membrane-destabilizing domains.

Based on this biologic design, synthetic polymers have been developed as means of facilitating cytosolic delivery of intracellular therapeutics. These materials employ the same bioinspired pH-sensing strategy by incorporating both carboxylic acids and hydrophobic alkyl segments throughout the polymer backbone. Under normal extracellular conditions (pH 7.4), these materials have sufficient negative charge to render them hydrophilic, but upon exposure to acidic endosomal compartments, the acid-base equilibrium is shifted triggering a hydrophilic–hydrophobic conformational change. This transition renders the polymeric materials membrane interactive allowing them to disrupt endosomal membranes. The pH-responsive membrane-destabilizing activity of these biologic drug delivery systems can conveniently be evaluated using a red blood cell hemolysis assay. In this assay, red blood cells are isolated and resuspended in buffers chosen to closely mimic physiological conditions as well as conditions found in the early and late endosomes. Spectroscopic analysis of hemoglobin in the supernatant can then be employed to quantitate the degree of red blood cell lysis. This assay has been shown to be a good indicator of successful intracellular delivery with materials that display high levels of red blood cell lysis under acidic conditions, showing high levels of cytosolic delivery. Specifically, polyalkylacrylic acids such as poly (ethylacrylic acid) (PEAA) and poly (propylacrylic acid) (PPAA) have been shown to significantly enhance the intracellular delivery of proteins to the cytoplasm both in vitro and in vivo.

As an alternative to the alkylacrylic acids, particle-based delivery systems have been developed that contain a hydrophobic pH-sensing endosomolytic segments surrounded by a hydrophilic corona. This technology is based on the incorporation of both a hydrophobic membrane-interactive component (i.e., butyl methacrylate, BMA) and a pH-responsive component. These systems employ propylacrylic acid (PAA) and dimethylaminoethyl methacrylate (DMAEMA) in approximately equal stoichiometric ratios as the pH-sensing component with between 30 % and 50 % BMA content. Concurrent protonation of both carboxylic acid and amine residues throughout the tercopolymer shifts the overall charge from approximately neutral at pH 7.4 to a net cationic conformation at

S

acidic pH values. In this conformation, the micelle morphology is disrupted and the resulting unimers become highly membrane disruptive. In an iteration of this design, both the PAA and DMAEMA residues are replaced with diethylaminoethyl methacrylate (DEAEMA). The increased hydrophobicity of DEAEMA coupled with the BMA content effectively sequesters the membrane-interactive segment from the aqueous phase until an acidic environment is encountered. The optimum composition of DEAEMA to BMA has been determined to be 60 mol % DEAEMA and 40 mol % BMA. At this stoichiometric composition, the polymeric micelles undergo the transition from inactive to membrane disruptive at approximately pH 6.8. Manipulation of this stoichiometry has been shown to allow precise tuning of the pH at which the polymer becomes membrane disruptive. Under extracellular pH conditions, these materials spontaneously self-assemble to form micelles ~30–50 nm in size.

Cell-Specific Targeting

Targeted delivery of biologic and small molecule drugs has been studied extensively as a way of improving therapeutic efficiency through the mitigation of off-target effects and reduction in effective dose. Targeting functionality is especially important for applications such as chemotherapy where the therapeutic agent may have strong cytotoxic properties. Targeting agents may be coupled to nanoparticle-based delivery systems through the use of activated ester-containing compounds resulting in conjugates linked via stable amide bonds. Typical activated esters include succinimidyl and pentafluorophenyl esters as well as mercaptothiazoline. For example, the controlled RAFT polymerization of *N*-hydroxysuccinimide acrylate (NHSAc) and its copolymerization with a variety of hydrophilic comonomers has been reported as a means of preparing protein-reactive polymers that can be dissolved directly in water without any tedious (seems better) postpolymerization modifications. This approach is especially versatile for preparing therapeutic and theranostic polymer–protein nanoparticles in

that conjugation reactions can be conducted directly in aqueous solution under mild pH conditions so as not to disrupt secondary and tertiary protein structures. Folic acid, which mediates enhanced uptake in many cancers, has also been coupled to polymeric nanoparticles. This approach involves the preparation of functional polymeric scaffold (e.g., amine or hydroxyl) to which folic acid is then coupled using carbodiimide chemistry. Folate functionalized nanoparticles may also be prepared using folate functionalized or (coupled/linked) RAFT CTAs which eliminates the need postpolymerization conjugation and purification steps. Similar to protein-reactive scaffolds, these materials are generally composed primarily of a neutral hydrophilic monomer such as *N*-(2-hydroxypropyl) methacrylamide (HPMA) or poly(ethylene glycol) methacrylate (PEGMA) with amine or hydroxyl functional comonomers (e.g., aminopropyl methacrylamide or hydroxyethyl methacrylate) added as a minor component. Manipulation of this stoichiometric ratio provides a means by which multidentate materials with controlled distribution of the targeting groups throughout the polymeric backbone can be synthesized.

Cell-specific antibodies and proteins may also be incorporated into therapeutic/theranostic nanoparticles by taking advantage of the strong noncovalent interaction between biotin and streptavidin (SA). This strategy involves the synthesis of polymers/nanoparticles that contain biotin residues, distributed throughout the polymer backbone or at the chain terminus, that bind spontaneously to SA-antibody conjugates (Fig. 2). This approach has been employed to target polymeric nanoparticles carrying therapeutic RNA drugs to lymphoma cells. Here antibodies targeting the CD22 receptor were integrated into the delivery system resulting in substantially higher levels of protein knockdown (i.e., 70 % mRNA reduction versus 20 % for negative control antibodies).

Circulation Stability and Biocompatibility

Conjugation of biologic drugs to water-soluble polymers and nanoparticles has been shown to

Fig. 2 Spontaneous
assembly of streptavidin-
antibody conjugates to
polymers containing
telechelic biotin groups
prepared via RAFT
polymerization with
a biotin-functional chain
transfer agent
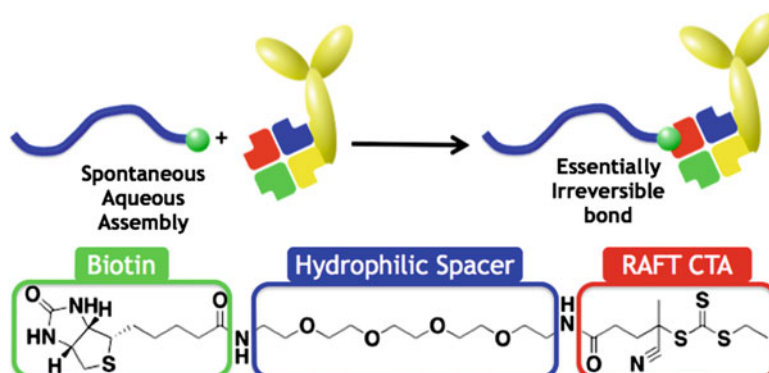
prolong circulation half-life and promote tumor accumulation [4–6]. Polyethylene glycol (PEG) conjugates have successfully been used clinically for cytokine and enzyme delivery. Alternative polymers to PEG have also been used to impart protein stability and enhanced circulation time in vivo including HPMA [7], poly-L-glutamic acid (PGA) [8], styrene maleic anhydride copolymers [9], and PEGMA. PEGMA is a polymerizable PEG containing macromonomer that has been widely employed as a precursor for the preparation of therapeutic nanoparticles. The wide variety of bioapplications of these polymers stem from their water-soluble and biocompatible properties and nonadhesive nature to proteins and cells. Previously, various polymerization techniques such as anionic, cationic, ring-opening metathesis, and free radical polymerization have been employed to polymerize PEG macromonomers. The advent of CRP methods such as atom transfer radical polymerization (ATRP) and reversible addition–fragmentation chain transfer (RAFT) polymerization has further broadened the scope of available PEG-based macromolecular architectures. The solution properties of PEGMA depend on its fine balance between hydrophilic and hydrophobic groups. While the ether oxygen atoms on the polyethylene oxide segment form stabilizing hydrogen bonds with water, the apolar carbon–carbon backbone increases hydrophobicity. As a result, poly(PEGMA) with short PEG side chains is only mildly hydrophilic, whereas poly(PEGMA) with 10 or more ethylene oxide units has enhanced hydrophilicity [10].

Stimuli-Responsive Bioconjugates for In Vitro Diagnostic Applications

Stimuli-responsive bioconjugates are utilized for biomolecules separation to improve clinical diagnostic tests and life science research (Fig. 3). Immunoassay, one type of clinical diagnostic tests, which detects trace amounts of certain proteins in human plasma, has enabled clinicians to identify harmful populations of cells and troublesome cellular processes and change clinical management. Improved assay analytical sensitivity can help identify those individuals that need immediate intervention and effectively rule out disease, and as a result is very useful in screening situations, where a second-line diagnostic strategy can be used to diagnose disease. Therefore, manufacturers are constantly improving the assay sensitivity on their immunoassay analyzers. For example, every generation of thyroglobulin assay made improvements in sensitivity, which resulted in better outcomes for patients after treatment of thyroid cancer.

Immunoassay utilizes the specific binding between immobilized antibodies at solid surfaces and protein biomarkers in the sample fluid. Antibody-biomarker binding for the immunoassay occurs at a solid–liquid interface, resulting in mass transport barriers. Therefore, the mainstream immunoassays with solid-phase supports suffer from slow reaction kinetics due to the presence of an unstirred surface layer that limits the flux of biomolecules to the surface. Additionally, large solid–liquid interface is utilized to promote biomarker recognition but also to

S
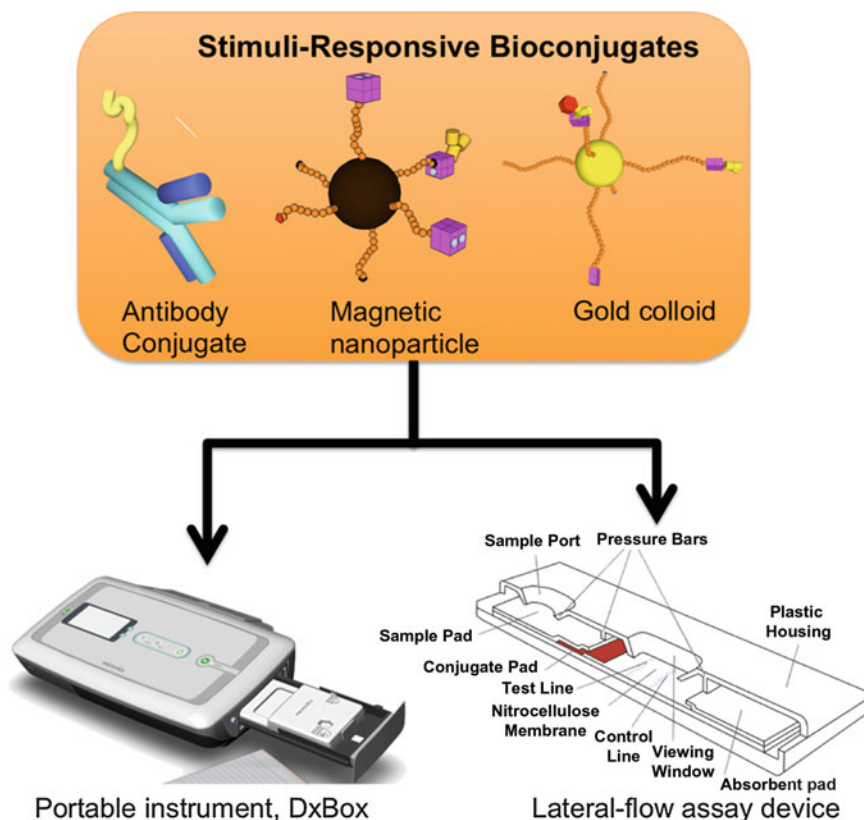
Stimuli-Responsive Bioconjugate, Fig. 3 Stimuli-responsive bioconjugates for diagnostic applications

increase the nonspecific binding, which raises the assay background noise and compromises the limit of detection. Specimen quality and quantity are intrinsically associated with assay performance because the biomarker concentration and the specimen volume define the absolute mass quantity available for detection. The rarity of disease antigens or nucleic acids in a broad sample background can lead to crippling signal-to-noise problems due to nonspecific interactions between contaminating biomolecules and device surfaces. Additionally, the rare antigens and nucleic acids themselves can be lost at various places when they are adsorbed nonspecifically to the device surfaces. Therefore, chromatography has been employed for purifying and concentrating biomarkers prior to diagnostic testing [11, 12].

Stimuli-responsive polymer–biomolecules conjugates have been utilized in achieving liquid-phase/homogeneous affinity separation of target molecules to facilitate chromatography and immunoassays. Reagents containing stimuli-responsive polymers such as pNIPAAm-antibody conjugates also exhibit reversible temperature responsiveness. Stimuli-responsive reagents can replace the antibodies immobilized at solid surfaces to overcome the mass transport limitations associated with heterogeneous immunoassays because the biomarker binding occurs in a homogeneous solution where molecular diffusion of the reagents facilitates rapid mass transport equilibration. Therefore, assay incubation times can be reduced from hours to minutes in many cases without compromising sensitivity. Since a large bulk solid phase is not present during the immunospecific capture step, nonspecific binding is also minimized, which can reduce the assay background noise to improve the limit of detection. Thermally, responsive

polymers and recognition molecules such as antibody are prepared in various formats (e.g., polymer–antibody conjugates, magnetic nanoparticles) to facilitate applications in biomarker separation and detection.

pNIPAAm–IgG Conjugates

pNIPAAm–IgG conjugates were developed to facilitate enzyme-based immunoassay for detecting a wide range of analytes, including clinically relevant biomarkers such as hepatitis B surface antigen (HB-Ag) with analytical sensitivity comparable to conventional ELISA [13, 14]. The IgG–pNIPAAm conjugates are mixed with a biological sample containing the target biomarker and peroxidase-conjugated antibodies (enzyme-antibody detection conjugate). After the sandwich immunocomplex was formed in solution, the solution temperature was increased to above the polymer LCST for aggregating the polymer conjugates and co-aggregating the associated antigen and enzyme-antibody conjugates. The immunocomplex aggregates were isolated via centrifugation. The amount of the captured enzyme-antibody conjugates is then measured and quantitatively correlated with the amount of target biomarker in the original sample.

In addition to centrifugation/precipitation, utilizing membranes for isolating the conjugate aggregates and the bound analytes is also an appealing approach [14, 15]. Golden et al. [16] developed a system of pNIPAAm–antibody conjugates and porous membranes grafted with pNIPAAm for separating and concentrating immunocomplexes within a microfluidic channel. After biomarker binding, heating above the polymer LCST transitioned/transformed the polymers on the membranes and conjugates to the collapsed state, hydrophobic polymer–polymer interaction directed the capture of antibody conjugates with bound biomarkers at the membrane. Upon lowering the temperature, the transition to a hydrophilic state rapidly released the bound polymer conjugates into the flow stream, resulting in a sharp conjugate release profile. Using fluorescently labeled streptavidin as a model antigen, the system showed ca. 80 % capture efficiency and enabled sharp release, 80 % for 15 µl. The system was also

utilized for concentrating biomarkers ca. 40-fold, from 0.2 to 8.5 nM, by capturing antigens from a larger volume specimen. The system can also incorporate enzyme-antibody conjugates for detecting PfHRP2, a malaria antigen, via a sandwich immunoassay. The assay used anti-PfHRP2 IgM-polymer conjugates in conjunction with a horseradish peroxidase-linked antibody to form sandwich immunocomplexes via PfHRP2 binding. The quantity of released detection antibody was shown to be dependent on the PfHRP2 antigen concentration in the specimens. The assay could detect 20–100 ng/ml PfHRP2 from a 50 µl human plasma specimen, which is within the relevant range of antigen for patient samples and comparable to ELISA's detection dynamic [17]. Additionally, the stimuli-responsive membrane assay took less than 10 min.

Stimuli-Responsive Magnetic Nanoparticles

Magnetic beads have been utilized as the solid supports for immunoassays, wherein the antibodies are immobilized on the bead surface for recognizing the target biomarker [18, 19]. A detection conjugate is an antibody with optical labels such as fluorophore, enzyme, etc. that binds to a second epitope on the target biomarker, and the sandwich immunocomplex is separated using a magnetic field. The amount of the separated detection conjugate can then be quantitatively correlated with the amount of target biomarker in the original sample. In this style of immunoassay, particles consisting of polymeric micro-beads impregnated with iron-oxide nanoparticles are often used [20, 21]. These particles are paramagnetic and as such retain no residual magnetization after the magnetic field has been removed. Therefore, the particles can be suspended into a carrier fluid and remain soluble and do not remain magnetically agglomerated after magnetic capture/enrichment has taken place.

Small magnetic nanoparticles (mNPs) such as iron oxide act as single-domain net magnetic dipoles and experience an applied magnetic force in the presence of a magnetic field gradient. Parameters that influence mNP separation include magnetic dipole moment, diffusion

coefficient, the field gradient, etc. Particle size is a key parameter in designing magnetic particle separation systems for biodiagnostics. Small mNPs ca. 10 nm are desirable in affinity separations because their small size enables rapid diffusive mixing and binding to the target analyte. Additionally, smaller particles have larger surface area per unit mass. However, small mNPs are typically difficult to separate using modest magnetic fields because thermal diffusion dominates over the miniscule magnetic forces applied to the small magnetic dipoles of the individual solvated particles. Surface functionalizing the mNPs with pNIPAAm overcomes this size limitation on the magnetic separation because after biomarker binding, polymer-induced particle aggregation can be used to increase the effective magnetophoretic mobility and overcome thermal diffusion. The thermally triggered magnetophoresis [16, 22–25] of pNIPAAm-functionalized mNPs has been reported by several groups, and such particles are also sold commercially.

Lai et al. [23] demonstrated an approach to achieve continuous separation of fluorescently labeled streptavidin using biotinylated pH-responsive mNPs in conjunction with an H-filter microfluidic device to reversibly aggregate mNPs by changing the solution pH. The streptavidin and mNPs complexation was done via mixing, and then the solution pH was lowered to induce mNP aggregation outside of the microchannel. The system was designed to pull aggregated mNPs and the bound target analytes from one flow stream across the laminar fluid interface into an adjacent flow stream. The solution was introduced into the microfluidic channel in a laminar flow stream at low pH where the mNPs remained aggregated. As the aggregates flowed through a magnetic field, they were magnetophoresed laterally across the laminar fluid interface and into the adjacent higher pH buffer stream, carrying the fluorescently labeled streptavidin with them. Because the polymer coating was sharply pH responsive, the adjacent flow stream with an alkaline pH transitioned the

aggregates to individual soluble mNPs with low magnetophoretic mobility. The soluble mNPs continued to flow into the receiving stream rather than being captured at the channel surface near the magnet. Movement of other molecules into the second flow stream meanwhile was limited by diffusion due to the low Reynolds number (laminar) fluid flow thereby achieving continuous purification of the target in the device.

Stimuli-Responsive Gold Colloids

Gold colloid is a key reagent in the biodiagnostics field due to their unique nanoscopic physical and chemical properties. Gold colloids can be prepared in bulk quantities with very narrow size distributions (<10 % SD) and are readily functionalized with affinity ligands through a variety of conjugation schemes, including thiol chemisorption and nonspecific protein adsorption. Additionally, gold colloids are stable for long periods of time and can be stored in a dry format and later rehydrated with good preservation of specific binding activity. pNIPAAm-functionalized gold colloids have been utilized in tunable plasmonic devices and biodetection by controlling the red-shift of the LSPR via stimuli-responsive polymer-induced aggregation [26].

Recently, Nash et al. [27] demonstrated a novel two-particle reagent system for separating pNIPAAm-gold colloids via a magnetic field. The system consisted of a mixture of pNIPAAm-mNPs and pNIPAAm-gold colloids. Gold colloids ($\sim$25 nm diameter) were modified with an amine-containing diblock copolymer, and mNPs ($\sim$10 nm diameter) were synthesized directly with a homo-pNIPAAm polymer surface coating. When mixtures of these two particle types were heated above the polymer LCST, the particles co-aggregated driven by hydrophobic interactions between the collapsed pNIPAAm. The aggregates exhibit a strongly enhanced magnetophoretic mobility that allowed them to be rapidly co-separated in a modest applied magnetic field gradient. The magnetically captured aggregates were redissolved into a smaller

volume of fluid, which resulted in highly concentrated gold colloids.

Nash et al. utilized the two-particle reagent system for concentrating gold-labeled biomarkers to improve the detection limit for clinically relevant malaria biomarkers via lateral-flow tests. The pNIPAAm-gold colloids functionalized with streptavidin were used in conjugation with biotinylated Ab for recognizing and concentrating biomarkers via the two-particle reagent system. The system that can achieve magnetic separation and concentrate gold nanoparticle-biomarker "half immunosandwiches" was advantageous because it enabled direct enrichment of the active gold-biomarker detection reagent, analogous to what is formed after dissolution of the conjugate pad in a typical immunochromatographic biosensor. Magnetic enrichment of gold colloids was achieved via polymer-induced co-aggregation and separation with pNIPAAm-mNPs. After enrichment, the concentrated particle mixture was directly applied to the lateral-flow membranes, and the target biomarker was visualized by the eye at the test line of the immunochromatographic flow strip.

Conclusion

Bioconjugation that utilizes synthetic polymers to modify naturally produced macromolecules (e.g., protein, peptide, nucleic acid, etc.) has a relatively long history of being used within the area of drug delivery, imaging, diagnostics, etc. because the synthetic polymer can provide a mechanism to tune the bioactivity of the biomolecules or passively stabilizing the biomolecules. Stimuli-responsive polymers that can enhance the biomolecules stability and solubility, are utilized to simultaneously provide responsive behavior and numerous sites for subsequent functionalization. Therapies based on biologic drugs have the potential to revolutionize the treatment of many serious diseases but will require the creation of powerful new drug delivery technologies. RAFT polymerization methodology is facilitating the development of a new generation of polymeric drug delivery systems with previously unatainable molecular architectures. These materials can be synthesized easily without the need for protecting group chemistry or postpolymerization modification reactions. Because RAFT is tolerant of most common functional groups, sophisticated molecular architectures can be engineered that contain the numerous functional modules necessary to achieve biologic drug delivery. Immunoassay, one type of clinical diagnostic tests, which detects trace amounts of certain proteins in human plasma, has enabled clinicians to identify harmful populations of cells and troublesome cellular processes and change management. The mainstream immunoassays utilize antibodies immobilized on solid-phase support to recognize and separate biomarkers, which results in slow reaction kinetics and compromises assay limit of detection. Stimuli-responsive bioconjugates are also utilized to address the clinical diagnostic challenges associated with the biomarker separation via solid-phase supports. The conjugates can facilitate biomarker separation to enable rapid immunoassays. The stimuli-responsive bioconjugates can enhance assay analytical sensitivity to help identify those individuals that need immediate intervention and effectively rule out disease and as a result are very useful in screening situations, where a second-line diagnostic strategy can be used to diagnose disease.

Related Entries

References

1. Schild HG (1992) Poly(N-isopropylacrylamide)-experiment, theory, and application. Progr Polym Sci 17:163–249

2. Hentschel J, Bleek K, Ernst O et al (2008) Easy access to bioactive peptide-polymer conjugates via RAFT. Macromolecules 41:1073–1075

3. Xu JT, Boyer C, Bulmus V et al (2009) Synthesis of dendritic carbohydrate end-functional polymers via RAFT: versatile multi-functional precursors for bioconjugations. J Polym Sci Pol Chem 47:4302–4313

4. Cheng Z, Al Zaki A, Hui JZ et al (2012) Multifunctional nanoparticles: cost versus benefit of adding targeting and imaging capabilities. Science 338:903–910

5. O'brien ME, Wigler N, Inbar M et al (2004) Reduced cardiotoxicity and comparable efficacy in a phase III trial of pegylated liposomal doxorubicin HCl (CAELYX/Doxil) versus conventional doxorubicin for first-line treatment of metastatic breast cancer. Ann Oncol 15:440–449

6. Sparano JA, Makhson AN, Semiglazov VF et al (2009) Pegylated liposomal doxorubicin plus docetaxel significantly improves time to progression without additive cardiotoxicity compared with docetaxel monotherapy in patients with advanced breast cancer previously treated with neoadjuvant-adjuvant anthracycline therapy: results from a randomized phase III study. J Clin Oncol 27:4522–4529

7. Jia Z, Wong L, Davis TP et al (2008) One-pot conversion of RAFT-generated multifunctional block copolymers of HPMA to doxorubicin conjugated acid- and reductant-sensitive crosslinked micelles. Biomacromolecules 9:3106–3113

8. Li C (2002) Poly(ʟ-glutamic acid)–anticancer drug conjugates. Adv Drug Deliv Rev 54:695–713

9. Henry SM, El-Sayed ME, Pirie CM et al (2006) pH-responsive poly(styrene-alt-maleic anhydride) alkylamide copolymers for intracellular drug delivery. Biomacromolecules 7:2407–2414

10. Lutz JF (2008) Polymerization of oligo(ethylene glycol) (meth)acrylates: toward new generations of smart biocompatible materials. J Polym Sci Pol Chem 46:3459–3470

11. Krishnan M, Namasivayam V, Lin RS et al (2001) Microfabricated reaction and separation systems. Curr Opin Biotechnol 12:92–98

12. Ocvirk G, Verpoorte E, Manz A et al (1995) High-performance liquid-chromatography partially integrated onto a silicon chip. Anal Method Instrum 2:74–82

13. Lin P, Zheng H, Yang HH et al (2003) Enzyme-linked fluorescence immunoassay for human IgG by using a pH-sensitive phase separating polymer as carrier. Chem J Chin Univ Chinese 24:1198–1200

14. Monji N, Cole CA, Tam M et al (1990) Application of a thermally-reversible polymer-antibody conjugate in a novel membrane-based immunoassay. Biochem Biophys Res Commun 172:652–660

15. Monji N, Cole CA, Hoffman AS (1994) Activated, N-substituted acrylamide polymers for antibody coupling- application to a novel membrane-based immunoassay. J Biomater Sci-Polym Ed 5:407–420

16. Furukawa H, Shimojyo R, Ohnishi N et al (2003) Affinity selection of target cells from cell surface displayed libraries: a novel procedure using thermo-responsive magnetic nanoparticles. Appl Microbiol Biotechnol 62:478–483

17. Kifude CM, Rajasekariah HG, Sullivan DJ Jr et al (2008) Characterization of enzyme linked immunosorbent assay for plasmodium falciparum histidine-Rich Protein 2 in blood, plasma and serum. Clin Vaccine Immunol 15(6):1012–8. doi:10.1128/CVI.00385-07

18. Dittmer WU, Evers TH, Hardeman WM et al (2010) Rapid, high sensitivity, point-of-care test for cardiac troponin based on optomagnetic biosensor. Clinica Chimica Acta 411:868–873

19. Jain KK (2003) Nanodiagnostics: application of nanotechnology in molecular diagnostics. Expert Rev Mol Diagn 3:153–161

20. Ahn KC, Lohstroh P, Gee SJ et al (2007) High-throughput automated luminescent magnetic particle-based immunoassay to monitor human exposure to pyrethroid insecticides. Anal Chem 79:8883–8890

21. Tsai HY, Hsu CF, Chiu IW et al (2007) Detection of c-reactive protein based on immunoassay using antibody-conjugated magnetic nanoparticles. Anal Chem 79:8416–8419

22. Lai JJ, Hoffman JM, Ebara M et al (2007) Dual magnetic-/temperature-responsive nanoparticles for microfluidic separations and assays. Langmuir 23:7385–7391

23. Lai JJ, Nelson KE, Nash MA et al (2009) Dynamic bioprocessing and microfluidic transport control with smart magnetic nanoparticles in laminar-flow devices. Lab on a chip 9:1997–2002

24. Nash MA, Lai JJ, Hoffman AS et al (2010) "Smart" diblock copolymers as templates for magnetic-core gold-shell nanoparticle synthesis. Nano Lett 10:85–91

25. Wuang SC, Neoh KG, Kang ET et al (2006) Heparinized magnetic nanoparticles: in-vitro assessment for biomedical applications. Adv Funct Mater 16:1723–1730

26. Zhu MQ, Wang LQ, Exarhos GJ et al (2004) Thermosensitive gold nanoparticles. J Am Chem Soc 126:2656–2657

27. Nash MA, Yager P, Hoffman AS et al (2010) A mixed gold and magnetic nanoparticle system for purification, enrichment, and detection of biomarkers. Bioconjugate Chemistry 21:2197–2204

Stimuli-Responsive Polymer Films

Manfred Stamm
Leibniz-Institut für Polymerforschung Dresden and Technische Universität Dresden, Dresden, Germany

Synonyms

Adaptive surfaces; Responsive thin films; Switchable surfaces

Definition

Stimuli-responsive polymer films are thin polymer films that respond to external stimuli like temperature, solvent, pH, salt content, light, etc. by a change in properties of the film.

Principle

These changes in properties can be changes in wetting, charge, adhesion, friction, hardness, solubility, or optical absorption, for example, but also the release of drugs or particles. The changes can be frozen in after the application of stimulus or may only be present with the application of stimulus; they can be reversible or happen only in one direction. The response is from a physicochemical aspect in many cases connected with phase transitions like the collapse of the chain conformation triggered by solvent, temperature, pH, salt content, or by a phase segregation of one component at the surface, driven by surface energy for example. There are other cases where a nonequilibrium structure is frozen in, which then relaxes under the influence of a stimulus to the equilibrium state connected with a change in properties. Typical examples here are dewetting of a thin film during temperature or solvent-vapor treatment to form a rough surface or the crystallization and/or orientation of a material in a thin film during annealing which usually is also connected with a change in the optical,

mechanical, and topological properties. So the spectrum is extremely wide and there are plenty of possibilities and examples.

Properties

Stimuli-responsive polymer films on the other hand have gained significant interest because of their unique ability to change the (surface) properties of a material quite significantly by a stimulus, where just a thin film, maybe a nanoscopic layer at the surface, changes its properties, while the bulk material is not affected. They may also be used for sensing of the environment or to react or adapt to the environmental changes. So also the area of application is very wide. There are several recent reviews that provide a good survey of concepts and applications [1–5]. In the following, some examples will be given focusing on a specific kind of stimuli-responsive polymer films, so-called polymer brushes which again offer a wide spectrum of possibilities and applications.

Polymer Brushes

Thin polymer films may be prepared generally in different ways: (a) casting from solution by spin coating, dip coating, etc. (b) adsorption from solution for self-assembled mono- or multilayers or (c) chemical grafting from solution or melt. In the latter case, one can mainly distinguish between grafting-from, where polymerization is initiated from the surface, and grafting-to, where end-functionalized chains are chemically attached to the surface. Grafting procedures may result in thin monolayers of end-attached chains, so-called polymer brush layers (Fig. 1). This terminology is used in particular at high grafting densities where due to steric repulsion, chains adopt an extended conformation [1, 4]. It is quite common practice to also use it for intermediate grafting densities, where chains are only slightly stretched. On the other hand, one should note that typical stimuli-responsive polymer brush coatings are only 5–20 nm thick in dry state and mostly consist of a polymer monolayer at intermediate grafting

S
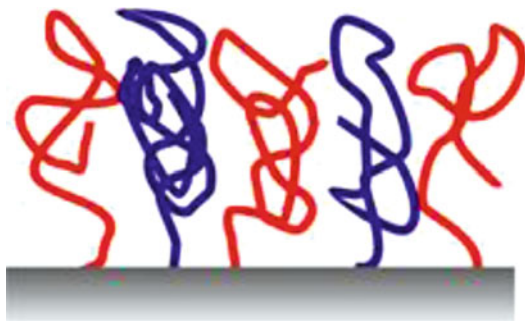
Stimuli-Responsive Polymer Films, Fig. 1 Stimuli responsive polymer brush layers

density with chains of molecular weights between 10 and 50 kg mol^{-1}. It turns out that responsiveness is best obtained in this range.

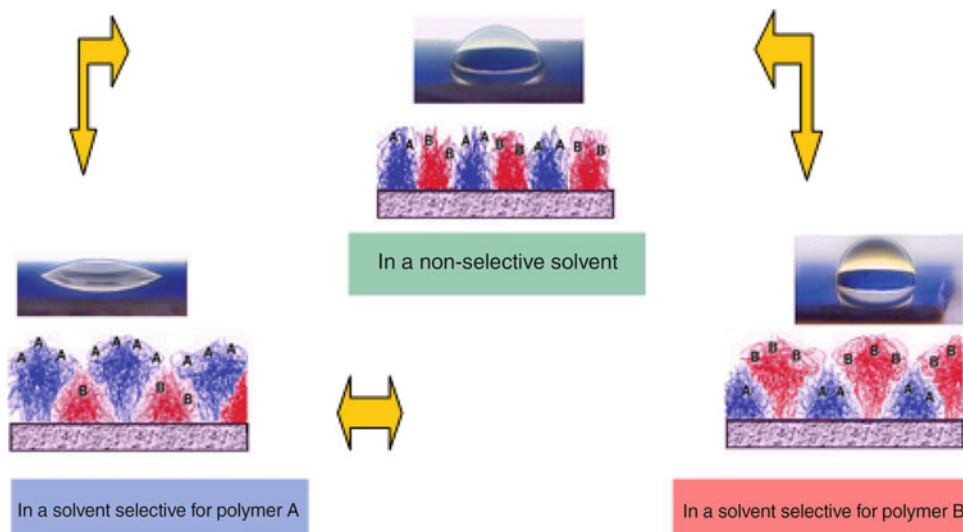## Stimuli-Responsive Polymer Brush Layers

Stimuli-responsive polymer films are obtained with polymer brushes when stimuli-responsive polymers are used as constituents of the brush layers. So already a homopolymer brush layer can be stimuli responsive. Prominent examples are PNIPAm brushes, which undergo with temperature a LCST behavior [6]. The chain conformations collapse in water at T > 32 °C, which causes a film thickness change for example from 50 nm at 20 °C to 10 nm at 50 °C, and at the same time the surface becomes more hydrophobic. As a consequence, for instance, the adsorption of polymer chains on the brush layer is influenced [7]. This transition is reversible with only small hysteresis. Similarly PAA brushes will be negatively charged at high pH and collapsed in neutral state at low pH, while P4VP brushes are positively charged at low pH and collapsed in neutral state at large pH. In all those cases the surface properties are modified by an external stimulus, temperature or pH, and for instance the adsorption of proteins or the adhesion of cells may be controlled in this way. PEO brushes on the other hand are essentially unaffected by both pH and temperature changes and may be considered as inert to those stimuli.

Binary Polymer Brush Layers

Using binary brush systems offers still further possibilities for stimuli-responsive polymer films. Typical examples are binary brush surfaces which can be switched from hydrophobic to hydrophilic behavior by solvent treatment (Fig. 2). The binary brushes consist of a hydrophobic and hydrophilic component, e.g., statistically grafted PS and P4VP chains, respectively. Utilizing a selective solvent like toluene the hydrophobic PS chains are swollen, while the hydrophilic ones are collapsed, thus exposing the hydrophobic chains to the surface. This state can be frozen in by fast evaporation of the solvent. With acidic water on the contrary, the hydrophilic P4VP chains are swollen and exposed to the surface, thus producing a hydrophilic coating upon drying. The different solvents act in this case as the external stimuli for switching of the film properties. This switching effect is largely amplified by further introduction of a surface roughness. The switching of binary brush systems on rough surfaces with external stimuli can take place between ultra-hydrophobic and ultra-hydrophilic states (water contact angles >150° and <10°). This is for instance also achieved on fabrics, where switching in the dryer (temperature >60 °C) goes to ultra-hydrophobic state and in the washing machine (basic environment, T > 60 °C) hydrophilic switching occurs [8]. Fabrics can be therefore highly water repellent in everyday use and still may be cleaned in the washing machine.

Particles with Attached Polymer Brushes

Also colloidal particles can be stimuli responsive when they are covered with polymer brushes. So they can be dispersed in quite diverse solvents or flocculated with temperature or pH (Fig. 3). They can also be used for coatings on solid flat substrates to introduce stimuli-responsive behavior. Colloidal particles are, for instance, functionalized with binary brushes for switching between hydrophobic and hydrophilic behavior. In a roll-to-roll process, they then can be coated

Stimuli-Responsive Polymer Films, Fig. 2 Switching of surface properties of binary polymer brush layers with selective solvents. Either the blue or red chains (left and right) are on the surface, which causes hydrophilic or hydrophobic behavior after drying. Water droplets on those surfaces are also shown where contact angles change significantly. In a non-selective solvent (middle) an intermediate behavior is obtained. Changes are fully reversible since they are only connected with changes of chain conformations at the surface

Stimuli-Responsive Polymer Films, Fig. 3 Cryo-TEM images of polymer brushes (polyacrylic acid PAA) attached to a colloidal silica particle at different pH (pH5 and pH10) causing collapse (left) or swelling (right) of the chains. The silica particle size is 100nm
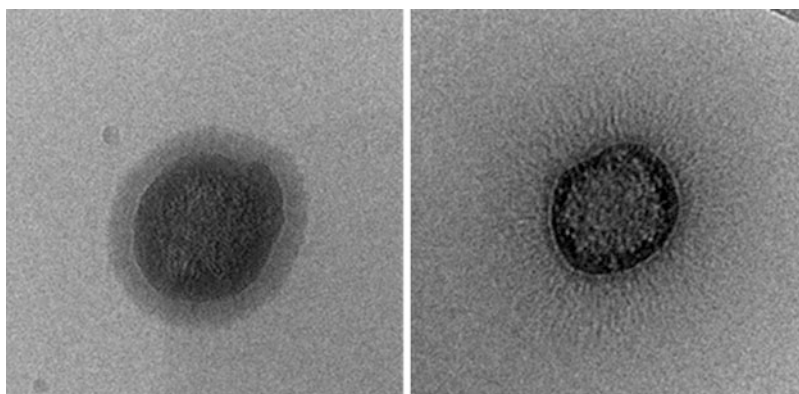
from water dispersion on a polymer foil to form an irregular rough surface. By temperature, this coating can be switched from hydrophilic to hydrophobic, and a flexible polymer foil with ultra-hydrophobic behavior is formed. After crosslinking, it still can be stimuli responsive, while colloidal particles are fixed at the surface. There are plenty of possibilities for functionalization of particles with polymers including Janus particles where two sides of the particles are functionalized with different polymers which then also can be stimulus responsive.

Control of Adhesion

It has been mentioned already that hydrophobic or hydrophilic nature of the brush layer can be changed by a stimulus, which also changes the interaction with polymer chains for adhesion. This is observed for a simple brush layer when a stimuli-responsive polymer is attached or with binary brush layers when two polymers with different behaviors are attached [7]. So a hydrophobic polymer shows higher adhesion when the brush layer exhibits hydrophobic behavior and

S

**Stimuli-Responsive
Polymer Films,
Fig. 4** Switching of
protein adhesion
(chymotrypsin) on pH-
responsive polymer brushes
(mixed polyacrylic acid
PAA/ poly-4-vinylpyridine
P4VP brush) as measured
by ellipsometry
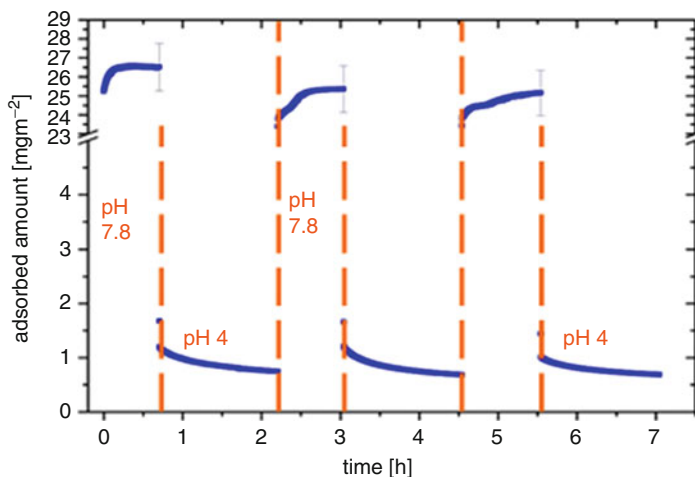
less adhesion when it is switched to the hydro-philic state. In this way, adhesion can be tuned and depends on an external stimulus.

Adsorption of Proteins

Also the adsorption of polyelectrolytes, proteins, and cells to surfaces can be controlled by stimuli-responsive polymer brush layers, which then should contain responsive polyelectrolytes (Fig. 4). The behavior is complex and difficult due to the combined response to pH, temperature, and salt content, where both the different constituents of the brush layer and the adsorbing species respond on those stimuli in a complex way [9]. So adsorption might even occur, when both the surface and the adsorbing molecules are positively charged, and one would expect Coulombic repulsion. Adsorption might occur, however, due to the so-called counterion evaporation effect, where by the adsorption of the chains in solution the counterions in the brush layer are replaced by the adsorbing molecules and thus produce an entropic driving force for adsorption via the counterions which then are free in solution ("evaporated"). This effect can compensate the repulsion from the charges. In addition, one should take into account that molecules like proteins may have a distribution of charges and adhesion sites along the molecule which then

could locally bind. So protein adsorption can be controlled by responsive polymer brushes causing e.g., adsorption and release of proteins to the surface by a change in pH, but properties are difficult to predict. Similarly one can also try to control the adhesion and release of cells to surfaces by responsive brush layers.

Sensing with Responsive Brush Layers

Polymer brushes can be further functionalized with nanoparticles, dyes or enzymes, for example for different applications, which are connected with the stimulus-responsive properties of the brushes. The responsive behavior is used for sensing at nanoscale for instance. So sensing of the swelling of the chains in different solvents can be detected optically, when quantum dots are attached to a brush layer (Fig. 5). The intensity of emitted light is modulated by interference effects when the brush is swelling at different levels in different solvents. This optical effect can be used for sensing of the solvents present at the surface. Similarly also the plasmon resonance of metallic nanoparticles attached to polymer brushes can be used for solvent or pH sensing with stimuli-responsive chains [10] or surface-enhanced Raman scattering for local chemical sensing [11]. Using those principles, functional particles, dyes, or drugs may be hidden in the brush layer or
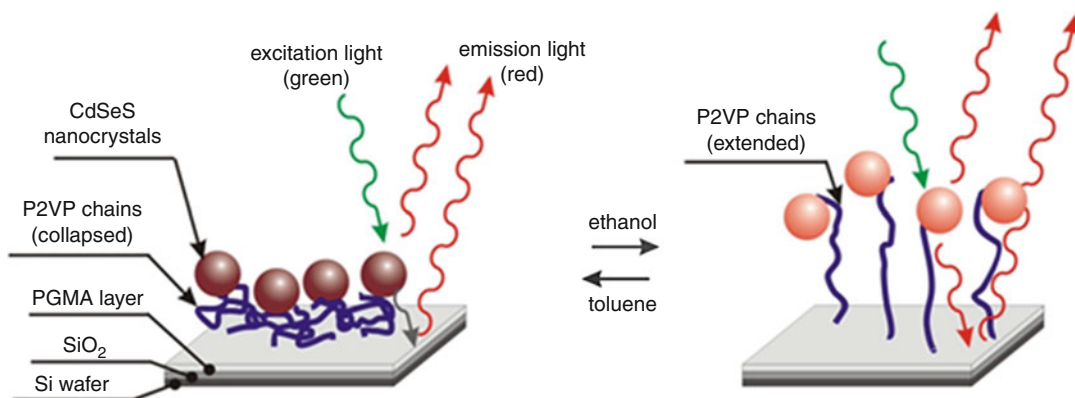
Stimuli-Responsive Polymer Films, Fig. 5 Sensing of swelling of P4VP polymer brush in different solvents by fluorescence of attached quantum dots. Depending on degree of swelling in different solvents the interference of fluorescent light will modulate the intensity which can be taken as a sensor for the degree of swelling

be exposed to the outside depending on an external stimulus, which offers many possibilities to control catalysis, enzymatic reactions, or drug delivery for example.

Related Entries

▶ Applications of Block Copolymers in Thin Films: Nanopatterning
▶ Biosensing Materials
▶ Controlling Wetting Properties of Polymers
▶ Polymer Brushes
▶ Polymer-Based Sensors
▶ Polymeric Coatings to Fight Biofouling
▶ Smart Materials
▶ Stimuli-Responsive Polymers
▶ Thermoresponsive Polymers

References

1. Cohen Stuart MA, Huck WTS, Genzer J, Müller M, Ober C, Stamm M, Sukhorukov GB, Szleifer I, Tsukruk VV, Urban M, Winnik F, Zauscher ST, Luzinov I, Minko S (2010) Emerging applications of stimuli-responsive polymer materials. Nat Mater 9:101–113
2. Urban MW (2005) Stimuli-responsive polymeric films and coatings, vol 912, ACS syposium series. ACS, Washington, DC
3. Urban MW (2011) Handbook of stimuli-responsive materials. Wiley-VCH, Weinheim
4. Knoll W, Advincula RC (2011) Functional polymer films, vols 1 and 2. Wiley/VCH, Weinheim
5. Advincula RC, Brittain WJ, Caster KC, Rühe J (2004) Polymer brushes. Wiley/VCH, Weinheim
6. Rauch S, Eichhorn K-J, Oertel U, Stamm M, Kuckling D, Uhlmann P (2012) Temperature responsive polymer brushes with *clicked* rhodamine B: synthesis, characterization and swelling dynamics studied by spectroscopic ellipsometry. Soft Matter 8:10260–10270
7. Synytska A, Svetushkina E, Martina D, Bellmann C, Simon F, Ionov L, Stamm M, Creton C (2012) Intelligent materials with adaptive adhesion properties based on comb-like polymer brushes. Langmuir 28:16444–16454
8. Messerschmidt M, Komber H, Häußler L, Hanzelmann CH, Stamm M, Raether B, da Costa d Silva O, Uhlmann P (2013) Amphiphilic ABC triblock copolymers tailored via RAFT polymerization as textile surface modifiers with dual-action properties. Macromolecules 46:2616–2627
9. Bittrich E, Rodenhausen KB, Eichhorn K-J, Hofmann T, Schubert M, Stamm M, Uhlmann P (2011) Protein adsorption on and swelling of polyelectrolyte brushes: a simultaneous ellipsometry-quartz crystal microbalance study. Biointerphases 5:159–167
10. Gupta S, Agrawal M, Uhlmann P, Simon F, Oertel U, Stamm M (2008) Gold nanoparticles immobilized on stimuli responsive polymer brushes as nanosensors. Macromolecules 41:8152–8158
11. Gupta S, Agrawal M, Conrad M, Hutter NA, Olk P, Simon F, Eng LM, Stamm M, Jordan R (2010) Poly(2-(dimethylamino)ethyl methacrylate) brushes with incorporated nanoparticles as a SERS active sensing layer. Adv Funct Mater 20:1756–1761

S

Stimuli-Responsive Polymers

Akihito Hashidzume and Akira Harada
Department of Macromolecular Science,
Graduate School of Science, Osaka University,
Machikaneyama, Toyonaka, Osaka, Japan

Synonyms

Intelligent soft materials; Smart soft materials

Definition

Stimuli-responsive polymers are polymers which dramatically change their properties, e.g., solubility or viscoelasticity, in response to external stimuli, including temperature, pH, and chemicals.

Background

In these decades, smart or intelligent materials have drawn considerable interest from researchers in materials science. In these materials, polymers, which change their properties responsive to external stimuli, play a vital role [1, 2]. This entry describes briefly stimuli and responses for stimuli-responsive polymers and overviews some typical examples of stimuli-responsive polymers.

Stimuli and Responses

Stimuli

Stimuli for stimuli-responsive polymer include temperature, pressure, pH, chemicals, light, and redox [3].

Temperature is the most common stimulus for stimuli-responsive polymers. Because all physical and chemical events proceed to thermally stable states, all materials are active against heat, and thus, their states depend on temperature. As the temperature of a polymer system is changed, the quality of medium may become better or worse, leading to alterations in the conformation of a polymer.

Pressure is another common stimulus for stimuli-responsive polymers because the state of materials is also dependent on pressure. However, these are fewer examples of pressure-responsive polymer systems presumably because of experimental difficulties in varying the pressure. Applying force or stress to polymers may cause changes in the structure or conformation or alteration in the solvent quality of supercritical fluid.

pH is a popular stimulus for stimuli-responsive polymers. As the pH of medium is increased, acids are converted from their neutral to anionic state, and bases are converted from their cationic and neutral state. Because these conversions switch the electrostatic interaction between the acid and base residues, leading to a change in the polymer conformation. Thus, polymers carrying acid or base moieties, e.g., carboxylic acid, hydroxyl, amine, and pyridine groups, act as pH-responsive polymers.

Chemicals are an important class of stimuli for stimuli-responsive polymers. Chemical stimuli can be categorized as either modifiers of the solvent quality or interacting molecules. Modifiers of the solvent quality contain solubilizers, precipitants, and salts. Interacting molecules contain hydrogen-bonding donors or acceptors, amphiphiles, and cyclodextrins. When the solvent quality is controlled by adding modifiers or interacting molecules are bound onto the polymer, the polymer may take a different conformation.

Light is a stimulus of increasing importance for stimuli-responsive polymers. The energy of light varies over a wide range, depending on the wavelength. Near-UV or visible light ($\lambda = 200$–750 nm) is usually used as a stimulus for photoresponsive polymers. Light-responsive (photoresponsive) polymers possess aromatic moieties that absorb light, leading to structural changes. Photoinduced structural changes include photoisomerization, photodimerization, and photoinduced decomposition.

Redox is a promising stimulus for stimuli-responsive polymers because the redox state can be controlled not only chemically but also electrically. Redox-responsive polymers contain redox-responsive residues, i.e., metal complexes, aromatic moieties, disulfides, and peroxides. When these residues undergo redox reactions, their charged states are switched, or bonds are cleaved or formed, leading to structural or conformational changes.

Responses

The responses of stimuli-responsive polymers are based on the change in polymer conformation, which is induced by alterations of interaction between the polymer and solvent or between polymer side chains. The change in polymer conformation finally results in switching properties, e.g., solubility and viscoelasticity.

Typical Examples of Stimuli-Responsive Polymer Systems

Temperature-Responsive (Thermoresponsive) Polymer Systems

Thermoresponsive polymers have been most widely investigated among stimuli-responsive polymers. Especially, polymers, whose aqueous solutions undergo phase separation by cooperative dehydration at a certain temperature (i.e., clouding point), have attracted significant interests from researchers in macromolecular science. When phase separation of an aqueous polymer solution occurs at higher temperatures, the solution system shows a lower critical solution temperature (LCST) (Fig. 1a). Whereas phase separation occurs at lower temperature, the solution system shows an upper critical solution temperature (UCST) (Fig. 1b). Typical examples of LCST-type polymers are poly(N-isopropylacrylamide) [4] and polymers carrying a number of oligo(ethylene glycol) grafts [5], whereas typical examples of UCST-type polymers are polybetains [6]. Recent developments of controlled polymerization techniques allow ones to synthesize various block copolymers possessing blocks of LCST- or UCST-type polymers [7]. These block copolymers form micellar aggregates at a limited temperature regime: block copolymers carrying LCST- and UCST-type blocks form aggregates at higher and lower temperatures, respectively. These block copolymers may be useful for controlled release systems.

Pressure-Responsive Polymer Systems

Supercritical fluids have been investigated as environmentally benign solvents. It is known that supercritical carbon dioxide is a solvent for various polymers, e.g., polystyrene, poly (dimethylsiloxane), and fluorinated polymers, and its solvent quality usually becomes better at a higher pressure [8]. Since fluorinated polymers are insoluble not only in water but also in many conventional organic solvents, block copolymers possessing fluorinated blocks form micellar aggregates in various solvents. It is noteworthy that the micellization of fluorinated block copolymers can be controlled in supercritical carbon dioxide by changing the pressure [9].
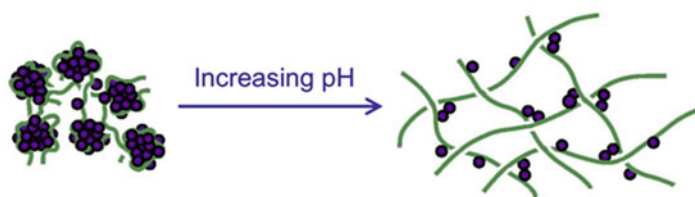
pH-Responsive Polymer Systems

A major class of water soluble polymers are polymers carrying carboxylic acids, e.g., poly(acrylic acid). Since carboxylic acid is a weak acid, it is neutral at lower pH and anionic at higher
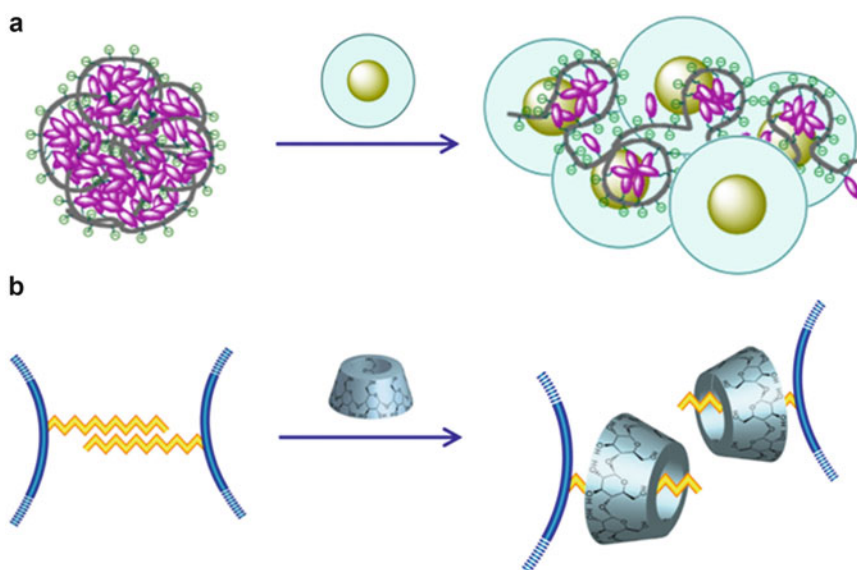
S

Stimuli-Responsive Polymers,
Fig. 1 Conceptual illustrations of the turbidity as a function of temperature for aqueous solutions of LCST-type (**a**) and UCST-type polymers (**b**)
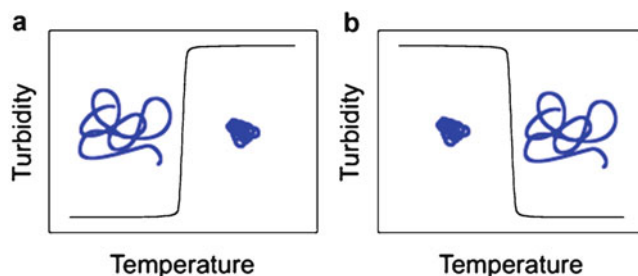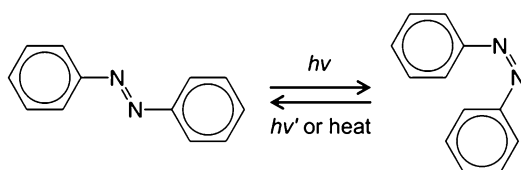
Stimuli-Responsive Polymers, Fig. 2 Conceptual illustration of the effect of pH on the aggregation behavior of hydrophobically modified polycarboxylic acid

Stimuli-Responsive Polymers, Fig. 3 Conceptual illustrations for the interaction of amphiphilic polymers with surfactant micelles (**a**) and with cyclodextrins (**b**)

pH. Thus, polycarboxylic acids take a compact conformation at lower pH and an expanded conformation at higher pH because of electrostatic repulsion between carboxylate residues. When polycarboxylic acids are modified with hydrophobic residues, they act as pH-responsive associative thickeners based on hydrophobic association (Fig. 2) [10]. A typical example of pH-responsive associative thickeners is hydrophobically modified alkali-swellable emulsion (HASE), i.e., terpolymers of methacrylic acid, ethyl acrylate, and a surfactant monomer [11]. Hydrophobically modified polycarboxylic acids have been widely utilized in industry.


Stimuli-Responsive Polymers, Fig. 4 *Trans*-to-*cis* photoisomerization of azobenzene

Chemical-Responsive Polymer Systems

Since the properties of all polymers can depend on some additives (i.e., chemical stimuli), all the polymers are chemical responsive. Chemical stimuli include precipitants, dispersants,

Stimuli-Responsive Polymers, Fig. 5 Redox reaction of ruthenium tris (2,2'-bipyridine) complex
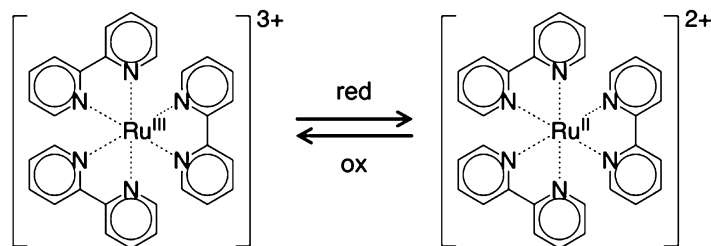
solubilizers, salts, surfactants, and cyclodextrins. Addition of precipitants, dispersants, solubilizers, or salts may alter the conformation of polymers in solvents. When surfactants or cyclodextrins are added to aqueous solutions of amphiphilic polymers, mixed micelles or inclusion complexes may be formed, in which the polymers take a different conformation, resulting in changes in the solution properties, e.g., viscosity. Interaction of amphiphilic polymers with surfactants [12] or with cyclodextrins [13, 14] has been widely studied (Fig. 3).

Light-Responsive (Photoresponsive) Polymer Systems

Photoresponsive polymers carry photoresponsive residues in their backbone or side chains. The most popular photoresponsive residue may be azobenzene. Azobenzene takes the *trans* form under ambient conditions. Azobenzene is isomerized from *trans* to *cis* under photoirradiation with UV light and from *cis* to *trans* under photoirradiation with visible light or at higher temperatures (Fig. 4). Azobenzene can act as a mesogen in the *trans* form because of its rigid-rod structure, whereas it cannot in the *cis* form. Azobenzene residues have been utilized for photoresponsive movement of liquid crystalline polymer films [15].

Redox-Responsive Polymer Systems

Redox-responsive polymers carry redox-responsive residues in their backbone or side chains. An important class of redox-responsive residues is transition metal complexes because transition metals can take different oxidation numbers. When transition metal complex residues in polymers are reduced or oxidized, the

electrostatic interactions between the complex residues are changed, leading to alteration in the polymer conformation. It was reported that poly(*N*-isopropylacrylamide) gels carrying ruthenium tris(2,2'-bipyridine) complex residues exhibited redox-responsive expansion-contraction motions because of the LCST depending the oxidation state of ruthenium complex (Fig. 5). Using this system, molecular actuators have been prepared by combination with the Belousov–Zhabotinsky reaction [16].

Related Entries

▶ Calixarenes-based Supramolecular Polymers
▶ Crown ethers-based Supramolecular Polymers
▶ Cucurbiturils-based Supramolecular Polymers
▶ Cyclodextrins-based Supramolecular Polymers
▶ Micelles and Vesicles
▶ Supramolecular Hydrogels
▶ Supramolecular Network Polymers
▶ Supramolecular Polymers (Coordination bonds)
▶ Supramolecular Polymers (Host-guest interactions)
▶ Supramolecular Polymers (Hydrogen bonds)

References

1. McCormick CL (ed) (2001) Stimuli-responsive water soluble and amphiphilic polymers. ACS symposium series, vol 780. American Chemical Society, Washington, DC
2. Roy D, Cambre JN, Sumerlin BS (2010) Future perspectives and recent advances in stimuli-responsive materials. Prog Polym Sci 35(1–2):278–301. doi:10.1016/j.progpolymsci.2009.10.008

S

3. Hashidzume A, Harada A (2012) Stimuli-responsive systems. In: Harada A (ed) Supramolecular polymer chemistry. Wiley-VCH, Weinheim, pp 231–267. doi:10.1002/9783527639786.ch11

4. Schild HG (1992) Poly(*N*-isopropylacrylamide): experiment, theory and application. Prog Polym Sci 17(2):163–249

5. Weber C, Hoogenboom R, Schubert US (2012) Temperature responsive bio-compatible polymers based on poly(ethylene oxide) and poly(2-oxazoline)s. Prog Polym Sci 37(5):686–714. doi:10.1016/j.progpolymsci.2011.10.002

6. Kudaibergenov S, Jaeger W, Laschewsky A (2006) Polymeric betaines: synthesis, characterization, and application. Adv Polym Sci 201(1):157–224. doi:10.1007/12_078

7. Aoshima S, Kanaoka S (2009) A renaissance in living cationic polymerization. Chem Rev (Washington, DC) 109(11):5245–5287. doi:10.1021/cr900225g

8. Kirby CF, McHugh MA (1999) Phase behavior of polymers in supercritical fluid solvents. Chem Rev (Washington, DC) 99(2):565–602. doi:10.1021/cr970046j

9. George DW (1999) Neutron scattering studies of polymers in supercritical carbon dioxide. J Phys Condens Matter 11(15):R157–R177. doi:10.1088/0953-8984/11/15/006

10. Hashidzume A, Morishima Y, Szczubialka K (2002) Amphiphilic polyelectrolytes. In: Tripathy SK, Kumar J, Nalwa HS (eds) Handbook of polyelectrolytes and their applications, vol 2. American Scientific Publishers, Stevenson Ranch, pp 1–63

11. Jenkins RD, DeLong LM, Bassett DR (1996) Influence of alkali-soluble associative emulsion polymer architecture on rheology. In: Glass JE (ed) Hydrophilic polymers. Performance with environmental acceptance. Advances in chemistry series, vol 248. American Chemical Society, Washington, DC, pp 425–447

12. Kwak JCT (ed) (1998) Polymer-surfactant systems. Surfactant science series, vol 77. Marcel Dekker, New York

13. Harada A, Hashidzume A, Yamaguchi H, Takashima Y (2009) Polymeric rotaxanes. Chem Rev (Washington, DC) 109(11):5974–6023

14. Hashidzume A, Harada A (2011) Recognition of polymer side chains by cyclodextrins. Polym Chem 2(10):2146–2154

15. Barrett CJ, Mamiya J-i, Yager KG, Ikeda T (2007) Photo-mechanical effects in azobenzene-containing soft materials. Soft Matter 3(10):1249–1261. doi:10.1039/b705619b

16. Yoshida R (2011) Self-oscillating polymer gels. In: Nakanishi T (ed) Supramolecular soft matter: applications in materials and organic electronics. Wiley, Hoboken, pp 237–253. doi:10.1002/9781118095331.ch12

Structure of Liquid Crystal Display

Hiromu Saito
Department of Organic and Polymer Materials Chemistry, Tokyo University of Agriculture and Technology, Koganei-shi, Tokyo, Japan

Synonyms

Optical and electric materials for liquid crystal display

Definition

Optical and electric materials are developed for liquid crystal displays.

Introduction

Liquid crystal displays (LCDs) are now extensively used from small mobile phones and microdisplays to medium-sized notebook and desktop computers and large-panel TVs. Since the first calculators using LCD were introduced in the 1970s, performance of LCDs has progressed over the years. LCDs became slimmer, more portable, and more compact. Their image resolution, viewing angle, color, contrast ratio, brightness, and speed of moving image have been improved. The improvement of the performance owes to vigorous progress of optical and electric materials for the elements of LCD structure, such as the liquid crystal layer, thin-film transistor (TFT), and backlight system; e.g., the LCD's viewing angle characteristics are improved by optical compensators and various liquid crystal alignment modes [1–7]. Due to the improvement of the performance of LCDs, LCDs are now widely acceptable and will be a mainstream of the display for the time being, though various excellent displays such as organic light-emitting diodes (OLEDs) display are manufactured. In this report, optical and electric

materials for the elements of LCD structure are briefly reviewed.

Structure of Liquid Crystal Display (LCD)

Figure 1 shows schematic drawings of basic elements of liquid crystal displays (LCDs). LCDs include a liquid crystal layer and polarizer for an optical shutter to modulate light, thin-film transistor (TFT) and electrode for a switch of an optical shutter of the liquid crystal layer, color filters for displaying color image, and antireflective coating for preventing the reflection of light. Three types of LCDs have been developed for different applications: (1) transmissive, (2) reflective, and (3) transflective LCDs. Since liquid crystals do not themselves emit light, external illumination is required. In transmissive LCDs, a light-emitting diode (LED) is embedded as the light source to display the image, and the backlight propagated in the light-guide plate is extracted into the front direction by reflection sheets, diffuser sheets, and prism sheets (Fig. 1a) [1–7]. Most of the light from the light source is lost through the LCD elements, i.e., the loss of the light through the LCD elements is above 95 %. On the other hand, reflective LCDs rely on external light to display the image by using the reflected light, so that it has power consumption and good sunlight readability. The external light is reflected by the reflector, and the polarizer and quarter-wave plate form a crossed-polarizer configuration for incident light (Fig. 1b) [4, 5].

Transmissive LCDs work well indoors, but ambient light gets so bright that the display image would become invisible. On the other hand, reflective LCDs work well under bright external light, but it is invisible under low external light. As a consequence, transflective LCDs are designed to combine both transmissive and reflective LCDs, i.e., the backlight is turned on and the image is displayed in the transmissive mode under dark or low external light state,
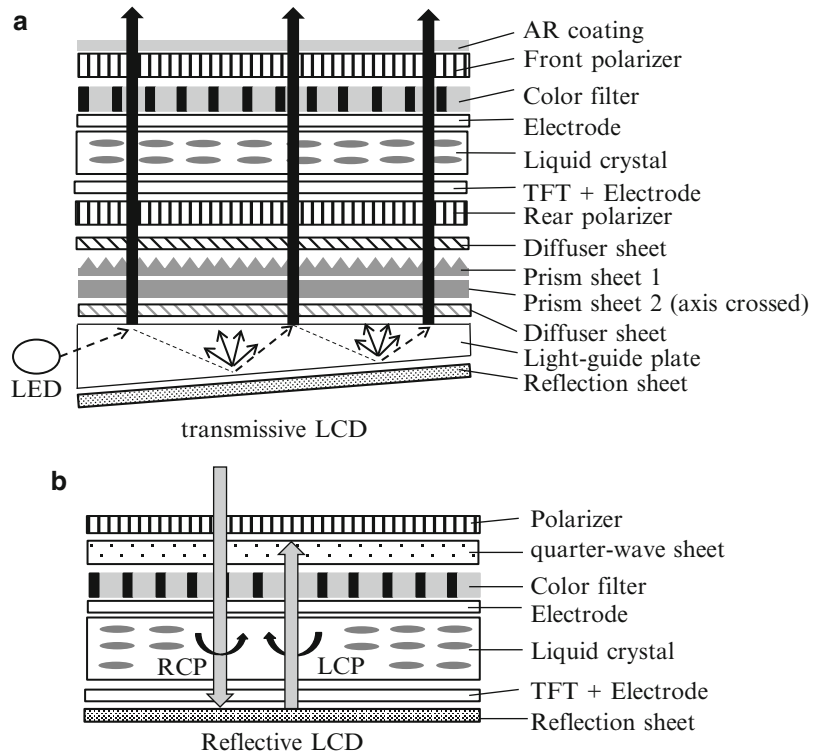
Structure of Liquid Crystal Display, Fig. 1 Schematic drawing of basic elements of LCDs
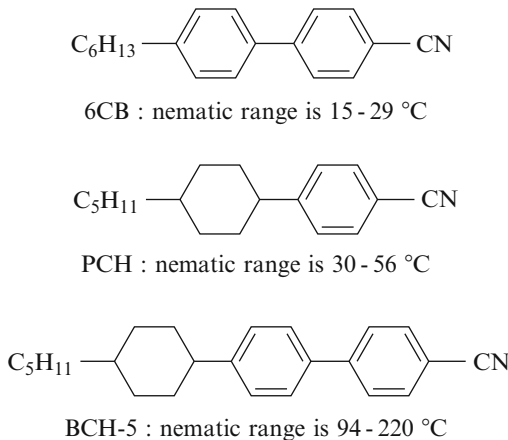
while the backlight is turned off and the image is displayed in the reflective mode under a bright external light state [4, 5].

Liquid Crystal Layer

Liquid crystal is a material that is intermediate between the crystalline solid and the amorphous liquid. Liquid crystals have rodlike molecules and align by applying electric field; liquid crystal with positive dielectric anisotropy aligns parallel to the direction of the applied electric field, while the negative one aligns normal to the direction of the electric field. Figure 2 shows examples of chemical structure of liquid crystals which are used for LCDs [3, 5]. Liquid crystals are usually used by mixing different liquid crystals for four criteria which are required for application of LCDs: (1) temperature operating range from below zero to body temperature, (2) hydrolytic and chemical stability, (3) low viscosity, and (4) colorless.
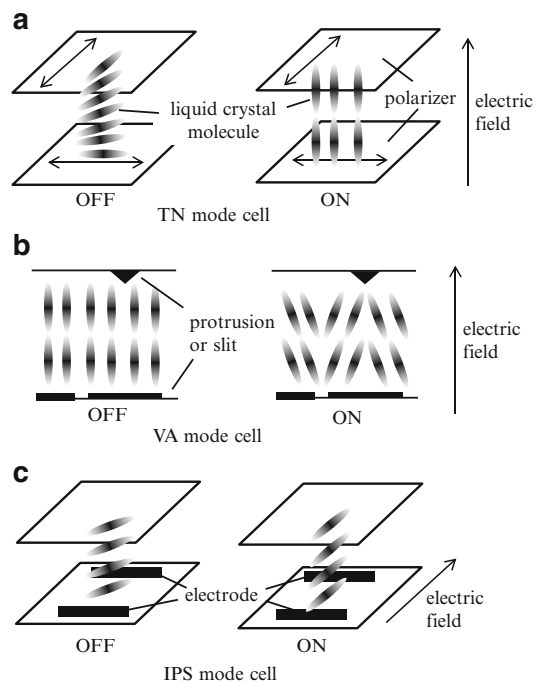
The liquid crystals respond to very low voltage and it plays a role of an optical shutter to modulate the light intensity supplied from an external light source. Figure 3 shows three examples of liquid crystal cell alignments which are widely used for LCDs [2–5].

Twisted nematic (TN) alignment mode cell is the most commonly used for small- and

medium-sized LCD panels. The front and rear substrates attached to the liquid crystal layer are rubbed at an angle difference of 90°; thus the optical axis of the liquid crystal gradually twists by 90° from the rear to the front substrate when no voltage is applied, so that the light is transmitted (Fig. 3a: left). When a voltage is applied, the vertical electric field between the rear and front substrates makes the liquid crystal directors tilt vertically in the bulk region, so that the light is blocked (Fig. 3a: right). The drawbacks of a TN mode cell are its narrow viewing angle and gray level inversion. The narrow viewing angle results from optical anisotropy of liquid crystals by the tri-layered structure in the dark state and off-axis light leakage from two crossed linear polarizers. To increase the viewing angle, a compensation film is needed. For instance, FUJIFILM Corporation employed a wide-view compensation film, i.e., triphenylene discotic derivative is coated on an alignment layer of a substrate. The discotic material is in a hybrid alignment configuration; (1) it exhibits a discotic nematic phase at a low

Structure of Liquid Crystal Display, **Fig. 2** Chemical structure of liquid crystal materials for LCDs

6CB : nematic range is 15 - 29 °C

PCH : nematic range is 30 - 56 °C

BCH-5 : nematic range is 94 - 220 °C

Structure of Liquid Crystal Display, Fig. 3 Liquid crystal cell alignments for LCDs

temperature and (2) it has π-electrons spread in a disklike shape which gives rise to a high birefringence [4].

Vertical alignment (VA) mode cell is used for super high-contrast LCDs. In a VA cell, the liquid crystal directors are almost perpendicular to the surface alignment layers; thus the axial light leakage between two crossed linear polarizers is quite low. In the voltage-off state, the incident light maintains its polarization when traversing the liquid crystal cell and is then blocked by the front linear polarizer independent of the incidence wavelength, leading to a good dark state for all wavelengths, causing deep black background (Fig. 3b, c: left). Since a single-domain VA cell exhibits a narrow viewing angle and severe gray level inversion, a multi-domain VA cell is developed by using zigzag-shaped electrode or protrusion surface. When a voltage is applied, liquid crystal molecules tilt away from the slits by generating fringe electric fields in the vicinity of the slits, and the tilt from the rear slits along with the adjusting effect from the front slits or the protrusion surface automatically forms multi-domain cells (Fig. 3b: right). The zigzag-shaped electrode generates fringe fields deeper into the central part of the liquid crystal cell [4, 5].

In-plane switching (IPS) mode cell and the fringe-field switching (FFS) one use horizontal electric fields to drive the homogeneously aligned liquid crystal molecules, i.e., interdigitated electrodes formed on the same rear glass substrate to generate transverse electric fields to reorient the liquid crystal molecules horizontally, leading to a symmetrical viewing angle because liquid crystal molecules are arranged in parallel with a substrate (Fig. 3c) [3–5]. However, vertical electric fields generated in the region in front of the electrode stripes tend to tilt the liquid crystal molecules in the vertical direction, causing a loss of phase retardation and low transmittance. To overcome the low transmittance of IPS mode LCD, FFS mode LCD is developed in which the distance between the adjacent pixel electrodes is narrower than or close to the cell gap to form a fringe field on the electrodes. The strong horizontal electric field generated near the electrode edges to rotate the liquid crystals in the horizontal direction, and this rotation propagates in other regions where vertical fields dominate, causing high transmittance. The transmittance of an FFS can be much improved by using a liquid crystal with negative dielectric anisotropy than by using a positive one, though the higher operating voltage is required [4, 5].
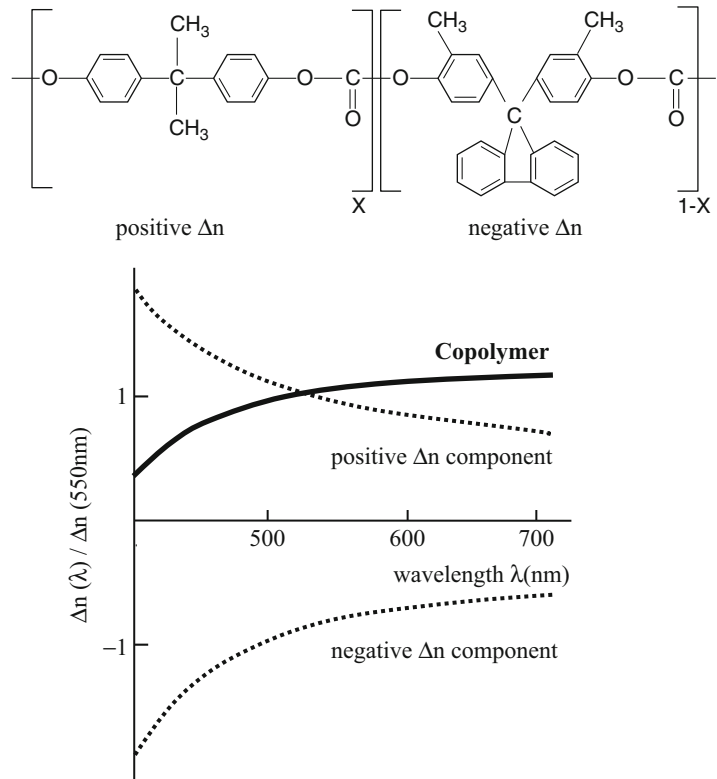
Polarizer

Polarizers are used with liquid crystal cell for an optical shutter to modulate light. Linear polarizers are made from a poly(vinyl alcohol) (PVA) film with iodine compounds using the wet-dyeing method. By stretching the PVA film, dichroic species such as I_3 and I_5 complexes are aligned along the stretching direction. Thus light polarized along the stretching direction is strongly absorbed, while light polarized perpendicular to the stretching direction is transmitted. The degree of polarization and transmittance of the PVA-stretched polarizer is highly dependent on the dichroism and the amount of dichroic species. By controlling these parameters, the transmittance and color balance of the polarizers can be adjusted [5].

The transmittance of light through the iodine-doped PVA polarizer is low, below 50 %, because half of the light is absorbed. To reduce the light loss by the polarizer, various types of polarizers are designed and developed. For example, by depositing periodic aluminum stripes on a reflector sheet at the bottom of the light-guide plate, polarized light can be extracted by reflecting as a nano-wire grid when the periodic length of the aluminum stripes is smaller than the wavelength of incident light [2, 4]. Hence, the reflecting light is converted to polarized light and the rear polarizer can be removed.

For reflective LCDs, a circular polarizer needs to be placed in front of the liquid crystal cell to obtain a cross-polarized state. A circular polarizer consists of a linear polarizer and a quarter-wave sheet. Linearly polarized light from the front polarizer is converted to right-handed circular polarization (RCP) by the quarter-wave sheet, and then the RCP light is

S

**Structure of Liquid
Crystal Display,**
Fig. 4 Chemical structure
of wide-wavelength
quarter-wave
polycarbonate copolymer
and the wavelength
dependence of
birefringence Δn.
Retardation δ is related to
Δn: $\delta = \Delta n \times d$ (d is the
thickness of the sheet)

reflected by the reflector, and its polarization becomes left-handed circular polarization (LCP) as the propagation direction is reversed. The LCP light is then converted by the quarter-wave sheet into linearly polarized light perpendicular to the transmission axis of the front polarizer and is blocked by the polarizer (Fig. 1b). However, the retardation of the quarter-wave sheet usually decreases with increasing wavelength, while the quarter-wave sheet for covering the whole wavelength of visible light requires the reverse retardation dispersion in which the retardation increases linearly with increasing wavelength. Hence, light leakage is prevented only at specific wavelength and large light leakage occurs at wide wavelength other than specific wavelength. To suppress the light leakage at wide wavelength, a quarter-wave sheet with reverse retardation dispersion can be designed by stacking several retardation films with different optical axis alignment to compensate the wavelength dispersion [4]. Recently, a simple quarter-wave sheet with reverse retardation dispersion was manufactured

by TEIJIN Limited as a wide-wavelength quarter-wave sheet in polycarbonate copolymer consisting of a positive birefringence Δn component and a negative one (Fig. 4) [7].

Color Filter

To display color image, an array of color filters is coated on the surface of the glass plate. Each individual pixel of the display is divided into three sub-pixels which are colored red (R), green (G), and blue (B). Color materials are made from dyes or pigments dispersed in photosensitive resins containing gelatin, glue, or polyvinyl alcohol. The color materials are coated on the glass plate by photolithography, printing, or electroplating. To avoid light leakage from the edge of the RGB color sub-pixels and the external light induced by the photoelectrons in thin-film transistors (TFTs), black resin containing carbon black and fluorine is used as a black matrix material. Color filters using dye allow fine patterning

and high freedom of color tone, while that using pigments can provide high heat and light resistance. However, color filters exhibit large absorption, leading to the low transmittance of about 30 % or less. To improve the transmittance, low-loss filters such as dielectric interference filters and polarization interference color filters are developed [2, 5].

Thin-Film Transistor (TFT)

On the rear substrate attached to the liquid crystal layer, a thin-film transistor (TFT) array is formed to provide an independent switch for each color pixel. Each color pixel consists of an array of color filters and a small liquid crystal cell that can be turned on or off electrically by TFT. In each time frame, signals from the gate lines turn on the TFTs, and the voltages from the data lines are applied to drive each individual liquid crystal pixel. An active-matrix LCD incorporates a two-dimensional array matrix of circuits to provide the electrical addressing of the individual pixels, and it has an individual active device in each pixel defined by the crossover of the row and column bus electrode lines [1, 2, 5].

Amorphous silicon (a-Si) or polysilicon (p-Si) is usually used as semiconductor of TFT. Electron mobility of a-Si is low (0.5–1.5 cm^2/Vs), while that of p-Si is high (30–300 cm^2/Vs). Hosono et al. invented a transparent amorphous oxide semiconductor of InGaZnO$_4$ (a-IGZO) which exhibits large electron mobility (10–50 cm^2/Vs). Since a-IGZO has 20–50 times the electron mobility of a-Si, it can be used to make transparent transistors [8]. Owing to huge electron mobility, IGZO transistor can be much smaller, allowing for higher pixel densities and lower power operation. Due to their transparency, image quality is improved and can reduce power consumption. Hence, IGZO TFT is used for fine-imaging LCDs such as the iPad Retina model and 4K television.

Organic semiconductor printable by using solvent is regarded as a promising alternative to silicon semiconductors for manufacturing flexible, low-cost, and large-area electronic devices.

However, high crystallinity is a prerequisite for obtaining sufficient semiconducting properties of organic materials; e.g., large mobility of 18–40 cm^2/Vs is achieved in purified rubrene single crystals obtained by physical vapor transport, while the mobility of amorphous organic material is quite low, below 10^{-3} cm^2/Vs [9]. Versatile printing techniques are investigated to manipulate soluble functional materials and fabricate electronic components. For example, single crystals of the organic semiconductor 2,7-dioctyl[1] benzothieno[3,2-*b*] [1] benzothiophene (C$_8$-BTBT) with an average carrier mobility of 16.4 cm^2/Vs were obtained by double-shot inkjet printing method, i.e., (1) the antisolvent ink of anhydrous DMF is first inkjet-printed, (2) solution ink of C$_8$-BTBT in DCB is overprinted sequentially to form intermixed droplets confined to a predefined area, (3) crystallization of C$_8$-BTBT grows at liquid–air interface of the droplet, and (4) a single-crystal C$_8$-BTBT semiconducting thin film is obtained by evaporating the solvent [10].

Transparent Conducting Electrode

Widely used transparent electrodes for LCDs are tin-doped indium oxide (ITO). Methods for their fabrication mostly incorporate photolithography using chemical etching and cleaning procedures. ITO has a sheet resistance of less than 100 Ω^{-1} and optical transparency around 90 %. However, ITO has several critical drawbacks [1, 11]. Since ITO is a ceramic material, it can crack and fracture at relatively low strains of 2–3 %, yielding drastic decrease in the electrical conductivity. Owing to the brittleness, ITO is limited on the durability and lifetime of flexible devices. The refraction index of ITO is high at around 2.0, which leads to high reflection when lower-index materials such as polymers are attached. The price of ITO is drastically fluctuated because the material for ITO is a rare element and is supplied by limited areas. Hence, alternative materials to ITO are extensively investigated.

One of the candidates for alternative material to ITO is conducting polymers such as

S

polyethylene dioxythiophene doped with polystyrene sulfonate (PEDOT-PSS) [11, 12]. The conductivity of PEDOT-PSS results from polaron and soliton species formed from the charged doping in the polymer backbone. Line patterned PEDOT-PSS electrode with several $k\Omega^{-1}$ could be fabricated by coating onto the PET film with a solution of PEDOT-PSS using spray, dip, and roller coating. The conductivity of PEDOT-PSS can be significantly improved up to two or three orders of magnitude by adding solvents such as ethylene glycol, glycerol, dimethyl sulfoxide, and sorbitol, and the subsequent heating treatment also enhances the conductivity. Conductivities higher than $1,000\ Scm^{-1}$ have been reported for vapor phase-polymerized PEDOT. The problem of conducting polymers is the instability of the doped state, which decreases the conductivity by exposure to high temperature, humidity, or UV light, though it is less susceptible to damage from bending.

Another alternative candidate to ITO is carbon-based material such as carbon nanotube (CNT) [11]. Printable CNT ink has been developed by dispersing the CNT into solvent. Transparent conductive CNT films have been made by many techniques including both dry and wet methods. Highly conducting large CNT films with high homogeneity were obtained by polydimethylsiloxane-based transfer printing (PDMS stamping) technique with vacuum filtration, e.g., conductivity is 175 S/cm and transmittance is 80 %. Printable elastic conducting materials with a conductivity of more than 100 S/cm and stretchability of more than a strain of 100 % were manufactured by comprising single-walled carbon nanotubes (SWNTs) uniformly dispersed in a fluorinated rubber using an ionic liquid and jet milling [13]. The high conductivity is attributed to the well-developed conducting networks of large and fine SWNT bundles in the rubber.

Backlight System

Transmissive LCDs require a backlight system. The light source (e.g., LED) is located at the edge of the system to minimize the thickness of the LCD. The light rays are irradiated from the edge surface of the light-guide plate (LGP), propagated by reflection from the surface of the wedge-shaped LGP, and then scattered by the microstructure patterns of the reflection sheet at the bottom of the LGP (Fig. 1a). A thin LGP is required for lightweight and thin LCDs, so flowable polycarbonate, poly(methyl methacrylate), or poly(ethylene terephthalate) are used for precise molding manufacture.

At least one diffuser sheet is laminated above the LGP to obtain uniform output light for uniform brightness over the entire area and all viewing angles. The diffuser sheet is usually made of a bulk material mixed with tiny particles having a refractive index difference. To collimate light into the front direction and enhance the brightness, two crossed prism sheets are placed above the diffuser sheet (Fig. 1a) [2]. A reflector with high reflectivity is laminated behind the LGP to reduce the optical loss from the LGP bottom surface. A diffusive-type reflector in which a bumpy structure is formed on the flat surface is widely used. The bumpy structure is made from micro-grating by photolithographic method or a biaxial-drawn two-phase polymer blend sheet with micro-debonding structure.

Recently, various backlight systems are developed for high efficiency of illumination. For example, an LGP made by a highly scattering optical transmission (HSOT) polymer is developed, though transparent polymers are usually used for LGP. Light scattering occurs in the HSOT polymer by a refractive index difference of two-phase system. The HSOT backlight system achieves higher brightness compared with conventional backlight system because the scattering light is controlled to propagate into the front direction [14].

To reduce large transmittance loss due to the existence of a rear polarizer, the polarized LGP system in which polarized light is extracted without a rear polarizer is also developed. A birefringent sheet made of uniaxially aligned liquid crystalline polymer with the same extraordinary refractive index to the substrate is placed above the LGP. Only s-polarized light is

extracted into the front direction through the birefringent film, while the p-polarized light continues to propagate inside the LGP substrate. The p-polarized light is converted to the s-polarized one by the quarter-wave sheet at the edge of the LGP, and then the rest of light propagated inside the LGP is extracted into the front direction [2].

Antireflective (AR) Coating

LCD usually reflects about 4 % of ambient light from its surface and the background is mirrored on the display. Reflection of light occurs at any surface between two mediums with different refraction indices. This reflection is not desirable for viewing images on displays. To reduce the reflection of light, antireflective (AR) coating is used on the outer surface of the display [6, 15]. Simplest AR coating consists of a single quarter-wave layer of transparent material whose refractive index is the square root of the substrate's refractive index. This reduces reflection almost to zero at a specific wavelength by destructive interference of the reflected light at the upper and lower surface of the AR coating film. The AR layer can be produced by vacuum/vapor deposition, like sputtering or chemical vapor deposition (CVD), or by wet processing using sol–gel chemistry. Multiple coatings stacked with alternating thin layers of a high and low refractive index are used for high-end products. However, a large number of thin-film layers are needed to achieve antireflection at relatively wide-wavelength regions, and color effects often appear at oblique angles.

It is known that the eye of the night-flying moth reflects little light owing to the graded refractive index of the moth's cornea; the refractive index continuously changes from 1 at the air to 1.4 at the optical nerve. The graded refractive index is caused from an array of cones arranged in domains with hexagonal packing; the cone distance is 180–240 nm and the cone height extends up to 230 nm. Recently, moth eyelike coatings have been manufactured in large scale by roll-to-roll process [15]. Graded-index moth eye AR coatings can be made by nano-imprint

lithography using nanostructured mold fabricated by the hexagonal array of cones with a size of about 200 nm. A nanostructured mold prepared by anode oxidation of aluminum or lithographic method is pressed into a softened polymeric surface or a wet UV-curable resist layer. The resulting moth eye AR coatings have antireflective properties at wide-wavelength regions with light reflection of below 0.5 %, low angular dependence of the reflection, and excellent color.

Related Entries

▶ Refractive Index

References

1. Crawford GP (2005) Flexible flat panel display. Wiley, Chichester
2. Bhowmik AK, Li Z, Bos PJ (2008) Mobile displays: technology and applications. Wiley, Chichester
3. Yeh P, Gu C (2010) Optics of liquid crystal displays, 2nd edn. Wiley, Hoboken
4. Ge Z, Wu S-T (2010) Transflective liquid crystal displays. Wiley, Chichester
5. Chen RH (2011) Liquid crystal displays: fundamental physics and technology. Wiley, Hoboken
6. Hainich RR, Bimber O (2011) Displays: fundamentals & applications. CRC Press, Boca Raton
7. The Society of Polymer Science, Japan (2012) Materials for displays (Japanese). Kyoritsu shuppan, Tokyo
8. Nomura K, Ohta H, Takagi A, Kamiya T, Hirano M, Hosono H (2004) Room-temperature fabrication of transparent flexible thin-film transistors using amorphous oxide semiconductors. Nature 432:488–492
9. Takeya J, Yamagishi M, Tominari Y, Hirahara R, Nakazawa Y, Nishikawa T, Kawase T, Shimoda T, Ogawa S (2007) Very high-mobility organic single-crystal transistors with in-crystal conduction channels. Appl Phys Lett 90:102120
10. Minemawari H, Yamada T, Matsui H, Tsutsumi J, Haas S, Chiba R, Kumai R, Hasegawa T (2011) Inkjet printing of single-crystal films. Nature 475:364–367
11. Hecht DS, Hu L, Irvin G (2011) Emerging transparent electrodes based on thin films of carbon nanotubes, graphene, and metallic nanostructures. Adv Mater 23:1482–1513
12. Kirchmeyer S, Reuter K (2005) Scientific importance, properties and growing applications of poly (3,4-ethylenedioxythiophene). J Mater Chem 15:2077–2088

S

13. Sekitani T, Nakajima H, Maeda H, Fukushima T, Aida T, Hata K, Someya T (2009) Stretchable active-matrix organic light-emitting diode display using printable elastic conductors. Nat Mater 8:494–499

14. Tagaya A, Koike Y (2012) A novel LCD structure using transparent polymers free of birefringence and scattering polymers free of wavelength dependency. SID Symp Dig Tech Rep 43:737–740

15. Burghoorn M, Roosen-Melsen D, Jd R, Sabik S, Vroon Z, Yakimets I, Buskens P (2013) Single layer broadband anti-reflective coatings for plastic substrates produced by full wafer and roll-to-roll step-and-flash nano-imprint lithography. Materials 6:3710–3726

Structures in CL/P Nanocomposites

Mitsuhiro Shibayama
Institute for Solid State of Physics, The
University of Tokyo, Kashiwa, Chiba, Japan

Synonyms

CL/P NCs; CL/P, NC; Clay/polymer nanocomposites

Definition

Clay/polymer nanocomposites (CL/P NCs) are inorganic/organic composites consisting of intercalated clay platelets and polymer. Due to their strong interactions and molecular-scale mixing, CL/P NCs exhibit much improved physical properties, such as high tenacity, drawability, transparency, etc., than those that are obtained by a simple addition of the physical properties of the components.

Introduction

As discussed in ▶ Mechanical Behavior of CL/P Nanocomposites, organic/inorganic nanocomposites (NCs) have attracted continuous attention. In the 1990s, a sol-gel process for preparation of transparent organic-inorganic composites became a topic, where NCs were prepared by

dissolving preformed polymers into sol-gel precursor solutions and then allowing the tetraalkyl orthosilicates to hydrolyze and condense to form glassy SiO_2 phases of different morphological structures [1]. This offered a new approach to the synthesis of composite materials with domain sizes approaching the molecular level. Incorporation of organic/oligomeric/polymeric materials into organic/inorganic networks by sol-gel process made it possible to optimize selected properties independently, such as mechanical flexibilities by incorporation of flexible polymers, new electric properties by conducting polymers, and optical properties by organic dye or π-conjugated polymers [2]. One of the most attractive points of NCs is that the properties of these composites can vary greatly and range from elastomeric rubbers to high-modulus materials. Since NCs are optically transparent, they were applied to optical devices. NCs have also been applied to various optical devices [3]. In 2002, a new class of gels called NC gels, prepared by radical polymerization of poly(N-isopropylacrylamide) (NIPA) in the presence of inorganic clay (CL), laponite, was reported [4]. NC gels have opened another field of clay/polymer nanocomposites (CL/P NCs). In this section, the structures of bulk, aqueous dispersion, and gels of CL/P NCs are overviewed.

Structure of CL/P NC Fibers and Films

CL/P NCs consist of intercalated clay platelets with large aspect ratio and polymer matrix. Typical polymer matrices are polystyrene, polycaprolactone, poly(ethylene oxide), polyamide, polyimide, epoxy, polysiloxane, polyurethane, etc. As a CL, montmorillonite $(Na_xSi_4(Al_{2-x}Mg_x)O_{10}(OH)_2 \cdot nH_2O)$ has been widely used, which is of particular importance in CL/Ps. Montmorillonite is a crystalline, 2:1 layered clay mineral in which a central alumina octahedral sheet is sandwiched between two silica tetrahedral sheets [5]. The layers are continuous in their crystal a and b directions and are stacked one above the other in the c direction.
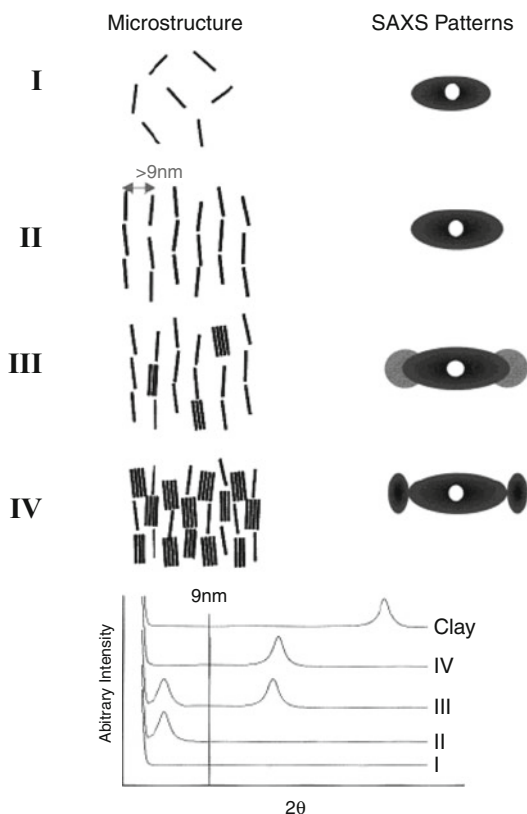
Structures in CL/P Nanocomposites, Fig. 1 Schematic representation of the evolution of the microstructure and their SAXS patterns as a function of CL concentration (Reprinted with permission from C. M. Koo, Macromolecules, 2002, 35, 5116. Copyright (2002) American Chemical Society)

The structure of CL/P has been extensively investigated with electron microscopy (EM), polarized optical microscopy (POM), atomic force microscopy (AFM), small-angle X-ray (SAXS) and neutron scattering (SANS), and others. Many of EM photographs show that exfoliated CL platelets are dispersed in polymer matrix and are aligned in a direction to stack. SAXS patterns of CL/Ps show peaks, indicating lamellar structure. Figure 1 shows a typical SAXS pattern of extruded fiber samples of maleated polyethylene (MAPE)/organically modified clay nanocomposites [6]. The upper patterns show 2D SAXS patterns (right) and the corresponding cartoons of CL orientation (left), and the lower shows SAXS intensity functions as a function of

the scattering angle, 2θ. Stage I indicates the disordered and exfoliated state. The individual silicate layer is randomly distributed because individual layers could keep the interlayer distance as far as they could not interact sterically. Nevertheless, the artificially oriented extrudate shows the layer spacing, which is shown as a slightly anisotropic X-ray pattern. Stage II indicates the ordered and exfoliated state. The ordering of stage II is not due to particular attraction or repulsion but due to the steric interaction of silicate layers. Stage III shows the dual morphologies of exfoliation and intercalation. It implies that there is a critical distance between silicate plates, below which the attractive interaction (van der Waals force) between CL platelets overwhelms the favorable interaction between silicate plate and polymer chain. CL/Ps show optical anisotropy above a certain clay concentration, e.g., 12 vol% in this particular case, due to the ordering of silicate layers. The optical anisotropy becomes stronger with the content of silicate. The d-spacing, i.e., the inter-silicate plate distance, is a decreasing function of the CL concentration. For disk-shaped particles having alternative parallel arrangement, the d-spacing is given by [6]

$$d \equiv H + a = \frac{\pi R^2 H}{(2R + b)^2 \phi} \tag{1}$$

where ϕ is the volume fraction of the disk-shaped particles; R and H are the radius and the thickness of the disk, respectively; and a and b are the separation gap between adjacent disks (a, face-to-face; b, edge-to-edge, respectively). Figure 2 shows clay volume fraction dependence of the d-spacing of the same system [6]. The solid line is the theoretical function obtained with Eq. 1. I to IV denote the states as introduced in Fig. 1. Note that there is a discrete transition in Stage III, suggesting exfoliation region to intercalation region.

A similar system, i.e., MAPE/clay nanocomposite system but in extruded thin-film form, shows interesting two-dimensional (2D) SAXS and 2D wide-angle X-ray scattering (WAXS) patterns as shown in Fig. 3 [7]. Here, corrected 2D SAXS and WAXS patterns for
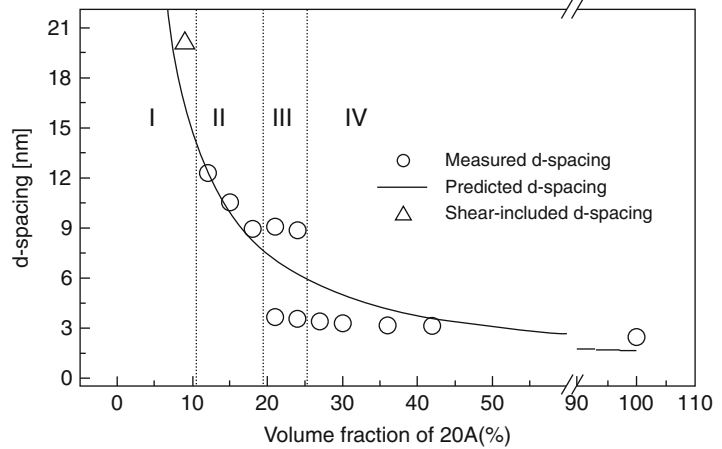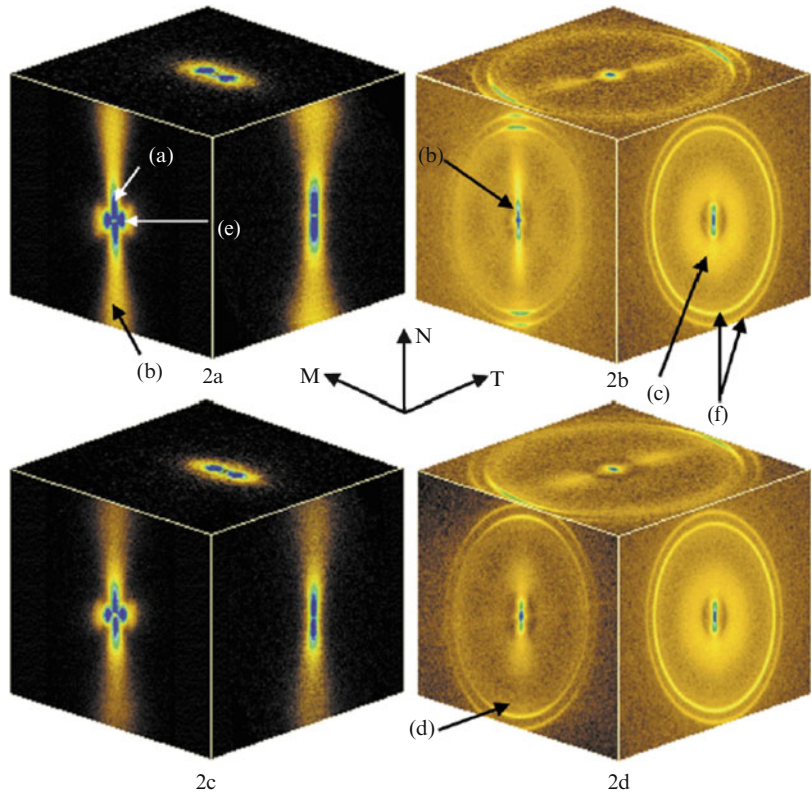
the different orientations are shown (left, SAXS; right, WAXS), in which M, T, and N denote the machine, transverse, and normal directions, respectively. The symbols in the figure, i.e., (a) to (f), denotes the periodicity (dispersion) of (a) CL tactoids, (b) modified/intercalated CL platelets, (c) unmodified CL platelets, (d) CL (110) and (020) planes, (e) polymer lamellar, and (f) polymer unit cell (110) and (200) planes. These nanoscale-layered CLs with very high aspect ratios and high strength can play an important role in forming effective CL/P NCs owing to their intercalation chemistry.

CL/P in Aqueous Media

Discotic laponites are known to form a gel phase at mass concentrations as low as a few percent in distilled water with "house of cards" three-dimensional structure [8]. Strong attractive interaction between polymer and CL as demonstrated by polymer adsorption to CL platelets in water is one of key factors for advanced properties of CL/P NCs. As already introduced, synthetic laponite clays (Rockwood Ltd.: $[Mg_{5.34}Li_{0.66}Si_8O_{20}–(OH)_4]Na_{0.66}$) are made of microcrystalline magnesium silicate-, disk-, or coin-like platelets. The laponite platelets carry a negative charge due to isomorphous substitution of fraction of Mg^{2+} by Li^+ ions, resulting in a unit cell of –0.7e charge [9]. These elementary charges (roughly –700e) are uniformly distributed over the disks, while a smaller positive charge, originating from broken bonds, is concentrated along the rim. The overall negative charge of the platelets is compensated by Na^+ counterions, which form electric double layers around the laponite disks suspended in water. This is due to polymer adsorption that holds the key to an understanding of formation and properties of CL-polymer mixtures. Addition of hydrosoluble polymers to this intriguing CL system either prevents gelation or slows it down extremely depending on the polymer weight, concentration, or the laponite concentration. Suspensions of CL particles (laponite), mixed with poly(ethylene oxide) (PEO), undergo a dramatic shear thickening when subjected to vigorous shaking, which transforms them from a low-viscosity fluid into a "shake-gel" [10]. The shake-gel is reversible, relaxing back to a fluid with a relaxation time that is strongly dependent on PEO concentration. Shake-gels are observed for PEO concentrations slightly below the threshold for complete saturation of the laponite particles by the polymer. Light scattering measurements confirm that the PEO is adsorbed on the surface of the laponite particles, which suggests that shear induces a bridging between the colloidal particles, resulting in a gel network that spans the system. Desorption of the polymer reduces the bridging and thus relaxes the network.
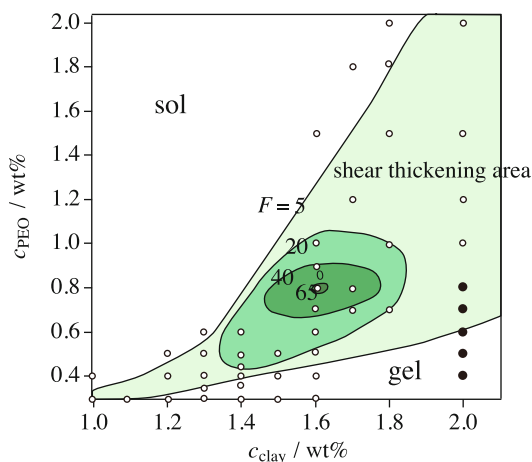
Structures in CL/P Nanocomposites, Fig. 4 Shear-thickening map for clay/PEO mixtures in water. F denotes the "shear-thickening factor" meaning the viscosity ratio after/before shaking (Reprinted with permission from Takeda, et al., Macromolecules 2010, 43, 7793–7799. Copyright (2010) American Chemical Society)

Figure 4 shows contour map of the shear-thickening factor for PEO/laponite mixtures in water as a function of CL and PEO concentrations [11]. The shear-thickening factor, F, defined here is the ratio of viscosities after and before shaking. As shown in the map, the concentration region where a strong shear thickening occurred was limited in a small concentration window, where the size of polymer chains is slightly smaller than the inter-CL distance but bridging occurs by shearing. As a matter of fact, simultaneous measurements of SANS and rheology showed a sudden change in SANS pattern at the critical shear rate for shear thickening. Figure 5 shows SANS patterns of laponite/PEO in deuterated water under shear [11]. SANS patterns are observed under steady shear rate. When the shear rate was increased step by step, the viscosity increases drastically at a critical shear rate, e.g., the shear rate = 400 s^{-1}. At the same time, the SANS patterns change from isotropic to anisotropic, indicating clay orientation along the flow direction. This kind of observation confirms the abovementioned mechanism of shear thickening, i.e., shear-induced bridging.

It was observed that SANS curves for mixtures of CL/PEO in deuterated water are very similar to

S

Col/SDD = 4 m/4 m
C2P08 $\phi_{D2O} = 1$
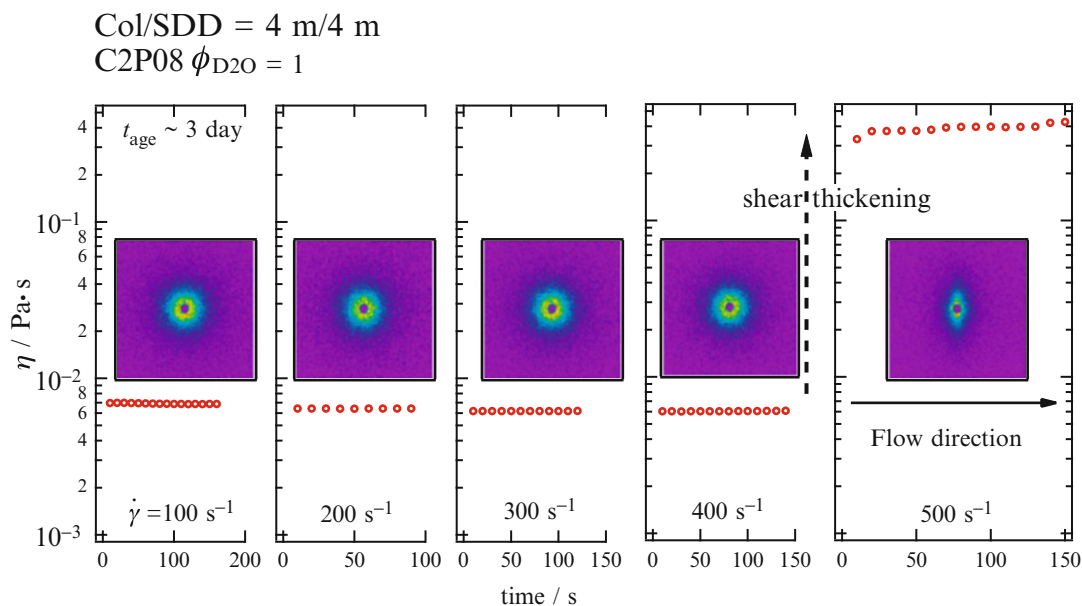
Structures in CL/P Nanocomposites, Fig. 5 Simultaneous measurements of SANS and rheology for clay/PEO mixtures in D_2O. SANS measurements were carried out under steady shear with various shear rates. The *open* *circles* denote viscosity and 2D SANS patterns are displayed (Reprinted with permission from Takeda, et al., Macromolecules 2010, 43, 7793–7799. Copyright (2010) American Chemical Society)

those of simple CL platelet dispersions in water, differing only in the magnitude of the scattering intensity [12]. Since CL/polymer mixture in water is a three-component system, conventional scattering methods cannot extract the necessary information, particularly about polymer-clay interactions. Contrast-variation (CV) SANS is a method to obtain SANS functions at different scattering contrasts. This can be achieved by using mixtures of D_2O/H_2O of various compositions as a solvent. Observation of SANS functions at different solvent mixtures and partial structure factors corresponding to polymer-CL correlation in addition to polymer-polymer and CL-CL correlations are obtained. CV-SANS was employed for CL/PEO in aqueous media and confirmed the presence of strong polymer-adsorbed layer on CL platelets [12].

Structure of CL/P Nanocomposite Gels (CL/P Gels)

CL/polymer nanocomposite hydrogels (NC gels) were firstly reported in 2002 with exiting

demonstrations [4]. NC gels are prepared by in situ free-radical polymerization of NIPA in the presence of water-swollen inorganic clay platelets and without using any organic cross-linker. Inorganic clay is synthetic hectorite (laponite, Rockwood Ltd.: $[Mg_{5.34}Li_{0.66}Si_8O_{20}–(OH)_4]$ $Na_{0.66}$) with lateral dimension of 20–30 nm and 1 nm thickness. Here, the term inorganic clay is used in contrast to organophilic clay as discussed above, which contains substantial amounts of organic surfactant and is widely used in the preparation of CL/P NCs as discussed above. Figure 6 shows (a) the structure of laponite, (b) clay platelets and NIPA monomers, (c) NC gels during polymerization of NIPA, and (d) resultant NC gels. The NC gels are transparent, not soluble but swollen in water, and stretchable more than ten times [13]. NC gels exhibit extraordinary mechanical, optical, and swelling/deswelling properties, such as large deformability, transparency, and negligible sol fractions [14].

SAXS/SANS studies on dilute CL dispersions in water showed that clay platelets are randomly dispersed in water and are described with a scattering function for disk [15].
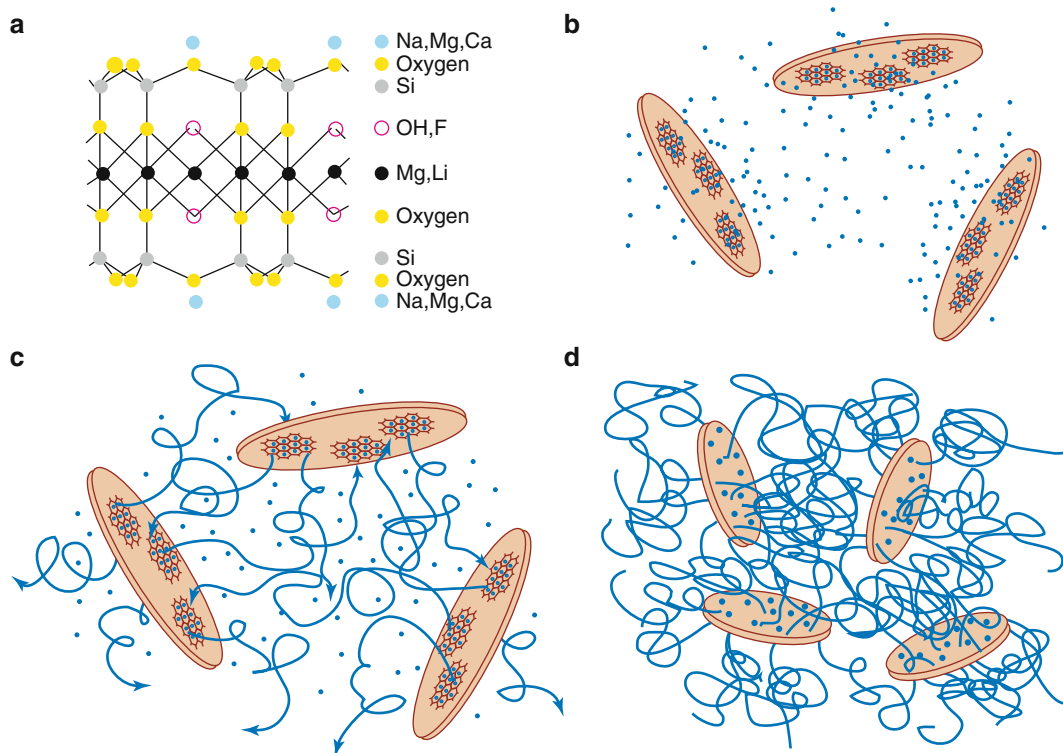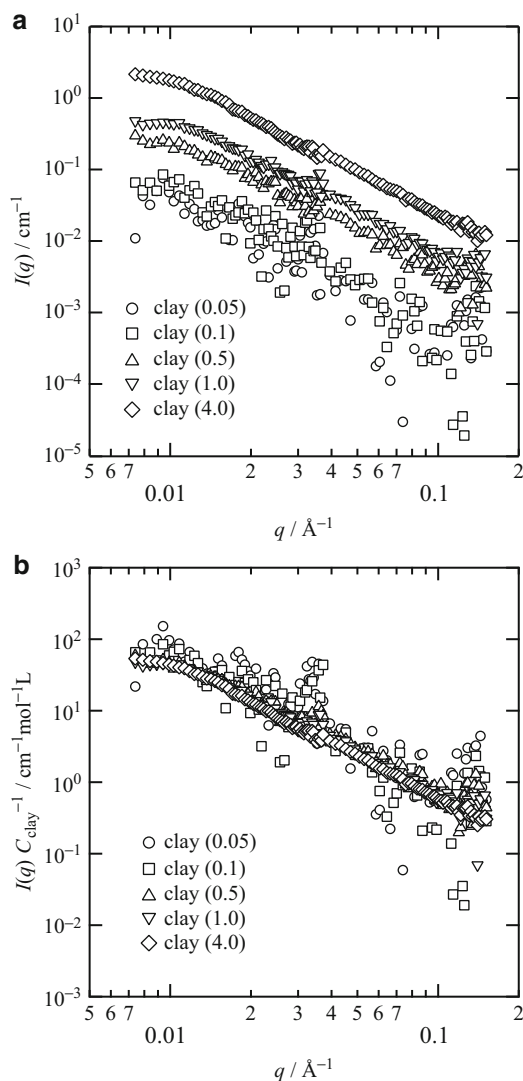
Structures in CL/P Nanocomposites, Fig. 6 Schematic representation of (**a**) clay, (**b**) a mixture of clay and NIPA monomer in water, (**c**) NC gel during polymerization, and (**d**) NC gel after completion of gelation

(Reprinted with permission from Shibayama, et al. Macromolecules, 2005, 38, 10772. Copyright (2005) American Chemical Society)
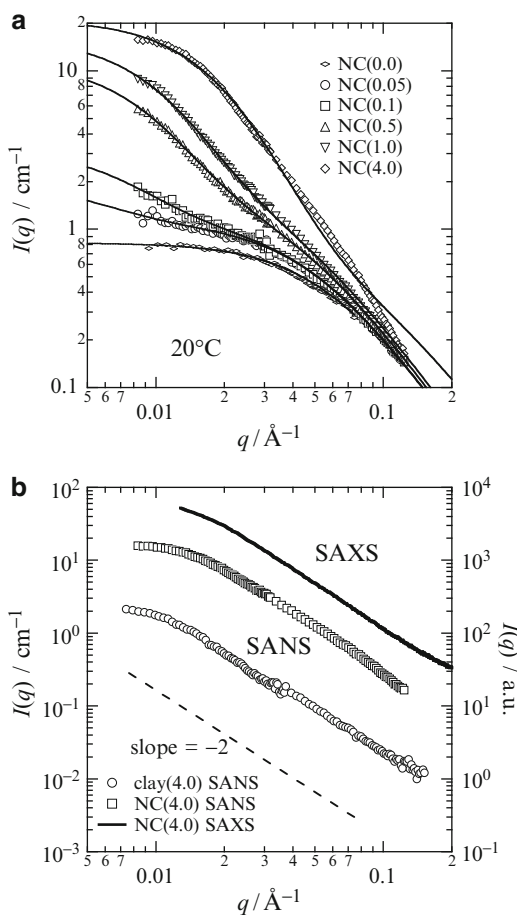
Figure 7a shows a series of SANS curves, $I(q)$s, for CL dispersion of water, and (b) their reduced plot with respect to the CL concentration, C_{clay}. Here, q is the magnitude of the scattering vector. The sample code is defined by the ratio of the CL and water, e.g., clay(1.0) and NC(1.0) indicating 0.01 mol of clay (=7.62 g) in 1 L of H_2O or D_2O for the CL dispersion and NC gel, respectively. The structure factors of clay dispersion do not change significantly by sol-gel transition. $I(q)$s are superimposed by normalizing with C_{clay} as shown in Fig. 7b. Note that the CL dispersions were in sol state for clay (2.0) and below within the time range of the experiments, while clay(4.0) was in gel state. This indicates that CL platelets form a self-similar aggregate structure irrespective of its concentration and the sol-gel transition is nothing but a volume-filling phenomenon of the CL aggregates.

SANS functions for NC gels show a systematic change from polymer-dominant scattering to CL-dominant scattering by increasing CL content from zero as shown in Fig. 8a, resulting in a similar scattering function to those of simple clay dispersions [15]. However, the scattering intensity for NC gels is much larger than that for simple CL dispersion. This is due to an increase of scattering contrast by polymer adsorption onto CL surface as described in a previous subsection. The neutron scattering length densities, ρ, are to be $\rho_{clay} = 39.2 \times 10^9 cm^{-2}$, and $\rho_{PNIPA} = 9.33 \times 10^9 cm^{-2}$, and $\rho_{D2O} = 63.4 \times 10^9 cm^{-2}$ according to the observed mass densities $d_{clay} = 2.65$ g/cm^3 and $d_{PNIPA} = 1.26$ g/cm^3 [15]. Since the difference in ρ's between PNIPA and D_2O is larger than that between clay and D_2O, adsorption of PNIPA results in a significant

Structures in CL/P Nanocomposites, Fig. 7 SANS intensity functions of (**a**) clay dispersions in water and (**b**) their reduced plot with respect to the clay concentration. The *number of parenthesis* denotes clay concentration (Reprinted with permission from Shibayama, et al. Macromolecules, 2004, 37, 9606. Copyright (2004) American Chemical Society)

Structures in CL/P Nanocomposites, Fig. 8 SANS intensity functions of (**a**) NC gels with different clay concentrations and (**b**) comparison of SANS of clay dispersion (*open circles*), SANS (*square*), and SAXS functions of NC gel (*dots*) (Reprinted with permission from Shibayama, et al. Macromolecules, 2004, 37, 9606. Copyright (2004) American Chemical Society)

increase in the SANS intensity as shown in Fig. 8b. Figure 8b also shows comparison of SANS and SAXS intensities for NC gels together with SANS of CL dispersion. On the other hand, the electron densities, ρ_e, are calculated to be $\rho_{e,clay} = 7.98 \times 10_{23}$ e/cm^3, $\rho_{e,PNIPA} = 4.16 \times 10^{23}$ e/cm^3,

and $\rho_{e,H2O} = 3.34 \times 10^{23}$ e/cm^3. These values indicate that SAXS is much more sensitive to clay than PNIPA chains. As a matter of fact, the SAXS function in Fig. 8b is effectively the same as the SANS of clay dispersion except for the magnitudes. Therefore, it can be concluded that SANS and SAXS are complimentary and detect the PNIPA network structure and CL structure, respectively.

In order to elucidate the structure of NC gels, information about the interfacial structure has to
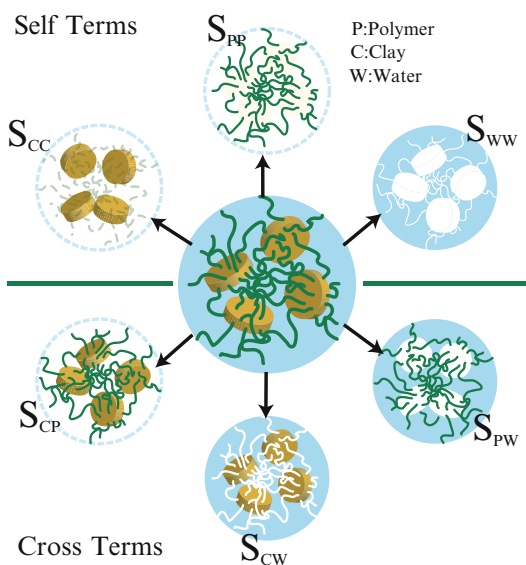
Structures in CL/P Nanocomposites, Fig. 9 Schematic representation of contrast variation for three-component system, C, P, and W (Reprinted with permission from Shibayama, Polym. J., 2011. Copyright (2011) Nature Publishing Group)

be obtained. CV-SANS allows ones to decompose the scattering function to the CL-CL, polymer-polymer, and CL-polymer scattering functions. Figure 9 shows schematic representation of partial structure factors obtained by CV-SANS [16]. In the case of three-component systems, there are six components as shown in the figure; three self-terms ($S_{CC}(q)$, $S_{PP}(q)$, and $S_{WW}(q)$) and three cross terms ($S_{CP}(q)$, $S_{PW}(q)$, $S_{CW}(q)$). Here, C, P, and W denote clay, polymer, and water, respectively. Here, $S_{WW}(q)$ is trivial since it corresponds to the solvent-solvent correlation. Detailed studies on NC gels with CV-SANS method have elucidated that there exists a strongly adsorbed polymer layer with about 1 nm thickness on CL platelets irrespective of C_{clay} [17]. Based on this observation, it is concluded that nanoparticles serve as two-dimensional cross-linker in NC gels. This is one of the reasons why NC gels are very tough and highly deformable. Another reason is that the molecular weight of PNIPA in NC gels is extraordinarily large ($\approx 5.5 \times 10^6$ g/mol) [18]. That is,

each CL platelet bundles a large number of long PNIPA chains and behaves like a node of bamboo.

Figure 10 shows 2D partial scattering functions (PSFs) of NC gels, $S_{CC}(q)$, $S_{CP}(q)$, and $S_{PP}(q)$, at various draw ratios, i.e., $\lambda = 1, 3, 5,$ and 9 [19]. At $\lambda = 1$, the scattering intensities are weak and the patterns are isotropic, suggesting that both clay platelets and polymer chains are oriented randomly in the NC gel. By stretching to $\lambda = 3$, anisotropy appears in all PSFs.

The elliptic pattern in $S_{CC}(Q_{\parallel}, Q_{\perp})$ does not seem to change noticeably on further stretching. This behavior in $S_{CC}(Q_{\parallel}, Q_{\perp})$ may indicate that clay orientation is saturated by $\lambda = 3$. This is due to inter-blocking of CL platelets themselves because the inter-clay platelet distance is shorter than the diameter of the platelets (≈ 300 Å). The SANS result is consistent with their result by optical birefringence measurements [20]. $S_{PP}(Q_{\parallel}, Q_{\perp})$, on the other hand, becomes more anisotropic by increasing λ. At $\lambda = 9$, a strong streak pattern appears in the perpendicular direction, indicating that polymer chains are highly stretched in the parallel direction. It is quite important to note that $S_{CP}(Q_{\parallel}, Q_{\perp})$ is positive and looks similar to $S_{CC}(Q_{\parallel}, Q_{\perp})$ at $\lambda = 3$. This indicates that there exists a strong correlation between CL and polymer and the clay-polymer cross term behaves similar to the CL-CL self-term. A most plausible scenario explaining this phenomenon is that there exists a polymer-enriched layer on the surface of CL platelets and the layer itself orients simultaneously with the CL platelets. However, such synchronized orientation is lost by further increasing $\lambda > 3$ as seen by fading out of the pattern in $S_{CP}(Q_{\parallel}, Q_{\perp})$ at $\lambda = 9$. Hence, it is deduced that the polymer-enriched layer is peeled off by stretching.

Summary

The structure of CL/Ps is characterized by a large aspect ratio of CL, exfoliated to sheet by sheet, and preferential orientation along machine direction. This results in a fibrillar or layer structure of

Structures in CL/P Nanocomposites,
Fig. 10 2D SANS patterns for deformed NC gels at different stretching draw ratios, λ's. S_{CC}, S_{CP}, and S_{PP} denote clay-clay, clay-polymer, and polymer-polymer partial structure factors, respectively (Reprinted with permission from Nishida, et al., PRE, 2009. Copyright (2009) American Institute of Physics)
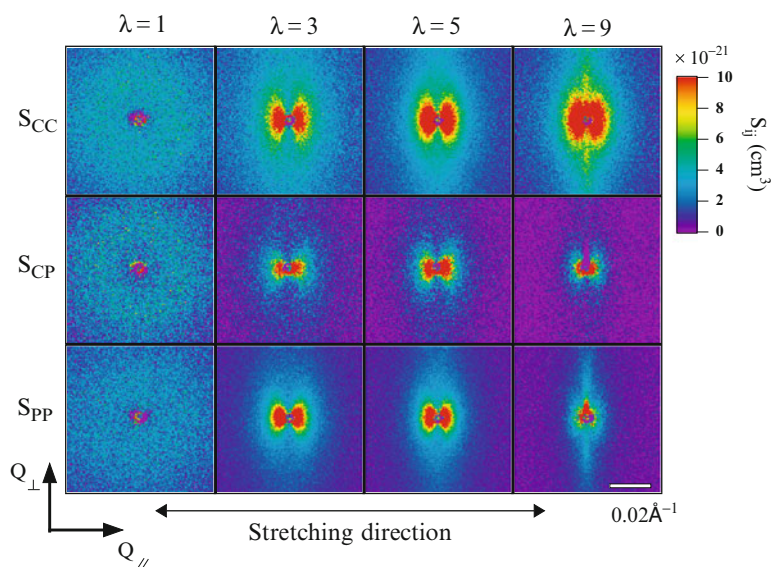
intercalated clay platelets with large aspect ratio and polymer matrix. Fine dispersion of CL is attained by surface modification of CL, i.e., organic clay, and chemical modification of polymer, e.g., maleated polyethylene. However, various kinds of polymers, such as PEO and polyamides, have strong attractive interaction with CL, resulting in polymer adsorption on CL platelets. Structural analyses of CL/P have been carried out with electron microscopy (EM), polarized optical microscopy (POM), atomic force microscopy (AFM), small-angle X-ray (SAXS) and neutron scattering (SANS), and others. Among them, detailed studies on the structure and the deformation mechanism of NC gels have revealed that the optical transparency of NC gels is ascribed to fine dispersion of exfoliated nano-sized CL platelets and the toughness of NC gels is due to 2D cross-linking of clay platelets on which long polymer chains are strongly adsorbed. By stretching NC gels, CL platelets orient along the stretching direction. Further stretching/retracting can be attained by peeling off/on of the reservoir polymer chains. Because of these unique mechanical/optical properties, NC gels have been attracting much attention for various applications. This is one of the advanced achievements of CL/P nanocomposites.

Related Entries

▶ Application of CL/P Nanocomposites
▶ Polysilanes
▶ Supramolecular Hydrogels
▶ Supramolecular Network Polymers
▶ Supramolecular Polymers (Hydrogen Bonds)

References

1. Novac BM (1993) Hybrid nanocomposite materials-between inorganic glasses and organic polymers. Adv Mater 5:422–433. doi:10.1002/adma.19930050603
2. Wen J, Wilkes GL (1996) Organic/inorganic hybrid network materials by the sol-gel approach. Chem Mater 8:1667–1681. doi:0.1021/cm9601143
3. Beecroft LL, Ober CK (1997) Nanocomposite materials for optical applications. Chem Mater 9:1302–1317. doi:10.1021/cm960441a
4. Haraguchi K, Takehisa T (2002) Nanocomposite hydrogels: a unique organic-inorganic network structure with extraordinary mechanical, optical, and swelling/de-swelling properties. Adv Mater 14:1120–1124. doi:10.1002/1521-4095(20020816) 14:16<1120::AID-ADMA1120>3.0.CO;2-9
5. Chin IJ, Thurn-Albrecht T, Kima HC, Russell TP, Wang J (2001) On exfoliation of montmorillonite in epoxy. Polymer 42:5947–5952. doi:10.1016/S0032-3861(00)00898-3
6. Koo CM, Ham HT, Kim SO, Wang KH, Chung IJ, Kim DC, Zin WC (2002) Morphology evolution and anisotropic phase formation of the maleated

polyethylene-layered silicate nanocomposites. Macromolecules 35:5116–5122. doi:10.1021/ma011770d

7. Bafna A, Beaucagea G, Mirabellab F, Mehta S (2003) 3D Hierarchical orientation in polymer–clay nanocomposite films. Polymer 44:1103–1115. doi:10.1016/S0032-3861(02)00833-9

8. van Olphen H (1977) Clay colloid chemistry. Interscience Publishers/Wiley, New York

9. Dijkstra M, Hansen JP, Madden PA (1995) Gelation of a clay colloid suspension. Phys Rev Lett 75:2236–2239. doi:10.1063/1.3673877

10. Zebrowski J, Prasad V, Zhang W, Walker LM, Weitz DA (2003) Shake-gels: shear-induced gelation of laponite-PEO mixtures. Coll Surf A 213:189–197. doi:10.1016/S0927-7757(02)00512-5

11. Takeda M, Matsunaga T, Nishida T, Endo H, Takahashi T, Shibayama M (2010) Rheo-SANS studies on shear thickening in clay-poly(ethylene oxide) mixed solutions. Macromolecules 43:7793–7799. doi:10.1021/ma101319j

12. Lal J, Auvray L (2000) Interaction of polymer with clays. J Appl Crystallogr 33:673–676. doi:10.1107/S0021889899013308

13. Loizou E, Butler P, Porcar L, Kesselman E, Talmon Y, Dundigalla A, Schmidt G (2005) Large scale structures in nanocomposite hydrogels. Macromolecules 38:2047–2049. doi:10.1021/ma0517547

14. Shibayama M, Karino T, Miyazaki S, Takehisa T, Haraguchi K (2005) Small-angle neutron scattering study on uniaxially stretched poly(N-isopropylacrylamide)-clay nanocomposite gels. Macromolecules 38:10772–10781. doi:10.1021/ma051979h

15. Shibayama M, Suda J, Karino T, Okabe S, Takehisa T, Haraguchi K (2004) Structure and dynamics of poly(N-isopropylacrylamide)-clay nanocomposite gel. Macromolecules 37:9606–9612. doi:10.1021/ma048464v

16. Shibayama M (2011) Small-angle neutron scattering on polymer gels: phase behavior, inhomogeneities and deformation mechanisms. Polym J 43:18–34. doi:10.1038/pj.2010.110

17. Miyazaki S, Endo H, Karino T, Haraguchi K, Shibayama M (2007) Gelation mechanism of poly (N-isopropylacrylamide)-clay nanocomposite gels. Macromolecules 40:4287–4295

18. Haraguchi K, Xu Y, Li G (2010) Molecular characteristics of poly(N-isopropylacrylamide) separated from nanocomposite gels by removal of clay from the polymer/clay network. Macromol Rapid Commun 31:718–723. doi:10.1002/marc.200900819

19. Nishida T, Endo H, Osaka N, Li H, Haraguchi K, Shibayama M (2009) Deformation mechanism of nanocomposite gels studied by contrast variation small-angle neutron scattering. Phys Rev E 80:30801. doi:10.1103/PhysRevE.80.030801

20. Murata K, Haraguchi K (2007) Optical anisotropy in polymer-clay nanocomposite hydrogel and its change on uniaxial deformation. J Mater Chem 17:3385–3388. doi:10.1039/b707570g

Structures in Filled Rubbers

Yoshinobu Isono
Department of Materials Science and Technology, Graduate School of Engineering, Nagaoka University of Technology, Nagaoka, Niigata, Japan

Synonyms

Structures in nanocomposites

Definition

Filled rubbers are mixtures of polymers having low glass transition temperatures and inorganic fillers such as carbon black and silica. Nanoparticle-filled rubbers include hierarchical network structures due to polymer-polymer, polymer-filler, and filler-filler interactions. Change in network structures exhibit strain-sensitive nonlinear viscoelasticity.

Introduction

Polymeric materials including rubbers are characterized by several characteristic features: (a) high specific strength, (b) network structure, (c) time-dependent response, and (d) relatively low modulus at temperatures above the glass transition temperatures, T_g. Of course, these materials are frequently subjected to large and/or fast deformation when they are in industrial processes and also when they are practically utilized as final products. Those materials are heavy duty because of some network structures therein. Usual polymers show practical mechanical strength when their degrees of polymerization exceed around 1,000. Degree of polymerization of the chains between adjacent entanglements is about 100. Therefore, existence of entanglement network is required for achieving practical strength. Crystalline polymers or thermoplastic elastomers are fairly strong,

S

because crystallites or high-T_g domains play a role of effective cross-links in a quasi-network structure [1]. Nanoparticle-filled rubbers include some hierarchical networks due to polymer-polymer, polymer-filler, and filler-filler interactions. Among these networks, those sustained by physical interactions exhibit dissociation and reformation. Therefore, filled rubbers show structural nonlinearity (in addition to usual nonlinearities of homopolymers simply attributable to chain orientation/stretch). Furthermore, those rubbers show viscoelastic nature because of their long relaxation times. Hence, their hierarchical structures need to be discussed/analyzed from wide viewpoints, e.g., from static to dynamic and also from microscopic to macroscopic viewpoints.

Structures in Cross-Linked Network

Chemical networks of rubbers are formed by chemical cross-linking reactions that have been reviewed elsewhere [2]. Chemical networks exhibit entropy elasticity [3]. It was well accepted, in a traditional way of thinking, that fairly homogeneous chemical networks are obtained through the cross-linking reactions, because the reactions should occur statistically and polymer chains take statistically random arrangements in space. But the actual networks are not homogeneous. Deep interest has been placed on the cross-linked network structures in the nonequilibrium, deformed state (where the rubbers are actually used), in addition to the interest on the equilibrium network density. However, it has been difficult to detect the structures in the deformed states. Recently, extremely strong energy beam (such as synchrotron radiation) becomes available to enable simultaneous measurements of rheological data and time-resolved scattering data, the latter detecting the change in structure. Toki et al. have observed extension-induced crystallization and extension hardening in the stress-strain curves from such simultaneous measurements and reported that the unoriented amorphous fraction in

sulfur-vulcanized natural rubbers remains to be 50–70 % even at 600 % extension [4]. Ikeda et al. have compared extension-induced crystallization behavior of peroxide-vulcanized and sulfur-vulcanized natural rubbers and found that the extension ratio at the onset of crystallization in the former samples decreases with increasing network-chain density ν, whereas this onset extension ratio in the latter samples hardly changes with ν [5]. Both results indicate that the sulfur-vulcanized natural rubber has fairly inhomogeneous distributions in the spatial positions of cross-linking points and in the length of network chains. Actual cross-linked rubbers are composed of effective cross-linked network chains and dangling chains, the latter having one end free from the network. The network and dangling chains, respectively, contribute to storage and loss moduli [6].

Structures in Filled Rubbers

Filled rubbers, consisting of polymer and filler, include three types of networks sustained by three different interactions, the polymer-polymer, polymer-filler, and filler-filler interactions. The first type of the network is the cross-linked and entangled network. The second type, referred to as the bridged filler network, is a network of filler particles such as carbon black particles bridged by polymer chains that are attached more or less firmly to the particles through, for example, entanglements trapped at the filler-polymer interface [7–9]. The third type, the contact filler network, is a network of directly contacting particles [8, 10] that can be formed at the particle content above the percolation threshold. The contact filler network of carbon black particles exhibits a significant decrease in its electrical resistivity and an increase in the modulus with increasing particle content, as shown in Fig. 1.
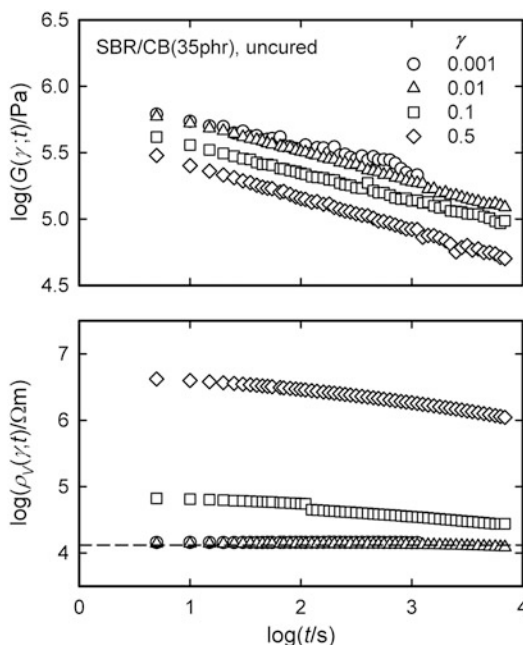
Simultaneous measurements of viscoelastic functions and electrical resistivity give a powerful route for studying the correspondence between a change in the contact filler network structure and the nonlinear viscoelasticity of
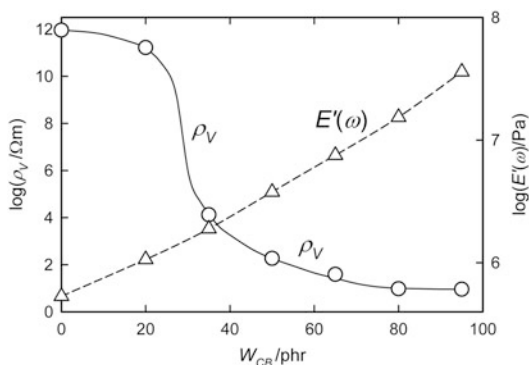
Structures in Filled Rubbers, Fig. 1 Filler concentration (W_{CB}) dependence of electrical volume resistivity ρ_V and tensile storage modulus $E'(\omega)$ of carbon black-filled and uncured SBR at no deformation. $W_{CB} = 0$ stands for the unfilled SBR

Structures in Filled Rubbers, Fig. 2 Double logarithmic plots of relaxation modulus (*upper panel*) and electrical volume resistivity (*lower panel*) against time for 35phr carbon black-filled, uncured SBR subjected to step shear strain γ as indicated. The measurements were made at 313 K. The *dashed line* in the *lower panel* denotes the value of electrical volume resistivity measured before straining

carbon black-filled rubbers under deformation, as demonstrated in Fig. 2. After imposition of step shear strain γ up to 0.5, the rubber shows just a minor decrease of the shear relaxation modulus, but its electrical resistivity exhibits orders-of-magnitude increases due to rupture of the contact filler network at large strains [10]. The Payne effect observed at higher particle concentrations also originates from rupture of the contact filler network. However, it is well known that nonlinearity of viscoelasticity emerges even at low particle concentrations below the percolation threshold (where the contact filler network is not formed). This nonlinearity may originate from a change in the bridged filler network [10].

As for the time-temperature superposition of viscoelastic data of filled rubbers, it was found that horizontal and vertical shift factors are governed by the matrix polymer and filler network, respectively [11]. The contact filler network of carbon black particles and hierarchical structures at smaller length scales have been detected statistically at the scattering vector q ranging from 3×10^{-4} to 2 nm^{-1} with the aid of combined scattering methods that include ultra-small-angle neutron and X-ray scattering (USANS and USAXS) and ordinary small-angle X-ray scattering (SAXS) [12]. The bound rubber phase near the filler surface, where the segmental

motion is suppressed, has been found by wide-line NMR [13]. The image of carbon black network is obtained by transmission electron microscopy (TEM) [7]. More realistic local images and detailed information on the carbon black network can be obtained with 3D-TEM, a technique that combines TEM with computerized tomography [14, 15]. For example, 3D-TEM has shown that a rubber phase of 3 nm thickness exists between CB aggregates, and this phase may correspond to bound rubber. 3D-TEM also revealed that elongation of SBR samples cured with a two-step process leads to disruption of the carbon black network therein [16]. In addition, silica network structures in rubber matrix have been observed [15, 17, 18]. However, further investigations are required for clear understanding of those structures. Recently, the atomic force

microscopy mapping techniques are applied to rubbers to directly detect local distributions in viscoelasticity and filler particles therein [19].

Summary

Filled rubbers include three different types of networks sustained by polymer-polymer, polymer-filler, and filler-filler interactions. The first type of network is characterized by average mesh size and inhomogeneity in distribution of cross-linking points. The latter two types of network, sustained by physical interactions, show dissociation and reformation. In addition, filled rubbers are of viscoelastic nature. The structures of the three types of network are being investigated with advanced experimental techniques that include high-energy beam scattering, viscoelasticity, electrical resistivity, and 3D-TEM at equilibrium and under deformation.

Related Entries

▶ Controlling Performance of Filled Rubbers
▶ Mechanical Behavior of Filled Rubbers
▶ Viscoelastic Relaxation and Morphology of Blends of Rubbery Polymers

References

1. Graessley WW (2004) Polymeric liquids & networks; structure and properties. Garland Science, New York
2. Choi W (2006) The main mechanism and cross-linking structure for accelerated sulfur vulcanization. J Soft Mater 2:47–55. doi:10.2324/ejsm.2.47
3. Mark JE, Erman B (2007) Rubberlike elasticity. A molecular primer, 2nd edn. Cambridge University Press, Cambridge
4. Toki S, Fujimaki T, Okuyama M (2000) Strain-induced crystallization of natural rubber as detected real-time by wide-angle X-ray diffraction technique. Polymer 41:5423–5429. doi:10.1016/S0032-3861(99)00724-7
5. Ikeda Y, Yasuda Y, Hijikata K, Tosaka M, Kohjiya S (2008) Comparative study on strain-induced crystallization behavior of peroxide cross-linked and sulfur cross-linked natural rubber. Macromolecules 41:5876–5884. doi:10.1021/ma800144u
6. Urayama K, Miki T, Takigawa T, Kohjiya S (2004) Damping elastomer based on model irregular networks of end-linked poly(dimethylsiloxane). Chem Mater 16:173–178. doi:10.1021/cm0343507
7. Klüppel M (2003) The role of disorder in filler reinforcement of elastomers on various length scales. Adv Polym Sci 164:1–86
8. Isono Y, Ferry JD (1984) Stress relaxation and differential dynamic modulus of carbon black-filled styrene-butadiene rubber in large shearing deformations. Rubber Chem Technol 57:925–945. doi:10.5254/1.3536050
9. Sternstein SS, Zhu AJ (2002) Reinforcement mechanism of nanofilled polymer melts as elucidated by nonlinear viscoelastic behavior. Macromolecules 35:7262–7273. doi:10.1021/ma020482u
10. Satoh Y, Fujii S, Kawahara S, Isono Y, Kagami S (2007) Differential dynamic modulus of carbon black filled, uncured SBR in single-step large shearing deformations. e-J Soft Mater 3:29–40. doi:10.2324/ejsm.3.29
11. Isono Y, Aoyama T (2013) Filler effects on temperature shift factors in viscoelastic properties of carbon black filled rubbers. Nihon Reoroji Gakkaishi (J Soc Rheol, Jpn) 41:137–144. doi:10.1678/rheology.41.137
12. Koga T, Hashimoto T, Takenaka M, Aizawa K, Amino N, Nakamura M, Yamaguchi D, Koizumi S (2008) New insight into hierarchical structures of carbon black dispersed in polymer matrices: a combined small-angle scattering study. Macromolecules 41:453–464. doi:10.1021/ma071867l
13. Kaufman S, Slichter WP, Davis DD (1971) Nuclear magnetic resonance study of rubber: carbon black interactions. J Polym Sci A2(9):829–839. doi:10.1002/pol.1971.160090505
14. Kojiya S, Kato A, Suda T, Shimanuki J, Kojiya S, Ikeda Y (2006) Visualization of carbon black networks in rubbery matrix by 3D-TEM image. Polymer 47:3298–3301. doi:10.1016/j.polymer.2006.03.008
15. Kojiya S, Kato A, Ikeda Y (2008) Visualization of nanostructure of soft matter by 3D-TEM: nanoparticles in a natural rubber matrix. Prog Polym Sci 33:979–997. doi:10.1016/j.progpolymsci.2008.06.001
16. Kato A, Isono Y (2013) Structural change in the carbon black network in carbon-black-filled styrene-butadiene rubber samples cured with a two-step process. J Appl Polym Sci 128:2498–2507. doi:10.1002/app.38356
17. Shinohara Y, Kishimoto H, Inoue K, Suzuki Y, Takeuchi A, Uesugi K, Yagi N, Muraoika K, Mizoguchi T, Amemiya Y (2007) Characterization of two-dimensional ultra-small-angle X-ray scattering apparatus for application to rubber filled with spherical silica under elongation. J Appl Crystallogr 40:S397–S401. doi:10.1107/S0021889807011697
18. Takenaka M, Nishitsuji S, Amino N, Ishikawa Y, Yamaguchi D, Koizumi S (2009) Structure analysis of swollen rubber-filler systems by using constant

variation SANS. Macromolecules 42:308–311. doi:10.1021/ma8019046

19. Watabe A, Komura M, Nakajima K, Nishi T (2005) Atomic force microscopy of mechanical property of natural rubber. Jpn J Appl Phys 44:5393–5396. doi:10.1143/JJAP.44.5393

Structures in Ion-Containing Polymers

U. Hyeok Choi[1] and James Runt[2]
[1]Functional Composites Department, Korea Institute of Materials Science, Changwon, South Korea
[2]Department of Materials Science and Engineering, Pennsylvania State University, University Park, PA, USA

Synonyms

Morphology of ion-containing polymers; Morphology of ionomers

Definition

An ion-containing polymer is a polymer – either inorganic or organic – which contains both covalent and ionic bonds in its chain or network structure [1–3]. A classic example is the ionomer introduced in 1965 by Du Pont, a class of thermoplastic materials consisting of random copolymers of ethylene and a relatively small fraction of methacrylic acid, in which the acid functionality is partially (or, in principle, completely) neutralized by a metal cation such as Zn^{++} or Na^+ (Surlyn). One of the most interesting features of ionomers is the state of aggregation of the ionic species. Some of the questions that have been intensely investigated are as follows: (i) whether the ionic species are uniformly distributed or are aggregated in domains, (ii) if ions do indeed aggregate, how large are the corresponding domains, and (iii) whether the state of aggregation is dependent on the concentration of ionic
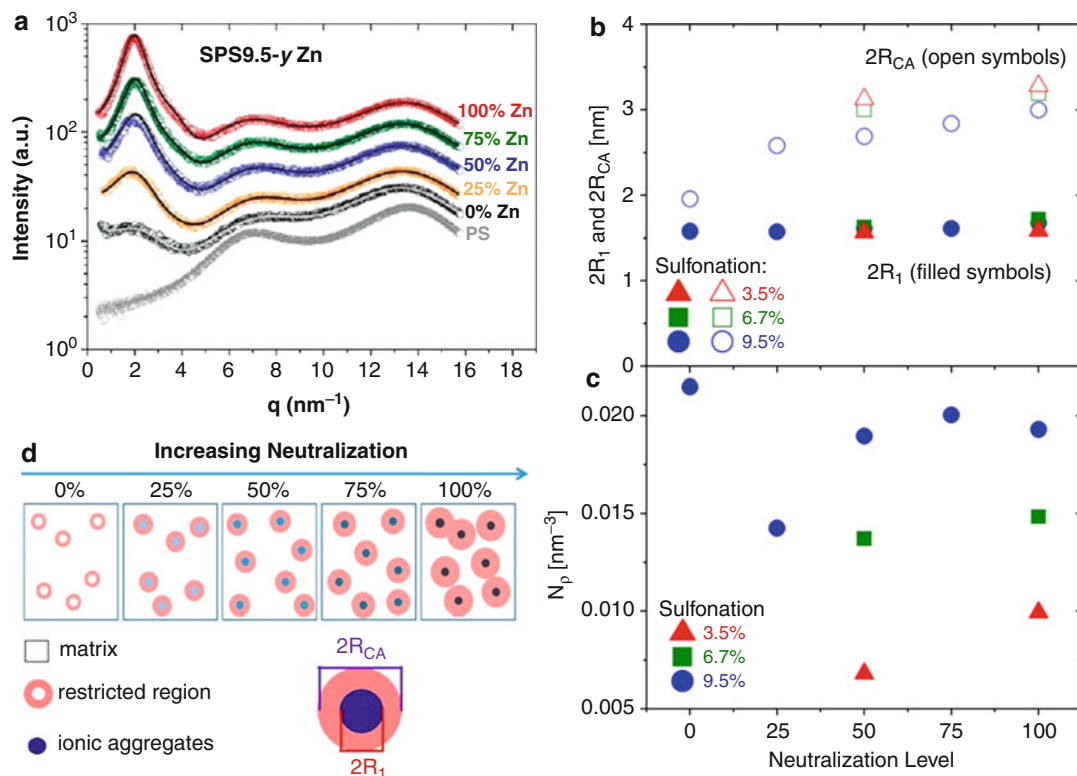
species. Central to the structure of ion-containing polymer is therefore the mode of association between the charged polymer and the counterions.

Introduction

It is well known that ion association takes places in media of low dielectric constant. As Bjerrium [4] first pointed out, in media of low dielectric constant, ions associate to form ion pairs and calculations show that the interaction energy is orders of magnitude greater than the thermal energy (kT). Thus, a simple view of ion-containing polymers would regard association in terms of ion pairs, triplets, or even multiplet formation. The most convincing evidence for the existence of ion aggregates of some type comes from the analysis of small-angle X-ray scattering (SAXS) data as well as high-magnification electron microscopy images. The scattering of X-rays is due to electron density fluctuations within a material. It has been found that partial neutralization of the acid groups in the ionomers (Surlyn) [5], and even acid groups in sulfonated polystyrene [6] or precisely sequenced poly(ethylene-co-acrylic acid) [7] copolymers, gives rise to a SAXS peak, which in the case of ionomers has since been termed the "ionomer peak," with a Bragg spacing of ~2–3 nm. It is sometimes underappreciated that a detailed molecular interpretation of the ionomer scattering peak depends on the choice of a suitable scattering model, generally requiring information on the microstructure (e.g., from electron microscopy) before doing so [2]. The most popular model used to gather quantitative information from the ionomer peak was introduced by Yarusso and Cooper, which approximates the aggregates as monodisperse spheres of ionic groups with liquid-like packing in the polymer matrix [8]. A modification to this model by Kinning and Thomas proposed a corona composed of polymer segments with restricted mobility surrounding the aggregates and imposing a separation of closest approach between

S

them [9]. The ultimate goal is to form a complete picture of the material from the nm to the μm length scales. A detailed understanding of the local environment inside the aggregates is required, as well as description of the size, shape, and spatial arrangement of the aggregates.

As examples of the structuring in ion-containing polymers, this chapter focuses on the application of X-ray scattering to the study of ionomer microstructure. Three case studies are provided: (i) the effect of extent of neutralization in sulfonated polystyrene-based ionomers, (ii) the effect of placement of functional group spacing (precise vs random) in poly(ethylene-*co*-acrylic acid) ionomers, and (iii) the investigation of thermally induced ionic aggregates in poly(ethylene oxide)–sulfonate polyester ionomers.

Effect of Neutralization

Winey [10, 11] and Weiss [12], among others, have explored ion aggregation in ionomers with different acid contents and neutralization levels using X-ray scattering and electron microscopy. Figure 1a compares the room temperature X-ray scattering profiles for a random Zn-neutralized sulfonated polystyrene (SPS) acid copolymer (having 9.5 mol-% sulfonation) at different neutralization levels (0 %, 25 %, 50 %, 75 %, and 100 %) [11]. Three distinct scattering peaks are observed: the higher-angle peak at the scattering wavevector $q \sim 13$ nm^{-1} corresponds to the polystyrene amorphous halo, the more subtle intermediate-angle peak at $q \sim 7$ nm^{-1} has been attributed to the polystyrene "polymerization

Structures in Ion-Containing Polymers, Fig. 1 (**a**) X-ray scattering intensity as a function of scattering wavevector q for polystyrene (PS) and Zn-neutralized sulfonated (9.5 mol-%) polystyrene ionomer (SPS) with different percent neutralization (0 %, 25 %, 50 %, 75 %, and 100 %), and the corresponding best fit of the scattering data using the Kinning-Thomas modified hard-sphere model (*solid lines*) [11]. (**b**) Radius of aggregates (R_I, *filled symbols*) and of closet approach (R_{CA}, *open symbols*) and (**c**) number density of the aggregates (N_p) as a function of neutralization level [11]. (**d**) Illustration of neutralization effect on matrix volume fraction, restricted region, and aggregates [11] (Reprinted with permission from Ref. [11]. Copyright 2011 ACS)

peak," and the lower-angle peak at $q \sim 1–2 \text{ nm}^{-1}$ is indicative of ion aggregation, the peak position indicating the mean spacing between ion aggregates (the "ionomer peak"). For the SPS ionomers, the intensity of the ionomer peak relative to the polystyrene amorphous halo increases significantly with increasing neutralization, which is consistent with enhanced electron density contrast as Zn ions are incorporated into the aggregates. Spherical, uniformly distributed bright features, corresponding to Zn-rich ionic aggregates within a matrix of lower average atomic number elements, are also observed in scanning transmission electron microscopy images of these ionomers [11]. To characterize the ionomer scattering in more detail, the Kinning–Thomas (K–T) modified hard-sphere model was utilized with four parameters: the aggregate radius R_1, the radius of closet approach R_{CA}, the number density of the aggregates N_p, and the amplitude A of the scattering maxima (see solid lines in Fig. 1a) [11, 13].

The corresponding K–T fit parameters (R_1, R_{CA}, and N_p) are displayed in Fig. 1b, c for three SPS sulfonation levels and various degrees of neutralization. Degree of sulfonation does not have a substantial effect on R_1 and R_{CA}, but a significant increase in N_p is observed. Degree of neutralization also does not have an appreciable effect on R_1, while R_{CA} systematically increases. The fact that the size of the ionic aggregates is independent of acid content and neutralization level suggests that the aggregate size in these strongly segregated ionomers is mainly controlled by the chemical structure of the acid copolymer (i.e., polymer backbone and acid type). For a fixed aggregate size, the region around the aggregates contains more polystyrene chain segments tethered to the aggregate by their anion resulting in a less mobile region of restricted mobility. With increasing degree of neutralization, therefore, the restricted region increases, corresponding to a decrease in the unrestricted matrix, while aggregates remain constant (see Fig. 1d). Furthermore, a second slower segmental relaxation (associated with T_g-like motion) arises from segments in the region of restricted mobility, and the

relaxation strength increases with neutralization and fits rather well with the microstructure picture from X-ray scattering [11].

Effect of Placement of Functional Group Spacing (Precise vs. Random)

Figure 2a provides a schematic representation of the possible placement of acid or charged groups in Zn-neutralized polyethylene (PE)–acrylic acid (AA) copolymers: (i) linear precise copolymers, (ii) linear pseudorandom copolymers, and (iii) branched random copolymers [14].

Linear poly(ethylene-*co*-acrylic acid) copolymers with acid groups separated by a precisely controlled number of carbon atoms ((i) in Fig. 2a) and with acid groups with pseudorandom spacings ((ii) in Fig. 2a) can be synthesized via acyclic diene metathesis (ADMET) and ring-opening metathesis polymerization (ROMP), respectively [7]. On the other hand, branched poly(ethylene-*ran*-methacrylic acid) copolymers with randomly spaced groups ((iii) in Fig. 2a) are commercially produced using high-pressure polymerization [16]. Neutralizing acid copolymers with a metallic salt produces ionomers and allows sufficiently high electron density contrast for X-ray scattering.

Random ionomers typically have a wide distribution of aggregate separations, leading to broad scattering features, which complicate efforts to draw quantitative conclusions about aggregate composition. On the other hand, precise ionomers yield more uniform aggregate distribution with better-defined scattering features. This chemical precision can in some cases lead to the self-assembly of ionic aggregates onto a lattice, as observed in block copolymers. These homogenous materials can be simulated to complement the experiments and gain molecular-level knowledge of morphology and dynamics.

Figure 2b displays X-ray scattering intensity versus q for linear precise PEpAA$_{13}$-Zn82, linear pseudorandom PErAA$_{13}$-Zn81, and branched random BPErMAA$_4$-Zn78 (having similar degrees of Zn neutralization level) at
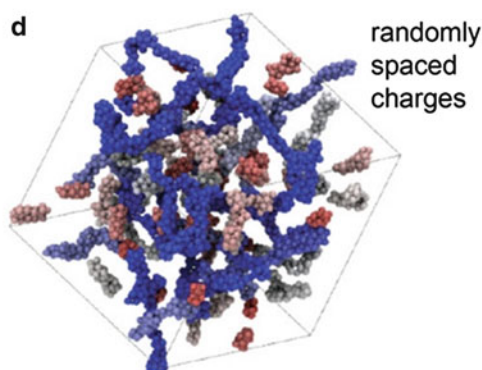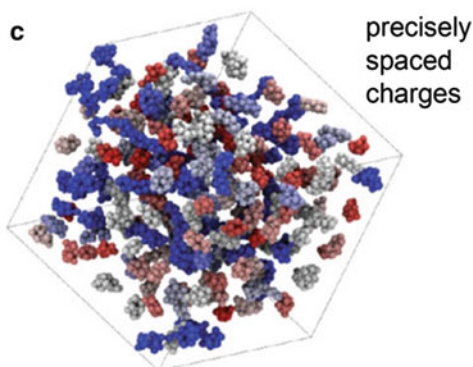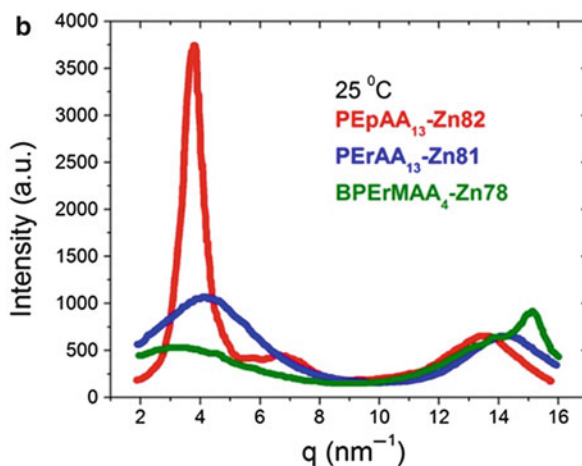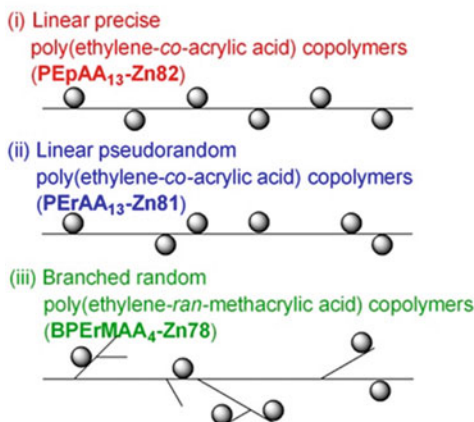
Structures in Ion-Containing Polymers, Fig. 2 (**a**) Schematic representation of placement of acid or charged groups (*circles*) in Zn-neutralized polyethylene (*PE*) – acrylic acid (*AA*) copolymers:[14] linear poly(ethylene-*co*-acrylic acid) copolymers with (i) precise acid placement in a linear chain, (ii) pseudorandom acid placement in a linear chain and (iii) branched poly(ethylene-*ran*-methacrylic acid) copolymers with randomly spaced groups (the precursor architecture of commercial ionomers like Surlyn) [14]. (**b**) X-ray scattering intensity versus scattering vector q for Zn-neutralized linear precise

PEpAA$_{13}$-Zn82 (13 mol % acid and 82 % Zn neutralization), linear pseudorandom PErAA$_{13}$-Zn81, and branched random BPErMAA$_4$-Zn78 at 25 °C plotted on a linear scale [14]. Snapshots of Na ionomers with (**c**) precise and (**d**) random charged groups by coarse-grained molecular dynamics simulations: only counterions and charged beads are shown, not but polymer backbones, and ionic aggregates are colored from *red* to *white* to *blue* in order of increasing number of ions in the aggregate [15]. (Reprinted with permission from Refs. [14] and [15]. Copyright 2010 and 2012 ACS)

room temperature. The precise ionomer exhibits dramatically sharper and more intense ionomer peak at $q \sim 4$ nm^{-1}, while the random ionomers exhibit a weaker and broad ionomer peak at $q \sim 4$ nm^{-1}. The more intense and well-defined peak indicates that the spatial distribution of the ionic aggregates is more uniform in the precise materials. Moreover, simulations provide a microscopic 3-dimensional picture of ionic aggregate morphology that can support for the experimental

scattering signatures. Figure 2c, d, respectively, presents snapshots of the simulated ionic aggregate morphology of ionomers with precise and random charged groups using coarse-grained molecular dynamics simulations [15]. The precise system displays discrete, roughly spherical aggregates with a relatively narrow size distribution. The random system also has discrete aggregates, but with a much wider range of aggregate size: in particular, the larger aggregates resemble short strings [15].

Thermally Driven Ion Aggregation

Investigations of thermally induced changes in the X-ray patterns of ionomers have been fairly common, partially motivated by the search for an ionic aggregate dissociation temperature. In general, this has been unsuccessful as X-ray studies have shown that ionic aggregates persist up to high temperatures. The effect of in situ heating on X-ray scattering has been extensively studied in SPS ionomers [12, 17, 18]. Heating of Zn-neutralized SPS ionomers (ZnSPS) leads to an increase in the intensity of the ionomer peak below the glass transition temperature (T_g) of the relatively nonpolar matrix phase, while above the T_g the intensity was unchanged. In addition, the scattering peak shifted to lower q as temperature increased up to T_g and remained at constant position thereafter. For Na-neutralized SPS ionomers (NaSPS), the intensity of the ionomer peak increased monotonically with temperature, while the peak position monotonically shifted toward lower q. By slowly cooling the ZnSPS ionomers from 260 °C, the original room temperature X-ray pattern was recovered; however, the high-temperature X-ray pattern was maintained in NaSPS, demonstrating that the effect of annealing on the microstructure at elevated temperatures is reversible for ZnSPS, but irreversible for NaSPS. The difference in the behavior for the two salts is presumably related to the difference in packing of the ionic species in aggregates: i.e., a tighter packing of sodium sulfonates in the nonpolar PS matrix than zinc sulfonates may account for the strong temperature resistance of the aggregates in NaSPS.

The effect of temperature on X-ray scattering has also been investigated in poly(ethylene oxide)-based ionomers [19]. In contrast to polystyrene and polyethylene, poly(ethylene oxide) is well known to solvate salts (cations), facilitated by the lone pair of electrons on ether oxygen atoms. Figure 3 shows the variable-temperature X-ray scattering of poly(ethylene oxide)–sulfonate polyester ionomers with Li^+, Na^+, and Cs^+ counterions [19, 20]. After heating from 25 °C to 120 °C, the identical scattering patterns at 25 °C before (black, 25-I) and after

(gray, 25-II) heating are observed, indicating that the morphology transformations are fully reversible in all of the materials (T_gs are all below 25 °C). In addition, heating these ionomers leads to a slight shift to lower q in the amorphous halo ($q \sim 15$ nm^{-1}) due to thermal expansion. In the Li ionomer, the scattering peak ($q \sim 2.6$ nm^{-1}) associated with ionic aggregates persists at all temperatures, indicating that the ionic aggregates are stable up to 120 °C (Fig. 3a). In contrast, both Na and Cs ionomers, wherein there are no well-defined ionic aggregates at room temperature, develop ionic aggregates upon heating (Fig. 3b, c). The Na ionomer displays an emerging aggregate peak at $q \sim 2.8$ nm^{-1} as temperature is raised, suggesting that upon heating a variety of local ion-pair environments transform into well-defined ionic aggregates.

For the Cs ionomer, the intensity of scattering peak at $q \sim 7$ nm^{-1}, corresponding to inter-pair scattering from isolated ion pairs ($SO_3^- Cs^+$) at room temperature, decreases with increasing temperature as a new scattering peak develops at $q \sim 3$ nm^{-1}, corresponding to interaggregate scattering from ionic aggregates. In particular, at 60 °C and 80 °C, the Cs ionomer exhibits both isolated ion pairs and ionic aggregates containing multiple ion pairs. This transformation is driven by the decrease in dielectric constant as temperature is raised, enhancing the Coulomb interactions between ions.

Summary

The incorporation of acid or ionic groups causes a fundamental change in morphology as the polar groups aggregate into domains. The morphological change undoubtedly plays an important role in modifying macroscopic properties. The effect of ion content was summarized for ZnSPS ionomers where the basic morphology was determined to be spherical ionic aggregates dispersed in a continuous polymer matrix; the number density of aggregates increased with increasing sulfonation but only weakly with degree of neutralization. The radius of closest approach increased with increasing neutralization,
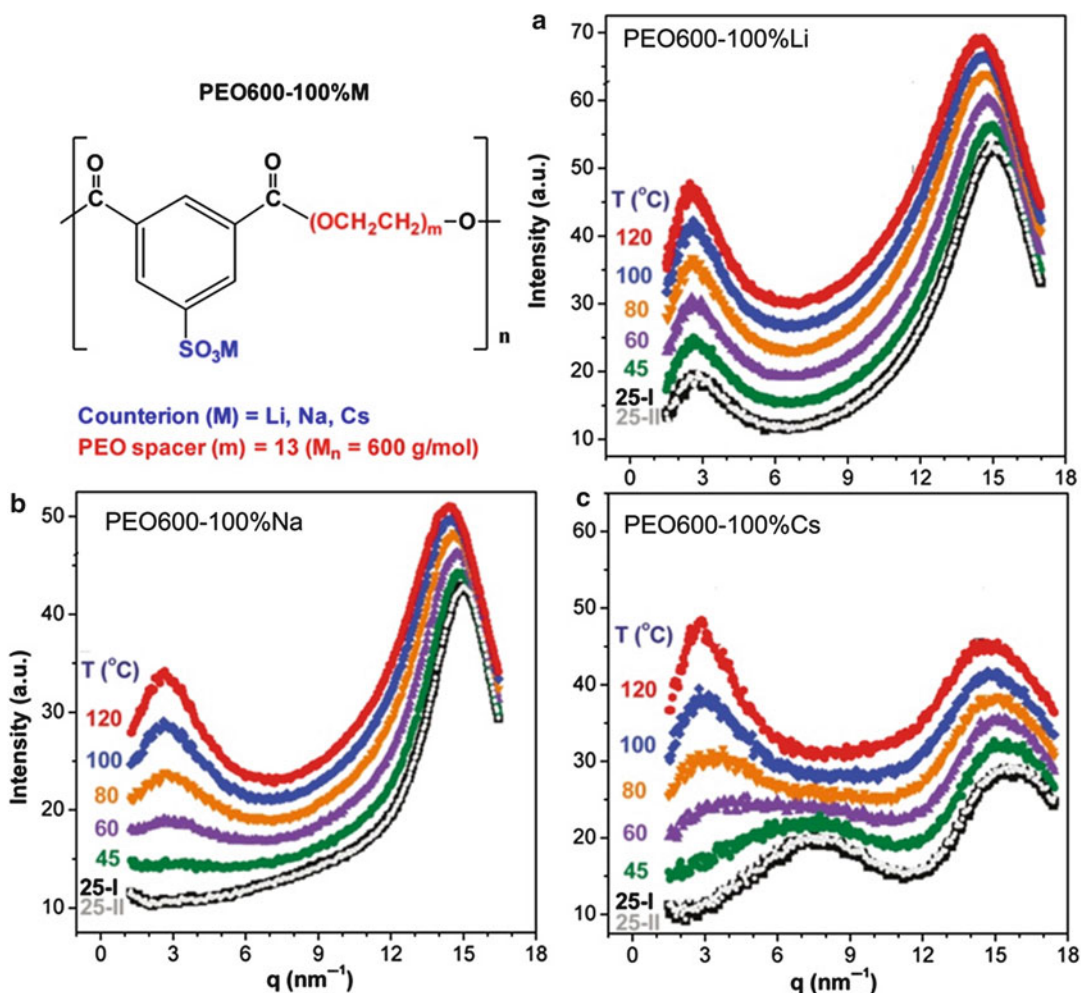
Structures in Ion-Containing Polymers, Fig. 3 X-ray scattering intensity versus scattering vector q for poly (ethylene oxide) (*PEO*) – sulfonate polyester ionomers with (**a**) Li$^+$ (PEO600-100 %Li), (**b**) Na$^+$ (PEO600-100 %Na), and (**c**) Cs$^+$ (PEO600-100 %Cs) counterions, each at six temperatures [19]. The scattering data were vertically shifted for clarity (Reprinted with permission from Ref. [19]. Copyright 2011 ACS)

indicating that with increasing neutralization the aggregates are becoming more ionic and the volume fraction of restricted region increases. Further, placement of ionic groups along the backbone, whether distributed precisely or randomly, has a significant influence on the morphology. The microstructural homogeneity of precise ethylene-based materials results in morphologies with unprecedented aggregate order, producing in some instances periodic aggregate structures in 1 and 3 dimensions. In situ heating studies on PEO-based ionomers showed that aggregation of the ion pairs increases with increasing temperature in these materials. In particular, Na and Cs ionomers exhibit thermally reversible transformation upon heating from 25 °C to 120 °C as isolated ion pairs aggregate. This seemingly counterintuitive aggregation of ions on heating is driven by the fact that the dielectric constant of all polar liquids decreases on heating, enhancing Coulomb interactions between ions.

Related Entries

▶ Effect of Crystallization on Morphology in Polymer Blends

▶ Morphology in Blends of Rubbery and Glassy Polymers

▶ Structures in CL/P Nanocomposites

References

1. Holliday L (1975) Classification and general properties of ionic polymers. In: Holliday L (ed) Ionic polymers. Applied Science, London

2. Eisenberg A, King M (1977) Ion-containing polymers: physical properties and structure. Academic, New York

3. Eisenberg A, Kim JS (1998) Introduction to ionomers. Wiley, New York

4. Fuoss RM, Kraus CA (1993) Properties of electrolytic solutions III the dissociation constant. J Am Chem Soc 55:1019–1028. doi:10.1021/ja01330a023

5. Schlick S (1995) Ion aggregation and its effect on ionomer properties. In: Kim JS, Eisenberg A (eds) Ionomers characterization: theory and applications. CRC Press, New York

6. Castagna AM, Wang W, Winey KI, Runt J (2010) Influence of the degree of sulfonation on the structure and dynamics of sulfonated polystyrene copolymers. Macromolecules 43:10498–10504. doi:10.1021/ma102206f

7. Baughman TW, Chan CD, Winey KI, Wagener KB (2007) Synthesis and morphology of well-defined poly(ethylene-*co*-acrylic acid) copolymers. Macromolecules 40:6564–6571. doi:10.1021/ma070841r

8. Yarusso DJ, Cooper SL (1983) Microstructure of ionomers: interpretation of small-angle x-ray scattering data. Macromolecules 16:1871–1880. doi:10.1021/ma00246a013

9. Kinning DJ, Thomas EL (1984) Hard-sphere interactions between spherical domains in diblock copolymers. Macromolecules 17:1712–1718. doi:10.1021/ma00139a013

10. Wang W, Chan TT, Perkowski AJ, Schlick S, Winey KI (2009) Local structure and composition of the ionic aggregates in Cu(II)-neutralized poly(styrene-*co*-methacrylic acid) ionomers depend on acid content and neutralization level. Polymer 50:1281–1287. doi:10.1016/j.polymer.2009.01.007

11. Castagna AM, Wang W, Winey KI, Runt J (2011) Structure and dynamics of zinc-neutralized sulfonated polystyrene ionomers. Macromolecules 44:2791–2798. doi:10.1021/ma2001614

12. Lu X, Steckle WP, Weiss RA (1993) Ionic aggregation in a block-copolymer ionomer. Macromolecules 26:5876–5884. doi:10.1021/ma00074a008

13. Zhou NC, Chan CD, Winey KI (2008) Reconciling STEM and X-ray scattering data to determine the nanoscale ionic aggregate morphology in sulfonated polystyrene ionomers. Macromolecules 41:6134–6140. doi:10.1021/ma800805m

14. Seitz ME et al (2010) Nanoscale morphology in precisely sequenced poly(ethylene-*co*-acrylic acid) zinc ionomers. J Am Chem Soc 132:8165–8174. doi:10.1021/ja101991d

15. Hall LM et al (2012) Ionic aggregate structure in ionomer melts: effect of molecular architecture on aggregates and the ionomer peak. J Am Chem Soc 134:574–587. doi:10.1021/ja209142b

16. Grady BP (2008) Review and critical analysis of the morphology of random ionomers across many length scales. Polym Eng Sci 48:1029–1051. doi:10.1002/pen.21024

17. Weiss RA, Lefelar JA (1986) The influence of thermal history on the small-angle X-ray scattering of sulfonated polystyrene ionomers. Polymer 27:3–10. doi:10.1016/0032-3861(86)90349-6

18. Register RA, Sen A, Weiss RA, Cooper SL (1989) Effect of thermal treatment on cation local structure in manganese-neutralized sulfonated polystyrene ionomers. Macromolecules 22:2224–2229. doi:10.1021/ma00195a040

19. Wang W, Tudryn GJ, Colby RH, Winey KI (2011) Thermally driven ionic aggregation in poly(ethylene oxide)-based sulfonate ionomers. J Am Chem Soc 133:10826–10831. doi:10.1021/ja201405v

20. Dou S, Zhang S, Klein RJ, Runt J, Colby RH (2006) Synthesis and characterization of poly(ethylene glycol)-based single-ion conductors. Chem Mater 18:4288–4295. doi:10.1021/cm0603699

Superabsorbent Polymers

Fusayoshi Masuda[1] and Yusuke Ueda[2]
[1]Sanyo Chemical Industries, Kyoto, Japan
[2]SDP Global Co., Ltd., Higashiyama-ku, Kyoto, Japan

Synonyms

Superabsorbent materials; Superabsorbents

Definition

Superabsorbent polymers are cross-linked hydrophilic polymers which can retain absorbed water under pressure due to an equilibrium balance of

dissolution and thermodynamically favored expansion of polymer chains constrained by cross-linking structure.

Historical Background

Superabsorbent polymers (SAPs) are defined as a class of cross-linked hydrophilic polymers which retain substantial amounts (>10 g/g) of absorbed water under pressure (>0.67 g/cm^2) (JIS, Japanese Industrial Standards). Until SAP was reported in the 1970s, naturally occurring materials like cotton and pulp had been used and applied to wide-ranging fields (e.g., sanitary goods) as absorbents for many years. These naturally occurring materials contain pores and absorb water primarily through capillary action, and under pressure, water is released as the volume of the internal pores is reduced.

A polymer derived from polyacrylonitrile grafted to starch followed by saponification could absorb 1,000 times its weight in water (in the absence of external pressure) was reported by the US Department of Agriculture Northern Regional Research Laboratory (NRRL) in 1974 [1, 2]. Since this discovery, various water-absorbing polymers such as polysaccharide-grafted polymers [3] and cross-linked sodium polyacrylate have been developed. These polymers became known as SAP. The majority of SAP produced today is a cross-linked sodium polyacrylate [4]; its cross-linked structure is an important factor for SAP absorbency as described below.

Since the SAP developed by NRRL was not a polymer with an added cross-linker, it was originally questioned whether the absorption mechanism for the NRRL polymer was the same as the water absorption mechanism of polymers with deliberately added cross-linker. It was later determined that a three-dimensional structure formed upon saponification; thus, the mechanism of water absorption was undoubtedly similar. Upon saponification, cross-linking was achieved mainly via imide formation by condensation of carboxylic acids and amide groups generated during saponification of nitrile groups. That is, a saponified

starch–*graft*–polyacrylonitrile was transformed into a strongly hydrophilic, cross-linked structure composed of polymer-supported sodium carboxylate salt and cross-linking imides [2]. Thereafter, commercial production of SAP, which was starch grafted with sodium polyacrylate, began in 1978 for use as sanitary goods [2, 4] and ultimately led to the current cross-linked sodium polyacrylate SAP.

Principle of Absorption by SAP

The mechanism of water absorption by SAP can be classified as physical rather than chemical absorption. Physical absorption of water proceeds by three mechanisms [2, 4]: (i) entrapment of water by capillary force inside macroporous structure (e.g., sponges), (ii) adsorption of water by capillary force and retention through formation of hydrogen bonds between water and hydrophilic functional groups (e.g., tissue paper), and (iii) a mechanism anticipated by the combination of (i) and (ii). *In SAP, equilibrium is established between natural dissolution of hydrophilic polymer segments and thermodynamically favored expansion of polymer chains limited by cross-linking.*
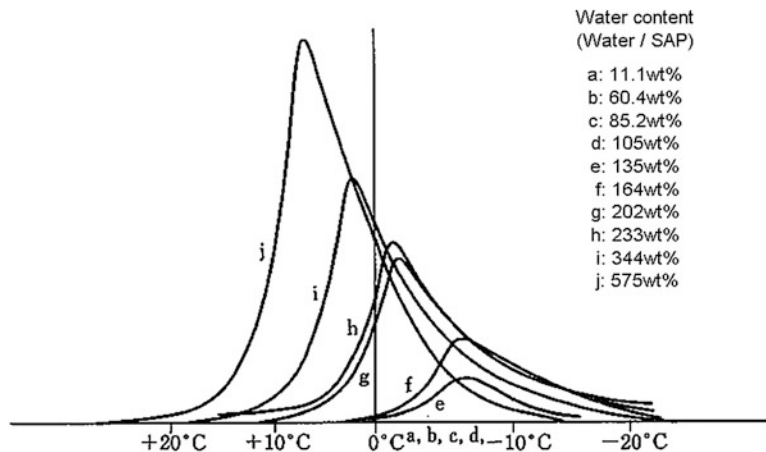
The theoretical basis of the equilibrium balance between absorption and retention of water under pressure was developed primarily by Flory and coworkers by using the Flory–Huggins model of the thermodynamics of polymer and solvent mixtures [5]. Enhanced absorption of water by lightly cross-linked polymer was predicted by Flory–Rehner swelling theory derived by introducing rubber elasticity to the Flory–Huggins model. The equilibrium swelling ratio, Q, can be expressed as shown in Eq. 1 by adding osmotic pressure effect to the Flory–Rehner theory:

$$Q^{5/3} \fallingdotseq \left\{ \left[i/\left(2V_u S^{*1/2}\right) \right] 2 + (1/2 - \chi_1)/V_1 \right\} (V_0/v_e) \tag{1}$$

where i/v_u is fixed charge density in polymer chain, S^* is ionic strength of solvent, v_1 is solvent molar volume, χ is an empirically derived

Fig. 1 Differential thermal
analysis of water-absorbing
cross-linked sodium
polyacrylate SAP. Cross-
linker, trimethylolpropane
triacrylate

Water content
(Water / SAP)

a: 11.1wt%
b: 60.4wt%
c: 85.2wt%
d: 105wt%
e: 135wt%
f: 164wt%
g: 202wt%
h: 233wt%
i: 344wt%
j: 575wt%

interaction parameter expressing polymer–solvent affinity, v_e is the number of polymer chains comprising the network structure, and V_0 is the polymer volume before swelling (v_e/V_0 = density of cross-linking).

In summary, the factors contributing to the capacity of a SAP are:

1. Density of cross-linking
2. Affinity between polymer and solvent
3. Osmotic pressure caused by polyelectrolyte counter ions

Nature of Water Absorbed by SAP

Water in the presence of a hydrophilic polymer shows different behaviors depending on its local structure imposed by interaction with the polymer. The behaviors are different from those of bulk water; absorbed water is classified into three groups depending on its structure [2].

1. Free water
2. Freezing bound water
3. Nonfreezing bound water

Free water is similar to bulk water. Its thermal motion (correlation time, τ_c: 10^{-12} s) is not restricted by the hydrophilic polymers and has the freezing point at 273 K. In contrast, nonfreezing bound water is water of hydration in association with hydrophilic polymers via

hydrogen bond. The motion of nonfreezing bound water is strongly restricted (τ_c: 10^{-5}–10^{-6} s) and does not freeze even at temperatures as low as 80 K. Freezing bound water shows properties intermediate to free water and nonfreezing bound water. Motion of freezing bound water is restricted (τ_c: 10^{-8}–10^{-9} s) and has a lower freezing point (253–263 K) than does free water. Freezing bound water arises from the interaction of water with nonfreezing water.

The nature of water absorbed by cross-linked sodium polyacrylate SAP was investigated by differential thermal analysis (Fig. 1). SAP with different amounts of absorbed water was cooled to 253 K, and the endothermic energy accompanying subsequent melting of water was measured. Although SAP with low amounts of absorbed water (<1.05 g distilled water/1 g SAP) did not show endothermic reaction, SAP began to show endothermic reaction from the point where the amount of absorbed distilled water was over 1.3/1 g SAP. The peak temperature of endothermic reaction shifted from 267 to 280 K as the amount of absorbed water increased, which means that free water became dominant in absorbed water. Table 1 shows the amount of free water, freezing bound water, and nonfreezing bound water. The amount of nonfreezing bound water in cross-linked sodium polyacrylate SAP is about 1.2/1 g SAP. This result means that almost all water (>98 %) is free water (small portion is freezing bound water) in fully swelled SAP (800 g distilled water/1 g SAP).

Superabsorbent Polymers, Table 1 The amount of nonfreezing bound water in swelled SAP

EXP	Water content (wt%) (water/ SAP)	Endothermic energy ΔH (J/g)	Peak temperature of endothermic reaction (K)	Free and freezing bound water content (wt%)	Nonfreezing bound water content (wt %)
a	11.1	0	–	0	11.1
b	60.4	0	–	0	60.4
c	85.2	0	–	0	85.2
d	105	2	–	0.6	104
e	135	47.1	265.8	14.1	121
f	164	127	266	38	126
g	202	309	271.9	93	109
h	233	384	272.2	115	118
i	344	732	276.5	219	125
j	575	1,472	279.5	441	134
				Average (EXP: d–j)	120

Superabsorbent Polymers, Table 2 Classification of SAP

| Gel type	Cross-linking mechanism	Backbone polymer		Example
Chemical gel	Covalent bond and ionic bond	Synthetic polymer		Cross-linked sodium polyacrylate
				Cross-linked sodium poly(vinyl sulfonate)
				Cross-linked poly(methacryloxyethyl ammonium chloride)
				Cross-linked poly(ethylene glycol)
		Natural polymer	Polysaccharide	Cross-linked carboxymethyl cellulose
				Cross-linked hyaluronic acid
				Cross-linked chitosan
				Cross-linked hydroxyethyl cellulose
			Polyamino acid	Cross-linked poly(glutamic acid)
				Cross-linked poly(lysine)
				Cross-linked poly(aspartic acid)
		Natural/synthetic hybrid		Starch–*graft*–sodium polyacrylate
				Saponified starch–*graft*–polyacrylonitrile
Physical gel	Hydrogen bond and others	The same as above		Poly(vinyl alcohol) treated by freezing and thawing
				Saponified poly(vinyl acetate-co-methyl [meth] acrylate)
				Mixture of poly(vinyl benzyl trimethylammonium chloride) and sodium polymethacrylate

Classification of SAP

SAP can be categorized into two groups according to whether the mechanism of cross-linking to form a gel is chemical or physical. The cross-linked structure of a chemical gel is retained over long periods ($>10^6$ s) because it is the result of covalent bonds (strong bond or ionic bond by multivalent metals). In contrast, the cross-linked structure of a physical gel is reversible ($<10^0$ s) and weak because it is the result of non-covalent bonds such as hydrogen bonds, hydrophobic interactions, or van der Waals forces. The ratio of water absorbed by a chemical gel is often more than ten times that of a physical gel because of its strong cross-linked structure. Table 2 further characterizes various types of SAP on the basis of the origin

Superabsorbent Polymers, Fig. 2 Morphologies of polymer particles produced by aqueous solution (*left*) and inverse suspension radical polymerization (*right*)
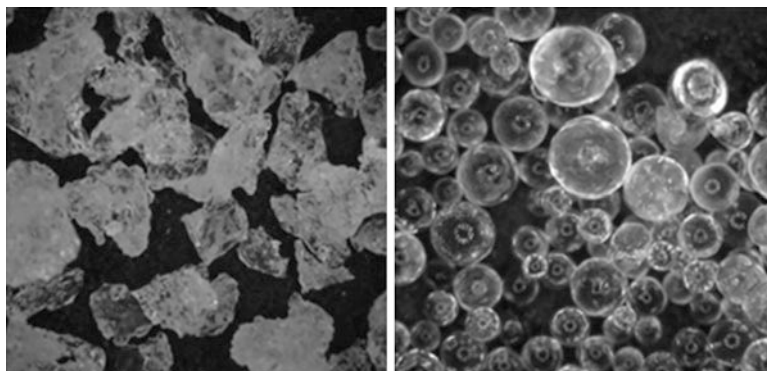
and chemistry of the polymer backbone [4, 6, 7] in addition to the above criteria.

1. Synthetic polymers
2. Natural/synthetic hybrid polymers
3. Natural polymers

SAPs classified as chemical gels are mainly described in this entry because of their high absorbency.

Synthetic Polymer Based SAP

Cross-linked sodium polyacrylate, sodium poly (vinyl sulfonate), and poly(ethylene glycol) are classified as synthetic polymer type SAP. Although all hydrophilic monomers (even nonionic monomers such as ethylene glycol) can be considered as monomers for SAP, the monomer most frequently used today is acrylic acid or sodium acrylate. Acrylic acid or sodium acrylate is especially preferred because of the ease of synthesizing high molecular weight polymers and the high charge density of the polymers. As described above, both features are important factors for polymer chain expansion, leading to large network structures in the presence of water. The most practical methods for synthesizing SAP on an industrial scale are the aqueous solution radical polymerization and inverse suspension radical polymerization methods. Today the predominant method to prepare sodium polyacrylate is based on radical polymerization of aqueous solutions of acrylic acid (or sodium acrylate); only a limited number of plants use the inverse suspension radical polymerization

method. One of the most characteristic differences between SAP produced by the aqueous solution radical polymerization method and the inverse suspension radical polymerization method is the morphology of the isolated polymer, as shown in Fig. 2 [2, 8]. The main industrial processes for SAP are shown schematically in Fig. 3 and discussed below.

Aqueous Solution Radical Polymerization

Acrylic acid monomer (or sodium acrylate monomer) is polymerized in aqueous solution (20–30 wt% in deoxygenized water) in the presence of a cross-linker and initiator. Depending on the monomers used, the detailed reaction conditions can change significantly [2, 4, 8].

Polymerization of Acrylic Acid Monomer As discussed below, the molecular weight of poly (acrylic acid) is strongly dependent on the pH during polymerization; higher molecular weight polymers are obtained at lower pH. Moreover, the lower the initial pH, the higher the rate of the polymerization of acrylic acid monomers. Despite some advantages in polymerization of acrylic acid monomers, the neutralization process after polymerization presents some challenges due to difficulties in handling poly(acrylic acid) gel. After neutralization, sodium polyacrylate gel is dried and pulverized into 300–600 μm particles.

Polymerization of Sodium Acrylate Monomer The use of sodium acrylate monomers avoids difficulties in the neutralization

S

Superabsorbent Polymers, Fig. 3 Synthetic routes for sodium polyacrylate SAP
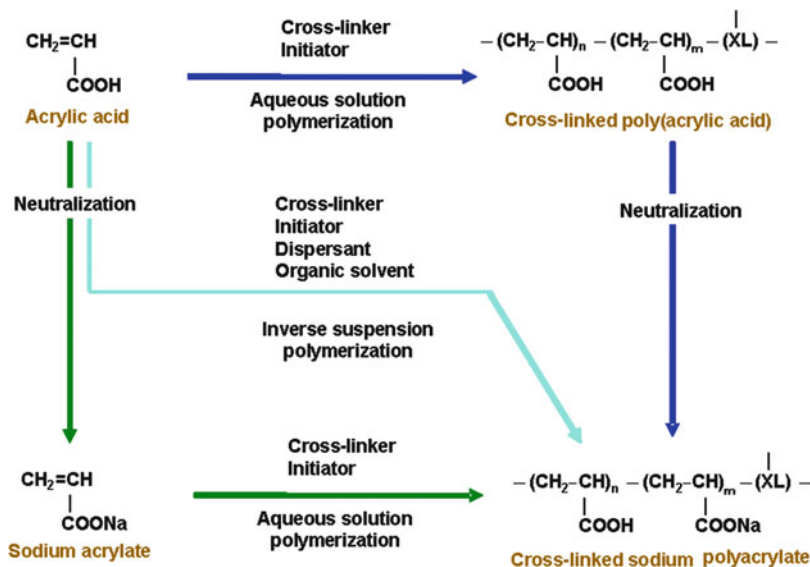
after polymerization, because the acrylic acid monomer is neutralized prior to polymerization. However, there are disadvantages; i.e., the resulting polymers possess lower molecular weight and the rate of polymerization is slower. In practice, sodium acrylate monomer is polymerized under kneader shearing conditions. After polymerization, the sodium polyacrylate gel is dried and pulverized into 300–600 μm particles.

Inverse Suspension Radical Polymerization

An organic solvent is used in inverse suspension radical polymerization to control reaction temperature, morphology, and particle size. The important points in inverse suspension radical polymerization are stabilization of an aqueous solution of sodium acrylate monomer in the organic solvent, optimization of mixing conditions, and recycle of organic solvent. In a typical industrial process, an aqueous solution of sodium acrylate monomer (30–50 wt% in deoxygenated water) and an initiator are fed into an organic solvent containing dissolved dispersant. Polymerization occurs at the boiling point of the organic solvent under mixing conditions. After polymerization, the cross-linked sodium polyacrylate particles and organic solvent are separated by centrifugation. Cross-linked

sodium polyacrylate particles are dried and the organic solvent is recycled for use in the next batch polymerization.

Radical polymerization initiators; redox pair initiators such as Fe^{2+}–H_2O_2 (Fenton reagent) and ammonia persulfate (APS)–sodium sulfite; thermal initiators such as potassium persulfate (KPS), APS, and 2,2′-azobis(isobutyronitrile) (AIBN); and photo-initiators such as gamma ray radiation are frequently applied [2, 4, 8]. Cross-linkers are classified into two groups, (a) multiple vinyl monomers which can copolymerize with the acrylic acid derivatives and (b) multifunctional reagents which can react with carboxyl groups. N,N'-methylenebisacrylamide (MBA), ethylene glycol dimethacrylate (EGDMA), 1,1,1-trimethylolpropane triacrylate (TMPTA), and tetraallyloxy ethane (TAOE) are the most frequently used multiple vinyl monomers [4, 8]. Multifunctional reagents include multifunctional glycidyl ethers such as ethylene glycol diglycidyl ether, polyols such as ethylene glycol, and polyamines such as ethylene diamine which form multicationic species in the presence of acrylic acid [2, 8]. As explained above, almost all SAP (>90 %) currently manufactured is cross-linked sodium polyacrylate, a synthetic chemical gel, because this type of SAP is superior to all other

known types of SAPs in absorbency. Notwithstanding, there is one SAP which shows exceptionally high absorbency despite its classification as a synthetic physical gel (which generally shows lower absorbency than chemical gels).

The finding that SAP, e.g., saponified copolymer of vinyl acetate and methyl (meth)acrylate (Table 2), can be synthesized without cross-linkers is of great interest. This SAP forms a sea–island structure where a noncontinuous phase (island) of sodium poly(meth)acrylate is surrounded by a continuous phase (sea) of noncrystalline poly(vinyl alcohol). In this microphase-separated structure, the continuous phase of poly(vinyl alcohol) is stretched and crystallizes as the noncontinuous phase of sodium polyacrylate absorbs water. While molecular rearrangement in the noncrystalline solid requires little energy, rearrangement within the crystal requires much more energy. Hence, this crystal structure can no longer be considered to belong to SAPs containing reversible weak bonds; the energy associated with crystal formation acts as the cross-linker for sodium polyacrylate phase [2].

Natural/Synthetic Hybrid Polymer Based SAP

Almost all SAP belonging to this group is polysaccharide–*graft*–polyacrylates. Because polysaccharides are the most abundant and inexpensive naturally occurring polymer and have the additional benefit of being biodegradable, they are fascinating resources as SAP raw materials. Various polysaccharide–g*raft*–polyacrylics using starch, cellulose, chitin, chitosan, guar gum, xanthan, and alginate have been reported [4, 7]. Starch–*graft*–poly(acrylic acid) was the first natural synthetic hybrid SAP to be produced on an industrial scale and remains widely used today [2, 7]. As explained above, the SAP developed by NRRL was produced by saponification of starch–*graft*–polyacrylonitrile to generate amide groups and carboxylic acids which condensed to form imides that served as the cross-linker.

In contrast, starch–*graft*–sodium polyacrylate is produced by polymerization of acrylic acid monomer directly on starch with cross-linker followed by neutralization to generate free carboxylic sodium salts distinct from the starch forming cross-linked structure. The principal purpose of graft polymerization on starch is to combine multiple high molecular weight poly(acrylic acids) with starch (also a polymer) to create very large three-dimensional network structures leading to high water absorbency. The high molecular weights can be attained by polymerization of acrylic acids using starch as a template because of the hydrogen bonding between acrylic acid and starch prior to the initiation of polymerization. This onto-starch graft-polymerization is initiated from radicals generated on starch molecules by added radical initiators; the nature of the graft copolymer is strongly influenced by the type of initiator and whether the starch has been subjected to pretreatment. The effects of initiators such as Fenton reagent, cerium ammonium nitrate (CAN) and KPS, and starch pretreatments (non-treated, swelling, and gelatinization) on grafting efficiency and molecular weight of poly (acrylic acids) were investigated [2]. Graft polymerization initiated with CAN gave especially high grafting efficiency and high molecular weight poly(acrylic acids) (Fig. 4). CAN is now used frequently to initiate grafting of acrylic acid to many kinds of polysaccharides in addition to initiating grafting of acrylic acid to starch.

Natural Polymer Based SAP

SAPs in this category are classified into two groups, (a) cross-linked natural polymers with charges on the polymer chain and (b) cross-linked natural polymers modified via substitution reactions to introduce low molecular weight substituents possessing charge. Polysaccharides such as alginate [4, 6, 9], hyaluronic acid [6, 9, 10] and chitosan [6, 7, 9], carboxymethyl-modified polysaccharides such as carboxymethyl cellulose [4, 11] and carboxymethyl starch [11], proteins such as collagen [6], and poly(amino acid) such as poly(glutamic acid) [9], poly(aspartic acid) [7, 9] and polylysine [9] are all reported to be used for SAP. Cross-linking can be achieved by coupling of radicals generated by electron or gamma ray irradiation [11] or multifunctional reagents such as ethylene glycol diglycidyl ether and glutaraldehyde which react with functional groups on different polymer chains.

S

Superabsorbent Polymers,
Fig. 4 Grafting efficiency of starch–*graft*–sodium polyacrylate in various grafting polymerization conditions
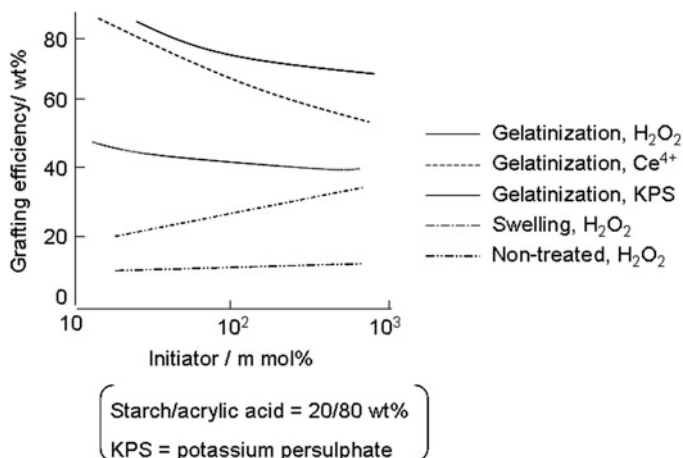
Water Absorption Ability of SAP

Absorption of water by hydrophilic polymers is primarily dependent on three factors, the density of cross-linking, the affinity between polymer and water, and the osmotic pressure generated by the presence of electrolytes.

Density of Cross-Linking

Depending on its degree of cross-linking (covalent bonding), a hydrophilic polymer may be soluble in water, swell in water, or remain an undissolved solid (e.g., an ion-exchange resin) [2]. SAP is a water-swelling resin which attains the targeted amount of water absorption by controlling density of cross-linking (Fig. 5). For each type of hydrophilic polymer, maximum water retention is achieved at a specific level of cross-linking. Water absorption increases as cross-linking increases, reaches a maximum, and then decreases as the cross-linking increases further. This is why hydrophilic polymer expansion in water is limited severely by increased cross-linking and too high density of cross-linking cannot form large network structure by water absorption.

Affinity Between Polymer and Solvent

As mentioned above, water absorption of SAP is derived from the force generated by the tendency of hydrophilic polymers to expand in water. Affinity between the polymer comprising SAP

and solvent is also very important for absorption [6]. Sodium polyacrylate type SAP shows poor absorbency for organic solvent immiscible with sodium polyacrylate such as methanol, acetone, and ethylene glycol. Figure 6 shows solvent absorption of sodium polyacrylate type SAP as a function of the organic solvent/water ratio. In this case, the SAP undergoes phase transition at a specific organic solvent/water ratio (threshold) resulting in a rapid decrease in the amount of water which can be absorbed by the SAP. The ratio at which the phase transition occurs varies according to the type of SAPs.

Osmotic Pressure Generated by Counter Ions of Polyelectrolytes

SAP containing polyelectrolytes exhibits much higher water absorption than SAPs without polyelectrolytes because the presence of the polyelectrolytes creates an affinity for water and also creates an osmotic force resulting from electrostatic repulsion and consequent expansion of the polymer network (Fig. 7). However, pH changes and the presence of salts in water have large effects on the water absorption capacity of polyelectrolyte type SAP [2, 6, 9] (Fig. 8). For example, sodium polyacrylate type SAP shows a dramatic decrease in water absorption capacity in the presence of multivalent metal ions, because sodium polyacrylate type SAP chelates the ions and forms over cross-linked structure [6, 9].
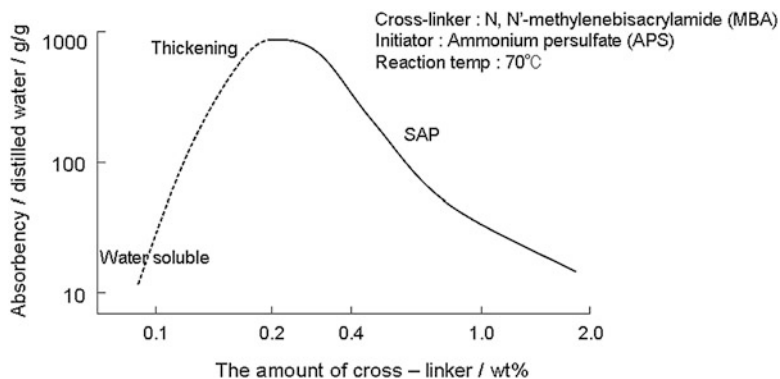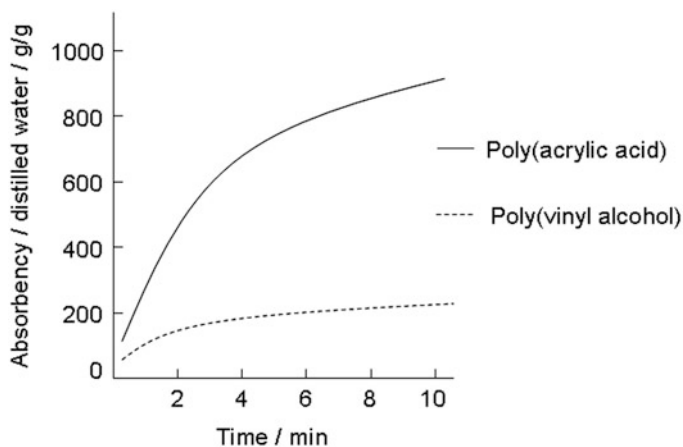
Superabsorbent Polymers, Fig. 5 Effect of cross-linker density on water absorbency of cross-linked sodium polyacrylate SAP. Cross-linker, *N*, *N*'-methylenebisacrylamide (*MBA*); initiator, ammonium persulfate (*APS*); reaction temperature, 70 °C. Absorbency is measured by the centrifuge method


Superabsorbent Polymers, Fig. 6 Effect of the organic solvent/water ratio on absorbency of cross-linked sodium polyacrylate SAP
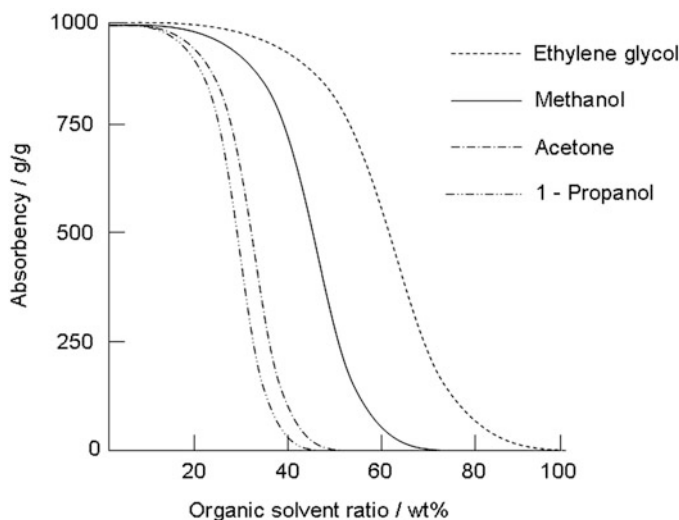
Superabsorbent Polymers, Fig. 7 Absorption of SAP composed of polyelectrolyte or nonionic polymer. Absorbency is measured by the centrifuge method (CRC)

S

Superabsorbent Polymers, Fig. 8 Effect of addition of salts on water absorbency of cross-linked sodium polyacrylate SAP
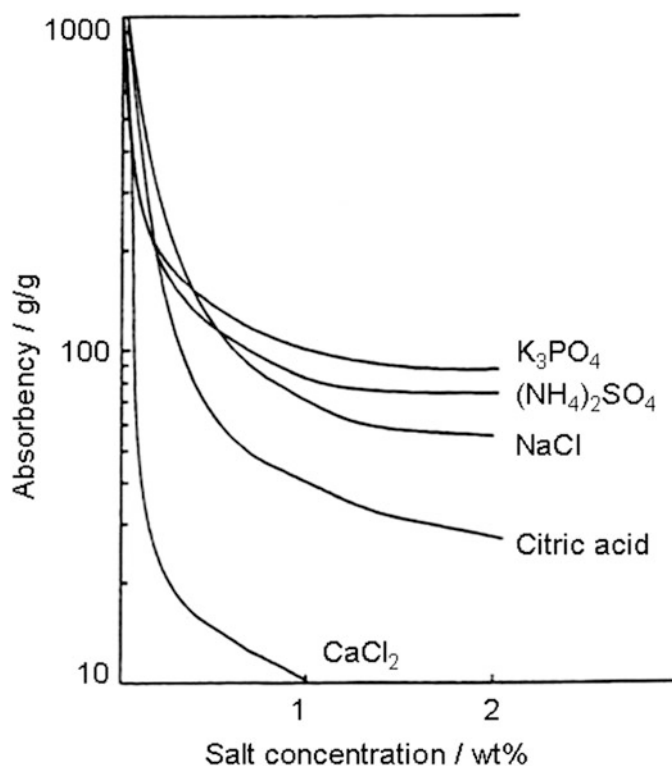
Superabsorbent Polymers, Table 3 Analytical evaluation of SAP property

Object	Analytical evaluation	Outline
Absorbency	**Centrifuge method**	SAP put in tea bag is immersed in excess amount of water and spun by centrifuge
	Tea bag method	SAP put in tea bag is immersed in excess amount of water and hanged to drop off excess water
	Demand wettability	SAP placed on stage with open hole is allowed to absorb water in burette with zero hydrostatic head
Absorption capacity under pressure	**Demand wettability**	**SAP is placed in a cylinder with nylon mesh bottom and pressure is applied. The amount of absorbed water is measured by demand wettability method**
Absorption speed	**Vortex method**	SAP put in beaker with 50 g saline water is stirred with a magnetic stirrer and measuring the time from addition of SAP to gelation
	Lockup method	SAP placed on a petri dish is allowed to absorb water without stirrer and measuring the time from addition of SAP to gelation
	Demand wettability	SAP placed on stage with open hole is allowed to absorb water in burette with zero hydrostatic head and measuring the amount of absorbed water with real time

Analytical Evaluation of SAP

Table 3 lists the analytical methods for measuring the kinetics of water absorption (one of the most characteristic properties for SAP) and total water absorption capacity [2, 4, 6, 8, 12].

Absorption Capacity Under Free Pressure

When the term absorbency or absorption without specific condition is used, "absorption" implies uptake of distilled water or saline (0.9 wt% sodium chloride in distilled water) under free pressure.

Centrifuge Method

A known weight ($W_1 = 0.3$–1 g) of SAP is placed in a tea bag, the total weight is measured (W_2), and the tea bag containing the SAP is immersed in excess distilled water/saline for 1 h. The tea bag/SAP is transferred to a centrifuge and then spun at 1,000–1,600 rpm for a few minutes to separate the water/saline not retained in the SAP. The tea bag/SAP/water is then weighed (W_3). The same procedure is carried out with only a tea bag (W_4) for reference, and the tea bag/(water/saline) sample is weighed (W_5). The amount of retained water is calculated as follows:

$$\text{Absorbency } (g/g) = [(W_3 - W_2) - (W_5 - W_4)]/W_1 \quad (2)$$

Tea Bag Method

In this conventional method, a SAP sample ($W_1 = 0.3$–1.0 g) is weighed in a tea bag with fine mesh, the total weight is measured (W_2), and the sample is immersed in an excess of distilled water/saline for 1 h. The recovered tea bag is hung until free excess water/saline is no longer observed, and then, the tea bag/SAP/(water/saline) sample is weighed (W_3). The same procedure is carried out with only a tea bag (W_4) for reference and the tea bag/(water/saline) sample is weighed (W_5). Absorbency is calculated in the same way as in the centrifuge method (*vide supra*).

Demand Wettability Method

A constant hydrostatic head is maintained by a vertical burette filled to a known level with an air-tight top and an air bleed system at a point in the lower portion of the burette, as shown in Fig. 9 [12]. The test is usually run at near-zero hydrostatic head. The liquid delivery hole is positioned at the same height as the tip of the air bleeder. The SAP sample of a known weight is placed on the stage with open hole, and valve (B) is opened to bleed air into the burette after valve (A) is opened. Water/saline flows through the tube (as indicated by the blue arrows), and the water is absorbed by the SAP. The amount of absorbed water within a predetermined time is conveniently measured by observing the decrease in the burette water level.
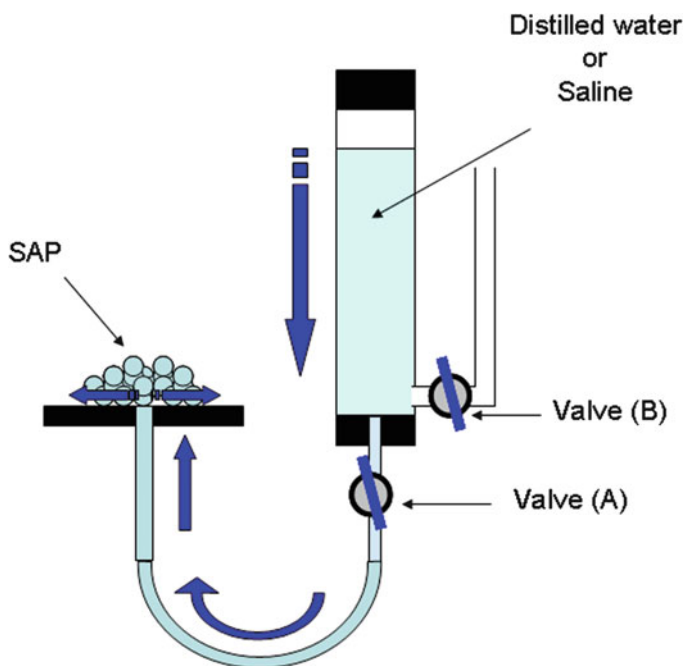
Superabsorbent Polymers, Fig. 9 Demand wettability (*DW*) test method

Absorption Capacity Under Pressure

As explained below, SAP is required to absorb water under pressure, and absorption capacity under pressure is one of the most important indexes for SAP absorption capacity.
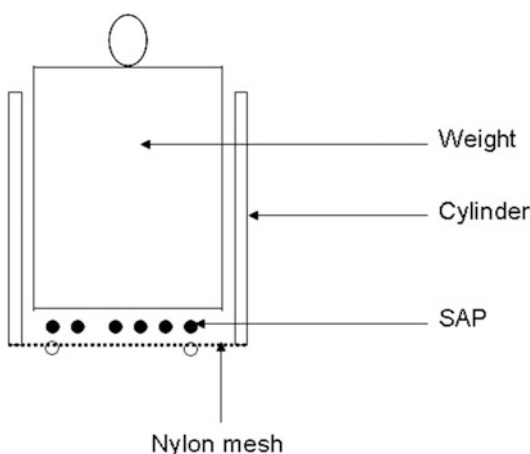
Absorption Capacity Under Pressure

A SAP sample (W_1 = 0.1–0.2 g) is placed in a cylinder with nylon mesh bottom (Fig. 10), and a pressure of 46.7 g/cm^2 is applied. The total weight is measured (W_2), the sample is put on the stage of DW test method explained above for 1 h (Fig. 9), and then, the total weight is measured (W_3). Absorption capacity under pressure is calculated as follows (Eq. 3):

$$\text{Absorption capacity under pressure } (g/g) = (W_3 - W_2)/W_1 \quad (3)$$

Absorption Speed

Vortex Method

In this conventional (relative and unique to each laboratory) method, distilled water/saline (50 g) is poured into a 100 ml beaker. The liquid is stirred at 600 rpm with a magnetic stirrer, and a SAP sample (W_1 = specified quantity) is added to the beaker at the starting time (t_0). The elapsed time (t) from the addition of SAP to gelation is

Superabsorbent Polymers, Fig. 10 Evaluation of absorption capacity under pressure. Water absorbency is measured on the stage of DW test method

measured. The absorption rate is calculated as follows:

$$\text{Absorption speed } (g/g \cdot s) = (50/W_1)/t \quad (4)$$

Lockup Method

A SAP sample is first spread uniformly in a petri dish, and then, a fixed amount of distilled water/saline is poured into the dish and left without stirring. The elapsed time from the addition of water to gelation is measured.

Modification of SAP

Efforts continue to improve both SAP water absorption capacity and the rate of SAP water absorption.

Absorption Under Free Pressure

Given that SAP is based on cross-linked network structures, increasing the molecular weight of the polymers which form the network continues to hold promise for creating high absorption SAP [2, 13]. In addition to efforts to increase molecular weight, strategies based on gel swelling theory to increase osmotic pressure are actively pursued.

Molecular Weight

Figure 11 shows the water absorption capacity of SAPs which are cross-linked poly(acrylic acids) with different molecular weights as indicated by changes in intrinsic viscosity under the constant cross-linker concentration. Absorption increases as the molecular weight of poly(acrylic acids) increases. The molecular weight of the poly (acrylic acids) is strongly dependent on the pH during polymerization [14]. Much higher molecular weight of poly(acrylic acids) is produced under low pH conditions compared with neutral and high pH conditions. The polymerization rate of acrylic acid monomers is also highest at low pH [14].

Other ultrahigh molecular weight ($M_w > 3*10^7$) polymers have been prepared by radical polymerization under plasma irradiation [13, 15]. For example, a copolymer of acrylamide and 2-acrylamide-2-methyl-1-propane sulfonic
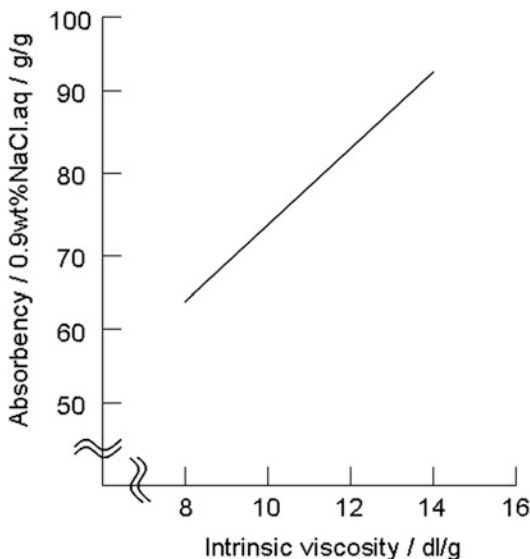
Superabsorbent Polymers, Fig. 11 Effect of molecular weight of poly(acrylic acids) on absorbency. Poly (acrylic acids) are cross-linked by ethylene glycol diglycidyl ether. Absorbency is measured by the centrifuge method. Intrinsic viscosity is used to evaluate the molecular weight of polymer

Superabsorbent Polymers, Table 4 Dissociation degree of synthetic polymer and polysaccharide

Polyelectrolyte	Example	Apparent dissociation degree (m)
Synthetic polymer	Poly(styrenesulfonic acid) sodium salt	0.2
	Poly (dimethylaminoethyl methacrylate) hydrochloride	0.13–0.2
	Partially saponified poly(methyl methacrylate)	0.25
Polysaccharide	Chitosan	0.61
	Keratinic acid sodium salt	0.92
	Chondroitin-6-sulfate	0.48

acid polymerized in water showed high water absorption capacity (molecular weight is evaluated by measuring reduced viscosity which is the value of specific viscosity divided by polymer concentration) [13].

Osmotic Pressure
In order to increase osmotic pressure, introduction of strong acid groups such as sulfonic acid on polymer chain has been investigated [2]. Although strong acid containing monomers such as 2-acrylamide-2-methyl sulfonic acid and styrene sulfonic acid would seem to be promising candidates to increase osmotic pressure even in saline, copolymers composed of acrylic acid monomers and these sulfonic acid monomers actually displayed reduced water absorbency [2, 9]. The decrease in water absorption was attributed to the difficulty in achieving the synthesis of high molecular weight copolymers of sulfonic acid monomers with acrylic acids [2]. On the other hand, SAP containing sulfonic acids shows tolerance against water with dissolved multivalent metal ions, e.g., seawater,

because sulfonic acids do not chelate multivalent metal ions in contrast to poly(acrylic acids) which chelate multivalent metal ions to form an over cross-linked structure [6, 9].

Another approach for improvement of osmotic pressure is cross-linking polysaccharide with ionic groups. Polysaccharides containing ionic groups exhibit a higher degree of counter ion dissociation than poly(acrylic acids). The difference is attributed to the difference in flexibility of the underlying polymer chain; poly(acrylic acids) is flexible while the polysaccharide backbone is stiff. The stiffness increases the distance between ionic groups and lowers the surface charge density, thus effectively lowering the ionic strength (Table 4) [2, 16]. Carboxymethyl cellulose and carboxymethyl starch cross-linked by radiation are known to exhibit higher water absorption than sodium polyacrylate type SAP [11].

Absorption Under Pressure
Increasing molecular weight of the polymer and osmotic pressure are promising approaches to improve absorption capacity as explained above. Under pressure condition, however, water diffusion inside of SAP has larger effects on water absorption than molecular weight of the polymer and osmotic pressure because of gel formation at the surface which inhibits diffusion

S

of water to the interior of the particle (gel blocking) and slowing of water uptake by gel blocking becomes even more serious under pressure. Notwithstanding, SAP is often required to absorb water under pressure in practical use (e.g., diaper). To avoid gel blocking, surface cross-linking is a promising approach.

Water Diffusion Inside of SAP

If compression of the surface occurs under pressure, the diameters of surface voids are reduced and the density of the surface gel is subsequently increased. If the gel density is high, diffusion of water through the gel to the interior of the particle is reduced, and thus, regardless of the structure of the interior of the particle, total water absorption is decreased. In order to take advantage of improved internal water diffusion and absorption under pressure by increasing internal cross-linkers, reduction of the diameters of surface pores must be prevented. Cross-linking specific to the surface has been shown to be effective in maintaining surface void structures even under pressure and without loss of the potential for polymer chains to expand inside of the SAP as water absorption under pressure increases as shown in Fig. 12 [8, 9, 17].
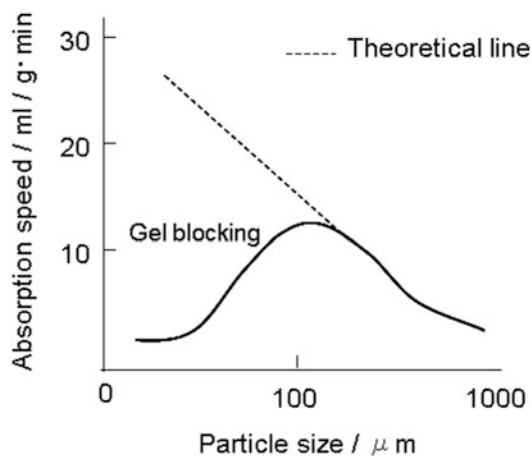
Absorption Speed

Absorption speed is influenced more by physical factors rather than chemical composition. The main factors for improving absorption speed are (i) increasing surface area and (ii) suppressing gel blocking.

Increasing Surface Area

To increase the effective surface area of SAP particles, SAP particles are reduced in size [2, 18]. Absorption speed increases as the SAP particle diameter decreases; however, at diameters less than about 100 μm, absorption speed begins to decrease because of gel blocking (Fig. 13). Increasing the surface area of the SAP particle by forming porous or botryoidal structures [2] is an effective approach for increasing absorption speed and obviates the need to reduce particle size.
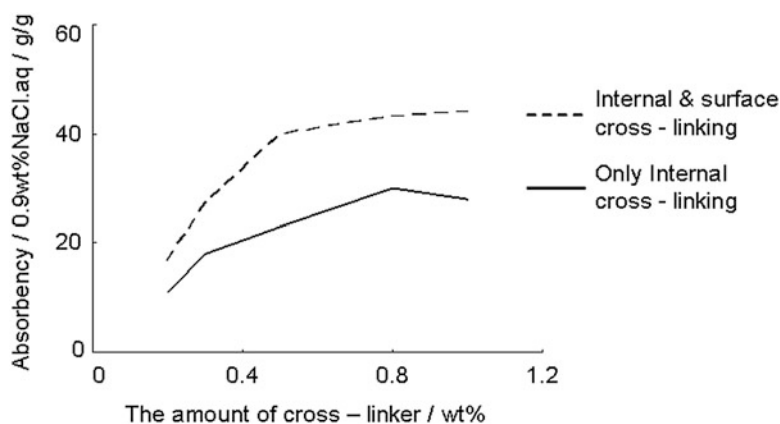
Suppression of Gel Blocking

As described above, gel blocking is a state where initially adsorbed water on surface of a SAP particle forms a hydrogel which inhibits water
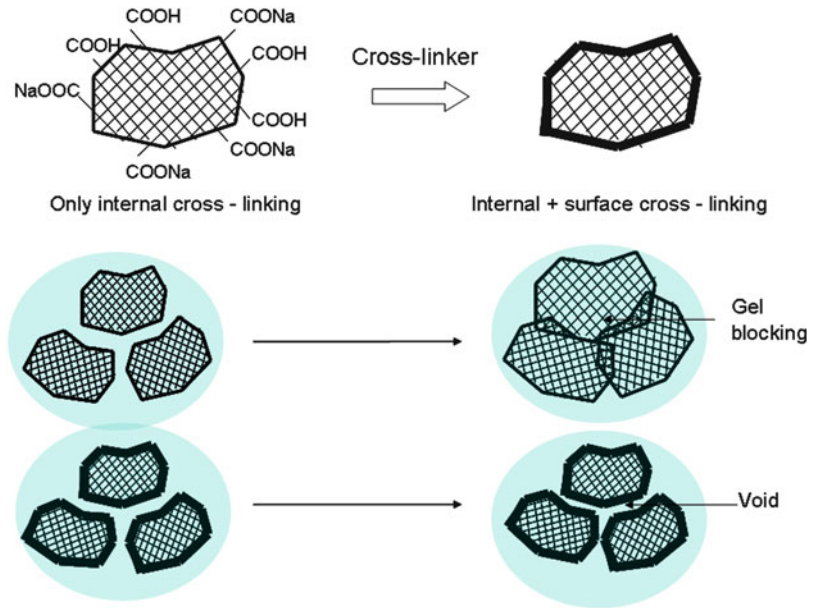

Superabsorbent Polymers, Fig. 13 Effect of particle size of cross-linked sodium polyacrylate SAP on absorption speed

Superabsorbent Polymers, Fig. 12 Effect of surface cross-linking of sodium polyacrylate SAP on absorbency under pressure

Superabsorbent Polymers,
Fig. 14 Suppression of gel blocking by surface cross-linking

diffusion to the interior of the SAP particle. Gel blocking can be suppressed through addition of inorganic particles (e.g., silica, talc, kaolin) to SAP and surface cross-linking (vide supra). The inorganic particles promote the formation of voids within any gel that forms and consequently promote water diffusion to the interior of the particle [2, 17]. If the density of cross-linking on the particle surface is higher than the interior of the particle, the swelling ratio on the surface of SAP will be suppressed relative to the particle interior. Under such conditions, the particles retain their shape and voids that permit diffusion of water to the interior [2, 8, 9, 17] (Fig. 14).

Future Development

The concept of cross-linked polyelectrolytes has given birth to the study of gels undergoing discontinuous volume phase transitions in response to small changes in their environment (e.g., solvent composition, temperature, electrical stimulus) [6, 19] and has formed the basis for recent intelligent materials research such as artificial muscle, actuator, shape memory elements, drug delivery system (DDS), and so on. Tanaka [19] expanded on the Flory–Rehner theory to include

absorption and phase transition phenomena. The generalized swelling state equation was derived from the combination of four kinds of force:

1. Interaction between polymer and solvent
2. Osmotic pressure derived from polyelectrolyte counter ions
3. Entropy of mixing polymer and solvent
4. Rubber elasticity of a cross-linked polymer

The overall swelling state equation is derived from the combination of forces against the polymer network above and shown below (Eq. 5),

$$P = -(NkT/v)\{\phi + \ln(1-\phi) + (\Delta F/2k)\phi^2\}$$
$$+ vkT\{(\phi/2\phi_0) - (\phi - \phi_0)^{1/3}\}$$
$$+ fvkT(\phi/\phi_0)$$

$$(5)$$

where P is the force against the polymer network, N is Avogadro's constant, k is Boltzmann's constant, T is absolute temperature, v is solvent molar volume, ϕ is volume fraction of polymer at swelling state, ϕ_0 is volume fraction of polymer at standard state (ϕ_0/ϕ is swelling ratio), ΔF is free energy change via interaction between polymer

chains and solvents, ν is the number of polymer chains per unit volume, and $f\nu$ is the number of counter ions of polyelectrolytes per unit volume.

SAP continues to be aggressively researched and applied to wide ranging fields due to their unique property. Among all the potential uses, application of SAP to desert reforesting is one of the most exciting and challenging. SAP is expected to hold promise for breakthrough leading to solution of global warming.

Summary

SAPs are slightly cross-linked polymers which can quickly absorb and retain water due to an equilibrium balance of natural dissolution and thermodynamically favored expansion of polymer chains constrained by cross-linking. Because of their unique ability to absorb and retain water and the possibility to tune other properties, SAPs have been designed for application in fields ranging from hygiene products to civil engineering, construction, and agriculture. SAPs are expected to play an important role as intelligent materials (e.g., actuator, drug delivery system, artificial organ) in the future.

Related Entries

▶ Cross-Linked Polymer Synthesis
▶ Stimuli-Responsive Polymers
▶ Supramolecular Hydrogels

References

1. (1974) Chemical week July 24: 21
2. Masuda F (1987) Super absorbent polymer, 1st edn. Kyoritsu – Publication, Tokyo, ISBN: 432004228X, 978432004228
3. Masuda F, Nishida K, Nakamura A(1976) Polysaccharide graft polyacrylate type SAP in US. Inventors: Fusayoshi Masuda, Kazuo Nishida and Akira Nakamura, US patent 4, 076, 663 29 March 1976
4. Zohuriaan-Mehr MJ, Kabiri K (2008) Superabsorbent polymer materials: a review. Iran Polym J 17(6):451–477, http://journal.ippi.ac.ir
5. Flory PJ (1953) Principle of polymer chemistry. Cornell University Press, Ithaca, New York
6. Masuda Y (2003) Superabsorbency. In: Osada Y, Kajiwara K (eds) Gel handbook, 1st edn. NTS, Tokyo
7. Wang A, Wang W (2009) Superabsorbent materials. Kirk Othmer Encycl Chem Technol. John Wiley & Sons Inc, Hoboken, New Jersey, US.doi:10.1002/0471238961.supewang.a01
8. Frank M (2012) Superabsorbents. Ullmann's Encycl Ind Chem. doi:10.1002/14356007.f25_f01
9. Adachi Y, Mitsugami Y (2004) Application development of super absorbent polymer. In: Shibayama M, Kajiwara K (eds) Advances in polymer gels – preparation, characterization, and application, 1st edn. CMC, Tokyo
10. Yanaki T (2003) Hyaluronic acid gel. In: Osada Y, Kajiwara K (eds) Gel handbook, 1st edn. NTS, Tokyo
11. Yoshii F (2004) Application of hydrogel synthesized with radiation. In: Shibayama M, Kajiwara K (eds) Advances in polymer gels – preparation, characterization, and application, 1st edn. CMC, Tokyo
12. Chatterjee PK, Nguyen HV (1985) Mechanism of liquid flow and structure property relationships. In: Chatterjee PK (ed) Absorbency. Elsevier, Amsterdam
13. Osada Y (1983) Preparation of polymer gels by the plasma – initiated polymerization and their properties of adsorbing water and metal ions. Nippon Kagaku Kaishi 3:439–444
14. Omori E (1978) Acrylic acid and its polymer. Shokodo, Tokyo
15. Osada Y (1981) Novel polymerizations initiated by plasma exposure. J Soc Fiber Sci Technol Jpn 37(7):243–251. doi:10.2115/fiber.37.7_P243
16. Nakagawa T (1973) Rheology of polysaccharide. In: Harada T, Koizumi T (eds) Sogo-tatorui-kagaku, 1st edn. Kodan-sha, Tokyo
17. Wang L, Rezai E (2003) Sanitary products. In: Osada Y, Kajiwara K (eds) Gel handbook, 1st edn. NTS, Tokyo
18. Buchholz FL (1990) Kinetics of swelling of absorbent polymers. In: Brannon-Peppas L, Harland RS (eds) Absorbent polymer technology. Elsevier Science Publishing Co, New York
19. Tanaka T (1986) Phase transition of polymer gels. Journal of the Physical Society of Japan (JPSJ), Phys Soc Jpn (JPS), Tokyo. 41(7):542–552, http://ci.nii.ac.jp/naid/110002075947

Supramolecular Catalysis

Yoshinori Takashima and Akira Harada
Department of Macromolecular Science,
Graduate School of Science, Osaka University,
Machikaneyama, Toyonaka, Osaka, Japan

Synonyms

Artificial enzyme; Catalytic reaction; Molecular receptor; Non-covalent bond interaction; Selectivity

Definition

Supramolecular catalyst is the catalytic reaction systems capable of mimicking the catalytic ability of natural enzymes. Supramolecular catalysts have molecular receptors with a catalytic site to bind selectively the substrate and to promote the reaction.

Introduction

At ambient temperature, enzymes in nature form products from substrates selectively and efficiently. Biological enzymes have a precise substrate-recognition site, and a deft reaction site controls the flexible structure due to non-covalent bonds. The substrate selectively recognizes the receptor site; the behavior is similar to a "lock and key" with a steric fit where the guest has a geometric size or shape that is complementary to the receptor or host. Enzymes selectively promote the transition state and intermediates of a particular reaction.

On the other hand, supramolecular structures, such as rotaxanes, occasionally play an important role in enzymatic activities. For example, DNA polymerases have a sliding clamp where the ring-shaped protein assembly forms supramolecular complexes. Although the clamp does not have an active site, replication of polynucleotides is difficult without a clamp. Inspired by biologically enzymatic systems, many chemists have developed innovative syntheses (supramolecular catalyses) using chemical processes that take advantage of biological systems [1]. This essay focuses on the development of novel supramolecular catalyses through host–guest systems that mimic certain aspects of enzymatic catalysts.

## Cyclic Host Molecules as Enzyme Models

Supramolecular catalyses using synthetic host molecules have been well studied. Early studies realized a hydrolysis reaction for ester derivatives using modified cyclodextrins (CDs) [2–5]. CDs are suitable for the study of two-substrate supramolecular catalysis in the synthesis of artificial enzymes. 2-Benzyimidazoleacetic acid–modified α-cyclodextrin hydrolyzes *m-tert*-butylphenyl acetate at an accelerated rate. An imidazole has a benzoate group in a position to imitate the function of the aspartate ion with the catalytic triad characteristics of serine proteases such as chymotrypsin (Fig. 1) [6–8].

The catalytic reaction by using CDs was studied as artificial enzyme models (model ribonuclease A). β-CD with two imidazole is prepared from β-CD diiodides (Fig. 2) [9]. Enzyme ribonuclease A uses two imidazole groups of histidines 12 and 119 as its principal catalytic groups in the hydrolysis of RNA.

Cavitands are armed with catalytic active sites, such as Zn salen, porphyrin, phenanthroline, and pyridone complexes [10]. These synthetic host molecules have catalytically active functional groups, and the position of catalytic groups, which is determined by estimating the transition state, is important for the catalytic activity.
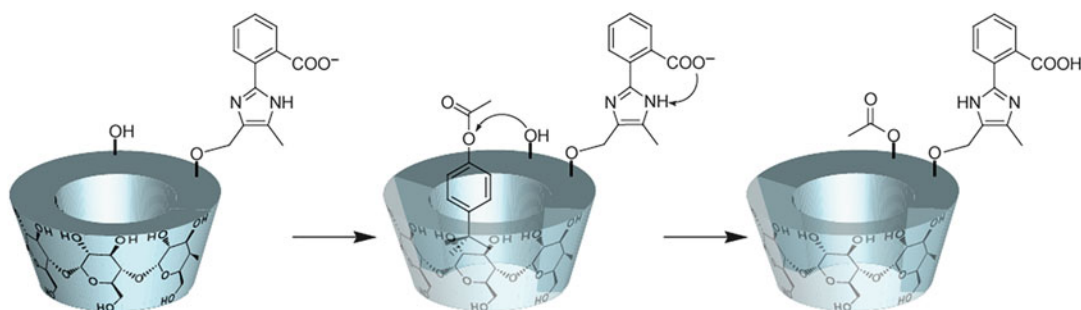
Supramolecular Catalysis, Fig. 1 Cyclodextrin supramolecular catalyst designed to mimic the catalytic triad in chymotrypsin
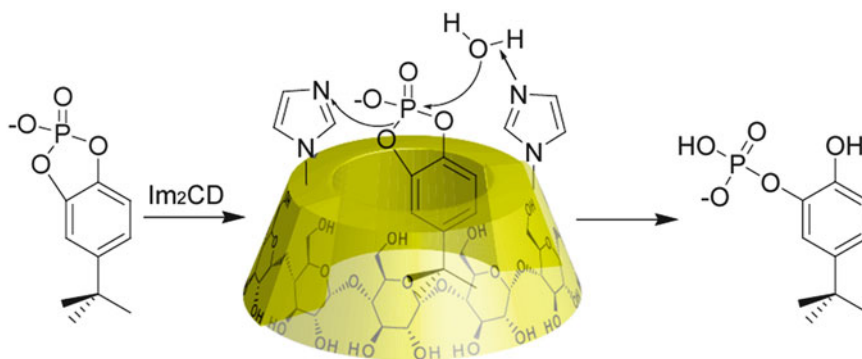
Supramolecular Catalysis, Fig. 2 Cyclodextrin bis(imidazoles) catalyzing the hydrolysis of the phosphate substrate

Cavitand has an affinity for alkylammonium ions. When the salen cavitand with zinc(II) hydrolyzes *p*-nitrophenyl choline carbonate (PNPCC), the Lewis acid zinc(II) activates the well-positioned carbonyl group of PNPCC. The reaction rate is accelerated more than 50-fold with a stoichiometric amount of catalyst. The cation-p interactions and $C = O \ldots Zn$ coordination bond likely reduce the activation energy barrier in the reaction [11, 12].

Self-Assembled Coordination Cages

Supramolecular assemblies using metal–ligand interactions produce effective catalytic active cages, which encapsulate guest molecules based on size, shape, charge, and functional group availability.
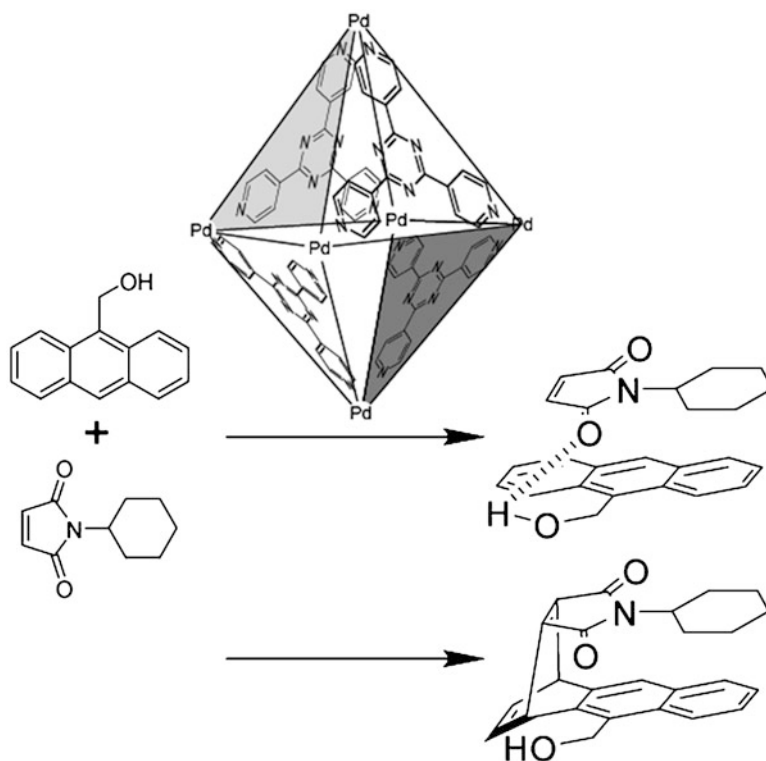
A self-assembled octahedral $[M_6L_4]$ ($M = \{Pd^{II}(tetramethylethylenediamine)\}$, $L =$ tris-(3pyridyl)triazine) cage catalyzes the Diels–Alder reaction of anthracene and maleimide to give a specific regioselective product because the cage constrains the arrangement of substrates and cycloaddition selectively occurs with the 1,4-positions of the anthracene molecule (Fig. 3). The Diels–Alder reaction of anthracene derivatives without a cage only yields the 9,10-adduct and not the 1,4-adduct. However, the reaction using the cage does not have a turnover ability due to inhibition by strongly bound products [13].

A cavity-containing tetrahedral metal–ligand assembly (M_4L_6) [$M = Ga^{III}$, Al^{III}, In^{III}, Fe^{III}, Ti^{IV}, or Ge^{IV}, $L = N,N'$-bis(2,3-dihydroxylbenzoyl)-1,5-diaminonaphthalene] forms a tetrahedral structure with the ligands spanning each edge and the metal ions occupying the vertices. The M_4L_6 assembly as a catalytic host preferentially includes cationic guests over neutral ones because the assembly is negatively charged. $Ga^{III}L_6$ encapsulates half-sandwich ruthenium complexes with diastereoselectivities of up to 85:15 [14]. The encapsulated iridium cations in $Ga^{III}L_6$ exhibit C–H activation of aldehydes to give diastereoselectivities up to 70:30 [15].

## Artificial Biomacromolecules for Asymmetric Catalysts

A metal complex with a host protein using a combination of avidin as a protein and biotin with a rhodium–diphosphine complex is prepared as a supramolecular asymmetric catalysis. Avidin shows a high affinity for biotin ($K =$ ca. 10^{15} M^{-1}), indicating that the rhodium–diphosphine complex quantitatively binds into the chiral space of avidin. Hydrogenation of N-acetamidoacrylate with the avidin–biotin and the rhodium–diphosphine complex shows a moderate enantioselectivity, yielding (*S*)-*N*-acetamidoalanine in 41 % ee (Fig. 4) [16]. Later, an artificial metalloenzyme system using a combination of biotinylated diphosphine with mutated streptavidin showed a high enantioselectivity. This catalytic system quantitatively yields high enantioselective products ((*R*) = 94 %) [17].
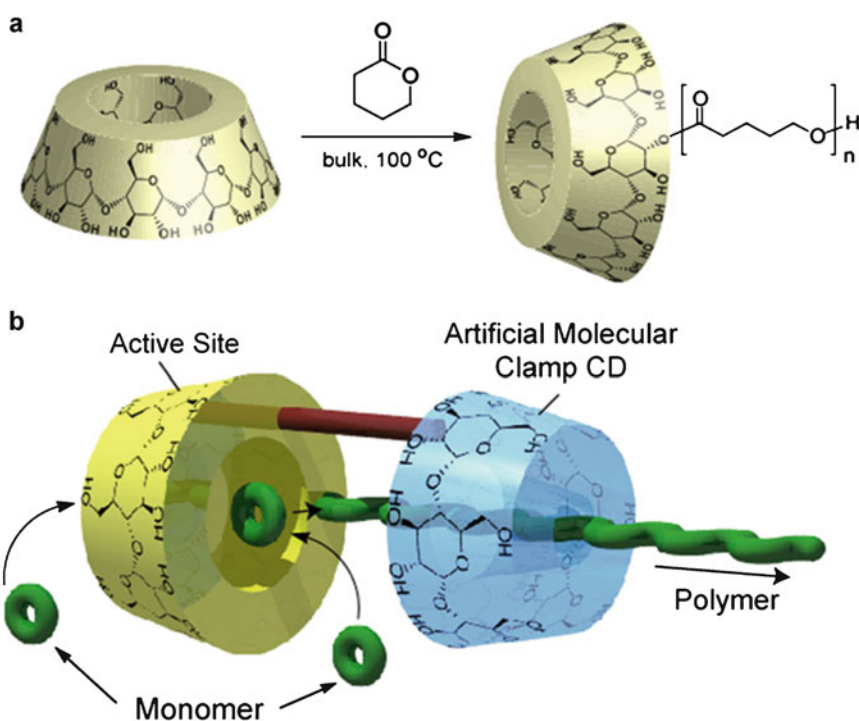
Supramolecular Catalysis, Fig. 3 Diels-Alder reaction of anthracene and maleimide derivatives catalyzed by the M_6L_4 (M = {Pd^{II}(tetramethylethylenediamine)}, L = tris-(3pyridyl)triazine) self-assembled coordination cage
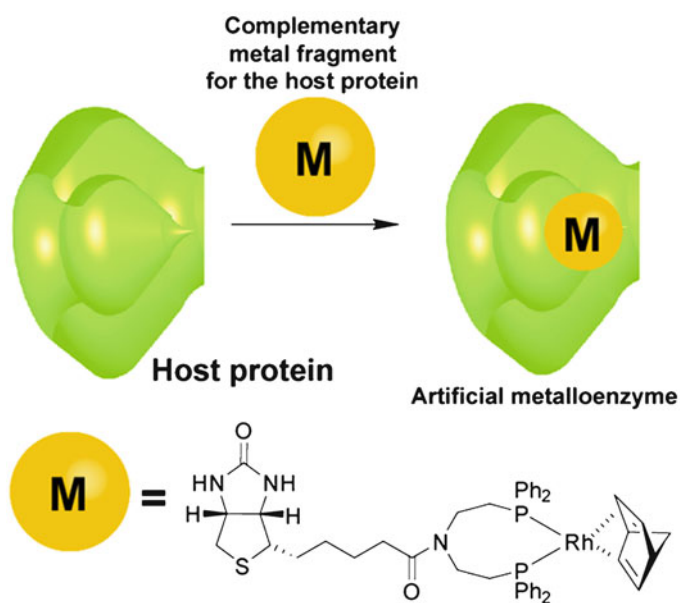
Supramolecular Catalysis, Fig. 4 Strategy to incorporate a catalytically active artificial metalloenzymes with avidin
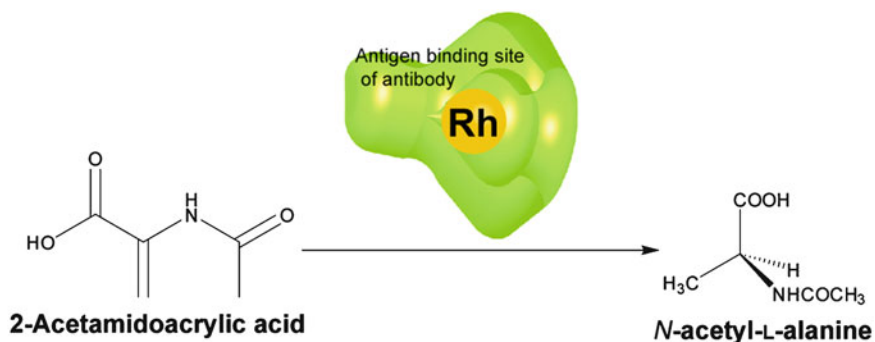
Supramolecular Catalysis, Fig. 5 Schematic structural representation of the complex between antibody 1G8 and the Rh catalyst to show substrate specificity

Supramolecular Catalysis, Fig. 6 Schematic illustration of the supramolecular catalyst using native CDs (**a**) and CD dimers (**b**) for δ-valerolactone

An artificial metalloenzyme for the asymmetric hydrogenation has been successfully created. Monoclonal antibodies as a host protein exhibit an extremely high affinity for antigen. An antibody has an achiral rhodium complex. Although the achiral rhodium complex does not show enantioselectivity for the hydrogenation of 2-acetamidoacrylic acid, the complex in the presence of the resultant antibody shows catalytic hydrogenation to produce *N*-acetyl-L-alanine in a high (>98 %) enantiomeric excess (Fig. 5) [18].

Supramolecular Polymerization Catalysis

Supramolecular catalysts that mimic the ability of processive enzymes have a macrocycle with manganese (III) porphyrin as a catalytic active site. The catalytic macrocycle binds a polymer substrate (polybutadiene), which is included in the cavity, and the macrocycle oxidizes polymer substrate complexes. The bulky ligand of the catalytic macrocycle is attached outside of the porphyrin, preventing the macrocycle from oxidizing the substrate outside the cavity [19].

CDs selectively initiate ring-opening polymerizations of cyclic esters (lactones and lactides) to give polyesters in high yields without a solvent and cocatalyst. The polymer yield depends on the cavity size of the CDs and monomer structure, indicating that the reaction occurs via the inclusion of lactones in the CD cavity. The monomers are activated by CD to give CD-tethered polyesters [20]. The propagating polymer chain forms a poly-*pseudo*-rotaxane structure between the propagating polymer chain and CDs. The poly-*pseudo*-rotaxane plays an important role in the polymerization activity (Fig. 6a).

As a novel concept for supramolecular catalysis, an artificial molecular clamp is attached to the activation site. Synthetic polymerases with an artificial molecular clamp yield high molecular weight polymers without solvents or cocatalysts. The CD dimers behave as polymerases for cyclic esters where one CD moiety initiates ring-opening polymerization, while the other propagates polymerization by serving as a molecular guide. Although the molecular guide CD does not exhibit polymerization activity for δ-VL, it assists in polymerization by anchoring the polymer chain and securing the active site. Thus, another new δ-VL is accessible to the β-CD at the end of polymer chain (Fig. 6b) [21].

Related Entries

▶ Organocatalytic Polymerization
▶ Ring-Opening Metathesis Polymerization

References

1. van Leeuwen PWNM (2008) Supramolecular catalysis. Wiley-VCH Verlag GmbH & Co. KGaA, Weinheim. doi:10.1002/9783527621781

2. Bender ML, Komiyama M (1978) Cyclodextrin chemistry. Springer, Berlin. ISBN 10: 3642668445

3. Breslow R (1986) Artificial enzymes and enzyme models. In: Meister A (ed) Advances in enzymology and related areas of molecular biology, 58th edn. Wiley, New York, pp 1–60. doi:10.1002/9780470123041.ch1

4. Komiyama M (1996) Cyclodextrins as enzyme models. In: Atwood JL, Davies JE, MacNicol DD, Vogtle F (eds) Comprehensive supramolecular chemistry, 3rd edn. Pergamon, Oxford, UK, pp 401–421. ISBN 9780080406107

5. Breslow R (2005) Artificial enzymes. Wiley-VCH Verlag GmbH & Co. KGaA, Weinheim. doi:10.1002/3527606645

6. Bender ML (1984) An artificial acyl-enzyme and an artificial enzyme. J Incl Phenom 2:433–444. doi:10.1007/BF00662210

7. D'Souza VT, Bender ML (1987) Miniature organic models of enzymes. J Acc Chem Res 20:146–152. doi:10.1021/ar00136a004

8. Komiyama M, Breaux EJ, Bender ML (1977) The use of cycloamylose to probe the "charge-relay" system. Bioorg Chem 6:127–136. (http://dx.doi.org/10.1016/0045-2068(77)90015-3)

9. Breslow R, Doherty J, Guillot G, Lipsey C (1978) β-Cyclodextrinylbisimidazole, a model for ribonuclease. J Am Chem Soc 100:3227–3229. doi:10.1021/ja00478a052

10. Jr Rebek J (1999) Reversible encapsulation and its consequences in solution. J Acc Chem Res 32:278–286. doi:10.1021/ar970201g

11. Richeter S, Jr Rebek J (2004) Catalysis by a synthetic receptor sealed at one end and functionalized at the other. J Am Chem Soc 126:16280–16281. doi:10.1021/ja045167x

12. Purse BW, Jr Rebek J (2005) Supramolecular structure and dynamics special feature: functional cavitands: chemical reactivity in structured environments. Proc Natl Acad Sci U S A 102:10777–10782. doi:10.1073/pnas.0501731102

13. Yoshizawa M, Tamura M, Fujita M (2006) Diels–Alder in aqueous molecular hosts: unusual regioselectivity and efficient catalysis. Science 312:251–254. doi:10.1126/science.1124985

14. Fiedler D, Leung DH, Bergman RG, Raymond KN (2005) Selective molecular recognition, C–H bond activation, catalysis in nanoscale reaction vessels. Acc Chem Res 38(4):349–358. doi:10.1021/ar040152p

15. Fielder D, Bergman RG, Raymond KN (2004) Supramolecular catalysis of a unimolecular transformation: Aza-Cope rearrangement within a self-assembled host. Angew Chem Int Ed 43(8):6748–6751

S

16. Wilson ME, Whitesides GM (1978) Conversion of a protein to a homogeneous asymmetric hydrogenation catalyst by site-specific modification with a diphosphinerhodium (1) moiety. J Am Chem Soc 100:306–307. doi:10.1021/ja00469a064

17. Skander M, Humbert N, Collot J, Gradinaru J, Klein G, Loosli A, Sauser J, Zocchi A, Gilardoni F, Ward TR (2004) Artificial metalloenzymes: (Strept) avidin as host for enantioselective hydrogenation by achiral biotinylated rhodium-diphosphine complexes. J Am Chem Soc 126:14411–14418. doi:10.1021/ja0476718

18. Yamaguchi H, Hirano T, Kiminami H, Taura D, Harada A (2006) Asymmetric hydrogenation with antibody-achiral rhodium complex. Org Biomol Chem 4(19):3571–3573. doi:10.1039/B609242J

19. Thordason P, Bijsterveld EJA, Rowan AE, Nolte RJM (2003) Epoxidation of polybutadiene by a topologically linked catalyst. Nature 424:915–918. doi:10.1038/nature01925

20. Takashima Y, Osaki M, Harada A (2004) Cyclodextrin-initiated polymerization of cyclic esters in bulk: formation of polyester-tethered cyclodextrins. J Am Chem Soc 126(42):13588–13589. doi:10.1021/ja047171e

21. Takashima Y, Osaki M, Ishimaru Y, Yamaguchi H, Harada A (2011) Artificial molecular clamp: a novel device for synthetic polymerases. Angew Chem Int Ed 33:7524–7528. doi:10.1039/C1CC11115ASSS

Supramolecular Hydrogels

Akira Harada
Department of Macromolecular Science,
Graduate School of Science, Osaka University,
Machikaneyama, Toyonaka, Osaka, Japan

Synonyms

Host–guest interaction; Hydrogels; Noncovalent interaction; Sol–gel phase transition

Definition

Supramolecular hydrogels are one of the hydrogels consisting of a solid three-dimensional network with noncovalent bonds such as hydrogen bond, hydrophobic interaction, and cation–π and π–π interactions. Although a morphology of chemical gels is stabilized by chemical cross-linker, that of supramolecular hydrogels is stabilized by the noncovalent bonds, which form macromolecular polymer and three-dimensional network gel. Supramolecular hydrogels are synthesized from hydrophilic molecules. Supramolecular hydrogels constructed by reversible bonds are expected to show stimuli responsiveness and self-healing properties.

Introduction

Hydrogels have recently received much attention due to their potential in medical fields, such as drug delivery, tissue cultures, medical treatments, etc. [1]. In addition to being classified as chemical or physical gels [1–4], they are either natural or synthetic hydrogels. Natural ones include collagen and polysaccharide gels, such as curdlan gels, while synthetic chemical gels include polyacrylic acid and polyacrylamide gels. In this entry, supramolecular gels formed by host–guest interactions are described.

Supramolecular Hydrogels Formed by Proteins

A famous example of a hydrogel formed by proteins is collagen [5]. Collagen forms a triple helix in the solid state, but upon heating in water, some of its triple helices dissolve, forming a gel after cooling. This is because the triple helices play a role in hydrogel cross-linking. This process is reversible, and heating the gel restores the sol.

Supramolecular Hydrogels Formed by Polysaccharides

Some polysaccharides form hydrogels in water. The most well-known example is agar [6], which consists of a mixture of agarose and agaropectin (Fig. 1a). Agar is soluble in hot water, but cooling an aqueous solution of agar restores the gel. This heating–cooling process is reversible.

a

Agarose polymer

b

Curdlan

c

Carrageenan
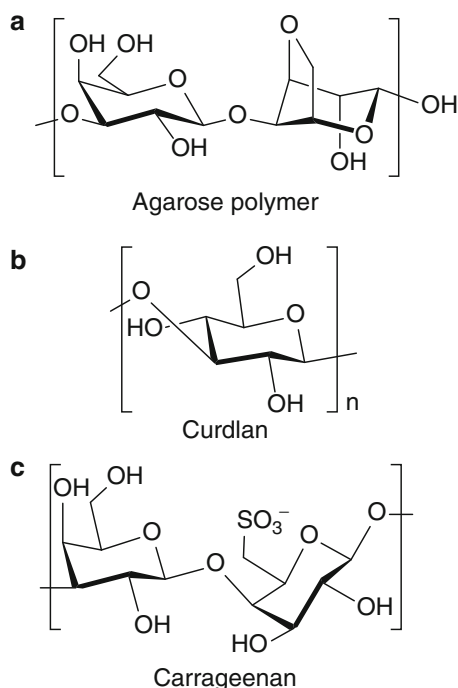
Supramolecular Hydrogels, Fig. 1 Chemical structures of the polysaccharides

Curdlan, β-1-3 glucan, forms a gel upon heating an aqueous suspension or neutralizing a basic solution of curdlan (Fig. 1b). In this case microfibrils form assemblies to give the gel [7]. Cooling or placing the gel in a basic solution does not cause the gel to go back into solution. Hydrogen bonds play an important role in this irreversible gel formation.

Some other anionic polysaccharides are known to form gels under certain conditions. For example, carrageenans, which are sulfated polysaccharides derived from seaweed, form a gel at room temperature in water [8] (Fig. 1c).

Supramolecular Hydrogels Formed by Cyclodextrin Derivatives

Chemical Gels Containing Cyclodextrins

Cross-linking reactions of cyclodextrins (CDs) realize hydrogels containing CDs. For example, CDs are cross-linked by epichlorohydrin to give

a hydrogel. This gel has been used in column chromatography to separate racemic molecules of mandelic acid derivatives [9].

Gels Formed by CD and PEG

CDs are water-soluble crystalline compounds with a molecular weight of about 1,000. CDs react with various guest molecules to give inclusion complexes [10], which are typically crystalline or water-soluble compounds. Although most inclusion complexes do not form a gel, the inclusion complexes of α-CD with poly(ethylene glycol) (PEG) of high molecular weight formed a gel in high concentrations (Fig. 2) [11].

Hydrogels Containing CD

Mixing poly(acrylic acid) (PAA) containing β-CD and PAA containing ferrocene in water forms a hydrogel [12]. In this case, the CD ring includes a ferrocene group to give a cross-linking part. This process is reversible. Treating the gel with an oxidizing reagent (NaClO) forms a sol, but the gel is restored upon treating the sol with a reducing reagent (GSH; glutathione). In this case, oxidation changes ferrocene into a ferrocenium cation, and a reducing agent restores ferrocene (Fig. 3).

Although a gel can be cut in half by a knife, when the cut surfaces are brought into contact with each other, the pieces adhere to give a single gel. The cut surface disappears after several hours, and the gel strength is recovered to almost 85 % after 20 h. Similarly, the pieces rebind after treating a cut surface with a reducing reagent. However, the gel does not rebind after treating a cut surface with an oxidizing reagent.

Polymers have also been obtained by copolymerization of acrylamide, β-CD acrylamide monomer, and a guest monomer. For example, an aqueous solution of adamantane forms a gel [13], which exhibits self-healing properties. Even when the gel is cut in half and allowed to sit for 20 h, the gel pieces bind to each other when they are brought into contact. In this particular case, the gel strength is almost 100 % restored after 24 h.

S

Fig. 2 Proposed structure of the supramolecular hydrogel with α-CD and poly(ethylene glycol)
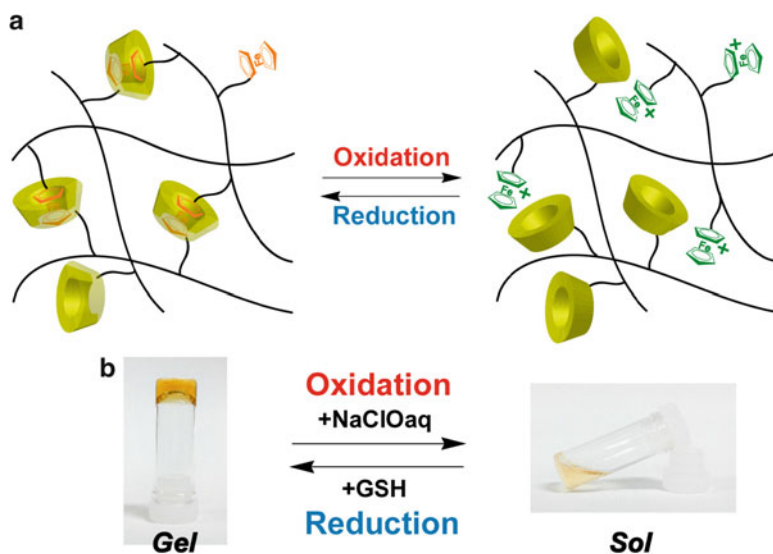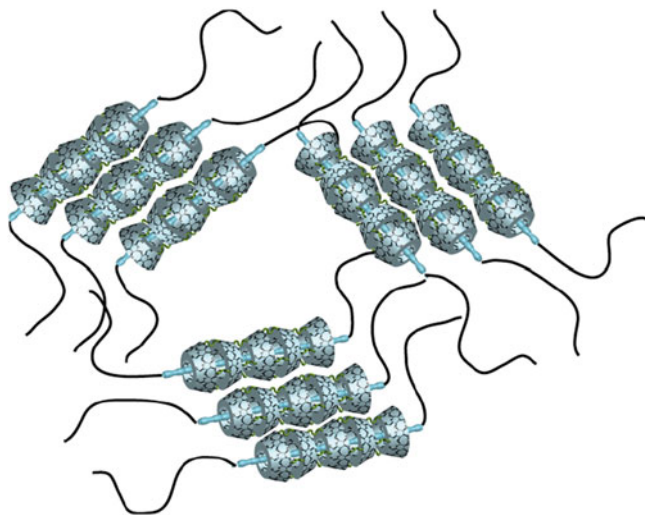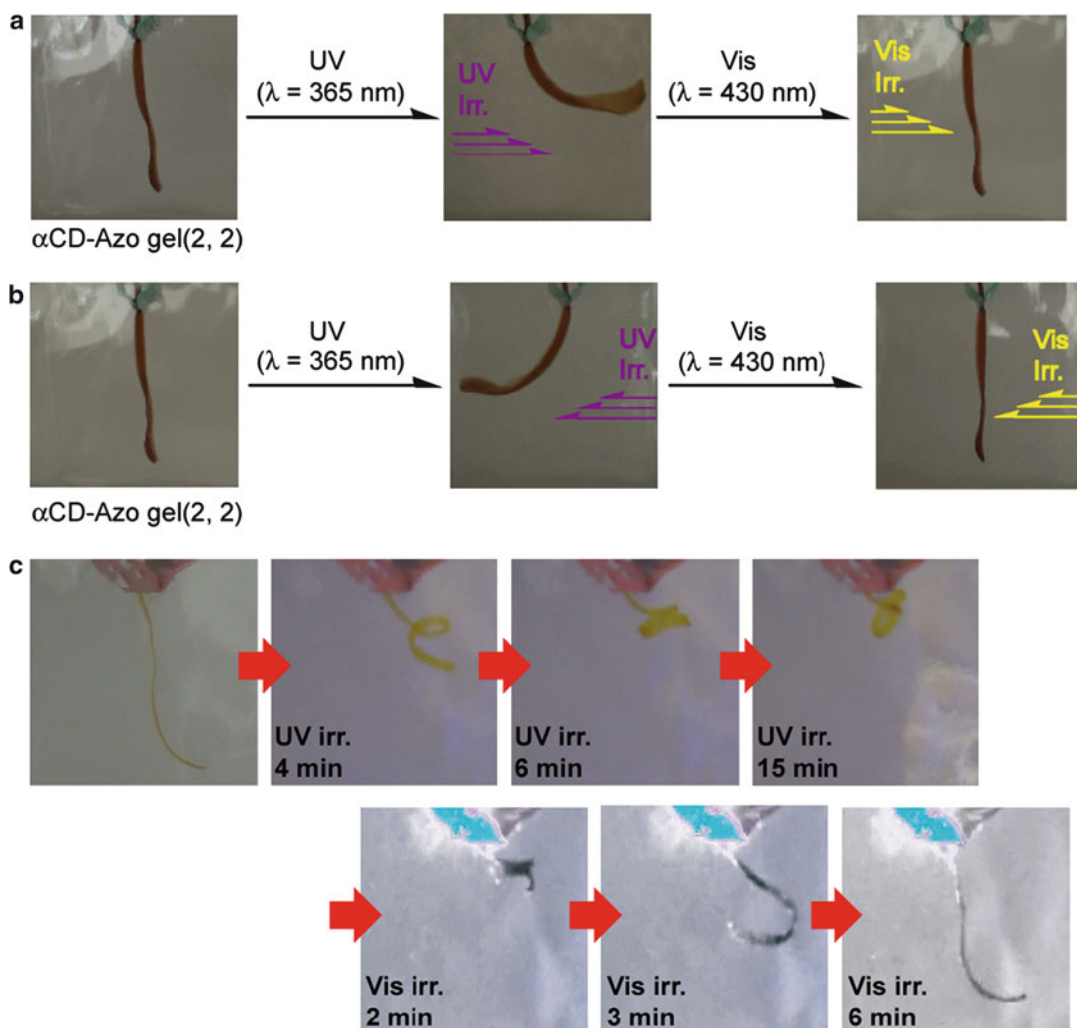

Supramolecular Hydrogels,
Fig. 3 Schematic illustration of the sol−gel transition (**a**). Sol−gel transition experiment using chemical reagents (**b**)

Partially Chemical Cross-Linked Host–Guest Gels

A mixture of a host polymer having α-CD and a guest polymer containing azobenzene (Azo) forms a supramolecular hydrogel. Photoirradiating with UV light (λ = 365 nm) isomerizes the *trans*-azo group in the guest polymer to the *cis*-azo group, whereas irradiating with visible light (λ = 430 nm) isomerizes the azo group from *cis*- to *trans*-. Irradiating the supramolecular hydrogel consisting of α-CD/Azo with UV light (λ = 365 nm) decreases the viscosity upon isomerization of the t*rans*-azo group to give the sol. In contrast, irradiating the sol with UV light at λ = 430 nm (or heating) recovers the viscosity and gives the hydrogel [14].

Partially chemically cross-linking a host gel containing CD and guest gels containing guest parts realizes unique gels. Irradiating a gel strip containing both CD and azobenzene parts as host and guest parts with UV light causes the strip to bend (Figs. 4a and b), but irradiating with visible

Supramolecular Hydrogels, Fig. 4 Photoresponsive actuator of the αCD-Azo gel in water. (**a**). Light irradiation from the *left* side of the αCD-Azo gel for an hour. After UV irradiation, the αCD-Azo gel bends to the *right*. Subsequent irradiation with visible light restores the initial state. (**b**). Light irradiation from the *right* side of the αCD-Azo gel for an hour. After UV irradiation, the αCD-Azo gel(2, 2) bends to the *left*. (**c**). Light irradiation from the *left* side of the ribbon shaped αCD-Azo gel for 15 min. After UV irradiation, the αCD-Azo gel forms a coil. Subsequent irradiation with visible light restores the initial state

light straightens the gels. This process is reversible [15]. When a thin-sliced gel strip is irradiated with UV light, it coils and forms a compact conformation. The gel shows shape memory effects, and irradiating the coil gel with visible light restores the original shape (Fig. 4b).

Similarly, polyacrylamide containing ferrocene and β-CD partially cross-linked by chemical bonds forms a gel. Treating this gel with oxidizing reagents expands the gels, but treating with reducing reagents shrinks the gel to the original size. These changes are reversible [16].

Supramolecular Hydrogels Formed by Cucurbituril Derivatives

Supramolecular polymeric hydrogel based on guest polymers and cucurbituril [n] (CB[n]) is prepared by mixing the viologen guest and

Supramolecular Hydrogels, Fig. 5 Schematic representation of the supramolecular hydrogel from methyl-viologen-functionalized polymer and naphthoxy functionalized polymer crosslinked by cucurbit[8]uril (CB[8])
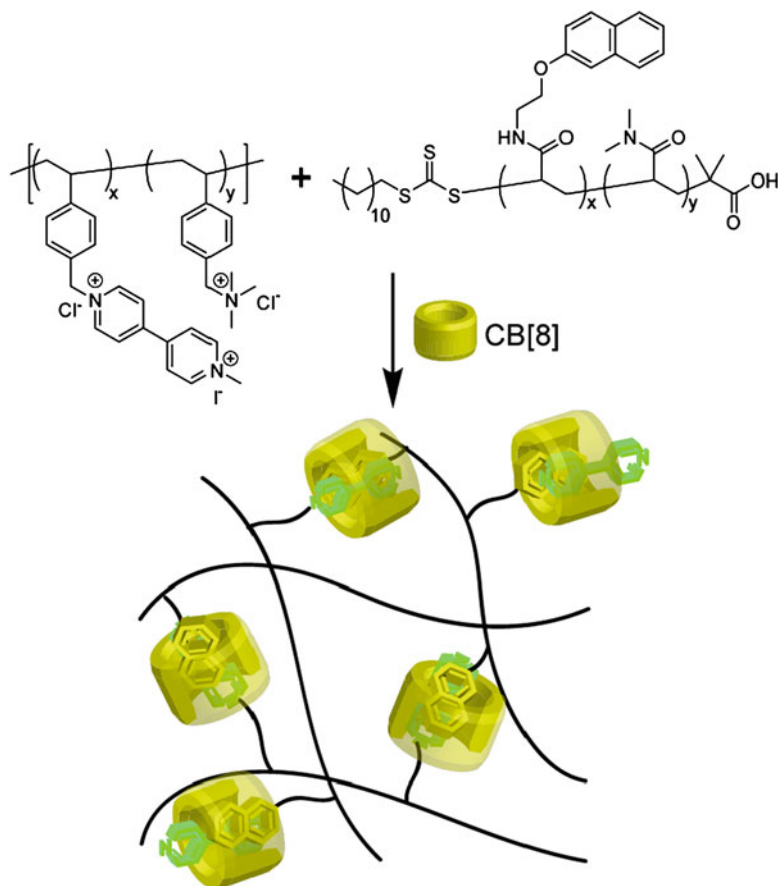
naphthoxy guest polymers with CB[8]. Although the viologen guest and naphthoxy guest polymers do not form a supramolecular hydrogel, the addition of CB[8] gives a hydrogel by cross-linking the pendant guest molecules. The obtained hydrogel shows a thermo-responsiveness, which is designed using CB[8] to facilitate a reversible cross-linking of multivalent copolymers (Fig. 5). The dynamic cross-links (1:1:1 supramolecular ternary complexes of CB[8]/viologen/naphthoxy) produce a thermo-responsive sol–gel switching property [17].

Kim and coworkers demonstrated a supramolecular hydrogel by utilizing functional CB[6] with an alkylammonium guest derived from 1,6-diaminohexane. Mixing solutions of the CB[6]-containing polymer and a DAH-containing hyaluronic acid (around 50 mol% of the functionalized repeating

units) produces a hydrogel after two min. The addition of excess SPM to the hydrogel results in a phase transition from the gel to the sol within ten min, suggesting that the cross-links of the polymer network are due to specific host–guest interactions [18]. The addition of excess amount of spermine to the hydrogel induces a phase transition from the gel to the sol, indicating that specific host–guest interactions stabilize the supramolecular polymeric hydrogel.

Related Entries

▶ Double-Network Hydrogels: Soft and Tough IPN
▶ Molecular Self-Organization
▶ Topological Gels

References

1. Marek WU (ed) (2011) Handbook of stimuli-responsive materials. Wiley-VCH Verlag GmbH, Weinheim. doi:10.1002/9783527633739. ISBN 9783527327003

2. Steed JW, Gale PA (eds) (2012) Supramolecular chemistry: from molecules to nanomaterials, 8 Volume Set. Wiley, Hoboken. ISBN 9780470746400

3. Yan X, Wang F, Zheng B, Huang F (2012) Stimuli-responsive supramolecular polymeric materials. Chem Soc Rev 41:6042–6065. doi:10.1039/C2CS35091B

4. Appel EA, del Barrio J, Loh XJ, Sherman OA (2012) Supramolecular polymeric hydrogels. Chem Soc Rev 41:6195–6214. doi:10.1039/C2CS35264H

5. Ward AG, Courts A (1977) The science and technology of gelatin (food science & technology monographs). Academic Press, London. ISBN 0127350500

6. Selby H, Whistler RL (1993) Agar. In: Whistler RL, BeMiller JN (eds) Industrial gums. Academic Press, New York. ISBN 0127462538

7. Harada T, Harada A (1993) Curdlan. In: Whistler RL, BeMiller JN (eds) Industrial gums. Academic Press, New York. ISBN 0127462538

8. Dea ICM (1989) Industrial polysaccharides. Pure Appl Chern 61:1315–1322. doi:10.1351/pac198961071315

9. Harada A, Furue M, Nozakura S (1978) Optical resolution of mandelic acid derivatives by column chromatography on cross-linked cyclodextrin gels. J Polym Sci Polym Chem Ed 16:189–196. doi10.1002/pol.1978.170160119

10. Harada A, Hashidzume A, Yamaguchi H, Takashima Y (2009) Polymeric rotaxanes. Chem Rev 109:5974–6023. doi:10.1021/cr9000622

11. Li J, Harada A, Kamachi M (1994) Sol-gel transition during complex formation between α-cyclodextrin and poly(ethylene glycol) of high molecular weight. Polym J 26:1019–1026, ISSN:00323896

12. Nakahata M, Takashima Y, Yamaguchi H, Harada A (2011) Redox-responsive self-healing materials formed from host-guest polymers. Nat Commun 2:511. doi:10.1038/ncomms1521

13. Kakuta T, Takashima Y, Nakahata M, Otsubo M, Yamaguchi H, Harada A (2013) Preorganized hydrogel: self-healing properties of supramolecular hydrogels formed by polymerization of host–guest-monomers that contain cyclodextrins and hydrophobic guest groups. Adv Mater 25:2849–2853. doi:10.1002/adma.201205321

14. Tamesue S, Takashima Y, Yamaguchi H, Shinkai S, Harada A (2010) Photoswitchable supramolecular hydrogels formed by cyclodextrin and azobenzene polymers. Angew Chem Int Ed 49:7461–7464. doi:10.1002/anie.201003567

15. Takashima Y, Hatanaka S, Otsubo M, Nakahata M, Kakuta T, Hashidzume A, Yamaguchi H, Harada A (2012) Expansion–contraction of photoresponsive artificial muscle regulated by host–guest interactions. Nat Commun 3:1270. doi:10.1038/ncomms2280

16. Nakahata M, Takashima Y, Hashidzume A, Harada A (2013) Redox-generated mechanical motion of a supramolecular polymeric actuator based on host–guest interactions. Angew Chem Int Ed 52:5731–5735

17. Appel EA, Biedermann F, Rauwald U, Jones ST, Zayed JM, Scherman OA (2010) Supramolecular cross-linked networks via host-guest complexation with Cucurbit[8]uril. J Am Chem Soc 132:14251–14260. doi:10.1021/ja106362w

18. Park KM, Yang J-A, Jung H, Yeom J, Park JS, Park K-H, Hoffman AS, Hahn SK, Kim K (2012) In situ supramolecular assembly and modular modification of hyaluronic acid hydrogels for 3D cellular engineering. ACS Nano 6:2960–2968. doi:10.1021/nn204123p

Supramolecular Network Polymers

Toshikazu Takata and Hiromitsu Sogawa
Department of Organic and Polymeric Materials, Tokyo Institute of Technology, Meguro-ku, Tokyo, Japan

Synonyms

Polyrotaxane networks; Rotaxane-cross-linked polymers; Supramolecular gels

Definition

Supramolecular network polymers are defined as polymeric networks that are brought together by noncovalent interactions. A typical example of supramolecular network polymers is a polyrotaxane network bearing rotaxane structures at cross-link points, a typical interlocked supramolecule, of which components are linked mechanically on the cross-link points. These structures are characterized in terms of both its topological linkage and specific property based on the unique mobility of the noncovalently bonded components in their special polymer structures. The movable polymer chain at the cross-link points of network polymer is capable

S

of equalizing mechanical tensions given by external stimuli or stress, eventually affording high swelling ability with solvents, high elasticity, and high stress-releasing ability.

Introduction

Supramolecules characterized by their molecular topology have attracted great interest experimentally and theoretically. Rotaxane and its polymers can be regarded as a supramolecular system from the viewpoint of the cooperative effect of the components. The components are so strongly linked in spite of the extraordinarily high mobility that it requires covalent bond energy to break the mechanical linkage or to separate the components. A polyrotaxane network (PRN) is a supramolecular network stabilized by not only the intercomponent interactions but also the mechanical restriction, providing specific properties and functions that have never been attained with any physically or chemically cross-linked polymers [1–7].

Synthetic methods of such PRNs are divided into several approaches. One approach is the statistical method, in which monomers with sufficiently large macrocycles are polymerized or copolymerized with linear comonomers to give mechanically cross-linked polymers through the accidental penetration in situ, which eventually leads to the cross-linking (Fig. 1, (I)). Another method is the strategic synthetic method, being divided into several approaches. The first approach is to link wheel components of main chain-type polyrotaxane with cross-linker which directly produces cross-linked polymers holding the main chain mobility (Fig. 1, (II-A)), as de Gennes suggested in his paper entitled "sliding gels." [8] The second one involves precise rotaxanative cross-linking, i.e., rotaxane-forming cross-linking, of main chain-type polymacrocycle with axle components via initial threading followed by end-capping of the axles (Fig. 1, (II-B)). Effective cross-linking can be achieved using dynamic covalent chemistry: dumbbell-shaped molecule possessing dynamic covalent bond enters into the cavity of the macrocycle during the equilibrium to form rotaxane structure. This approach advantageously requires no pre-synthesis of polyrotaxane. The third approach is to link pendant wheel components of side chain-type polymacrocycle using cross-linker which forms a pseudo-rotaxanative structure (Fig. 1, (II-C)). The formed PRNs possess effective degradation and reforming abilities. The last approach uses cross-linker that can introduce cross-link points into polymers during polymerization of monomers. This type of "indirect" approach has so wide versatility in monomer structure that most polymers can be converted to PRNs (Fig. 1, (II-D)).
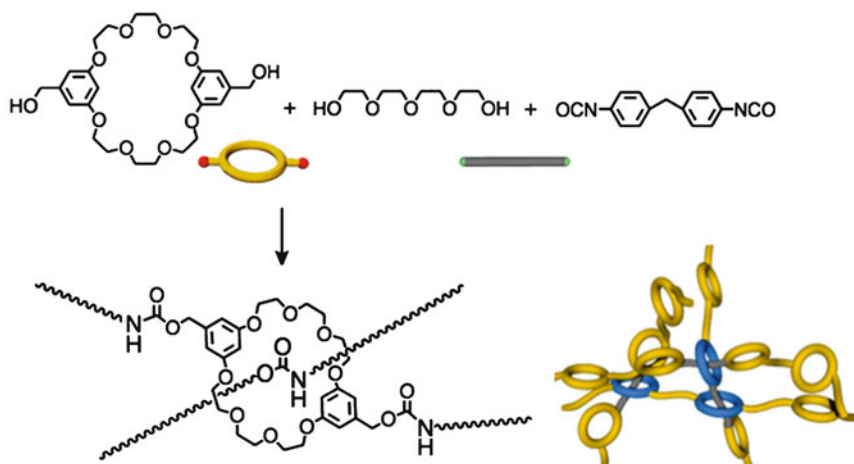
Formation of PRNs via Statistical Cross-Linking

Gibson et al. reported the first PRNs as mechanically networked polymers containing the rotaxane structures on the cross-linking points [9]. The polyamide-type PRN was formed as a gelled product by the polycondensation of a ditopic amine and a 32-membered macrocyclic dicarboxylic acid (Fig. 2). In this case, the propagation end was accidentally threaded to form 3D PRNs. Zilkha's groups, Tezuka's group, and Kubo's group also reported the synthesis of mechanically cross-linked polymers through the radical copolymerizations of vinyl monomers with large macrocycles.

Formation of PRNs via Cross-Linking of Wheels

Ito et al. prepared polyrotaxane with a sparse population of α-cyclodextrin (α-CD) where the most poly(ethylene glycol) (PEG) chain was "naked," by the Harada method [10] using a PEG bisamine. The cross-linking by linking the wheel components was carried out by the reaction with cyanuric chloride to yield the PRN as a transparent gel (Fig. 3). The gelled polymer, a superabsorbent, could take up about 400 times water to the dry weight. Yui et al. also utilized this approach for the development of biodegradable hydrogels [11].

Statistical Method (I): Threading into macrocycles

Accidental Threading
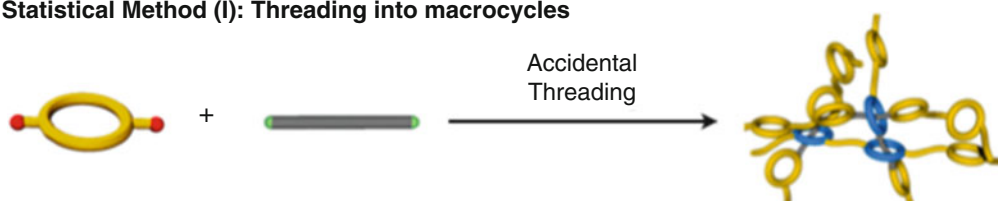
Strategic Method (II-A): Linking of Wheels of Main Chain-Type Polyrotaxane

Connection of Wheel Moieties
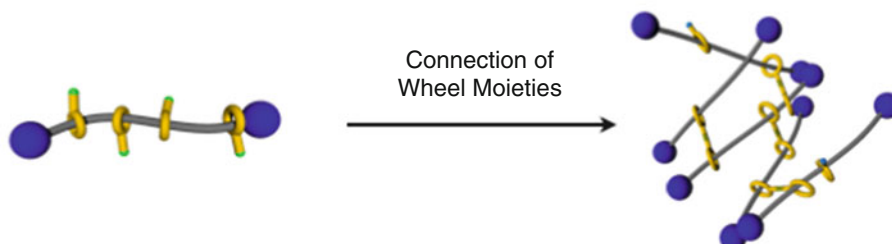
Strategic Method (II-B): Linking of Macrocyclic Unit of Main Chain-type Polymacrocycle

1) Pseudorotaxane Formation

2) Connection of Axle Moieties
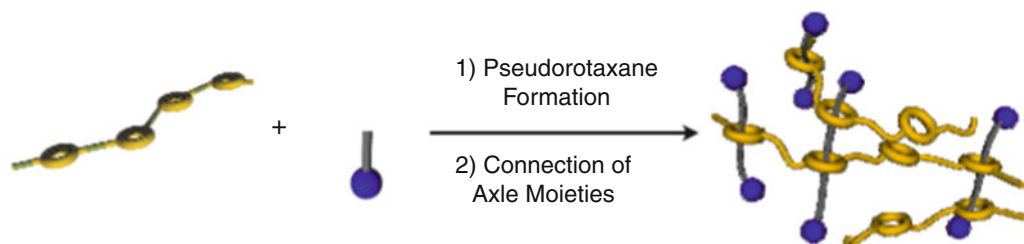
Strategic Method (II-C): Linking of Polymacrocycle Using Psudo-rotaxanative Cross-linker

Psudo-rotaxanative Cross-linking
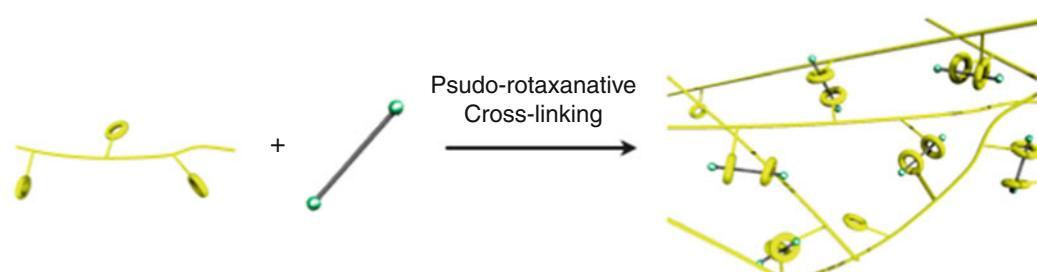
Strategic Method (II-D): Cross-linking Using Vinylic Rotaxane Cross-linker

Radical Polymerization
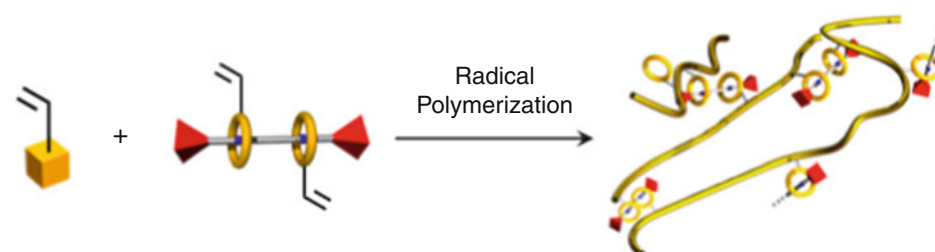
Supramolecular Network Polymers, Fig. 1 Typical synthetic methods of PRNs

Supramolecular Network Polymers, Fig. 2   Synthesis of PRNs via statistical method
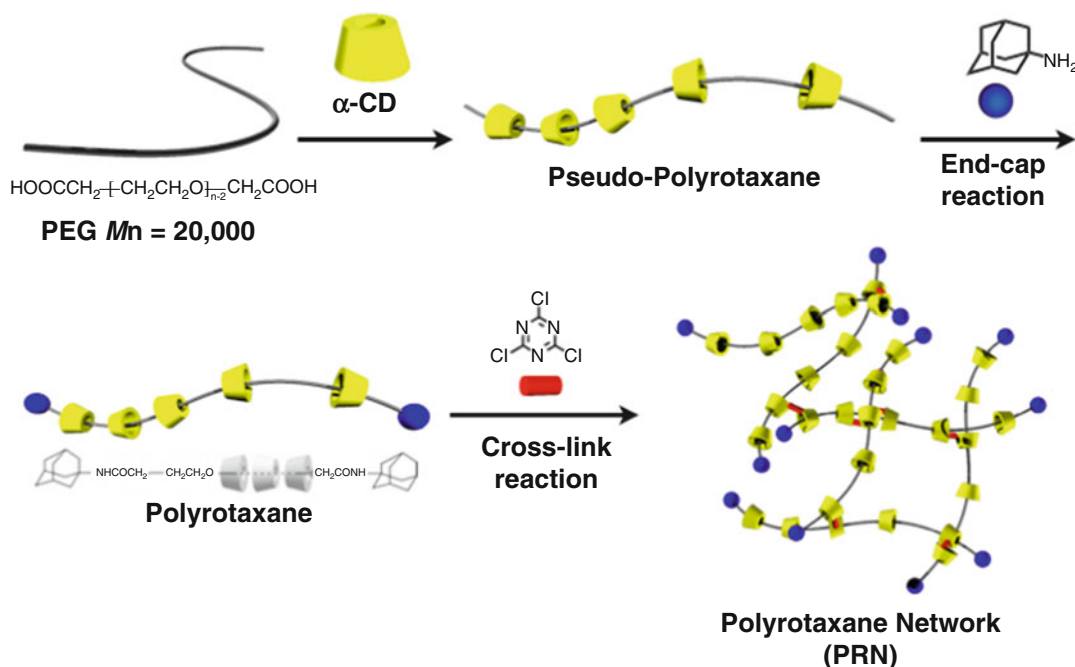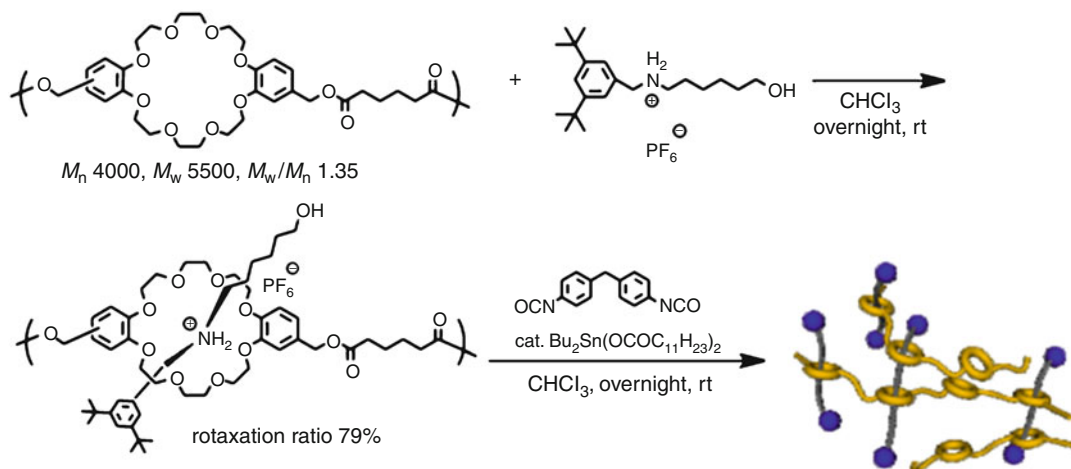

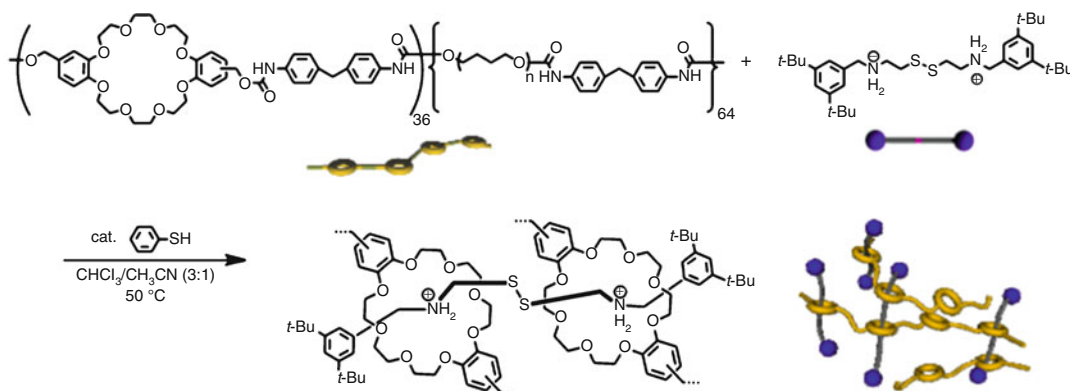**Supramolecular Network Polymers, Fig. 3**   PRNs prepared by the cross-linking of main chain-type polyrotaxane

Takata et al. synthesized a similar type of structurally definite PRN using a polyrotaxane with monohydroxy permethylated α-CDs (PMα-CDs) to limit one OH group that participates the cross-linking to avoid the occurrence of chemical cross-linking by linking two or more OH groups of one α-CD [12]. The structurally defined PRN showed remarkable swelling properties despite the fairly high degree of cross-linking.

Formation of PRNs via Cross-Linking of Macrocyclic Units of Main Chain-Type Polymacrocycle

Novel type of PRNs based on the *sec*-ammonium salt/crown ether rotaxane chemistry was developed by Takata et al. Treatment of a main chain-type poly(crown ether) with a *sec*-ammonium hexafluorophosphate bearing bulky end-cap and

Supramolecular Network Polymers, Fig. 4 Synthesis of PRN by linking the axle terminal of polypseudorotaxane

Supramolecular Network Polymers, Fig. 5 Synthesis of PRN using reversible cleavage of disulfide linkage

hydroxy groups at the both termini afforded the polypseudorotaxane, in which the axle components were threaded into the macrocyclic cavities of the two polymer chains to cross-link. Subsequent connection of the axle hydroxy terminals with a bifunctional linear linker gave the corresponding PRN (Fig. 4) [13].

A novel reversibly cross-linkable PRN was also demonstrated by exploiting dynamic covalent chemistry [14]. Treatment of poly(crown ether) as the main chain polymer with a bifunctional *sec*-ammonium salt as the axle component or cross-linker bearing a central disulfide linkage and two bulky end-caps afforded the PRN as a thermally equilibrated mixture in a less polar solvent in the presence of a catalytic

amount of benzenethiol (Fig. 5). The translucent hard gel swelled well in N,N-dimethylformamide (DMF) and DMSO. Exposure of the product to a small amount of an alkane thiol having a half structure of the disulfidic cross-linker enabled the smooth decross-linking to afford a homogeneous mixture.

It gave a new impulse for the chemical recycling of cross-linked polymers, but it suffered from the disadvantage that it was a sluggish reaction. Takata's group further developed a novel method that enables the efficient decross-linking of PRNs without any cleavage of covalent bonds using size-complementary rotaxane cross-linker [15]. The stability of PRNs was controllable by the size of the end

groups of the axle components. The bulky *t*Bu- and 4-*t*BuC$_6$H$_4$-terminated axle-tethering PRNs showed good stability and suitable degradability. The occurrence of the selective dissociation of the rotaxane skeleton without any destruction or damage to the polymer backbone produced very high recyclability.

Formation of PRNs via Cross-Linking of Polymacrocycles Using Pseudo-Rotaxanative Cross-Linker

Huang et al. synthesize PRNs by treating a poly (methyl methacrylate) copolymer with pendent crown ether groups with a bisammonium cross-linkers at high concentrations (Fig. 6) [16]. The reversible sol–gel transition took place utilizing the pH-controllable interaction between the *sec*-ammonium salt and the crown ether moieties. Furthermore, the self-healing property was studied using rheological measurements, showing 100 % recovery over several cycles.

Formation of PRNs from Vinyl Monomers via Polymerization Using Vinylic Rotaxane Cross-linker

Number and type of polyrotaxanes are still limited because of the difficulty of polyrotaxane synthesis. Meanwhile, introduction of rotaxane cross-links into common polymers, especially polymers formed by radical polymerization, seems most essential from viewpoint of developing a variety of PRNs. To address this issue, several rotaxane-based cross-linkers capable of yielding rotaxane-cross-linked polymers (RCPs) as PRNs were investigated. Takata's groups obtained cross-linked vinyl polymers using various [3] rotaxane cross-linkers having two vinyl groups. Although the PRNs having a small amount of rotaxane cross-link points were stable under normal conditions, the PRNs became stimuli degradable, when size-complementarity between axle and macrocycle cavity or dynamic covalent bond character was endowed [17].
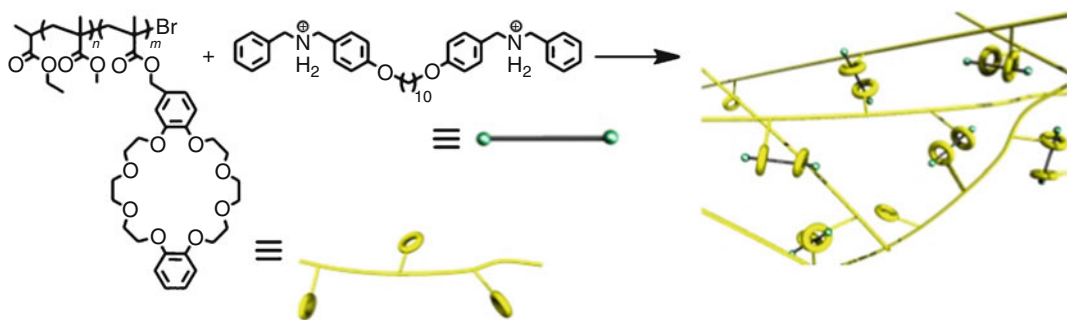
Supramolecular Network Polymers, Fig. 6 Synthesis of PRN using pseudo-rotaxanative cross-linker
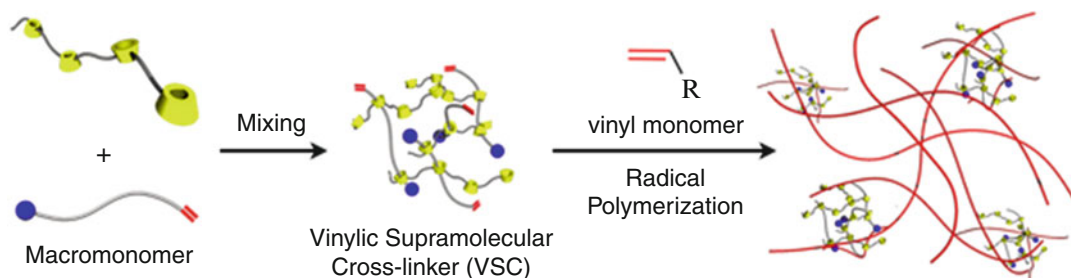
Supramolecular Network Polymers, Fig. 7 Strategy for the synthesis of VSC and PRN

Moreover, a CD-based vinylic supramolecular cross-linker (VSC) capable of facilitating the synthesis of PRNs through radical polymerization of a vinyl monomer was also reported (Fig. 7) [18]. To prepare the VSC, oligocyclodextrin as the oligomacrocycle and the macromonomer, a terminal bulky group-tethering polyethylene glycol (PEG)-type methacrylate, were prepared. Mixing of these components became a white gel, indicating the formation of polypseudorotaxane, originating from the pseudo-cross-linking reaction based on the multiple penetrations of the macromonomer to the CD cavities. A mixture of DMAAm as a typical vinyl monomer, VSC, and a photoinitiator was UV irradiated to afford a transparent gelled product.

Summary

A variety of synthetic methods of PRNs have been reported as mentioned above. Beside them, cross-linkers possessing two or more macrocycles are also reported to date which afford PRNs via accidental or controlled penetration of the propagation ends into the macrocycle cavities [19]. Recently a PRN material has been practically used as the surface coating materials for mobile phone and automobile, which is being notified as the first commercial-level application. This is an epoch-making event in the fields of science of rotaxane and related materials. Continuous improvements are ongoing to prepare supramolecularly cross-linked polymers by effective and efficient procedure. Further effective and significant applications utilizing characteristic properties of PRNs are also expected at both molecular and bulk levels.

Related Entries

▶ Crown Ethers-Based Supramolecular Polymers
▶ Cyclodextrins-Based Supramolecular Polymers
▶ Polyrotaxanes: Synthesis, Structure, and Chemical Properties
▶ Supramolecular Hydrogels
▶ Topological Gels

References

1. Gibson HW, Marand H (1993) Polyrotaxanes: molecular composites derived by physical linkage of cyclic and linear species. Adv Mater 5:11
2. Sauvage JP, Dietrich-Buchecker C (1999) Molecular catenanes, rotaxanes, and knots. Wiley-VCH, New York
3. Takata T (2006) Polyrotaxane and polyrotaxane network: supramolecular architectures based on the concept of dynamic covalent bond chemistry. Polym J 38:1
4. Huang F, Pederson AM, Gibson HW (2007) Polyrotaxanes. In: Mark JE (ed). Physical properties of polymers handbook. Springer, New York, p 693
5. Araki J, Ito K (2007) Recent advances in the preparation of cyclodextrin-based polyrotaxanes and their applications to soft materials. Soft Matter 3:1456
6. Harada A, Hashidzume A, Yamaguchi H, Takashima Y (2009) CD-based polymeric rotaxanes. Chem Rev 109:597
7. Takata T, Arai T, Kohsaka Y, Shioya M, Koyama Y (2012) Polyrotaxane Network as a topologically cross-linked polymer: synthesis and properties. In: Harada A (ed). Supramolecular polymer chemistry. Wiley-VCH, Weinheim, p 331
8. De Gennes PG (1999) Sliding gels. Phys A 271:231
9. Gong C, Gibson HW (1997) Controlling polymeric topology by polymerization conditions: mechanically linked network and branched poly(urethane rotaxane)s with controllable polydispersity. J Am Chem Soc 119:8585
10. Okumura Y, Ito K (2001) The polyrotaxane gel: a topological gel by figure-of-eight cross-links. Adv Mater 13:485
11. Ichi T, Watanabe J, Ooya T, Yui N (2001) Controllable erosion time and profile in poly(ethylene glycol) hydrogels by supramolecular structure of hydrolyzable polyrotaxane. Biomacromolecules 2:204
12. Kihara N, Hinoue K, Takata T (2005) Solid–state end–capping of pseudopolyrotaxane possessing hydroxy-terminated axle to polyrotaxane and its application to the synthesis of a functionalized polyrotaxane capable of yielding a polyrotaxane network. Macromolecules 38:223
13. Bilig T, Oku T, Furusho Y, Koyama Y, Asai S, Takata T (2008) Polyrotaxane networks formed via rotaxanation utilizing dynamic covalent chemistry of disulfide. Macromolecules 41:8496
14. Oku T, Furusho Y, Takata T (2004) Novel concept for recyclable crosslinked polymer: topologically networked polyrotaxane capable of undergoing reversible crosslinking and decrosslinking. Angew Chem Int Ed 43:966
15. Kohsaka Y, Nakazono K, Koyama Y, Asai S, Takata T (2011) Size-complementary rotaxane cross-linking for the stabilization and degradation of a supramolecular network. Angew Chem Int Ed 50:4872

S

16. Zhang M, Xu D, Yan X, Yan X, Chen J, Dong S, Zheng B, Huang F (2012) Self-healing supramolecular gels formed by crown ether based host–guest interactions. Angew Chem Int Ed 51:7011
17. Koyama Y, Yoshii T, Kohsaka Y, Takata T (2013) Photodegradable cross-linked polymer derived from a vinylic rotaxane cross-linker possessing aromatic disulfide axle. Pure Appl Chem 85:835
18. Arai T, Jang K, Koyama Y, Asai S, Takata T (2013) Versatile supramolecular cross-linker: a rotaxane cross-linker that directly endows vinyl polymers with movable cross-links. Chem Eur J 19:5917
19. Ogawa M, Kawasaki A, Koyama Y, Takata T (2011) Synthesis and properties of a polyrotaxane network prepared from a Pd-templated bis-macrocycle as a topological cross-linker. Polym J 43:909

Supramolecular Polymers (Coordination Bonds)

Yuji Suzaki and Kohtaro Osakada
Chemical Resources Laboratory, Tokyo Institute of Technology, Yokohama, Japan

Synonyms

Coordination polymers

Definition

Supramolecular polymer is defined as the polymer whose repeating units are connected with non-covalent bonds such as coordination bond, π-π interaction, and hydrogen bonding [1]. The definition of the "coordination polymers" is a polymer whose repeating units are connected with coordination bond.

Introduction

Most organic supramolecular polymers are composed of the organic repeating units with dual or multiple hydrogen bonds. Coordination bonds, in particular, bind bifunctional organic ligands with metals to form the (supramolecular) coordination polymer. The coordination bonds of transition metals are directional and form the polymers with ordered structures. A number of linear polymers (1D system), sheet-type polymers (2D system), and metal-organic frameworks (MOFs, 3D system), containing the coordination bonds, were known and studied extensively in the solid state and/or in solution. In July 2013, ca. 39000 references are selected by using "coordination polymer" as the keyword (SciFinder, online search of Chemical Abstracts Service (CAS) database of chemical and bibliographic information).

This entry focuses on supramolecular coordination polymers composed of the mechanically interlocked molecules (MIMs) such as rotaxane, formed by macrocyclic molecule and threading dumbbell-shaped molecule, and catenane, formed by two or more macrocyclic molecules [2, 3].

Figure 1 summarizes the typical strategy for synthesis of a MIM-functionalized coordination polymer. A stoichiometric reaction of metal ions with the pseudorotaxane which contains linear-shaped component with coordinating units at the both ends yields the MIM-functionalized supramolecular coordination polymer. Structure of the resulting supramolecular varies from linear, square planer to tetrahedral, depending on the
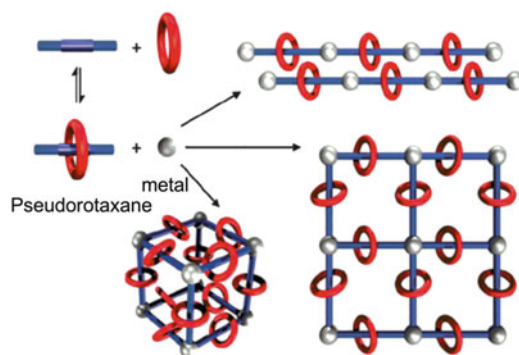
Supramolecular Polymers (Coordination Bonds), Fig. 1 Typical strategy for supramolecular coordination polymer (The artwork is reproduced from Scheme 1 of Ref. [3b])
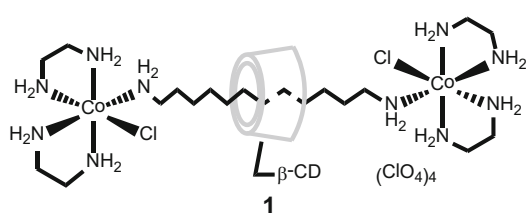
coordination number of the metal ions, as well as the stoichiometry between the metal ions and pseudorotaxane. Critical analysis of the structure of the compounds was conducted by single crystal and powder XRD analysis.

Kim reported the first supramolecular coordination polymer, which contains the rotaxanes of cucurbituril and linear organic molecule, and showed unique properties based on its flexible interlocked structure [3a].

Linear Polymers

The first rotaxane containing coordination bonds was reported by Ogino in 1981 (Fig. 2). The reaction of the Co complex with β-cyclodextrin and α, ω-diaminoalkane, or their pseudorotaxane yields [2]rotaxane **1** [4].

Liu et al. reported a supramolecular coordination polymer from an inclusion complex of β-cyclodextrin and 4,4′-bipyridine (β-CD-4,4′-bpy) by coordination with Ni(II)(2,2′-bpy) [5], Ru(II) (2,2′-bpy)$_2$ [6], CoCl$_2$ [7], ZnCl$_2$ [7], CuCl$_2$ [8], and NiCl$_2$ [8] (2,2′-bpy = 2,2′-bipyridine) (Fig. 3). The coordination polymer of Ru(II) (2,2′-bpy)$_2$ and β-CD-4,4′-bpy shows emission derived from the ruthenium units. Spectroscopic studies using NMR, UV, and induced circular dichroism (ICD), scanning tunneling microscopy (STM), and transmission electron microscopy (TEM) of the polymers revealed the structure of the molecules in solution and the aggregates in the solid state. The reaction of α-, β-, and

γ-CD-4,4′-bpy with Ni(II)Cl$_2$ and Cu(II)Cl$_2$ formed the coordination polymers, {NiCl$_2$(α-CD-4,4′-bpy)}$_n$ (**2**), {MCl$_2$(β-CD-4,4′-bpy)}$_n$ (M = Co (**3**), Zn (**4**)), and [CuCl$_2$\{γ-CD-(4,4′-bpy)$_2$\}]$_n$ (**5**), and then ICD spectroscopy analysis revealed the effect of the cyclodextrin size on the stoichiometry and morphology of the polymers [8]. {NiCl$_2$(α-CD-4,4′-bpy)}$_n$ (**2**) and {MCl$_2$(β-CD-4,4′-bpy)}$_n$ (M = Co (**3**), Zn (**4**)) include 4,4′-bpy in the cavity of α-CD with vertical and oblique orientation, respectively. [CuCl$_2$\{γ-CD-(4,4′-bpy)$_2$\}]$_n$ (**5**) is composed of copper and 1:2 complex of γ-CD and 4,4′-bpy in which two 4,4′-bpy molecules are included in a parallel orientation.

Li et al. synthesized Ag nanoparticle modified with β-CD-4,4′-bpy and used for colorimetric detection of Yb^{3+} ions in aqueous solution with
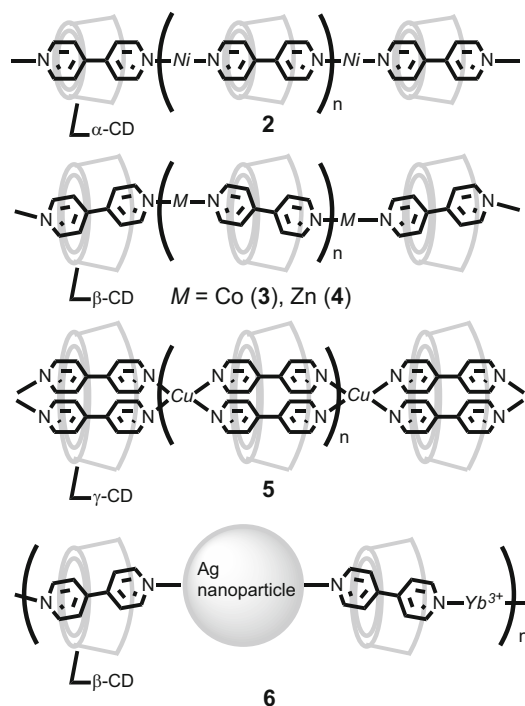
Supramolecular Polymers (Coordination Bonds), Fig. 3 The assembly behaviors of the pseudorotaxane of α−, β−, and γ−CDs and 4,4′-bipyridine (4,4′-bpy) through the coordination linkage by Ni(II) (**2**), Co (II) (**3**), Zn(II) (**4**), Cu(II) (**5**), and Yb(III) and Ag nanoparticle (**6**)

Supramolecular Polymers (Coordination Bonds), Fig. 2 Ogino's rotaxane **1** composed of β-cyclodextrin threaded by α, ω-diaminoundecane coordinated to cobalt (III) complexes
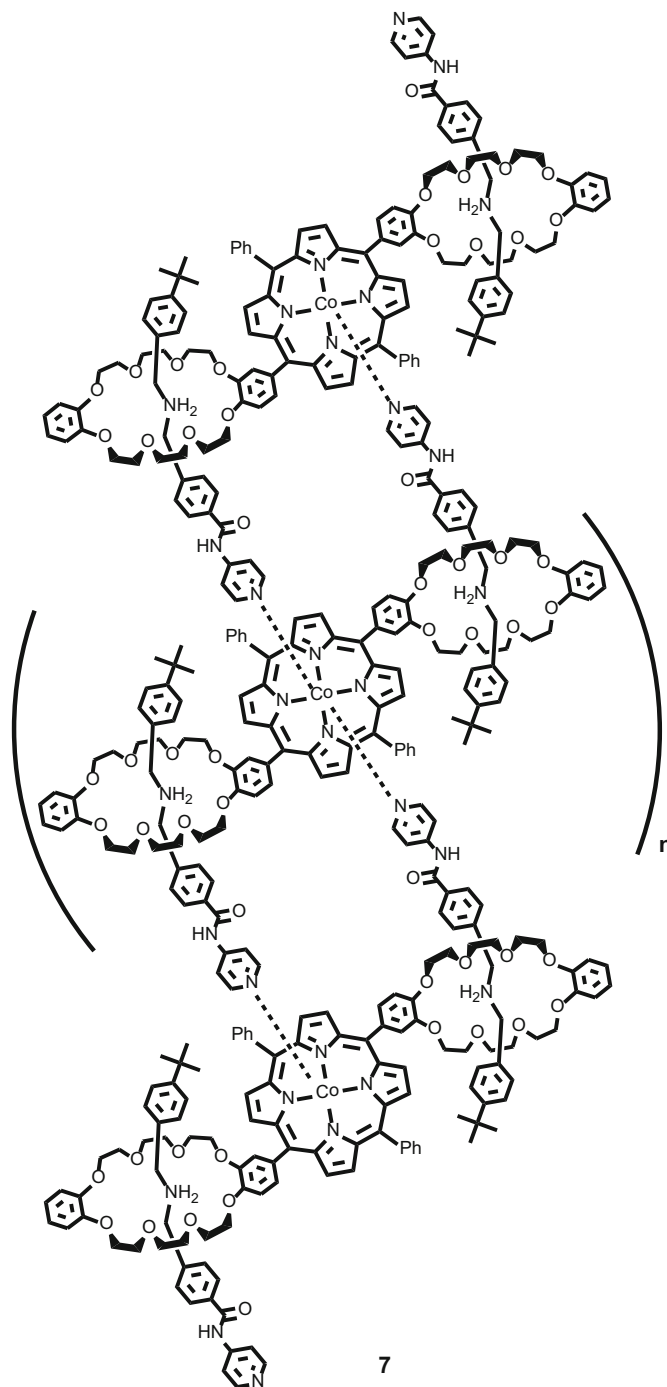
Asakawa's supramolecular coordination polymer **7** whose repeating units were connected by hydrogen bonding as well as the coordination bond

7

high sensitivity ($>2 \times 10^{-7}$ M by visual detection) [9]. The sensing of Yb^{3+} ions was assigned to the formation of supramolecular coordination polymer formulated as [(Ag-nanoparticle)-

(β-CD-4,4′-bpy)-(Yb^{3+})-(β-CD-4,4′-bpy)-]$_n$ (**6**) (Fig. 3). Aqueous reaction of Yb^{3+} ions with β-CD-4,4′-bpy-modified Ag nanoparticle induced a distinct color change from yellow to
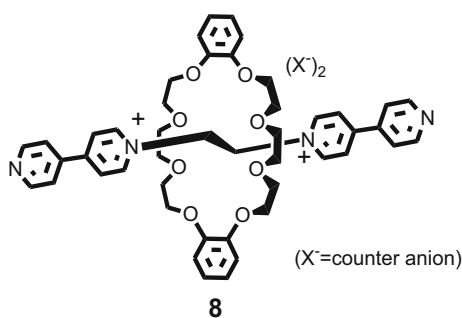
red, while a similar reaction using Pr^{3+}, Eu^{3+}, Sm^{3+}, La^{3+}, Nd^{3+}, and Ce^{3+} does not change its visible solution color.

Asakawa and Shimizu et al. reported supra-molecular coordination polymer **7** composed of dialkylammonium and porphyrin-functionalized crown ethers (Fig. 4) [10, 11]. Both the hydrogen bond between ammonium hydrogens and oxygen atoms of crown ether and the coordination bond between pyridyl group and Co-porphyrin support the structure. Averaged number of the repeating units, *n*, in **7** was estimated to be ca 100.
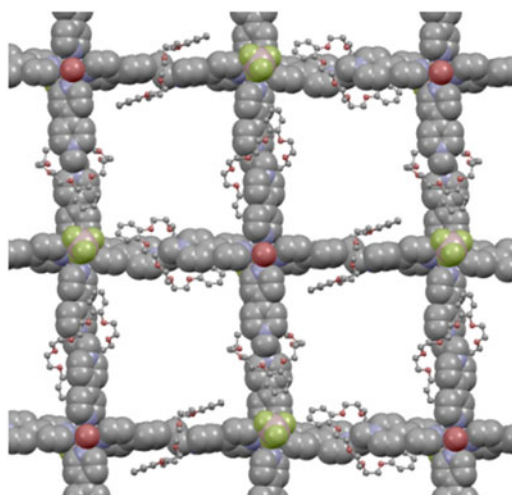
Metal-Organic Frameworks (MOFs)

Metal-organic frameworks (MOFs, 3D system) have become the most important field in coordination chemistry because of its possible application including gas storage. Metal-organic rotaxane frameworks (MORFs) are defined by Loeb as a subclass of MOF [3b]. Until 2000, Kim et al. synthesized a series of MORFs composed of metal ions, such as Cu^{2+}, Ni^{2+}, Co^{2+}, Ag^+, Cd^{2+}, Tb^{3+}, and pseudorotaxane of cucurbituril and dialkyldiamine, and reported their 1D, 2D, and 3D polyrotaxane network [3a].

Loeb et al. employed pseudorotaxane **8** composed of $[4,4'$-bpy-N-CH_2CH_2-N-$4,4'$-bpy$]^{2+}$ and dibenzo[24]crown-8-ether as a linker of the transition metals (Fig. 5). 1D (Ag^+, Co^{2+}, Zn^{2+}), 2D

Supramolecular Polymers (Coordination Bonds), Fig. 6 MORFs **9** based on **8** and Cd^{2+}
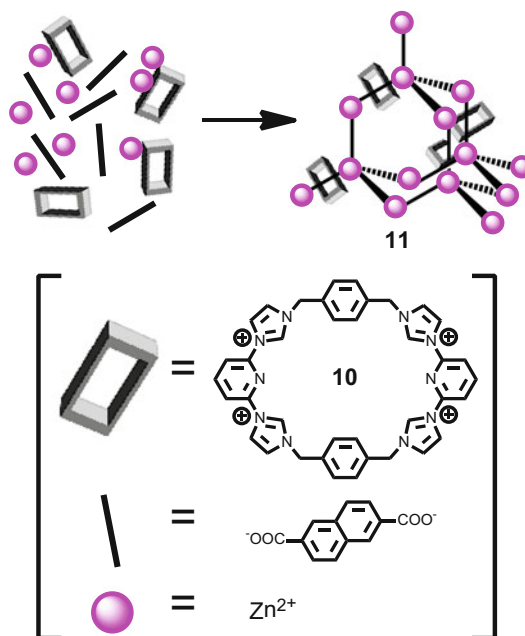
Supramolecular Polymers (Coordination Bonds), Fig. 7 Structure of "Texas-sized" molecular box (**10**) and the MORF (**11**) formed from **10**, disodium 2,6-naphthalenedicarboxylic acid, and Zn^{2+} (The artwork is reproduced from Fig. 1 in Ref. [13])

(Ag^+, Cu^{2+}, Cd^{2+}, Ni^{2+}), and 3D (Sm^{3+}, Eu^{3+}, Gd^{3+}, Tb^{3+}) MORFs were obtained by reaction of pseudorotaxane **8** with the metal ions [3b], [12]. Figure 6 depicts crystal structure of MORF

Supramolecular Polymers (Coordination Bonds), Fig. 5 Pseudorotaxane **8** composed of dibenzo[24] crown-8-ether and 1,2-bis(dipyridyl)ethane

S

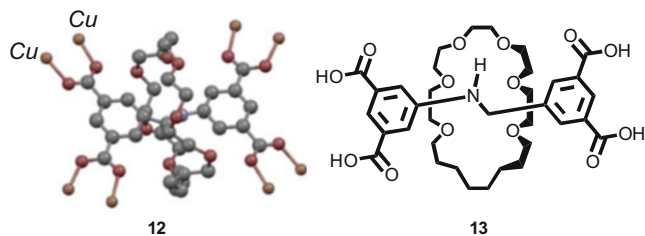**Supramolecular Polymers (Coordination Bonds), Fig. 8** Structure of the single unit of the [2]rotaxane coordinated to four Cu(II) paddle wheel clusters in **12** and [2]rotaxane **13** (The artwork of **12** is reproduced from Fig. 3a in Ref. [15])
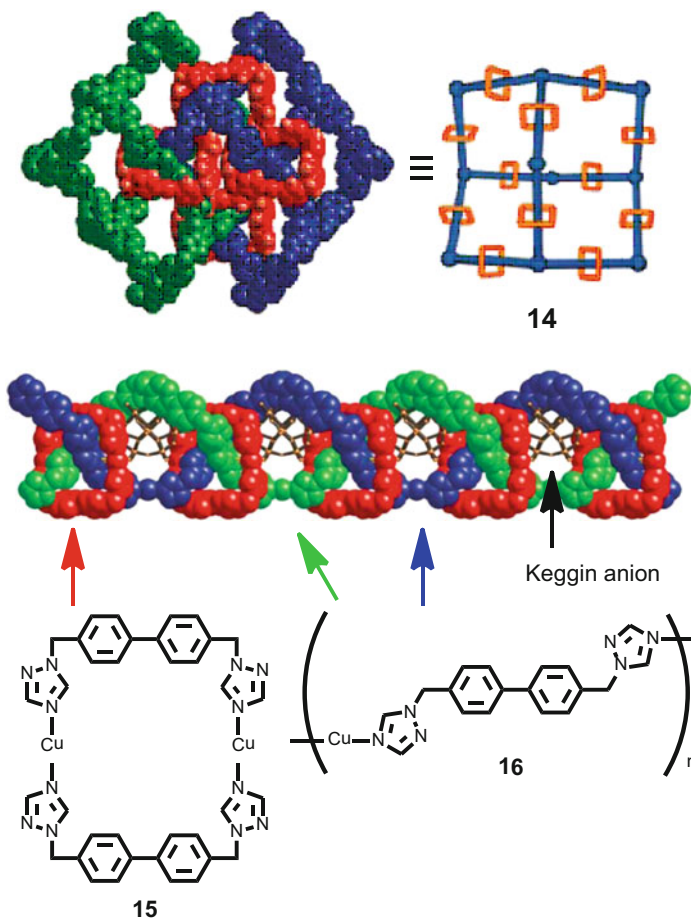
Supramolecular Polymers (Coordination Bonds), Fig. 9 The structure of MORF **14**, $[Cu_2(L)_2]^{2+}$ macrocycle (**15**) and linear $[Cu(L)]^+$ (**16**) (The artwork of **14** is reproduced from Fig. 2 of Ref. [17])

9 obtained from **8** and Cd^{2+}. The Cd ions adopt square planar coordination whose apical positions are occupied by BF_4 and H_2O.

Oh and Sessler reported an anion-directed assembly of a 3D MORF of tetracationic imidazolium macrocyclic molecule **10**, which is named as "Texas-sized" molecular box, with zinc(II) 2,6-naphthalenedicarboxylate. The resulting MORF contains Zn(II) with twisted tetrahedral coordination (**11**) (Fig. 7) [13].

Supramolecular Polymers (Coordination Bonds), Fig. 10 Structure of crown ether-incorporating MOFs **17,** bifunctional crown ether **18**, and [2]catenane **19** (The artwork is reproduced from Fig. 2 of Ref. [18] (**17** and **18**) and Scheme 14 of Ref. [19] (**19**))
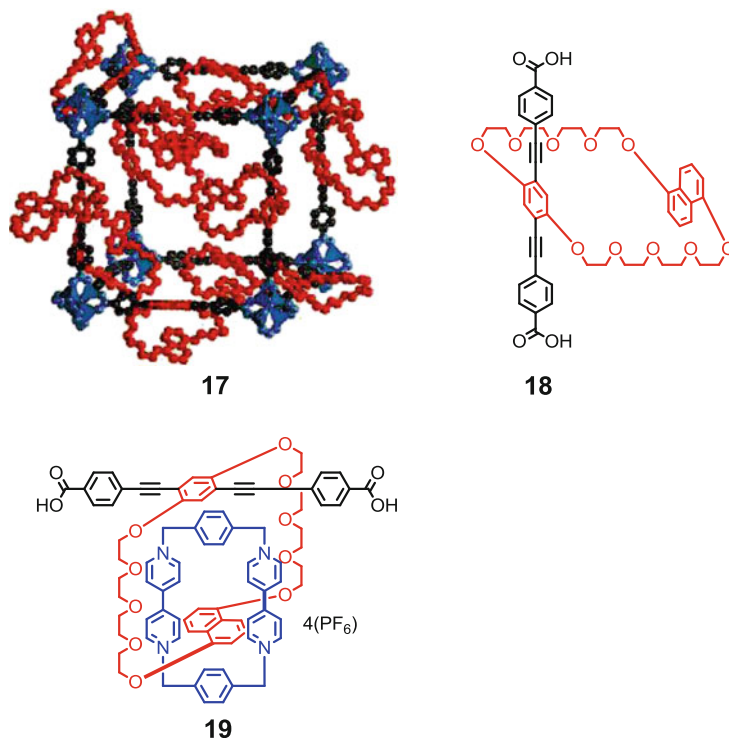
The trivalent Ln salts (M(NO$_3$)$_3$; M = Y(III), Gd (III), Er(III), Tm(III), or Lu(III)) were also applied for the synthesis of luminescent MORFs in which nature of the lanthanide cations influences the optical properties of the MORF–Ln complexes. In particular, the MORF–Eu was found to be highly luminescent [14].

More recently, MORFs **12** of dinuclear Cu complex and rotaxane **13**, composed of arylalkylamine and [24]crown-6-ether (Fig. 8), were found to undergo rotation of the crown ether in the solid state (10 MHz at 373 K and above), which was investigated by variable temperature solid-state NMR technique [15]. In this study, MOF structure creates free space which allows dynamic motion of the macrocyclic crown ether.

Su et al. reported MORF**14** of macrocyclic [Cu$_2$(L)$_2$]$^{2+}$(L = 4,4′-bis(1,2,4-triazol-1-ylmethyl) biphenyl) (**15**) threaded by linear [Cu(L)]$_n$ chain (**16**) which encapsulates ball-shaped polyoxometalate (Keggin anion [PMo(V)Mo (VI)$_{11}$O$_{40}$]$^{4-}$) (Fig. 9) [16, 17].

Recently, Yaghi, Stoddart, and their coworkers have reported MOF **17** having macrocyclic polyethers as recognition modules for relatively large guest molecules such as paraquat dication (Fig. 10) [18]. **17** is synthesized from crown ether **18** and Zn(NO$_3$)$_2$. Similar reaction using the bifunctional catenane, **19**, was employed also for synthesis of [2]catenane-incorporating MOFs [19].

Yaghi, Stoddart, and Sauvage reported MORFs incorporating copper-complexed rotaxanes. The MORF, MOF-1040 (**20**), is obtained by the reaction of Zn(NO$_3$)$_2$ and copper-complexed pseudorotaxanes **21**. The reaction of **21** with oxone and with KCN causes oxidation and demetalation of the Cu (I) center, respectively, to yield MOF-1041 and MOF-1042. The topological structure is maintained even after oxidation of Cu or demetalation [20].

Outlook

This entry focused on recent successful incorporation of rotaxane (or catenane) structure to the supramolecular coordination polymer, which fixed flexible MIMs to the rigid coordination polymer having highly ordered arrangement in the solid state. It can be regarded as a new step for further application of supramolecules and MIMs toward molecular devices and versatile materials and toward clear understanding of the motions of MIMs group in the solid state as well as the control of process in the crystal phase.

Related Entries

▶ Calixarenes-Based Supramolecular Polymers
▶ Stimuli-Responsive Polymers
▶ Supramolecular Polymers (Host-Guest Interactions)
▶ Supramolecular Polymers (Hydrogen Bonds)

References

1. Brunsveld L, Folmer BJB, Meijer EW, Sijbesma RP (2001) Supramolecular polymers. Chem Rev 101:4071–4097. doi:10.1021/cr990125q
2. In this essay, (pseudo)rotaxanes and catenanes are not called as supramolecule to avoid confusion with supramolecular polymer, although rotaxanes and catenanes are often classified as supramolecules
3. Excellent reviews of this area: (a) Kim K (2002) Mechanically interlocked molecules incorporating cucurbituril and their supramolecular assemblies. Chem Soc Rev 31:96–107. doi:10.1039/A900939F; (b) Vukotic VN, Loeb SJ (2012) Coordination polymers containing rotaxane linkers. Chem Soc Rev 41:5896–5906. doi:10.1039/C2CS35141B
4. Ogino H (1981) Relatively high-yield syntheses of rotaxanes. Syntheses and properties of compounds consisting of cyclodextrins threaded by α, ω-diaminoalkanes coordinated to cobalt(III) complexes. J Am Chem Soc 103:1303–1304. doi:10.1021/ja00395a091
5. Liu Y, Zhao Y-L, Zhang H-Y, Song H-B (2003) Polymeric rotaxane constructed from the inclusion complex of β-cyclodextrin and 4,4'-dipyridine by coordination with nickel(II) ions. Angew Chem Int Ed 42:3260–3263. doi:10.1002/anie.200351128
6. Liu Y, Song S-H, Chen Y, Zhao Y-L, Yang Y-W (2005) The construction of a supramolecular polymeric rotaxane from bipyridine-ruthenium and cyclodextrin. Chem Commun :1702–1704. doi:10.1039/B415930F
7. Zhao Y-L, Zhang H-Y, Guo D-S, Liu Y (2006) Nanoarchitectures constructed from resulting polypseudorotaxanes of the β-cyclodextrin/4,4'-dipyridine inclusion complex with Co^{2+} and Zn^{2+} coordination centers. Chem Mater 18:4423–4429
8. Yang Y-W, Chen Y, Liu Y (2006) Linear polypseudorotaxanes possessing many metal centers constructed from inclusion complexes of α-, β-, and γ-cyclodextrins with 4,4'-dipyridine. Inorg Chem 45:3014–3022. doi:10.1021/ic0601438
9. Han C, Zhang L, Li H (2009) Highly selective and sensitive colorimetric probes for Yb^{3+} ions based on supramolecular aggregates assembled from β-cyclodextrin-4,4'-dipyridine inclusion complex modified silver nanoparticles. Chem Commun :3545–3547. doi:10.1039/B904787E
10. Asakawa M, Yamanishi H, Shimizu T (2002) Monomers having rotaxane structure and polymers and processes for production of both. PCT Int Appl, WO 2002098956, A1 20021212
11. Asakawa M, Yamanishi H, Shimizu T (2004) Preparation of pseudorotaxane-type dibenzocrown ether-containing transition metalloporphyrinsecondary ammonium salt aggregates by self association. Jpn Kokai Tokkyo Koho, JP 2004083725, A 20040318
12. Reviews, (a) Loeb SJ (2007) Rotaxanes as ligands: from molecules to materials. Chem Soc Rev 36:226–235. doi:10.1039/B605172N; (b) Loeb SJ (2005) Metal–organic rotaxane frameworks; MORFs. Chem Commun :1511–1518. doi:10.1039/B416609D
13. Gong H-Y, Rambo BM, Cho W, Lynch VM, Oh M, Sessler JL (2011) Anion-directed assembly of a three-dimensional metal–organic rotaxane framework. Chem Commun 47:5973–5975. doi:10.1039/C1CC10272A
14. Gong H-Y, Rambo BM, Nelson CA, Cho W, Lynch VM, Zhu X, Oh M, Sessler JL (2012) Multi component self-assembly: supramolecular organic frameworks containing metal–rotaxane subunits (RSOFs). Dalton Trans 41:1134–1137. doi:10.1039/C1DT11495F
15. Vukotic VN, Harris KJ, Zhu K, Schurko RW, Loeb SJ (2012) Metal–organic frameworks with dynamic interlocked components. Nature Chem 4:456–460. doi:10.1038/nchem.1354
16. Pang P-J, Peng J, Zhang C-J, Li Y-G, Zhang P-P, Ma H-Y, Su Z-M (2010) A polyoxometalate-encapsulated 3D porous metal–organic pseudorotaxane framework. Chem Commun 46:5097–5099. doi:10.1039/C003048A

17. Wang X-L, Qin C, Wang E-B, Su Z-M (2007) An unusual polyoxometalate-encapsulating 3D polyrotaxane framework formed by molecular squares threading on a twofold interpenetrated diamondoid skeleton. Chem Commun :4245–4247. doi:10.1039/B709563E

18. Li Q, Zhang W, Miljanić OŠ, Sue C-H, Zhao Y-L, Liu L, Knobler CB, Stoddart JF, Yaghi OM (2009) Docking in metal-organic frameworks. Science 325:855–859. doi:10.1126/science.1175441

19. Zhao Y-L, Liu L, Zhang W, Sue C-H, Li Q, Miljanić OŠ, Yaghi OM, Stoddart JF (2009) Rigid-strut-containing crown ethers and [2]catenanes for incorporation into metal–organic frameworks. Chem Eur J 15:13356–13380. doi:10.1002/chem.200902350

20. Coskun A, Hmadeh M, Barin G, Gándara F, Li Q, Choi E, Strutt NL, Cordes DB, Slawin AMZ, Stoddart JF, Sauvage JP, Yaghi OM (2012) Metal–organic frameworks incorporating copper-complexed rotaxanes. Angew Chem Int Ed 51:2160–2163. doi:10.1002/anie.201107873

Supramolecular Polymers (for Organic Electronics and Optoelectronics)

Dongzhong Chen[1] and Leyong Wang[2]
[1]Key Lab of High Performance Polymer Materials and Technology and Key Lab of Mesoscopic Chemistry, Ministry of Education, Department of Polymer Science and Engineering, School of Chemistry and Chemical Engineering, Nanjing University, Nanjing, Jiangsu, P. R. China
[2]Key Laboratory of Mesoscopic Chemistry of MOE, Center for Multimolecular Organic Chemistry, School of Chemistry and Chemical Engineering, Nanjing University, Nanjing, Jiangsu, P. R. China

Synonyms

Molecular assemblies; Noncovalent associated polymer; Self-assembled polymer; Supramolecular organization; Supramolecular structure

Definition

Supramolecular chemistry is the chemistry of the entities produced through intermolecular noncovalent interactions beyond covalent bonds-based molecular chemistry as pioneered by Lehn [1]. The generalized definition of a supramolecular polymer (SP) is that of a system based on the association of many component units through secondary (noncovalent) interactions [2], such as hydrogen bonds, coordination, charge transfer, electrostatic and host–guest interaction, and van der Waals interactions rather than the primary covalent bonds found in conventional polymeric materials [1, 2].

The most restrictive definition for SP was proposed by Meijer and coworkers that supramolecular polymers are defined as polymeric arrays of monomeric units via reversible and highly directional secondary interactions, behaving according to well-established theories of polymer physics and exhibiting polymeric properties [3].

Engineered supramolecular polymer or supramolecular engineering generates the nanostructures or molecular assemblies and patterns in such as layers, films, membranes, micelles, gels, and particulate solids through recognition-directed association, self-assembly, and self-organization [2].

Introduction

Polymer chemistry is currently a worldwide beneficial multibillion dollar industry, and supramolecular chemistry deals with many of the hottest scientific topics and locates at the multidisciplinary interface such as chemistry, physics, biology, nanotechnology, and materials science. Thus, supramolecular polymers have great potential in the construction of new materials with unique structures and functions imparting some of the important features of polymer in virtue of innovative ideas from supramolecular chemistry. Especially supramolecular polymers or molecular assemblies have a great influence on the

S

design of advanced functional materials, the construction flexibility, and error correction (self healing) capability empowered by the characteristics of noncovalent interactions, such as π–π stacking, which is specifically an attractive feature for organic electronics and optoelectronics, since the performance of organic electronic materials in the solid state is determined not only by the property of individual molecules but also by properties of ensembles of molecules [4].

On the other hand, miniaturization of the operating optoelectronic devices is currently of broad interest in both the academic and industrial community; thus, *supramolecular electronics* of 5–100 nm dimensions intermediating between single molecular electronics of angstroms (Å) scale and bulk devices ($>$ μm) has aroused intensive attentions due to some intriguing characteristics such as much increased amount of volume information storage, faster operation rate, manipulation at micro- or nanoscale, and development of novel and more specific functionalities [5, 6].

Supramolecular (Noncovalent) Interactions and Supramolecular Structures Take Crucial Effect in Organic Electronics and Optoelectronics

As symbolized by the awarding of 2000 Nobel Prize in Chemistry to Heeger, Macdiarmid, and Shirakawa [7], remarkable research progress on conjugated materials (including small conjugated organic molecules and conjugated oligomers and polymers) with conducting and semiconducting characteristics useful for electronics and optoelectronics devices manufacturing has been achieved, and some novel organic electronic products have been commercialized. However, some unsatisfactory performance of the present generation of conjugated materials when used in working devices presses for new strategies to improve materials functionalities and device properties. For organic optoelectronics, supramolecular polymers themselves and also many engineered assemblies based on the control of the supramolecular structures seem to be very

promising for the improvement of carrier mobility, luminescence efficiency, and device performance and stability [8].

## Semiconducting Polymers and Doped Conducting Polymers

For polymers composed of fully saturated σ bonds, the excitation energy is above 7 eV, while in conjugated systems with an alternated pattern of single and double bonds, the excitation energy is lowered to 1.5–4 eV, values typical for the semiconducting state. Conjugated polymers possess both specific electronic and macromolecular properties; they are stiff and usually not soluble and processable without adding proper side chains or dopants. A conjugated polymer can theoretically be considered as natural quantum wires, provided with complete π-electron delocalization along the backbone in a quasi-one-dimensional geometry, with lateral confinement of about 0.5 nm. While the fully conjugated metallic system is unstable due to Peierls dimerization, thus bond alternation spontaneously occurs stabilizing the system in the semiconducting state. Fortunately, the conjugated semiconducting polymers can be modified into a supramolecular complex to achieve the metallic state through a so-called doping process which is a kind of solid-state redox reaction; the preparation of stable conducting polymers with conductivities up to few hundreds of S cm^{-1} is currently achieved [8].

However, practically π-electrons in conjugated polymers are seldom delocalized along the whole macromolecule chain but usually existing with discrete segments (persistent conjugation lengths) separated each other by chain twisting or defects [8]. Such structure features endow conjugated polymers with distinctive characters in electronic structure and dynamics intermediating between large organic molecules and low dimensional semiconductors, which constitutes the basis for finely tuning and enhancing their optoelectronics performance from the supramolecular polymer standpoints. Side chain substitution, regioregular polymer preparation, orientation, and thus resulted anisotropy are all

utilized to modify their supramolecular structure and then improve their electronic properties. Such as polythiophene (PT) and its derived poly (alkylthiophene) (PAT) are typical examples (Fig. 1) [9]. The unsubstituted PT itself is insoluble, the introduction of substituents in the 3 or 4 position of the thiophene rings promotes solubility, and different relative orientations can be realized which exert a crucial effect on the macromolecular and electronic properties of the material. Compared with the one-dimensional ones for regiorandom PATs, both excitons and polarons are delocalized over several conjugated chains thus possessing two-dimensional characteristics with reduced electron–phonon coupling in regioregular PAT.

Doping is a widely adopted means to attain conducting polymers, the doping process is very similar to a redox reaction with the dopant agent closer to the π-electron system donating or withdrawing an electron, and the transport properties of obtained doped polymers are strongly dependent on the dopant molecule characteristics, the morphology, and the polymer supramolecular structure. To achieve significant bulk conductivity, charges moving not only along the chain but also through interchain hopping to sustain macroscopic drifts under an applied electrical field are required. The hopping process is determined by intermolecular interactions thus dependent on the doped complex supramolecular structure, and the conductivity is achieved by percolating the conducting polymer. The poly (3,4-ethylenedioxythiophene) (PEDOT, see Fig. 1) possesses rather high-conductivity properties of σ up to 300 S cm^{-1} with reduced optical
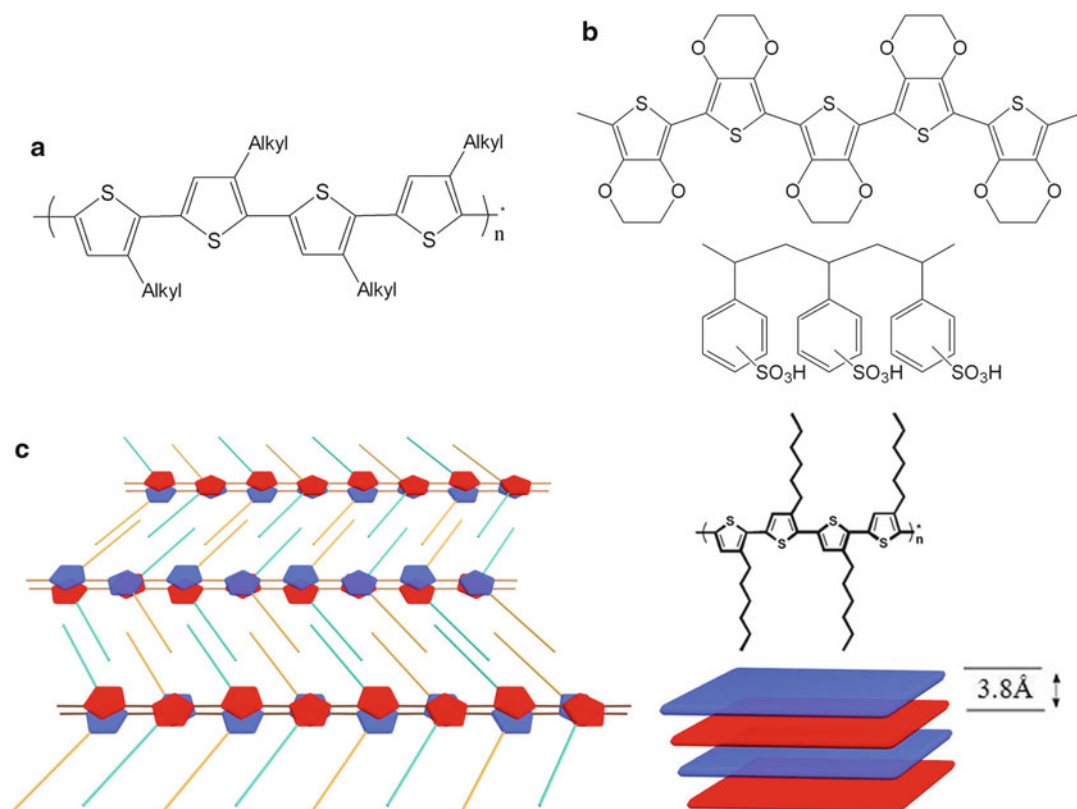
**Supramolecular Polymers (for Organic Electronics and Optoelectronics), Fig. 1** (**a**) Poly(alkylthiophene), PAT; (**b**) poly(3,4-ethylenedioxythiophene) (*PEDOT*) and polystyrene sulfonic acid (*PSS*) and PEDOT:PSS complex; (**c**) regioregular poly(3-hexylthiophene), P3HT, and its supramolecular structure (Adapted in color with permission from Fig. 1 in Ref. [9], copyright Wiley-VCH (1998))

S

Supramolecular Polymers (for Organic Electronics and Optoelectronics), Fig. 2 Typical discotic liquid crystalline compounds of substituted triphenylene (*TP*) and hexabenzocoronene (*HBC*) and the construction of supramolecular columns by π-stacking
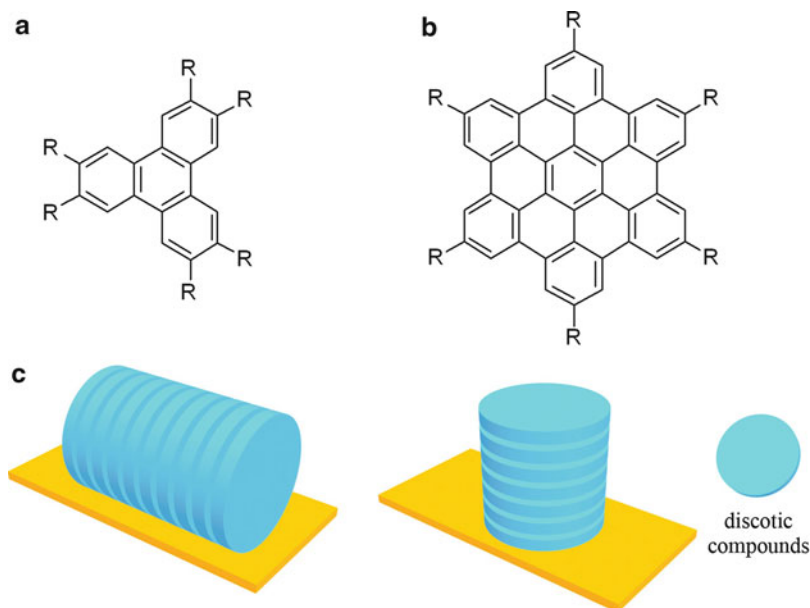
gap, while PEDOT itself is insoluble with poor processability; fortunately, the in situ polymerization of ethylenedioxythiophene in the presence of polystyrene sulfonic acid (PSS) offers PEDOT/PSS transparent films which are highly conductive and of good mechanical quality; thus broad commercial applications such as in antistatic, corrosion protection, and batteries are implemented [8], also often employed as modifying conducting layer for electrodes in device fabrication and as conducting ink in transistors prepared by ink-jet printers [10].

Transport Properties and OFET

Unlike conducting polymers, for semiconducting polymers, no carriers are available except those thermally excited across the gap. Therefore, negative (positive) carriers are needed to inject into the material through overcoming the barrier between the metal work function and the LUMO (HOMO) molecular levels. Then under an applied bias field, the injected carriers move inside the semiconductor, such injection of carriers and their transport is of fundamental importance for all electronic devices and especially for organic field effect transistors (OFETs).

The interest in organic thin film transistors (OTFTs) is related to their low-cost and low-temperature solution processing, mechanical flexibility, and suitability for large-area preparation and also driven by the broad technological applications such as flat-panel display devices, electronic paper, electronic identification tags, and smart cards [8].

For OFETs, the transport properties of active semiconductor materials of either small π-conjugated molecules or polymers are of primary concern. When the π-conjugated molecules are stacked along a direction, then π-orbitals of nearby molecules can interact with each other thus delocalizing electrons along the stacking direction to form a kind of main-chain SP. Some typical examples of such systems are conjugated calamitic liquid crystals (LCs) in their smectic phases or discotic LCs to create supramolecular columns, conjugated oligomers, and charge transfer salts [8]. As shown in Fig. 2, the typical discotic LC compounds of substituted triphenylene (TP) and hexabenzocoronene (HBC) can form supramolecular columns by π-stacking in parallel to or perpendicular with the substrate. For instance, the HBC-based discotic LCs generated columnar self-assembled SPs showing quite high carrier mobility (μ), and

the mesophase assembly order was further increased by adopting epitaxy techniques; furthermore, the highly oriented discotic LC sample exhibited anisotropic mobility with the maximum value parallel to the stacking direction up to 0.5 cm^2 V^{-1} s^{-1} [11]. Based on these data, 0.5 μm was estimated for the carrier diffusing length before trapping, which was obviously smaller than the typical channel width of several tens μm in typical OFET devices; thus, an enhanced carrier mobility of discotic LC and remarkably improved OTFT performance may be expected provided that the order improvement of the assembled SPs by more than one order of magnitude the carrier diffusing length is to be larger than the typical OTFT channel width.

The scenario for covalent polymeric systems is much more complicated owing to their larger dimension and intrinsic disorder. Some theoretical conclusions from the corresponding oligomers may still be circumspectly applicable for engineering the proper polymeric assembly, but different properties must be considered. To improve carrier mobility, to take full advantage of both the intramolecular carrier drift along the conjugated backbone and the interchain carrier hopping is the effective pathway; thus, fine-tuning of the intramolecular properties of the conjugated polymer in combination with their supramolecular organization control usually makes sense to enhance carrier mobility. For example, for regioregular PATs, their intrachain regioregularity increases the planarity of the backbone, which also decreases the interchain separation, thus resulting in the lamellar structure of very short intermolecular separation (3.8 Å) showing much increased bulk mobility and transport properties. Furthermore, the electron–phonon coupling in regioregular PAT is reduced in contrast with the one-dimensional case in regiorandom PAT thus diminishing the carrier localization due to self-trapping. Moreover, the possibility to align polymer chains further increases both planarity and intermolecular interactions [8]. Fully organic field effect transistors with organic electrodes in addition to organic active semiconducting materials have also been reported, even with complicated circuitry

structures [12]. Based on the exploitation of the supramolecular properties of active materials, the use of new generations of conjugated polymers allows to reach μ values comparable with those of amorphous silicon, as the development in the field, the semiconductor materials, and OFET devices enough for industrial applications can be envisaged [8].

Organic Light-Emitting Diode (OLED)

Organic light-emitting diode (OLED) is one of the most attractive optoelectronics application of conjugated organic molecules and polymers, which may serve as a promising novel generation for flat display technology. Compared with LC-based displays, OLED possesses wide viewing angle, high brightness, desirable mechanical flexibility, low power consumption, and low cost. Before analyzing how supramolecular polymers or supramolecular structure of conjugated materials enhance their OLED properties, the fundamental principles of OLEDs are briefly introduced.

As shown in Fig. 3a, an organic semiconductor layer sandwiched between two electrodes of different work functions with a supporting transparent substrate constitutes the simplest OLED. The work function of the different electrode metals should be well matched with the HOMO and LUMO levels of the organic semiconducting materials for injecting carriers into the devices. Transparent conductive materials such as indium tin oxide (ITO) and sometimes surface modified with a PEDOT:PSS layer or polyaniline are adopted as an anode, calcium with a work function of 2.9 eV is usually selected as the electron injector covered with another metal due to its high reactivity, and aluminum is often used though with a higher work function of 4.3 eV [8]. When the device is applied, a positive bias, electrons from the cathode, and holes from the anode are injected into the device; then the opposite carriers drift inside the semiconducting layer, meet and recombine each other, and thus radiate the excess energy as photons. The physical processes involved in OLED mainly include charge
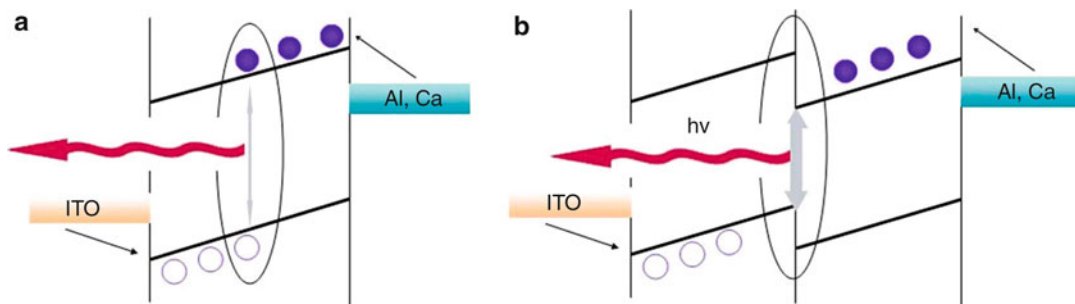
Supramolecular Polymers (for Organic Electronics and Optoelectronics), Fig. 3 Schematic representation of device structure and working principle of OLED. (**a**) Simple monolayer device; (**b**) two-layer device. *Blue full* *circles* stand for electrons; *gray open circles* symbolize holes (Adapted in color from Fig. 12 in Ref. [8] with permission of Taylor & Francis, 2005; permission conveyed through Copyright Clearance Center, Inc.)

injection, transport, recombination, and light emission. The polymeric semiconductors are usually solution processable and deposited by spin coating in contrast with the usual vacuum evaporation for small organic molecules. The chemical and physical properties of the organic semiconductors, especially their supramolecular structure and the film quality, are crucial factors influencing the performance of OLED. For enhancing the OLED device efficiency and lowering the operating voltage thus reducing the power consumption, multilayer depositions of small organic molecules with different electronic properties are often employed to improve the matching with the metal's work function as well as alter the color emission. While for conjugated polymers, substitution with proper electron-donating or electron-withdrawing side groups allows modifying the material ionization potential and electron affinity thus promotes the performance.

Typical energy transfer distances in organic materials are tens of angstroms, in comparison with few angstroms for carriers hopping, which imply that a proper engineering of the supramolecular structure of the semiconducting active layer may be useful to improve carrier transport and emitting properties of OLED devices. For achieving the radiative recombination, after carriers are injected in the device, they must travel along the organic semiconductor layer. For conjugated polymers possessing the emission functionality with good hole mobility, while usually

poor transport properties for electrons, an inefficient recombination close to the cathode often occurs due to the unbalanced carrier flux, which may be resolved by adopting a two-layer structure as shown in Fig. 3b, to create a potential barrier for storing up both electrons and holes before their radiative recombination. For small molecule OLED, the transport and emission functionalities may be fully separated, and then proper transport layers can be evaporated. While for semiconducting polymers, considering opposite carriers may hop on different molecules and then recombine at the intermolecular interface, blending with electron deficient molecules may be a solution, though the macroscopic phase separation between the two physically blended components is an obvious limit to this approach. Properly designed diblock copolymers containing electron transporting and/or hole transporting/light-emitting functional blocks giving rise to complex nanostructured microphase separation morphologies are a group of promising materials for organic optoelectronics [13]. Recent developments in living radical polymerization methods facilitate a suitable control of the block copolymer structure and the possibility of introduction of variant functional blocks.

The key process of an OLED device is charge recombination, which is responsible for the efficient formation of the emitting centers (singlet excitons) and the exclusion of the parasitic nonradiative decay channels, such as intersystem crossing (ISC), which leads to the formation of

triplet excitons [8]. Formation of triplet excitons in molecular solids may give rise to phosphorescence while seldom observed in conjugated polymers. The OLED emission efficiency is not only affected by ISC but also by supramolecular interactions of the material. Two strategies can be assumed to achieve highly luminescent polymers in the solid state: increase separation of the conjugated backbones or synthesize polymers having highly delocalized π-electrons, thus mimicking an infinite ordered one-dimensional system [8]. From the viewpoint of isolated molecule properties, rodlike conjugated systems are useful, and chemical substitution of the conjugated backbone with bulky side groups promotes the polymer solubility and also increases the interchain separation resulting in increased luminescence efficiency. Intermolecular interactions can also be suppressed by using sp^3-carbon atom spiro-linked structure of steric repulsion in organic small molecules or polymers. Another way to prevent intermolecular interactions is realized by threading conjugated polymers within a molecular shield such as cyclodextrins, which result in supramolecular wires separated by jacketed macrocycle compounds thus showing isolated molecule optical properties. Furthermore, even though the intermolecular interactions are shielded, they do not modify too much the frontier orbitals of the threaded molecule and preserve carrier transport; thus, better OLED performances exhibit by threaded polymers compared with the nonthreaded ones.

At last, polarized emission is requested for some specific applications; polarized OLED sources from oriented organic semiconducting systems may be then the candidates for a new generation of displays [8].

Organic Solar Cells (OSCs) or Photovoltaic Cells (PVCs)

Sunlight is the most abundant source of energy, solar fuel production such as photosynthesis often starts with the capture of sunlight by an assembly of molecules, and thus produced electronic excitation by energy absorption is subsequently transferred to a suitable acceptor [14]. Organic solar cells (OSCs) or photovoltaic cells (PVCs) utilize energy from sunlight efficiently to produce solar fuels; it seems the optimal efficiency for charge photogeneration can be obtained only in donor–acceptor-like mixed systems.

Intensively investigated systems for photovoltaic applications are the composites of conjugated polymer–fullerene derivatives. Fullerene (C_{60}) is an excellent electron acceptor able to capture several electrons; photoexcitation of the conjugated polymers induces an electron transfer to fullerene resulting in a stable positive carrier (polaron or radical cation) in the polymer and an ionized C_{60} molecule (radical anion) in a well-mixed polymer–fullerene system [8]. The transfer of the electron from the conjugated polymer to the acceptor occurs in an ultrafast rate almost two order of magnitude larger than competing radiative or nonradiative processes with an almost perfect high efficiency. Based on such photoinduced electron transfer character, several photophysical processes can be exploited in devices such as luminescence quenching-based sensors, photoconductivity sensitization, photovoltaic phenomena, and nonlinear processes [8]. Although potential applications in different fields vary, the main application of the photoinduced electron transfer process is related to photovoltaic cells, with rapidly expanding commercial market and particularly fascinating when employing disposable organic materials with low-cost solution processing.

The operating principle of photovoltaic devices is schematically illustrated in Fig. 4. Figure 4a depicts the simplest structure with one active conjugated polymer layer sandwiched between metals of different work function (e.g., ITO and Al or Ca). If a bias field is applied, such a construction can work like OLEDs in forward bias, while in reverse bias, injection of carriers from electrodes is strongly inhibited; under photoexcitation charged carriers (polarons) can be generated; thus, a current is detected endowing the device with the function of a photodetector. In photovoltaic devices without any external field applied, upon photon absorption the potential
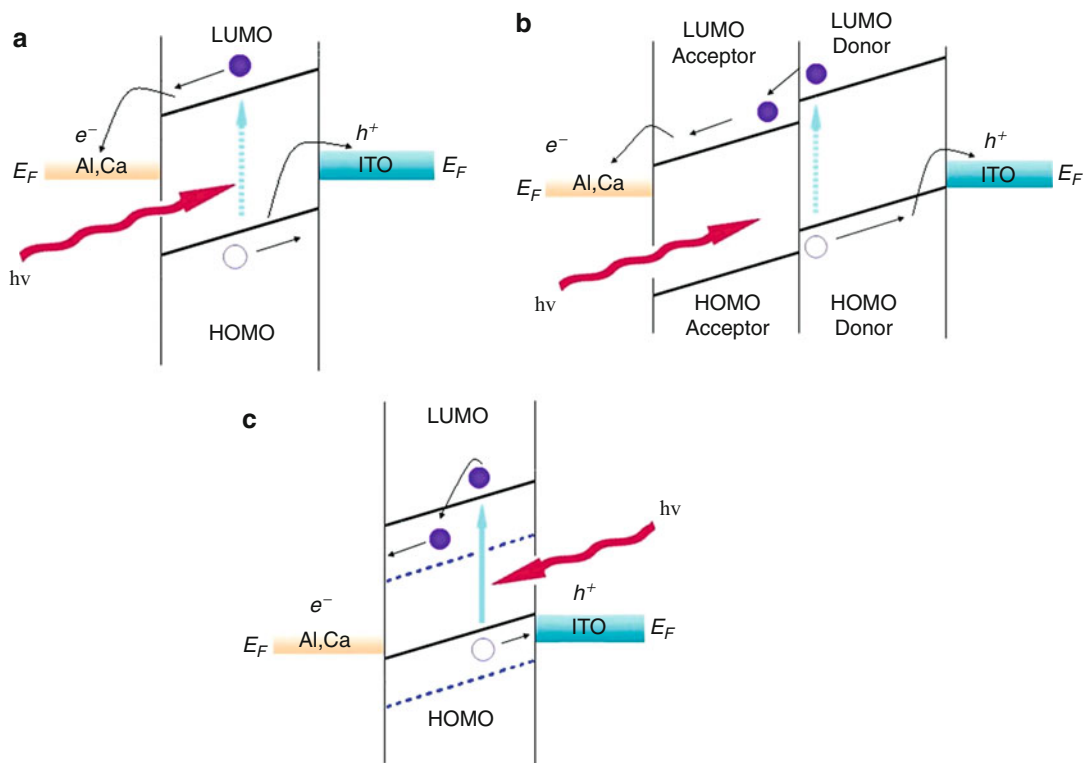
Supramolecular Polymers (for Organic Electronics and Optoelectronics), Fig. 4 Schematic illustration of photovoltaic devices structure and working principle. (**a**) Single layer; (**b**) double layers; (**c**) interpenetrating donor/acceptor (bulk heterojunction, *BHJ*) organic solar cells (*OSCs*). *Blue full circles* stand for electrons; *gray open circles* symbolize holes (Adapted in color from Fig. 17 in Ref. [8] with permission of Taylor & Francis, 2005; permission conveyed through Copyright Clearance Center, Inc.)

between the electrodes of different work functions separates the excited states into a pair of oppositely charged carriers, while the efficiency of single layer devices is quite inferior due to the very low work function difference. As shown in Fig. 4b, a bilayer structure with donor–acceptor materials superimposed can remarkably promote the photovoltaic performance. When donor (polymer) and acceptor (fullerene) molecules are very close to each other such as the interface contacts between the two layers, electrons can jump from the polymer to the fullerene, so in bilayer cells, the charge transfer process offers an efficient channel for breaking the excitons into carriers besides the potential from the electrode work function difference thus enhancing their performances.

The main drawback of the bilayer structure is the limited interface contact between the donor and acceptor components; morphological problems in the mixed system are crucial for prompting effective charge transfer, where supramolecular polymer strategies may be useful to solve the typical problem of macrophase separation in blending. Blending donor and acceptor at a molecular scale through supramolecular interactions can obviously promote the interface contacts. The newly structured bulk heterojunction (BHJ) photovoltaic cell as sketched in Fig. 4c, works in similar manner to the bilayer one but with much promoted efficiency due to the enhanced donor–acceptor interface with interpenetrating donor–acceptor network (BHJ). Power conversion efficiency of 1.7 % is reported

under air mass (AM) 1.5 global solar conditions using BHJ blends of regioregular PAT with improved hole mobility and CdSe nanorods possessing excellent electron mobility [15]. Remarkable improvements in carrier mobility have also been observed by adopting BHJ blends of one-dimensional positive carrier discotic LCs (hexaphenyl-substituted hexabenzocoronene) and perylene derivatives providing a crystalline network for negative carrier drift. Well-performed solar cells and photodetectors with blending morphology of continuous smooth texture and dimension-reduced perylene crystallites have been produced by facile solution processing [16]. Block copolymer-based nanophase separation and even regular micropatterning formation on a larger scale constitute another supramolecular approach to enhance transport properties of devices [13]. The microphase separation achieved in this way based on some rod–coil block copolymers or with a block possessing the acceptor functionality strongly enhances the probability of carrier hopping and improves the transport properties of carriers in photovoltaic device thus promoting the performance of solar cells. Nowadays, through markedly improving light collection and enhancing transport properties of carriers, BHJ organic solar cells with conversion efficiency higher than 10 % can be readily fabricated, which is an important step toward commercial application of OSCs.

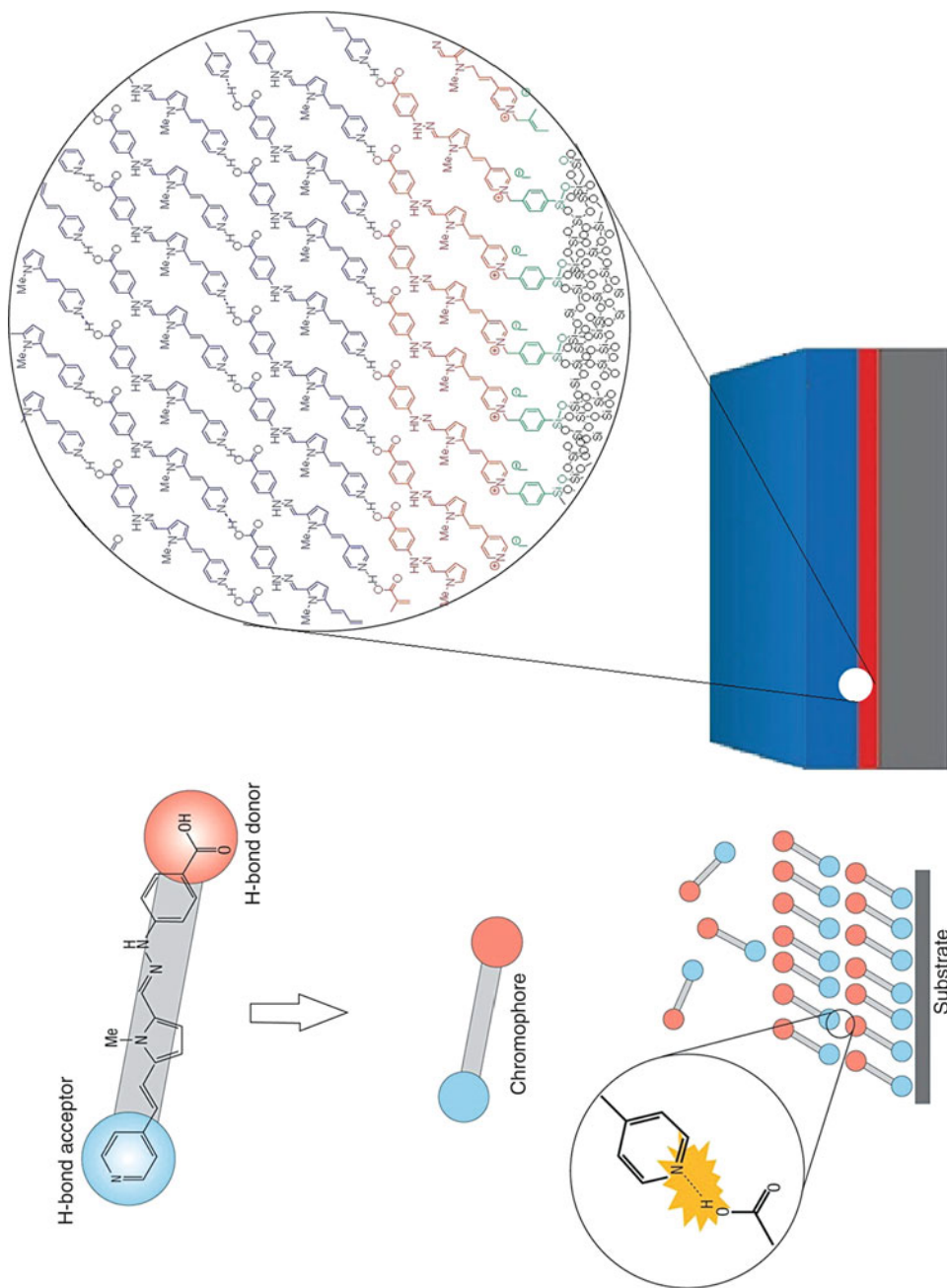## Engineered Supramolecular Polymers for Optoelectronic Applications

Supramolecular engineering using self-assembly targets at developing complex functional materials and devices [17]. Herein an example of supramolecular engineering for nonlinear optical (NLO) materials and device application is illustrated. As shown in Fig. 5, secondary interactions such as hydrogen bonding can construct complex supramolecular architectures by self-assembly, enabling the preparation of materials with nanoscale morphologies that optimize their optical

and electronic properties [17]. Without electric field poling, the fabrication of acentric micrometer-thick organic films by self-assembly using physical vapor-phase deposition is achieved. By using hydrogen bonding, high-response heteroaromatic organic chromophores have been straightforwardly self-organized from the vapor phase into intrinsically acentric, high-quality π-conjugated electrooptically active films (with second-order susceptibilities up to ~100 pm V^{-1}), which are thermally stable and promising for applications in telecommunications [18]. Many other impressive examples based on supramolecular self-assembly are reported such as the supramolecular liquid crystals by the self-assembly of fluorinated tapered dendrons through their core π-stacks of donors, acceptors, or donor–acceptor charge transfer complexes to create supramolecular nanometer-scale columns exhibiting high charge carrier mobilities, demonstrating promising optoelectronic properties from a wide range of organic materials [19].
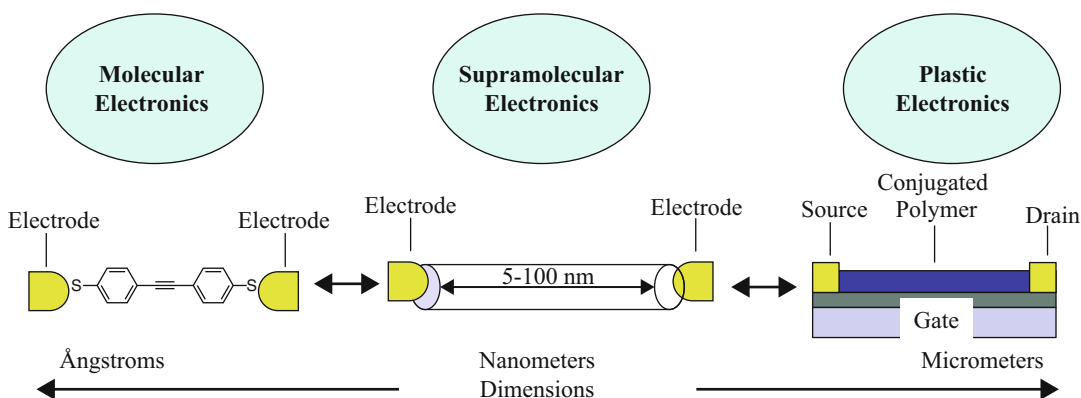
Supramolecular Electronics

As discussed above, supramolecular interactions between organic molecules not only enable them to self-organize into large regular assemblies but also enhance their electronic and luminescent properties thus improving the performance of organic devices, which constitute so-called supra solutions for organic electronics [20].

As shown in Fig. 6, the construction of nanosized electronic components through supramolecular assemblies of π-conjugated systems on the 5–100 nm length scale is referred to as supramolecular electronics, which bridges the gap between single-molecule electronics of angstroms (Å) scale and bulk organic "plastic" electronics (>μm) [5]. Contact problems existing between molecule and electrode and the thermal noise due to orientational and conformational motion of the molecule are the main drawbacks and concerns for applications of single-molecule

Supramolecular Polymers (for Organic Electronics and Optoelectronics), **Fig. 5** Self-assembly of nonlinear optical molecules end-capped by a hydrogen bond acceptor group (pyridine) at one end and a donor (COOH group) at the other end through vapor deposition into acentric films with head-to-tail geometries via hydrogen bonding (Adapted by permission from Macmillan Publishers Ltd.: [Nature Materials] (from Fig. 1 and 2 in Ref. [17]), copyright (2004))

Supramolecular Polymers (for Organic Electronics and Optoelectronics), Fig. 6 Schematic illustration of supramolecular electronics on the 5–100 nm length scale bridging the gap between molecular electronics of angstroms (Å) scale and bulk organic "plastic" electronics larger than micrometer dimension (Reproduced from Fig.1 in Ref. [5] with permission of The Royal Society of Chemistry, copyright (2005))

devices. While the performance of bulk materials used for macroscopic plastic devices is often limited by the dimension of the "crystalline" domains of typically smaller than 100 nm and showing remarkable domain boundary effects. It is proposed that self-assembled structures with the dimensions of 5–100 nm falling within supramolecular electronics are the ideal building blocks [5]. Nano-sized optoelectronic devices can be created through the programmed self-assembly of almost any polymeric and oligomeric π-conjugated system. Self-assembly is an attractive and efficient bottom-up strategy to position well-defined shape-persistent objects under thermodynamic control at predefined locations [5]. Both the construction of 1D-nanostructures exhibiting optimized transport properties and their precise connections to electrodes are the main challenges in the field of supramolecular electronics. Very recently important advances are achieved using external stimuli to realize addressability; by externally controlling light-responsive supramolecular polymerization processes in combination with appropriate methods of casting under an applied electric field, it becomes possible to predetermine the accurate positioning of organic interconnects within patterned nano-circuitry, demonstrating promising technological applications in nanosciences [6].

Related Entries

▶ Molecular Self-Organization
▶ Supramolecular Polymers (Coordination Bonds)
▶ Supramolecular Polymers (Host-Guest Interactions)
▶ Supramolecular Polymers (Hydrogen Bonds)

References

1. Lehn J-M (2005) Chapter 1. Supramolecular polymer chemistry. In: Ciferri A (ed) Supramolecular polymers, 2nd edn. Taylor & Francis, New York
2. Ciferri A (2005) Chapter 2. Growth of supramolecular structures. In: Ciferri A (ed) Supramolecular polymers, 2nd edn. Taylor & Francis, New York
3. Brunsveld L, Folmer BJB, Meijer EW, Sijbesma RP (2001) Supramolecular polymers. Chem Rev 101:4071–4097. doi:10.1021/cr990125q
4. Sugiyasu K, Shinkai S (2012) Chapter 3. Supra-macromolecular chemistry: toward design of new organic materials from supramolecular standpoints. In: Harada A (ed) Supramolecular polymer chemistry. Wiley-VCH, Singapore
5. Schenning APHJ, Meijer EW (2005) Supramolecular electronics, nanowires from self-assembled π-conjugated systems. Chem Commun 3245–3258. doi: 10.1039/B501804H
6. Moulin E, Cid J-J, Giuseppone N (2013) Advances in supramolecular electronics –from randomly self-assembled nanostructures to addressable self-organized interconnects. Adv Mater 25:477–487. doi:10.1002/adma.201201949

S

7. http://www.nobelprize.org/nobel_prizes/chemistry/laureates/2000/. Accessed 30 Sept 2013

8. Comoretto D (2005) Chapter 14. Supramolecular properties of polymers for plastic electronics. In: Ciferri A (ed) Supramolecular polymers, 2nd edn. Taylor & Francis, New York

9. McCullough RD (1998) The chemistry of conducting polythiophenes. Adv Mater 10:93–116. doi:10.1002/(SICI)1521-4095(199801)10:2<93::AID-ADMA93>3.0.CO;2-F

10. Sirringhaus H, Kawase T, Friend RH, Shimoda T, Inbasekaran M, Wu W, Woo EP (2000) High-resolution inkjet printing of all-polymer transistor circuits. Science 290:2123–2126. doi:10.1126/science.290.5499.2123

11. van de Craats A, Warman JM, Fechtenkotter A, Brand JD, Harbison MA, Mullen K (1999) Record charge carrier mobility in a room-temperature discotic liquid-crystalline derivative of hexabenzocoronene. Adv Mater 11:1469–1472. doi:10.1002/(SICI)1521-4095(199912)11:17<1469::AID-ADMA1469>3.0.CO;2-K

12. Brown AR, Pomp A, Hart CM, de Leeuw DM (1995) Logic gates made from polymer transistors and their use in ring oscillators. Science 270:972–974. doi:10.1126/science.270.5238.972

13. Segalman RA, McCulloch B, Kirmayer S, Urban JJ (2009) Block copolymers for organic optoelectronics. Macromolecules 42:9205–9216. doi:10.1021/ma901350w

14. Scholes GD, Fleming GR, Olaya-Castro A, van Grondelle R (2011) Lessons from nature about solar light harvesting. Nat Chem 3:763–774. doi:10.1038/NCHEM.1145

15. Huynh WU, Dittmer JJ, Alivisatos AP (2002) Hybrid nanorod-polymer solar cells. Science 295:2425–2427. doi:10.1126/science.1069156

16. Schmidt-Mende L, Fechtenkotter A, Mullen K, Moons E, Friend RH, MacKenzie JD (2001) Self-organized discotic liquid crystals for high-efficiency organic photovoltaics. Science 293:1119–1122. doi:10.1126/science.293.5532.1119

17. Kippelen B (2004) Optical materials, self-assembly reaches new heights. Nat Mater 3:841–843. doi:10.1038/nmat1273

18. Facchetti A, Annoni E, Beverina L, Morone M, Zhu PW, Marks TJ, Pagani GA (2004) Very large electro-optic responses in H-bonded heteroaromatic films grown by physical vapour deposition. Nat Mater 3:910–917. doi:10.1038/nmat1259

19. Percec V, Glodde M, Bera TK, Miura Y, Shiyanovskaya I, Singer KD, Balagurusamy VSK, Heiney PA, Schnell I, Rapp A, Spiess HW, Hudsonk SD, Duan H (2002) Self-organization of supramolecular helical dendrimers into complex electronic materials. Nature 419:384–387. doi:10.1038/nature01072

20. van de Auweraer M, de Schryver FC (2004) Organic electronic, supra solutions. Nat Mater 3:507–508. doi:10.1038/nmat1182

Supramolecular Polymers (Host-Guest Interactions)

Akira Harada
Department of Macromolecular Science, Graduate School of Science, Osaka University, Machikaneyama, Toyonaka, Osaka, Japan

Synonyms

Host-guest polymers; Non-covalent polymers; Polyrotaxanes

Definition

Supramolecular polymers are defined as polymers formed by non-covalent bonds. Non-covalent bonds include hydrogen bonds, coordination bonds, donor-acceptor bonds, and host-guest interactions.
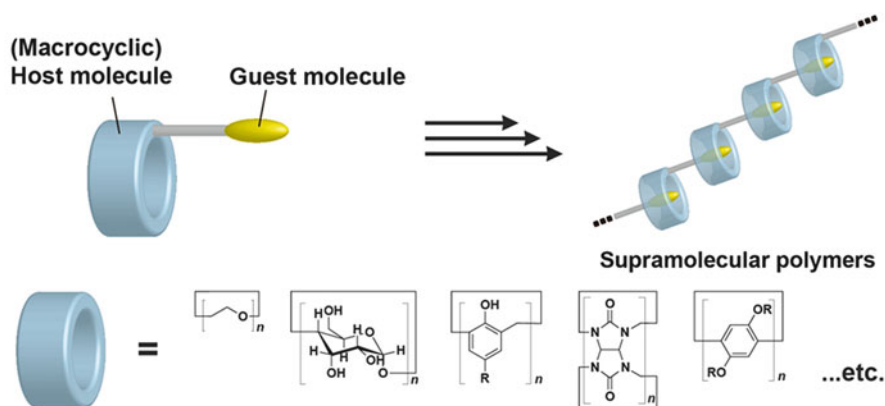
Supramolecular Polymers (Definition)

Supramolecular polymers are defined as polymers linked by intermolecular non-covalent interactions among molecules. Intermolecular interactions are involved in hydrogen bonds, metal-ligand interactions, donor-acceptor bonds, and host-guest interaction. Here in this chapter, supramolecular polymers formed by host-guest interactions are mainly focused on. (Supramolecular polymers involved in cyclodextrins are described in detail in another chapter, so the description of such supramolecular polymers is limited to the overview.)

The term "supramolecular polymers" was first proposed by J. Lehn in his book on Supramolecular Chemistry [1].

There are various types of supramolecular polymers in nature. Microtubules, for example, are supramolecular polymers in biological systems comprising subunits α- and β-tubulins. Microfilaments (in sarcomere) are supramolecular polymers
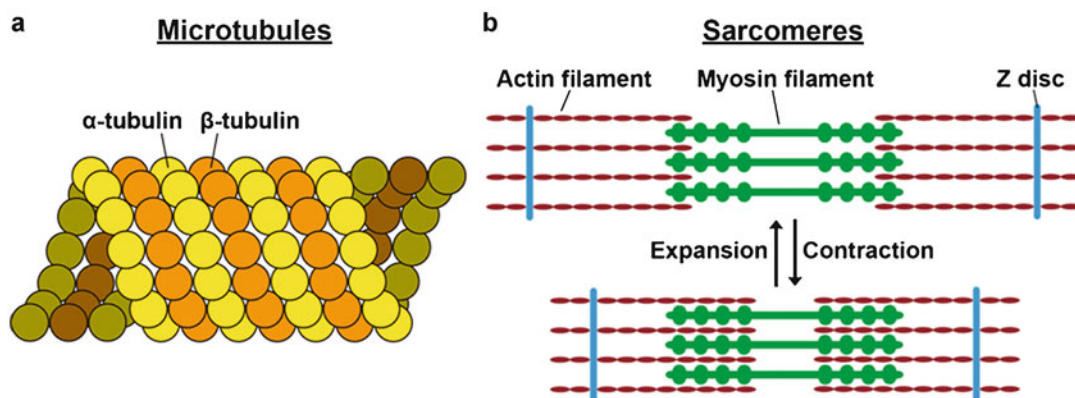
Supramolecular Polymers (Host-Guest Interactions), Fig. 1 Typical examples of supramolecular polymers in biological systems, microtubules (*left*), and sarcomeres (*right*)

Supramolecular Polymers (Host-Guest Interactions), Fig. 2 Schematic illustration of a formation of supramolecular polymers consists of macrocyclic host molecule modified with guest molecule (*upper*) and typical examples of macrocyclic host molecules (*lower*)

containing myosin and actin which form muscle systems (Fig. 1).

In this chapter, supramolecular polymers comprising mainly synthetic units through host-guest interactions are described.
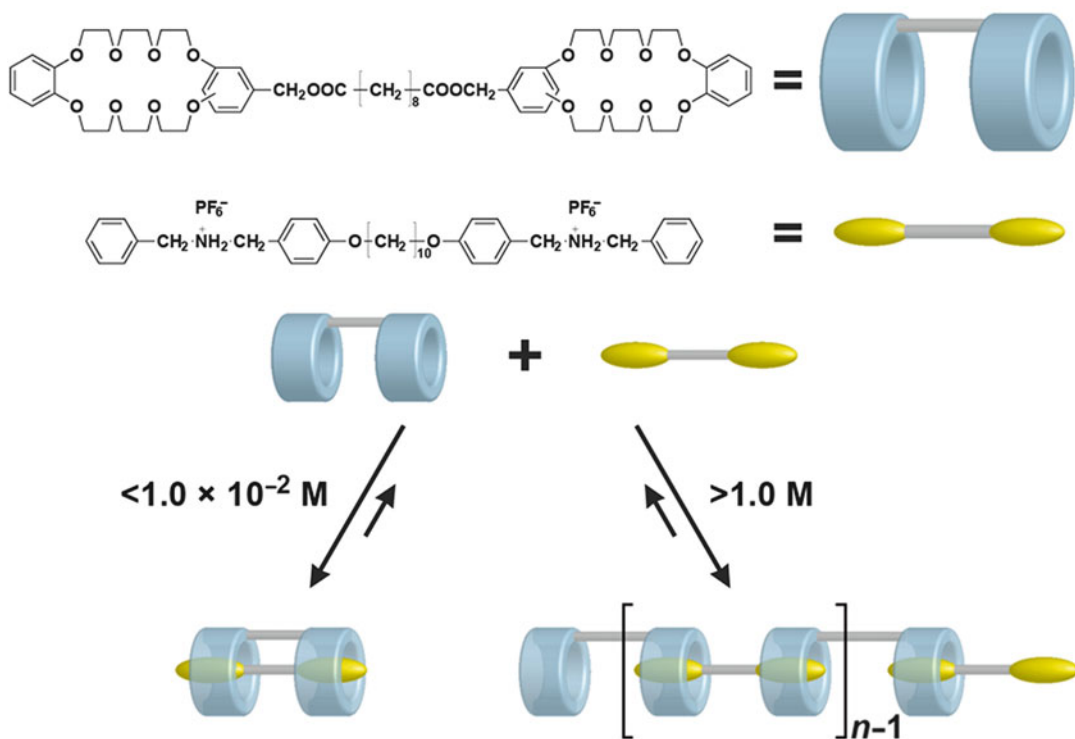
Supramolecular Polymers (Classification)

Supramolecular polymers may be classified by their interactions: hydrogen bonding, metal-ligand interactions, donor-acceptor interactions, and host-guest interactions. Host molecules include crown ethers, calixarenes, cyclodextrins, cucurbiturils, and other cyclic molecules (Fig. 2).

Crown Ethers

Crown ethers are typical host molecules which are able to bind not only alkali metal ions but also ammonium ions. The interactions between crown ethers and ammonium groups are strong enough to form supramolecular polymers.

Stoddart et al. used a monomer carrying dibenzo24-crown-8 as a host and a benzylammonium group as a guest part. In this

Supramolecular Polymers (Host-Guest Interactions),
Fig. 3 Chemical structure and schematic illustration of
the supramolecular polymers formed from homoditopic
molecules with secondary ammonium ions and crown
ether moieties

case, the monomer was found to form cyclic
dimer in the solid state by X-ray studies of the
single crystal [2,3].

Gibson et al. used ditopic crown hosts and
ditopic guest cations as monomers [4–7]
(Fig. 3). In this case at high concentrations
(ca. 2 M), they formed supramolecular polymers
with MW of about 18,000, which corresponds to
the degree of polymerization of about 9. When
the mixture of two kinds of cationic hosts
appended by dibenzo crown ether was used as
a monomer, the supramolecular polymers with
alternating copolymers were obtained from self-
sorting complexation of monomers.

Cyclodextrins

When a hydrophobic guest part is covalently
attached to a cyclodextrin host, they form

intramolecular complexes or supramolecular poly-
mers depending on the structure of the host and
guest moieties.

Calixarenes

Calixarene derivatives have been found to form
supramolecular oligomers and polymers.
Calixarene dimers form supramolecular
polymers with ditopic guests. (Calixarenes
having guest part form supramolecular
oligomers and polymers in solutions.) Guo and
Liu summarized calixarene-based supramolecu-
lar polymerization in solution in Chem. Soc. Rev.
in 2012 [8].

Dalcanale et al. reported that ditopic cavitand
monomers form supramolecular polymers with
ditopic guest molecules [9] (Fig. 4).
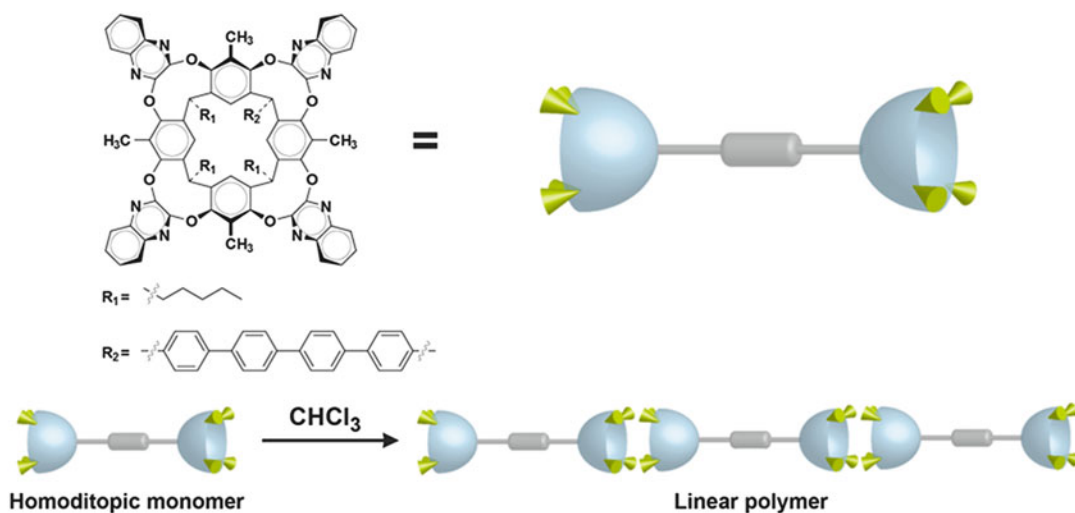
Supramolecular Polymers (Host-Guest Interactions), Fig. 4 Chemical structure and schematic illustration of the linear supramolecular polymers formed from homoditopic cavitand-based monomer self-assembling through self-complementary solvophobic π-π stacking interactions
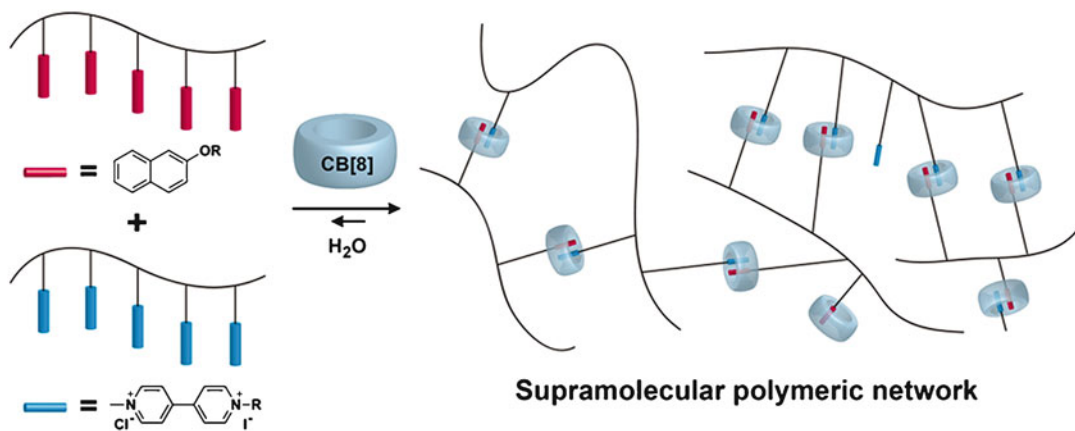
Supramolecular Polymers (Host-Guest Interactions), Fig. 5 Schematic illustration of the supramolecular polymeric network based on 2:1 complex formation of guests at the side chain of polymer by cucurbituril [8] (CB[8])

Cucurbiturils

Recently, cucurbiturils have been frequently used as host molecules to form supramolecular polymers [10–14]. In this case, the host molecules are soluble in acidic aqueous solutions and form complexes with cationic guest in water.

Kim Kimoon et al. reported 2D supramolecular framework using cucurbiturils as host molecules [15].

Steinke et al. found that 1,3-dipolar cycloaddition between alkyne and azide inside the cavity of cucurbituril [6] can be used to prepare polyrotaxanes [15].

Cucurbiturils form 2:1 complexes with cationic guests. Sherman's group reported that supramolecular polymeric network is formed by side-chain inclusion of polymer by cucurbiturils to give a gel [16] (Fig. 5).

Pillararenes

Recently, Ogoshi et al. prepared some pillararene hosts. Pillararenes are composed of hydroquinone units linked in para-position [17]. They found that pillararene forms supramolecular polymers and oligomers and polyrotaxanes in solutions [18].

Related Entries

▶ Molecular Self-Organization

▶ Supramolecular Polymers (Coordination Bonds)

▶ Supramolecular Polymers (Hydrogen Bonds)

References

1. Lehn J-M (1995) Supramolecular chemistry. VCH, Weinheim
2. Ashton PR, Baxter I, Cantrill SJ, Fyfe MCT, Glink PT, Stoddart JF, White AJP, Williams DJ (1998) Supramolecular daisy chains. Angew Chem Int Ed 37:1294–1297
3. Ashton PR, Parsons IW, Raymo FM, Stoddart JF, White AJP, Williams DJ, Wolf R (1998) Self-assembling supramolecular daisy chains. Angew Chem Int Ed 37:1913–1916
4. Yamaguchi N, Gibson HW (1999) Formation of supramolecular polymers from homoditopic molecules containing secondary ammonium ions and crown ether moieties. Angew Chem Int Ed 38:143–147
5. Yamaguchi N, Gibson HW (1999) Stabilities of cooperatively formed cyclic pseudorotaxane dimers. Chem Commun 9:789–790
6. Gibson HW, Yamaguchi N, Jones JW (2003) Supramolecular pseudorotaxane polymers from complementary pairs of homoditopic molecules. J Am Chem Soc 125:3522–3533
7. Jr Price T, Gibson HW (2012) Crown ether-based polymeric rotaxanes. In: Harada A (ed) Supramolecular polymer chemistry. Wiley-VCH, Weinheim
8. Guo DS, Liu Y (2012) Calixarene-based supramolecular polymerization in solution. Chem Soc Rev 41:5907–5921
9. Tancini F, Dalcanale E (2012) Polymerization with ditopic cavitand monomers. In: Harada A (ed) Supramolecular polymer chemistry. Wiley-VCH, Weinheim
10. Lee JW, Samal S, Selvapalam N, Kim H-J, Kim K (2003) Cucurbituril homologues and derivatives: new opportunities in supramolecular chemistry. Acc Chem Res 36:621–630
11. Huang F, Scherman OA (2012) Supramolecular polymers. Chem Soc Rev 41:5879–5880
12. Rauwald U, Scherman OA (2008) Supramolecular block copolymers with cucurbit[8]uril in water. Angew Chem Int Ed 47:3950–3953
13. Kim K, Ko YH, Selvapalam N (2013) Cucurbiturils: chemistry, supramolecular chemistry and applications. Imperial College Press, London
14. Regen N, Isaacs L (2009) Toward supramolecular polymers incorporating double cavity cucurbituril hosts. Tetrahedron 65:7249–7258
15. Kim K (2002) Mechanically interlocked molecules incorporating cucurbituril and their supramolecular assemblies. Chem Soc Rev 31:96–107
16. Appel EA, Biedermann F, Rauwald U, Jones ST, Zayed JM, Scherman OA (2010) Supramolecular cross-linked networks via host − guest complexation with Cucurbit[8]uril. J Am Chem Soc 132: 14251–14260
17. Ogoshi T, Kanai S, Fujinami S, Yamagishi T, Nakamoto Y (2008) para-bridged symmetrical Pillar [5]arenes: their Lewis acid-catalyzed synthesis and host-guest property. J Am Chem Soc 130:5022–5023
18. Ogoshi T, Yamagishi T (2013) Pillararenes: versatile synthetic receptors for supramolecular chemistry. Eur J Org Chem 2013:2961–2975. doi:10.1002/ejoc. 201300079

Supramolecular Polymers (Hydrogen Bonds)

Gordon Armstrong
Irish Centre for Composites Research, Materials and Surface Science Institute, University of Limerick, Limerick, Ireland

Synonyms

Self-assembly of hydrogen bonded polymers

Definition

A supramolecular polymer is an assembly of small molecules bound together by secondary interactions (e.g., hydrogen bonds) rather than the covalent bonds found in conventional polymeric materials.

Introduction

From the watershed that was Wöhler's synthesis of urea in 1828, organic chemistry has progressed to the point where the total synthesis of complex molecules has become a reality. However, the larger the target molecule, the more challenging its synthesis becomes. In contrast to this "total synthesis" approach, supramolecular chemistry is concerned with preparing assemblies of molecules using a combination of secondary chemical interactions rather than covalent bonding.

Therefore, a *supramolecular polymer* may be defined as an assembly of small repeat unit molecules bound together by secondary interactions rather than the covalent bonds found in conventional polymeric materials. The comparatively simple molecules used in these assemblies are driven to spontaneously self-assemble and then hold together via such noncovalent interactions as hydrogen bonds, metal coordination sites, and van der Waals forces. This may appear to contradict the conventional definition of a polymer first proposed by Carothers in 1929, whereby a polymer's structural units are linked together via covalent bonds to form giant "macromolecules" long enough to entangle with each other, and it is the entanglements that are primarily responsible for the unique properties of polymers. However, because a supramolecular polymer remains an extended structure formed from recurring repeat units, it may reasonably be expected to exhibit similar properties to conventional macromolecules.

Lehn [1, 2] and Lawrence et al. [3] have reviewed the advantages offered by this self-assembly approach in the context of synthetic chemistry and biological systems, respectively, including strategies to promote formation of small molecular assemblies and recurring problems in characterizing them. Also, numerous strategies besides hydrogen bonding have been pursued to prepare supramolecular polymers (e.g., ionomers, crown ethers, macrocycles, ligands), but these are outside the remit of this entry. For a discussion of these, the reader is referred to the recent comprehensive textbooks by Ciferri [4] and Steed and Atwood [5].

The Role of Hydrogen Bonding in Supramolecular Polymer Chemistry

The noncovalent interactions that hold linear supramolecular polymers together must be specific and directional so that the monomers only interact with their intended partners to allow the assembly form as intended. The interactions should also be reversible, so that the finished assembly may be annealed or undergo self-healing of defects. Due to the limited strength of individual interactions (typically less than 20 kJ/mol), additional stabilization (e.g., crystallization) is often needed to obtain useful material. However, if combined carefully, these interactions give rise to a bonding system that is sufficiently strong and long-lived to be a reasonable alternative to covalent bonds. Hydrogen bonding has proven especially suitable for supramolecular polymer synthesis because it is easier to control the direction of hydrogen bonds than ionic interactions, and though metal coordination bonds are highly directional, their shape changes with each new bond formed. Whereas covalent bonds typically have energies of 250–800 kJ/mol, the strongest hydrogen bonds have energies of 210 kJ/mol, with 12–25 kJ/mol being more usual for OH...O and NH...N bonds. In contrast, the bond energy of a van der Waals force is typically less than a kilojoule.

Reversible hydrogen bonds behave like entanglements in linear polymers, allowing a dense, thermodynamically determined network to assemble, yet adjust its configuration immediately in response to external stimuli. In systems where there is no anisotropy, strong, highly directional, reversible interactions are necessary as a reasonable alternative to covalent bonding in order to prepare linear supramolecular polymers with high degrees of polymerization (Dp) [6]. Otherwise, the polymer gels or forms microphase-separated structures. Single- or double-hydrogen bonds are not sufficiently stable to fulfill this role. Avoiding unspecific aggregation allows a high level of control over polymer networks as the degree of association, degree of branching, and distance between crosslinks (if present) can all be tuned by modifying the

S

spacers chemically or by varying the hydrogen bonding functionality. Also, the sequence of hydrogen bond donor and acceptor sites in multiple hydrogen bonded repeat units has a marked effect on K_{dim}, the rate of dimerization. High-purity monomers must be used in preparing supramolecular polymers because monofunctional impurities or unreacted monomer caps the growing polymer chain. However, high Dp values are only obtained at high monomer concentrations [7].

Despite the variety of supramolecular polymers reported in the literature, much of the early emphasis in the field was on demonstrating that hydrogen bonding arrays formed as anticipated rather than investigating the resulting assembly's suitability for use as a novel material. Successfully exploiting the principles of molecular assembly offers the potential to give rise to novel polymeric materials, and supramolecular polymers show promise across a broad range of emerging applications, as will be discussed later. Here, the discussion will be concentrated on two representative classes of supramolecular polymer commonly encountered in the literature: benzoic acid/pyridyl complexes and self-complementary ureidopyrimidinones. Many other systems have also been reported and have been reviewed in detail [6, 8–10].

Liquid Crystalline Hydrogen Bonded Supramolecular Polymers

Figure 1 shows an early example of a supramolecular liquid crystalline polymer reported by Lenz and co-workers [11]. The development of liquid crystalline molecular assemblies stemmed from attempts to stabilize anisotropic phases of small molecules: increasing the axial ratio (length/diameter) of a liquid crystal improves the mesophase's stability, which could be achieved by synthesizing liquid crystals from small molecules using noncovalent interactions [6].

It is widely accepted that the first truly "supramolecular" polymer was an extended linear assembly composed of an equimolar mixture of
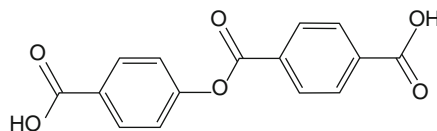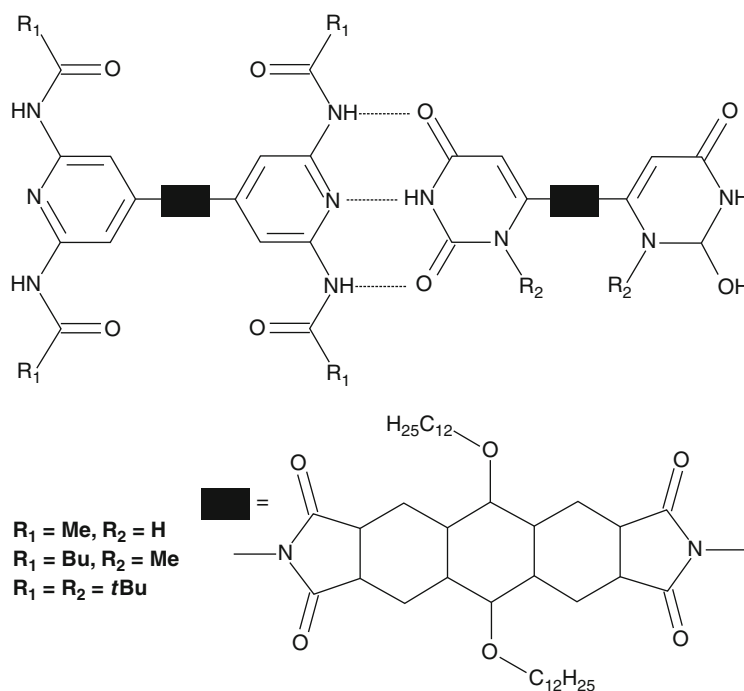

Supramolecular Polymers (Hydrogen Bonds), Fig. 1 Aromatic ester triad mesogen capable of hydrogen bonding

2,6 diaminopyridine and uracil, derivatized to bear long aliphatic chains as shown in Fig. 2 [1, 12]. These associated via triple hydrogen bonding to yield the polymer. Though the individual components did not display liquid crystalline behavior, they stacked to produce a columnar hexagonal mesophase. The mechanism compared closely with that of base pairing in double-stranded DNA. Condensing these diaminopyridine and uracil groups with long-chain derivatives of tartaric acid gave complementary repeat units from which the assembly was formed. The assembly process brought about spontaneous resolution of the racemic mixture. Microscopy revealed that this supramolecular polymer had the aspect of a birefringent glue. If a film of the polymer was spread across a surface, it formed fibers, just as a conventional polymer would.

Unlike many of the liquid crystalline supramolecular polymers described in the literature, Lehn's adopts a well-defined structure, and no complications have been reported regarding its long-term stability. Furthermore, the final assembly is chiral, still a unique feature among supramolecular polymer liquid crystals. Subsequently, the same triple hydrogen bonding motif was used to synthesize supramolecular rigid rods (examples are shown in Fig. 3) which displayed polymeric characteristics and were found to be reasonably soluble in common organic solvents [1, 13]. However, to prepare useful quantities of these supramolecular polymers starting from commercially available reagents, 12 steps are necessary to produce both monomers shown in Fig. 2, with an overall yield of 25 %. Also, two-component systems such as these require exact stoichiometric quantities of both components for successful assembly, which can prove
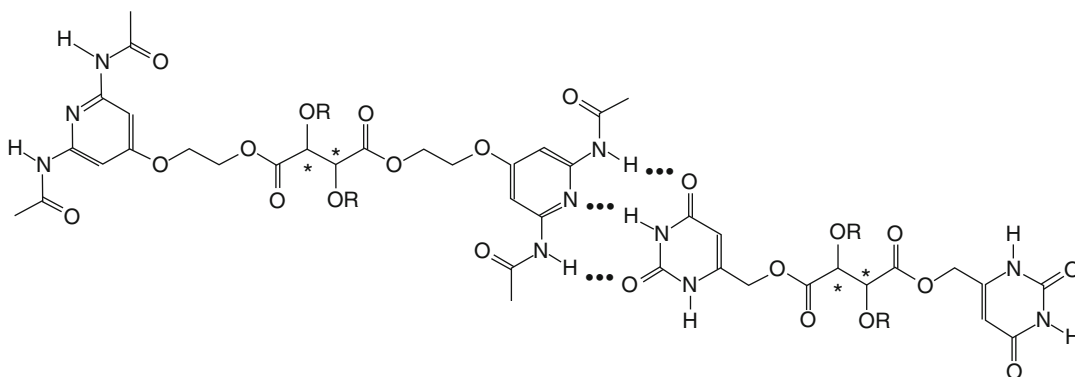
Supramolecular Polymers (Hydrogen Bonds), Fig. 2 Lehn's diaminopyridine-uracil molecular assembly. The hydrogen bonds between repeat units are indicated by *dotted lines* and chiral centers are marked *
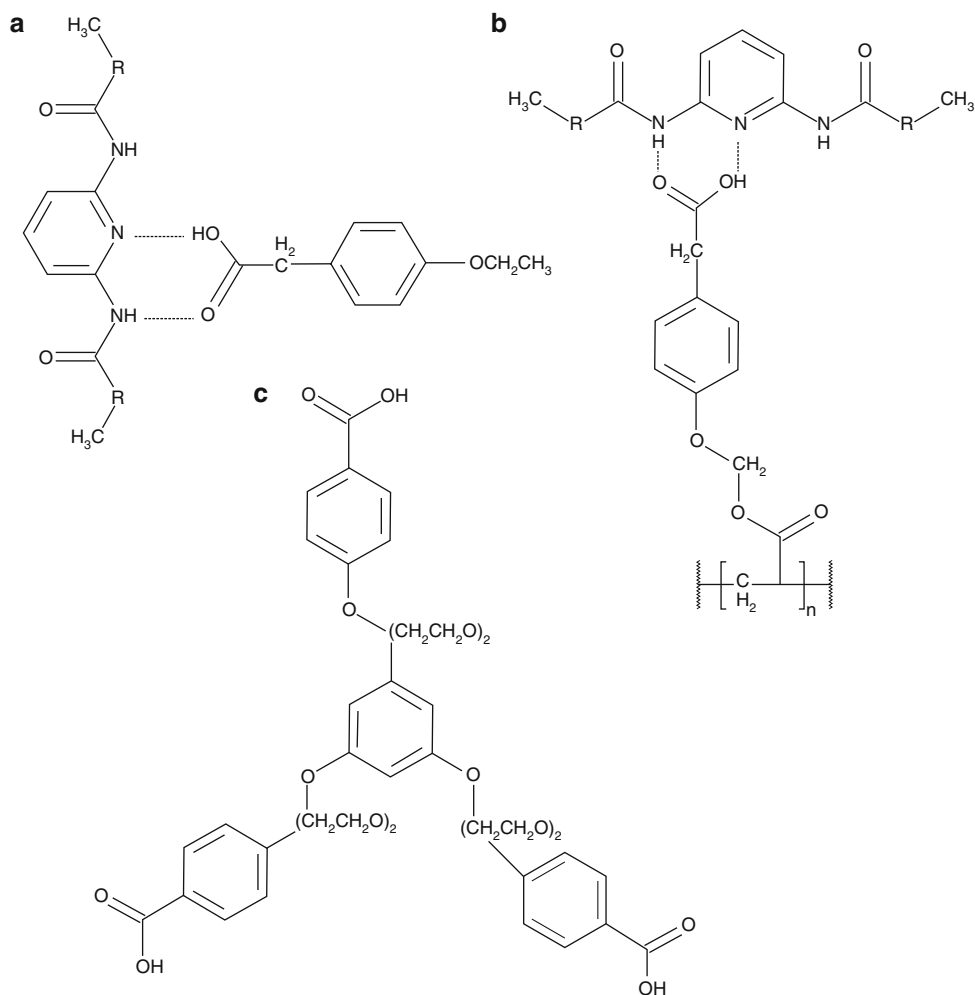

Supramolecular Polymers (Hydrogen Bonds), Fig. 3 Supramolecular rigid rods. The hydrogen bonds between repeat units are indicated by *dotted lines*

a R_1 = Me, R_2 = H
b R_1 = Bu, R_2 = Me
c R_1 = R_2 = tBu

difficult to prepare in practice. As a result, simpler routes to prepare polymers with comparable properties were sought.

Several groups have studied hydrogen bonded complexes involving benzoic or carboxylic acid and pyridine. Because these complexes can form no more than two hydrogen bonds between repeat units, the resulting polymers inevitably depend on liquid crystallinity to align the repeat units so that bonding can occur. In many cases, small

molecules have been grafted onto a conventional preformed polymer main chain via hydrogen bonds to give, or modify, liquid crystalline properties. Of greater relevance to this entry are those systems which use hydrogen bonding alone to form the polymer main chain.

Benzoic acid and 2-aminopyridine functionalities (without ortho-substituents) were used to prepare 1:1 complexes via double-hydrogen bonds, as illustrated by the structures shown in
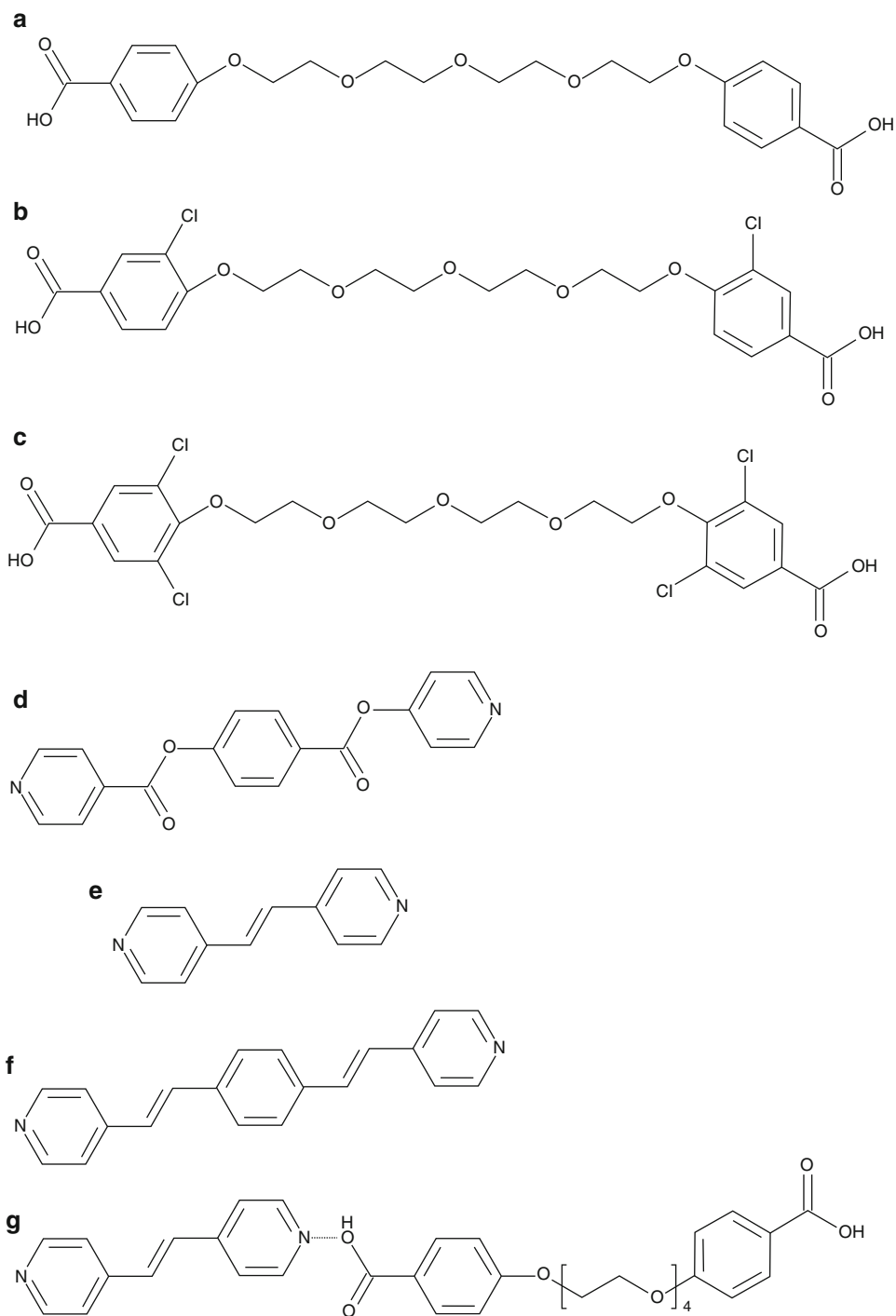
Supramolecular Polymers (Hydrogen Bonds), Fig. 4 Liquid crystalline polymers prepared by Kato and Frecht – 1:1 liquid crystalline complex (**a**), side chain liquid crystalline complex (**b**), and network polymer (**c**)

Fig. 4 [14]. These 1:1 complexes exhibited sharp melting transitions, indicating that they behaved as single molecules, and displayed liquid crystalline mesophases not observed for the individual components. Even network polymers were obtained by the self-assembly of a star-shaped repeat unit with small bifunctional molecules such as 1,2-di(4-pyridyl)ethylene (Fig. 4c).

Using similar chemistry, Lee and co-workers prepared liquid crystals by reacting molten dipyridine and dicarboxylic acid monomers (Fig. 5) in the isotropic phase [15–17]. At low Dp and high temperatures, such main chain liquid crystals tend to crystallize as oligomers. To overcome this, lateral substitution of the polymer chain retarded crystallization by restricting close packing of adjacent chains. This allowed hydrogen bonding to occur and a mechanically coherent chain to form as the material cooled to ambient temperature. Substituted polymers prepared from 1:1 stoichiometric mixtures of dipyridine and dicarboxylic acid monomers gave a glassy nematic phase from which fibers could be drawn. For a more detailed discussion of such liquid crystalline supramolecular polymers, the reader is referred in particular to the reviews by Zimmerman et al. [6] and Armstrong and Buggy [9].

a

b

c

d

e

f

S

g

Supramolecular Polymers (Hydrogen Bonds), Fig. 5 Bis-benzoic acid (**a**–**c**) and dipyridl (**d**–**f**) functionalized monomers that form liquid crystals via single hydrogen bonds, yielding 1:1 liquid crystalline association complexes such as tetraethyleneglycoxybis (4-benzoic acid):1,2-di(4-pyridyl)ethylene (**g**). "Carbuncle monomers" **b** and **c** bear chlorine side groups that retard crystallization

Quadruple Hydrogen Bonded Self-Complementary Ureidopyrimidinone Polymers

Among attempts to develop molecular assemblies which display polymeric behavior without the need for liquid crystallinity, the family of materials originally reported by Meijer and co-workers [18–20] all based on the ureidopyrimidinone (UPy) hydrogen bonding motif have proven especially successful. The UPy function is more readily synthesized than the majority of hydrogen bonding motifs, and, because it is self-complementary, the problem of preparing stoichiometric mixtures discussed earlier is avoided. The pattern of hydrogen bond donor and acceptor sites in these dimers is donor-donor-acceptor-acceptor (DDAA), which is a particularly stable arrangement because it gives rise to fewer repulsive secondary interactions between adjacent donor/acceptor pairs. Representative examples of these materials are shown in Fig. 6; note that the aspect of the polymer depends on the choice of spacer between the UPy functions. For example, whereas a hexamethylene spacer (Fig. 6a) results in a crystalline solid, substituting the spacer with methyl groups (2,2,4/2,4,4 trimethylhexane, Fig. 6b, c) yields a transparent solid that displayed elastic properties at room temperature. A trifunctional spacer (Fig. 6d) yielded a two-dimensional network structure.

Ureidopyrimidinones exhibit keto-enol tautomerism, and the dimers may adopt at least three crystal structures, all with similar dimer geometry [18, 19]. All three crystal structures pack in layers, differing mainly in the position of the layers with respect to each other. These dimers have a high k_{dim} ($>10^6$ M^{-1} for 6-methyl dimer) and exist in solution as a single tautomer. k_{dim} is a function of the solvent; nonpolar solvents such as chloroform favor hydrogen bonding more than apolar solvents such as dimethyl sulfoxide (DMSO). Crystallographic studies of annealed UPy compounds suggest that this tautomerism should have no adverse effects on their material properties. High-temperature solid-state 1H nuclear magnetic resonance spectroscopy confirmed that the UPy motif's hydrogen bonding remains unchanged until the onset of molecular motion at 140 °C, confirming this species' high thermal stability [21].

Towards Industrial Supramolecular Polymers

Supramolecular polymers such as those discussed here can adjust quickly to changing environmental stresses, thanks to their selective, reversible bonding. For example, ureidopyrimidinones exhibit low melt viscosity typical of organic compounds at elevated temperatures but display the mechanical properties of conventional polymers upon returning to room temperature [22]. Both acid/bipyridyl- and UPy-based supramolecular polymers have been found to remain thermally stable to temperatures exceeding those of conventional engineering polymers, but, once thermal degradation begins, it proceeds rapidly [23, 24].

As previously mentioned, trifunctional repeat unit 6D has been reported to self-assemble into a network (or "hyperbranched") polymer structure [25]. The resulting polymer was found to be transparent and exhibited a glass transition (T_g) at −70 °C but was too brittle to allow dynamic mechanical thermal analysis (DMTA) to be performed. As might be expected, the network did not exhibit typical polymer rheology; the change in storage modulus vs. frequency indicated that this supramolecular polymer network relaxed completely – which is not possible for covalently bonded polymer networks. Also, the supramolecular network's dynamic viscosity reached a plateau at low frequencies. These differences with respect to covalently bonded polymer networks were explained by assuming that the hydrogen bonds between repeat units dissociated and then reformed to allow stress relaxation to occur at temperatures below T_g.

For such supramolecular polymers to be industrially useful, they must exhibit good mechanical and thermal properties and be synthesized using scalable chemistry and readily available starting materials. Starting from commercially available starting materials,
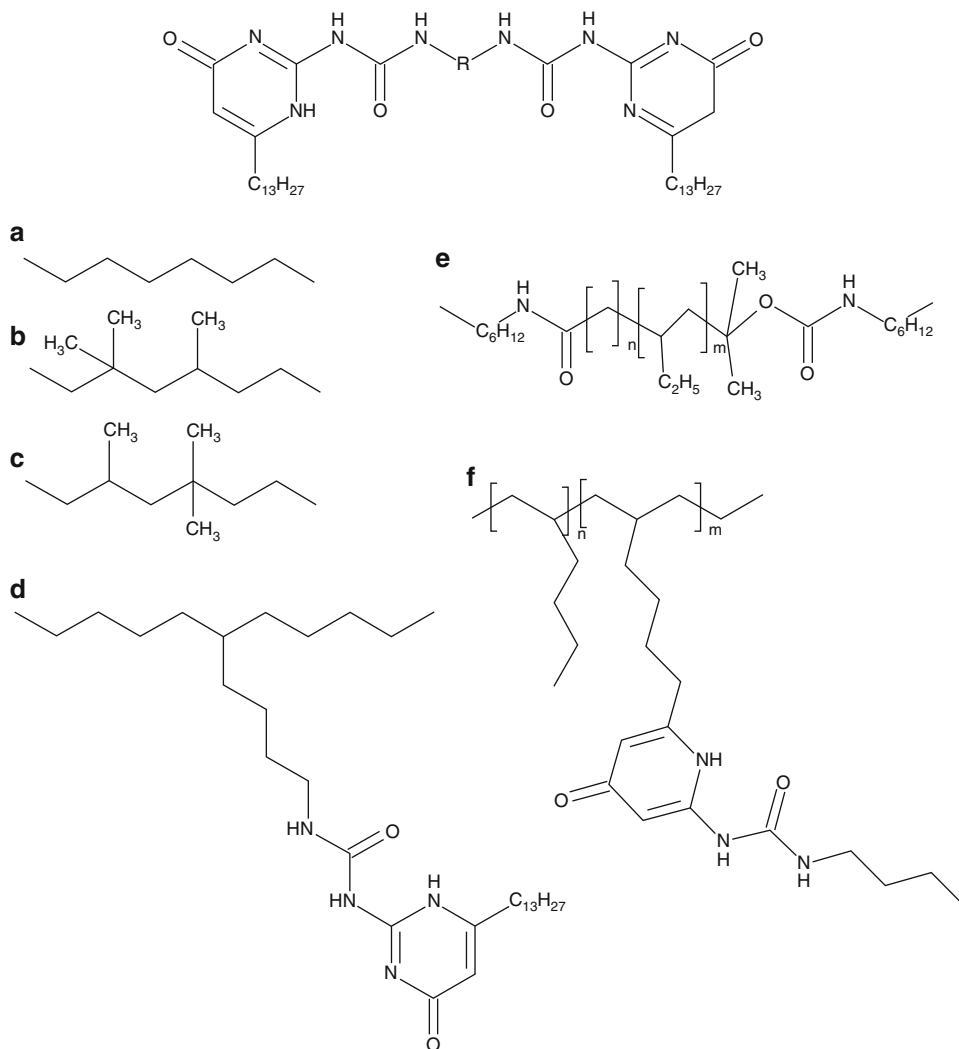
Supramolecular Polymers (Hydrogen Bonds), Fig. 6 Representative ureidopyrimidinone (*UPy*) supramolecular polymer structures: crystalline N^w,N^w-(1,6-hexanediyl)-bis-(2-ureido-6-tridecyl-4-[1H]-pyrimidininone) (**a**); elastomeric N^w,N^w-(2,2,4/2,4,4-trimethyl-1,6-hexanediyl)-bis-(2-ureido-6-tridecyl-4-[1H]-pyrimidinone) (**b/c**); trifunctional repeat unit bearing UPy groups (**d**); UPy-functionalized telechelic poly (ethylenebutylene) (**e**); UPy-functionalized poly (1-hexane) copolymer (**f**)

Folmer et al. [26] grafted the UPy motif to various telechelic (i.e., end-group functionalized) polyol oligomers (e.g., Fig. 6e) which assembled into chains of high virtual molecular weight. The synthesis has been successfully scaled up to produce kilogram-scale batches in good yield [27]. The telechelic UPy-functionalized repeat unit self-assembled to give a fully amorphous clear elastic solid which formed highly viscous solutions in chloroform. The resulting polymer's rheological properties were similar to those of the supramolecular network polymer prepared from trifunctional repeat unit 6D. It displayed very strong temperature and frequency dependence; for example, its zero-shear melt viscosity decreased fourfold between 40 °C and 50 °C. Whereas the precursor telechelic oligomers were viscous liquids or waxy solids, the UPy-functionalized oligomers formed supramolecular polymers that displayed typical

elastomeric properties. For example, dilute solutions of 6E in chloroform were highly viscous, and it formed elastic solids. In contrast, a low-molecular-weight homopolymer analogue displayed tensile properties typical of a viscous liquid. Both 6E and the homopolymer exhibited similar behavior at high molecular weight; these differences were attributed to the increased intermolecular interaction of the longer polymer chains. Similarly, Coates and co-workers [28] synthesized a polyolefin copolymer (Fig. 6f) with a random branched architecture bearing ~2 % UPy side chains that acted as reversible cross-links.

In recent years, the ureidopyrimidinone chemistry has been commercialized by SupraPolix, a joint venture between DSM and Eindhoven Technical University to apply the approaches discussed here to self-healing polymers and coatings [22, 29]. In principle, a wide range of synthetic and bio-based polymers can be functionalized with ureidopyrimidinone groups, resulting in comparable temperature-, concentration- and frequency-dependent properties as described for Fig. 6d, e above. Biocompatible hydrogels for drug delivery based on UPy-modified poly(ethylene glycol) that forms transient networks which form nanoscale micelles in solution have also been investigated for use in drug delivery applications [30].

The principle of self-assembly via hydrogen bonding has also been exploited to enhance conventional polymers, leading to useful improvements in their material properties. For example, urethane polymers have also been reported that exploit the principles of supramolecular polymer chemistry to promote atomic interaction between chains that allow control of crystallization behavior and chain flexibility. These are of particular importance in controlling the properties of linear thermoplastic materials [31]. Recently, the self-healing ability of supramolecular polyurethane coatings, in which up to 25 % of the covalent bonds were substituted with hydrogen bonds, was investigated. These coatings were shown to exhibit partial self-healing

of scratches in the coating after thermal treatment, to restore the barrier properties of the coating [32]. Indeed, considering the ease of synthesis and processing offered by hydrogen bonded supramolecular polymers with the valuable properties of the resulting materials, it can only be a matter of time before this novel class of polymers achieves their first successful commercial applications.

Related Entries

- ▶ Calixarenes-Based Supramolecular Polymers
- ▶ Crown Ethers-Based Supramolecular Polymers
- ▶ Cucurbiturils-Based Supramolecular Polymers
- ▶ Cyclodextrins-Based Supramolecular Polymers
- ▶ Dendrimer-Like Star Branched Polymers
- ▶ Molecular Self-Organization
- ▶ Self-Assembly of Hyperbranched Polymers
- ▶ Self-Healing Polymers
- ▶ Supramolecular Hydrogels
- ▶ Supramolecular Network Polymers
- ▶ Supramolecular Polymers (Coordination bonds)
- ▶ Supramolecular Polymers (Host-Guest Interactions)
- ▶ Surfactant Assemblies (Micelles, Vesicles, Emulsions, Films, etc.), An Overview
- ▶ Synthesis and Self-assembly of Linear-Dendritic Hybrid Polymers

References

1. Lehn JM (1993) Makromol Chem Macromol Symp 69:1–17
2. Lehn JM (1995) Supramolecular chemistry. VCH, Weinheim
3. Lawrence DS, Jiang T, Levett M (1995) Chem Rev 95:2229–2260
4. Ciferri A (ed) (2005) Supramolecular polymers, 2nd edn. CRC Press, Durham
5. Steed JW, Atwood JL (2009) Supramolecular chemistry, 2nd edn. Wiley, Chichester
6. Zimmerman N, Moore JS, Zimmerman S (1998) Chem Ind 604–610

7. Beijer FH (1998) Cooperative multiple hydrogen bonding in supramolecular chemistry. PhD thesis, Eindhoven Technical University
8. Sherrington DC, Taskinen KA (2001) Chem Soc Rev 30:83–93
9. Armstrong G, Buggy M (2005) J Mater Sci 40:547–559
10. Shimizu LS (2007) Polym Int 56:444–452
11. Hoshino H, Jin JI, Lenz RW (1984) J Appl Poly Sci 29:547–554
12. Fouquey C, Lehn JM, Levelut AM (1990) Adv Mater 5:254–257
13. Kotera M, Lehn JM, Vigneron JP (1995) Tetrahedron 51:1953–1972
14. Kato T (1996) Supramol Sci 3:53–59
15. Alexander C, Jariwala CP, Lee CM, Griffin AC (1994) Macromol Symp 77:283–294
16. Lee CM, Jariwala CP, Griffin AC (1994) Polymer 35(21):4550–4554
17. Lee CM, Griffin AC (1997) Macromol Symp 117:281–290
18. Sijbesma RP, Beijer FH, Brunsveld L, Folmer BJB, Hirschberg JHK, Lange RFM, Lowe JKL, Meijer EW (1997) Science 278:1601–1604
19. Beijer FH, Sijbesma RP, Kooijman H, Spek AL, Meijer EW (1998) J Am Chem Soc 120:6761–6769
20. Sijbesma RP, Meijer EW (1999) Curr Op Colloid Interface Sci 4:24–32
21. Armstrong G, Alonso B, Massiotand D, Buggy M (2005) Magn Reson Chem 43:405–410
22. de Greef TFA, Meijer EW (2008) Nature 453(8):171–173
23. Armstrong G, Buggy M (2001) Mater Sci Eng C 18:45–49
24. Armstrong G, Buggy M (2002) Polym Intl 51:1219–1224
25. Folmer BJB (2000) New polymers based on the quadruple hydrogen bonding motif, Ph.D. thesis, Eindhoven Technical University
26. Folmer BJB, Sijbesma RP, Versteegen RM, van der Rijt JAJ, Meijer EW (2000) Adv Mater 12:874
27. Keizer HM, van Kessel R, Sijbesma RP, Meijer EW (2003) Polymer 44(19):5505–5511
28. Rieth LR, Eaton RF, Coates GW (2001) Angew Chem Int Ed 40(11):2153–2156
29. van Gemert GML, Peeters JW, Söntjens SHM, Janssen HM, Bosman AW (2012) Macromol Chem Phys 213:234–242
30. Dankers PYW, Hermans TM, Baughman TW, Kamikawa Y, Kieltyka RE, Bastings MMC, Janssen HM, Sommerdijk NAJM, Larsen A, van Luyn MJA, Bosman AW, Popa ER, Fytas G, Meijer EW (2012) Adv Mater 24:2703–2709
31. Ulrich H (2006) Urethane polymers. In: Kirk-Othmer encyclopedia of chemical technology, vol 25. Wiley, New York. doi:10.1002/0471238961.2118052021121809.a01.pub2
32. Deflorian F, Ross S, Scrinzi E (2013) Corros Eng Sci Technol 48(8):147–154

Surface Active Nanoparticles for Interfacial Catalysis

Hengquan Yang[1], Xia Rong[1] and Dayang Wang[2]
[1]School of Chemistry and Chemical Engineering, Shanxi University, Taiyuan, People's Republic of China
[2]Ian Wark Research Institute, University of South Australia, Mawson Lakes, SA, Australia

Synonyms

Aqueous reaction; Interface catalysis pickering emulsions

Definition

Due to the large reaction interface area, Pickering emulsions are emerging as a new platform to design a variety of aqueous reaction systems. The catalysis efficiency and selectivity can be significantly enhanced with the unique oil/water interface.

Background

Using water as reaction solvent is a long-standing goal in view of the fact that all reactions in living systems occur in water and of its unique properties such as low toxicity, noninflammability, low volatility, high heat capacity, and easy separation from most organics [1, 2]. In past decades, researchers have attempted to utilize water as reaction medium in place of organic solvents. Many important reactions such as hydrogenation, oxidation, hydroformylation, C–C coupling, Diels–Alder cycloadditions, Claisen rearrangements, and Fischer–Tropsch (F-T) synthesis have been carried out in water. Among these reactions, aqueous hydroformylation and selective hydrogenation of benzene to cyclohexene have been successfully applied in

S

industry. Moreover, it was found that several reactions, for example, Diels–Alder cycloadditions and Claisen rearrangements, showed much higher reaction efficiency in water than in organic solvents or solvent-free systems due to the unique properties of water. The asymmetric desymmetrization of meso-epoxides with amines showed a higher enantiomeric excess (ee) in water than in organic solvents. Such significantly positive influences have been attributed to the unique properties of aqueous phase systems such as the hydrophobic effects and hydrogen bonding interactions. These achievements sufficiently underline that water is an appealing reaction solvent for practical applications.

Since most organics have poor solubility in water, the aqueous reaction systems usually involve at least two phases: an organic phase (oil) and an aqueous phase. In the presence of solid catalysts, the reaction consists of three phases (oil–water–solid) or even four phases (gas–oil–water–solid). The phase separation in the reaction systems gives rise to high mass transport resistances. As a consequence, most of aqueous reactions proceed sluggishly and the reaction efficiency is often much lower than the reaction in organic solvents. To address this obstacle, cosolvents, surfactants, and phase transfer catalysts are added into the reaction systems to mitigate the mass transport resistance. Although these methods can improve the reaction efficiency, extra procedures are required to separate these additives from the final products.

It is well known that submicron or micronsized solid particles with a proper wettability prefer to attach to the oil/water interface, leading to Pickering emulsions [oil in water (o/w) or water in oil (w/o)] [3–6]. Such particles are interfacially active like surfactant molecules. Should the surfaces of these particles be catalytically active, the prepared as-Pickering emulsion systems are envisioned as oil–water–solid three-phase catalytic systems. Although Pickering emulsions have been recognized about a century ago [7, 8], their exploitation for catalysis commences only in recent years. The recognition of the potential of Pickering emulsions in catalytic application brings new opportunities to

green catalysis because they can exhibit large oil/water interface areas and thereby significantly reduce the mass transfer resistances. Recent 5 years have witnessed the successful adoption of Pickering emulsions in diverse aqueous reactions. Novel catalysis effects, arriving from Pickering emulsions, are unraveled, which are hardly achieved for catalysis in organic or conventional organic/aqueous biphasic reaction systems.

Pickering Emulsion Catalysis

Aqueous Pickering Emulsion Catalysis

Hydrogenation

Hydrogenation is a widely used catalysis reaction in laboratory and industry. The use of water as hydrogenation medium is preferable because it can effectively absorb the heat released by hydrogenation besides its green contents.

The pioneering works of Pickering emulsion catalysis are done by Resasco's group [9]. Oxide nanoparticles are usually hydrophilic while carbon nanotubes are hydrophobic. Resasco et al. blended these two components together to form hybrid nanocomposites, in which the hydrophilic–hydrophobic balance is dependent on the composition. After depositing palladium onto as-prepared hybrid nanocomposites, they fabricated interfacially active catalysts for hydrogenation. By simply changing the formulations of the composites, two interfacially active catalysts $Pd/SiO_2/CNT$ and $Pd/CNT/MgO$ were obtained, in which Pd nanoparticles were positioned on the hydrophilic part and hydrophobic part, respectively. With decalin as oil phase, Pickering emulsion systems were formulated in the presence of these interfacially active catalysts, as shown in Fig. 1. In hydrogenation of vanillin (4-hydroxy-3-methoxybenzaldehyde) that is a common component of pyrolysis oil derived from the lignin fraction, $Pd/SiO_2/CNT$ gave higher reaction efficiency than the commercial Pd/C catalyst. The chemoselectivity of this reaction was significantly varied with the reaction conditions such as reaction temperature and reaction time.
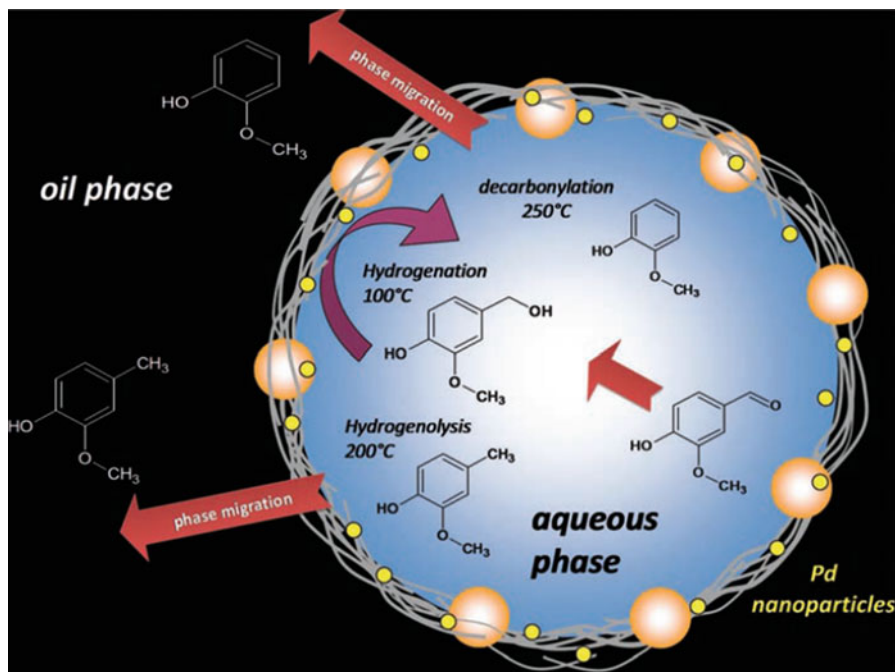
Surface Active Nanoparticles for Interfacial Cataly-sis, Fig. 1 Schematic illustration of the reactions taking place at the water/oil interface in solid-stabilized em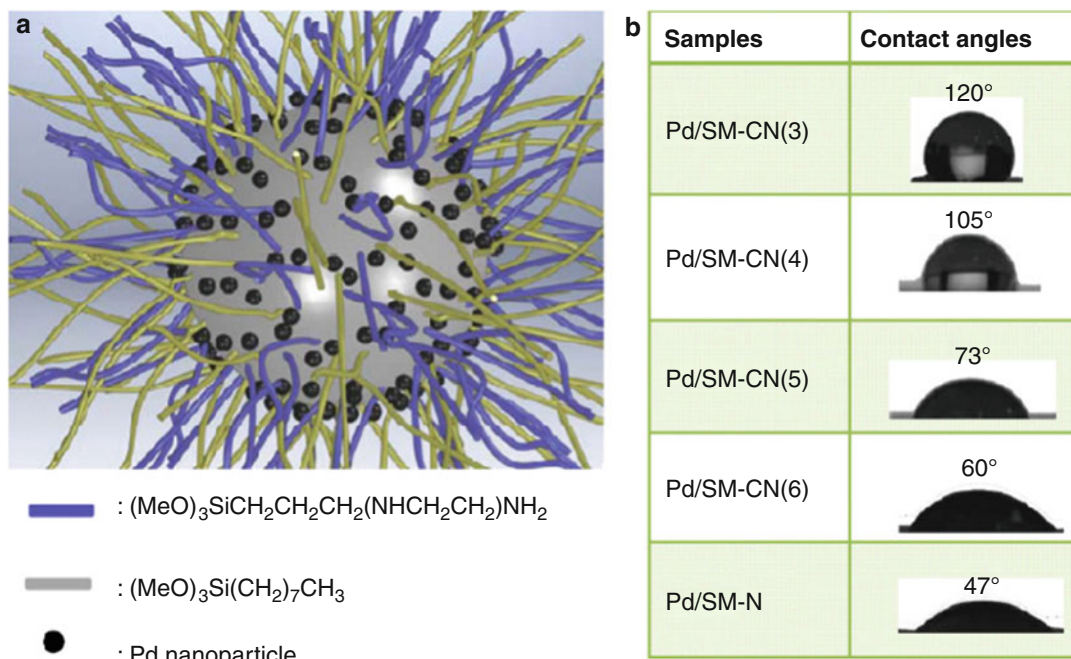ulsions. Depending on the reaction temperature, the prevailing reactions are hydrogenation, hydrogenolysis, or decarbonylation, and depending on the relative solubilities, the products remain in the aqueous phase or migrate to the oil phase (Copyright 2010 Science)

The changes are different from the results obtained in the conventional monophasic reaction. These effects were partly explained by the fact that in the Pickering emulsion catalysis system, driven by relative solubility change, the intermediate products migrated from water droplets to the continuous phase (oil), and the catalysis reaction is then stopped, because the catalytically active Pd nanoparticles are selectively located on the hydrophilic parts. This unique feature of Pickering emulsion catalysis was further highlighted by comparison with the single aqueous phase system. The Pickering interface catalysis gave high selectivity, which was not obtained with the single-phase reaction.

More interestingly, the Pickering emulsion catalysis system can promote a tandem reaction sequence [9]. The concept was demonstrated by the cascade of aldol condensation and hydrogenation in the presence of Pd/CNT/MgO hybrid catalysts. MgO acted as a hydrophilic part whereas CNT served as a hydrophobic part where Pd nanoparticles were deposited. As a base catalyst, MgO promoted the aldol condensation of 5-methylfurfural with acetone. Due to the carbon chain increase and functionality change during the reaction, the resultant intermediate4-(5-methylfuran-2-yl)buten-2-one became relatively hydrophobic, in propensity to shift from the water phase to the oil one. This shift triggered the second step hydrogenation reaction, which is catalyzed by the Pd nanoparticles deposited on the hydrophobic carbon nanotube.

This type of hybrid catalysts was further extended to the single-walled (SWCNTs), multiwalled carbon nanotubes (MWCNTs), and micrographitic platelets that were fused to silica or alumina particles [10–12]. These interfacially active hybrid catalysts can stabilize high internal phase Pickering emulsions with the emulsion droplets less than 40 μm. In the hydrogenation of phenanthrene, glutaraldehyde, and benzaldehyde and the oxidation of tetralin, these interfacially active hybrid catalysts also gave

a

: (MeO)$_3$SiCH$_2$CH$_2$CH$_2$(NHCH$_2$CH$_2$)NH$_2$

: (MeO)$_3$Si(CH$_2$)$_7$CH$_3$

: Pd nanoparticle

b

Samples	Contact angles
Pd/SM-CN(3)	120°
Pd/SM-CN(4)	105°
Pd/SM-CN(5)	73°
Pd/SM-CN(6)	60°
Pd/SM-N	47°

Surface Active Nanoparticles for Interfacial Catalysis, Fig. 2 The proposed structure of Pd/SM–CN(x) and their surface wettability. (**a**) The proposed structure; (**b**) the images of water contact angles and the measured values (Copyright 2014 Wiley-VCH)

higher conversion and better selectivity in comparison with the reactions that occurred in the single phase.

Yang's group has developed interfacially active silica-based catalysts. Silica microparticles were modified with a mixture of triamine silane and octylsilane via silylation [13]. The resulting particles are denoted as SM-CN(x), where x represents the molar fraction of the triamine silane. The air–water–solid three-phase contact angle of silica was varied from 47° to 120°, depending on x (Fig. 2). The subsequent deposition of Pd nanoparticles onto the functionalized silica particles led to the hydrogenation catalysts. With these catalysts, Pickering emulsions were formulated with various olefins as oil (without need for extra organics). Depending on the surface composition of silica particles, the sizes of the resulting Pickering emulsion droplets were changeable in a wide range.

Although the as-prepared Pd-decorated silica particle catalysts displayed almost equal catalysis activity in single organic phase, they showed remarkably different catalytic activities in Pickering emulsion systems. Their catalysis efficiency was closely dependent on the emulsion droplet sizes. Small droplets led to high catalysis efficiency. The maximum catalysis efficiency was obtained with Pd/SM-CN(5) catalyst, 4.2 times higher than that of the conventional biphasic system. The dependence of catalysis efficiency for the Pickering emulsion systems on the stirring input power is remarkably different from that of the conventional biphasic system. The catalysis efficiencies increased with increasing stirring input power, and notably, the catalysis efficiency of the Pickering emulsion systems was always much higher than that of the conventional biphasic system. A much lower stirring input power was found sufficient for the Pickering emulsion systems to reach the maximum catalysis efficiency in comparison to the conventional biphasic system. Furthermore, the catalysis efficiency slightly increased with the catalyst amount in Pickering emulsion systems. In contrast, the catalysis efficiency usually decreased

with increase of the catalyst amount in the conventional biphasic system. These comparisons underline the fundamental difference in the reaction nature between Pickering emulsion and conventional biphasic reaction systems.

TiO$_2$-based and mesoporous silica-based interfacially active catalysts have been developed for the hydrogenation in Pickering emulsion systems by Yang's group. A commercial TiO$_2$ was first loaded with Pt nanoparticles, followed by modification with $(CH_3O)_3SiCH_3$ for hydrophobization, leading to interfacially active Pt/TiO$_2$–C catalysts. The catalysis efficiency in the Pickering emulsion systems stabilized with Pt/TiO$_2$–C catalysts was much higher than that of the conventional biphasic system with Pt/TiO$_2$ catalyst, 61 % conversion in the former case versus 25 % in the latter. With a modified delayed condensation method, mesoporous silica nanosphere-based Pd/MSN–C catalysts were synthesized. The Pickering emulsion systems stabilized with Pd/MSN–C exhibited 4.8 times higher catalysis efficiency than the conventional organic/aqueous system bearing Pd/MSN (Pd was supported on nonfunctionalized MSNs).

Oxidation and Epoxidation

Qiu et al. prepared interfacially active Ru-decorated carbon nanotubes, denoted as Ru/CNT [14]. The catalytic activity of Ru/CNTs in pure water was much higher than that in toluene, but the main product is benzoic acid. Using toluene as solvent, however, the selectivity to produce benzaldehyde is higher than that in water. In the toluene/water biphasic system, Ru/CNT was observed to self-assemble at the surfaces of water droplets and thus stabilize Pickering emulsions. The catalytic activity of Ru/CNTs in the Pickering emulsion was significantly enhanced in comparison to the toluene system, and the selectivity for benzaldehyde production is much higher than that obtained in water. As displayed in Fig. 3, the large interfacial area of the emulsion droplets also favored the quick mass transfer of intermediate molecules between the dispersed phase and continuous phase. The benzaldehyde is more soluble in toluene than benzyl alcohol. Once being formed, the
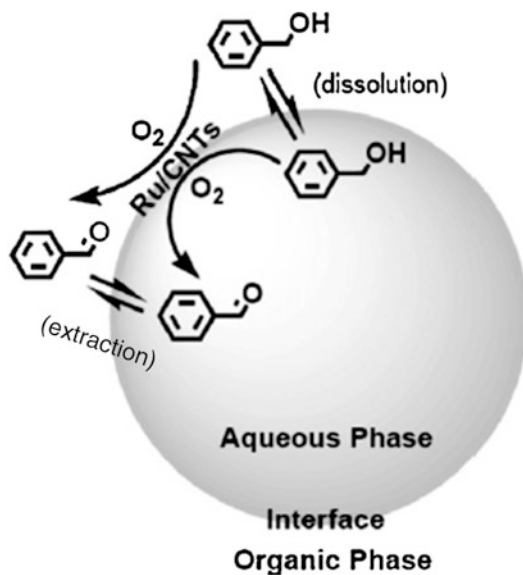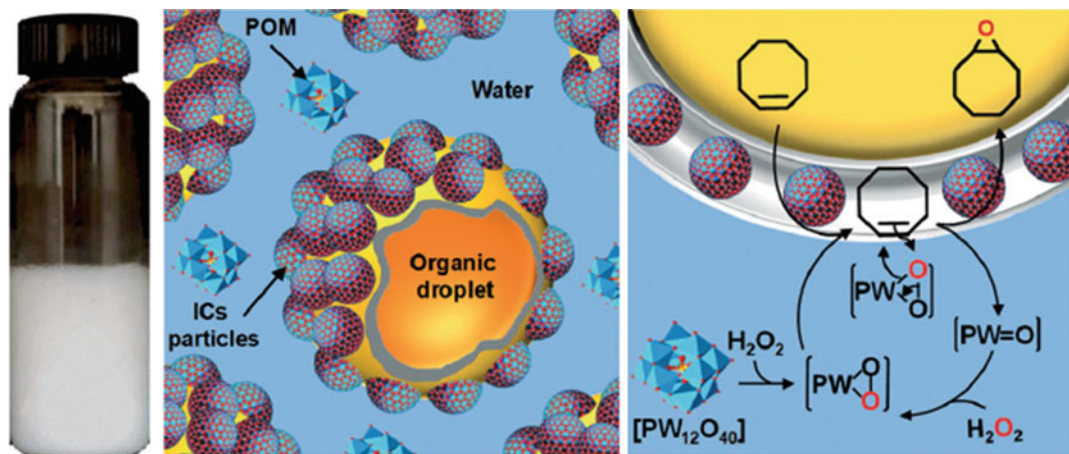

Surface Active Nanoparticles for Interfacial Catalysis, Fig. 3 Schematic model of Pickering emulsion reaction system for the selective oxidation of benzyl alcohol to benzaldehyde over Ru/CNTs (Copyright 2010 Elsevier)

intermediate benzaldehyde is readily transferred from the aqueous phase to the organic phase, avoiding further oxidation.

Qiu et al. prepared interfacially active catalyst Ru/CNT–TiO$_2$ nanohybrids [15]. The Pickering emulsions stabilized by the resulting nanohybrids could be altered from the oil/water (o/w) type to the water/oil (w/o) type by changing the CNT content in the nanohybrids. When as-prepared Pickering emulsions were applied for aerobic oxidation of benzyl alcohol to benzaldehyde, the reaction selectivity was as high as 99 %, while the conversion depended greatly on the chemical nature of the catalysts, which gradually increased with the CNT content in the supports. The conversions of benzyl alcohol over Ru/CNT–TiO$_2$-60 and Ru/CNT–TiO$_2$-75 are above 95 %, much higher than that over Ru/TiO$_2$ and Ru/CNT catalysts.

Nardello-Rataj and coworkers prepared interfacially active polyoxometalate (POM) nanoparticles by electrostatically coupling $[PW_{12}O_{40}]_3$ anions to alkyltrimethyl ammonium cations, which is soluble neither in water nor in organic solvents [16]. These hybrid nanoparticles

Surface Active Nanoparticles for Interfacial Catalysis, Fig. 4 Proposed mechanism for eco-friendly catalytic epoxidation in 1/water/b-CD Pickering emulsions (Copyright 2013 Wiley-VCH)

could stabilize water droplets in aromatic solvents to form Pickering emulsions. In the case of epoxidation of cyclooctene, the conversion reached to 98 % after 3 h, which was much higher than obtained in the conventional biphasic system. Cyclodextrin-stabilized Pickering emulsion systems were developed and successfully applied to epoxidation, as shown in Fig. 4 [17]. In the presence of hydrogen peroxide as a green oxidant and $[Na]_3 [PW_{12}O_{40}]$ as a catalyst, a high reaction efficiency was obtained for the epoxidation of olefins, organosulfurs, and alcohols. These reactions could proceed at competitive rates (up to 400 h^{-1}) with straightforward separation of the phases by centrifugation or heating. In comparison with immobilization on silica, this strategy does not require multiple synthetic steps.
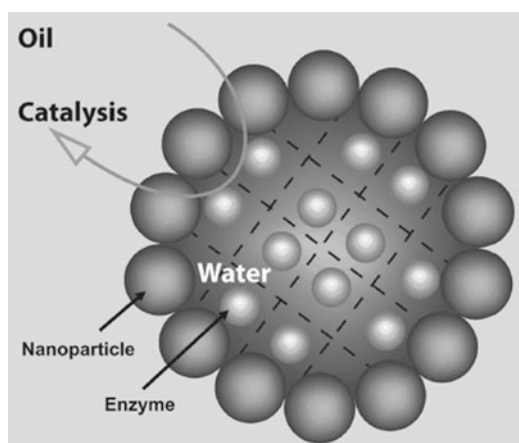
Fischer–Tropsch Synthesis

Fischer–Tropsch synthesis (FTS) is an important reaction to produce predominately aliphatic straight-chain hydrocarbons from syngas (CO/H_2). It has gained growing interest in recent decades because of the ever-increasing demands for sustainable and alternative sources.

By fusing the carbon nanotube (CNT) with $MgO–Al_2O_3$, Resasco et al. [18, 19] prepared interfacially active $Ru/CNT–MgO–Al_2O_3$ hybrid

catalysts and utilized them to stabilize Pickering emulsions for FTS. When a lower H_2 to CO ratio of 1.2 was used, a complex variety of products, consisting of alkanes, alkenes, and long-chain alcohols, were obtained. After 6 h of reaction at 200 °C and 600 psi of initial pressure, the CO conversion was 38.1 % at the catalyst concentration of 5 mg/mL. When a higher H_2 to CO ratio of 3.5 was used and the FTS reaction period was extended to 12 h, the predominant product was found to be alkanes. The CO conversion was determined to be 96 %, and liquid hydrocarbons represent more than 80 wt% of the total hydrocarbon products. In single decalin phase, the CO conversion in the single-phase system was drastically lower, i.e., only 34.1 % after 12 h, with almost no hydrocarbon products larger than C10. The formation of small water droplets dispersed in oil dramatically increases catalyst dispersion and interfacial surface areas. This facilitated the contact between the catalysts and the reactants and mass transport between the two phases. As a result, produced molecules can be continuously removed from one phase to the other in the Pickering emulsions based on the differences in solubility. In addition, the differences in solubility could enhance the tolerance against impurities and catalyst poisons in the syngas feedstock.

Biocatalysis

Biocatalyst enzymes typically prefer an aqueous reaction while many substrates are poorly soluble in water. Pickering emulsion can serve as an efficient platform to immobilize biocatalysts (Fig. 5) [20]. Lipase B from Candida antarctica (CalB) was confined within the Pickering emulsion droplets stabilized by hydrophobic SiO_2 nanoparticles. In the esterification of 1-octanol and octanoic acid, the specific activity of CalB confined in these liquid Pickering emulsion droplets (238.82 U mg^{-1}) is more than 300 times higher than that of native CalB in a liquid biphasic system (0.76 U mg^{-1}), as shown by Fig. 5. Although the specific activity of the confined CalB is slightly decreased after the emulsion droplets were gelled with agarose, the specific activity of the confined CalB is still 150 times higher than native CalB in a liquid biphasic system. This method was extended to immobilize an ordinary enzyme, benzaldehyde lyase, from Pseudomonas fluorescens Biovar I (BAL), that is extremely sensitive to the microenvironment change and tend to deactivate upon immobilization. After emulsification of their aqueous solutions in organic reaction media using hydrophobic silica particles, BAL shows an apparent activity of 7.73 μ mol h^{-1}, wh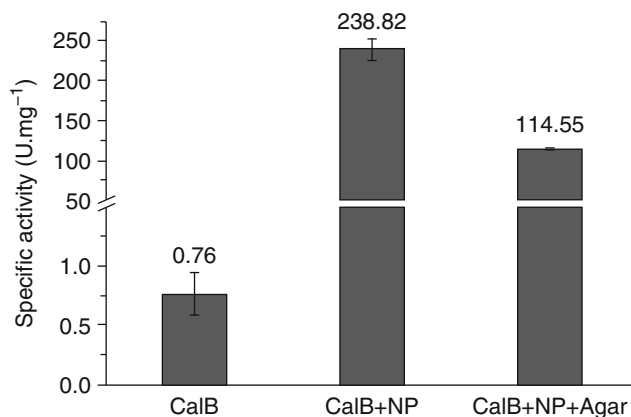ich is more than eight times higher than that of native BAL in the conventional biphasic system (Fig. 6). Such an enhancement of the catalytic performance of BAL has never been achieved with any other immobilization techniques to date. The significant enhancement of biocatalyst activity is a result of the considerably increased interfacial area of SiO_2 particle-stabilized enzyme droplets, which improves mass transfer and accessibility of the enzyme catalyst in the reaction system. Impressively, in opposition to the negative influence on the catalytic activity, it was observed that the jellification can maintain BAL at a comparably long operational stability, which is a key objective for any application of a vulnerable enzyme.

Using thermo-sensitive microgel particles as emulsifying agents, Richtering and coworkers present a conceptually novel approach to perform enzyme catalysis and recycle the enzyme [21]. As shown in Fig. 7, a two-phase mixture system for emulsification contains the organic (oil) phase loaded with organic substrates and the aqueous phase loaded with enzymes and microgel particles. After emulsification, the microgel particles are located at the droplet surface and the enzymes confined in the droplets can convert the substrate to the products at the interfaces. At the end of the reaction, the emulsion is broken by increasing the temperature above the volume phase transition temperature (VPTT) of the microgel, thereby leading to macroscopic phase separation. The organic phase containing the product can easily be separated while the aqueous phase still contains the enzymes and the microgel particles. Such reversible stabilization and breakage of emulsions allow simple product separation as well as recycling of biocatalyst and emulsifier.

Van Hest et al. employed polymersomes as colloidal nanoparticles to stabilize Pickering emulsions [22, 23]. Two different strategies were used to introduce CalB into the Pickering emulsion system, as shown in Fig. 8. One was to directly emulsify the aqueous solution of the enzymes by polymersomes. The other was to first encapsulate the enzyme into the lumen of polymersomes and then use as-prepared enzyme-loaded polymersomes to stabilize
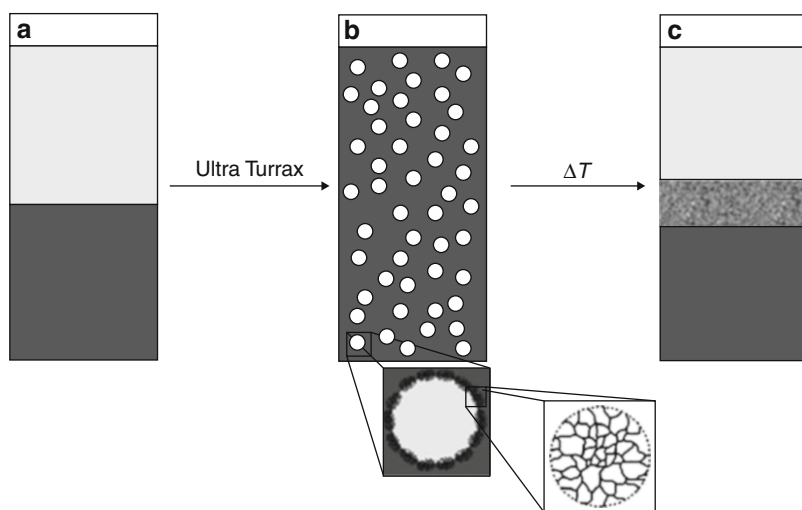

Surface Active Nanoparticles for Interfacial Catalysis, Fig. 5 A typical Pickering emulsion for enzymatic catalysis (Copyright 2011 Wiley-VCH)

S

Pickering emulsions. The catalytic performance of the two types of CalB-loaded Pickering emulsions was tested in esterification of 1-hexanol and hexanoic acid. A biphasic water/toluene system containing free CalB was utilized as control experiment for comparison. The conversion reached 80–90 % at equilibrium with both Pickering emulsions, while less than 25 % conversion was observed for the biphasic system under the same conditions. The specific activity achieved with the second method is higher than that with the first method (70.8 vs. 25.2 U mg^{-1}). For the second method, the CalB in polymersomes was distributed at the interface of the Pickering emulsion; the effective use of the enzyme was enhanced compared to the former case.

Another apparent advantage of polymersome-stabilized Pickering emulsions for biphasic enzymatic reactions is the ease of enzyme separation from products in the organic phase. The Pickering emulsions, stabilized by CalB-loaded polymersomes, were reused to catalyze the esterification of 1-hexanol and hexanoic acid for ten times without a significant loss in the specific activity.

Nonaqueous Pickering Emulsion Catalysis

Besides organic/aqueous biphasic systems, some reactions often involve organic/organic immiscible biphasic systems, for example, glycerol/organics that is common in the glycerol transformation and ionic liquid/organics. Like the
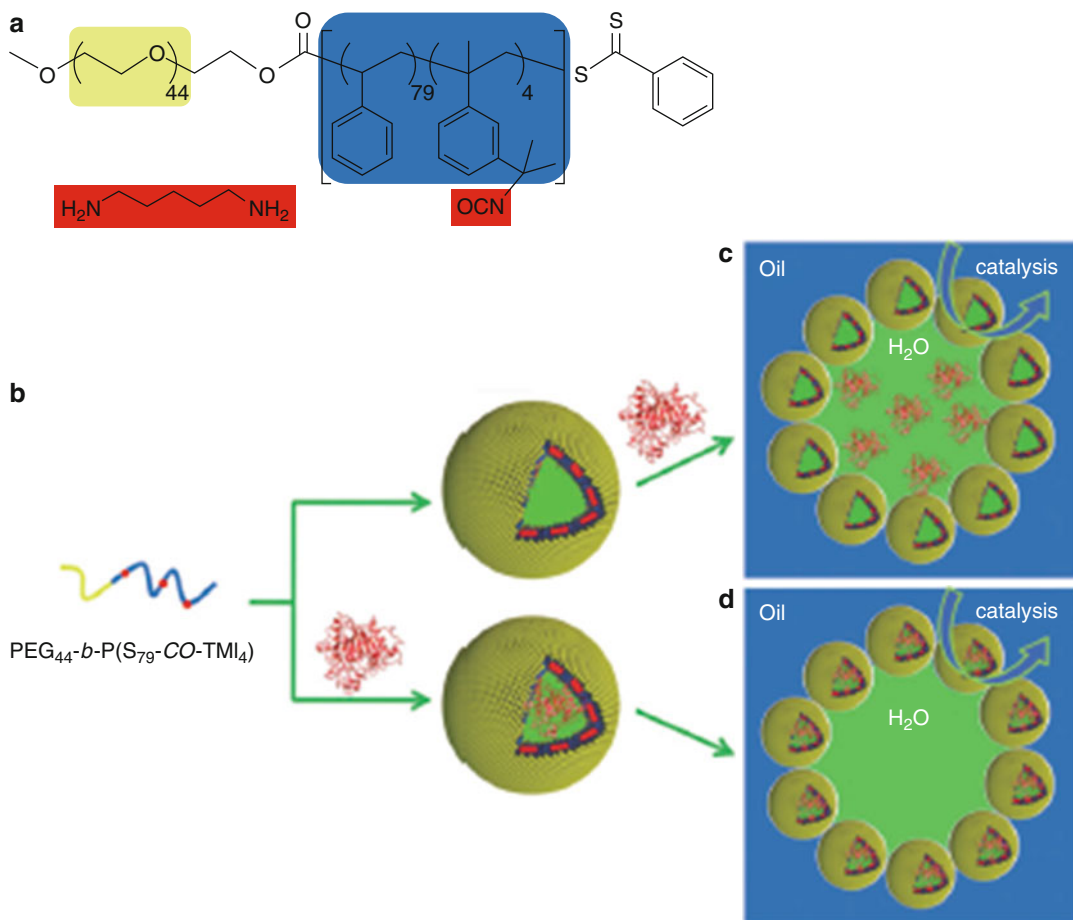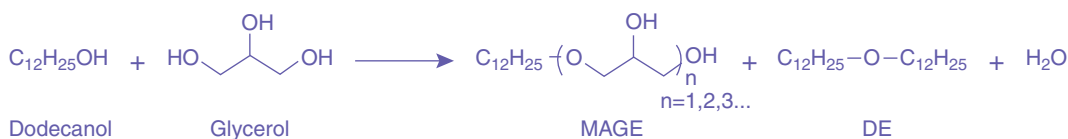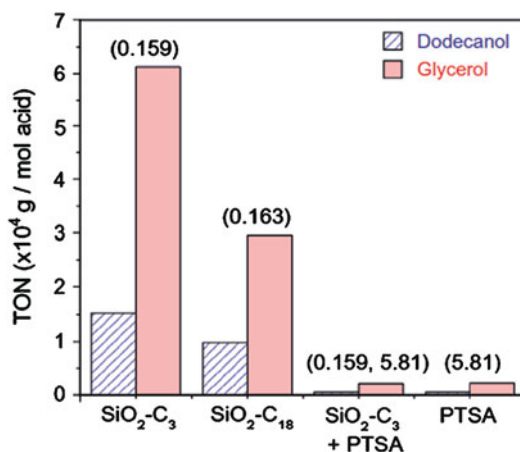
Surface Active Nanoparticles for Interfacial Catalysis, Fig. 8 (**a**) The chemical structure of the block copolymer of which the polymersome is constructed. (**b**) Representation of the cross-linking process to prepare stabilized polymersomes. Schematic representation of a Pickering emulsion with the enzyme in the water phase (**c**) or with the enzyme inside the polymersome lumen (**d**) (Copyright from 2012 Wiley-VCH)

organic/aqueous biphasic system, the organic/organic immiscible biphasic systems often have extremely high mass transfer resistance. Recently, Wang et al. have successfully tackled this issue through nonaqueous Pickering emulsions [24, 25]. By modifying silica nanoparticles with alkyl chains and alkyl sulfonic groups, they prepared interfacially active solid acid catalysts for etherification reaction of glycerol with dodecanol. The hydrophilic–lipophilic balance on the catalysts was tuned by the alkyl chains [methyl(TM), propyl (C3), and octadecyl (C18)]. These interfacial active nanoparticles showed much higher emulsifying ability for the glycerol/dodecanol mixture than the

conventional surfactants in terms of emulsion stability. The most stable emulsions were obtained with the silica particles with the surfaces decorated with methyl (TM) or propyl (C3) chains, denoted as SiO_2–TM and SiO_2–C3. The time evolution of the emulsion volume was very slow and kept almost constant after 500 min using 1 wt% particles for emulsification. Figure 9 summarizes the catalytic activity and selectivity of production of monododecyl glyceryl ether (MAGE1) and dodecyl ether (DE) in the glycerol/dodecanol Pickering emulsions stabilized by different solid catalysts. The yield is almost two times higher in SiO_2–C3-stabilized emulsions (2.9 %) than that via conventional homogeneous

S

Surface Active Nanoparticles for Interfacial Catalysis, Fig. 9 Pickering interfacial catalysis in the etherification reaction of glycerol with dodecanol for samples SiO$_2$–C3 and SiO$_2$–C18 together with control PTSA and SiO$_2$–C3 + PTSA systems. TON numbers computed from dodecanol and glycerol conversion and acidity (value in parentheses on top of the bars, in mmol/g). Experimental conditions: 150 °C, 16 h, 4:1 glycerol/dodecanol molar ratio, 5 mol% modified silica loading (4 wt%), with or without 0.1 eq. PTSA to dodecanol (Copyright 2014 Elsevier)

catalysis using *p*-toluenesulfonic acid (PSTA) (1.8 %). More interestingly, the turnover numbers (TON) were 30 times higher in SiO$_2$–C3-stabilized emulsion than that via conventional homogeneous catalysis using PTSA or the mixtures of SiO$_2$–C3 and PTSA.

Pickering Emulsions for Stirring-Free Heterogeneous Catalysis

Organic/aqueous biphasic reactions are commonly implemented for laboratory- and industry-scale synthesis. Due to the incompatibility of reaction reagents with either or both of bulk phases and the use of solid particles as catalysts in particular, vigorous stirring is required for better dispersion of the solid catalyst particles and sufficient mixing of the reactants to facilitate mass transport. However, vigorous stirring not only needs a large energy input but also causes catalyst particle fragmentation, because of repeated collision and persistent abrasion. Yang's group has

recently demonstrated that different from conventional biphasic systems, Pickering emulsions may enable catalytic reactions to be implemented in a stirring-free manner [26]. As shown in Fig. 10, a given organic/aqueous biphasic mixture is completely transformed into a Pickering emulsion, which can be envisioned as a stable three-dimensional network with huge interfacial areas where the catalysts are selectively reside. In this scenario, the whole reaction system is compartmentalized into micrometer-scaled domains. This significantly shortens the diffusion distance of both the reactant A molecules dissolved in the interspace of the adjacent emulsion droplets and the reactant B molecules dissolved in the interior of emulsion droplets, leading to sufficiently mixing on micrometer scale. This enables the reaction to proceed efficiently through the self-diffusion of reactant molecules.
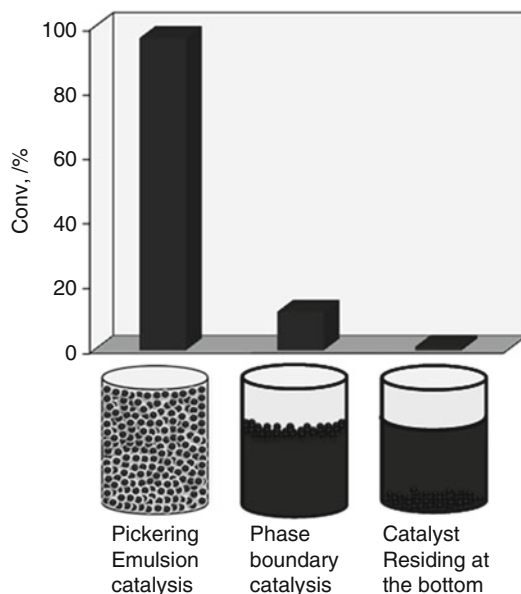
Yang et al. tested the catalytic performance of Pickering emulsions stabilized by Pd/SM–CN (5) in nitroarene reduction with NaBH$_4$ in the absence of stirring. Figure 11 shows that the
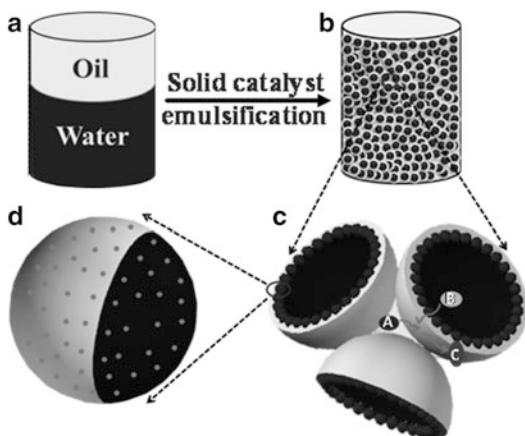
Surface Active Nanoparticles for Interfacial Catalysis, Fig. 10 Pickering emulsion reaction systems, where reactants A and B react to yield product C, catalyzed by catalysts located at interfaces. (**a**) A given organic/aqueous biphasic reaction. (**b**) The formulated Pickering emulsion phase in the presence of an interfacially active solid catalyst. (**c**) The reactant A and B molecules compartmentalized in the interspace of the adjacent droplets and in the droplet meet at the catalyst-covered interface through molecular self-diffusion. (**d**) One of the catalyst particles. The gray dots on the particle represent catalytically active centers. The catalyst particle is partly immersed in organics and water (Copyright 2014-VCH)

Surface Active Nanoparticles for Interfacial Catalysis, Fig. 11 Reactivity comparison of m-nitrotoluene reduction in three different systems in the absence of stirring. Reaction conditions: 2 mL of H_2O, 0.7 mL of toluene, 1 mmol of *m*-nitrotoluene, 2 mmol of $NaBH_4$, solid catalyst containing 1 μmol Pd. Pickering emulsion catalysis: Pd/SM-1 is dispersed at the surface of emulsion droplets. Phase-boundary catalysis: Pd/SM-1 is located at the two-phase boundary. Biphasic catalysis: Pd/SM-2 is deposited at the bottom of the reaction vessel (Copyright from Wiley)

conversion in the Pickering emulsion is one order of magnitude higher than that in phase-boundary catalysis and two orders of magnitude higher than that in the conventional biphasic system when the reaction is implemented without stirring. The catalyst mass-normalized efficiency increases as the droplet diameter decreases, underlining that the significantly shorter molecular diffusion distance is responsible for the high reaction efficiency of the Pickering emulsion system.

The reaction efficiency of the Pickering emulsion reaction systems implemented without stirring was also compared with those implemented under stirring and with conventional biphasic systems implemented under stirring. The reaction rates of the Pickering emulsion systems implemented in the absence and presence of stirring (800 rpm) are comparable, while the reaction in stirring-free Pickering emulsion systems proceeds faster than in conventional biphasic systems implemented under stirring. Only when conventional biphasic systems are used under

vigorous stirring (2,200 rpm), their reaction efficiency becomes comparable to that of stirring-free Pickering emulsion systems. At the end of the reaction, the interfacially active catalyst can be recovered from the Pickering emulsion phase through centrifugation. The reaction efficiency had no significant decrease during the consecutive reaction cycles.

Pickering emulsions were successfully applied to effectively catalyze the epoxidation of allylic alcohols with H_2O_2 in the absence of stirring. [3-(Trimethoxysily)propyl]-octadecyldimethylammonium chloride was used to modify the surfaces of silica microspheres. The quaternary ammonium sites on the silica microsphere surfaces were used to immobilize POM via ionic exchange, yielding interfacially active catalysts. As-prepared catalysts were used to emulsify the mixture of ethyl acetate and the

aqueous solution of H_2O_2. The reaction efficiency of the resulting Pickering emulsion systems in the absence of stirring is comparable to or higher than that in conventional biphasic reactions under stirring (800 rpm).

In addition of low energy input, high reaction efficiency, and simple workup, the stirring-free feature makes Pickering emulsion reaction systems superior to conventional biphasic ones, thus resulting in a technological leap toward more green and sustainable heterogeneous catalysis.

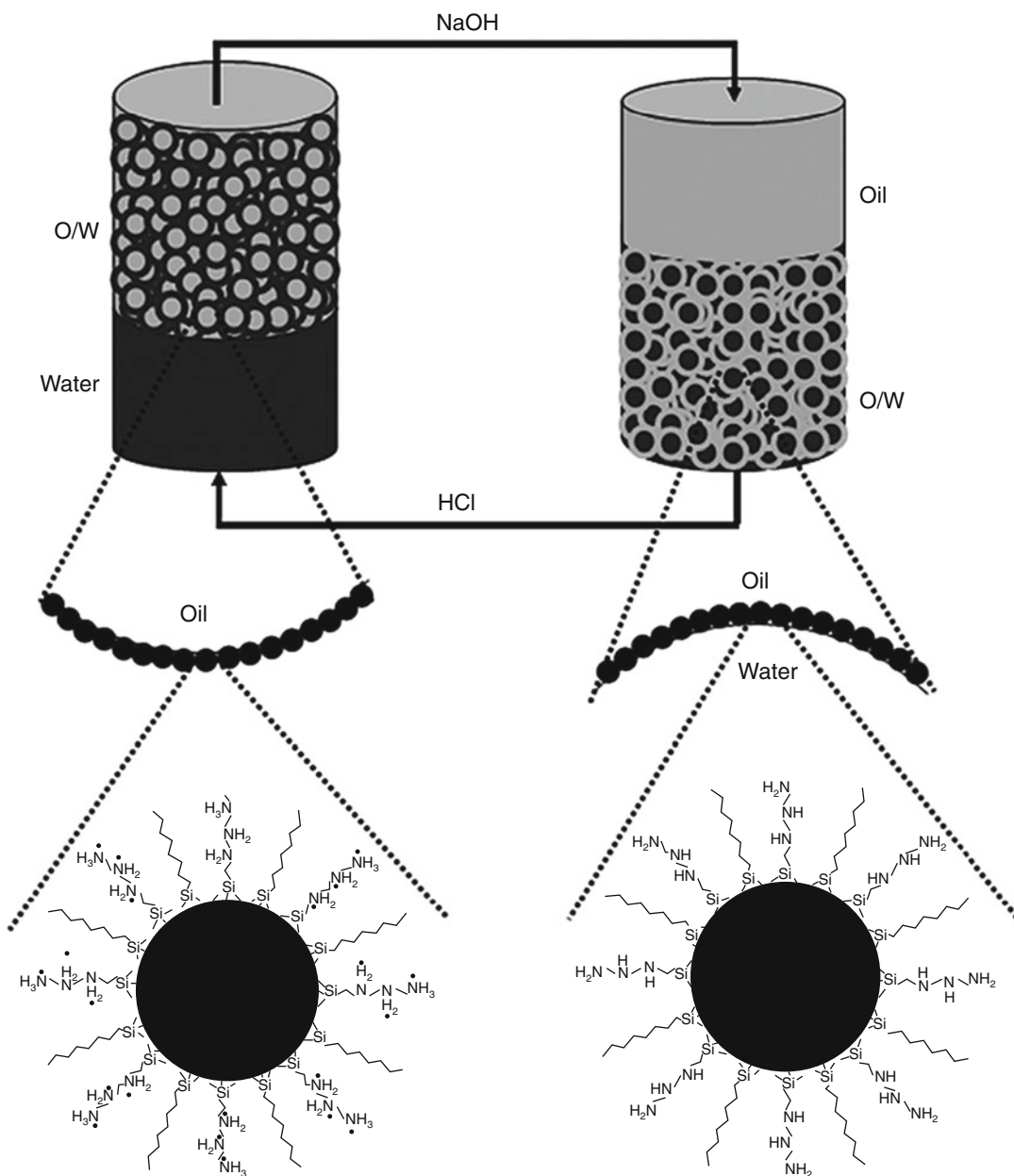## Catalyst Separation and Recycling in Pickering Emulsion Systems

Due to the high surface area, nanoparticle catalysts are highly active in many reactions for the synthesis of various fine chemicals. The applications of nanoparticle catalysts are often hampered by the difficulties in separation and recycling. In laboratory-scale research, the separation and recycling of nanoparticle catalysts require transfer of the reaction mixture from a reaction vessel to other vessels for filtration or centrifugation. Afterwards, the catalysts are collected and transferred back to the reaction vessel for the next batch. Such repeated transfers and operations inevitably cause catalyst loss and exposure to air and are time and energy consuming, which significantly limited the success of nanoparticle catalysts. Furthermore, conventional filtration and centrifugation are not applicable for separation of the catalysts with sizes below 50 nm, which needs more expensive techniques such as ultrafiltration and nanofiltration.

Catalyst Recycling in Pickering Emulsions: Phase Inversion Strategy

Yang et al. have recently demonstrated that pH-triggered Pickering emulsion inversion can be an appealing strategy for separation and recycling of nanoparticle catalysts, as schematically described in Fig. 12 [27]. The aforementioned SM–CN(4) particles were found to be the best stabilizers for Pickering emulsions. After adding an equal volume of toluene to an aqueous

solution containing 0.8 wt% of SM–CN(4) (with respect to water), and subsequent shaking or vigorous stirring, w/o Pickering emulsions were easily formed. After adding HCl dropwise to adjust the pH to 3–4 under gentle stirring, SM–CN(4) particles were transferred to the upper oil layer and in turn Pickering emulsions were inverted from the o/w type to the w/o one. Adjusting the pH of the aqueous phase back to 7–8 by NaOH, the SM–CN(4) particles were rapidly transferred back to the aqueous phase and the Pickering emulsions were inverted back to the w/o type. The phase inversion was accomplished within a few minutes under stirring, which was reversible at least for ten cycles and general for a range of organic solvents including toluene, ethyl acetate, benzene, ether, dichloromethane, and chloroform. Yang et al. carefully assessed the volume fraction of oil in o/w Pickering emulsions and that in the w/o emulsions recovered after phase inversion, respectively. In all the o/w emulsions obtained at pH 3–4, the oil volume fractions in the emulsion phase were in the range of 83.0–91.7 %. The high fraction of internal oil phase favors sufficient contact between catalysts and reactants. When the pH was adjusted to pH 7–8, 68.8–83.8 % of the original emulsion phase oil can be recovered after emulsion phase inversion. A high fraction of resolved oil should be favorable for separation of more products from the catalyst-containing emulsion phase. Moreover, after removing the recovered oil layer, the remaining emulsion still exhibits good stability without any coalescence.

After loading with Pd nanoparticles on their surfaces, SM–CN(4) served as smart Pickering emulsion stabilizers for the aqueous hydrogenation of styrene. Firstly, the reaction media pH was adjusted at 3–4 to obtain o/w Pickering emulsions for catalytic reactions. After the reaction was completed, the reaction media pH was adjusted to 7–8, which caused the phase inversion of the Pickering emulsions. The conversion of styrene was determined as >99 % within 0.5 h. The o/w and w/o Pickering emulsion systems had the same intrinsic activity. However, they exhibited different stirring rate dependence. At lower stirring rates, the reaction efficiency of the o/w

Surface Active Nanoparticles for Interfacial Catalysis, Fig. 12 The proposed strategy for catalyst separation and recycling based on the pH-triggered emulsion inversion (Copyright 2013 Wiley-VCH)

emulsion systems was much higher than that of the (w/o) emulsion system.

The pH-induced stabilization/destabilization cycle of Pd/SM–CN(4)-stabilized Pickering emulsion catalysis systems was repeated for 36 reaction cycles. The ethylbenzene yield was 77 % in the first reaction cycle, which was increased to the range of 86–108 % with the repetition of the reaction cycle. Furthermore, the catalyst loss study confirmed that the residual Pd concentration was determined as 0.1 ppm in the first reaction cycle and below 0.1 ppm after

Surface Active Nanoparticles for Interfacial Catalysis, Fig. 13 The Pickering emulsion/organics biphasic system (PEOBS) for recycling of nanoparticle catalysts (Copyright 2014 Wiley-VCH)
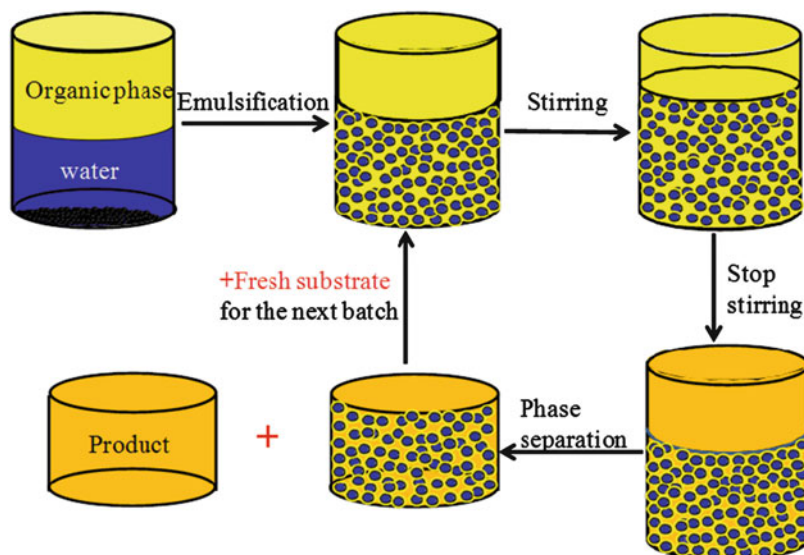
36 reaction cycles. These results highlight the high yield and excellent recyclability of the presented strategy.

Nanoparticle Catalyst Recycling in PEOBS

Although the above Pickering emulsion inversion strategy can realize the recycling of nanoparticle catalysts, it requires addition of acid/base to adjust the pH at each reaction cycle. Yang's group recently simplified the recycling procedure by taking advantage of the irreversible adsorption of nanoparticles at oil/water interfaces [13]. As illustrated in Fig. 13, PEOBS comprises two phases : w/o Pickering emulsion phase (the lower phase) and excessive oil phase (the upper phase), where the continuous oil phase in the Pickering emulsion phase and the upper oil phase are obviously integrated as one continuous oil phase. During reaction, organic substrates dissolved in the organic phase can freely diffuse from the upper oil phase to the continuous oil phase of the lower Pickering emulsion phase and, at the same time, are in direct contact with the nanoparticle catalysts strongly attached on the surfaces of the water droplets in the Pickering emulsion phase. At the end of the reaction, once the stirring is stopped, the upper oil phase containing organic products can be removed simply via decantation, for example, which leave the lower Pickering emulsion phase for the next batch without need for other operations.

The recyclability of Pd/SM–CN(5) was examined with styrene hydrogenations in PEOBS. At the end of each reaction cycle, the Pickering emulsion phase and organic phase were automatically separated into two distinct phases. After the removal of the upper oil phases dominantly containing the product ethylbenzene, the lower Pickering emulsion phase was directly used to the next batch. After adding fresh styrene, a new PEOBS was formed without the need for further emulsification. The morphologies and sizes of the emulsion droplets are little changed after repetition of reaction cycles. Although the isolation efficiency of the first reaction cycle was ca. 70.5 %, it was increased up to 94–99 % after the second reaction cycle. The residual Pd in the resolved organic layer was determined with ICP-AAS (inductively coupled plasma atomic absorption spectroscopy). In the first reaction cycle, the residual Pd concentration in the organic product was 0.25 ppm, suggesting only 0.32 % solid catalysts leached into the upper layer. In the second reaction cycle, the residual Pd concentration was as low as 0.12 ppm. In the tenth cycle, the residual Pd concentration was further decreased down to 0.1 ppm.
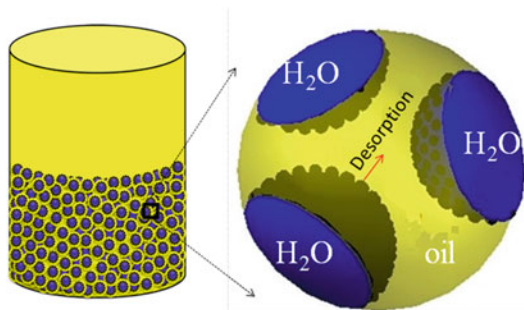
Surface Active Nanoparticles for Interfacial Catalysis, Fig. 14 The schematic description of anchoring nanoparticle catalysts by PEOBS (Copyright 2014 Wiley)

The effectiveness and efficiency of catalyst recycling in PEOBS stem from the stability of Pickering emulsions against coalescence under the reaction conditions. It is well documented that particle-stabilized emulsions have extremely high stability. As displayed in Fig. 14, the desorption of a particle from the droplet surface must overcome an energy barrier that can be calculated from the following equation:

$$E = \pi R^2 \gamma_{ow} (1 \pm \cos\ \theta)^2$$

where R is the particle radius, γ_{ow} is the interfacial tension of oil/water, and θ is the contact angle of the particle at the interface. For nanoparticle catalysts used to stabilize Pickering emulsions, E is estimated to be as high as $10^4 - 10^6\ K_B T$ (K_B is Boltzmann constant), several orders of magnitude higher than the thermal energy. Thus, the nanoparticle catalysts, adsorbed on the surfaces of Pickering emulsion droplets, can move laterally on the surface, but cannot desorb from the droplet surface. This irreversible interfacial adsorption of particles enables Pickering emulsions to be treated as a stationary phase to recycle nanoparticle catalysts.

Concluding Remarks and Directions

Organic/aqueous biphasic systems are increasingly popular for chemical synthesis, because water is proved to be a promising alternative to organic solvents under the ever-increasing pressure of green and sustainable chemistry. The high mass transfer resistance is the major obstacle for biphasic reaction systems especially when solid catalysts are present. This technical challenge may be readily solved by developing heterogeneous catalysis formulations based on Pickering emulsions. Increasing evidence has demonstrated that in Pickering emulsion reaction systems stabilized by nanoparticle catalysts, the diffusion distances of organic and aqueous substrates are remarkably shortened and the interfacial area for catalysis is dramatically enlarged. In the reactions involving gas phase such as H_2 and O_2, the transport of the gas molecules in the continuous organic phase in w/o Pickering emulsions is substantially improved, and the apparent activation energy is significantly lowered in comparison to the single aqueous phase. This rate enhancement enables efficient interfacial catalysis in Pickering emulsions even in the absence of stirring. For oil–water–solid three-phase reactions, the reaction efficiency of Pickering emulsion reaction systems conducted without stirring is comparable to that of conventional biphasic systems performed under stirring and at least one order of magnitude higher than that of phase-boundary catalysis systems. The short diffusion distance, arising from compartmentalization of oil/water biphasic mixtures to densely packed droplets, is the rationale for the reaction efficiency enhancement.

In addition to the catalysis activity, the reaction selectivity has been influenced in Pickering emulsion reaction systems because the pronounced increase in the organic/aqueous interface not only changes the diffusion and transport way of reactants and intermediates, but also facilitates the extraction of the intermediates from the one phase to the other due to the difference in their solubility in either of the bulk phases. The in situ partitioning can prevent further transformation of the intermediates if they have different reactivities in the dispersed phase and in the continuous phase. This is of particular importance for the reactions involving multistep transformation.

The phase inversion of Pickering emulsions stabilized by stimuli-responsive nanoparticle catalysts leads to innovative stimuli-responsive ways

of separation and recycling of nanoparticle catalysts without the aid of centrifugation or filtration. Taking the advantage of irreversible interfacial adsorptions, PEOBSs allow easy separation of the w/o Pickering emulsion catalytic phase from the oil phase bearing organic products. These two methods show high product separation efficiency and high catalyst recycling efficiency.

In contrast to the more than a century of research history in colloid and interface science, the research of using Pickering emulsions for interface catalysis is just in its infancy and its impact is unfolding. Many fundamental aspects need to be addressed before practical applications. The interfacially active nanoparticle catalysts, reported in literature, are limited to carbon nanotubes and silica-based catalysts. For other widely used catalyst supports such as Al_2O_3, carbon, and ZnO, tuning their surface wettability for better emulsification is rarely studied to date. At present, organic solvents are needed to act as oil phase for Pickering emulsions in most cases. Using organic reactant liquids directly as oil phase to form Pickering emulsions may need more deliberate control of the surface hydrophobicity of nanoparticle catalysts, which needs to be carefully explored.

At present, the number of studies of using Pickering emulsions for interfacial catalysis is limited but increasing, which, no doubt, opens up promising prospects. However, it is still too early to predict if Pickering emulsions will lead to big success in industrial application and commercialization. We indeed believe that this research theme is worthy of further investigation and exploration because of the solid research foundation of Pickering emulsions in colloid and interface science and their unprecedented integration of many appealing features in one, which become essential in the context of green and sustainable chemistry.

References

1. Chanda A, Fokin VV (2009) Organic synthesis "on water". Chem Rev 109:725–748
2. Minakata S, Komatsu M (2009) Organic reactions on silica in water. Chem Rev 109:711–724
3. Aveyard R, Binks BP, Clint JH (2003) Emulsions stabilised solely by colloidal particles. Adv Colloid Interface Sci 100:503–546
4. Tsuji S, Kawaguchi H (2008) Thermosensitive Pickering emulsion stabilized by poly(N-isopropylacrylamide)-carrying particles. Langmuir 24:3300–3305
5. Yan NX, Gray MR, Masliyah JH (2001) On water-in-oil emulsions stabilized by fine solids. Colloids Surf A 193:97–107
6. Fielding LA, Armes SP (2012) Preparation of Pickering emulsions and colloidosomes using either a glycerol-functionalised silica sol or core-shell polymer/silica nanocomposite particles. J Mater Chem 22:11235–11244
7. Pickering SU (1907) CXCVI. – Emulsions. J Chem Soc 91:2001–2021
8. Ramsden W (1903) Separation of solids in the surface-layers of solutions and 'suspensions' (observations on surface-membranes, bubbles, emulsions, and mechanical coagulation). – Preliminary account. Proc R Soc 72:156–164
9. Crossley S, Faria J, Shen M, Resasco DE (2010) Solid nanoparticles that catalyze biofuel upgrade reactions at the water/oil interface. Science 327:68–72
10. Shen M, Resasco DE (2009) Emulsions stabilized by carbon nanotube-silica nanohybrids. Langmuir 25:10843–10851
11. Drexler S, Faria J, Ruiz MP, Harwell JH, Resasco DE (2012) Catalysts for reactions at the water/oil interface in subsurface. Reservoirs Energy & Fuels 26:2231–2241
12. Zhang L, Balzano L, Resasco DE (2005) Single-walled carbon nanotubes of controlled diameter and bundle size and their field emission properties. J Phys Chem B 109:14375–14381
13. Liu HF, Zhang ZM, Yang HQ, Cheng FQ, Du ZP (2014) Recycling nanoparticle catalysts without separation based on a Pickering emulsion/organic biphasic system. ChemSusChem 7:1888–1900
14. Yang XM, Wang XN, Qiu JS (2010) Aerobic oxidation of alcohols over carbon nanotube-supported Ru catalysts assembled at the interfaces of emulsion droplets. Appl Catal A Gen 382:131–137
15. Yu C, Fan LM, Yang J, Shan YY, Qiu JS (2013) Phase-reversal emulsion catalysis with CNT-TiO_2 nanohybrids for the selective oxidation of benzyl alcohol. Chem Eur J 19:16192–16195
16. Leclercq L, Mouret A, Proust A, Schmitt V, Bauduin P, Aubry JM, Nardello-Rataj V (2012) Pickering emulsion stabilized by catalytic polyoxometalate nanoparticles: a new effective medium for oxidation reactions. Chem Eur J 18:14352–14358
17. Leclercq L, Company R, Muhlbauer A, Mouret A, Aubry JM, Nardello-Rataj V (2013) Versatile eco-friendly Pickering emulsions based on substrate/native cyclodextrin complexes : a winning approach for solvent-free oxidations. ChemSusChem 6:1533–1540

18. Zapata PA, Faria J, Ruiz MP, Resasco DE (2012) Condensation/hydrogenation of biomass-derived oxygenates in water/oil emulsions stabilized by nanohybrid catalysts. Top Catal 55:38–52

19. Zapata PA, Faria J, Ruiz MP, Jentoft RE, Resasco DE (2012) Hydrophobic zeolites for biofuel upgrading reactions at the liquid–liquid interface in water/oil emulsions. J Am Chem Soc 134:8570–8578

20. Wu CZ, Bai S, Ansorge-Schumacher MB, Wang DY (2011) Nanoparticle cages for enzyme catalysis in organic media. Adv Mater 23:5694–5699

21. Wiese S, Spiess AC, Richtering W (2013)) Microgel-stabilized smart emulsions for biocatalysis. Angew Chem Int Ed 52:576–579

22. Scott G, Roy S, Abul-Haija YM, Fleming S, Bai S, Ulijn RV (2013) Pickering stabilized peptide gel particles as tunable microenvironments for biocatalysis. Langmuir 29:14321–14327

23. Wang ZP, C. M. van Oers M, P. J. T. Rutjes F, C. M. van Hest J (2012) Polymersome colloidosomes for enzyme catalysis in a biphasic system. Angew Chem Int Ed 51:10746–10750

24. Fan ZY, Tay A, Pera-Titus M, Zhou WJ, Benhabbari S, Feng XS, Malcouronne G, Bonneviot L, Campo FD, Wang LM, Clacens JM (2013) Pickering Interfacial Catalysts for solvent-free biomass transformation: Physicochemical behavior of non-aqueous emulsions. J Colloid Interface Sci 427:80–90

25. Zhou WJ, Fang L, Fan ZY, Albela B, Bonneviot L, Campo FD, Pera-Titus M, Clacens JM (2014) Tunable catalysts for solvent-free biphasic systems: Pickering Interfacial catalysts over amphiphilic silica nanoparticles. J Am Chem Soc 136:4869–4872

26. Zhang WJ, Fu LM, Yang HQ (2014) Micrometer-scale mixing with Pickering emulsions: Biphasic reactions without stirring. ChemSusChem 7:391–396

27. Yu YH, Fu LM, Zhang FW, Zhou T, Yang HQ (2014) Pickering-emulsion inversion strategy for separating and recycling nanoparticle catalysts. ChemPhysChem 5:841–848

Surfactant Assemblies (Micelles, Vesicles, Emulsions, Films, etc.), an Overview

Shinji Yamada
New Industry Creation Hatchery Center,
Tohoku University, Sendai, Japan

Synonyms

Self-assembly of amphiphilic molecules

Definition

Spontaneous organization of materials (commonly amphiphilic molecules such as low-molecular-weight surfactants and polymeric surfactants) into highly ordered structures through non-covalent interactions without adding external energy.

Introduction

Amphiphilic molecules or surfactants can self-assemble into a variety of ordered structures. The self-assembly of low-molecular-weight surfactants has been studied for many decades; the principle that determines the morphologies of ordered aggregates in solutions is explained primarily from the concept of packing parameter [1]. The packing parameter, p ($= v/a_0 l_c$), indicates the geometry or packing property of a surfactant molecule into ordered aggregates, where v is the volume of the hydrophobic chain, a_0 is the optimum head-group area, and l_c is the length of the hydrophobic chain. Evaluation of p enables us to estimate the morphology of aggregates such as spheres, cylinders, flexible lamellae or vesicles, and planar lamellae.

Polymeric surfactants have received particular attention during the last three decades. There are three types of polymeric surfactants that consist of hydrophilic and hydrophobic segments, which are as follows [2]:

(i) Molecules that have a hydrophilic backbone and hydrophobic side chains
(ii) Molecules that have a hydrophobic backbone and hydrophilic side chains
(iii) Molecules that consist of hydrophilic and hydrophobic blocks (block copolymers)

All of these types of polymeric surfactants have ability to adsorb onto hydrophilic/hydrophobic interfaces and exhibit surface activity. They are actually used in many practical applications in order to stabilize dispersions and/or

S

control rheological properties of the systems. In general, most of the polymeric surfactants in types (i) and (ii) are only moderately surface active. For example, the ability to reduce surface tension between oil and water interfaces is not so high compared with low-molecular-weight surfactants. On the other hand, the block copolymers type (iii) have great similarities with low-molecular-weight surfactants from the views of surface activity and self-assemble properties. Block copolymers self-assemble into a variety of ordered structures in bulk and in solutions [3, 4]. The morphology of the ordered structures is governed by the geometric factor of the molecule, which is quite similar to the packing parameter concept for low-molecular-weight surfactants. In this section, self-assembly of polymeric surfactants, particularly the block copolymers, will be described.

Self-Assembly of Block Copolymers in Bulk

Figure 1 schematically shows the geometries (conformations) of a molecule of a simplest A–B block copolymer (a) and morphologies of its self-assembled structures (b) in the bulk state. The A and B blocks are immiscible, and the molecules aggregate into ordered structure via microphase separation in which the contact between the same blocks is maximized and that between different blocks is minimized. The conformation of the molecule and morphology of the self-assembled structures (microdomains) are governed by the following factors:

(i) The volume fraction f of the A and B blocks (f_A and $f_B, f_A + f_B = 1$)
(ii) The total degree of polymerization N (= $N_A + N_B$, N_A and N_B are the degree of
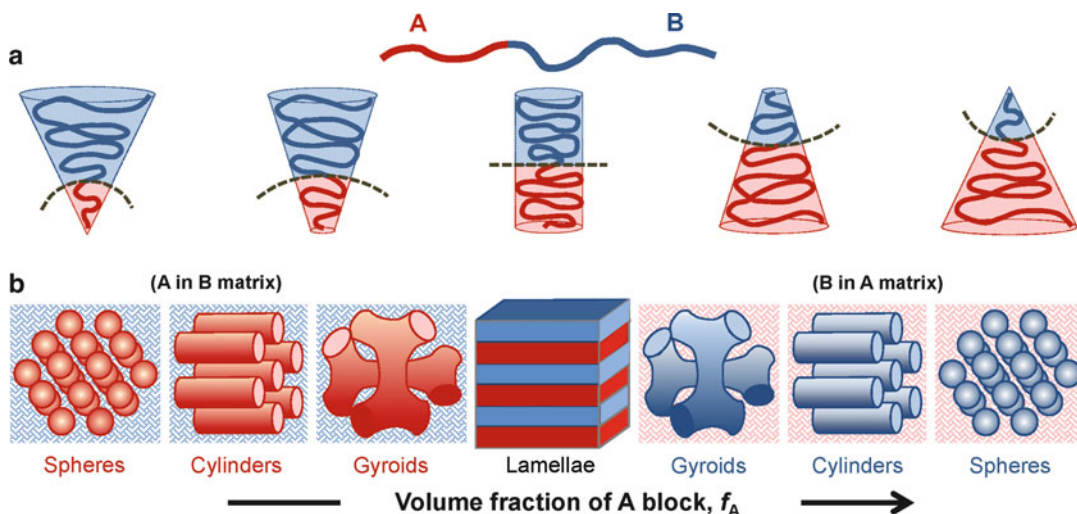
Surfactant Assemblies (Micelles, Vesicles, Emulsions, Films, etc.), an Overview, Fig. 1 Possible chain rearrangements or molecular conformations of block A–B diblock copolymers in bulk and resulting morphologies of self-assembled microdomains. (**a**) The curvature of the interface between A and B domains in the molecule is determined by the geometric factor, basically the same as the packing parameter concept for low-molecular-weight surfactants (sometimes referred to as cone-column mechanisms). Small f_A gives a cone-like molecular conformation; increasing f_A increases the curvature of the domain interface. When $f_A \approx f_B$ (≈ 0.5), cylinder-like molecular conformation is attained (flat domain interface). Further increase of f_A leads to the conformational changes from cylinder to cone, but the orientation of the cone shape is reversed. (**b**) Morphological transitions of microdomain structures as a function of f_A. Cone-like conformation gives spheres or cylinders; increasing f_A (increasing the curvature of the domain interface) leads to gyroids and then flat lamellae when $f_A \approx f_B \approx 0.5$. The block that has small volume fraction constitutes the microdomains and the other block constitutes the matrix in the system

polymerization of A block and B block, respectively)

(iii) The Flory–Huggins parameter χ_{AB} that describes the free energy cost of contact between A and B blocks

The A–B block copolymer with small f_A tends to have a cone-like conformation. Increasing f_A increases the radius of curvature of the interface between the A and B domains and the geometry of the molecule shifts from a cone-like to a cylinder-like conformation. This conformational change of the molecule as a function of f_A directly alters the morphology of the self-assembled microdomains. The morphology is determined by the balance between (a) interfacial energy between A block and B block (an enthalpic contribution) and (b) chain stretching (an entropic contribution). The microdomain structure shifts from spheres to cylinders, to bicontinuous gyroids, and to lamellae along with the increase of f_A. In the region where $f_A < f_B$, the A blocks constitute the microdomain structures in the matrix of the B blocks. The lamellae morphology appears where $f_A \approx f_B$ (≈ 0.5). A further increase of f_A shifts the geometry of the molecule from a cylinder-like to cone-like conformation, but the orientation of the cone shape is reversed compared to that in the low f_A region. This conformation change of the molecule results in the transition of the self-assembled microdomains from lamellae to gyroids, to cylinders, and to sphere; the B blocks constitute the microdomains in the matrix of the A blocks (where $f_A > f_B$).

Increasing the number of blocks in block copolymers induces much complex morphological transitions of the self-assembled microdomains. For example, ABC linear triblock copolymers contain three different blocks. Then, the system has three χ parameters (χ_{AB}, χ_{AC}, and χ_{BC}) and three volume fraction parameters (f_A, f_B, and f_C; $f_A + f_B + f_C = 1$). In addition, the sequences of the three segments (ABC, BCA, or CAB) also affect the morphology of the aggregates. As a result, a wide variety of ordered structures could be formed; experiments and theories indicate the possibility of more than 30 different morphologies available for triblock copolymer aggregates.

Much higher complexity should be expected for the copolymers having more than three different blocks.

Self-Assembly of Block Copolymers in Solutions

The addition of solvent induces much complex phase behaviors for A–B block copolymer systems depending on the solvent quality for the both block units. If the solvent is a good solvent for both block units, the configuration of molecules in the solution should be not very different from that of a homopolymer in a good solvent. If it is a poor solvent for both block units, the polymer will not dissolve in the solution. When the solvent is a good solvent for either of the block unit but is a poor solvent to another unit, the molecule exhibits amphiphilicity and aggregates into a variety of ordered structures. The ordered shapes include spherical micelles, rods, bicontinuous structures, lamellae, vesicles, large compound micelles, large compound vesicles, tubules, onions, eggshells, baroclinic tubules, pincushions, etc.; more than twenty kinds of morphologies have been identified. Some of the morphologies are not thermodynamically equilibrium structures but kinetically induced structures due to the long relaxation time of the systems.

The morphology of the self-assembled structures of block copolymers in solution is affected by the following factors: copolymer composition, copolymer concentration, solvent quality, presence of additives, and temperature. Increasing the number of block units and/or increasing the number of solvents in the systems (systems often include two or more solvents) induces much complex morphological transitions of the self-assembled aggregates.

Block Copolymer Micelles

As with low-molecular-weight surfactants, block copolymers in a selective solvent form micelles above a concentration called the critical micelle concentration (CMC). The CMCs of block

copolymer systems are sometimes very low, which is one of the reasons of the high stability of polymer micelles.

The physicochemical properties of block copolymer micelles are described by their CMC, morphology, size (aggregation number), solubilization behaviors, and chain dynamics of the polymers [5]. In most case, characterization techniques that are commonly used for low-molecular-weight surfactant micelles are applicable to block copolymer systems. However, it should be noted that, due to the very low diffusion coefficient (very long relaxation time) of the polymeric surfactants, it takes a very long time to reach equilibrium conditions of the systems. Therefore, as was already mentioned, some thermodynamically nonequilibrium (kinetically induced) phases or structures could be observed in experimental time scales.

Micellization of block copolymers occurs both in aqueous solutions and in organic solvents. In the former case, hydrophilic–hydrophobic block copolymers form micelles, and they can be classified into three categories by the structure of hydrophilic blocks, such as nonionic, anionic, and cationic (similar to low-molecular-weight surfactant systems). Among these three categories, nonionic type block copolymers are extensively studied due to their importance as novel carriers in the field of drug delivery. Block copolymer micelles are suitable for this purpose because of their high drug-loading capacity (large solubilization capacity), high stability, sizes, and surface properties. Poly(ethylene glycol) (PEG) is the most common hydrophilic block for this application due to the advantage of its adjustable water solubility with temperature, nontoxic, and non-immunogenic features.

As is the case with low-molecular-weight surfactants, the addition of oil to block copolymer micelles in aqueous solutions can lead to the formation of o/w microemulsions. Likewise, the addition of water to reverse micelles can lead to w/o microemulsions. One of the big advantages of using block copolymers for microemulsion formation is the large solubilization capacity in the micelle core as was mentioned; a wide variety of pharmaceutical and cosmetic applications have been reported [6, 7].

Block Copolymer Vesicles

As with low-molecular-weight surfactants and lipids, block copolymers tend to self-assemble into vesicles if the time average geometry of the molecules is the form of a cylinder [4, 8]. Poly (ethylene glycol)–polybutadiene (PEG–PBD), polyacrylic acid–polystyrene (PAA–PS), and PS–poly(isocyano-L-alanine-L-alanine) are the typical examples of block copolymers to form vesicles under suitable solution conditions. Block copolymers generally have lower CMC than small amphiphiles and lipids because of their large molecular weight of their hydrophobic parts in the molecules; low CMC is an advantage for the stability of vesicles. Amphiphile exchange rate between aggregates is also an important parameter for the stability, and it is directly proportional to CMC. Very low CMC of block copolymers have much smaller exchange rates than low-molecular-weight surfactants and lipids, indicative of kinetic quenching and stable vesicle aggregates.

Polydispersity in molecular size, which comes from the polydispersity of the chain length in the molecule, is an intrinsic feature of polymeric amphiphiles, and this is also closely related to the vesicle stability. For both vesicle bilayers and multilamellar vesicles, flip-flop of molecules is important to relax the strain within the bilayer films. Polydispersity of block copolymers contributes to the flip-flop mechanism and stability as follows. Molecules with short chains could tend to segregate into the inner leaflet of the bilayer, and those with long chains segregate into the outer leaflet, which induces different repulsion strength (steric and/or electrostatic) on the leaflets [8]. This mechanism leads to a thermodynamically stable curvature of the bilayer and contributes to the vesicle stability.

From the viewpoint of practical applications such as drug delivery, permeability of vesicle bilayers is another important character. Permeability is dependent on the fluidity of the bilayer, and the fluidity decreases with the increase of the molecular weight of the polymer amphiphiles (increase of bilayer thickness). If the molecular weight is long enough to entangle with each other, fluidity of the bilayers drastically decreases.

Vesicle stability and fluidity (permeability) are generally incompatible with each other, and it is important to select the best suitable amphiphiles to fit the needs of applications.

Emulsification by Block Copolymer Amphiphiles

Polymeric surfactants that have the ability to adsorb at oil/water interfaces work as good emulsifiers. For oil-in-water (O/W) emulsion, hydrophilic (A block)–hydrophobic (B block) diblock copolymers can be used; hydrophobic B block adsorbs on oil droplet surfaces and hydrophilic A chain spreads in water and produces effective steric stabilization against flocculation, coalescence, and Ostwald ripening [9].

Not only block copolymers but also graft copolymers (AB_n type) can be used to prepare stable emulsions. The B chains work as multi-anchor attachments to oil/water interfaces and the long A chain produces steric stabilization.

For some polymeric emulsifiers, strong viscosifying effect contributes to the emulsion stability [10]. For example, hydrophobically–hydrophilically modified hydroxyethylcellulose (HHM-HEC) forms a strong gel network structure in aqueous solutions. Oil droplets dispersed in the HHM-HEC solution are trapped in the three-dimensional network structure, and the system exhibits excellent stability against creaming and coalescence. This type of emulsification technique is widely used in the field of foods, cosmetics, and drug delivery applications.

Self-Assembly in Thin Films

Polymeric surfactants (block copolymers) in bulk and in solutions have the ability to self-assemble into a variety of ordered aggregates as was described. The morphology of the aggregates is mainly controlled by the block–block interactions, block compositions, and molecular architectures. Here the block copolymers in thin film on rigid substrate (surface of the film is in contact with an atmosphere) are described. Besides the intrinsic parameters listed above, extrinsic factors such as structural frustration and surface–polymer interactions should have large effects on the self-assembled morphologies in thin films [11, 12].

When thickness of the film approaches to the size of a polymer domain spacing, polymer chains in the molecule are stretched or compressed that produces entropic penalty. Then, molecules in the block copolymer film self-assemble into ordered structures to relieve the entropic penalty and obtain favorable enthalpic interactions at the substrate or free surface. Molecules in the film form self-assembled structures such as islands, holes, cylinders, and lamellar morphologies depending on the interactions between molecules and substrate interfaces.

Surface energy of substrate is one of the most important parameters for the self-assembled structures of block copolymers in thin films. The stability of the structures is of course sensitive to the wettability of surfaces by the blocks in the polymer molecules. In addition, some block copolymers form lamellae or cylinders on surfaces, and their orientation is primarily determined by the surface energy of the substrates.

Self-assembly of block copolymers in thin films is closely related to a variety of practical applications. For example, highly ordered hexagonal dot pattern obtained from a thin film having cylindrical or spherical self-assembled morphology of block copolymers can be effectively used in memory applications; the inverse morphology is applied to nanoporous membranes. Due to the importance in many industrial applications, designing of self-assembled block copolymer structures in thin films (and sometimes also in 3D confinement [13]) is a very active research area in these decades.

Related Entries

▶ Biomembrane as a Soft Matter
▶ Block Copolymers
▶ Microphase Separation (of Block Copolymers)
▶ Molecular Self-Organization
▶ Polymer Surfactant
▶ Self-Assembled Monolayer

References

1. Israelachvili J (2011) Intermolecular and surface forces, 3rd edn. Academic, Amsterdam
2. Holmberg K, Jönsson B, Kronberg B, Lindman B (2002) Surfactants and polymers in aqueous solution, 2nd edn. Wiley, West Sussex
3. Evans DF, Wennerström H (1999) The colloidal domain: where physics, chemistry, biology, and technology meet, 2nd edn. Wiley-Vch, New York
4. Mai Y, Eisenberg A (2012) Self-assembly of block copolymer. Chem Soc Rev 41:5969–5985. doi:10.1039/c2cs35115c
5. Riess G (2003) Micellization of block copolymers. Prog Polym Sci 28:1107–1170. doi:10.1016/S0079-6700(03)00015-7
6. Blanazs A, Armes SP, Ryan AJ (2009) Self-assembled block copolymer aggregates: from micelles to vesicles and their biological applications. Macromol Rapid Commun 30:267–277. doi:10.1002/marc.200800713
7. Kataoka K, Harada A, Nagasaki Y (2012) Block copolymer micelles for drug delivery: design, characterization and biological significance. Adv Drug Deliv Rev 64:37–48. doi:10.1016/J.addr.2012.09.013
8. Discher DE, Eisenberg A (2002) Polymer vesicles. Science 297:967–973
9. Tadros T (2009) Polymeric surfactants in disperse systems. Adv Colloid Interface Sci 147–148: 281–299. doi:10.1016/j.cis.2008.10.005
10. Rodrigues-Abreu C, Lazzari M (2008) Emulsions with structured continuous phases. Curr Opin Colloid Interface Sci 13:198–205. doi:10.1016/j.cocis.2007.09.004
11. Albert JN, Epps TH (2010) Self-assembly of block copolymer thin films. Mater Today 13:24–33
12. Zoelen WV, Brinke GT (2009) Thin films of complex block copolymers. Soft Matter 5:1568–1582. doi:10.1039/b817093b
13. Shi AC, Li B (2013) Self-assembly of diblock copolymers under confinement. Soft Matter 9:1398–1413. doi:10.1039/c2sm27031e

Synthesis and Self-Assembly of Linear-Dendritic Hybrid Polymers

Ivan Gitsov
SUNY College of Environmental Science and Forestry, Syracuse, NY, USA

Synonyms

Dendritic-linear polymer; Dendronized polymer; Hybrid copolymer; Linear-dendritic copolymer

Definition

A "linear-dendritic hybrid polymer" (LDHP) is a macromolecule composed of polymeric fragments with two dissimilar architectures: (a) a linear chain with nominal molecular weight higher than 1,000 Da and (b) a perfectly branched (dendritic) moiety with number of branching layers exceeding two [1, 2].

Classification

Linear chains (L) and dendrons or dendrimers (D) are the only two types of building blocks, contained in the LDHPs, but they can be arranged in several distinct combinations, due to the multifunctional character of both fragments. The simplest members of the series are DL (Fig. 1, **1**), DLD (Fig. 1, **2**), and LDL (Fig. 1, **3**) copolymers where the linear chain (L) is linked to a D - dendron (**1**, **2**) or a dendrimer (**3**). Their main characteristic is structural flexibility, which potentially would enable their architectural rearrangement upon changes in their environment.

The second group of macromolecules unifies structures with many D blocks (dendrons and dendrimers) in the copolymer. They can be grafted/grown onto the backbone to produce L-*graft*-D hybrid (Fig. 2, **4**) or "inserted" between the individual linear segments yielding an alternating $(LD)_n$ copolymer (Fig. 2, **5**).

Depending on the size of the building blocks, these LDHPs can change their profile from a relatively flexible coil/globule (long chains and small dendrimers) to more rigid, tubular structure (short chains and large dendrimers).

The third variety of linear-dendritic block copolymers has symmetrical starlike architecture with two subgroups: (a) a dendrimer is placed in the middle and serves as the core of the star, $D(L)_n$ (Fig. 3, **6**), or (b) the star has dendrons attached at every arm's end, *star*-$(LD)_n$ (Fig. 3, **7**). These LDHPs could change their size and shape depending on their chemical composition and the nature of the surrounding medium.

Synthesis and Self-Assembly of Linear-Dendritic Hybrid Polymers,
Fig. 1 Schematic representation of LD, DLD, and LDL linear-dendritic hybrid polymers
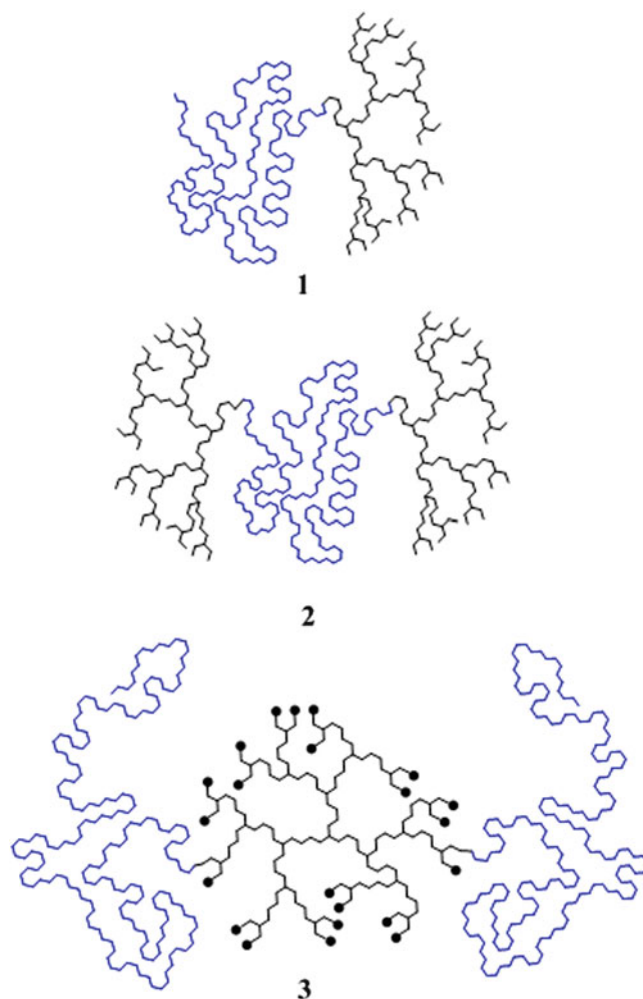
LDHPs with infinite molecular mass, arranged in the form of covalent or physical polymer networks, constitute the fourth group, which has been reported. The construction uses dendrimers as large, shape-persistent cross-linking moieties (Fig. 4, **8**), interconnected with linear blocks of identical chain length. The hybrid gels would swell or shrink depending on the solubility of their constituents in the chosen medium.

Variations in the character and size of the building elements will possibly expand those four groups, but the final set of LDHPs, which await practical construction, are the "dendritic dendrimers" having a dendritic core and dendrons as branching elements (Fig. 5, **9**).

Synthesis

The construction of LDHPs necessitates precise and quantitative repetitive placement of the two building blocks at specific sites in the hybrid macromolecules. While many organic reactions can be used to produce linear-dendritic block copolymers, the hybrid architectures shown in Figs. 1, 2, 3, 4, and 5 can be formed via few synthetic pathways. They include (a) coupling of preformed linear and dendritic blocks with complimentary functionalities, (b) growth of dendrons on linear chains with suitable reactive groups located in the repeating units or at the

S

**Fig. 2** Schematic representation of L-*graft*-D and (LD)$_n$ linear-dendritic hybrid polymers
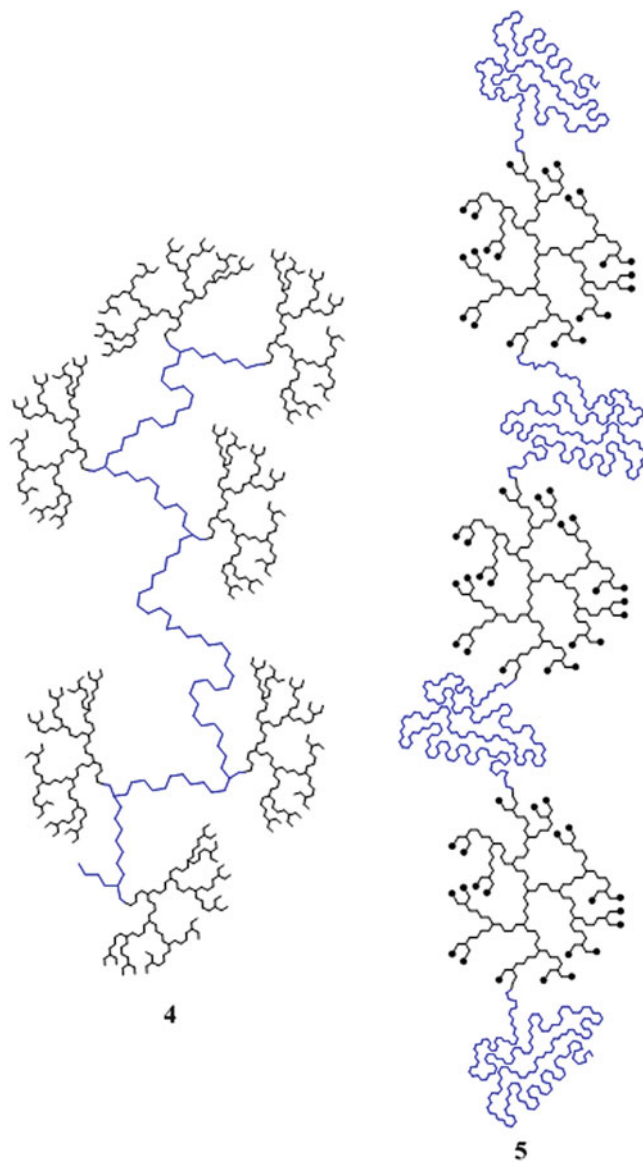
chain ends, and (c) growth of linear chain(s) from initiating sites located at the focal point of a dendron or at the periphery of a dendrimer [3].

Coupling of Preformed Linear and Dendritic Blocks

The synthetic approach, based on direct coupling of both constituents, is probably the simplest method for the construction of LDHPs within the four classes of hybrid macromolecular architectures. The main benefit of the method is that the hybrid copolymers are formed in one stage by a single chemical reaction. In many cases the linear block is commercially available and can be used as is or can be modified by standard synthetic techniques. The significant difference in molecular masses and solubility between the starting materials and the final products greatly simplifies their isolation and purification. The molecular size of the reagents usually does not affect the outcome of the coupling reaction, which is influenced mostly by the chemical reactivity of the functional groups in both blocks.
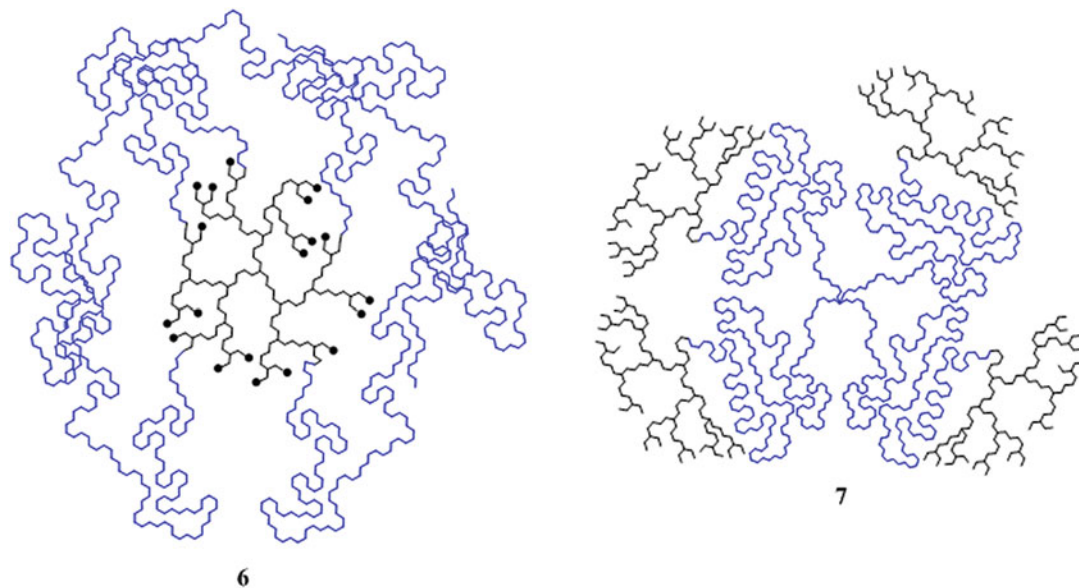
Synthesis and Self-Assembly of Linear-Dendritic Hybrid Polymers, Fig. 3 Schematic representation of $D(L)_n$ and *star*-$(LD)_n$ linear-dendritic hybrid polymers
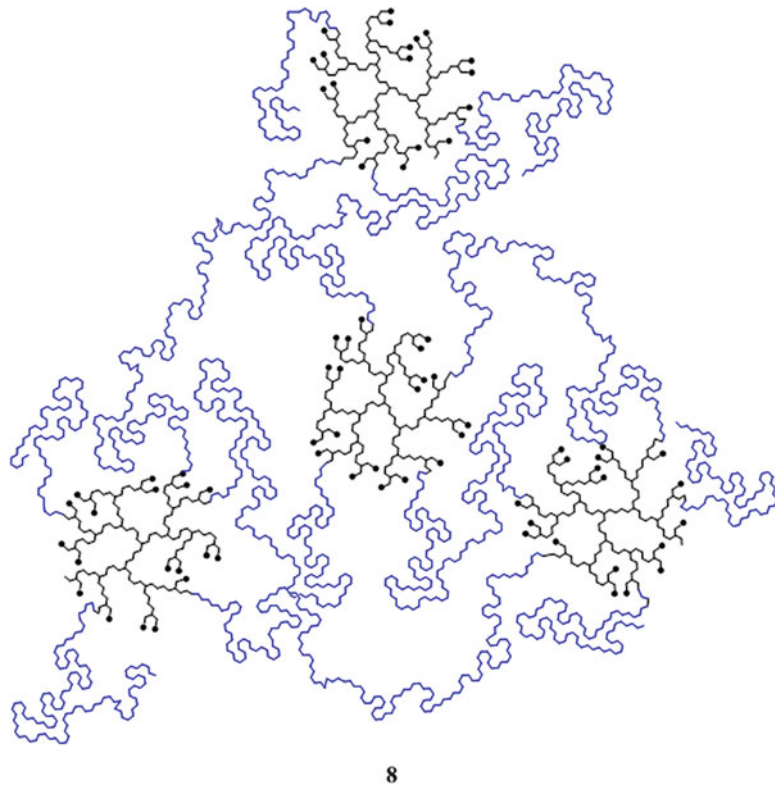
Synthesis and Self-Assembly of Linear-Dendritic Hybrid Polymers, Fig. 4 Schematic representation of linear-dendritic hybrid network

Synthesis and Self-Assembly of Linear-Dendritic Hybrid Polymers,
**Fig. 5** Schematic representation of a hypothetical linear-dendritic hybrid dendrimer
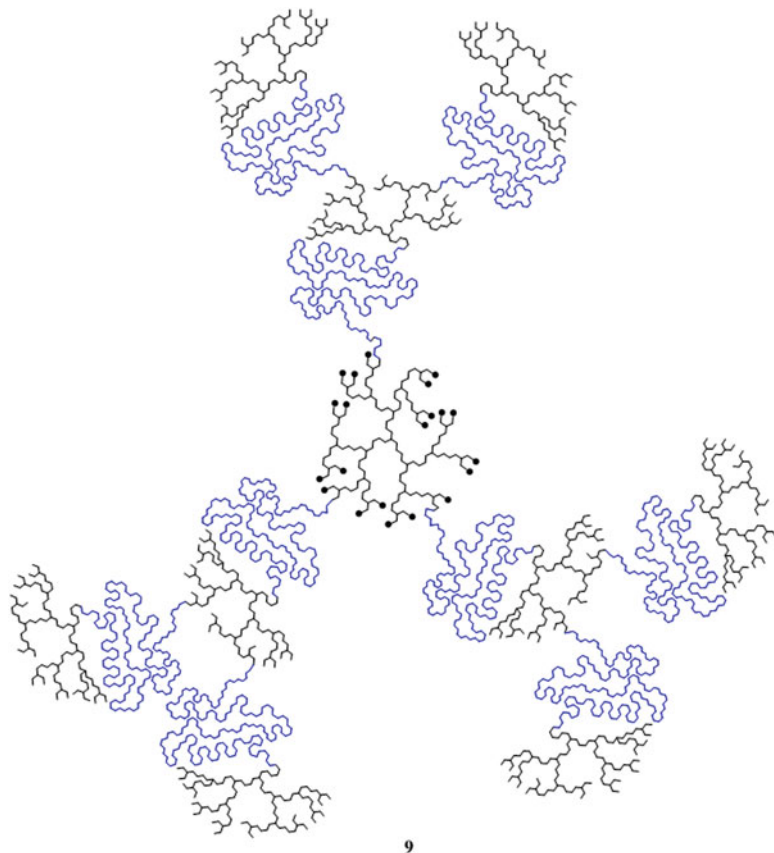
The size of the reagents becomes a yield-determining factor only in those cases where the synthesis targets LDHPs with voluminous components (linear or dendritic) and high dendritic content. The analysis of the formed linear-dendritic macromolecules, based on size-sensitive analytical techniques (size-exclusion chromatography, dynamic light scattering, or MALDI-TOF), provides unambiguous evidence for the purity of the isolated hybrids. On the other side, the classic spectroscopic methods are not sufficiently sensitive and discriminating to trace the quantitative formation of a single or few linkages between the two building fragments.

The synthetic strategy is exemplified by the procedure, shown in Fig. 6.

The first stage involves the in situ formation of reactive bifunctional poly(styrene) by polymerization with potassium naphthalide, followed by the actual coupling reaction with two 4th generation poly(benzyl ether) dendrons possessing benzyl bromide functionalities. The metal-halogen exchange side reactions are suppressed by reducing the reactivity of the polystyryl potassium with 1,1-diphenylethylene [4]. The resulting LDHPs are of DLD type (Fig. 1, 2) and can contain linear blocks of different chain length due to the good molecular mass control, provided of the "living" anionic polymerization. Other frequently used coupling reactions include Williamson ether synthesis, esterifications of different type, "click" chemistry, and others. The polymerization of preformed dendritic macromonomers could also be considered part of this strategy. An example is shown in Fig. 7.

These interesting amphiphilic copolymers are formed in good yields by Suzuki cross-coupling of dendritic macromonomers with dibromobenzene moiety and phenylene diboronic acid under the action of Pd[P(p-Tol)$_3$]$_3$ [5].
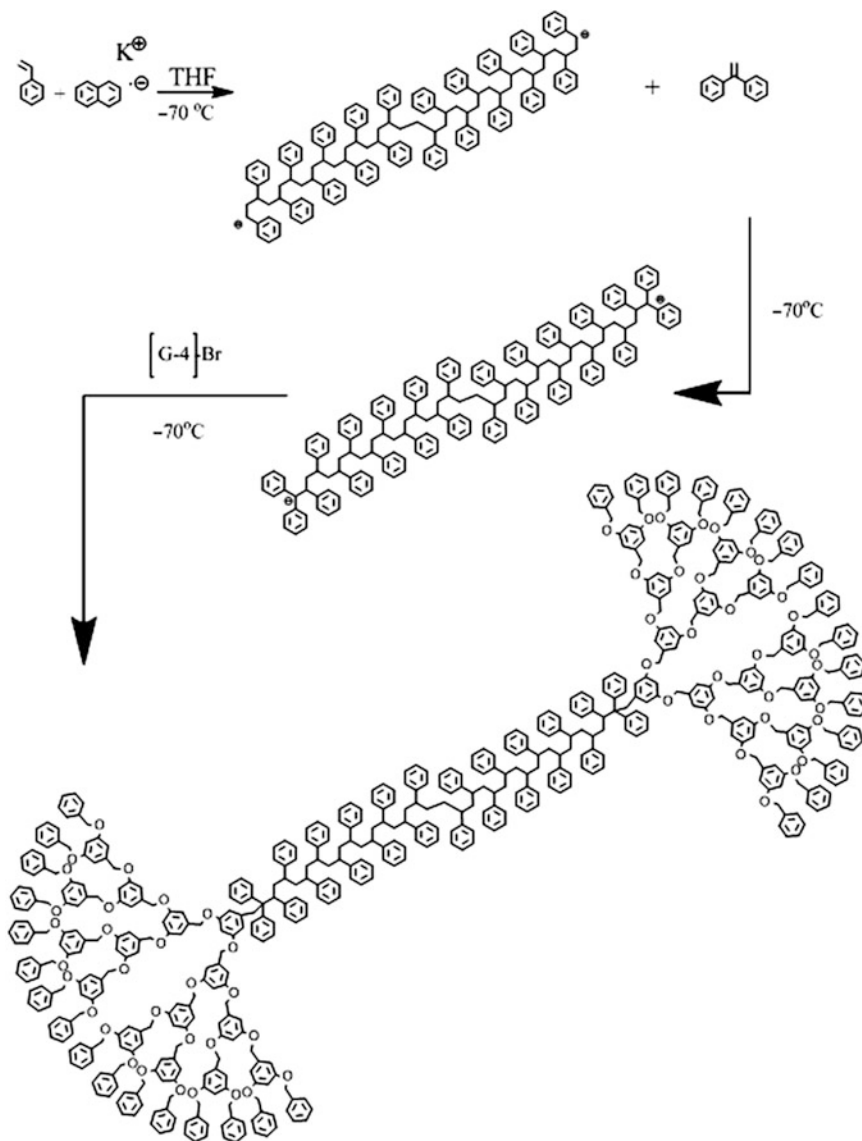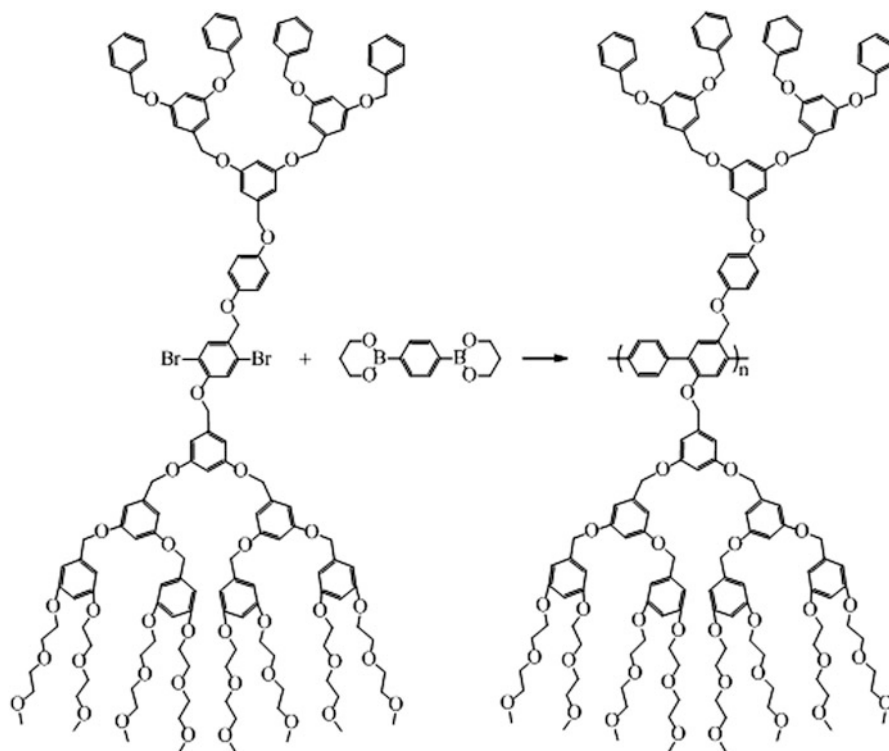
Synthesis and Self-Assembly of Linear-Dendritic Hybrid Polymers, Fig. 6 Synthesis of DLD hybrid copolymer by coupling of preformed blocks [4]

Growth of Dendrons on Linear Chains

Following the original divergent dendrimer synthesis, dendrons could be grown at the last unit of a linear chain or on specific reactive moieties along a polymer backbone. The method has been applied for the construction of macromolecular structures like **1** and **2** (Fig. 1), **4** (Fig. 2), or **7** (Fig. 3). Other combinations are also possible. Practically all common dendrimers could be divergently grown on a single polymer chain.

The advantage of this approach in comparison to the first strategy is that it enables the incorporation of more diverse functionalities on the surface of the dendrons formed. In many occasions the linear precursor facilitates the synthesis and the purification of the resulting copolymers by changing their solubility in selective solvents. Notably, the largest LDHPs (dendronized polymers of type **4**) are obtained using this method [6]. On the other side, the preformed polymer

Synthesis and Self-Assembly of Linear-Dendritic Hybrid Polymers, Fig. 7 Polycondensation of dendron macromonomers via Suzuki cross-coupling [5]

usually "screens" the small reactive group at the chain end and thus necessitates the application of large reagents excess and prolonged reaction times. Because of this "polymer effect," the typical molecular mass range of the linear chains is rather narrow – almost all published studies use polymers with molecular masses between 500 and 10,000. In addition, long linear blocks make the spectral proof of defect-free dendron formation particularly difficult because of the overwhelming intensity of the characteristic signals from the chain repeating units.

Type **1** structure is shown in Fig. 8 as an example of the possibilities offered by this synthetic approach. This new class of amphiphilic LDHPs containing poly(styrene) and poly(propylene imine) dendrons [7] is formed by a two-stage procedure. Initially amino-terminated poly(styrene) of molecular weight 3,000 is formed by classic anionic polymerization, and

the fifth generation dendron is constructed (Fig. 8) by five consecutive cycles of acrylonitrile coupling via Michael addition and catalytic hydrogenation. Careful selection of the reaction conditions is imperative to ensure high yields at each synthetic step. The abovementioned advantage of subsequent chemical transformation has been demonstrated since the dendron in the hybrid structure can be selectively modified not only at the periphery (CN- to COOH groups) [7] but also throughout the entire structure (quaternization of the primary and tertiary amines with methyl iodide) [8].

Growth of Linear Chain(s) on Dendritic Macroinitiators

This synthetic strategy enables the single step construction of hybrid copolymers of DL- or $D(L)_n$ type (Fig. 1, **1** and Fig. 3, **6**, respectively). Linear blocks with well-defined molecular mass characteristics could be formed on a dendritic
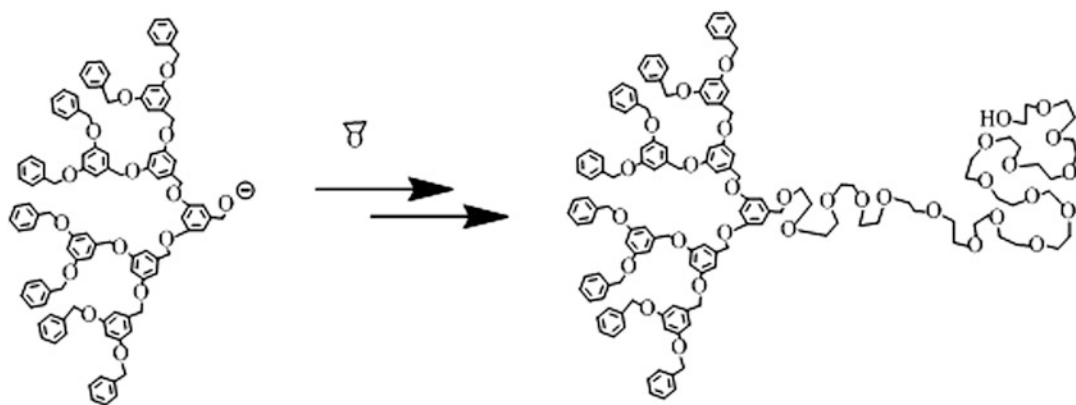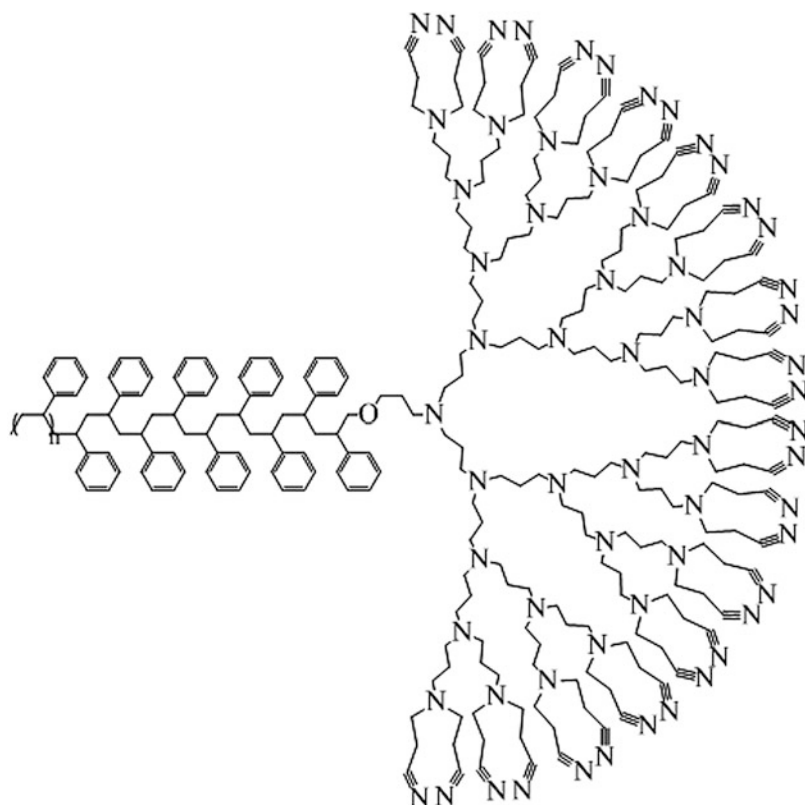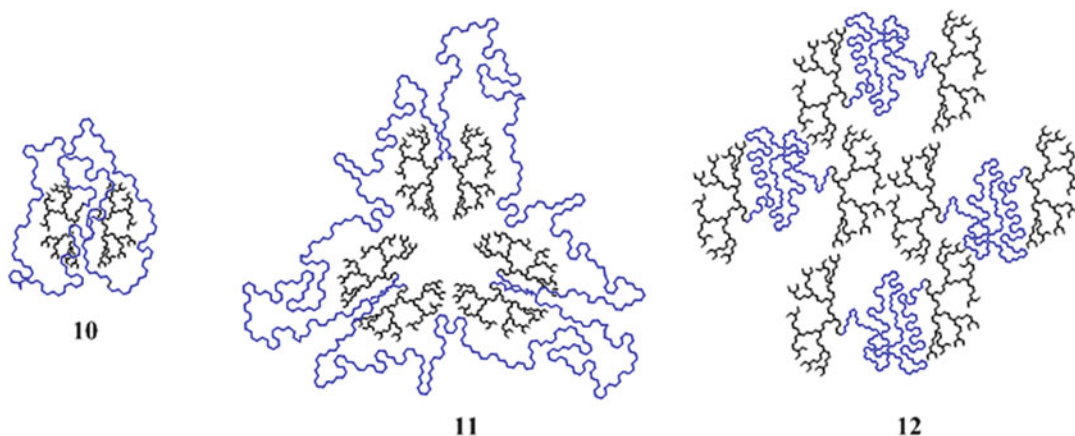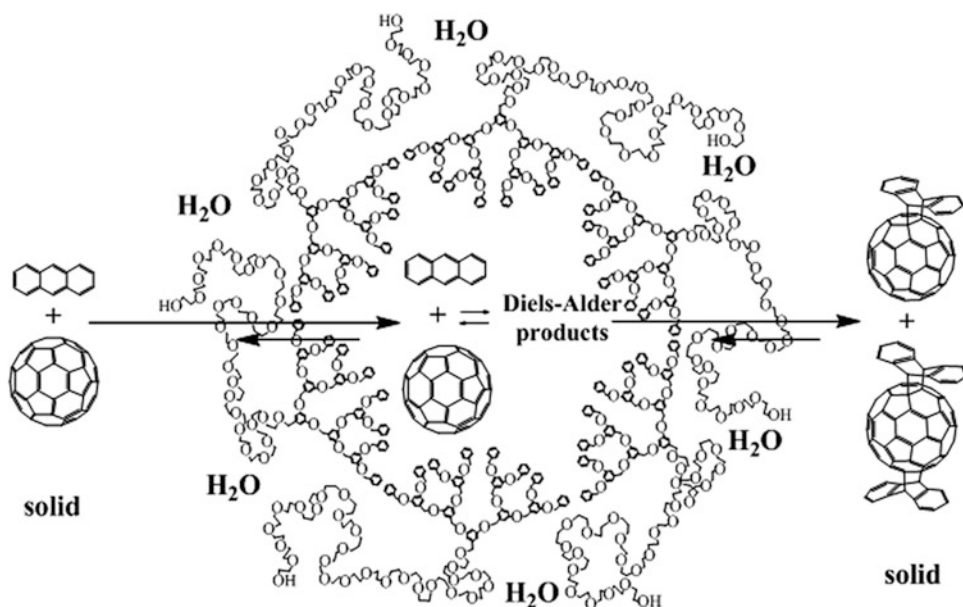
Synthesis and Self-Assembly of Linear-Dendritic Hybrid Polymers, Fig. 9 Synthesis of dendritic-linear copolymer by "living" anionic polymerization [9]

fragment by various chain-growth polymerization processes including anionic, controlled radical and ring-opening polymerizations. Notable advantages of this method are the possibility to control the chain growth, the chemical composition of the chain and chain end. The relatively simple purification and structure elucidation should not be overlooked, as well. Restrictions in the type of the peripheral groups in the dendron could be considered as minor disadvantages. The synthetic process is exemplified by the polymerization presented in Fig. 9. The procedure yields

Synthesis and Self-Assembly of Linear-Dendritic Hybrid Polymers, Fig. 10   Self-assembly patterns for linear-dendritic copolymers in linear-block-selective media

Synthesis and Self-Assembly of Linear-Dendritic Hybrid Polymers, Fig. 11   Linear-dendritic nano-sized reaction vessels facilitate Diels-Alder reactions of strongly hydrophobic substances in water [12]

LDHPs of controllable molecular mass and narrow polydispersity [9].

The presence of reactive functional groups at the end of the linear block provides additional avenues for the creation of asymmetric tri-block copolymers via a few subsequent steps [9]. Other linear chains successfully grown on reactive dendrons include poly(lactide)s, poly(styrene), and poly(methyl methacrylate), among others.

Self-Assembly

Naturally the presence of dendrons and linear chains with often different solvent affinity would potentially trigger the self-assembly of the LDHPs into supramolecular nano- and microstructures in block-selective media [1, 2]. In an environment, where the linear portions are soluble, the balance between the size of the dendrons

and the length of the linear chains directs the micellization via end-to-end association towards monomolecular species (Fig. 10, **10**), true supermolecules (Fig. 10, **11**), or physical networks (Fig. 10, **12**). Similar association pattern could be achieved with type **1** LD copolymer. Self-assembly is also possible with structures **3**, **6**, and **7** and under special conditions and circumstances with LDHPs of types **4** and **5** depending on the size of the two building blocks.

The incorporation of two or more non-entangled dendrons creates a nano-porous compartmentalized core in the hybrid micelles, which can possibly accommodate substantial amounts of substrates with similar affinity to the surrounding medium. This mechanism differs favorably from the binding pattern of the common micelles, constructed by linear copolymers or low molecular mass amphiphiles, where the majority of encapsulated molecules reside at the interface between the micellar core and the corona. Indeed, the partition equilibrium coefficients (K_v) of some linear-dendritic micelles were found superior to the conventional linear-linear copolymer micelles [10, 11]. This peculiar feature of the hybrid supermolecules has been utilized for the construction of nano-sized reaction vessels and their use in environmentally friendly reactions. Such a process is shown in Fig. 11 [12].

In this application strongly hydrophobic substances – C_{60}, anthracene (shown), or tetracene – undergo a Diels-Alder reaction in aqueous medium and at ambient temperature with apparent kinetic rate constants and product yield, which are significantly higher than those observed in organic solvents (toluene, naphthalene) and elevated temperatures [12]. This approach has been further expanded with the incorporation of oxidative enzymes in the same type of nano-reactor for the unprecedented oxidation of fullerene in water under mild reaction conditions [13].

Summary

Since the inception of the linear-dendritic hybrid polymers more than 20 years ago, the research on this class of nano-structured materials has witnessed steady increase and expansion. Besides the introduction of new efficient synthetic methodologies ("click" chemistry [14]), the exploration of the solution and solid-state behavior has intensified due to the rather limited data available and the promising potential of the LDHPs as nano-transporters through interfaces and cell membranes [15], as enzymatic nano-reactors in "green chemistry" applications [16], and as substances for tissue regeneration and repair [17].

Related Entries

- ► Dendrimer-Like Star Branched Polymers
- ► Dendronized Block Copolymers
- ► Dendronized Copolymers
- ► Dendronized Homopolymers
- ► Stimuli-Responsive Polymers
- ► Supramolecular Hydrogels
- ► Supramolecular Network Polymers
- ► Supramolecular Polymers (Host-Guest Interactions)

References

1. Gitsov I (2008) Hybrid linear dendritic macromolecules: from synthesis to applications. J Polym Sci Part A Polym Chem 46:5295–5314
2. Wurm F, Frey H (2011) Linear-dendritic block copolymers: the state of the art and exciting perspectives. Prog Polym Sci 36:1–52
3. Gitsov I (2002) Linear-dendritic block copolymers. Synthesis and characterization. In: Newkome GR (ed) Advances in dendritic macromolecules, vol 5. Elsevier, Amsterdam, pp 45–87
4. Gitsov I, Fréchet JMJ (1994) Novel nanoscopic architectures. Linear-globular ABA copolymers with polyether dendrimers as A blocks and polystyrene as B block. Macromolecules 27:7309–7315
5. Bo Z, Rabe JP, Schlüter AD (1999) A poly(paraphenylene) with hydrophobic and hydrophilic dendrons: prototype of an amphiphilic cylinder with the potential to segregate lengthwise. Angew Chem Int Ed 38:2370–2372
6. Zhang B, Wepf R, Fischer K, Schmidt M, Besse S, Lindner P, King BT, Sigel R, Schurtenberger P, Talmon Y, Ding Y, Kröger M, Halperin A, Schlüter AD (2010) The largest synthetic structure with molecular precision: towards a molecular object. Angew Chem Int Ed 50:737–740

S

7. van Hest JCM, Baars MWPL, Elissen-Román C, van Genderen MHP, Meijer EW (1995) Acid-functionalized amphiphiles derived from polystyrene-poly(propylene imine) dendrimers, with a pH-dependent aggregation. Macromolecules 28:6689–6691

8. Elissen-Román C, van Hest JCM, Baars MWPL, van Genderen MHP, Meijer EW (1997) Amphiphilic block copolymers based on quaternized poly(propylene imine) dendrimers. Polym Mat Sci Eng 77:145

9. Gitsov I, Simonyan A, Vladimirov NG (2007) Synthesis of novel asymmetric dendritic-linear-dendritic block copolymers via "Living" anionic polymerization of ethylene oxide initiated by dendritic macroinitiators. J Polym Sci Part A Polym Chem 45:5136–5148

10. Gitsov I, Lambrych KR, Remnant VA, Pracitto R (2000) Micelles with highly branched nanoporous interior: solution properties and binding capabilities of amphiphilic copolymers with linear dendritic architecture. J Polym Sci Part A Polym Chem 38:2711–2727

11. Chang Y, Park C, Kim KT, Kim C (2005) Synthesis and micellar characteristics of dendron-PEG conjugates. Langmuir 21:4334–4339

12. Simonyan A, Gitsov I (2008) Linear-dendritic supramolecular complexes as nano-scale reaction vessels for "Green" chemistry. Diels Alder reactions between fullerene C_{60} and polycyclic aromatic hydrocarbons in aqueous medium. Langmuir 24:11431–11441

13. Gitsov I, Simonyan A, Wang L, Krastanov A, Tanenbaum SW, Kiemle D (2012) Polymer-assisted biocatalysis: unprecedented enzymatic oxidation of fullerene in aqueous medium. J Polym Sci Part A Polym Chem 50:119–126

14. Lundberg P, Walter MV, Montañez MI, Hult D, Hult A, Nyström A, Malkoch M (2011) Linear dendritic polymeric amphiphiles with intrinsic biocompatibility: synthesis and characterization to fabrication of micelles and honeycomb membranes. Polym Chem 2:394–402

15. Gillies ER, Fréchet JMJ (2002) Designing macromolecules for therapeutic applications: polyester dendrimer-poly(ethylene oxide) "bow-tie" hybrids with tunable molecular weight and architecture. J Am Chem Soc 124:14137–14146

16. Gitsov I, Hamzik J, Ryan J, Simonyan A, Nakas JP, Omori S, Krastanov A, Cohen T, Tanenbaum SW (2008) Enzymatic nano-reactors for environmentally benign biotransformations. 1. Formation and catalytic activity of supramolecular complexes of laccase and linear dendritic block copolymers. Biomacromolecules 9:804–811

17. Grinstaff MW (2002) Biodendrimers: new polymeric biomaterials for tissue engineering. Chem Eur J 8:2838–2846

Synthesis of Hyperbranched Polymers

Mario Smet
Department of Chemistry, Division of Polymer Chemistry and Materials, University of Leuven, Heverlee, Belgium

Synonyms

Branched polymers; Synthesis of dendritic polymers

Definition

Hyperbranched polymers are macromolecules that are densely branched (but typically not as densely as dendrimers) and that are typically obtained in one synthetic step (like linear polymers and in contrast to dendrimers).

Introduction

Hyperbranched polymers are a relatively new class of densely branched macromolecules [1]. They differ from linear polymers a.o. in their low viscosity and high end group density in which they resemble dendrons and dendrimers. An example of a hyperbranched polymer and a dendron derived from an AB_2 monomer, which is among the simplest monomers from which branched polymers can be obtained, is given in Fig. 1. A dendrimer is a conjugate of several dendrons attached to a central core. In contrast to dendrimers, which are even more densely branched, monodisperse, and perfectly symmetric structures, the synthesis of hyperbranched polymers does not rely on a multistep sequence but usually consists in a one-step process like for regular linear polymers. Consequently, they are often considered readily available and cheap substitutes for dendrimers.
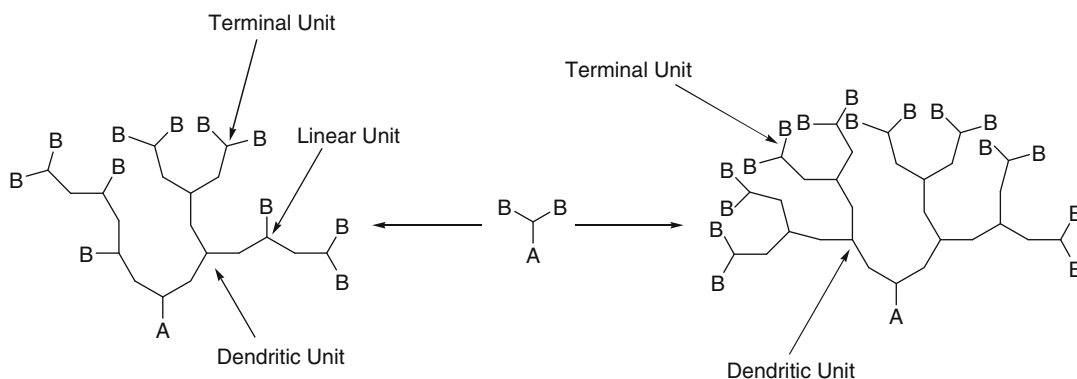
Synthesis of Hyperbranched Polymers, Fig. 1 Schematic representation of a hyperbranched polymer (*left*) and a dendron (*right*), both derived from the same AB_2 monomer

An important characteristic of hyperbranched polymers is the degree of branching (DB), which is a measure for the branching density and which is usually defined according to Eq. 1 proposed by Fréchet in which D equals the number of dendritic units (both B functionalities have reacted), L the number of linear units (one of the B functionalities has reacted), and T the number of terminal units (none of the B functionalities has reacted), respectively (Fig. 1) [1]:

$$DB = \frac{D + T}{D + T + L} \qquad (1)$$

An alternative definition put forward by Frey is given in Eq. 2 [1]. Linear polymers have a DB of 0 and dendrimers have a DB of 1. Hyperbranched polymers can have variable DB, in many cases around 0.5. It should be noted that both definitions mentioned here are, in the strict sense, only valid for hyperbranched structures derived from AB_2 monomers:

$$DB = \frac{2D}{2D + L} \qquad (2)$$

In general, hyperbranched polymer synthesis can be subdivided in the following main strategies [1–7]: (i) polycondensation of AB_n monomers ($n \geq 2$); (ii) polycondensation of symmetric monomer pairs such as a combination of A_2 and B_n monomers ($n \geq 3$); (iii) polymerization of asymmetric monomer pairs, which can suppress gel formation which is a potential undesired side effect of the second strategy; and (iv) self-condensing chain-growth polymerization of AB* monomers of which ring-opening multibranching polymerization (ROMBP) and self-condensing vinyl polymerization (SCVP) are the main instances. Besides these strategies, in what follows, a few more special approaches will be discussed.

Polycondensation of AB_n Monomers

Polycondensation of an AB monomer obviously yields a linear polymer with one A and one B terminal group. Analogously, polycondensation of an AB_n monomer yields hyperbranched macromolecules with one free A functionality and numerous B terminal groups. The number of terminal B groups per macromolecule theoretically equals $x + 1$, with x the number of monomeric units in the macromolecule under consideration. It should be noted that the term polycondensation is used rather generally in this context, although also, e.g., addition reactions and even cycloadditions [8] between AB_n have been explored to obtain hyperbranched polymers of similar structure.

The number average molar mass typically grows in a stepwise fashion like in a classical polycondensation toward linear polymers, i.e., high molar masses are typically only formed at high conversions (Table 1) [1]. Cyclization often

complicates this synthetic strategy [9]: as polycondensation proceeds, the chance that an A functionality **intramolecularly** reacts with one of the B functionalities increases dramatically (obviously becoming much higher than in the case of linear polycondensation polymers as in this case there are only two end groups which necessarily have to find each other for cyclization) resulting in the formation of a cyclic structure without A functionality (Fig. 2). This phenomenon strongly reduces the molar mass built up, as the only way by which the average molecular weight can grow is by **intermolecular** reactions of an A and a B functionality.

Cyclization can be suppressed by the use of multifunctional core molecules (B_n monomers with $n \geq 3$) as this creates a stoichiometric excess of B groups, decreasing the chance that A groups intramolecularly react. The use of core molecules has been found particularly effective in this respect if the monomer is slowly added to the polymerization mixture containing the core. Also control of the molar mass is possible by varying the ratio of monomer to core. Moreover, the use of a core reagent usually allows to obtain narrower polydispersities.

It should be noted that although network formation is theoretically impossible if only

condensation between A and B groups occurs, in practice, gelation can be observed if side reactions (for instance coupling between B groups) happen. The polydispersity of the polymers obtained is often very broad; typically, PDI are in the range of 2–3. When the reactivity of the two B functionalities is equal (hence, e.g., for an AB_2 monomer, the reactivity of the residual B functionality is not influenced by the reaction of the first), the DB reaches 0.5 according to Eq. 3, with x the conversion of the A groups:

$$\mathrm{DB} = \frac{2x}{5 - x} \qquad (3)$$

Among the numerous examples of polymerization reactions of AB_n monomers, nucleophilic substitutions are one of the most widespread. An important type of monomers fit for this strategy is, for instance, structures **1a–d**, which undergo polymerization through nucleophilic aromatic substitution due to the activation of the aromatic ring by the electron withdrawing substituents yielding the respective hyperbranched polymers **2a–d** (Fig. 3).

Mostly oxygen has been used as the nucleophilic center, but also sulfur has been explored due to its higher nucleophilicity and the specific functional properties of the sulfur connecting bridges (e.g., possibility for oxidation to sulfoxides and sulfones) in the final polymer. For nonactivated aromatic rings, the Ulmann-type coupling has been explored, but also nucleophilic substitution of aliphatic or benzylic halogenides is possible. Another type of nucleophilic substitution which is well suited for hyperbranched polymer formation is the formation of esters or amides from carboxylic acids. In general, thermal

Synthesis of Hyperbranched Polymers, Table 1 Theoretical degree of polymerization and polydispersity in polycondensations of A-R-B_{f-1}-type monomers

Monomer type	A-R-B_{f-1}[a]	AB_2[a]
DP_n	$\frac{1}{1-p}$	$\frac{1}{1-p}$
DP_w	$\frac{1-p^2/(f-1)}{(1-p)^2}$	$\frac{1-p^2/2}{(1-p)^2}$
DP_n/DP_w	$\frac{1-p^2/(f-1)}{1-p}$	$\frac{1-p^2/2}{1-p}$

[a]p: conversion of A functionality

Synthesis of Hyperbranched Polymers, Fig. 2 Cyclization in AB_2 polycondensation
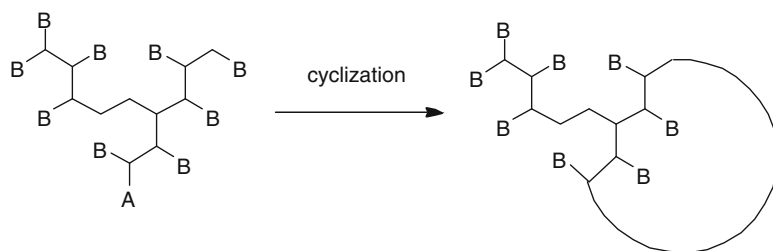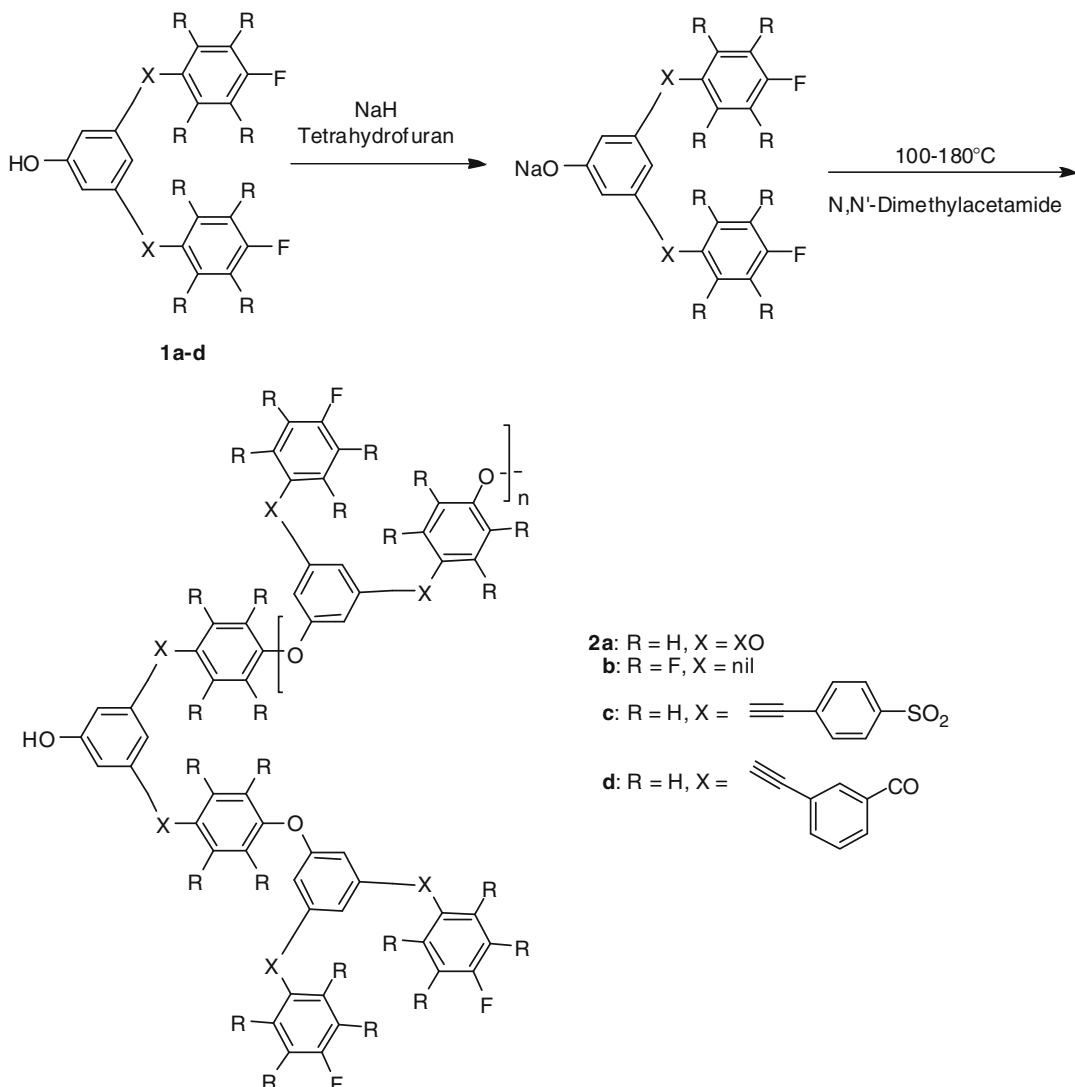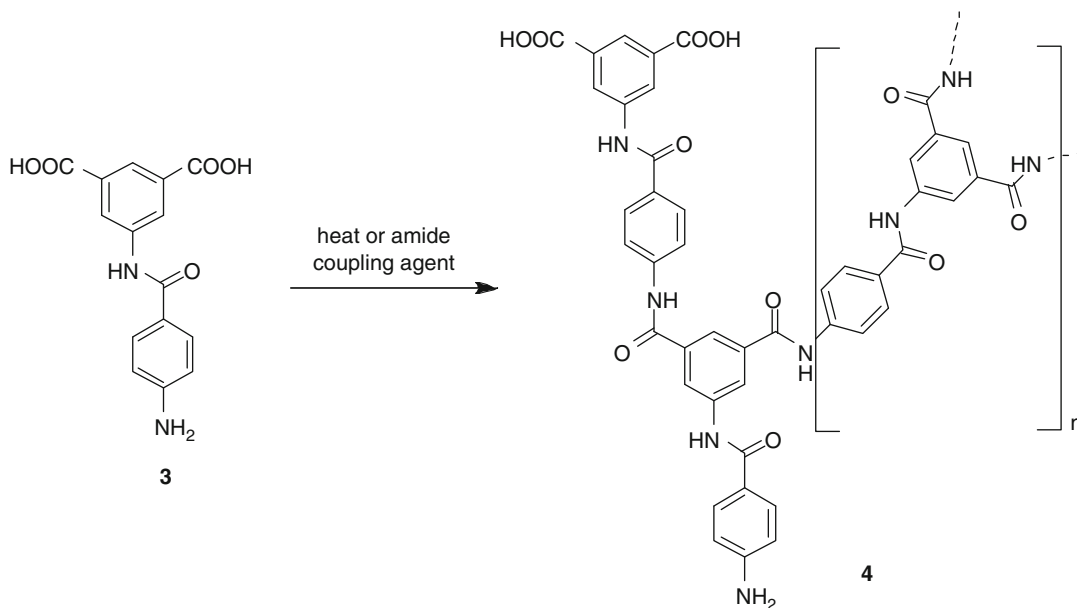
Synthesis of Hyperbranched Polymers, Fig. 3 Polycondensation by nucleophilic aromatic substitution

activation or special dedicated coupling agents can be used to promote condensation. Figure 4 shows the synthesis of an aromatic polyamide **4** starting from an AB_2 monomer **3**, featuring an amino and two carboxylic acid groups.

The formation of polyurethanes from isocyanates and alcohols has been very fruitful for both academic and industrial applications [10]. Hence, it is not surprising that also this reaction has been applied for hyperbranched polymer synthesis. Due to the high reactivity of

the isocyanate, which would result in undesired early polymerization, the isocyanate moiety is typically present as a precursor which is thermally converted in situ such as in the case of monomers **5** and **6** in which an acyl azide and a phenol urethane act as the masked isocyanate, respectively (Fig. 5).

Also silicon has been proven a very useful building block for polymers due to the remarkably different physical properties of the materials. The incorporation of silicon in the
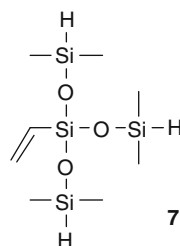
Synthesis of Hyperbranched Polymers, Fig. 4 Formation of a hyperbranched polyamide
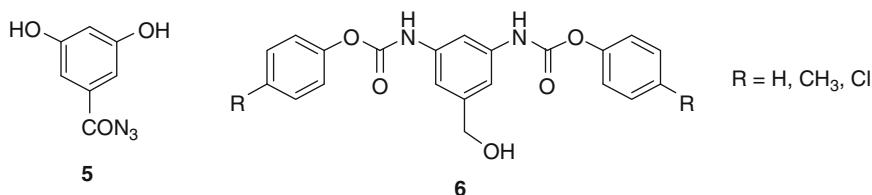
Synthesis of Hyperbranched Polymers, Fig. 5 AB$_2$ monomers for hyperbranched polyurethane synthesis with masked isocyanate precursor functionalities

Synthesis of Hyperbranched Polymers, Fig. 6 AB$_3$ monomer for hyperbranched polysilane synthesis via hydrosilylation

required AB$_n$ monomer also allows the facile construction of the monomer for $n = 3$, 4, and 6. Especially the hydrosilylation reaction has been explored as an attractive strategy for hyperbranched polysilanes using, for instance, monomers such as **7** (Fig. 6).

Polycondensation of Symmetric Monomer Pairs

The main advantage of hyperbranched polymers over dendrimers is their much easier synthesis. However, the use of AB$_n$ monomers does not fully exploit this potential as monomers of this type are in many cases not commercially and/or readily available. Therefore, a combination of A$_2$ and B$_n$ monomers ($n \geq 3$) seems even more attractive as the required monomers are usually commercially available at low prices. Hence, it is not surprising that especially the A$_2$ + B$_3$ approach has been explored extensively. However, according to the theoretical consideration of Flory [11], a polycondensation of this type

gives rise to gelation, i.e., the formation of an insoluble "infinite" 3-dimensional network, if the following conditions are met: (i) the reactivity of the A and B functional groups remains constant during the course of the polymerization, (ii) no cyclization occurs, and (iii) the polymerization only relies on the reaction between A and B groups. It seems not very difficult to find settings and conditions which sufficiently deviate from these theoretical requirements to avoid gelation, and indeed this has been widely experimentally confirmed, resulting in many new approaches to hyperbranched macromolecules which are, especially from an industrial point of view, more attractive than the traditional AB_2 polycondensates.

According to the aforementioned Flory theory, the gel point, characterized by p_{Ac} and p_{Bc}, i.e., the conversion of A and B functions at which gelation occurs, can be calculated. These conversions also reflect the reciprocal of the actual residual number of the respective functional groups in the polymer. (For soluble macromolecules, these values are actually the limits as they hold for the network at the gel point.) For a $A_2 + B_3$ system, its dependence of the stoichiometric ratio of the two monomers in the feed (with $r = A:B$, the stoichiometric ratio of the actual functional groups) varies as displayed in Table 2.

Using Frey's definition of the degree of branching, DB has been simulated as a function of the conversion of A groups and for different monomer ratios as depicted in Fig. 7 up to the gel point [1]. In general, it is more easy to avoid gelation when a lower A:B ratio is taken. Consequently, however, the degree of branching will be lower. It should be noted that also higher initial monomer concentrations favor gelation. Obviously, cyclization can also occur in $A_2 + B_3$ systems. In contrast to AB_2-based systems, multiple cyclization can occur. In the typical case of an $A_2:B_3$ ratio of 1:1, most of the macromolecules contain a cyclic structure. Higher $A_2:B_3$ ratios typically tend to give more multicyclic systems [9]. So it should be noted that the actual structural details of $A_2 + B_3$ derived hyperbranched macromolecules can be variable

Synthesis of Hyperbranched Polymers, Table 2 Calculation of the gel point in $A_2 + B_3$ polycondensation for various monomer ratios

$A_2:B_3$	$r = A:B$	p_{Ac}	p_{Bc}
0.75:1.00	0.50	1.000	0.500
0.90:1.00	0.60	0.913	0.548
1.00:1.00	0.67	0.866	0.577
1.25:1.00	0.83	0.775	0.645
1.50:1.00	1.00	0.707	0.707
2.00:1.00	1.33	0.612	0.816
3.00:1.00	2.00	0.500	1.000

Synthesis of Hyperbranched Polymers, Fig. 7 Simulation of DB versus conversion of A functionalities p_A for various $A_2:B_3$ ratios
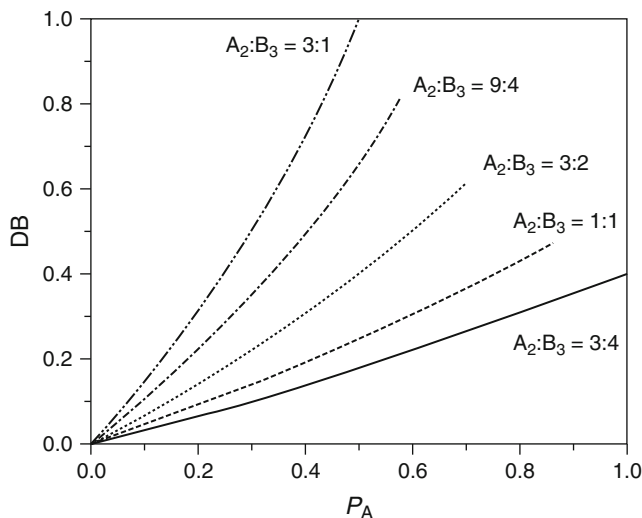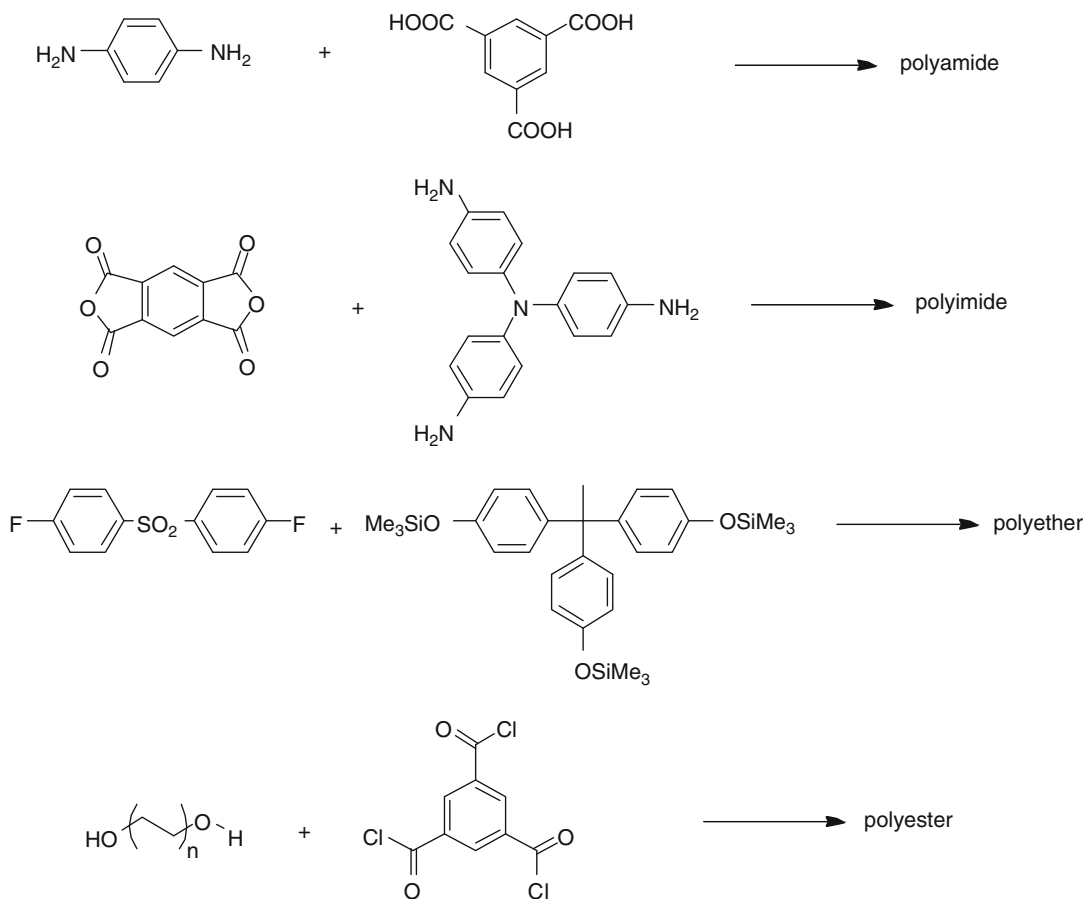
Synthesis of Hyperbranched Polymers, Fig. 8 Several A_2 + B_3 combination that have been applied for hyperbranched polymer synthesis

and in general also quite different from their AB_2 counterparts.

The main types of hyperbranched polymers that have been prepared using this strategy are polyamides, polyimides, polyethers, and polyesters. Some examples of monomer combinations have been given in Fig. 8.

A remarkable example of a A_2 + B_3 system features isatins **8** as the A_2 monomer (Fig. 9) [12]. The 3-carbonyl group of this heterocycle can be doubly arylated by electron-rich aromatic moieties. The second arylation is much faster than the first, thus creating a strong reactivity difference between the A functionalities which suppresses the gelation tendency almost completely, resulting in the polymers **9** which can easily be

functionalized further via electrophilic aromatic substitution.

Polycondensation of Asymmetric Monomer Pairs

Comparing the AB_2-based strategy with the A_2 + B_3 strategy, it seems attractive to explore modifications which favor in situ formation of a AB_2 monomer out of the initial monomers as illustrated in Fig. 10. Such an approach can consist in the use of an AA′ monomer, in which A′ is more reactive than A, in combination with a symmetric B_3. Alternatively, a B′B_2 monomer can be combined with a symmetric A_2. The latter approach not only
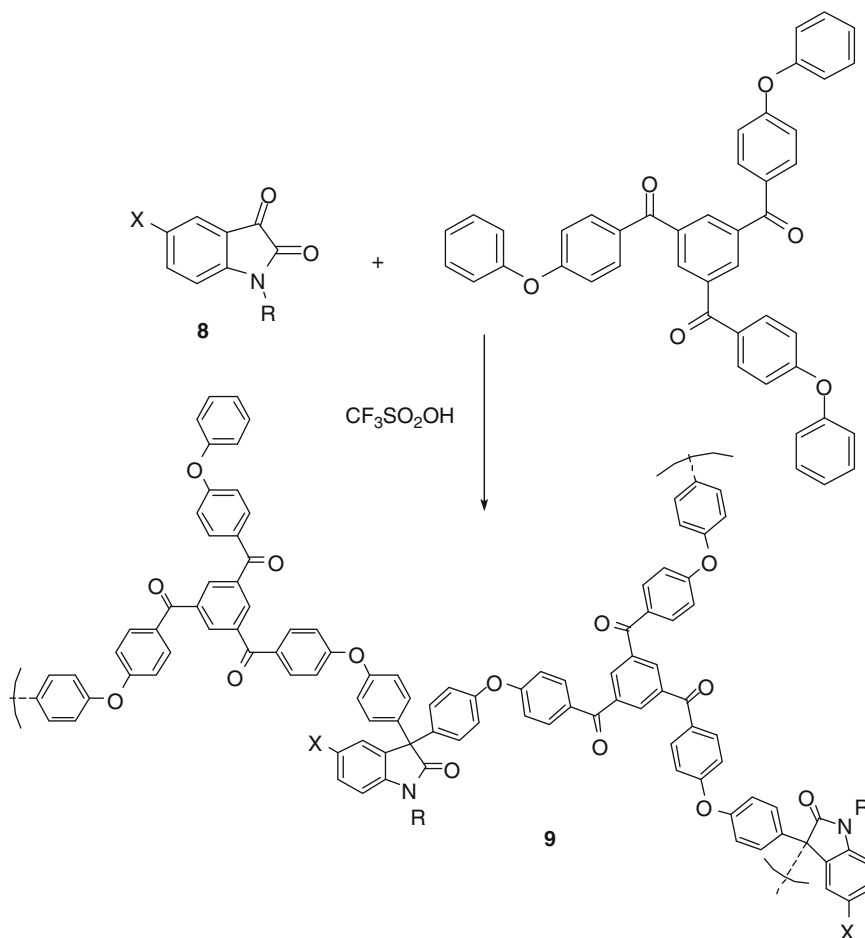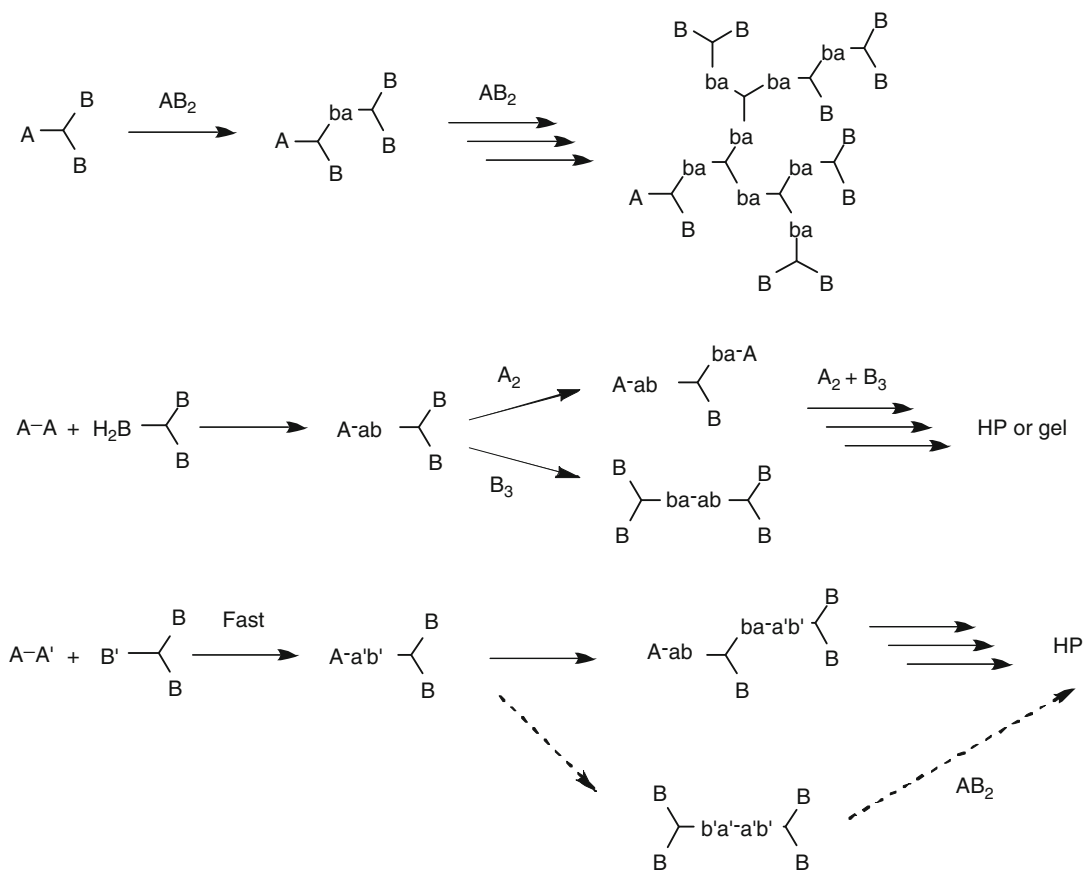
Synthesis of Hyperbranched Polymers, Fig. 9 $A_2 + B_3$ synthesis using isatins as the A_2 partner

favors the in situ formation of AB_2-type monomers. Reaction of A_2 with two $B'B_2$ monomers indeed gives rise to a B_4-type species (Fig. 10) which acts as a core and hence may lead to a narrower molecular weight distribution.

Both phenomena have been observed in the polymerization of a mixture of divinyl sulfone (DVS) and an asymmetric diamine with a secondary and a primary amino group such as 1-(2-aminoethyl)piperazine (AEPZ) (Fig. 11). The secondary amino (B') group was found to react much faster with the DVS than the primary (which itself acts as a bifunctional unit B_2 or BB'' as both functionalities are not quite equivalent).

Obviously, it is possible to use monomer combinations in which one or both of the A' or/and the B' functionalities have a completely different

nature than the A and B functions, respectively. In such a case, the feed system is usually denoted as an $AC + DB_2$ polymerization, although this largely remains a matter of interpretation. It is interesting to mention that in the latter case, the polymer backbone consists of two different functional linkages, which can bring additional functionalities to the final polymer. Hyperbranched poly(amide amine)s, poly(amine ester)s, and poly(ester amide)s are typical examples, prepared by combination of the monomers shown in Fig. 12. In the latter case, the second A functionality is only created upon reaction of the first; hence, the monomer is denoted as A*. It should be noted that one of the few hyperbranched polymers that have been prepared on a (semi) commercial scale, i.e., DSM's Hybrane

Synthesis of Hyperbranched Polymers, Fig. 10 Schematic comparison of the AB_2 polycondensation, the $A_2 + B_3$ strategy, and an asymmetric combination $AA' + B'B_2$
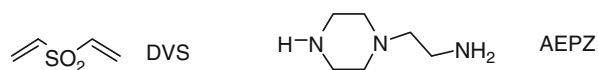
Synthesis of Hyperbranched Polymers, Fig. 11 Example of a monomer combination for a $AA' + B'B_2$ ($BB'B''$) approach

hyperbranched poly(ester amide), also belongs to this category, using cyclohexane 1,2-dicarboxylic acid anhydride (**10**) in combination with diisopropanolamine (**11**).
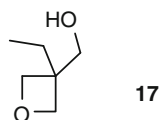
An additional advantage of the so-called couple-monomer methodology is the possibility to tune the molar mass by varying the ratio of the two monomers: a higher AA'-to-$B'B_2$ ratio favors higher molar masses and vice versa. Concomitantly, the ratio of residual A and B groups in the resulting polymer will be modified.

Ring-Opening Multibranching Polymerization

A particularly elegant way to obtain hyperbranched polymers is the use of a so-called inimer, which is a monomer which contains both a polymerizable unit and a functionality capable to initiate the polymerization of the former. This polymerization can be considered as a combination of a chain-growth mechanism (for instance a ring-opening polymerization) and

Synthesis of Hyperbranched Polymers, Fig. 12 Selected examples of asymmetric monomer combinations from the literature

Synthesis of Hyperbranched Polymers, Fig. 13 ROMBP of glycidol using pentaerythritol as the core yielding polyglycerol

a step-growth mechanism (for instance the ring-opening by the side group, hence the initiation of a new chain). The example given here is commonly denoted as ring-opening multibranching polymerization (ROMBP). Glycidol (12) is among the best studied examples of monomers fit for this kind of hyperbranched polymer synthesis (Fig. 13) [13]. Anionic polymerization of glycidol (12) leads to remarkably moderate polydispersities and allows for the highly beneficial use of core reagents such as 13

and slow addition methodology. Besides the excellent control of the polymer structure, the obtained polyglycidols 14 (usually called polyglycerol) display also a low toxicity and good biocompatibility which may result in, e.g., in vivo sensing applications. A drawback of this polymer, although more significant from the characterization than the application point of view, is that these polyglycidols typically contain two kinds of linear units: one with a free primary alcohol and one with a free secondary alcohol

**Synthesis of
Hyperbranched
Polymers,
Fig. 14** ROMBP of
aziridine yielding poly
(ethyleneimine)
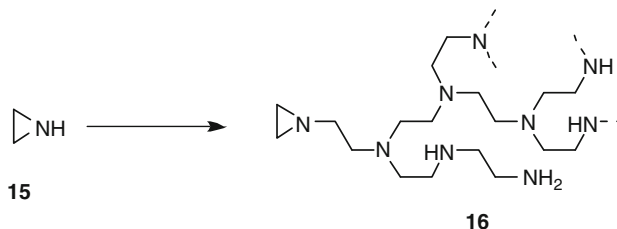
Synthesis of Hyperbranched Polymers, Fig. 15 A
less toxic, however, less versatile monomer for ROMBP
yielding polyethers

(in a terminal unit obviously both have not reacted). Obviously, this is usually the case when an AB* strategy is applied.

Of maybe even more importance nowadays is the ring-opening polymerization of aziridine (**15**), which indeed can be considered as an inimer and yields poly(ethyleneimine)s **16** with various degree of branching depending on the polymerization conditions (Fig. 14). Also poly (ethyleneimine)s have been extensively studied in the biomedical application context, mainly as gene delivery vectors.

The typical inimers required for ring-opening multibranching polymerization may represent a lack of structural diversity as a main drawback. Also the toxicity of glycidol and aziridine is a point of concern. An obvious analog of glycidol which also has been explored for the synthesis of a hyperbranched polymer is 3-hydroxymethyl-3-ethyloxetane (**17**) (Fig. 15). Although far less toxic, the lower ring strain of this compound makes it a much less attractive monomer due to its lower reactivity. It typically allows only cationic polymerization which is more difficult to control.

## Self-Condensing Vinyl Polymerization

The ring-opening multibranching polymerization as discussed above relies on the combination of

an initiating and a (chain-growth) polymerizable moiety in one and the same molecule, the so-called inimer. The most important type of chain-growth polymerizable monomers giving rise to linear polymers, i.e., vinyl monomers, however, has not been discussed so far. Indeed, it is possible to combine also a vinyl monomer and an initiating moiety for the polymerization thereof in one inimer, giving rise to a species that can be polymerized under typical conditions also used for the preparation of linear vinyl polymers. Such inimers are commonly denoted as AB* in which the vinyl moiety is denoted as A and the group that is capable of being activated to initiate the polymerization as B*. Figure 16 represents the initial steps of a self-condensing vinyl polymerization of *p*-chloromethylstyrene (**18**). It should be noted that just like in the case of the ROMBP, two types of linear units can be expected, as clarified in Fig. 16 in which a possible hexamer from SCVB of *p*-chloromethylstyrene (**18**) is shown.

Mostly acrylate- and styrene-type monomers have been used in SCVP. Acrylate-based inimers such as the examples given in Fig. 17 have mainly been polymerized using the well-established atom transfer radical polymerization (ATRP) technique. Styrene monomers are more versatile allowing, besides ATRP, cationic polymerization, nitroxide-mediated polymerization (NMP), anionic polymerization, and other more specific techniques.

Cocondensation and Radical Copolymerization

Copolymerization strategies in general allow more structural diversity of the resulting
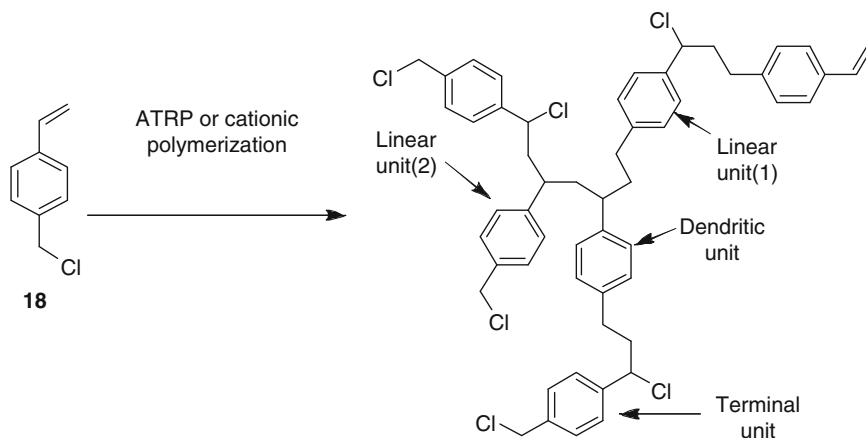
Synthesis of Hyperbranched Polymers, Fig. 16 SCVP of *p*-chloromethylstyrene and representation of the four different units present in the resulting hyperbranched polymer
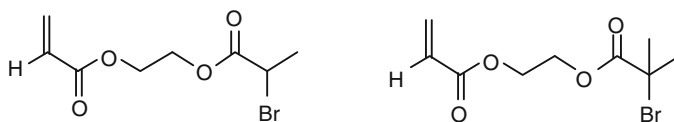
Synthesis of Hyperbranched Polymers, Fig. 17 Some examples of (meth) acrylate-based monomers for SCVP of hyperbranched poly(meth)acrylates
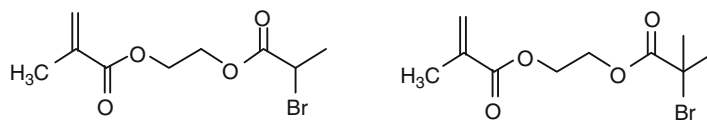
hyperbranched polymers with respect to both the nature of the monomer/backbone and the degree of branching. Probably the most straightforward application of such a strategy is the so-called AB_2 + AB strategy which is usually mainly applied to allow fine-tuning of the degree of branching. As the comonomer is non-branched, this strategy only allows to reduce the degree of branching to values lower than the typical statistical 0.5 for AB_2 polycondensations. Seen from the perspective of linear polymers, this strategy obviously is also an elegant method to incorporate a limited number of branching points in mostly linear polymers, which can be of interest to modify important material properties such as the solubility and the degree of crystallinity (and the related melting point).

Slightly more complex related applications are the combination of ring-opening

polymerization with AB_2 polycondensation and the combination of ring-opening multibranching polymerization with ring-opening polymerization featuring monomer combinations such as depicted in Fig. 18. The first strategy, for instance, allows the incorporation of a limited number of branching points in commercially interesting linear polymers such as poly(ε-caprolactone) and polylactide.

Also the double monomer strategy can readily be expanded to a copolymerization by adding a B_2 monomer, for instance, resulting in a A_2 + B_2 + BB'_2 approach for which a typical monomer combination is shown in Fig. 19.

A versatile strategy that allows the fine-tuning of the backbone properties without affecting too much the degree of branching is the combination of two different AB_2 monomers, in which, typically, the A and B functionalities of the two
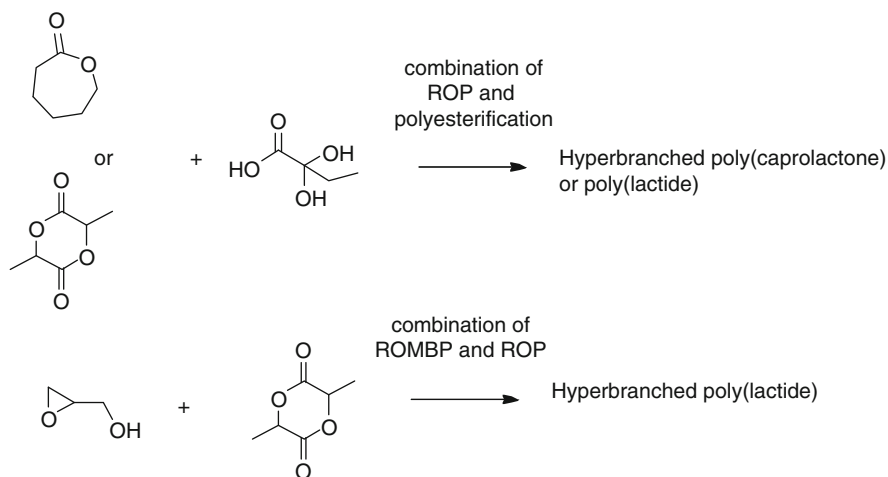
Synthesis of Hyperbranched Polymers, Fig. 18 Selected monomer combination for the introduction of branching in ROP
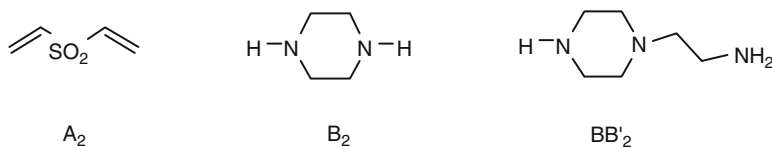
Synthesis of Hyperbranched Polymers, Fig. 19 Typical monomer combination for a $A_2 + B_2 + BB'_2$ approach
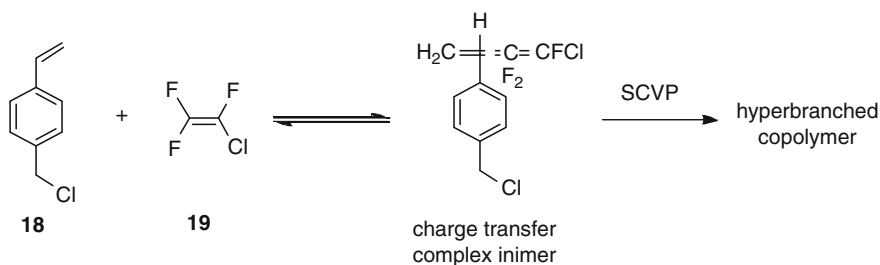
Synthesis of Hyperbranched Polymers, Fig. 20 SCVP of a charge transfer complex inimer

different monomers are the same but in which there is a different spacer in between (hardly affecting their intrinsic reactivity).

Finally, also the scope of the self-condensing vinyl polymerization can be significantly enhanced by using comonomers. This can be a monomer which is structurally similar to the polymerizable entity of the inimer, but also a kind of charge transfer complex polymerization has been explored, allowing the incorporation of structurally very different monomers, typically one being electron rich and the other electron deficient such as depicted in Fig. 20 for *p*-chloromethylstyrene (**18**) and chlorotrifluor-oethylene (**19**), respectively. Both comonomers form a charge transfer complex which acts as the inimer for the SCVP. This is particularly significant as the typical monomers for SCVP are usually not readily available (not commercial or rather expensive), and hence the structural diversity accessible by SCVP is limited if only homo-polymers are considered.

Related Entries

References

1. Yan D, Gao C, Frey H (2011) Hyperbranched polymers, synthesis, properties and applications. Wiley, New Jersey
2. Kim YH (1998) Hyperbranched polymers 10 years after. J Polym Sci Polym Chem 36:1685–1698. doi:10.1002/(SICI)1099-0518(199808)36:11
3. Voit B (2000) New developments in hyperbranched polymers. J Polym Sci Polym Chem 38:2505–2525. doi:10.1002/1099-0518(20000715)38:14
4. Jikei M, Kakimoto M (2001) Hyperbranched polymers: a promising new class of materials. Prog Polym Sci 26:1233–1285. doi:10.1016/S0079-6700(01)00018-1
5. Gao C, Yan D (2004) Hyperbranched polymers: from synthesis to applications. Prog Polym Sci 29:183–275. doi:10.1016/j.progpolymsci.2003.12.002
6. Yates CR, Hayes W (2004) Synthesis and applications of hyperbranched polymers. Eur Polym J 40:1257–1281. doi:10.1016/j.eurpolymj.2004.02.007
7. Voit B (2005) Hyperbranched polymers – all problems solved after 15 years of research? J Polym Sci Polym Chem 43:2679–2699. doi:10.1002/pola.20821
8. Voit B (2007) The potential of cycloaddition reactions in the synthesis of dendritic polymers. New J Chem 31:1139–1151. doi:10.1039/b615637c
9. Kricheldorf HR (2007) Polycondensation of 'a-b$_n$' or 'a$_2$++b$_n$' monomers – A comparison. Macromol Rapid Commun 28:1839–1870. doi:10.1002/marc.200700261
10. Bruchmann B (2007) Dendritic polymers based on urethane chemistry – syntheses and applications. Macromol Mater Eng 292:981–992. doi:10.1002/mame.200700119
11. Flory PJ (1953) Principles of polymer chemistry. Cornell University Press, Ithaca
12. Smet M, Fu Y, Zhang X, Schacht EH, Dehaen W (2005) A convenient A$_2$ + B$_3$ approach to hyperbranched poly(arylene oxindole)s. Macromol Rapid Commun 26:1458–1463. doi:10.1002/marc.200500386
13. Wilms D, Stiriba SE, Frey H (2010) Hyperbranched polyglycerols: from the controlled synthesis of biocompatible polyether polyols to multipurpose applications. Acc Chem Res 43:129–141. doi:10.1021/ar900158p

Synthesis of Star Polymers

Nikos Hadjichristidis[1], Kedar Ratkanthwar[2], Marinos Pitsikalis[3] and Hermis Iatrou[3]
[1]Division of Physical Sciences and Engineering, King Abdullah University of Science and Technology (KAUST), KAUST Catalysis Center, Polymer Synthesis Laboratory, Thuwal, Saudi Arabia
[2]School of Chemical Sciences, Swami Ramanand Teerth Marathwada University, Nanded, MS, India
[3]Department of Chemistry, University of Athens, Athens, Greece

Synonyms

Star-branched polymers

Definition

Star polymers are defined as polymers having at least three polymer chains (arms) radiating from a core. If all arms are identical, it is regular or symmetric star, and if all arms or some of them are different, it is miktoarm (*mikto* coming from the Greek word μικτός, meaning mixed) star or asymmetric star-branched polymer. There are three types of asymmetric star-branched polymers based on (1) molecular weight asymmetry, (2) topological asymmetry, and (3) functional group asymmetry (Fig. 1).

## Synthesis of Regular Star-Branched Polymers/Symmetric Stars

For the synthesis of well-defined symmetric star polymers so far three general methodologies have been developed [1], as shown in Fig. 2.

Multifunctional Initiators (MFIs)
The MFIs have to fulfill two requirements in order to yield well-defined star polymers: (i) the initiation sites must be equally reactive and

S

Fig. 1 Classification of
star-branched polymers
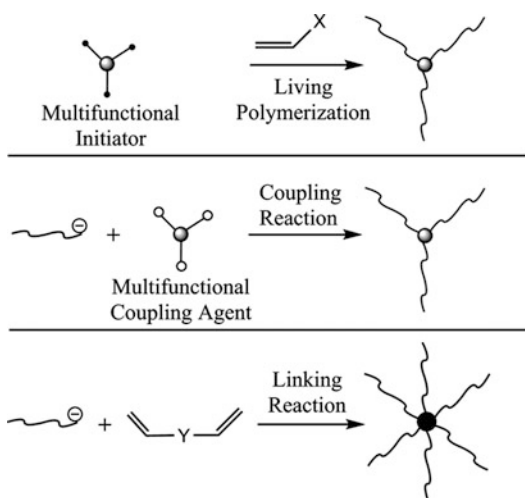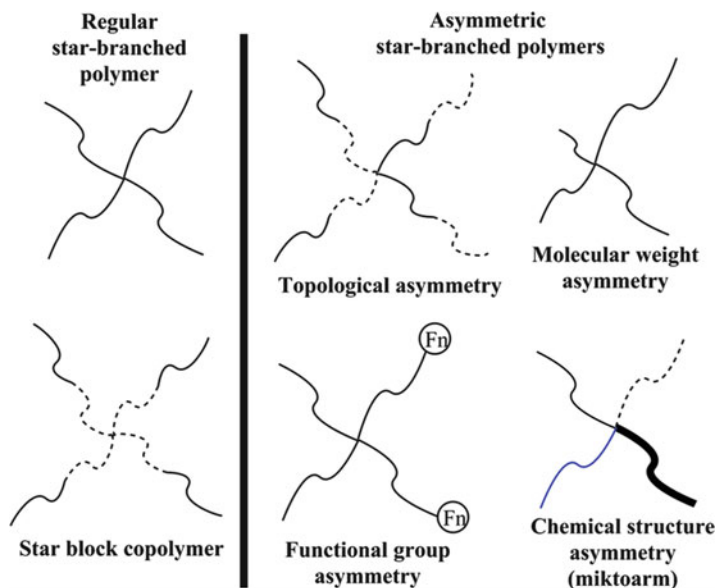
Synthesis of Star Polymers, Fig. 2 Different methodologies for the synthesis of symmetric stars

(ii) the initiation rate must be higher than the propagation rate. Only a very few multifunctional initiators satisfy these two requirements, and consequently, this method is not used very often.

Initially Burchard et al. demonstrated the use of divinylbenzene (DVB) to prepare multifunctional initiators. Later this method was further developed by Rempp and his coworkers. When DVB was reacted with *n*-butyllithium (*n*-BuLi) in benzene solution, stable microgel suspension was obtained covered by living anionic sites, serving subsequently as multifunctional initiators for the polymerization of styrene (S), isoprene (Is), or butadiene (Bd). Funke used low-molecular-weight living poly(*tert*-butylstyryl) lithium instead of *n*-BuLi in order to avoid the solubility problems arising from the strong association of the carbon–lithium functions in the nonpolar solvent. Rempp et al. synthesized poly(ethylene oxide) (PEO) and poly(*tert*-butyl acrylate) (P*t*BuA) stars, according to Fig. 3.

DVB was also reacted with naphthalene lithium to produce the MFIs by electron transfer instead of addition. For the synthesis of P*t*BuA stars using this MFI, the polymerization of *t*BuA was performed in the polar solvent tetrahydrofuran (THF) to minimize the strong association effect. It was carried out at $-55\,^{\circ}$C in the presence of LiCl and after the active centers have been reacted with a suitable amount of 1,1-diphenylethylene (DPE) to reduce their nucleophilicity. It was found that the mole ratio [DVB]:[Li^{+}] should be varied between 1.5 and 2.5 to obtain a stable microgel suspension. The molecular weight of the arms can be calculated from the ratio of the monomer consumed during the polymerization over the total Li concentration. The products were characterized by size
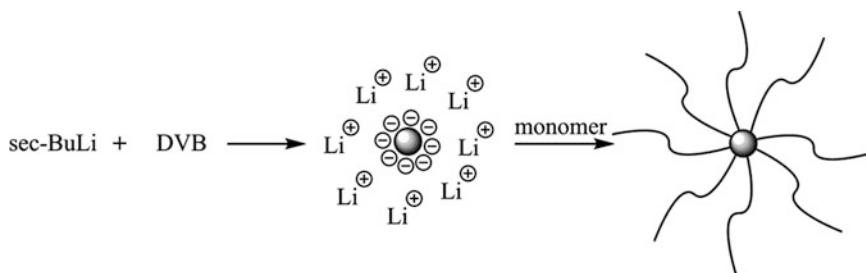
Synthesis of Star Polymers, Fig. 3 Use of DVB as a multifunctional initiator

exclusion chromatography (SEC) and light scattering (LS). The SEC results showed the presence of broad molecular weight distributions and even multimodal peaks. The formation of a rather small amount of aggregates was obtained in most cases, which was removed by filtration or centrifugation. The molecular characteristics of the final products and the calculated molecular weight of the arms revealed the existence of large numbers of arms, ranging from 22 to 1,300.

Potassium naphthalene was used to generate the multifunctional initiator for the synthesis of the PEO stars. In all cases, the molar ratio [DVB]:[K$^+$] was less than 3. As determined by LS measurements, the functionalities of the stars were rather large, ranging from 5 to 219. Alternatively, PEO stars were synthesized using cumylpotassium to polymerize DVB and thus prepare the multifunctional initiator. The products exhibited a large distribution of functionalities and molecular weights.

The MFI method provides the possibility to prepare end-functionalized stars by deactivating the living branches by suitable electrophilic terminating agents. PEO and PS stars having end hydroxyl groups were prepared by this method.

Another methodology was proposed by Lutz et al. in which *m*-diisopropenylbenzene (DIB) was polymerized anionically under such conditions that the second double bond remained unaffected. Linear polymers having molecular weights between 3,000 and 10,000 and pendent double bonds were prepared. The remaining double bonds were reacted with cumylpotassium to create active sites along the PDIB chain.

The polymerization of ethylene oxide was initiated from these active sites to produce PEO stars.

4-, 8-, and 16-arm star poly(ethylene oxides) were prepared using hydroxy-functionalized carbosilane dendrimers of several generations. The dendrimers were prepared starting from tetravinylsilane and using two reaction sequences, the hydrosilylation of the vinylsilane groups with dichloromethylsilane and the nucleophilic replacement of silicon chloride by vinylmagnesium bromide, as shown in Fig. 4.

The –Cl end groups were converted to hydroxy groups and activated by potassium naphthalene. The polymerization of ethylene oxide was initiated by these active sites to form well-defined star polymers. The tedious preparation of the dendrimer core molecules is the only drawback of this method.

Further, hyperbranched polyglycerol and polyglycerol modified with short poly(propylene oxide) chains, activated with diphenylmethylpotassium (DPMP) [2], were employed as multifunctional initiators for the synthesis of PEO stars, as depicted in Fig. 5.

Due to strong association of polar groups, hyperbranched polyglycerol was found to be an unsuitable initiator. The incorporation of the poly (propylene oxide) chains (degree of polymerization, 23–52) was crucial for the synthesis of the PEO stars. Moderate to large molecular weight distributions were obtained ranging from 1.4 up to 2.2. The functionalities of these stars were calculated to vary between 26 and 55.

A new hydrocarbon-soluble trifunctional initiator was proposed by Quirk et al. synthesized by

S

Fig. 4 Synthesis of the carbosilane dendrimer
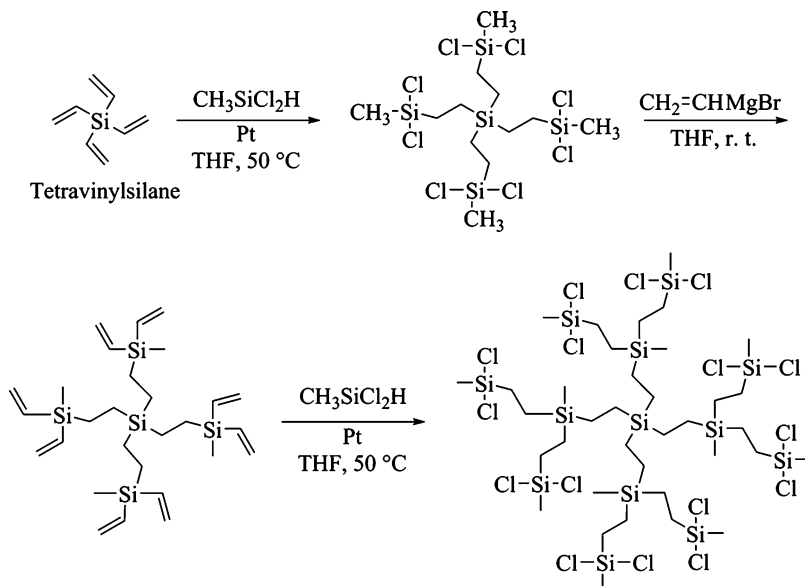
the reaction of *sec*-butyllithium (*sec*-BuLi) with 1,3,5-tris(1-phenylethenyl)benzene (tri-DPE), as shown in Fig. 6. This initiator was found to be efficient for the polymerization of styrene only when THF was also added in the reaction mixture in a ratio [THF]:[*sec*-BuLi] = 20.

This trifunctional initiator was also used for the synthesis of a three-arm star PBd. Complete monomer consumption was observed, but SEC analysis showed a bimodal distribution. This behavior was attributed to the strong association effects of the trifunctional initiator in a nonpolar solvent. To overcome this problem, *sec*-BuOLi was added in the reaction mixture in a ratio [*sec*-BuLi]:[*sec*-BuOLi] = 2. *sec*-BuOLi was shown to be capable of disrupting the initiator association without affecting appreciably the microstructure of the PBd chains. Therefore, a well-defined star polymer with low-molecular-weight distribution and the appropriate microstructure was obtained. The limitations of the method include the extreme care that should be exercised over the stoichiometry of the reaction between *sec*-BuLi and tri-DPE and the fact that a minimum arm molecular weight around 6×10^3 is required for a successful synthesis. For arm molecular weights lower than this limit, incomplete initiation was observed.

Eight-arm star polyisobutylenes (PIB) were synthesized, as shown in Fig. 7, using cationic polymerization and *tert*-hydroxy and *tert*-methoxy derivatives of 5,11,17,23,29,35,41,47-octaacetyl-49,50,51,52,53,54,55,56-octamethoxycalixarene as octafunctional initiator [1].

Tetrafunctional and hexafunctional initiators shown in Fig. 8 have been used for the polymerization of acrylates and styrene by atom transfer radical polymerization (ATRP). In addition, a six-arm star-block copolymer composed of poly (methyl methacrylate) (PMMA) as an internal block and poly(isobornyl acrylate) as an external block was synthesized (Fig. 8).

Another octafunctional calixarene derivative, as shown in Fig. 9, was prepared and used as a multifunctional initiator for the bulk ATRP of styrene at 100 °C in the presence of CuBr/2,2-bipyridyl, leading to the synthesis of eight-arm star polymers. Well-defined stars could be obtained only at low polymerization conversion (up to 20 %) since the irreversible coupling reactions taking place at higher concentrations are avoided.

The dendritic multifunctional reverse addition fragmentation termination (RAFT) initiators carrying 6 and 12 external 3-benzylsulfanylthiocarbonylsulfanylpropionic acid
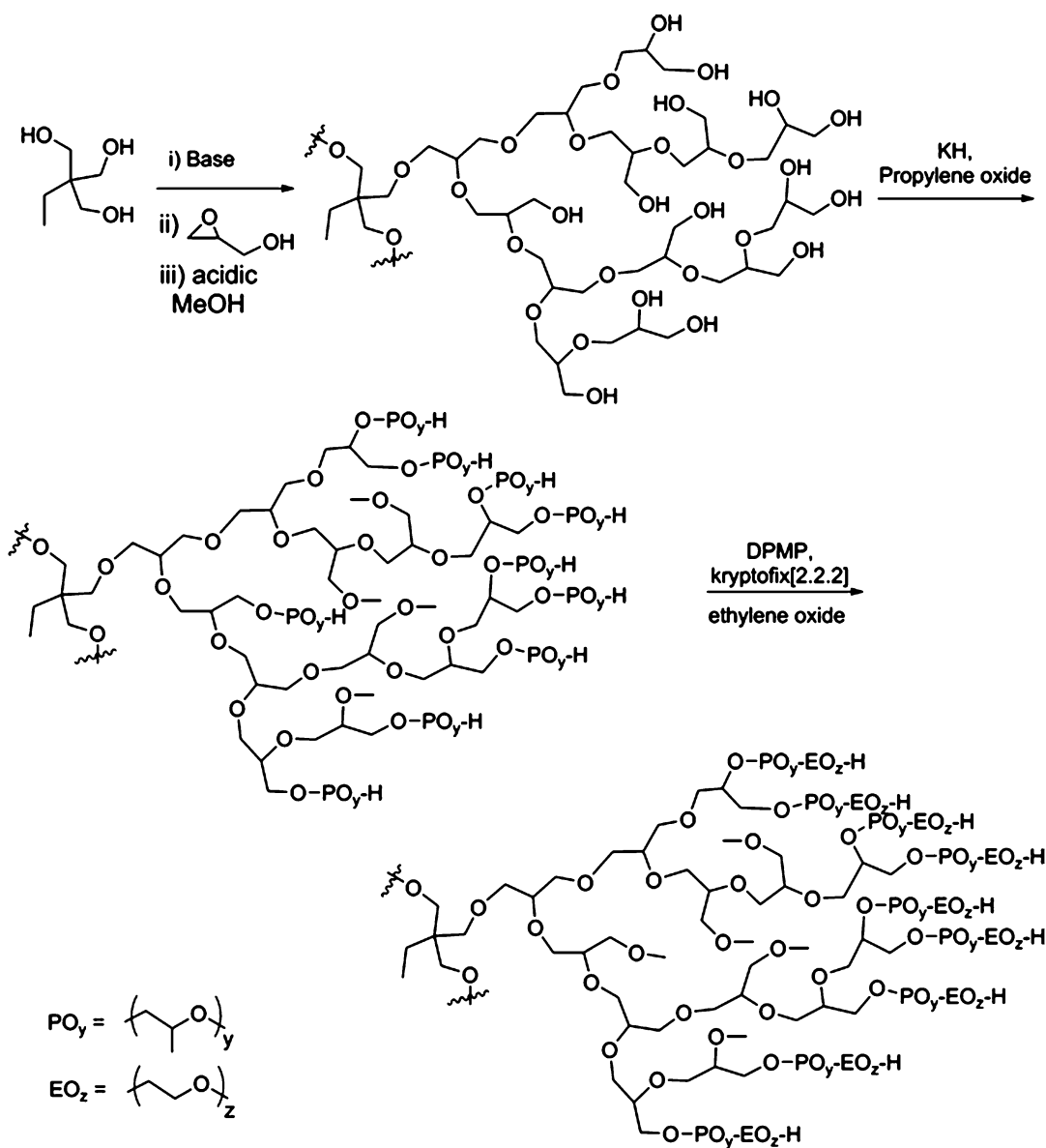
Synthesis of Star Polymers, Fig. 5 Hyperbranched polyglycerol as a MFI

$$PO_y = \left(\begin{array}{c} \\ \end{array} O \right)_y$$

$$EO_z = \left(\begin{array}{c} \\ \end{array} O \right)_z$$

Synthesis of Star Polymers, Fig. 6 Synthesis of a trifunctional initiator

3 *sec*-BuLi +
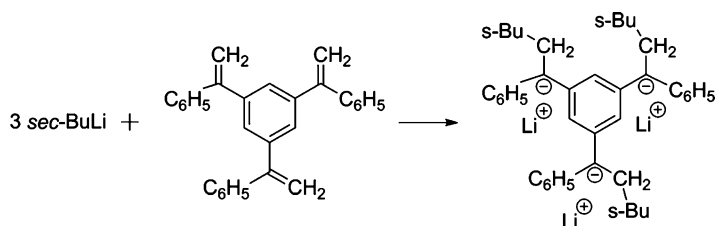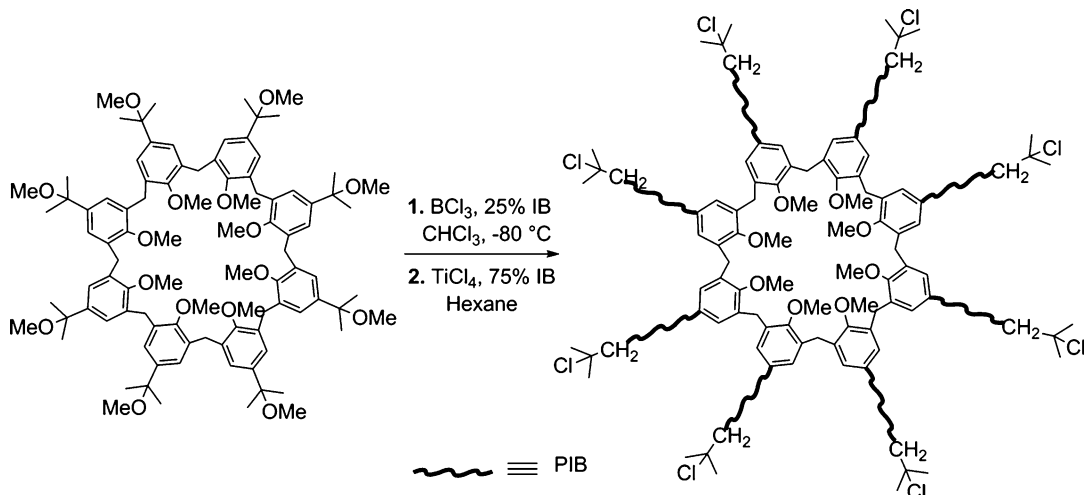
Synthesis of Star Polymers, Fig. 7 Synthesis of eight-arm star polyisobutylenes by cationic polymerization using an octafunctional initiator
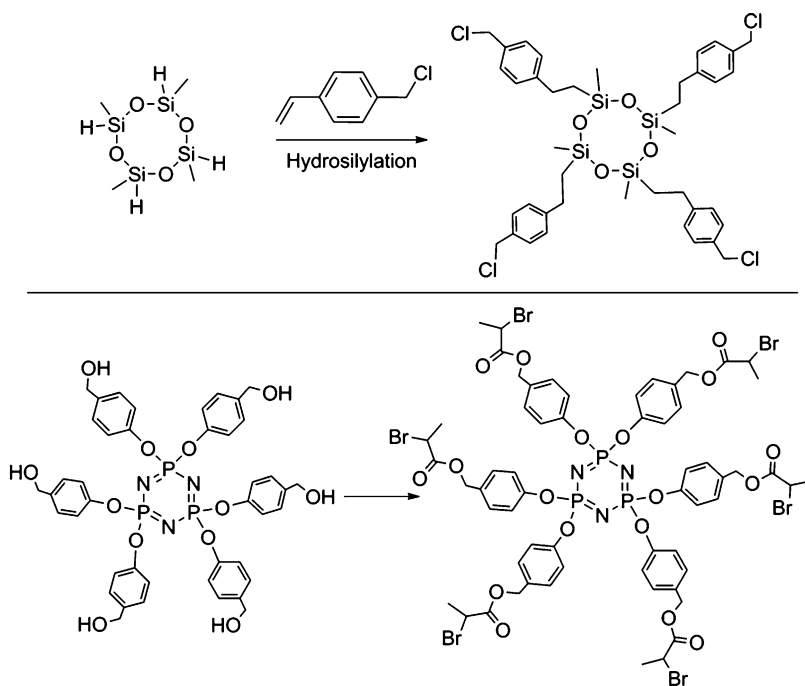
Synthesis of Star Polymers, Fig. 8 Tetrafunctional and hexafunctional initiators

groups were synthesized. In combination with azo-α,α′-diisobutyronitrile (AIBN), these compounds have been used to polymerize *n*-butyl acrylate (*n*BuA), in bulk at 60 °C, leading to star P*n*BuA with moderately low polydispersity (1.1–1.5). The star-shaped structure of the synthesized polymers has been confirmed through the cleavage of the arms from the core and characterization.

In the "arm-first" approach presented in Fig. 10, the fragmentation results in the formation of benzyl radicals, which are able to reinitiate

polymerization of linear chains. The arms of the star polymer are dormant and the growth of the arms always occurs away from the core. Using this methodology, four-arm PS and poly(methyl acrylate) stars were prepared.

A series of multi-thiocarbonyl thio compounds with 2, 4, 6, or 8 functional groups were prepared and subsequently employed as chain
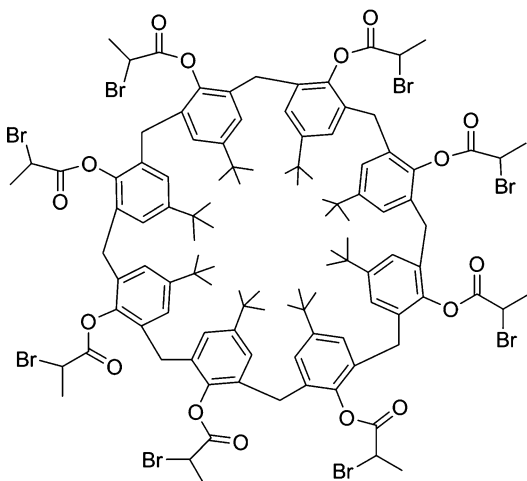
Synthesis of Star Polymers, Fig. 9 Octafunctional calixarene derivative as a MFI for ATRP

transfer agents for the synthesis of star polymers using the RAFT technique (Fig. 11).

Using pentaerythritol as the MF initiator, four-arm hydroxyl-terminated poly(ε-caprolactone) (PCL) stars were synthesized by ring-opening polymerization (ROP) of ε-caprolactone (Fig. 12). The hydroxyl end groups of the star were then reacted with an α-carboxy-functionalized poly(ethylene oxide) to afford the four-arm PCL-*b*-PEO star-block copolymer. The linking efficiency was approximately 95 %.

Multifunctional Linking Agents (MFLA)

Multifunctional linking agents (MFLA) are compounds with several reactive sites which can react with living chains. It is the most efficient way to synthesize well-defined star polymers, since there is absolute control in all the synthetic steps. The functionality of the linking agent determines the number of the arms of the star polymer, provided that the linking reaction is quantitative. The living arms can be isolated and characterized independently along with the final star product. Consequently, the functionality of the star can be measured directly and accurately. Disadvantages of the method are the sometimes long time required for the linking reaction and the need to
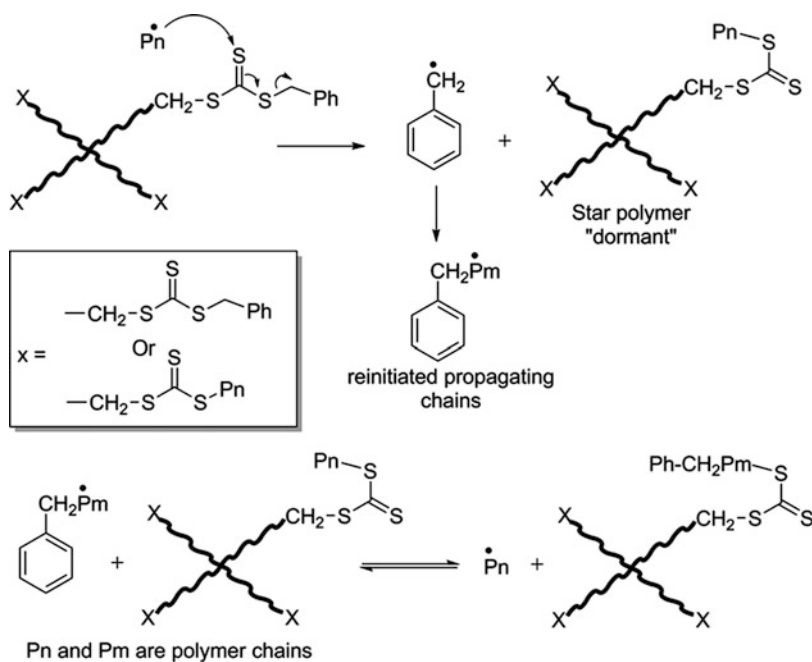
Synthesis of Star Polymers, Fig. 10 Four-arm star polymers synthesis using RAFT technique

Pn and Pm are polymer chains

Synthesis of Star Polymers, Fig. 11 Multi-thiocarbonyl thio compounds with 2 to 8 functional groups
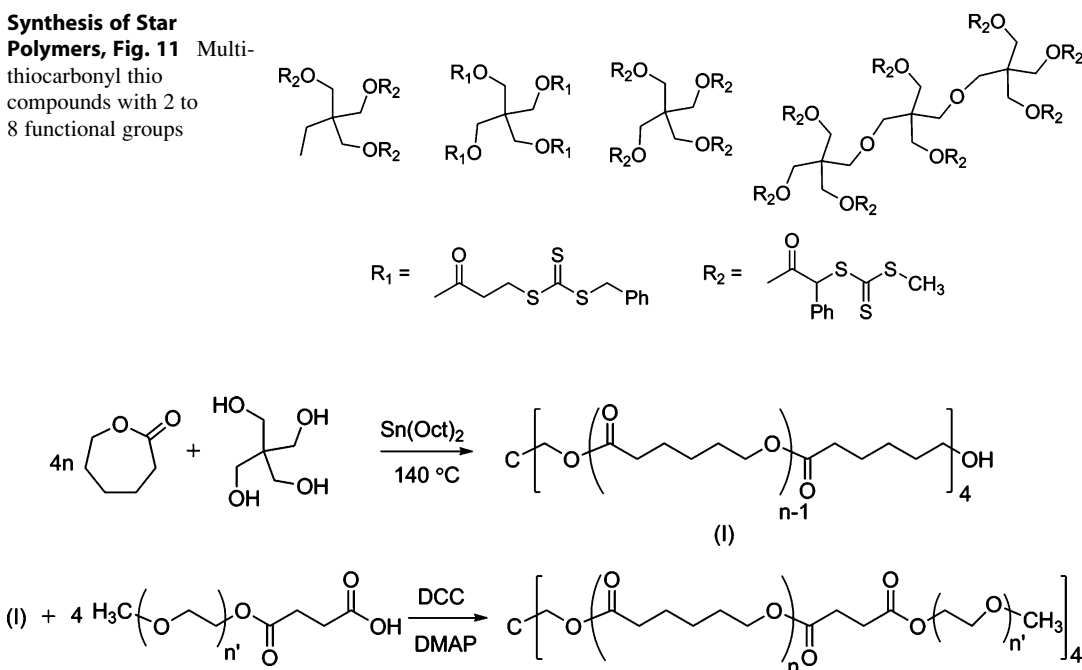
Synthesis of Star Polymers, Fig. 12 Synthesis of four-arm PCL-*b*-PEO star-block copolymer

perform fractionation in order to obtain the pure star polymer, since in almost all cases a small excess of the living arm is used to ensure complete linking.

For the synthesis of star polymers from living precursors synthesized by anionic polymerization, the most important linking agents are the chlorosilanes following by the chloromethyl or bromomethyl benzenes. The linking reactions of the living macroanionic chains with the chlorosilanes proceed very smoothly without any side reactions. However, the efficiency of the linking reaction depends on the steric-hindered character of the linking agent and the living macromolecular chain end. It was shown that the higher the steric hindrance of the reactants, the lower the linking efficiency. The linking efficiency can be improved by separating the Si–Cl groups by spacers, such as methylene groups, and/or by end-capping the living chains with a few units of butadiene in order to reduce the steric hindrance and facilitate the linking reaction. Under these conditions, well-defined stars have been prepared with functionalities ranging from 3 to 128 arms.

Advances in the synthesis of pure carbosilane dendrimers, an example is given in Fig. 13, led to the preparation of linking agents with functionalities as high as 128. These dendrimers were successfully used for the synthesis of PBd stars having 32, 64, and 128 branches.

The chlorosilane LAs cannot be used in the case of poly(meth)acrylates and polyvinylpyridines (PVP) because either they react with the pyridine ring or the produced stars have hydrolysable C–O–Si groups. In these cases, chloro(bromo)-methyl benzenes are the most appropriate linking agents.

1,3,5-tri(chloromethyl)benzene was used for the synthesis of three-arm P2VP stars. The samples were characterized by SEC and viscometry. This chloromethylbenzene method suffers from metal–halogen exchange which leads to LAs with more or fewer chloromethyl groups and consequently produces stars with more or fewer arms than the desired number of arms. The metal–halogen exchange can be avoided by using bromo- instead of chloro-derivatives in polar solvents and at low temperatures.
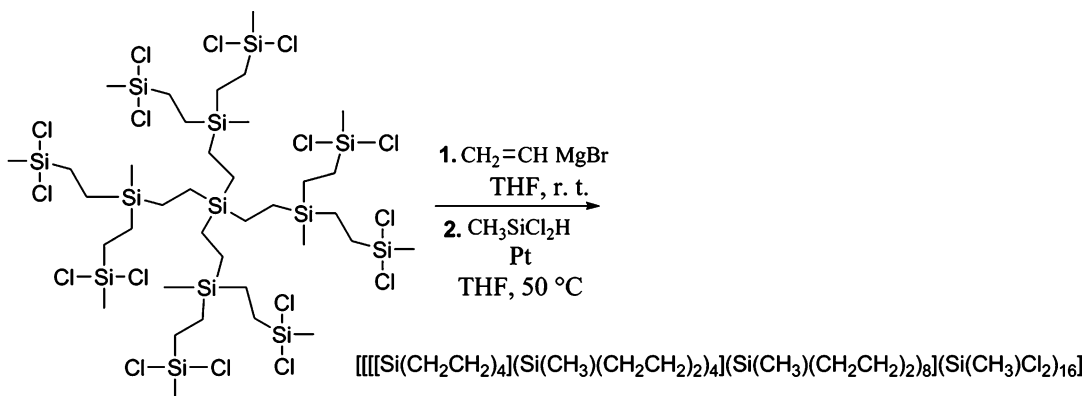
Synthesis of Star Polymers, Fig. 13 Carbosilane dendrimers as a MFLA

Synthesis of Star Polymers, Fig. 14 Synthesis of four-arm star polymer using 1,2,4,5-tetra(bromomethyl)benzene
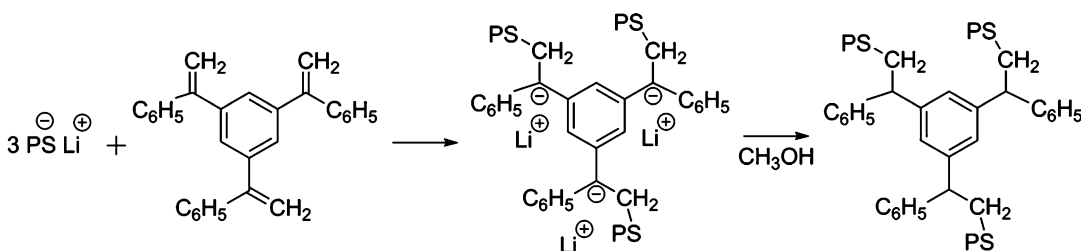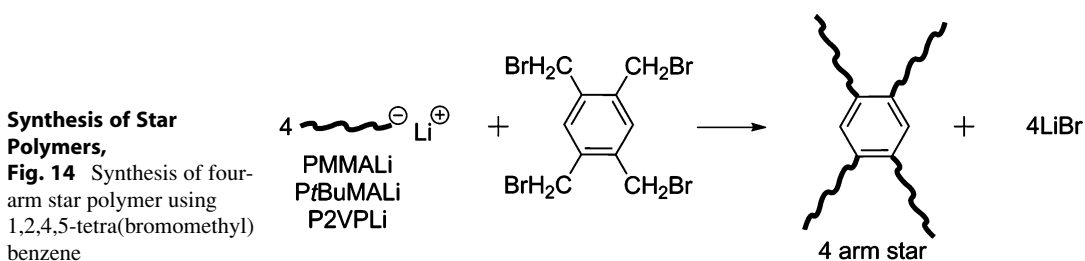
Synthesis of Star Polymers, Fig. 15 1,3,5-tris(1-phenylethenyl)benzene as a living LA

The synthesis of four-arm stars bearing poly(*tert*-butyl methacrylate) (P*t*BuMA), PMMA, or P2VP arms using 1,2,4,5- tetra (bromomethyl)benzene has been reported (Fig. 14). Combined characterization results by SEC and membrane osmometry (MO) revealed the formation of well-defined star polymers.

A three-arm PS star (Fig. 15) was synthesized using 1,3,5-tris(1-phenylethenyl)benzene as a living LA. Although the arm molecular weight used was rather low ($M_n = 8.5 \times 10^3$), there was no steric limitation for the synthesis of higher molecular weight three-arm PS stars.

Three- and four-arm poly(isobutyl vinyl ether) (PIBVE) star homopolymers have been synthesized by employing tri- and tetrafunctional silyl enol ethers as coupling agents and cationic polymerization (Fig. 16). The living arms were produced at $-15\ °C$, using the $HCl/ZnCl_2$ initiating system in methylene chloride. The coupling of relatively short chains of living PIBVE (DP $\sim$ 10) was shown to occur nearly quantitatively, affording the multi-armed polymers in high yield (>95 %). The yield decreased slightly (85–89 %) with a longer living chain (DP $\sim$ 50). The molecular weight distribution of the final stars was narrow.

Synthesis of Star Polymers, Fig. 16 Use of silyl enol ethers as coupling agents in cationic polymerization

Synthesis of Star Polymers, Fig. 17 Synthesis of three-arm star-block copolypeptides
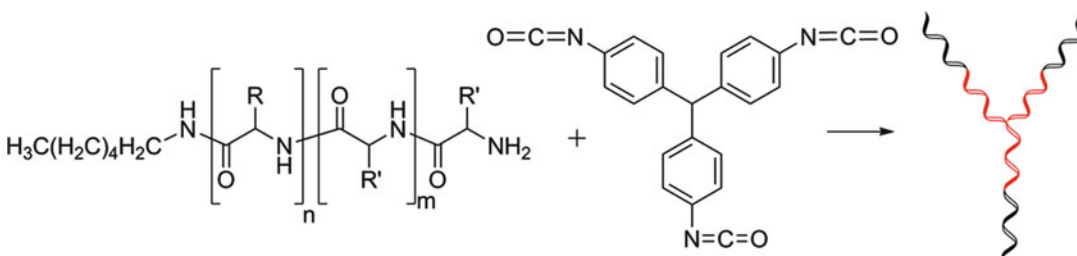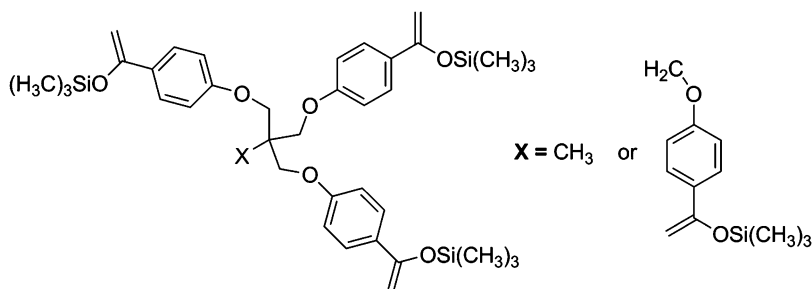
Three-arm star-block copolypeptides of poly(γ-benzyl-L-glutamate) (PBLG) and poly(ε-benzyloxycarbonyl-L-lysine) (PZLL), i.e., (PBLG)$_3$ and (PZLL)$_3$, were synthesized by the ring-opening polymerization (ROP) of the *N*-carboxyanhydride (NCA) of the corresponding α-amino acids and the linking methodology. The synthetic approach involves the preparation of the corresponding living arms, followed by linking with triphenylmethane 4,4′,4″-triisocyanate at room temperature (Fig. 17). The sequential copolymerization of the monomers γ-benzyl-L-glutamate NCA and ε-benzyloxycarbonyl-L-lysine NCA was performed using high-vacuum techniques, with *n*-hexylamine as the initiator, leading to high-molecular-weight, well-defined living polypeptides in $\sim$100 % yield with low polydispersity. A slight excess of living arms was used for the linking reaction and was subsequently fractionally removed. The copolypeptides were extensively characterized by membrane osmometry (MO) and SEC equipped with a LALLS detector, along with NMR spectroscopy. The polydispersity indices were lower than 1.1, and the observed molecular weights were very close to the theoretical ones.

The characterization results revealed that the stars exhibited a high degree of molecular and compositional homogeneity.

Three-arm PMMA stars were synthesized by reacting living PMMA chains obtained by group transfer polymerization with the linking agent 1,3,5-tris(bromomethyl)benzene (Fig. 18). A reexamination of the reaction revealed that the linking efficiency was not quantitative. This behavior can be attributed to the fact that the reaction of the –CH$_2$Br groups with the living chain ends occurs in a stepwise manner. Therefore, after each substitution of Br by a chain, the reactivity of the remaining –CH$_2$Br groups is reduced due to steric hindrance, thus leading to lower conversions.

Synthesis of three- and four-arm PS star has been reported by ATRP techniques and click linking chemistry, according to the procedure given in Fig. 19. Alkyne-containing multifunctional compounds were reacted with azido-terminated PS chains of low molecular weight to produce the desired star structures. The linking reactions were catalyzed by CuBr/N,N,N′,N″,N″-pentamethyldiethylenetriamine complex.
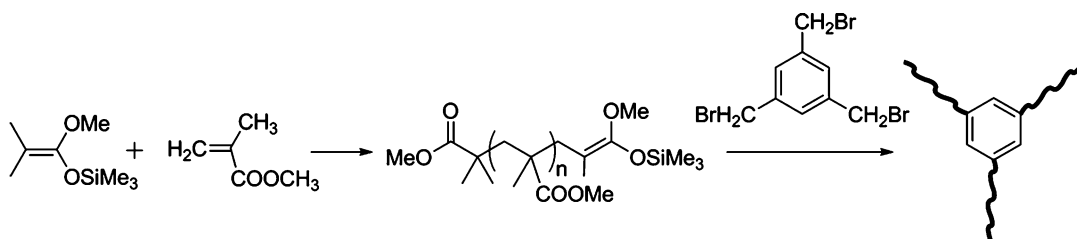
Synthesis of Star Polymers, Fig. 18 Synthesis of three-arm PMMA stars by group transfer polymerization and linking reaction
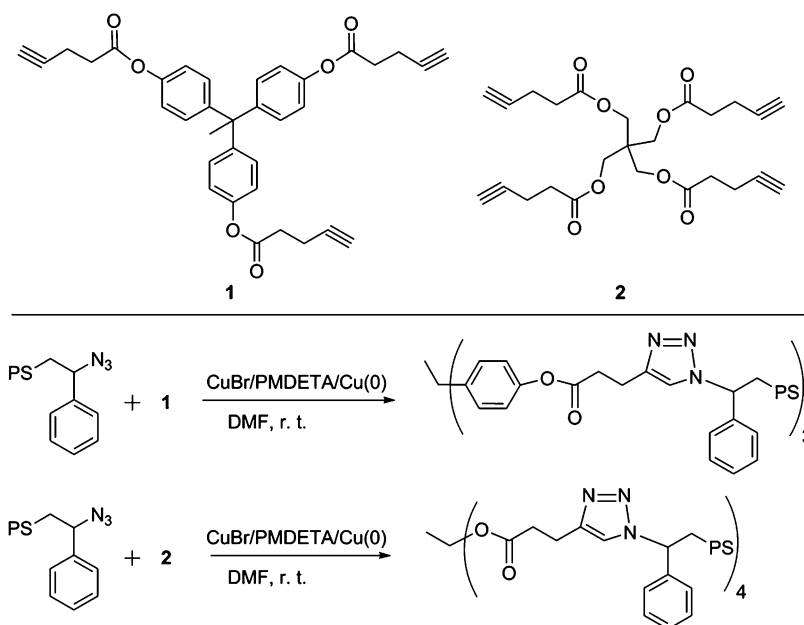
Synthesis of Star Polymers, Fig. 19 Combination of ATRP and click chemistry for star polymers synthesis

Difunctional Monomer (DFM)

For the synthesis of star polymers by this method, a living polymer precursor is used as initiator for the polymerization of a small amount of difunctional monomer, such as ethylene glycol dimethacrylate (EGDM) or divinylbenzene (DVB). Microgel nodules of tightly cross-linked polymer are formed upon the polymerization. These nodules serve as the junction moiety from which the arms emanate. The functionality of the stars prepared by this method can be determined by molecular weight measurements of the arms and the star product. However, it is very difficult to predict and control the number of arms. The number of arms incorporated in the star structure is influenced by many parameters. The most important is the molar ratio of the DFM over the

living polymer. The functionality of the stars increases by increasing this ratio.

For the synthesis of star polynorbornene, the norbornadiene dimer, *exo-trans-exo*-pentacyclo [7.02,8,8.2.1.14,9.03] tetradeca-5,11-diene, was used as a difunctional monomer by ring-opening metathesis polymerization (ROMP). Norbornene was polymerized to the corresponding living polymer using M(CHR)(NAr)(O-*t*-Bu)$_2$ (M = W or Mo; NAr = N-2,6-C$_6$H$_3$-^{i}Pr$_2$) as catalyst. The living polymer was then reacted with the DFM to produce the star polymers (Fig. 20). The linear living polymer was completely consumed, but the molecular weight distribution of the stars was broader than that of the corresponding arms (stars with different functionality). These stars are still living and bear active centers
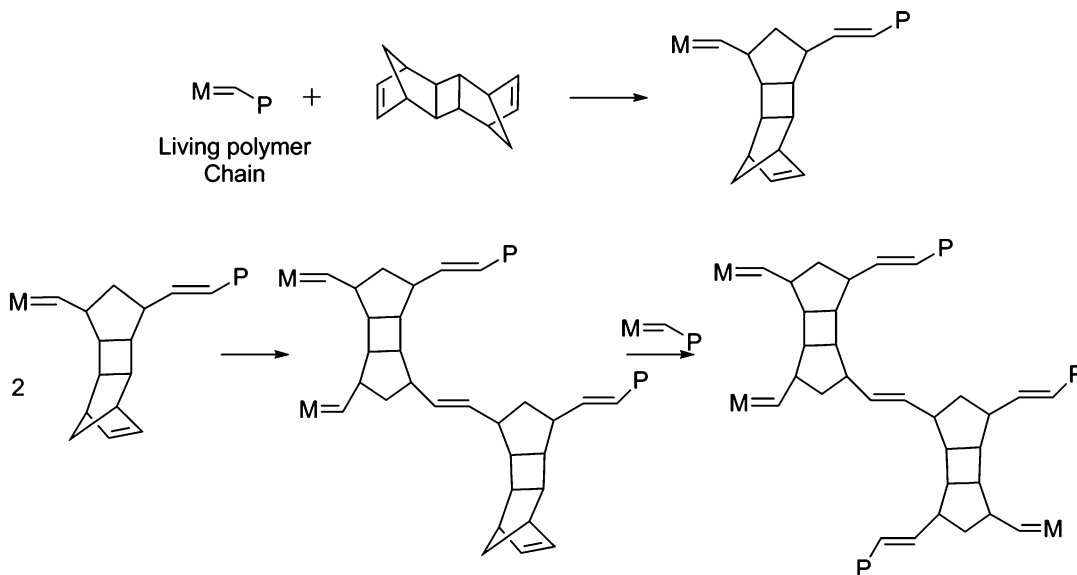
Synthesis of Star Polymers, Fig. 20 ROMP for the synthesis of star polynorbornene

at the core of the structure. New arms can grow from these living sites giving rise to the formation of asymmetric stars. However, products with bimodal distributions were obtained, due to the slower initiation at the core of the star and the faster propagation as the reacting alkylidene centers been away from the sterically crowded core.

Several star polymers have been prepared by reacting living polymeric chains, synthesized by anionic polymerization, with DVB. The method has been applied for the synthesis of PS and polydiene stars. Rather narrow molecular weight distribution PS stars were obtained when the [DVB]/[PSLi] ratio was varied from 5.5 to 30 and the corresponding functionality ranged from 13 to 39. A similar behavior was obtained for polydiene stars when the [DVB]/[PDLi] ratio was between 5 and 6.5 and the functionality of the star was varied from 9 to 13.

PMMA stars were also prepared by reacting PMMA chains, synthesized by anionic polymerization, with the difunctional monomer ethylene glycol dimethacrylate (EGDM). The polymers were characterized by SEC, LS, and viscometry. It was found that well-defined polymers can be prepared when the arm molecular weight was rather high (e.g., $M_w = 40,000$). It seems that

this high molecular weight is necessary to prevent intercore and gelation reactions. By reacting EGDM with isotactic living PMMA chains obtained using t-butyl magnesium bromide as initiator in the presence of 1,8-diazabicyclo [5.4.0]undec-7-ene, a star polymer with 20–30 arms was synthesized. SEC connected with LS and viscometry detectors was used to characterize the sample. A similar reaction using syndiotactic living PMMA chains, obtained with the t-BuLi-R$_3$Al initiator system, failed to give star polymers. However, when EGDM was replaced by the butane-1,4-diol dimethacrylate, a PMMA star was obtained bearing 50–120 arms.

For the synthesis of PS and PtBuA star homopolymers using DFMs, included DVB, 1,4-butanediol diacrylate, as well as with EGDM, and ATRP technique has been reported. Formation of monodisperse stars depends on several factors such as the choice of the exchanging halogen, the solvent, the addition of copper (II) species, the ratio of the coupling agent to the macroinitiator, and the reaction time. Using a 10–15-fold excess of the difunctional monomer over chain ends, the highest efficiency (~95 %) was obtained. PMMA star polymers were synthesized by reaction of living PMMA chains, produced by the RuCl$_2$(PPh$_3$)$_3$-catalyzed

$$\text{sec-BuLi} + \text{Styrene} \longrightarrow \text{PSLi} \xrightarrow{\text{Isoprene}} \text{(PS-}b\text{-PI)Li} \xrightarrow{\text{SiCl}_4} \text{(PS-b-PI)}_4\text{Si}$$

Synthesis of Star Polymers, Fig. 21 Synthesis of star-block copolymers of PS and PI

Synthesis of Star Polymers, Fig. 22 Synthesis of three-arm star-block copolymer containing fullerene

$$\text{sec-BuLi} + \text{Styrene} \xrightarrow[-78\ °C]{\text{THF}} \text{PS}^{\ominus} \text{Li}^{\oplus} \xrightarrow{\text{2VP}} \text{PS-}b\text{-P2VP}^{\ominus} \text{Li}^{\oplus} \xrightarrow{\text{C}_{60}}$$

(excess)

— : P2VP
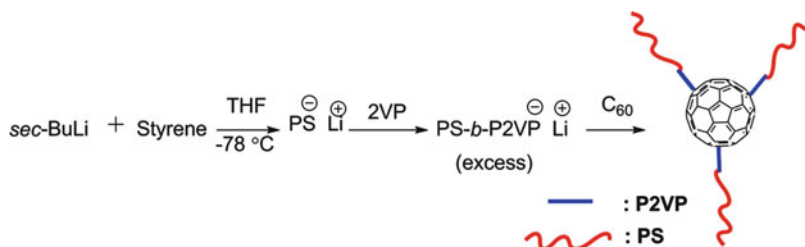
~~~ : PS

polymerization of MMA, with the difunctional monomer bisphenol A dimethacrylate (BPDMA). The functionality of the products ranged from 4 to 63. The yield of the linking reaction was found to depend on the concentration and the degree of polymerization of the living arms and the molar ratio of BPDMA over the living chains.

The DFM methodology and RAFT were employed for the synthesis of PS star. The linear macro-RAFT PS agent was synthesized in bulk at 110 °C using benzyl dithiobenzoate and AIBN. DVB was used as the difunctional monomer.

Synthesis of Star-Block Copolymers

Star-block copolymers are star polymers in which each arm is a diblock, triblock, or multiblock copolymer [3]. The preparation of star-block copolymers involves the linking reaction of a living block copolymer, prepared by sequential polymerization of the two or more monomers, with a suitable multifunctional linking agent (MFLA). Fetters and collaborators synthesized star-block copolymers (PS–b–PI)_n, where n = 4, 8, 12, 18, using anionic polymerization and chlorosilane linking agents as shown in Fig. 21.

Fullerene, $C_{60,}$ was also used for the synthesis of star-block copolymers. Living PS–b–P2VP diblocks, having short P2VP chains, were prepared by sequential anionic polymerization in

THF and were reacted with a suspension of C_{60} in THF leading to the formation of a three-arm star-block copolymer as per reaction given Fig. 22.

PS–b–P4VP star-block copolymers with 12 arms were also synthesized using dendritic dodecafunctional macroinitiators (Fig. 23) and TEMPO-mediated radical polymerization. These polymerization reactions were conducted in bulk at 120 °C and the synthesized stars showed low polydispersity indices (1.06–1.26).

The combination of difunctional monomer methodology and RAFT was successfully employed for the synthesis of PS–b–poly(N-isopropyl acrylamide) star-block copolymers. The synthesis of the block copolymer was performed by sequential polymerization in bulk at 110 °C, using benzyl dithiobenzoate and AIBN. DVB was used as the difunctional monomer. The stars were extensively characterized by NMR and IR spectroscopy, as well as SEC and dynamic light scattering (DLS). It was found that the molar ratio of DVB/PS and the polymerization time influenced the yield, molecular weight, and the polydispersity index of the stars.

Synthesis of Asymmetric Stars

Asymmetric star polymers belong to a special class of star polymers characterized by an asymmetry factor [4]. The following parameters have been considered as asymmetry factors:

S

Synthesis of Star Polymers, Fig. 23 Use of dendritic dodecafunctional macroinitiators for the synthesis of star-block copolymers with 12 arms

(a) **Molecular weight**: All the arms of the star are identical in chemical nature but have different molecular weights (Fig. 1).

(b) **Topology**: The arms of the star are block copolymers that may have the same molecular weight and composition but differ with respect to the polymeric block that is

$$PS_A \overset{\ominus}{} \overset{\oplus}{Li} \ + \ (CH_3)SiCl_3 \ \longrightarrow \ PS_A\text{-}Si(CH_3)Cl_2 \ + \ LiCl \ + \ (CH_3)SiCl_3 \uparrow$$
$$\text{(Excess)}$$

$$PS_A\text{-}Si(CH_3)Cl_2 \ + \ PS_B \overset{\ominus}{} \overset{\oplus}{Li} \ \longrightarrow \ PS_A\text{-}Si(CH_3)(PS_B)_2$$
$$\text{(Excess)}$$

Synthesis of Star Polymers, Fig. 24 Chlorosilane method for the synthesis of asymmetric PS stars

covalently attached to the core of the star (Fig. 1).

(c) **Functional group**: The arms are of the same chemical nature and have the same molecular weight, but they have different end groups or functional groups (Fig. 1).

Asymmetric stars can be synthesized by the same general methods described for the symmetric stars but in such way that a controlled incorporation of the arms which are different in molecular weight, end-functional groups, or topology.

Molecular Weight Asymmetry

Chlorosilane Method

The chlorosilane method, for the synthesis of asymmetric stars, was initially described by Fetters and was later developed by Hadjichristidis, Mays, and collaborators. In this method, different living polymer chains stepwise replaces the chlorines of chlorosilanes to form asymmetric stars [5]. This procedure can be achieved taking into account the different reactivity of the living polymer ends toward the Si–Cl bond, as this is determined by the steric hindrance effects, the charge localization on the terminal carbon atom, and the excluded volume of the living chain that is affected by the reaction solvent. The reactivity of the living chain end decreases by charge delocalization and by increasing the steric hindrance. The latter can be affected by both structures of the living chain end and the chlorosilane linking agent. The steric hindrance of the living end increases in the order BdLi < IsLi < SLi < DPELi. The closer the distance between the Si–Cl groups in the linking agent, the more sterically hindered is the reaction with the living chains. For example, overall $SiCl_4$ is less reactive

than $Cl_2Si\text{–}CH_2\text{–}CH_2\text{–}SiCl_2$. The reactivity is also influenced by other parameters such as the molecular weight of the living chain; the polarity of the solvent, where the reaction takes place; and the temperature. When all these factors are optimized, well-defined products are produced. However, the disadvantage of this method is that it is time-consuming and requires in most cases high-vacuum techniques.

The chlorosilane method was initially used for the synthesis of asymmetric PS stars composed of two arms of equal molecular weights, PS_B, and a third one, PS_A, with a molecular weight either half or twice that of the identical arms (Fig. 24). Latter, the same method was also applied in the synthesis of asymmetric PBd and PI stars.

Divinylbenzene (DVB) Method

As already discussed, when appropriate living polymer chains react with a small amount of DVB, a star polymer is formed consisting of a highly cross-linked polydivinylbenzene core from which the arms emanate. This is actually a living star since the core carries anionic centers. The number of these active sites is theoretically equal to the number of the arms of the star. Subsequent addition of a new monomer results in the growth of new arms from the core, and therefore the formation of an asymmetric star of the type $A_nA'_n$ can be achieved (A and A' chains with different molecular weight). This general procedure is depicted in Fig. 25.

Using this method $(PS_A)_n(PS_B)_n$ asymmetric stars were prepared. Living PS chains were obtained by *sec*-BuLi initiation and reacted with a small amount of DVB to give a living star polymer. The anionic sites of the star core were subsequently used to initiate the polymerization of a new quantity of styrene. This initiation step

Synthesis of Star Polymers, Fig. 25 DVB method for the formation of asymmetric stars

Synthesis of Star Polymers, Fig. 26 Formation of difunctional initiator reaction of living PS with MDDPE and PDDPE

was accelerated by the addition of a small quantity of THF.

In another example, mono-2-bromoisobutyryl PEO ester was used as macroinitiator for the ATRP of DVB, leading to the synthesis of the desired star polymers. Subsequent addition of styrene led to PEO_nPS_m miktoarm stars through the polymerization of styrene from the initiating sites located at the core of the PEO stars. The styrene conversion did not exceed 10 % to avoid star–star coupling reactions and, therefore, the production of gels.

Diphenylethylene Derivative Method
This method is based on the use of 1,1-diphenylethylene derivatives which are non-homopolymerizable monomers. Initially Quirk reacted living PS chains with either 1,3-bis(1-phenylethenyl)benzene (MDDPE) or 1,4-bis(1-phenylethenyl)benzene (PDDPE), according to Fig. 26.

It was shown that two moles of the living polymer reacts rapidly with the DPE derivatives to form the dilithium adduct in hydrocarbon solvents, whereas in THF monoaddition is reported. This reaction was monitored by UV-visible spectroscopy. The analysis showed that the stoichiometric addition of PSLi was quantitative. However, PDDPE exhibited lower tendencies to form the diadduct both in polar and in nonpolar solvents. This behavior can be attributed to the better delocalization of the negative charge in the "para" than in the "meta" isomer. Mainly, low-molecular-weight polystyrenes have been used for these studies. Therefore, by using PDDPE, a three-arm asymmetric PS star was successfully synthesized (Fig. 27). The monoaddition product was reacted with a second polystyryllithium chain, having different molecular weight, to form the coupled product. Finally, the addition of styrene leads to the formation of the asymmetric 3-arm PS star. The polymerization took place in the presence of THF to accelerate the crossover reaction.

Hirao developed a general method using DPE derivatives carrying protected chloromethyl groups [6]. Asymmetric PS stars of the types AA'_2, $AA'_2A''_2$, AA'_3, AA'_4, $AA'A''_2$, and $AA'_4A''_4$ were prepared by this method. The whole procedure is based on the reaction sequence shown in Fig. 28. Living PS was reacted with 1,1-bis(3-methoxymethylphenyl) ethylene followed by transformation of the methoxymethyl groups to chloromethyl groups

Synthesis of Star Polymers, Fig. 27 Synthesis of asymmetric three-arm PS star

Synthesis of Star Polymers, Fig. 28 DPE method for the synthesis of asymmetric star-branched polymers

using BCl$_3$ in CH$_2$Cl$_2$ at 0 °C for 10–30 min. Prior to the reaction with the BCl$_3$, the living end-functionalized PS is able to react with other compounds such as 1-(4′-bromobutyl)-4-methoxymethylbenzene as shown in Fig. 28.

More complex in-chain-functionalized structures with two or four chloromethyl groups were

prepared according to Fig. 29. The living end-functionalized PS with two methoxymethyl groups was reacted with a 10-fold excess of 1,4-dibromobutane to introduce a bromobutyl end group. The terminal bromobutyl group was subsequently coupled with living PS to afford a linear PS chain having two in-chain

Synthesis of Star Polymers, Fig. 29 DPE method for the synthesis of asymmetric star-branched polymer

methoxymethylphenyl groups. These groups were transformed to chloromethyl groups. Alternatively, the terminal bromobutyl group can be reacted with another living end-functionalized PS with two methoxymethyl moieties, resulting in the synthesis of a linear PS chain having four in-chain functional chloromethyl groups, after performing the transformation reaction. If the four functions are required at the middle of the polymer chain, it is easier to couple a small excess of the living end-functionalized PS having two methoxymethyl moieties with 1,3-dibromobutane. Unreacted polymer from the coupling reactions was removed by HPLC fractionation.

DPE-functionalized macromonomers were also used for linking reactions with living polymeric anions, followed by the coupling with

chloromethyl groups. Characteristic examples for the synthesis of $AA'_2A''_2$ and $AA'_4A''_4$ asymmetric star polymers are given in Figs. 30 and 31, respectively.

ATRP has also led to the preparation of asymmetric stars. ω-Bromopolystyrene was obtained using ethyl 2-bromoisobutyrate as initiator in the presence of the catalyst CuBr and the ligand pentamethyldiethylenetriamine (PMDETA). The end-bromine group was reacted with 2-amino-1,3-propanediol leading to PS chains bearing two hydroxyl groups at the same chain end. These hydroxyl groups were subsequently transformed to bromines after reaction with 2-bromoisobutyryl bromide. The new initiating sites were used for the polymerization of styrene, leading to of asymmetric $PS(PS')_2$ stars.

Functional Group Asymmetry

Three-arm PBd stars carrying one or two end-functional groups (Fig. 32) were synthesized by the chlorosilane method. The dimethylamino end groups were transformed to sulfozwitterions by reaction with 1,3-propane sultone.

The synthesis of asymmetric three-arm stars PBd with one end-standing dimethylamine group is given in Fig. 33. Butadiene was polymerized using the functional initiator dimethylaminopropyllithium (DMAPLi). The living end-functionalized polymer is then reacted with a large excess of methyltrichlorosilane ([Si–Cl]:

[C–Li] = 100) to produce the methyldichlorosilane end-capped amine-functionalized PBd. The excess silane was removed on the vacuum line. Purified benzene was then introduced to dissolve the silane-capped arm. Finally, a slight excess of PBd living chains, prepared by the nonfunctionalized initiator *sec*-BuLi, was reacted with the macromolecular linking agent, giving the functionalized PBd star with one dimethylamine end group.

A similar procedure was followed for the synthesis of three-arm stars carrying two functional groups. The only difference is that the nonfunctionalized arm was prepared first and reacted with the excess methyltrichlorosilane followed, after the removal of the excess silane, with the addition of a small excess of the living functionalized arms.

Topological Asymmetry

A new class of asymmetric stars, the so-called inverse star-block copolymers, were reported by Tselikas et al. [4]. These polymers are four-arm stars, with each of these arms being a diblock copolymer of isoprene and styrene. Two of these diblock copolymers are connected to the star's center with their PS end, while the other two diblock copolymers with their PI end. Consequently the asymmetry is due to the different topology of the arms. The synthetic procedure for the synthesis of the inverse star-block copolymers is given in Fig. 34.

Diblock copolymer arms (I) having the living end at the PS chain end were prepared by anionic

Synthesis of Star Polymers, Fig. 30 Synthesis of $AA'_2A''_2$ type asymmetric star polymer

Synthesis of Star Polymers, Fig. 31 Synthesis of $AA'_4A''_4$ type asymmetric star polymer

polymerization with sequential addition of monomers. In order to accelerate the crossover reaction from the PILi to the PSLi chain end, a small quantity of THF was added prior the addition of

Synthesis of Star Polymers, Fig. 32 3-arm PBd stars carrying end-functional groups

styrene. The living diblock (I) solution was added dropwise to a stoichiometric amount of $SiCl_4$ until two arms are linked to the silane. This step was monitored by SEC and is similar to a titration process. The end point of the titration was determined by the appearance of a small quantity ($\sim$1 %) of trimer in the SEC trace. The diblock (I) was selected over the diblock (II) due to the increased steric hindrance of the styryl anion over the isoprenyl anion, which makes easier the control of the incorporation of only two arms into the silane. The difunctional macromolecular linking agent was then reacted with a small excess of the living diblock (II) for the preparation of the inverse star-block copolymers. In order to facilitate the reaction with the macromolecular linking agent, the living diblock was end-capped with 3–4 units of butadiene.

Synthesis of Star Polymers, Fig. 33 The synthesis of asymmetric three-arm stars PBd with one end-standing dimethylamine group

Synthesis of Star Polymers, Fig. 34 Synthesis of inverse star-block copolymers

Synthesis of Star Polymers,
Fig. 35 Synthesis of PS (PI)$_2$ miktoarm star polymer

$$\overset{\ominus}{PS}\ \overset{\oplus}{Li}\ +\ (CH_3)SiCl_3\ \longrightarrow\ PS\text{-}Si(CH_3)Cl_2\ +\ LiCl\ +\ (CH_3)SiCl_3\uparrow$$
(Excess)

$$PS\text{-}Si(CH_3)Cl_2\ +\ \overset{\ominus}{PI}\ \overset{\oplus}{Li}\ \longrightarrow\ PS\text{-}Si(CH_3)(PI)_2$$
(Excess)

$$\overset{\ominus}{PS}\ \overset{\oplus}{Li}\ +\ Cl_3SiCH_2CH_2SiCl_3\ \longrightarrow\ PSCl_2SiCH_2CH_2SiCl_3\ \xrightarrow[\text{(Excess)}]{\overset{\ominus}{PI}\ \overset{\oplus}{Li}}\ PS(PI)_5\ +\ 5LiCl$$
$$+\ LiCl$$

Synthesis of Star Polymers, Fig. 36 Synthesis of PS(PI)$_5$ miktoarm star

Synthesis of Miktoarm Star Polymers

Star polymers having chemically different arms are usually called miktoarm stars. The term miktoarm comes from the Greek word μικτός, meaning mixed. Miktoarm star polymers can be synthesized by methods similar to those reported for the synthesis of asymmetric stars [7]. The most common examples of miktoarm stars are A$_2$B, A$_3$B, A$_2$B$_2$, A$_n$B$_n$ (n > 2), and ABC types. Other less common structures, like the ABCD, AB$_5$, AB$_2$C$_2$, etc., are also reported.

Anionic Polymerization Followed by Chlorosilane Coupling

This method is based on stepwise replacement of chlorine of multifunctional chlorosilane compounds, which act as linking agents (LA), with anionically prepared living polymer chains. Miktoarm star copolymers, terpolymers, and quarterpolymers of the type A$_2$B, A$_3$B, A$_5$B, A$_2$B$_2$, A$_8$B$_8$, (AB)$_2$B, (AB)$_3$B, ABC, and ABCD have been prepared by this method.

A$_2$B type of miktoarm star copolymer was first reported by Mays, where A represent PI and B is PS. For its synthesis, the living PS chains (PSLi) were reacted with an excess of methyltrichlorosilane to produce the monosubstituted macromolecular linking agent. The steric hindrance of the living polystyryllithium and 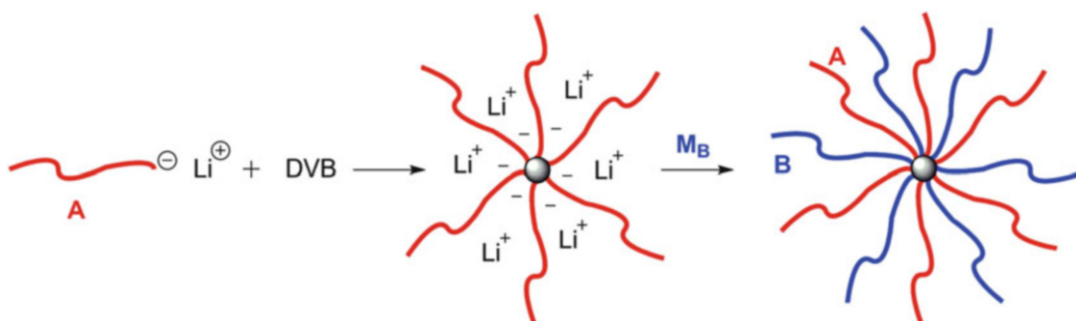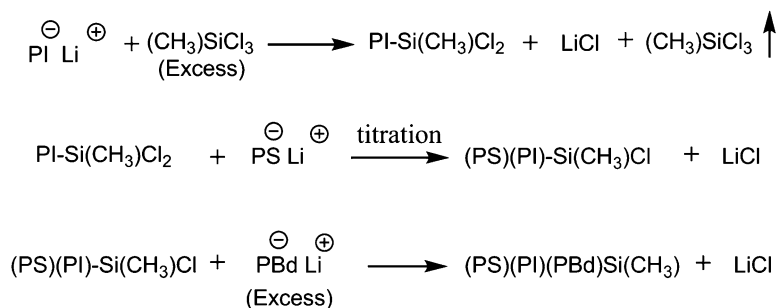the excess of the silane led to the absence of any coupled by-product. The excess silane was removed and then a slight excess of the living PI chains was added to produce the miktoarm star PS(PI)$_2$ (Fig. 35). Excess PI was then removed by fractionation, and final polymer was characterized by SEC and MO.

Using silicon tetrachloride, SiCl$_4$, instead of methyltrichlorosilane as the linking agent, the same method of A$_2$B miktoarm stars synthesis can be expanded to the synthesis of A$_3$B structures. The synthesis of PSPI$_5$ miktoarm stars was accomplished by the reaction sequence outlined in Fig. 36.

Using same chlorosilane chemistry, Hadjichristidis et al. [8] reported the synthesis of the (PS)(PI)(PBd) miktoarm star terpolymer. Living PI chains reacted with a large excess of methyltrichlorosilane to produce the dichlorosilane end-capped polyisoprene. After evaporation of the excess silane, the living PS arm was incorporated by a slow stoichiometric addition (titration). Samples were taken during the addition and were analyzed by SEC to monitor the progress of the reaction and determine the end point of the titration. When the formation of the intermediate product (PS)(PI)Si(CH$_3$)Cl was completed, a small excess of the living PBd chains was added to give the final product. The reaction sequence is outlined in Fig. 37. The order of linking of the various arms to the LA is crucial for the success of the synthesis. The less sterically hindered chain end, namely, PBdLi, has to be

S

Synthesis of Star Polymers, Fig. 37 Synthesis of (PS)(PI)(PBd) miktoarm star terpolymer

$$\text{PI}^{\ominus} \ \text{Li}^{\oplus} \ + \ (CH_3)SiCl_3 \longrightarrow \text{PI-Si}(CH_3)Cl_2 \ + \ LiCl \ + \ (CH_3)SiCl_3 \uparrow$$
$$\text{(Excess)}$$

$$\text{PI-Si}(CH_3)Cl_2 \ + \ \text{PS}^{\ominus} \ \text{Li}^{\oplus} \xrightarrow{\text{titration}} (PS)(PI)\text{-Si}(CH_3)Cl \ + \ LiCl$$

$$(PS)(PI)\text{-Si}(CH_3)Cl \ + \ \text{PBd}^{\ominus} \ \text{Li}^{\oplus} \longrightarrow (PS)(PI)(PBd)Si(CH_3) \ + \ LiCl$$
$$\text{(Excess)}$$

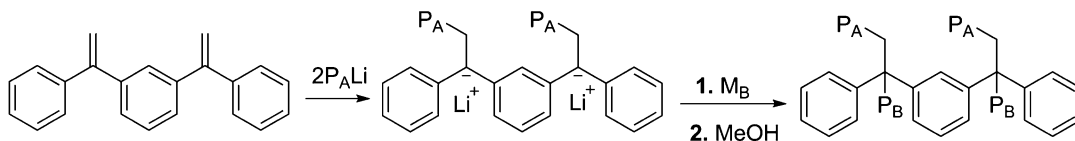**Synthesis of Star Polymers, Fig. 38** The synthesis of miktoarm stars by the DVB method

incorporated last, whereas the most sterically hindered, PSLi, is linked in the titration step.

Anionic Polymerization Method with Divinylbenzene (DVB)

The synthesis of miktoarm stars by the DVB method is a three-step procedure. The first step involves the preparation of the living arm by anionic polymerization using a suitable initiator. The living precursor then reacts in the second step with a small amount of DVB, leading to the formation of a star molecule bearing within its core a number of active sites, which is theoretically equal to the number of the A arms of the star polymer. Subsequent addition of another monomer, in the third step, results in the growth of B arms of the miktoarm stars, since the active star, prepared at the second step, acts as a multifunctional initiator for the polymerization of the second monomer. The growing B arms have anionic sites at their outer ends thus
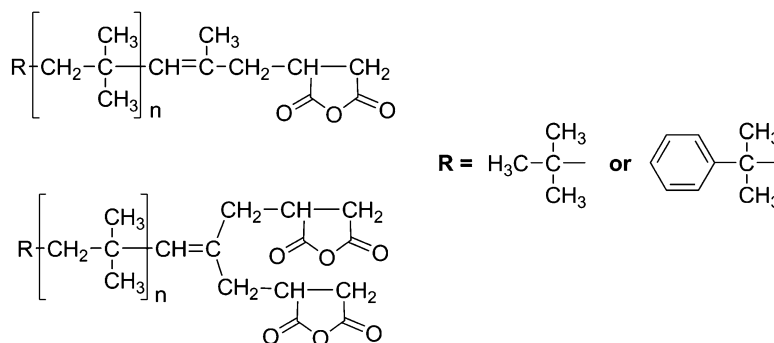
providing the possibility of reacting with electrophilic compounds or other monomers toward the preparation of end-functionalized stars or star-block copolymers. It was first reported by Okay and Funke and by Eschwey and Burchard and developed by Rempp and collaborators. Fig. 38 illustrates the DVB method.

In all cases published in the literature, the A arms are PS chains, whereas a variety of B chains such as PtBuMA, PtBuA, PEO, P2VP, and PEMA have been used. Special care was given to the synthesis of amphiphilic stars bearing hydrophobic and either cationic or anionic arms. The polymerization of styrene was initiated with *sec*-BuLi, except in the case of the PS_nPEO_n stars, where cumylpotassium was used. After the formation of the living PS star, the SEC analysis showed that a considerable part (as high as 15 %) of the PS chains was not incorporated in the star structure mainly due to accidental deactivation. When the second monomer was a (meth)acrylate,

Synthesis of Star Polymers, Fig. 39 The synthesis of A_2B_2 type of miktoarm star polymer

Synthesis of Star Polymers, Fig. 40 Macromolecular coupling agents

the active sites were first capped with a unit of DPE to reduce their nucleophilicity. The final stars usually had *n* values between 4 and 20.

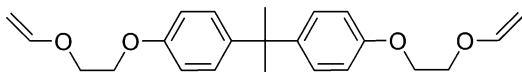## Anionic Polymerization with Diphenylethylenes (DPEs)

Quirk developed the method for the synthesis of miktoarm stars using 1,1-diphenylethylene (DPE) derivatives. Two moles of living polymer A react with one mole of 1,3-bis (1-phenylethenyl)benzene, DDPE, leading to the formation of the coupled product having two active sites. These active sites initiate the polymerization of another monomer to produce A_2B_2 type of miktoarm star polymer. The general reaction sequence is given in Fig. 39.

Polymers of the type A_2B_2 and ABC have been produced by this method so far. The crucial point of the procedure is the control of the stoichiometry of the reaction between the living A chains and the DPE derivative, otherwise a mixture of stars is produced. A major problem is the fact that the rate constants for the reaction of the first and second polymeric chain with the DPE derivative are different. This results in bimodal distributions because of the formation of both the monoanion and dianion. In order to

overcome this problem, polar compounds have to be added, but it is well known that they affect dramatically the microstructure of the polydienes that are formed in the last step. However, the addition of lithium *sec*-butoxide to the living coupled DPE derivative, prior to the addition of the diene monomer, was found to produce monomodal well-defined stars with high 1,4 content. Finally another weak point of the method is that the B arms cannot be isolated from the reaction mixture and characterized separately. It is therefore difficult to obtain unambiguous information about the formation of the desired products.

Living Cationic Polymerization Method

Lemaire et al. reported the amphiphilic miktoarm star copolymers of PIB and PEO bearing one PIB arm and two, three, and four PEO arms with identical length. Using cationic polymerization, end-chlorinated PIBs with controlled MW and narrow molecular weight polydispersity were prepared by cationic polymerization, and the *tert*-Cl ω-end group was quantitatively converted to anhydride or dianhydride (Fig. 40). These species were used as macromolecular coupling agents for α-methoxy-ω-hydroxy PEOs leading

Synthesis of Star Polymers, Fig. 41 Use of divinyl ether as the difunctional monomer

to star-shaped polymers. It was found that the best coupling efficiency was obtained with *p*-toluenesulfonic acid as catalyst in mesitylene at 155 °C. The final products, characterized by SEC and MALDI–TOF mass spectrometry, were mixtures of the stars with unreacted PEO and intermediate products.

Miktoarm star copolymers of the A_2B_2 type were prepared via cationic polymerization, where A is PIB and B is poly(MeVE). The synthetic strategy involved the reaction of 2,2-bis [4-(1-phenylethenyl)phenyl]propane (BDPEP) and 2,2-bis[4-(1-tolylethenyl) phenyl] propane (BDTEP) with living PIB, resulting in a dicationic in-chain initiator. This initiator was used for the polymerization of methyl vinyl ether to give the $(PIB)_2(PMVE)_2$ miktoarm copolymer. Purification of the crude A_2B_2 copolymer was performed on a silica gel column and the purity of the resulting star was 93 %.

Miktoarm stars of isobutyl vinyl ether (IBVE) and hydrolyzed 2-acetoxyethyl vinyl ether (AcOVE) or diethyl 2-(vinyloxy)ethyl malonate (VOEM) were prepared using the divinyl ether (as shown in Fig. 41) as the difunctional monomer. The living chains of IBVE were used as macroinitiators for the polymerization of the diether, resulting in a star IBVE with a microgel core. The living sites in the core were used for the sequential polymerization of the other monomers.

Living Anionic Polymerization and Stepwise Iterative Methodology

For the synthesis of asymmetric and miktoarm star polymers, Hirao has developed new conceptual methodology based on the "iterative approach" using living anionic polymerization [6]. The methodology involves two sets of the following reaction conditions for the entire iterative

synthetic sequence: (a) the introduction of polymer segment(s) together with the site(s), "Y," into the core by using reaction site(s), "X," and (b) the regeneration of "X" derived from "Y." The two reactions are repeated several times to successively synthesize star-branched polymers.
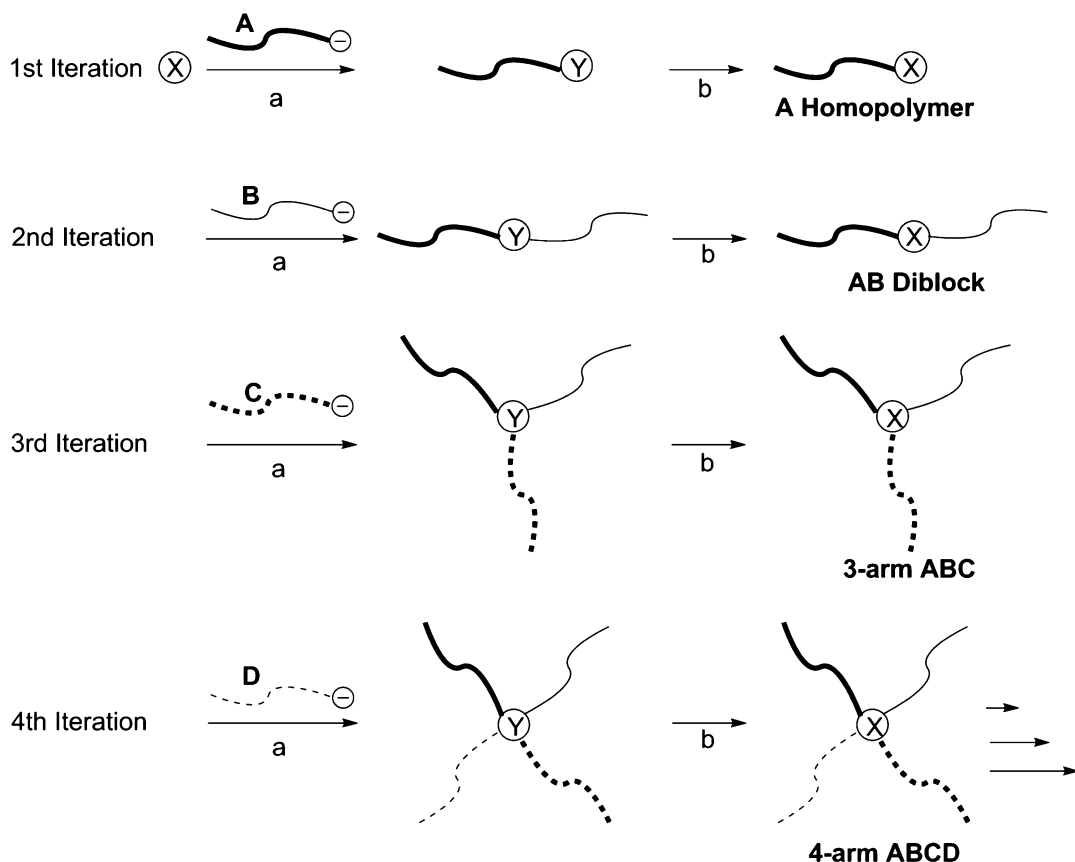
As can be seen in Fig. 42, a living anionic polymer (A) reacts quantitatively with the "X" reaction site to link the polymer chain with the change from "X" to "Y" in reaction step (a), resulting in a chain-end-Y-functionalized polymer (A). The "Y" is regenerated to "X" by reaction step (b). In the next iteration, another living anionic polymer (B) reacts with the chain-end-X-functionalized polymer (A) to link the two polymer chains, resulting in an in-chain-Y-functionalized AB diblock polymer. After again regenerating the "X" reaction site through "Y," the resulting in-chain-X-functionalized AB diblock polymer reacts with a living polymer (C) to synthesize a three-arm ABC star-branched polymer with "Y" at the core. It is possible to continue the same reaction sequence to successively synthesize four-arm ABCD, followed by five-arm ABCDE, and so on to many armed and multicompositional miktoarm star polymers.

Use of the iterative methodology led to the synthesis of miktoarm stars of the type AB_4, AB_8, A_2B_4, A_2B_8, A_2B_{12}, ABC_2, ABC_4, $A_2B_2C_2D$, $A_4B_4C_4D$, ABC, A_3B, A_2B_2, AB_3, A_2BC, AB_2C, ABC_2, and ABCD, where A is PS, B is PI or PαMS, C is PI or poly(4-(4–1,2:5,6-di-O-isopropylidene-α-glucofuranose-3-oxy)butoxy) styrene, and D is poly(4-trimethylsilylstyrene).

Methodology Based on ATRP
In addition to anionic polymerization, ATRP has also been used for the synthesis of miktoarm stars of the A_nB_m type. Using DVB, $(PnBuA)_n(PS)_m$ miktoarm stars were obtained (Fig. 43).

Bis(2-methacryloyloxyethyl)disulfide was also employed as a difunctional monomer for the synthesis of $(PMMA)_n(PnBuA)_m$ miktoarm stars (Fig. 44). In the last case, using suitable reducing agents, it is possible to degrade the core of the star structure. The formation of

Synthesis of Star Polymers, Fig. 42 Iterative methodology for the successive synthesis of asymmetric star-branched polymers

Synthesis of Star Polymers, Fig. 43 Synthesis of miktoarm stars of the A_nB_m type by ATRP

interstar and intrastar arm–arm coupling was observed. The initiating efficiency of the alkyl bromide sites in the core of the star polymers was determined after cleavage of the degradable stars and the corresponding miktoarm stars. It was found that only 19 % of the initiation sites were active for the polymerization of the second monomer.

S

Synthesis of Star Polymers, Fig. 44 Synthesis of $(PMMA)_n(PnBuA)_m$ using difunctional monomer

Related Entries

References

1. Hadjichristidis N, Iatrou H, Pitsikalis M, Mays J (2006) Macromolecular architectures by living and controlled/living polymerizations. Prog Polym Sci 31(12):1068–1132
2. Hadjichristidis N, Pitsikalis M, Pispas S, Iatrou H (2001) Polymers with complex architecture by living anionic polymerization. Chem Rev 101(12):3747–3792
3. Pitsikalis M, Pispas S, Mays JW, Hadjichristidis N (1998) Nonlinear block copolymer architectures. Adv Polym Sci 135:1–137
4. Hadjichristidis N, Pispas S, Pitsikalis M, Iatrou H, Vlahos C (1999) Asymmetric star polymers: synthesis and properties. Adv Polym Sci 142:71–127
5. Hadjichristidis N, Pispas S, Iatrou H, Pitsikalis M (2002) Linking chemistry and anionic polymerization. Curr Org Chem 6:155–176
6. Higashihara T, Hayashi M, Hirao A (2011) Synthesis of well-defined star-branched polymers by stepwise iterative methodology using living anionic polymerization. Prog Polym Sci 36(3):323–375
7. Hadjichristidis N (1999) Synthesis of miktoarm star (μ -Star) polymers. J Polym Sci Part A Polym Chem 37:857–871
8. Hadjichristidis N, Pitsikalis M, Iatrou H, Driva P, Sakellariou G, Chatzichristidi M (2012) Polymers with star-related structures: synthesis, properties, and applications. Polym Sci Compr Ref 6:29–110

Synthetic Rubbers

Sven Thiele and Michael Roessle
Development Anionic, R&D Synthetic Rubber,
Styron Deutschland GmbH, Merseburg,
Germany

Synonyms

Synthetic elastomers

Definition

In contrast to natural rubber obtained by coagulation from latex of plants such as *Hevea brasiliensis*, synthetic rubbers is a collective term for different elastomeric polymers of synthetic origin with properties tailor-made according to the application.

Historical Background

In 1900, J. Kondakow reported the potassium hydroxide initiated polymerization of 2,3-dimethylbutadiene in ethanol upon treatment of the monomers for 5 h's at 150 °C [1]. The same solvent free monomers were auto-polymerized in the presence of sunlight, yielding a white relatively high molecular weight rubber, which resembled natural rubber in terms of chemical resistance [2]. The development of a technically feasible rubber production technology was proposed by Fritz Hofmann in 1906. Germany, with no access to natural rubber plants, subsidized the technology development with 100,000 Reichsmark. An estimated total amount of 2.5 kt polydimethylbutadiene "Methyl-Kautschuk H" (hard rubber) and "Methyl-Kautschuk W" (soft rubber) was produced from 1914 to 1918. The more economic feasible processes of emulsion butadiene-styrene copolymerization and the process of sodium initiated butadiene polymerization (BuNa) were started in 1938 at the central German industrial complex of the I.G. Farbenindustrie at Schkopau ("Buna Werke").

Though cured synthetic rubber compositions were observed to outperform natural rubber comprising formulations in terms of oil, abrasion, and ozone resistance, the seven to eightfold polymer market price compared to natural rubber would not have justified commercialization under normal political conditions. Since the 1930s, synthetic rubber quality and production technology were constantly improved resulting in the volume of these products reaching the level of natural rubber production volumes [3].

Synthetic Rubber Production

In 2012, the worldwide capacity for synthetic rubbers amounted to about 17,000 kt per year. The majority of this volume is comprised of butadiene rubber (BR), random styrene-butadiene copolymer rubber made in solution or emulsion (SSBR or ESBR), solution-made styrene-butadiene block copolymers (SBC), isobutylene isoprene rubber (IIR), isoprene rubber (IR), ethylene propylene diene rubber (EPDM), and acrylonitrile butadiene rubber (NBR) (Fig. 1).

The production processes of rubber can be distinguished by the applied reaction media and/or by the chemical nature of the polymerization initiating agent. Below, commercially applied production processes are classified accordingly. They are:

(i) Solution-made BR (Ti-, Co-, Ni-, or Nd-based catalysts or anionic initiator), SSBR (anionic initiator), EPDM (Ti- or V-based catalyst), and IR (anionic initiator or Ti-based catalyst)
(ii) Emulsion-made chloroprene rubber (CR), ESBR, and NBR (cold- or warm-radical polymerization process)
(iii) Suspension-made EPDM and IIR
(iv) Gas phase-made EPDM (Ti-based catalyst) [5]

Tires – The Main Application for Synthetic Rubbers

The main applications for synthetic rubbers are tires (69 %), general rubber goods (25 %)

Synthetic Rubbers,
Fig. 1 2012 Global
Synthetic Rubber
Capacities in kt and % [4]

Synthetic Rubbers,
Fig. 2 Applications of
synthetic rubber [6]

including conveyor belts or automotive applications and high impact polystyrene (HIPS, 3 %) (Fig. 2).

The key performance requirements of tires are wet traction, abrasion resistance (corresponding to tire lifetime), and rolling resistance (relating to fuel consumption). CO_2 emissions from road transport have increased worldwide by 57 % from 1990 to 2011 and are now responsible for approximately 16 % of total CO_2 emissions (Table 1).

Therefore, world total CO_2 emissions rose by 49 % in the reported timeframe [7]. 20–30 % of total automobile driving resistance is caused by the rolling resistance of tires. In 2012 a tire label was introduced in the EU to rate fuel consumption, wet grip, and noise characteristics of commercially available tires (Fig. 3). Similar initiatives were established in Korea and Japan, while other countries announced similar plans.

Figure 3 below shows a difference of the fuel consumption between Class A and G tires in the

Synthetic Rubbers, Table 1 EU and World total CO_2 emissions

	1990 in Gt	2011 in Gt
EU total CO_2 emissions	4.05	3.54
World total CO_2 emissions	20.99	31.34

European labeling system of 0.66 l/100 km or 10 % of the total fuel consumption.

The average CO_2 emission from new passenger cars in 2011 in Europe (EU) was 135.7 g $[CO_2]$/km. In the following years, several national automobile CO_2 emission limits were announced. Exemplarily, the emission limits for the USA, EU, and China (CN) are listed below [9–12].

USA (g[CO_2]/km)	EU(g[CO_2]/km)	CN(g[CO_2]/km)
2016: 137–172	2015: 130	2020: 119–133
2020: 113–137	2022: 95	
2022: 93–124		

Synthetic Rubbers,
Fig. 3 Fuel consumption according to the EU tire label in L/100 km [8]

Synthetic Rubbers,
Fig. 4 Number of patents for SBR and BR

Patent Situation

Proposed legislative actions and rising oil prices compel tire manufacturers and rubber producers to develop new fuel saving materials. This is reflected in the increased number of patent publications in recent years, as shown below. The number of innovative technologies for SBR and BR increased from 1,243 in the 10-year period 1980–1989 to 1,075 in the single year 2012, representing a growth factor of 9 (Fig. 4) [13].

Innovative companies are responsible for the majority of new technologies, improving tire properties such as fuel consumption, abrasion resistance, ice and wet grip. These tire properties essentially depend on polymer-filler interactions. Those interactions can be achieved through chemical modification of the polymer macromolecules

through incorporation of polar functionalities. Further optimization for specific end-applications can be made by variations of the rubber microstructure and composition distribution.

Chemical Modifications

For optimization of the physical and chemical properties of rubber, there are 3 major concepts of chemical modification:

1. Functional initiators (e.g., deprotonated amines) (Fig. 5)
2. End modification and coupling with polar molecules (e.g., epoxides, nitriles, isocyanates, siloxanes, alkoxy compounds, organo- or metal halides) (Fig. 6)

Synthetic Rubbers, Fig. 5 Initiation of polymerization with deprotonated allylamine [14]

Synthetic Rubbers, Fig. 6 End modification and coupling with tetraethoxysilane [15]

Synthetic Rubbers, Fig. 7 Linear or star-shaped backbone modified polymer [16]

3. Backbone modification with functional monomers (e.g., amino or alkoxy substituted styrenes, vinyl heteroarenes) or by grafting reaction (e.g., epoxidation reactions) upon completed monomer polymerization (Fig. 7).

Reinforcement of rubbers is achieved through application of suitable filler systems. Depending on the type, particle size, and surface area of selected fillers, dynamic and mechanical properties are changed. Currently, the most often used fillers are silica in combination with silane coupling agents and carbon black. For tire applications (tread, inner liner, carcass), N110-N772 carbon black grades with specific surface areas from 32 to 127 m^2/g (nitrogen surface area) are applied. The nitrogen surface area of silica ranges from 115 to 235 m^2/g. Recently, new nano-filler materials such as carbon nanotubes and organoclays have been reported to further optimize rubber properties [17].

Evolution of SBR Grades

As an innovative major supplier of SBR, Styron is steadily improving the rubber architecture through application of novel modifying agents and technologies [18]. Figure 8 visualizes the development of functionalized synthetic rubber properties (filled with silica) with respect to non-modified Generation 0 SSBR.

The developmental process from Generation 0 to Generation 3 SSBR enabled a stepwise reduction of the rolling resistance performance indicator tan delta at 60 °C of approximately 40 % while improving the grip properties in parallel. Further steps towards an enhanced tire rolling resistance – grip – abrasion resistance performance balance are underway at Styron, along with SSBR production capacity expansions. Therefore, novel Styron synthetic rubber availability is enabling the development of high-performance tires with lower automobile fuel consumption and CO_2 emission.

Synthetic Rubbers, Fig. 8 Styron SSBR performance properties in silica relative values in %)

Related Entries

▶ Carbon Black Reinforced Elastomers
▶ Elastomer Blends: The Role of Nanoparticles on Properties
▶ Material Laws of Rubbers
▶ Mechanical Behavior of Filled Rubbers
▶ Natural Rubber
▶ Silica Reinforcement
▶ Vulcanization
▶ Wear and Abrasion of Tires

References

1. Kondakov I (1900) Über das anormale Verhalten der Poly-Haloidverbindungen zu alkoholischer Kalilauge. J Prakt Chem 62:166–188
2. Kondakov I (1901) Ein bemerkenswerter Fall von Polymerisation des Diisopropenyls. J Prakt Chem 64:109–110
3. Jünger W (1940) Kampf um Kautschuk. Wilhelm Goldmann, Leipzig
4. IISRP 2012 report
5. Röthemeyer F, Sommer F (2013) Kautschuktechnologie: Werkstoffe – Verarbeitung – Produkte. Carl Hanser, München
6. LMC report 2012
7. CO_2 emissions from fuel combustion highlights 2013, OECD/IEA 2013
8. Rollwiderstand http://www.vcd.org/rollwiderstand.html. Accessed 05 Dec 2013
9. Regulation (EC) No 443/2009 of the European Parliament and the council of 23 Apr 2009
10. Federal Register/vol 77, no 199/Monday, 15 Oct 2012/ Rules and regulations, 62623–63200 EPA
11. China state council (2012): http://www.gov.cn/zwgk/2012-07/09/content_2179032.htm
12. Conversion of 5 l/100 km: 1 l of Diesel fuel: 2650 g CO_2, 1 l of gasoline: 2380 g CO_2, source: http://www.deutsche-handwerks-zeitung.de/kraftstoffverbrauch-in-co2-ausstoss-umrechnen/150/3097/57956
13. Styron patent search with Thomson innovation, 3 Dec 2013
14. Styron Europe GmbH: Modified polymer compositions. WO 2011/076377 A1, 30 June 2011
15. Phillips Petroleum Company: Silicon-containing polymers. US 3,244,664 A, 5 Apr 1966
16. The Goodyear Tire & Rubber Company: Functionalized elastomers. US 6,664,328 B1, 16 Dec 2003
17. (a) The Goodyear Tire & Rubber Company: Tire with a component containing carbon nanotubes. EP 2 338 697 A1, date of publication: 29 June 2011; (b) Continental AG: Fahrzeugluftreifen. DE 10 2007 056 689 A1, 28 May 2009; (c) ContiTechAG: Polymer mixture, rubber mixture comprising the polymer mixture and process for preparing the rubber mixture. EP 2 650 325 A1, 16 Oct 2013; (d) Bridgestone Corporation: Orientated carbon nanotube composite,

S

process for Producing orientated carbon nanotube composite, and, produced using orientated carbon nanotube composite, pneumatic tire, wheel for vehicle, tire wheel, assembly and disk brake. WO 2004/031289 A1, 15 Apr 2004; (e) Hankook Tire Co. LTD.: Rubber composition for tread portion of pneumatic tire, contains rubber component containing carbon nanotube and organic compound and hardening filler. KR2009044637A; (f) Giannini L, Coombs M, Galimberti M, Conzatti L, Hybrid filler networks in hydrocarbon polymer compounds: the unexpected role of organoclay building blocks, Nanopolymers 2011, International conference, 3rd, Duesseldorf, Germany, 13–14 Sept 2011; (g) Seo BH, Kang YG, Jang SH, Kim W (Nexen Tire Corporation): Characterization of SBR/Nanoprene compounds, International Rubber Conference 2012, Bangkok, 16–18 Dec 2012

18. (a) Thiele SKH, Knoll S (2011) Novel functionalized SSBR for silica- & carbon black containing tires, Published at the conference of the rubber division of the ACS at the Fall 180th technical meeting 2011 at Cleveland, 10–13 Oct 2011; (b) Thiele SKH, Kiesekamp J, Rulhoff S, Bellgardt D (2011) Modified synthetic rubber for silica & carbon black containing tires. KGK 64:36–41; (c) Thiel SKH, Ruehmer T, Kiesekamp J (2013) Novel functionalized synthetic rubbers for tire applications. KGK 66:38–44; (d) Thiele SKH, Bellgardt D, Holzleg M (2008) Polymer functionalization – novel rubber for tire tread application. KGK 61:244–245; (e) Thiele SKH, Bellgardt D (2009) Novel functionalized SSBR for silica- & carbon black containing tires, Published at the conference of the rubber division of the ACS at the Fall 176th technical meeting 2009 at Pittsburg, 12–16 Oct 2009